AMIRA INTERNATIONAL

Final Report

Confidential

P700 - Predictive Magnetic Exploration Models for Porphyry, Epithermal and Iron Oxide Copper-Gold Deposits: Implications for Exploration

February 2004

CSIRO Exploration & Mining

AMIRA International Limited ACN 004 448 266 ABN 60 176 687 975
Level 2 271 William Street Melbourne 3000 Australia Phone: +61 3 8636 9999 Facsimile: +61 3 8636 9900

Exploration and Mining Report 1073R

PREDICTIVE MAGNETIC EXPLORATION MODELS FOR PORPHYRY, EPITHERMAL AND IRON OXIDE COPPER-GOLD DEPOSITS: IMPLICATIONS FOR EXPLORATION

D.A. Clark, S. Geuna and P.W.Schmidt

SHORT COURSE MANUAL FOR AMIRA P700

April 2003

CSIRO Exploration and Mining
PO Box 136, North Ryde, NSW, Australia

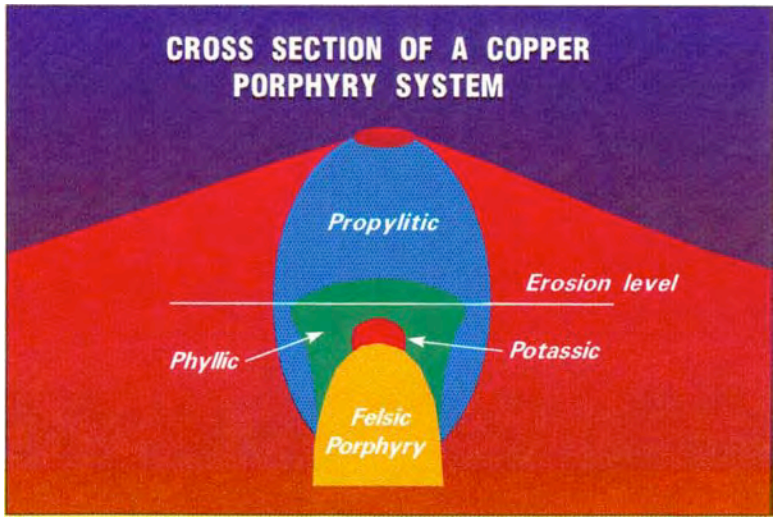

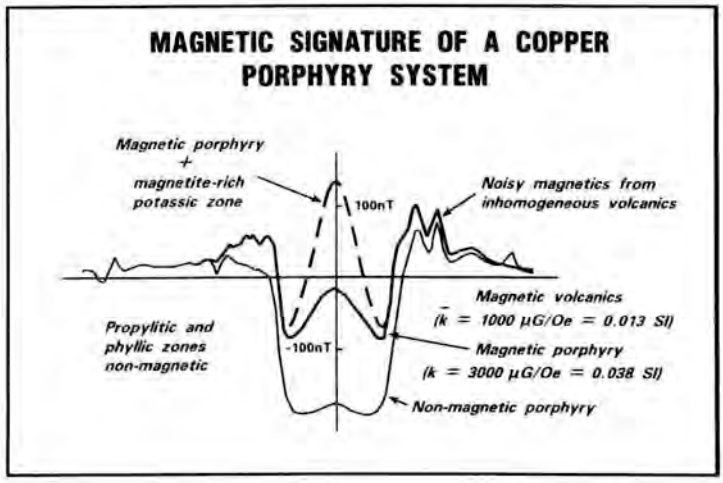

Idealised magnetic anomaly associated with a porphyry copper system, showing the noisy background associated with magnetic volcanics, the 'alteration low' associated with the propylitic and phyllic alteration zones, the high arising from the magnetic porphyry plus, in the case of gold-rich copper mineralisation, the magnetite-bearing potassic alteration zone.

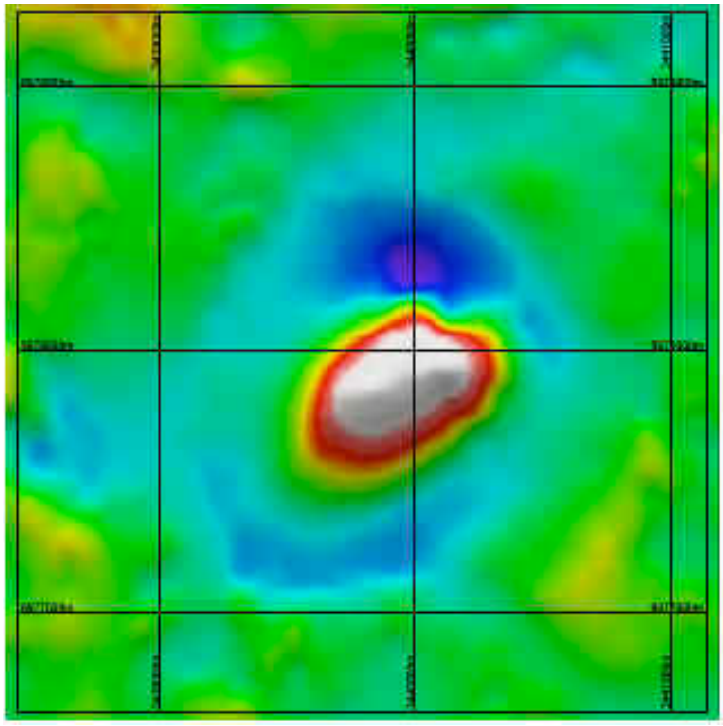

Distribution List

	Copy No.
AMIRA	1-8
Dr N. Phillips, Chief CSIRO Exploration and Mining	9
Mr D.A. Clark	10
Dr S. Geuna	11
Dr P.W. Schmidt	12
Records Section (North Ryde)	13

Copy no. ..... of 19 copies

Page no.

TABLE OF CONTENTS

1. INTRODUCTION

AMIRA project P700 was aimed at improving the utility of magnetic surveys in exploration for a number of deposit types: porphyry Cu (Au, Mo) and related deposits, the newly recognised category of reduced porphyry deposits, precious metal and Cu-Au volcanic-hosted epithermal deposits, and iron oxide Cu-Au deposits. In the course of the project predictive magnetic exploration models were developed for these types of deposit. The magnetic models are based on realistic geological models, a comprehensive magnetic property database, and magnetic petrological principles. Outcomes of the project include an Atlas of Predictive Magnetic Exploration Models for these types of deposit, in a wide range of geological settings, and a set of practical and easily understandable criteria for exploration using magnetics for porphyry and epithermal deposits.

Magnetics is the most widely used geophysical method in hard rock exploration and magnetic surveys are an integral part of exploration programmes for porphyry and epithermal deposits. However, the magnetic signatures of porphyry and epithermal deposits are extremely variable and exploration that is based simply on searching for signatures that resemble those of known deposits is rarely successful.

A number of well-known geological models of porphyry and epithermal deposits are routinely used in exploration, even though most deposits fail to match the idealised models closely, due to post-emplacement tectonic disruption and rotations, asymmetric alteration zoning due to emplacement along a contact between contrasting country rock types, and so on. These complications are taken into account by exploration geologists as geological information about a prospect accumulates.
The variability of magnetic signatures of these deposits reflects:

i. strong dependence of magnetic signatures on local geological setting,
ii. departures of real mineralised systems from idealised geological models,
iii. the direction and intensity of the geomagnetic field, which varies over the Earth,
iv. differing magnetic environments (host rock magnetisation, regional gradients, interference from neighbouring anomalies etc.).

Points (i)-(ii) are the most important reasons for variability of magnetic signatures of mineralised systems. Point (i) covers a number of significant geological factors, the most important of which are: tectonic setting and its influence on magma composition and mode of emplacement; influence of pre-existing structures on the geometry and depth of emplacement; and the crucial influence of host rock composition on alteration assemblages, including secondary magnetic minerals, and on the stability of primary magnetic minerals.

Many porphyry systems depart from idealised models due to emplacement along geological contacts with contrasting rocks on either side, producing asymmetric zoning patterns. Point (ii) reflects not only the local geological setting at the time of emplacement, but also post-emplacement modification of deposits. Post-emplacement tilting of porphyry and epithermal systems and dismemberment by faulting are very

common and drastically modify the geophysical signatures. Burial of a deposit by younger sedimentary or volcanic rocks also modifies the anomaly pattern. Conversely, exhumation and partial erosion of the system produces a very different magnetic signature. In older deposits, metamorphism can substantially modify the magnetic mineralogy of the deposits and host rocks, with concomitant changes in the magnetic anomaly pattern. Although the majority of porphyry and epithermal deposits are relatively young and, at most, weakly metamorphosed, some relatively ancient deposits in metamorphosed terrains are known. There is a strong possibility that some older porphyry and epithermal deposits occur that have not been recognised, because effects of metamorphism and deformation have obscured their true nature.

Points (i)-(ii) can only be satisfactorily addressed by an approach that integrates a knowledge base of magnetic properties, based on detailed sampling of a variety of deposits and modelling of their magnetic anomalies, combined with magnetic petrological principles to produce predictive magnetic exploration models that are specific to each geological setting. Given the magnetic petrophysical database and the understanding of the geological factors that create and destroy magnetic minerals in porphyry systems, however, the magnetic effects of the above-mentioned geological complications are quite predictable. The CSIRO Rock Magnetism Group is uniquely qualified to tackle predictive magnetic modelling of mineral deposit models, as it combines expertise in magnetic interpretation with extensive knowledge of magnetic petrophysics and magnetic petrology, acquired over a succession of AMIRA projects, as well as a long history of case studies of mineralised areas carried out for exploration companies.

Point (iii) above is routinely addressed by reduction-to-the-pole (RTP) processing of measured total magnetic intensity (TMI) data, which is generally successful in producing more intuitively interpretable magnetic signatures that are no longer skewed by the inclination of the geomagnetic field and can therefore be directly compared with signatures from other geomagnetic latitudes. Thus it is proposed to produce the predictive magnetic exploration models predominantly in the form of calculated RTP anomalies that can be compared with RTP processed surveys, although TMI signatures at other geomagnetic latitudes will be presented for selected models.

Once a generic predictive magnetic model has been produced for a particular *geological* setting, point (iv) above can be addressed by using the grid of predicted values as a template that can be superimposed on the measured values anywhere in the survey area to produce the predicted signature for the local *magnetic* environment. For example, in the presence of a steep regional field gradient, the generic signature can be grossly distorted and may easily elude recognition. Superimposing the grid values for the generic model on this gradient produces the anomaly that is to be expected at that specific locality, which may be quite different from the signature of an identical source in a different regional field.

The project provided the following products:

- An Atlas of Predictive Magnetic Exploration Models (and case histories), based on standard geological models for porphyry copper and copper-gold deposits (including associated skarn deposits and intrusive-related breccia-hosted Au deposits), volcanic-hosted epithermal precious metal and Au-Cu deposits, and iron oxide copper-gold deposits for a wide range of geological settings (RTP images, contour maps and profiles; supplemented by TMI equivalents at a range of latitudes, for selected models).
- Calculated grids for each of the models, in formats convenient for sponsors.
- An extensive review and classification of observed magnetic signatures of porphyry and epithermal deposits and an analysis of the geological factors that influence those signatures,
- A relational database (Access and/or Paradox) of geological, magnetic petrophysical, magnetic petrological and magnetic anomaly characteristics along with other geophysical characteristics of well-documented porphyry and epithermal deposits worldwide. An example of the type of query that can be made with such a database is ‘list all porphyry copper deposits that are rich in gold and that have a central magnetic high (i.e. abundant magnetite in the potassic zone) and an annular low (i.e. magnetite destruction in the surrounding rocks)’, another more quantitative query may be ‘what is the range of magnetic susceptibility for all potassic zones in porphyry copper deposits’.
- A set of practical and easily understood guidelines that can be applied by geologists and geophysicists to magnetic exploration for porphyry and epithermal deposits, e.g. favourable and unfavourable indicators for porphyry and epithermal systems from regional to local scale.
- A workshop at the end of the project to present the outcomes and transfer the knowledge base to sponsors. This workshop manual is aimed at geologists, as well as geophysicists, and includes a comprehensive treatment of the principles underlying the models and their application. Additional workshops are available at cost to each sponsor at a location of their choice.

2. MAGNETIC PETROPHYSICS AND MAGNETIC PETROLOGY: APPLICATION TO INTERPRETATION OF MAGNETIC SURVEYS AND IMPLICATIONS FOR EXPLORATION

2.1 Induced, Remanent and Viscous Magnetisation

Magnetised matter contains a distribution of microscopic magnetic moments. Unpaired electron spins are the most important sources of magnetic moment. Magnetisation **J** is defined as the magnetic dipole moment per unit volume of the material. *Induced magnetisation* $\mathbf{J_I}$ is the component of magnetisation produced in response to an applied field. The induced magnetisation varies sympathetically with changes in the applied field and vanishes when the field is removed. *Remanent magnetisation* or *remanence* $\mathbf{J_R}$ is the "permanent" magnetisation that remains when the applied field is removed, and is essentially unaffected by weak fields.

The total magnetisation is the vector sum of the induced and remanent magnetisations:

$$\mathbf{J} = \mathbf{J_I} + \mathbf{J_R} .$$

For sufficiently weak fields, such as the geomagnetic field, the induced magnetisation is approximately proportional to the applied field. The constant of proportionality is known as the *susceptibility*, k. Thus if the applied field is **F**, the induced and total magnetisations are given by:

$$\mathbf{J_I} = k\mathbf{F} ; \quad \mathbf{J} = k\mathbf{F} + \mathbf{M_R} .$$

For most rocks the induced magnetisation is essentially parallel to the applied field, irrespective of the field direction. In this case the susceptibility is a scalar quantity, i.e. it is characterised simply by its magnitude and is isotropic. The case of anisotropic susceptibility is discussed below.The *Koenigsberger ratio* (Q) is a convenient parameter for expressing the relative importance of remanent and induced magnetisations. It is given by:

$$Q = J_R / J_I = J_R / kF .$$

Thus Q > 1 indicates that remanence dominates induced magnetisation, whereas Q < 1 implies that induced magnetisation is dominant.

The distinction between induced and remanent magnetisations is not completely clear-cut because, strictly speaking, remanent magnetisation is metastable, not permanent. A wide range of time constants characterises the equilibration of magnetisation in many magnetic materials. Thus magnetisation responds over time to changes in the applied field. The time-varying part of the remanence is called *viscous remanent magnetisation*. Figure 2.1 illustrates the distinction between induced magnetisation, viscous remanence and stable remanence. Figure 2.1(a) shows the changes in magnetisation of an initially demagnetised sample in response to an applied field, which is switched on and off as shown in Figure 2.1(b). Small applied fields, comparable in strength to the geomagnetic field, produce small, reversible changes in magnetisation when they are applied briefly, i.e. the magnetisation vanishes on removal of the field. This induced magnetisation is approximately proportional to the strength of the applied field. Thus the susceptibility, which is defined as the induced magnetisation divided by the applied field, is approximately independent of the field. If a larger field is

applied and then removed an irreversible change in magnetisation occurs - an *isothermal remanent magnetisation* J_{IRM} has been imparted to the sample. This magnetisation can be regarded as permanent on the experimental time scale. Figure 2.1(c) illustrates this behaviour in terms of the hysteresis loop, plotting magnetisation J versus applied field H. The initial portion of the J-H curve is approximately linear and is traversed reversibly when a small field is applied and removed. When the larger field is applied and instantaneously removed, the sample follows the trajectory abc. At the point b the total magnetisation is the sum of the induced magnetisation, which by definition is the component that vanishes when the field is removed, and the isothermal remanence.

If the field is again switched on, the magnetisation follows the path cd and returns initially to its former value ($J_{IRM} + J_{IND}$). If the applied field remains on, however, the total magnetisation increases gradually with time, from d to e. After an initial period that depends on the grain size distribution, the increase in magnetisation is usually found to be approximately proportional to the logarithm of time, over several decades of t. When the field is removed this excess magnetisation, the viscous remanent magnetisation (VRM), remains and augments the isothermal remanence, but decays at a rate comparable to the acquistion rate. After sufficient time in zero field the VRM has decayed completely and only the stable IRM remains. Thus viscous remanence is a temporary magnetisation that is intermediate in character between induced magnetisation and more stable forms of remanence. The separation of magnetisation into induced, viscous and stable components is not exact, because the distinctions depend on the time scale under consideration.

In general the sample may not be initially in a demagnetised state. If the sample carries a stable remanence component initially the magnetisation plots in Figure 2.1(a) and 1(c) are simply shifted upwards.

2.2 Types of Remanent Magnetisation

The natural remanent magnetisation (NRM) of rocks reflects the history of the rock and the ambient field. Some rock samples carry isothermal remanent magnetisation as a result of exposure to magnetic fields. In this case the NRM is not representative of the remanence carried by the bulk of the rock unit. Lightning-affected samples often carry intense NRM, characterised by anomalously high Q and directions that are scattered for samples separated by a few metres or more. NRM measurements from surface exposures should therefore be regarded with caution. Drilling, logging with pencil magnets, mining activities and exposure to fields during or after collection can contaminate sample NRMs with IRM components that have no geological significance. Standard palaeomagnetic cleaning techniques are strongly recommended to detect and preferentially remove these sources of palaeomagnetic noise.

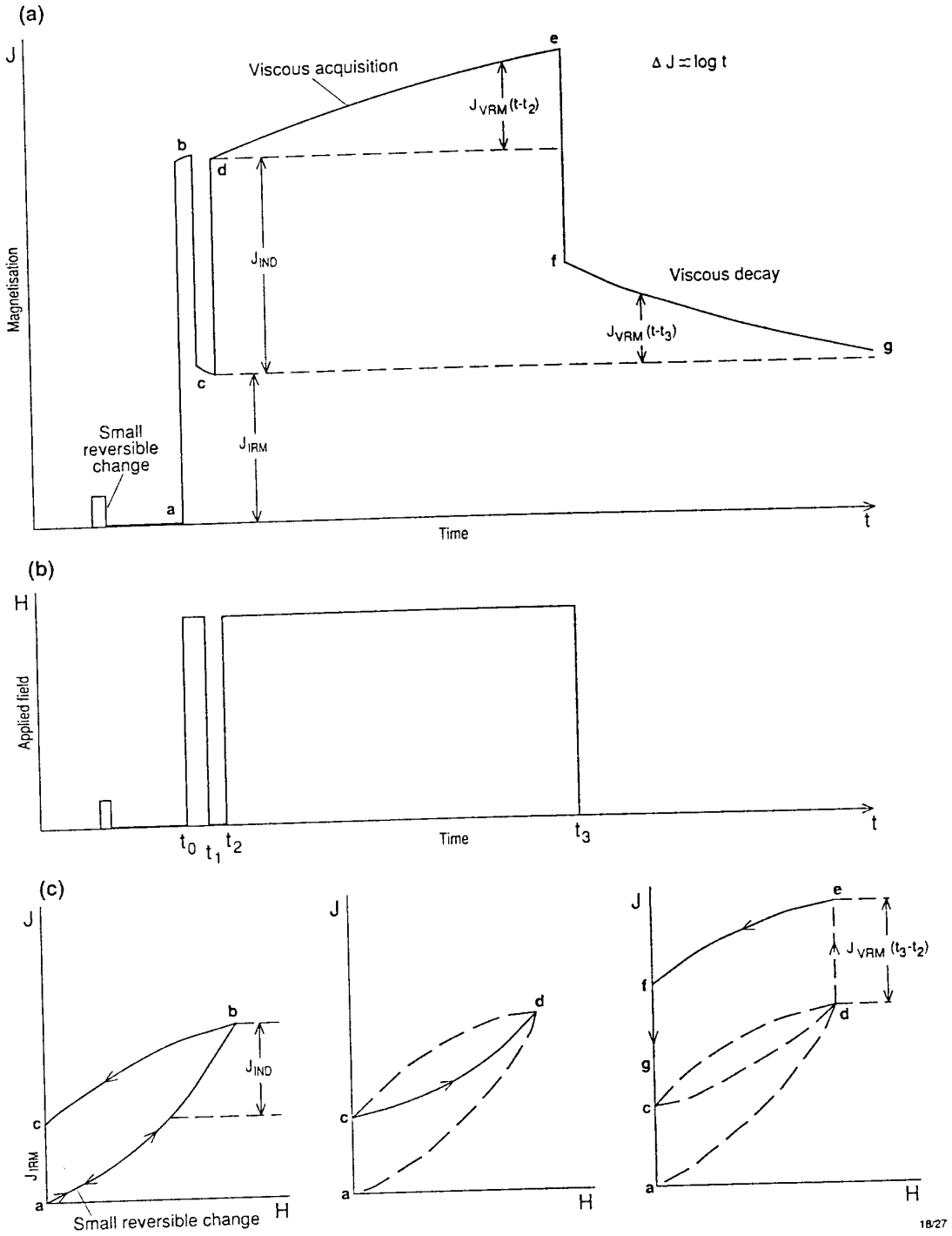

Figure 2.1. Distinction between induced, viscous and remanent magnetisations.

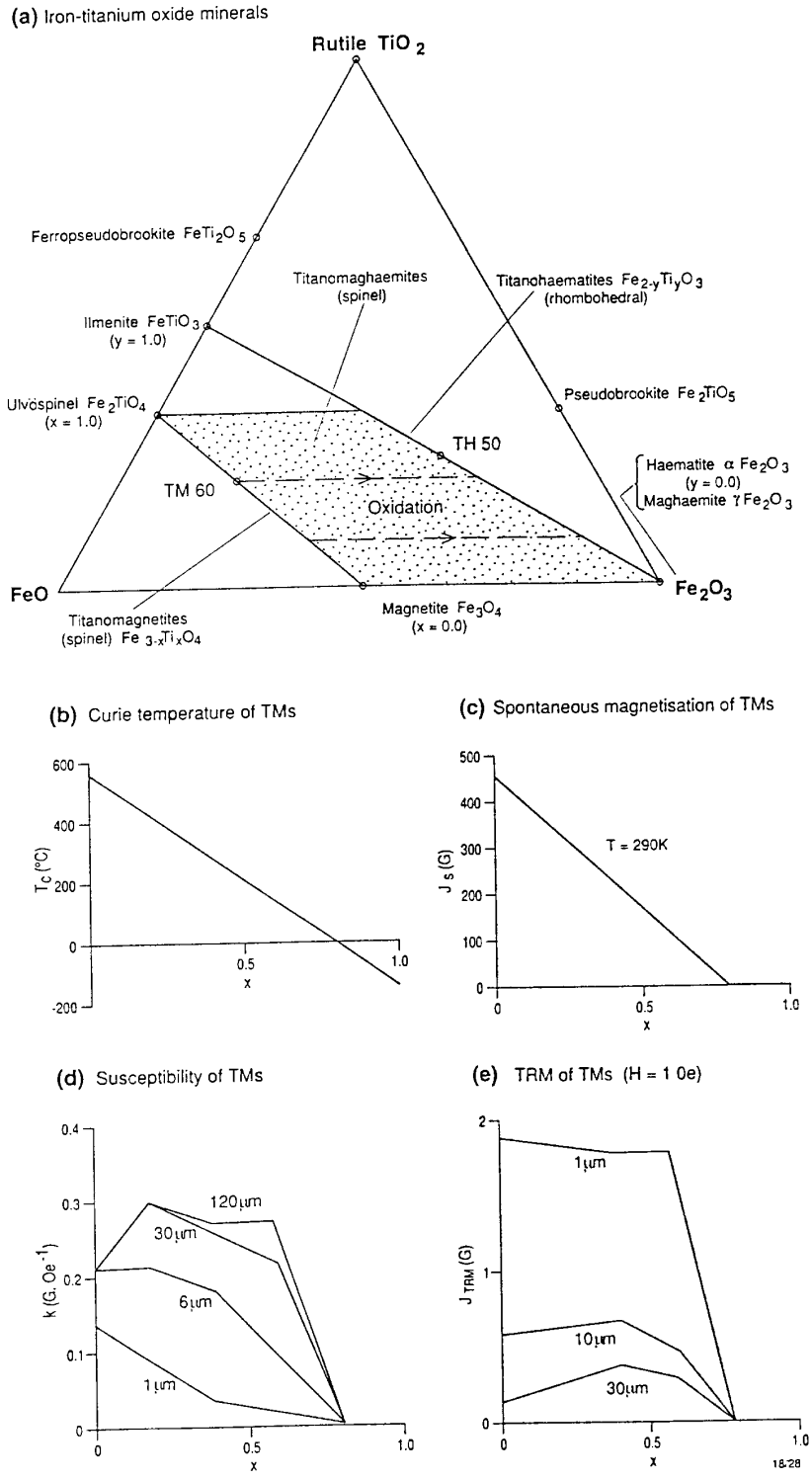

Figure 2.2(a) compositions of the Fe-Ti oxide minerals that play a major role in rock magnetism. Composition dependence of: (b) Curie temperature, (c) spontaneous magnetisation, (d) susceptibility and (e) specific remanent intensity of TRM for titanomagnetites. Note the grain size dependence of susceptibility and TRM intensity.

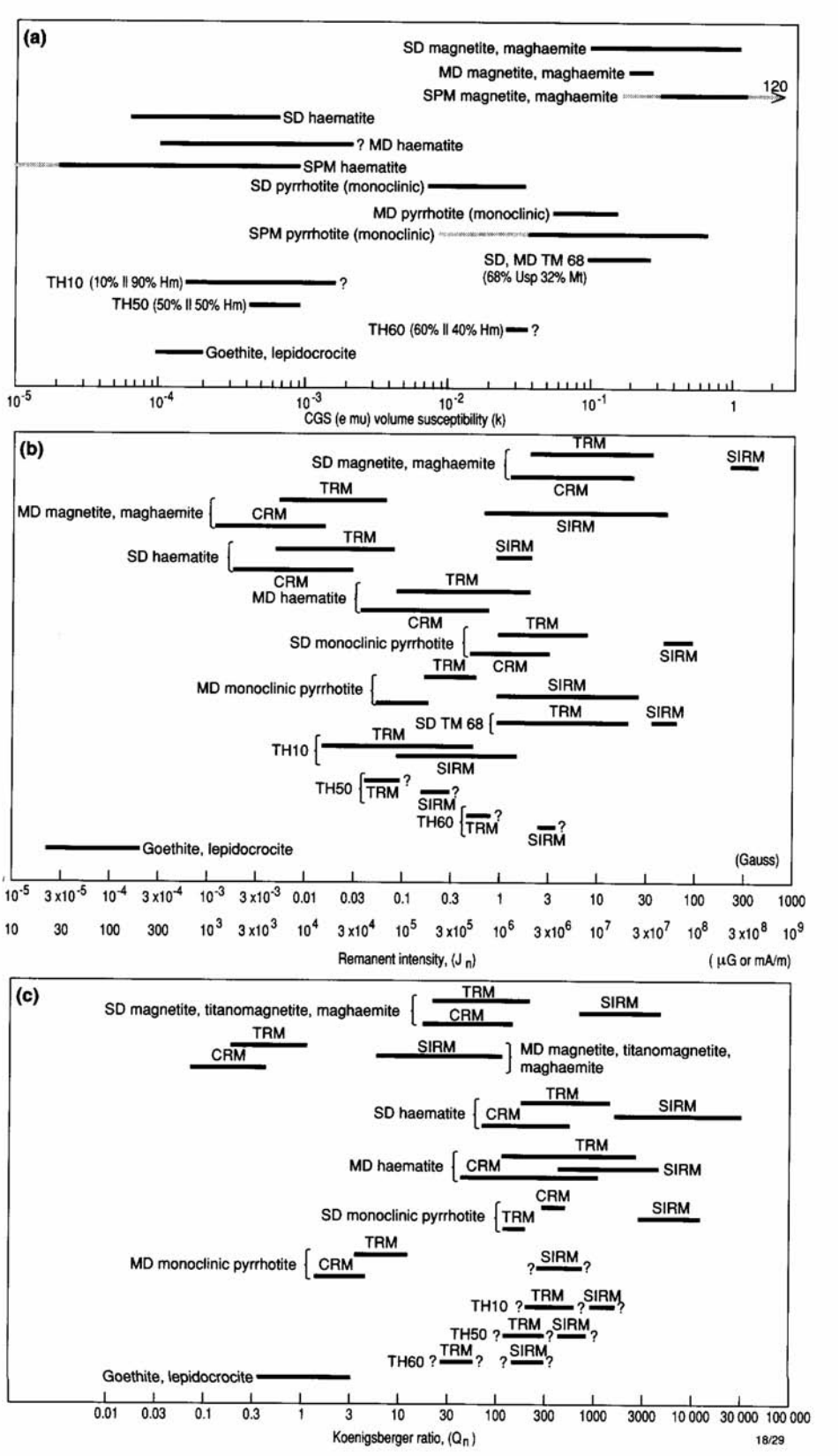

Figure 2.3. Typical values of susceptibility, remanent intensity and Koenigsberger ratio of various domain states for common magnetic minerals (from Clark, 1983).

During initial cooling of an igneous rock, magnetic mineral grains make the transition from paramagnetism to ferromagnetism as they cool through their Curie points. A spontaneous magnetisation appears that is initially in equilibrium with the applied field, but becomes "frozen in" or blocked at a somewhat lower temperature, called the blocking temperature, when the relaxation time of the grain's magnetic moment increases prodigiously. Below the blocking temperature the magnetisation is a stable remanence that is known as *thermoremanent magnetisation* (TRM). Chemical changes to these ferromagnetic minerals at elevated temperature, but below the Curie temperature, produce *thermochemical remanent magnetisation* (TCRM).

Detrital magnetic mineral grains align their magnetic moments with the ambient field as they settle through water. As a result, sediments acquire detrital remanent magnetisation (DRM) which is subparallel to, but slightly shallower than, the ambient field. Subsequent rotation of grains within pore spaces produces a *post-depositional remanent magnetisation* (pDRM) which more closely reflects the ambient field. Crystallisation of new magnetic minerals or physico-chemical changes to existing magnetic minerals during diagenesis produces *chemical remanent magnetisation* (CRM) in many sedimentary rocks. Neglecting anisotropy, TRM and CRM are acquired parallel to the ambient field at the time of acquisition. For each of these types of remanence the remanent intensity is approximately proportional to the magnitude of the field, for typical geomagnetic field strengths.

The NRM of a rock may consist of components, carried by different subpopulations of magnetic minerals, acquired at different times. For example low-grade or medium-grade metamorphism may overprint a primary remanence with a partial TRM. Alteration or weathering may superimpose a CRM on an earlier remanence.

2.3 Magnetic Minerals in Rocks

2.3.1 Diamagnetism, Paramagnetism and Ferromagnetism

Diamagnetism arises from the response of orbiting electrons in atoms to a magnetic field. The orbital motions adjust to oppose the applied field, i.e diamagnetism is characterised by a negative susceptibility. Diamagnetism is present in all materials, but is very weak and is overwhelmed by paramagnetism when permanent magnetic dipoles, usually due to unpaired electron spins, are present. Diamagnetic minerals (e.g. calcite and quartz) have very weak, negative susceptibilities (about -10^{-6} G/Oe or -10^{-5} SI) and can usually be regarded as nonmagnetic for geophysical purposes. Minerals that contain iron, manganese or a number of other transition metal and rare earth ions are paramagnetic, provided that the electron spins of adjacent ions are weakly correlated. Paramagnetic minerals (e.g. olivines, pyroxenes and pure ilmenite) have weak positive susceptibilities (maximum ~ 10^{-3} G/Oe ≈ 10^{-2} SI; generally less than 10^{-4} G/Oe ≈ 10^{-3} SI) and do not carry remanence. They were, therefore, normally unimportant for magnetic interpretation, given that most rocks only contain a few percent of these minerals. In recent times, however, the enhanced sensitivity of magnetometers and improved resolution of magnetic surveys permit detection of susceptibility contrasts between rocks of differing paramagnetic mineral contents.

Antiferromagnetism occurs when magnetic moments are parallel within a sublattice but antiparallel on different sublattices, such that the nett moment is zero, in the absence of an applied field. The susceptibility of antiferromagnetic minerals is low, similar to that of

paramagnetic substances, and they do not acquire remanence. Magnetically ordered phases that possess spontaneous magnetisations can be ferromagnetic *sensu stricto* (e.g. iron) or ferrimagnetic (e.g. magnetite). Ferromagnetism occurs when exchange interactions tend to align electron spins. Ferrimagnetism occurs when there is antiferromagnetic coupling, but the moments of the two magnetic sublattices are unequal. For simplicity, all these strongly magnetic minerals will be referred to hereafter as ferromagnetic. Ferromagnetic minerals lose their spontaneous magnetisation at a characteristic temperature, the Curie point (T_C), which is a function only of composition and which can therefore be used to detect particular ferromagnetic phases. Below its Curie temperature a ferromagnetic mineral has high susceptibility and can carry remanence. Above T_C the mineral becomes paramagnetic, with low susceptibility and no remanence. Paramagnetic minerals have greater susceptibility at low temperatures, reflecting a ~ 1/T dependence, and may become magnetically ordered, i.e. ferromagnetic or antiferromagnetic, below a transition temperature (the Curie point or the Néel point, respectively) which is composition dependent and can be used to determine the presence of particular paramagnetic minerals. Table 4.1 gives susceptibilities of common diamagnetic and paramagnetic minerals. The properties of ferromagnetic minerals are discussed below. Readers are referred to O'Reilly (1984) for detailed discussion of the atomic basis of magnetism and the properties of natural minerals.

Table 2.1 at the end of this chapter lists susceptibilities of common diamagnetic and paramagnetic minerals.

2.3.2 Intrinsic Magnetic Properties of Spinel Group Minerals

Banerjee (1991) has recently reviewed the magnetic properties of Fe-Ti oxide minerals. Bleil and Petersen (1982) have compiled extensive data on magnetic properties of natural minerals, including spinels. Figure 2.2(a) shows the compositions of the Fe-Ti oxide minerals that play a major role in rock magnetism. Many cations other than titanium can substitute into magnetite, with important effects on magnetic properties. Spontaneous magnetisation at room temperature (J_S) and Curie temperature (T_C), which are intrinsic properties dependent only on composition, are given in Table 4.2 for a number of minerals, including some end-member spinel phases. Titanomagnetites with less than ~80 mole% ulvospinel are ferromagnetic at room temperature. Although the spontaneous magnetisation and Curie temperature of titanomagnetites decrease steadily with increasing titanium content (Figure 2.2(b)-(c)), the susceptibility and specific remanent intensity of TRM are not strongly dependent on composition for the ferromagnetic phases. Thus moderate titanium content in magnetite does not generally produce weaker magnetic properties, contrary to popular opinion. In fact, grain size is a more important factor influencing magnetisation of titanomagnetite-bearing rocks (see Figure 2.2(d)-(e)).

Note that the Curie point of maghaemite cannot be observed directly because maghaemite inverts to haematite below its Curie temperature, at temperatures as low as ~300°C, depending on impurities. The Curie temperature of magnetite-bearing spinel minerals varies systematically with magnetite content. To a first approximation, the Curie point of a particular spinel composition can be estimated by linear interpolation between the T_C of the constituent end members. Diamagnetic minerals can be assigned a nominal T_C of absolute zero (-273°C)

for this purpose. For the titanomagnetite series, a more accurate expression relating Curie temperature to mole fraction of ulvospinel (x) is:

$Fe_{3-x}Ti_xO_4$: T_C (°C) = 578 - 580x - 150x².

The effect on T_C of substitution of Cr, Al and V into magnetite is broadly similar to that of Ti substitution. Substitution of Ni increases the Curie point slightly, as does cation deficiency. Thus cation-deficient magnetites ("kenomagnetite"), representing compositions intermediate between stoichiometric magnetite and maghaemite, can have T_C above 600°C.

Magnesioferrite is the only important spinel end member, other than magnetite, that is ferromagnetic at room temperature. The magnetic properties of magnesioferrite depend strongly on the cation distribution, which reflects thermal history. The Curie point of magnesioferrite is given by:

$MgFe_2O_4$: T_C (°C) = 417 - 490f,

where f is the fraction of Mg^{2+} ions on tetrahedral sites. Because of the elevated T_C and high spontaneous magnetisation, magnesioferrite-rich spinels and Mg-magnetites are strongly magnetic and can be important contributors to the magnetic properties of rocks (e.g. some kimberlites) in which they occur.

A note of caution concerning the magnetic properties of spinels needs to be sounded. Although a number of three component solid solution series have been studied, in most cases the compositions are restricted to the edges of the spinel prisms. Large portions of the interiors have not been systematically investigated. Although there is some theoretical basis for predicting the properties of complex spinel compositions, unusual behaviour has been found in special cases and it is conceivable that some of the exotic spinels that are found in some mafic and ultramafic rocks may have unexpected behaviour.

Table 2.2 at the end of this chapter lists intrinsic magnetic properties of common ferromagnetic minerals, including spinels. Table 2.3 lists densities of common minerals.

2.3.3 Intrinsic Magnetic Properties of Titanohaematites and Picroilmenites

The rhombohedral titanohaematites are second in importance only to the titanomagnetites. The magnetic phase diagram of the titanohaematite series is complex and the magnetic properties of the compositions that are ferromagnetic at room temperature are influenced by thermal history. $FeTiO_3$-Fe_2O_3 solid solutions have been thoroughly studied. The Curie temperature decreases approximately linearly with increasing ilmenite content. Titanohaematites containing between 50 mole% and 80 mole% ilmenite are strongly magnetic and are efficient carriers of remanence. An interesting property of titanohaematites that contain between 50 mole% and 73 mole% ilmenite is that they can acquire self-reversed thermoremanent magnetisation. Although full self-reversal of remanence is a rare phenomenon in rocks, the majority of well-documented cases are attributable to titanohaematites within this composition range. Compositions closer to ilmenite are paramagnetic at room temperature and haematite-rich compositions are only weakly magnetic.

Pure haematite has a diagnostic magnetic transition (the Morin transition) at -20°C. Below this temperature atomic magnetic moments are aligned with the crystallographic c-axis and haematite is antiferromagnetic. Above the transition the moments lie in the basal plane but are

slightly canted out of antiparallelism, giving rise to weak ferromagnetism and an increased susceptibility. The Morin transition can also be exploited for diagnosis of well-crystallised haematite by the effect of low temperature demagnetisation on remanence. As well as the intrinsic weak ferromagnetism due to spin-canting, haematite has an additional ferromagnetism associated with crystal defects. This defect moment is dependent on grain size, crystallinity and stress history, but is not affected by the Morin transition.

The magnetic properties of picroilmenites (solid solutions between ilmenite, haematite and geikielite, $MgTiO_3$) have not been systematically studied outside the former Soviet Union. Most of the data have been gathered from kimberlitic ilmenite megacrysts, but the Russian literature on this subject is often difficult to interpret, even in translation, and some inconsistencies between different studies are evident.

Results reported by Frantsesson (1970), Garanin *et al.* (1978) and Yakubovskaya and Ilyupin (1982) indicate that kimberlitic picroilmenites from particular pipes or clusters tend to have an inverse relationship between haematite and geikelite contents, with ilmenite approximately constant. The Curie temperature increases monotonically with haematite content. The picroilmenites in each case had somewhat different compositions. These studies found that the investigated picroilmenites became ferromagnetic at room temperature when the haematite content exceeded ~10 mole % (ilmenite ~68 mole %), ~15 mole % (ilmenite ~50 mole %) and ~20 mole % (ilmenite ~60 mole %) respectively. In all cases picroilmenites with less than 20 mole % haematite were found to have low T_C, below 200°C. The maximum Curie temperatures reported for the most haematite-rich picroilmenites were 230°C, 240°C and 220°C for these three studies respectively. Approximate Curie temperatures for picroilmenites with ~ 15 mole % haematite was found to be, respectively, 95°C, 0°C and -110°C. It seems established, therefore, that kimberlitic picroilmenites with < 10 mole% haematite are paramagnetic and those with > 20 mole% haematite are ferromagnetic at room temperature, but have relatively low Curie temperatures. The properties of intermediate compositions require further study.

2.3.4 Magnetic Properties of Iron Sulphide Minerals

The crystallography and mineralogy of the pyrrhotite group have been reviewed by Ward (1970), Ribbe (1974), Power and Fine (1976), Vaughn and Craig (1978) and Vaughn & Lennie (1991). The general formula of pyrrhotites is $Fe_{1-x}S$, with $0 \leq x \leq 0.13$. Crystal structures in the pyrrhotite group are all superstructures of the NiAs structure. At elevated temperatures, above 300°C, Fe vacancies in the structure are disordered and the $Fe_{1-x}S$ solid solution adopts the hexagonal NiAs structure, which is denoted 1C. At lower temperatures the random distribution of vacancies gives way to various vacancy ordering schemes (depending on composition and thermal history) accompanied by formation of superstructures, usually with a lowering of crystal symmetry.

The only common pyrrhotite type that is ferrimagnetic at ambient temperatures is monoclinic pyrrhotite with 4C superstructure and approximate composition Fe_7S_8. The ferrimagnetism of monoclinic pyrrhotite arises from the ordering of Fe vacancies onto alternate, antiferromagnetically coupled, layers of Fe atoms. The spontaneous magnetisation of monoclinic pyrrhotite is ~90 G (90 kA/m) and its Curie temperature is ~320°C. The spontaneous magnetisation is confined to the basal plane, except at cryogenic temperatures,

by strong magnetocrystalline anisotropy. Within the basal plane there is also substantial intrinsic anisotropy, which controls magnetic domain structure and structure dependent properties such as susceptibility, remanence intensity and stability of remanence. Other common types, such as 5C pyrrhotite with composition ~Fe_9S_{10} and 6C pyrrhotite (~$Fe_{11}S_{12}$), are antiferromagnetic at room temperature. The temperature dependence of crystal structure of pyrrhotite is very sensitive to composition. The variation of magnetic properties with temperature is therefore diagnostic of composition. Thermomagnetic analysis of pyrrhotites has been discussed at length by Schwarz and Vaughn (1972).

Monoclinic pyrrhotite with composition ~Fe_7S_8 is a relatively common ferromagnetic mineral, particularly in areas with sulphide mineralisation. The magnetic susceptibility of monoclinic pyrrhotite is less than that of magnetite, but is nevertheless substantial, and is strongly dependent on grain size. The susceptibility of monoclinic pyrrhotite decreases monotonically with decreasing grain size from ~ 0.1 G/Oe (1.3 SI) for very coarse (≥ 1 mm) grains, ~ 0.025 G/Oe (0.31 SI) for ~ 80 μm grains, 0.01 G/Oe (0.13 SI) for ~ 10 μm grains, to ~ 0.004 G/Oe (0.05 SI) for single domain (≤ 2 μm) grains (Clark, 1983). The grain size dependence of magnetic hysteresis properties of natural pyrrhotites have been studied by Clark (1983, 1984) and Dekkers (1988).

Rocks and ores containing monoclinic pyrrhotite often carry relatively intense remanent magnetisation, characterised by Koenigsberger ratios greater than unity (Kropacek, 1971; Kropacek and Krs, 1971; Schwarz, 1974; Clark, 1983; Thomson et al., 1991; Clark & Tonkin, 1994). Clark (1983) has shown that strong specific remanent intensities, high coercivity and high Koenigsberger ratios are predictable consequences of the intrinsic properties of monoclinic pyrrhotite, in particular the moderately high spontaneous magnetisation and the strong magnetocrystalline anisotropy. Theoretical, experimental and petrophysical studies have demonstrated that remanence carried by monoclinic pyrrhotite, particularly by fine grains, is magnetically hard and can be stable for geologically long periods at low temperatures (Clark, 1983). Remanence carried by monoclinic pyrrhotite is easily thermally reset, however, because of the low Curie temperature and the instability of the monoclinic phase with respect to antiferromagnetic pyrrhotite phases + pyrite above ~250^{o}C. It is quite common, therefore, for pyrrhotite-bearing rocks to have a magnetisation dominated by an ancient remanence, which dates from the last significant thermal event(s) experienced by the rocks and which may be highly oblique to the present field. Temperatures as low as ~100°C can superimpose an overprint remanence on an older magnetisation carried by monoclinic pyrrhotite (Clark, 1983). Interpretation of magnetic anomalies associated with such rocks may be seriously in error if the effects of remanence are ignored.

Because of the high intrinsic anisotropy of monoclinic pyrrhotite, any preferred orientation of pyrrhotite grains produces substantial susceptibility anisotropy of the rock or ore within which the pyrrhotite occurs. The effect of anisotropy on the magnitude and direction of induced and remanent magnetisations may also be significant for magnetic interpretation, particularly when the pyrrhotite is coarse-grained (Clark, 1983; Thomson et al., 1991).

Monoclinic pyrrhotite exhibits significant field dependence of susceptibility (Worm, 1991). Therefore susceptibilities of pyrrhotite-bearing rocks should be measured in fields that are comparable in intensity to the geomagnetic field. In addition, the susceptibility of massive sulphide ores with pyrrhotite, but not disseminated pyrrhotite-bearing rocks, is dependent on

measurement frequency, due to eddy currents induced in the specimens (Worm et al., 1993). Thus susceptibility of sulphide ores should be measured at the lowest practicable frequency. Frequencies of ~1 kHz or less are acceptable.

Greigite is iron thiospinel, Fe_3S_4, the sulphur analogue of magnetite. The spontaneous magnetisation and inferred Curie temperature of greigite are similar to those of monoclinic pyrrhotite. In recent times it has been realised that greigite is a common magnetic sulphide mineral in young sediments and in sedimentary rocks from a variety of environments (Snowball, 1991; Krs et al., 1990; Krs et al., 1992; Roberts & Turner, 1993; Reynolds et al., 1994). The magnetic properties of greigite have been characterised by Snowball (1991) and Hoffman (1992).

Smythite, which has approximate composition $(Fe, Ni)_9S_{11}$, is a relatively rare ferromagnetic mineral associated with some magmatic ores and is also present in some sedimentary rocks. The magnetic properties of smythite probably resemble those of monoclinic pyrrhotite. Krs et al. (1993) have studied magnetic properties of smythite from organic-rich Lower Miocene claystones of Bohemia.

2.3.5 Domain Structure

The bulk magnetic properties of rocks reflect the modal proportions, compositions and microstructure of the magnetic mineral grains, which are usually present in only minor amounts. Microstructure includes, *inter alia*, grain size and shape, degree of crystallinity and textural relationships and strongly influences the magnetic domain state of the grains. The most important control on domain structure is the effective grain size, which is equivalent to the actual grain size in a homogeneous grain, but is related to lamella size in grains with exsolution lamellae and the size of the ferromagnetic zone in a zoned grain.

Sufficiently small grains are uniformly magnetised, i.e. they have single domain (SD) structure. Ultrafine SD grains (< 0.03 μm for equant magnetite) are sufficiently perturbed by thermal fluctuations that the orientation of the spontaneous magnetisation flips rapidly between two or more easy directions. Such grains cannot retain a stable remanence and their magnetisations tend to relax rapidly towards any applied field, leading to a very high susceptibility. This behaviour is called superparamagnetism, and the grains are termed superparamagnetic (SPM). Rocks and soils that contain substantial quantities of SPM grains exhibit substantial frequency dependence of susceptibility, often greater than 10% and up to 24% decrease in susceptibility per decade of frequency (Thompson & Oldfield, 1986). Lateritic soils that contain SPM grains of cation-deficient magnetite or maghaemite are responsible for anomalous decays in coincident-loop TEM surveys (Buselli, 1982). The relaxation time for superparamagnetism increases exponentially with grain volume. Thus slightly larger grains have very long relaxation times, even on a geological time scale, and can retain remanent magnetisation indefinitely. These stable SD grains, typically in the submicron size range, are important carriers of remanent magnetisation in many rocks. Acicular grain shape, or elongated lamellar shape, favours SD behaviour and extends the maximum size for SD behaviour to the micron range.

With increasing size it becomes energetically favourable for the grain to subdivide into a number of magnetic domains with differently oriented magnetisations. These multidomain (MD) grains have susceptibilities, controlled by self-demagnetisation, which in the case of

strongly magnetic minerals, such as magnetite, are comparable to the susceptibilities of SD grains with similar composition. The remanence of MD grains is more easily demagnetised ("softer") than that carried by SD grains and is of lower specific intensity. The case of magnetite will be considered in some detail, but other magnetic minerals exhibit qualitatively similar behaviour. Magnetite grains larger than ~ 20 μm exhibit true MD behaviour. The coercivity, which is a measure of the ease of demagnetisation, and the remanent intensity decrease steadily with increasing grain size until they level out for grain sizes greater than ~ 100 μm.

Grains smaller than ~20 μm have properties intermediate between those of SD and true MD grains and are called pseudosingle domain (PSD). Small PSD grains, a few microns in size, are relatively hard and carry relatively intense remanence. For this reason, small PSD grains are the most important remanence carriers in many rocks, in spite of the fact that they constitute a minor proportion of the magnetic mineral assemblage and even though relatively large MD grains may dominate the susceptibility of the rocks.

The behaviour of some important magnetic properties with increasing grain size (above the SPM threshold size) can be summarised as: remanence, coercivity and Koenigsberger ratio (remanent/induced magnetisation) decrease; susceptibility increases slightly. Typical values of susceptibility, remanent intensity and Koenigsberger ratio of various domain states for a number of magnetic minerals are summarised in Figure 2.3 (from Clark, 1983). The theoretical maximum sizes for superparamagnetic and single domain behaviour for equant grains of a number of magnetic minerals are summarised below:

SUPERPARAMAGNETIC THRESHOLD AND CRITICAL SINGLE DOMAIN SIZES

Mineral	SPM threshold size (μm)	Critical SD size (μm)
Iron	< 0.008	0.023
Magnetite	0.03	0.06
Maghaemaite	0.02	0.06
Titanomagnetite (60% usp)	0.08	0.4
Haematite	0.03	15
Monoclinic pyrrhotite	0.018	1.6
Greigite	~0.04	~0.8

It has become apparent in recent years that magnetic grains frequently occupy metastable domain states of anomalously low domain multiplicity. The above values for the critical SD size assume equilibrium, i.e. that the grain is in the absolute energy minimum state. In fact, grains an order of magnitude larger than the theoretical size can remain in a metastable SD state, because formation of a domain wall requires an energy barrier to be overcome. Thus the effective upper limit for SD behaviour has been extended to ~ 1 μm for magnetite and by a similar factor for other minerals. The threshold sizes are also larger for elongated grains than

for equant grains. The domain structure transition sizes for titanomagnetites and other spinel phases with lower spontaneous magnetisations are larger than for magnetite. Thus the single domain/two domain transition, the upper limit of the PSD size range etc. occur at larger grain sizes for spinels with decreasing magnetite contents.

Taking metastable behaviour into account, the approximate size ranges and coercivities for SPM, (stable) SD, PSD and MD behaviour for magnetite are:

DOMAIN STATE SIZE RANGES AND COERCIVITIES FOR MAGNETITE

Domain state	Size (μm)	Coercivity (Oe)
SPM	< 0.05	0
(Acicular) SD	0.05-1	> 600
PSD	~1-20	100-600
MD	> 20	< 100

1 Oe = 0.1 mT (SI)

2.3.6 Palaeomagnetic Cleaning Techniques

Collinson (1983) and Butler (1992) describe demagnetisation techniques that are routinely used for resolving palaeomagnetic components and for characterisation of magnetic mineralogy. Alternating field (AF) demagnetisation is similar to degaussing of permanent magnetisation of ships or tape recorder heads. The sample is subjected to an alternating magnetic field that is gradually reduced to zero, thereby randomising the moments of all grains with coercivity less than the initial AF amplitude. This procedure is repeated at successively higher fields, demagnetising successively harder fractions of the magnetic mineral assemblage and isolating the most stable component of remanence. AF demagnetisation is particularly effective at removing isothermal remanent magnetisation (IRM) acquired by exposure to strong magnetic fields, such as those produced by mining equipment or lightning strikes etc. AF demagnetisation is sometimes effective in selectively removing VRM.

In thermal demagnetisation, the sample is heated and then cooled in zero field. This randomises the magnetic moments of all grains with unblocking temperetures less than the heating temperature. This procedure is repeated at successively higher temperatures, thereby demagnetising successively higher unblocking temperature fractions. Thermal demagnetisation is particularly effective at unravelling the thermal history of the rock, for instance by resolving primary TRM from a later metamorphic overprint. Thermal demagnetisation is especially useful for removing VRM components acquired at low temperatures, but is not so effective against IRM noise.

Low temperature demagnetisation involves cooling the sample to very low temperatures (e.g. the boiling point of liquid nitrogen) and rewarming to room temperature, in zero field. This technique exploits low temperature magnetic transitions of particular magnetic minerals, to isolate remanence components carried by different minerals or by different grain size fractions of magnetite, for example. The effect of low temperature demagnetisation can be characterised by the parameter R_K, which is the ratio of the remanence remaining at room temperature, after cooling to -196°C in zero field, to the original remanence.

Because different remanence components are carried by subpopulations of grains with different characteristics, they can usually be distinguished by their different responses to various demagnetisation techniques. Palaeomagnetic cleaning techniques have three main applications, which can be termed palaeomagnetic, petrophysical and rock magnetic respectively:

(i) Resolution of remanence components acquired at different times, allowing estimation of palaeofield directions and palaeopole positions at the time of formation, at the time of metamorphism etc.,

(ii) Removal of palaeomagnetic noise components, which are not representative of the bulk *in situ* properties, allowing characteristic NRMs of the rock to be determined,

(iii) Identification of magnetic minerals by their demagnetisation characteristics. Information on compositions, domain states and grain sizes of the magnetic minerals can be obtained.

When two or more components of remanence are present in a rock unit, the NRM directions and intensities of individual samples can be very variable, depending on the relative proportions of each component in the sample. Estimating the effective remanence of a large volume of rock from NRM measurements alone is difficult in these circumstances. Statistical techniques for estimating average vectors and errors in these circumstances are in their infancy. However, if the NRM of each sample is resolved into discrete components, a well-grouped set of directions and moderate range of intensities can be determined for each generation of remanence. Standard statistical techniques can then be used to estimate an average remanence vector, and its uncertainty, for each component. The estimated remanence vector for the rock unit can then be reconstructed from the components.

The differences in AF demagnetisation behaviour of acicular SD, small PSD and large MD magnetite is shown in Figure 2.4. The remanence that is being demagnetised is an artificially imparted saturation IRM (SIRM), produced by placing the samples in a very strong field. The plot shows the remanent intensity, normalised to the initial value before AF treatment, versus AF field. The corresponding coercivity spectra can be obtained from the demagnetisation curves by differentiation, as the coercivity spectrum is the magnitude of the slope of the demagnetisation curve. Thus the coercivity spectrum of the large MD grains peaks at low fields (less than 5 mT), the spectrum for the small PSD grains peaks at ~ 15 mT and that of the SD grains peaks above 40 mT. The Lowrie-Fuller test exploits the differences between AF demagnetisation behaviour of small and large grains. For SD and PSD grains weak field remanence, such as TRM, is more resistant to demagnetisation than strong field remanence, particularly SIRM. For true MD grains the relative stability of weak and strong field remanences is reversed.

Demagnetisation behaviour can be used to detect the presence of other magnetic minerals. For example, haematite is very hard (coercivity >> 1000 Oe) and does not thermally demagnetise until close to 670°C. Goethite has even greater coercivity than haematite, but has a Curie temperature of ~120°C, and is therefore very easily thermally demagnetised.

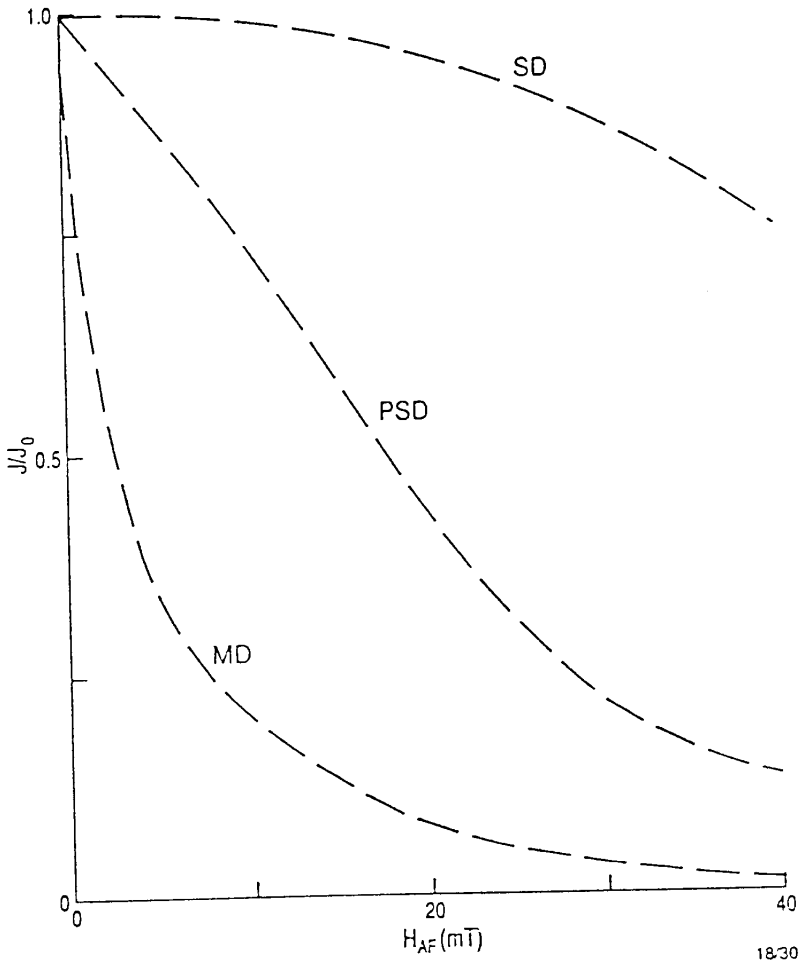

Figure 2.4. Characteristic AF demagnetisation behaviour of acicular SD, small PSD and large MD magnetite (Dunlop and Ozdemir, 1997).

Thermomagnetic Analysis of Magnetic Mineralogy

The variation of magnetic properties of magnetic minerals with temperature depends on composition and, in some cases, on domain state and microstructure. This variation can therefore be used for analysis of magnetic minerals and for optimising thermal demagnetisation steps (Schmidt, 1993). The variation of susceptibility with temperature is particularly useful, because of the rapid change in susceptibility close to T_C, which enables well-defined Curie points to be determined, and because of the sensitivity of susceptibility to domain state and microstructure.

The characteristic susceptibility (k) versus temperature (T) behaviour of different magnetic minerals is shown in Figure 2.5. The k-T curve for paramagnetic minerals is hyperbolic, reflecting the 1/T dependence of paramagnetic susceptibility. The k-T curve of magnetite with MD structure, including PSD grains as well as true MD, grains is very diagnostic. There is a prominent peak at -155°C, which corresponds to the isotropic point of magnetite. Below this temperature the easy magnetisation directions are along the <100> cubic axes, whereas above it the easy directions lie along <111> body diagonals of the cubic unit cell. At the isotropic point the magnetisation rotates freely to align with an applied field, giving rise to an increase in susceptibility. The susceptibility of MD grains is limited by self-demagnetisation and the observed susceptibility remains almost constant until just below the Curie temperature, when it plummets to paramagnetic values. The isotropic point is very sensitive to composition and substitution of cations other than iron, or departures from stoichiometry, tend to lower the isotropic point. Titanomagnetites containing more than ~10 mole% ulvospinel have isotropic points below liquid nitrogen temperature. Thus the presence of a well-defined peak around -155°C is diagnostic of the presence of nearly pure PSD and/or MD magnetite.

The titanomagnetite for which the k-T curve is shown has a Curie point of ~ 200°C and contains ~60 mole% ulvospinel. The k-T curve is irreversible on cooling from high temperature (not shown), due to exsolution of more magnetite-rich and magnetite-poor titanomagnetites than the original composition. Thus two Curie points, one above 500°C and the other shifted somewhat lower than the original T_C, would be seen in the cooling curve.

The k-T curve for SD magnetite does not exhibit a peak at the isotropic point because the properties of SD grains are controlled largely by shape anisotropy, rather than by magnetocrystalline anisotropy. The susceptibility is almost constant at low temperatures, but increases as the Curie temperature is approached. This increase in k reflects unblocking of fine grains below T_C.

The susceptibility of grains increases sharply at the unblocking temperature because the relaxation time suddenly decreases, allowing the magnetic moments of the grains to equilibrate rapidly with the applied field. Above the unblocking temperature the superparamagnetic susceptibility of grains of specified volume is proportional to J_S^2/T and is much higher than the room temperature susceptibility, until the Curie temperature is approached (at which point J_S ® 0, so k ® 0). Thus the presence of significant unblocking of remanence well below the Curie temperature may indicate that this portion of the remanence is carried by very fine (submicron) single domain grains.

Even smaller grains unblock at much lower temperatures and exhibit superparamagnetism at room temperature. The k-T curve shown for SPM grains is idealised for an assemblage of

identical grains. In rocks there is always a distribution of grain sizes and the superposition of unblocking peaks over a wide range of temperatures leads to a steady increase in susceptibility from below room temperature up to the maximum unblocking temperature of the ultrafine SPM + SD assemblage. This behaviour is commonly seen in soil samples, particularly lateritic soils.

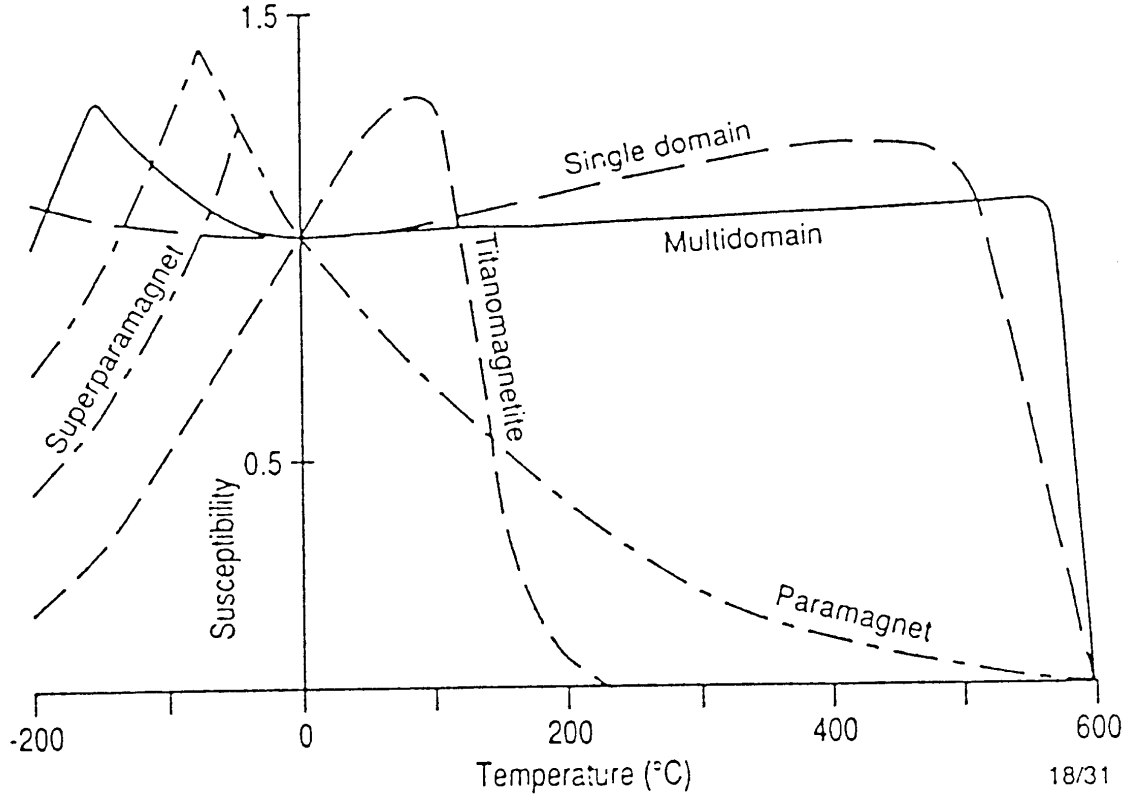

Figure 2.5. The characteristic susceptibility (k) versus temperature (T) behaviour of different magnetic minerals (after Thompson & Oldfield, 1986).

Large multidomain grains also exhibit substantial unblocking below the Curie temperature, due to rearrangements of domain structure with changes in temperature. The component unblocked below the Curie temperature has much lower coercivity if it is carried by MD grains than by SD grains. The unblocking behaviour of partial TRMs is quite diagnostic of SD versus MD carriers. For SD grains the maximum unblocking temperature for a PTRM acquired at a given temperature below the Curie point is approximately the maximum temperature of acquisition. For MD grains, on the other hand, unblocking occurs from low temperatures right up to the Curie point.

As the Curie temperature of a magnetic mineral is approached, there is a rapid decrease in spontaneous magnetisation and an even more rapid decrease in magnetocrystalline anisotropy. As a consequence the remanence of even the most stable grains unblocks, but without an increase in k. In fact, the susceptibility plummets until it attains paramagnetic values at T_C.

Thermal demagnetisation of remanence provides another analytical technique. MD grains exhibit a spectrum of unblocking temperatures right up to T_C, whereas the unblocking temperature spectrum of SD grains cuts off below the Curie point. However, given that the grain size range of a particular mineral extends at least to the upper end of the SD range, the maximum unblocking temperature lies just below T_C. Thus Curie points can also be estimated from thermal demagnetisation data. Prominent inflexions in the demagnetisation curve, corresponding to a sharp peak in the blocking temperature spectrum, indicate the approximate Curie temperature of a particular phase. Comparison of the blocking temperature spectra with k-T curves enable phases originally present in samples to be distinguished from phases created during heating. Low temperature demagnetisation also allows magnetic transitions characteristic of magnetite and haematite to be detected. Judicious application of a variety of rock magnetic techniques, including thermomagnetic analysis, allows the relative contributions to susceptibility and remanence of different compositions and grain size ranges to be estimated. Lowrie (1990) has presented an elegant technique for identifying magnetic minerals, even in trace amounts, which exploits differences in Curie temperature and coercivity for different minerals.

Magnetic Susceptibilities of Minerals and Rocks

Figure 2.3(a) plots the susceptibilities *for dilute dispersions* of common ferromagnetic minerals, in various domain states, normalised to 100% by volume. That is, if the specific volume susceptibility indicated is χ and the volume fraction of the mineral is f, the contribution of that mineral to the susceptibility of the rock is $\sim\chi f$, *provided* $f << 1$. For strongly magnetic minerals, such as magnetite, the susceptibility versus volume fraction relationship departs substantially from linearity for $f > 0.1$. This is because the effective susceptibility of isolated strongly magnetic grains is strongly controlled by self-demagnetisation and depends only weakly on the intrinsic susceptibility of the grain material. Thus the microstructure and size of the grains does not greatly affect the observed susceptibility of sparsely dispersed magnetite particles. At high concentrations, however, susceptibilities are influenced by interactions between grains and the susceptibility increases faster than the extrapolated linear relationship that applies for low concentrations. On the other hand, for weakly magnetic minerals, such as haematite, the contribution to the susceptibility is essentially proportional to the volume content, for all f.

A simple model of grain interactions adequately accounts for the concentration dependence of the susceptibility for magnetite-bearing rocks. Each magnetite grain can be regarded as residing in a cavity within a magnetised medium (see Figure 2.6). The environment of each grain is a magnetic "plum pudding" of randomly dispersed magnetic grains of average magnetisation J within a non-magnetic matrix. Replacing the actual environment with a continuous medium that has the same volume-averaged magnetisation *viz* fJ, the nett magnetic field within each grain is:

$$H' = H - NJ + NfJ,$$

where H' is the internal field of the grain, H is the applied field and N is the self-demagnetising factor of the grain. The second term on the RHS is the self-demagnetising field and the third term is the Lorentz field term, which corrects for the grain interactions.

Thus the induced magnetisation of each grain obeys:

$$J = \chi H' = \chi[H - N(1-f)J],$$

$$\therefore J = \chi H/[1+(1-f)N\chi].$$

The magnetisation of the *rock* is fJ, which implies that the observed susceptibility of the rock is:

$$k = fJ/H = f\chi/[1+(1-f)N\chi].$$

For low concentrations of magnetite, this reduces to:

$$k = f\chi/[1+N\chi]. \quad (f << 1)$$

For MD magnetite the intrinsic susceptibility depends on microstructure, but is always high ($\chi \geq 1$ G/Oe = 13 SI), and N is the order of 3-4 Oe/G (0.25-0.3 SI). Therefore $N\chi >> 1$ and the susceptibility of the rock is almost independent of χ at low concentrations of magnetite:

$$k \approx f/N. \quad (f << 1)$$

Thus the susceptibility of a rock containing low to moderate amounts of MD magnetite is approximately proportional to magnetite content, irrespective of the magnetite grain size or microstructure. Conversely, the susceptibility can be used to infer the magnetite content for moderately magnetic magnetite-bearing rocks. According to Puranen (1989) a reasonable average empirical relationship between susceptibility and magnetite content for magnetite contents up to a few percent is:

$$k \approx 0.276f \text{ G/Oe} = 2760v\ \mu\text{G/Oe} = 3.47f \text{ SI} = 3470v \times 10^{-5} \text{ SI},$$

where v = 100f is the volume percent magnetite content.

Significant departures from the linear k-f relationship occur for magnetite contents greater than about 10%. In the limit of 100% magnetite the susceptibility of the ore is simply the intrinsic susceptibility of the magnetite crystals, which depends on average grain size, crystallinity, dislocation densities etc. The susceptibility of pure magnetite ore approaches χ, which ranges from ~ 1 G/Oe (13 SI) for fine-grained, poorly crystalline, inhomogeneous or stressed grains to ~10 G/Oe (130 SI) for very coarse, well-crystallised magnetite. Parry (1980) estimated the average effective demagnetising factor, N, for MD magnetite grains to be 3 Oe/G (0.24 SI). Puranen's relationship is consistent with the theoretical relationship if a typical value of intrinsic susceptibility of natural magnetite grains in rocks is ~1.6 G/Oe (20 SI), which agrees well with Stacey & Banejee's (1974) estimates of intrinsic susceptibility of large multidomain magnetite grains. Figure 2.7 shows curves of susceptibility versus magnetic mineral content for magnetite and monoclinic pyrrhotite, based on the theory presented above and confirmatory experimental data.

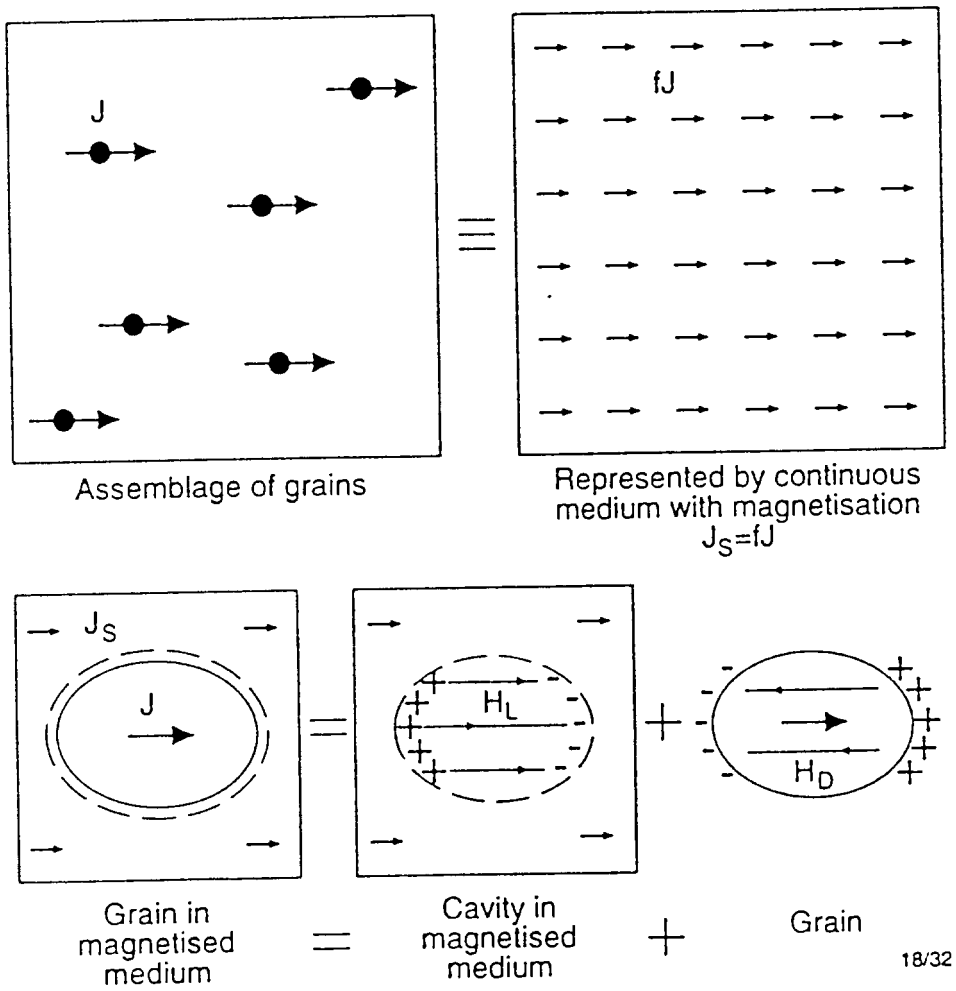

Figure 2.6. Simple model of effect of grain interactions on susceptibility of ferromagnetic mineral-rich rocks. The self-demagnetising field of each grain is opposed by the Lorentz field of the cavity occupied by the grain.

The paramagnetic susceptibility of rocks that contain no ferromagnetic minerals can usually be estimated simply and reasonably accurately from their total iron content (Puranen, 1989). In this case

$k_{SI} \approx 2.86 \times 10^{-8} \times$ wt% Fe $\times$ density (kg/m^3) $= 2.22 \times 10^{-8} \times$ wt% FeO^T $\times$ density (kg/m^3)

k (G/Oe) $\approx 2.27 \times 10^{-6} \times$ wt% Fe $\times$ density (g/cm^3) $= 1.77 \times 10^{-6} \times$ wt% FeO^T $\times$ density (g/cm^3).

As examples, a paramagnetic granite with 2 wt% total iron as FeO and a density of 2.65 g/cm^3 = 2650 kg/m^3 has a susceptibility of 9 μG/Oe = 12×10^{-5} SI, whereas a paramagnetic gabbro with 12 wt % total iron as FeO and a density of 3.0 g/cm^3 = 3000 kg/m^3 has a susceptibility of 64 μG/Oe = 80×10^{-5} SI (Clark & Emerson, 1991). The maximum anomaly that could be associated with a contact between rock units with these

susceptibilities is ~20 nT. Susceptibility contrasts between paramagnetic rock units with differing total iron contents are certainly easily detectable, if the background variation due to ferromagnetic rocks in the area is sufficiently subdued.

Figure 2.8 plots observed susceptibility ranges and common susceptibility ranges for various rock types. The implications of these data will be discussed below, in the section on magnetic petrology.

Remanent Magnetisation of Minerals and Rocks

The susceptibility of most rocks primarily reflects their magnetite content. Remanence intensity, whilst also correlated with modal magnetite, is sensitive to other factors, particularly grain size and microstructure of magnetic minerals and geological history. The natural remanent magnetisation of rocks is often multicomponent in character, i.e. it represents the sum of remanence components, each carried by a different subpopulation of magnetic grains, acquired at different times and therefore generally with differing directions. Variations in the relative proportions of remanence components throughout a rock unit produce scatter in the remanence direction, as well as variations in intensity. Specific remanent intensity is highest for acicular submicron magnetite grains in the single domain size range. Pseudosingle domain (titano)magnetite grains, up to ~20 μm diameter, also carry relatively intense remanence and are the dominant remanence carriers in many rocks. Larger magnetite grains have relatively weaker remanence, corresponding to Q values less than unity.

Remanence carried by haematite and monoclinic pyrrhotite is characterised by high Q values, but haematite is only weakly magnetic and therefore haematite-rich rocks are rarely responsible for substantial anomalies, unless the haematite is associated with magnetite and/or maghaemite. In cases where minor amounts of magnetite or maghaemite are intimately intergrown with haematite a relatively intense remanence, characterised by exceptionally high Q, may be present.

Pyrrhotite-bearing rocks often carry a relatively intense remanence, which may be ancient and quite oblique to the present field. Greigite also seems to be associated with high Q values (Reynolds et al., 1990b). The remanence carried by magnetically soft multidomain magnetite, which is the dominant magnetic phase in many rocks, is dominated by viscous magnetisation. This remanence is subparallel to the present field and therefore augments the induced magnetisation, enhancing the effective susceptibility. Thus most anomalies can be interpreted in terms of magnetisation by induction, even when typical Koenigsberger ratios are comparable to unity. However, for a given source geometry, the anomaly amplitudes may be larger than measured susceptibilities indicate,

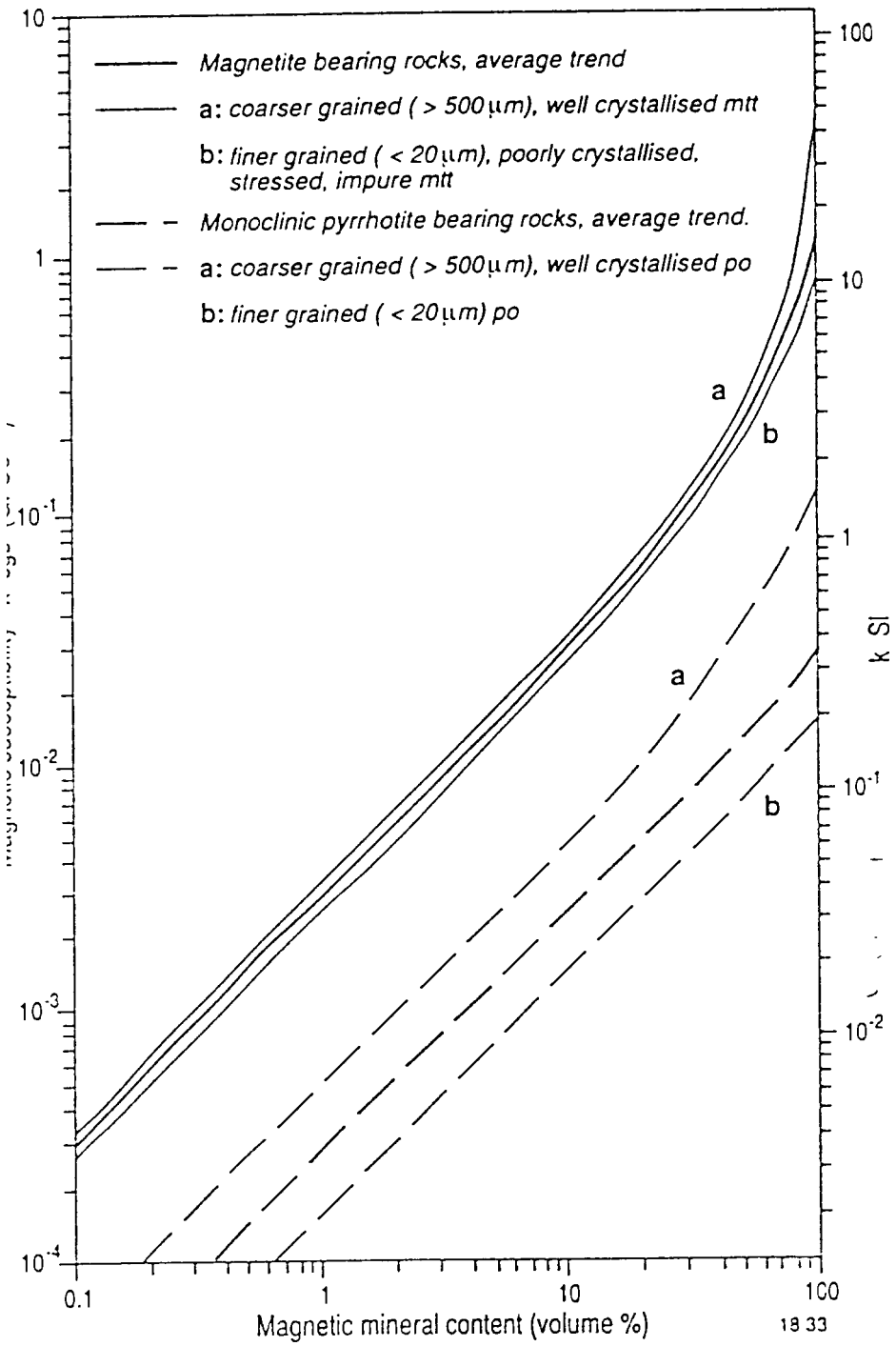

Figure 2.7. Susceptibility versus magnetic mineral content for magnetite and monoclinic pyrrhotite.

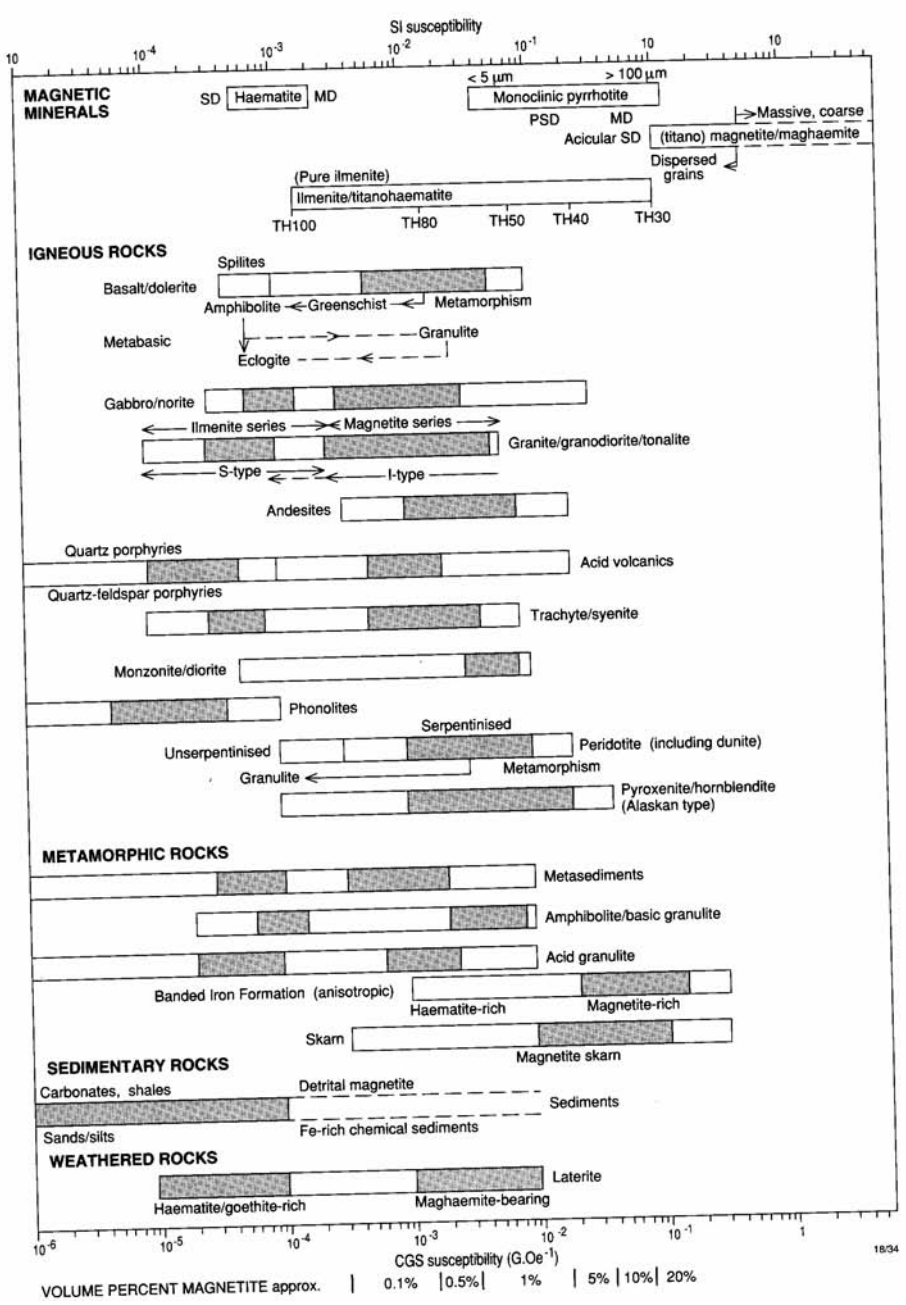

Figure 2.8. Observed susceptibility ranges and common susceptibility ranges for various rock types.

due to the viscous remanent magnetisation. Neglect of remanence may therefore mislead quantitative interpretation, even though the anomaly form is consistent with magnetisation parallel to the present field.

Koenigsberger ratios for viscous remanence carried by multidomain magnetite have an upper limit of approximately unity, but are typically much lower, averaging ~ 0.2. Rocks containing predominantly somewhat harder multidomain magnetite grains may carry a stable ancient remanence, characterised by a larger Q value. The Koenigsberger ratio of thermoremanence carried by an igneous rock that contains predominantly such multidomain grains is typically ~ 0.5. In this case the remanence direction records the geomagnetic field direction at the time of initial cooling. This direction can be of either normal or reversed polarity and may be highly oblique to the present field, depending on the age of the rock. Figure 2.3(c) summarises Koenigsberger ratios for various types of magnetisation carried by the major magnetic minerals, as a function of domain state. Figure 2.9 shows ranges of Koenigsberger ratio found for a variety of rock types.

Estimation of the bulk remanent magnetisation of a rock unit is not straightforward. The scatter of directions must be taken into account, as well as the distribution of intensities. Remanence makes a greater contribution to the anomaly associated with a unit that exhibits a consistent remanence direction and moderate Koenigsberger ratios than a unit that has highly scattered remanence directions on a mesoscopic scale, even though the samples may all have high Q values.

Measurements of raw NRMs can also be quite misleading. Surface samples are often affected by lightning, which imparts unrepresentatively high remanent intensities and Q values. Drill core samples may carry spurious remanence imparted by drilling. Estimation of representative remanence vectors requires palaeomagnetic cleaning of samples to remove spurious components and to identify the components that correspond to bulk *in situ* properties. The remanent magnetisations identified in this way should then be analysed statistically as vectors, rather than analysing directions and scalar intensities separately.

Magnetic Anisotropy of Minerals and Rocks

Anisotropic susceptibility cannot be described by a scalar quantity, but takes the form of a symmetric second order tensor. For any crystal, and similarly for any homogeneous but anisotropic rock, three mutually orthogonal axes can be defined, along which the susceptibility has maximum, intermediate and minimum values. These principal axes (the *major*, *intermediate*, and *minor axes*, respectively) define an ellipsoid, the *susceptibility ellipsoid* (Nye, 1957), which describes the behaviour of the susceptibility and induced magnetisation uniquely and also characterises the *magnetic fabric* of the rock. The *magnetic foliation* is the plane that contains the major and intermediate susceptibility axes. It reflects planar structures in the rock. The *magnetic lineation* coincides with the major susceptibility axis and reflects linear structures. Figure 2.10 illustrates the concept of the susceptibility ellipsoid.

The susceptibility of paramagnetic and diamagnetic minerals can differ along different crystallographic directions, depending on the crystal symmetry (Nye, 1957). Cubic minerals have isotropic susceptibility, whereas minerals with lower crystallographic symmmetry

exhibit anisotropy of susceptibility. The anisotropy can be characterised by the parameter A, which is the ratio of the major susceptibility to the minor susceptibility. Common paramagnetic minerals for which anisotropies have been measured have A ranging from ~ 1.1 to ~ 1.8. In highly deformed rocks for which paramagnetic phases such as micas dominate the susceptibility, the high degree of preferred orientation of the micas can produce substantial anisotropy of the rock. The orientations of the major susceptibility axes reflect, and can be used to infer, the planar and linear petrofabric elements in such rocks.

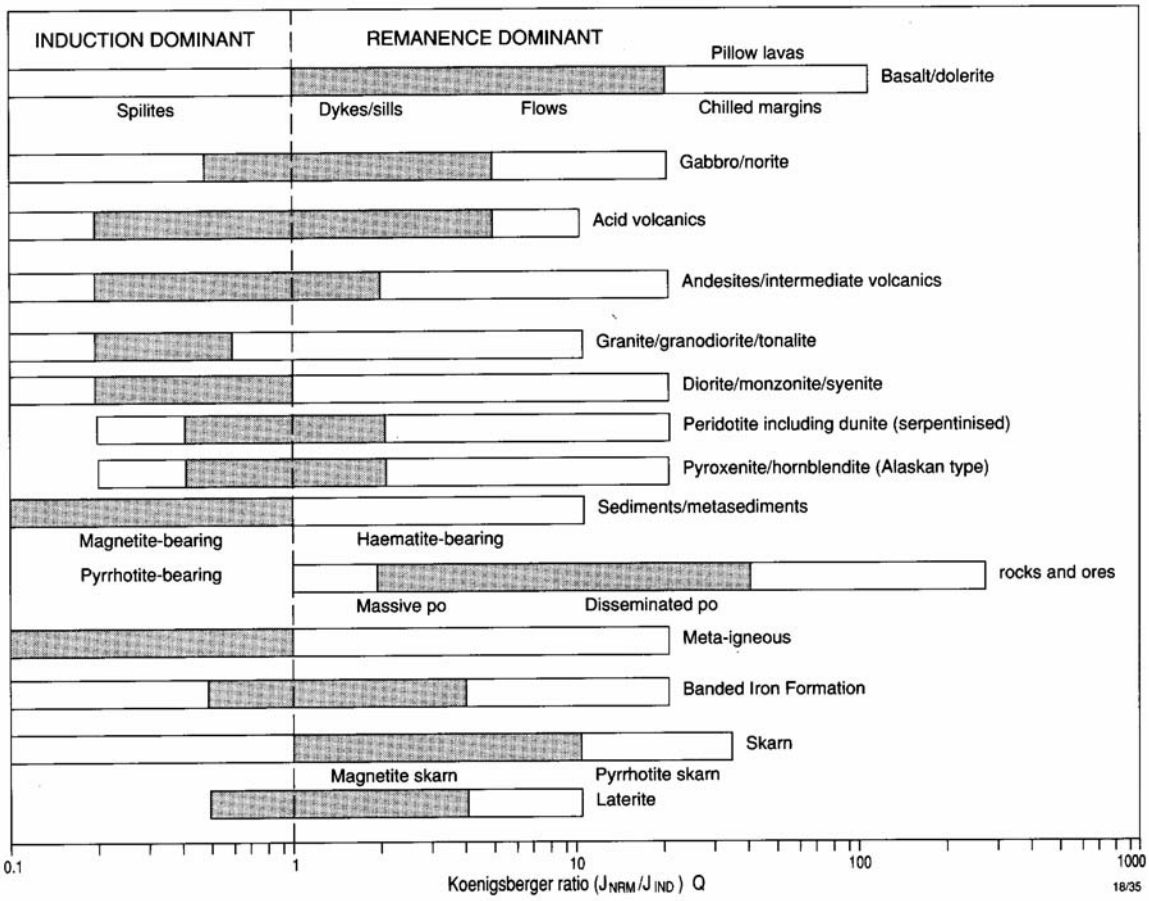

Figure 2.9. Observed ranges and common ranges for Koenigsberger ratios of various rock types.

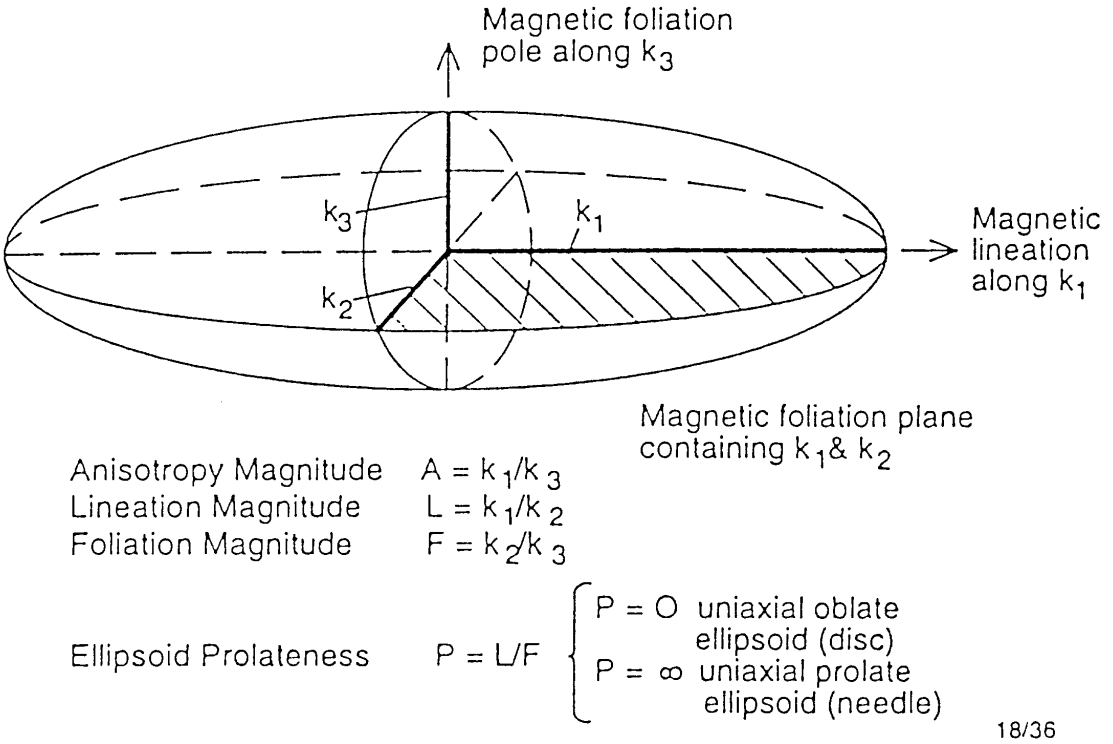

Figure 2.10. Relationship between the susceptibility ellipsoid and magnetic fabric elements.

Ferromagnetic minerals of low crystal symmetry, such as haematite and monoclinic pyrrhotite exhibit very strong susceptibility anisotropy. For both these minerals the susceptibility within the basal plane is orders of magnitude greater than the susceptibility along the c-axis. Therefore even a slight preferred crystallographic orientation of haematite or monoclinic pyrrhotite can produce a substantial anisotropy for the rock.

The susceptibility anisotropy of (titano)magnetite-bearing rocks arises from self-demagnetisation. In the case of dispersed grains, the effective susceptibility is greatest along the long axis of the grain and least along the short axis, because the grain demagnetising factor is least along the long axis and greatest along the short axis. Preferred dimensional orientation of magnetite grains therefore leads to anisotropic susceptibility of the rock, with maximum susceptibility parallel to the preferred alignment of long axes. When magnetite grains are inhomogeneously distributed, self-demagnetisation of the magnetite aggregates can produce strong anisotropy. The classic case is banded-iron formation with magnetite-rich bands alternating with weakly magnetic bands. The susceptibility normal to the banding is greatly reduced by self-demagnetisation, whereas the susceptibility parallel to the banding is unaffected by self-demagnetisation.

Although almost all rocks exhibit slightly anisotropic magnetic susceptibility, which can be interpreted in terms of petrofabric, the degree of anisotropy is generally insufficient to significantly influence the form of magnetic anomalies. Exceptions include banded iron formations and some rocks and ores that contain pyrrhotite with a strong preferred orientation. In rocks that have substantial magnetic anisotropy the susceptibility varies significantly with the field direction and, in general, the magnetisation is not parallel to the applied field,

because the magnetisation tends to be deflected away from an axis of relatively low susceptibility, towards an axis of higher susceptibility.

Acquisition of remanent magnetisation is also affected by anisotropy. The palaeomagnetic direction recorded by anisotropic rocks is deflected from the palaeofield direction. Thus palaeomagnetic results obtained from strongly anisotropic rocks are unreliable, unless they are corrected for anisotropy. Strong anisotropy can complicate magnetic interpretation in areas where remanence is important. If anisotropy effects are neglected, the inferred timing of remanence acquisition relative to folding can be misinterpreted (Clark & Schmidt, 1994).

A recent book (Tarling and Hrouda, 1993) is devoted the subject of magnetic anisotropy in rocks and readers are referred to this work for further information and a guide to the extensive literature on applications of magnetic anisotropy.

Properties of Strongly Magnetic Rocks and Ores

Magnetite-rich and monoclinic pyrrhotite-rich rocks and ores present particular difficulties for magnetic interpretation. Interpretation of structure and source geometry for these rocks is unreliable unless complicating factors are taken into account. These factors include:

(i) self-demagnetisation,
(ii) anisotropy of susceptibility,
(iii) Koenigsberger ratio,
(iv) palaeofield direction during remanence acquisition,
(v) anisotropy of remanence acquisition,
(vi) age of remanence with respect to deformation,
(vii) perturbation of the local geomagnetic field direction by intense anomalies.

It should be noted that existing commercial modelling packages do not address these problems and are unsuitable for interpreting structures in these environments.

In Australia, types of mineralisation where these considerations are important include BIF-derived supergene-enrichment iron ores, Tennant Creek type discrete ironstone Au-Cu orebodies, BIF-hosted gold in Archaean greenstone belts, magnetite-rich Archaean VMS deposits, pyrrhotite-rich metasediments and sulphide ores in many areas, including the Pine Creek Inlier, the Cobar District and the Paterson Province, and magnetite-rich ironstone-associated Cu-Au mineralisation and BIF-associated Pb-Zn-Cu-Ag mineralisation of the East Mount Isa Inlier. The function of replaceable iron-rich lithologies as chemical traps and the reducing power of magnetite are now recognised as important controls on mineralisation in the East Mount Isa Inlier, the Cullen Mineral Field of the Pine Creek Inlier, and other areas.

Rock magnetic research has concentrated on the properties of dilute dispersions of magnetic grains in rocks. The theoretical and experimental basis for understanding the magnetic properties of magnetite and pyrrhotite-rich rocks is therefore inadequate. In such rocks the properties are strongly influenced by grain interactions, greatly modifying the magnetic behaviour.

The magnetic petrophysics and petrology of iron-formations and ironstones is also a fertile area for research. Little is known about the magnetic properties of different facies of these rocks and the effects of alteration on their magnetic properties. The magnetic expression of

transitions from magnetite-facies to haematite-facies or to sulphide-facies iron formations in mineralised environments is poorly known.

Clark and Schmidt (1994) have reviewed the magnetic properties of BIFs. Magnetite grains in BIFs are in the large multidomain size range. In most rocks, for which magnetite is an accessory mineral that occurs as widely dispersed grains, large multidomain grains are associated with Koenigsberger ratios (Q values) less than unity, due to inhomogeneous magnetization and strong self-demagnetization of such grains. When magnetite occurs in very high concentrations, however, interactions between grains reduce the effective self-demagnetizing factors of the grains and enhance the specific susceptibility and, to an even greater extent, the specific remanence. Thus the Koenigsberger ratio exhibited by BIFs can be substantial. Q values vary widely for BIFs, but predominantly fall in the range 1-2, with higher values occurring occasionally. Because remanence contributes substantially to the total magnetisation, it should not be ignored in quantitative interpretation of magnetic signatures of BIFs.

The effective susceptibility of BIFs parallel to bedding exceeds the susceptibility normal to bedding, typically by a factor of 2-4. Bedding-parallel susceptibilities of magnetite-rich BIFs are typically 0.5-2.0 SI (0.05-0.16 G/Oe). Similarly, remanence is acquired more readily along the layering than across it, leading to deflection of the remanence direction away from the palaeofield direction, towards the bedding plane. The anisotropy of remanence acquisition generally exceeds the susceptibility anisotropy and can produce large deflections of palaeomagnetic directions acquired in moderate to high (but not polar) palaeolatitudes. For this reason remanence directions in BIFs usually lie fairly close to the bedding plane.

The strong anisotropy of BIFs means that the Q value of a BIF unit is sensitive to the orientation of the bedding with respect to the geomagnetic field. Remanence directions and the relative ages of remanence and folding are best determined by palaeomagnetic study of fresh BIF samples (from mines or drill core), backed up by detailed modelling of magnetic anomalies over BIFs with known structure.

Magnetic properties of outcropping BIFs are usually greatly modified by weathering, which substantially decreases the bulk susceptibility, the degree of anisotropy and the remanence intensity. Deeper and more intense weathering of BIFs is assisted by faulting and may be associated with reduced magnetic response over intensely faulted zones. The magnetisations of the haematite-rich supergene-enrichment iron ores are much lower than those of their BIF precursors.

Much magnetic modelling ignores the effects of anisotropy and remanence and proceeds on the assumption of magnetization parallel to the geomagnetic field. Dips of magnetic units are then interpreted from the shapes of the associated magnetic anomalies. This approach is inappropriate for interpretation of anomalies associated with BIFs, because anisotropy and remanence effects are demonstrably important and the direction of the resultant magnetization may depart substantially from geomagnetic field direction.

As an illustration, Figure 2.11 shows theoretical magnetic profiles over idealised fold structures, indicating the differences in anomalies produced by isotropic induced magnetization, anisotropic induced magnetization (for A = 2.5), and anisotropic induced magnetization plus pre-folding remanence (with intensity 1.5 times that of the isotropic induced magnetization). The anisotropy and Koenigsberger ratio used are typical values for

BIFs. Clearly, an interpretation of the magnetic signatures that ignores anisotropy and remanence will lead to serious errors, particularly in interpreted dips.

Magnetic Petrology

Magnetic petrology integrates rock magnetism and conventional petrology to characterise the composition, abundance, microstructure and paragenesis of magnetic minerals in order to define the processes that create, alter and destroy magnetic minerals in rocks. By relating magnetic mineralogy, bulk magnetic properties and petrology to observed magnetic anomalies an understanding of the geological factors that control magnetic signatures is obtained, which can be used to improve geological interpretation of magnetic surveys.

Magnetic properties of rocks reflect, above all else, the partitioning of iron in the rock between strongly magnetic oxides and/or sulphides and weakly magnetic phases (silicates, carbonates etc.). This partitioning depends on chemical composition, oxidation ratio of the iron and petrogenetic conditions. Thus a host of geological factors influence magnetic properties and simplistic correlations between magnetic properties and lithotype are generally unreliable. Rules-of-thumb, such as "susceptibilities go according to: basic extrusive > basic intrusive > acid igneous > sedimentary", have so many exceptions that they are almost useless. It is also dangerous to extrapolate empirical correlations between mapped geology and magnetics in one area to another area, ignoring changes in depositional environment, metamorphic grade or structural setting.

A magnetic petrological classification that can provide a sound basis for geological interpretation of magnetics in a given province must rely on an understanding of the factors that control partitioning of iron. The most direct approach to this problem is to characterise ferrous and ferric iron contents of whole rocks, and of all the minerals in the rocks, as a function of the geological variable that is being studied. This requires wet chemical determination of ferrous and ferric iron, petrographic determination of modal mineralogy and microprobe determinations of mineral chemistry of each phase, to produce a complete inventory of iron in the sample. As yet, such studies are in their infancy, due to the rarity of wet chemical analyses to determine whole rock ferrous and ferric iron and to difficulties in determining ferric/ferrous ratios in individual minerals, particularly hydrous silicates.

The data of Figures 2.8-2.9 are based on magnetic property measurements at the CSIRO Division of Exploration and Mining over the last 18 years and published studies and compilations.

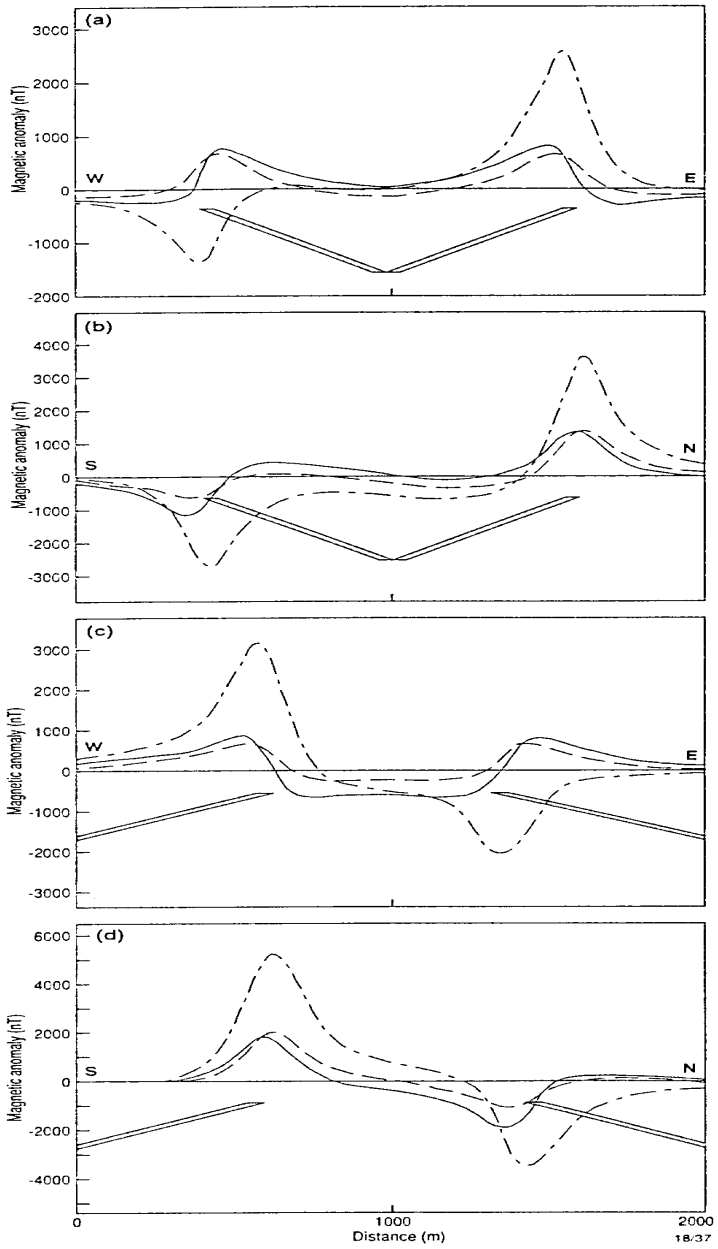

Figure 2.11. Magnetic anomalies of folded BIF units, showing the effects of anisotropy and pre-folding remanence on the total field anomalies. (a) E-W profiles over a N-S striking syncline, (b) N-S profiles over an E-W striking syncline, (c) E-W profiles over a N-S striking eroded anticline, (d) N-S profiles over an E-W striking eroded anticline. The regional geomagnetic field intensity is 54,000 nT, the field declination is 0° and the field inclination is -56°. Solid curves represent pure induced magnetisation with isotropic susceptibility (k = 0.754 SI = 0.06 G/Oe), dashed curves represent induced magnetisation with anisotropy (susceptibility parallel to bedding 0.942 SI = 0.075 G/Oe, A = 2.5), and dash-dot curves incorporate anisotropy and pre-folding remanent magnetisation (declination normal to strike, original inclination -10°, intensity 48.6 A/m = 0.0486 G). Because of the anisotropy, the Koenigsberger ratio depends on the field direction and bedding attitude, but it is about 1.5. After Clark & Schmidt (1994).

The systematic collection of petrophysical data by the Geological Surveys of Scandinavian countries, in particular, has greatly expanded the size and scope of the information available. It is evident from Figure 2.8 that each rock type exhibits a wide range of susceptibilities and that susceptibility values are not generally diagnostic of lithology. Classical rock names are in fact much too broad to be useful for classification of magnetic properties. This is because the susceptibility of most rocks reflects the abundance of accessory minerals, particularly magnetite (*sensu lato*), which are ignored in petrological classification. At a more refined level, however, there is significant geological information in basic magnetic properties, especially if the statistical characteristics of large collections are considered and if the measurements are supplemented by rock magnetic experiments to characterise the compositions and microstructures of the magnetic minerals. The magnetic minerals in a metaigneous rock, for example are sensitive to its geological history, including the bulk composition and petrogenetic affinities of the magma, the degree of differentiation, conditions of emplacement, degree and type of hydrothermal alteration and conditions of metamorphism (temperature, pressure, fugacities of oxygen, water, sulphur, CO_2 etc.). Differences in magnetic properties can therefore reflect subtle variations in some or all of these influences. More detailed clasification schemes, based on the most important of these factors, may therefore allow more meaningful interpretation of magnetic surveys in terms of geology. In some cases observed differences in magnetic anomaly patterns within single mapped units have indicated hitherto unsuspected heterogeneity, which has then been confirmed by remapping.

Bimodal Susceptibility Distributions Reflect Ferromagnetic and Paramagnetic Populations

The variations in magnetic properties for given lithologies are generally greater between geological provinces than within them, although large variations are also possible over smaller areas, even down to the outcrop scale. A notable feature of Figure 2.8 is that the susceptibilities of a number of rock types have distinctly bimodal distributions. More generally, bimodal susceptibility distributions represent distinct subpopulations within each rock type for which ferromagnetic minerals are absent and present respectively. Iron in the weakly magnetic subpopulation is incorporated into paramagnetic silicate minerals, predominantly as Fe^{2+}, whereas similar rocks that are moderately to strongly magnetic contain significant Fe^{3+}, which is incorporated into magnetite. Very highly oxidised rocks, however, tend to contain haematite rather than magnetite and are therefore also weakly magnetic. Puranen (1989) presents results from very large petrophysical sampling programs in Finland. His data show that all broad field names, such as "granite", "gabbro", "mica schist", "amphibolite" etc., exhibit distinctly bimodal susceptibility distributions.

Within each magnetic subpopulation susceptibility tends to increase with basicity. The greater abundance of paramagnetic mafic minerals in rocks with lower SiO_2 increases the paramagnetic contribution to the susceptibility. This produces a small, but systematic difference, in the susceptibilities of paramagnetic acid and basic rocks. The increasing sensitivity of modern magnetometers and the trend to more detailed magnetic surveys suggests that magnetic mapping may become useful even in very weakly magnetic terrains, where the rocks would hitherto have been classified as "non-magnetic" on the basis of their apparent flat and featureless magnetic patterns in low resolution surveys. More commonly,

however, the observed magnetic signatures reflect variations in the abundance of ferromagnetic minerals.

When varietal mineralogy is incorporated into the rock classification, the bimodal susceptibility distribution tends to resolve into a paramagnetic subpopulation associated with particular varietal minerals and a ferromagnetic subpopulation associated with a distinct mineralogy. Bimodality often also reflects the fact that important geological factors, such as geochemical affinity, alteration and metamorphic grade are not considered in the simple classification schemes used for most petrophysical summaries. A truly meaningful magnetic petrological classification scheme must include chemical and/or mineralogical data for protoliths, plus information on metamorphic grade and/or alteration.

Magnetic Properties of Igneous Rocks

In the case of granitoids, bimodal susceptibilities reflect the existence of two distinct categories, the magnetite-series and ilmenite-series granitoids of Ishihara (1977). Magnetite-series granitoids are relatively oxidised and correspond broadly to the I-type granitoids of Chappell & White (1974), whereas ilmenite-series granitoids are more reduced and are usually S-type. The new classifications, which have important petrogenetic and metallogenic implications, have led to the concept of mapping granitoid terrains using a hand-held susceptibility meter or a magnetometer and provide a good example of the utility of categories based on magnetics.

Although broad rock names such as "granodiorite" show only a weak correlation with magnetic properties, more detailed classifications that include varietal minerals are much more predictive. For example, hornblende-biotite granodiorites are predominantly ferromagnetic, with moderate susceptibilities, whereas muscovite-biotite granodiorites are usually paramagnetic. Accessory minerals that occur commonly in ferromagnetic felsic granitoids include sphene, epidote, allanite, pyrite and haemoilmenite or Mn-rich ilmenite. The biotite is Fe^{3+} and Mg-rich and is generally brown, black or olive green.

Accessory minerals that are often associated with paramagnetic granitoids include cordierite, garnet or aluminosilicate (which are characteristic of S-type granites), reduced (low Fe^{3+}) ilmenite, pyrrhotite, and biotite that is Fe^{2+} and Al-rich, often with a "foxy red" colour. Hornblende-bearing granitoids that are too reduced to contain magnetite are less common overall and tend to occur within specific provinces or "basement terranes", for which the source material at depth is relatively reduced (Chappell et al., 1988). Susceptibility of felsic granitoids also correlates with feldspar colour (Blevin, 1994). For granites that have white plagioclase, relatively oxidised ferromagnetic granites generally have salmon pink K-feldspar, whereas reduced paramagnetic granites have white K-feldspar. There is a systematic increase in susceptibility with increasing pinkness of the K-feldspar. On the other hand, brick red K-feldspar is usually indicative of hydrothermal alteration and is associated with low susceptibility. This simple relationship is disturbed if green plagioclase is present. The green colour reflects replacement of plagioclase by chlorite, sericite, albite, epidote and calcite. This alteration also tends to destroy magnetite. Granites with green plagioclase and pink K-feldspars exhibit variable susceptibilities, reflecting destruction of some or all of the magnetite originally present in the granite.

There is a clear association between granite metallogeny and oxidation state, which translates into a correlation between magnetic susceptibility of granitoids and their associated mineralisation (Ishihara, 1981; Blevin & Chappell, 1992). In order of reducing susceptibility, Cu and Au are associated with magnetite-series, intermediate I-type granitoid suites, Mo with more fractionated and oxidised magnetite-series I-type suites and Sn with paramagnetic, reduced, fractionated I- or S-type suites.

The overall tendency for magnetite content of ferromagnetic rocks to increase with basicity is somewhat obscured when igneous rocks from different provinces are compared. For consanguinous rocks, in particular, there is a general correlation between susceptibility and basicity. Andesites generally have similar, or slightly lower, susceptibilities than related basalts. Rhyolites have a distinctly bimodal susceptibility distribution. Ferromagnetic rhyolites tend to be somewhat less magnetic than the more basic members of the series, and many rhyolites are paramagnetic (e.g. fayalite rhyolites, strongly peraluminous and strongly peralkaline rhyolites). Trachyandesites and trachytes generally have moderate to high susceptibilities, comparable to or somewhat less than susceptibilities of related alkali basalts, but the corresponding phonolites are usually weakly magnetic. Within the ferromagnetic subpopulation of each lithology, magnetic properties can also be related to geochemistry. For tholeiitic rocks in both oceanic and continental settings iron and titanium-rich variants that are interpreted to be related to hotspots have been found to have substantially higher susceptibilities, reflecting greater modal titanomagnetite, than similar rocks with lower Fe and Ti contents (e.g. Anderson et al., 1975; de Boer & Snider, 1979).

Granitic rocks and metamorphic rocks with secondary magnetite usually contain relatively coarse grained multidomain magnetite, accounting for the generally low Q values of these rocks. On the other hand, young, rapidly chilled basaltic rocks (e.g. pillow lavas) exhibit very high Koenigsberger ratios, due to the fine grain size of the titanomagnetites. In basaltic rocks the Q value of the primary thermoremanence is essentially a function of cooling rate, being highest for subaqueous chilled margins and small pillows and decreasing with distance from the margin. However, even thick doleritic sills and dykes are characterised by relatively high Q values, typically 1-10, provided the primary remanence has not been substantially modified by thermal or chemical overprints.

Plutonic rocks generally have low Koenigsberger ratios, due to their coarse grain size, with the notable exception of some gabbroic to dioritic intrusives for which the remanence is dominated by SD and PSD grains of magnetite (*sensu lato)*. These efficient remanence carriers may be either fine (titano)magnetite inclusions in silicate grains or large, originally homogeneous, titaniferous magnetite grains that have undergone deuteric oxidation, which produces abundant oxyexsolution lamellae of ilmenite within relatively low-Ti magnetite. This subdivision of the magnetite grains by non-magnetic lamellae produces an effective grain size in the PSD range.

Ultramafic rocks (pyroxenites, hornblendites, serpentinised dunites etc.) in zoned Alaskan-type complexes are generally highly magnetic. The associated mafic and intermediate rocks (gabbro, diorite, monzonite) in these intrusions are also moderately to highly magnetic. Primary magnetite is the main magnetic mineral in these intrusive complexes. On the other hand, the primary spinel phase in unaltered komatiitic lavas (including spinifex textured peridotite, olivine orthocumulate and adcumulate (dunite) zones) and alpine-type peridotites is paramagnetic chromite and they are therefore weakly magnetic. However, komatiites are

usually serpentinised, as are alpine-type peridotites. Serpentinisation usually creates substantial quantities of magnetite, accounting for the high susceptibility of serpentinised ultramafic rocks. This magnetite is generally multidomain, well-crystallised, almost pure Fe_3O_4, which is magnetically soft and carries relatively weak remanence ($Q < 1$). The NRM of serpentinites is often dominated by viscous remanence, subparallel to the present field. Large dunite bodies sometimes have a weakly magnetic, unserpentinised core within an envelope of highly magnetic serpentinite.

Magnetic Properties of Sedimentary Rocks

"Clean" carbonates and clastic sediments have very low susceptibilities. Some immature sandstones are magnetic because they contain significant quantities of detrital magnetite. Sediments deposited in the presence of metal-bearing solutions, associated with volcanic activity for example, may contain appreciable magnetite, or possibly pyrrhotite, and therefore be magnetic. Such sediments may be transitional to syngenetic massive mineralisation or to banded iron formation. Magnetite-rich banded iron formations are not only strongly magnetic but are characterised by high anisotropy of susceptibility. The susceptibility values for banded iron formation shown in Figure 2.8 are bulk susceptibilities, i.e. the average of the susceptibilities along any three orthogonal directions.

Traditionally aeromagnetic surveys over sedimentary basins were used primarily to determine depth to basement. In recent times it has become evident that modern high resolution aeromagnetic surveys over sedimentary basins also provide considerable information about sedimentary lithologies and structures. Little is known about the intrasedimentary sources that are responsible for the observed anomaly patterns. There is an urgent need for research into the magnetic petrophysics and petrology of intrasedimentary sources, directed at improving understanding of the geological significance of the magnetic anomaly patterns. Gay (1992) gives examples of intrasedimentary anomalies associated with distributions of detrital magnetite. Reynolds et al. (1990a,b; 1994) demonstrate that diagenetic monoclinic pyrrhotite and greigite are possible sources of low amplitude, high frequency anomalies, that in some cases may be associated with hydrocarbon seepage, over some sedimentary basins. There is as yet no definitive evidence of diagenetic magnetite produced by hydrocarbon seepage in quantities sufficient to produce observable anomalies (Reynolds et al., 1990b), but Machel & Burton (1991) describe chemical and microbial processes that could in principle produce authigenic magnetite and pyrrhotite, at the expense mainly of haematite, in the presence of hydrocarbons.

Effects of Hydrothermal Alteration

Studemeister (1983) points out that the redox state of iron in rocks is a useful indicator of hydrothermal alteration. Large volumes of fluid or high concentrations of exotic reactants, such as hydrogen or oxygen, are required to shift Fe^{3+}/Fe^{2+}. When reactions associated with large water/rock ratios occur, the change in redox state of the rocks produces large changes in magnetic properties due to creation or destruction of ferromagnetic minerals.

Zeolite grade hydrothermal alteration of mafic to silicic igneous rocks tends to decrease the susceptibility of these rocks according to the degree of development of zeolites (Emerson & Welsh, 1987). Zeolite-rich rocks are generally paramagnetic, even when derived from strongly magnetic protoliths. Regional hydrothermal alteration of volcanic piles produces

progressive demagnetisation from zeolite grade to greenschist grade. For example, primary titanomagnetite and ilmeno-magnetite in basalts progressively develops ferrirutile granules at ~150°C, with sphene replacing ilmenite lamellae by ~250°C, and polycrystalline titanohaematite replacing titanomagnetite above 300°C (Ade-Hall et al., 1971). However, contact metamorphism of hydrothermally altered, demagnetised igneous rocks, for instance by dyke injection, may produce secondary magnetite (Hall & Fisher, 1987).

The available evidence suggests that both major types of alteration associated with epithermal systems, acid-sulphate and adularia-sericite alteration, tend to demagnetise volcanic rocks through replacement of magnetite by paramagnetic phases. Similarly phyllic alteration and intense propylitic alteration associated with porphyry intrusions tend to destroy magnetite in the intrusion and in surrounding rocks. On the other hand, the potassic alteration zone associated with oxidised, magnetic felsic intrusions is often magnetite-rich. This is commonly observed for Au-rich porphyry copper systems (Sillitoe, 1979). Early potassic (biotite-rich) alteration around the gold-mineralised Mount Leyshon Complex (Queensland), which comprises intrusive breccias, porphyry plugs and dykes, produced abundant magnetite in metsedimentary and doleritic host rocks and is largely responsible for the Mount Leyshon magnetic anomaly (Sexton et al., 1995).

Serpentinisation of olivine-rich ultramafic rocks tends to produce abundant magnetite. At low grades, initial serpentinisation of olivine produces Fe-lizardite plus brucite. With further serpentinisation, the maximum iron content of lizardite is exceeded and magnetite is produced, along with lizardite, chrysotile and brucite. At higher grades antigorite and magnetite are produced. For serpentinites there is generally an inverse relationship between density, which decreases with progressive serpentinisation, and susceptibility. Saad (1969) found that weakly (~10%) serpentinised peridotites are weakly magnetic (k ~ 100 μG/Oe = 126×10^{-5} SI), partially (~ 75%) serpentinised peridotites are moderately ferromagnetic (k ~ 500 μG/Oe = 6300×10^{-6} SI) and fully serpentinised peridotites are substantially more magnetic (k ~ 5000 μG/Oe = $63{,}000 \times 10^{-6}$ SI).

Carbonate alteration of serpentinised ultramafics initially redistributes magnetite, without destroying it, and has little effect on susceptibility. Intense talc-carbonate alteration, however, consumes the magnetite, with iron entering magnesite as a siderite component, and demagnetises the rock.

Effects of Metamorphism

Metamorphism has profound effects on magnetic properties. It follows that magnetic interpretation should take changes in metamorphic grade across the study area into account. Effects of metamorphism on magnetic properties have been discussed by McIntyre (1980), Grant (1985), Shive et al. (1988), Wasilewski and Warner (1988), Urquhart (1989), Frost (1991b), Olesen et al. (1991), Skilbrei et al. (1991) and Clark et al. (1992).

Fresh basalts and dolerites have moderate to high susceptibilities. Burial metamorphism of igneous rocks to zeolite or prehnite-pumpellyite grade does not demagnetise them, in the absence of circulating hydrothermal fluids, but regional metamorphism to greenschist and lower to mid-amphibolite grades tends to demagnetise basic igneous rocks. In gabbros the fine magnetic grains within silicates may be protected by their silicate hosts from

metamorphic breakdown, so that gabbros may be somewhat less sensitive to low and medium grade metamorphism than their extrusive and hypabyssal equivalents.

Where magnetite is an abundant cumulus phase, it appears to be much less prone to metamorphic breakdown than if it is present as a minor intercumulus mineral. Thus highly differentiated ferrogabbros and ferrodiorites, which contain abundant primary magnetite, remain strongly magnetic throughout medium to high grade metamorphism. This probably reflects the fact that secondary metamorphic minerals become rapidly saturated in Fe^{3+} when magnetite starts to break down, ensuring that the rest of the magnetite remains stable during metamorphism. Felsic plutons seem to be more resistant to metamorphic destruction of magnetite in the greenschist and amphibolite facies than mafic rocks and felsic volcanic rocks. Amphibolite grade metamorphism overall produces heterogeneous magnetic properties with bimodal susceptibilities, although dominated by weakly magnetic rocks. At this grade magnetic mafic rocks are more common than magnetic silicic rocks. Chlorite and/or biotite-bearing amphibolites tend to be weakly magnetic, whereas hornblende-rich amphibolites may have much higher susceptibilities.

Granulite facies metamorphism of mafic protoliths frequently produces secondary magnetite and large increases in susceptibility. High pressure granulites and eclogites are generally paramagnetic. Magnetite breakdown in these high pressure rocks generally occurs between 10 kbars and 20 kbars. The reactions occur at generally lower pressures for undersaturated basaltic rocks than for quartz tholeiites, for lower Mg/Fe ratios and for more reduced rocks.

These changes in properties reflect redistribution of ferric iron in metabasites during metamorphism. Ferric iron originally present in magnetite goes largely into haematite, epidote and chlorite during greenschist grade metamorphism, then into biotite and amphibole in the amphibolite facies, whence into metamorphic magnetite in the granulite facies and finally into paramagnetic silicates such as garnet and clinopyroxene in the eclogite facies. The magnetite-in isograd reflects P-T-t conditions and appears to occur within lower granulite facies, above the orthopyroxene-in isograd for prograde metamorphism, followed by isobaric cooling (Olesen et al., 1991). For retrograde metamorphism or for isothermal decompression during rapid uplift the magnetite-in isograd lies within the upper amphibolite facies, above the biotite isograd (Skilbrei et al., 1991). Decompression of high pressure granulites during rapid uplift can produce fine-grained magnetite by breakdown of garnet and clinopyroxene. This magnetite may carry relatively strong and stable remanence. In general, however, metamorphic magnetite is relatively coarse-grained, well crystallised and fairly pure, i.e. it occurs as magnetically soft MD grains, which are associated with low Q values and unstable, predominantly viscous, remanence.

Prograde metamorphism of serpentinised ultramafics causes increasing substitution of Mg and Al into the magnetite, eventually shifting the composition into the paramagnetic field. Thus metamorphism progressively demagnetises serpentinites, which become paramagnetic at granulite grade (Shive et al., 1988). Subsequent retrograde serpentinisation, if it occurs, can produce a magnetic rock again. Clark et al. (1992) note a progressive decrease in magnetic anomaly amplitude associated with a major serpentinised ultramafic unit as metamorphic grade increases from prehnite-pumpellyite facies to upper amphibolite facies.

The iron content of sediments (generally higher for pelites than for psammites) and the Fe^{3+}/ Fe^{3+} ratio, which reflects the redox conditions during deposition and diagenesis, have a major

bearing on the capacity of sedimentary rocks to develop secondary magnetite during metamorphism (McIntyre, 1980). Thus magnetic patterns over metasedimentary rocks tend to reflect sedimentary facies variations, as well as metamorphic conditions. These patterns can be very useful for mapping, although the relationship between the magnetic marker units and conventional lithological units may be quite tenuous (McIntyre, 1980).

Magnetite formation is favoured by high total iron and therefore tends to be associated with metapelites more frequently than metapsammites. Substantial chemical input by exhalative metal-bearing solutions, including iron, increase the potential for magnetite formation during subsequent metamorphism. Magnetite formation is favoured by intermediate redox state/ oxidation ratio. Low oxidation states are associated with ilmenite in metasediments and very high oxidation states are associated with haematite. Very iron oxide-rich assemblages, for example BIFs, are self-buffered during metamorphism, preserving fine layering with magnetite- and haematite-rich bands.

Organic rich sediments produce reduced graphitic metasediments, which are magnetite-free, but commonly contain pyrrhotite above greenschist grade. Red (haematite-bearing) sediments produce intermediate redox metasediments, which may be magnetite-bearing. Haematite goes to magnetite in the biotite or lower garnet zones for these rocks. The maximum ferromagnetic proportion in metasediments generally occurs at granulite grade.

Pyrrhotite is the main magnetic mineral in many metasedimentary rocks, particularly in mineralised areas. Clark & Tonkin (1994) discuss magnetic anomalies associated with monoclinic pyrrhotite in metasediments of the Cobar area, Australia. Remanent magnetisation and susceptibility anisotropy are often important in monoclinic pyrrhotite-bearing metasediments (Clark, 1983).

Conclusions

The aim of magnetic interpretation is to elicit *geological* information from magnetic survey data. There is a continuing need for magnetic petrophysical studies to constrain interpretation of magnetic surveys and for fundamental research in magnetic petrology to improve understanding of the geological factors that create, alter and destroy magnetic minerals in rocks. A large scale, systematic effort to create physical property databases, including comprehensive magnetic property data classified according to magnetic petrological principles and integrated with geological and geochemical databases, is required. New developments in 3D modelling, including inversion, and visualisation will assist efficient interpretation of large magnetic datasets. However, meaningful geological interpretation using these tools should allow incorporation of petrophysical information and magnetic petrological concepts.

TABLE 2.1. COMMON DIAMAGNETIC AND PARAMAGNETIC MINERALS
(data from Bleil and Petersen, 1982)

Mineral	Type of Magnetism	Susceptibility (G/Oe)	Susceptibility (SI)
Quartz*	Diamagnetic	-1.2×10^{-6}	-1.5×10^{-5}
Orthoclase*	Diamagnetic	-1.1×10^{-6}	-1.4×10^{-5}
Forsterite*	Diamagnetic	-1.0×10^{-6}	-1.3×10^{-5}
Calcite*	Diamagnetic	-1.0×10^{-6}	-1.3×10^{-5}
Gypsum*	Diamagnetic	-2.3×10^{-6}	-2.9×10^{-5}
Anhydrite*	Diamagnetic	-4.7×10^{-6}	-5.9×10^{-5}
Halite*	Diamagnetic	-0.8×10^{-6}	-1.0×10^{-5}
Galena*	Diamagnetic	-2.6×10^{-6}	-3.3×10^{-5}
Sphalerite*	Diamagnetic	-1.0×10^{-6}	-1.3×10^{-5}
Apatite*	Diamagnetic	-0.85×10^{-6}	-1.1×10^{-5}
Fayalite*	Paramagnetic	390×10^{-6}	490×10^{-5}
Ferrosilite*	Paramagnetic	260×10^{-6}	330×10^{-5}
Hedenbergite*	Paramagnetic	220×10^{-6}	270×10^{-5}
Olivine	Paramagnetic	$10...430 \times 10^{-6}$	$12...540 \times 10^{-5}$
Orthopyroxene	Paramagnetic	$10...260 \times 10^{-6}$	$12...330 \times 10^{-5}$
Clinopyroxene	Paramagnetic	$50...220 \times 10^{-6}$	$60...280 \times 10^{-5}$
Actinolite	Paramagnetic	40×10^{-6}	50×10^{-5}
Hornblende	Paramagnetic	$60...110 \times 10^{-6}$	$75...130 \times 10^{-5}$
Sodic amphiboles	Paramagnetic	270×10^{-6}	340×10^{-5}
Pyrope	Paramagnetic	40×10^{-6}	50×10^{-5}
Almandine	Paramagnetic	$210...530 \times 10^{-6}$	$260...660 \times 10^{-5}$
Spessartine	Paramagnetic	540×10^{-6}	680×10^{-5}
Andradite	Paramagnetic	$180...350 \times 10^{-6}$	$230...440 \times 10^{-5}$
Biotite	Paramagnetic	$70...260 \times 10^{-6}$	$90...330 \times 10^{-5}$
Phlogopite	Paramagnetic	$15...25 \times 10^{-6}$	$20...30 \times 10^{-5}$
Muscovite	Paramagnetic	$3...60 \times 10^{-6}$	$4...75 \times 10^{-5}$
Cordierite	Paramagnetic	$15...90 \times 10^{-6}$	$20...110 \times 10^{-5}$
Epidote	Paramagnetic	80×10^{-6}	100×10^{-5}
Sphene	Paramagnetic	20×10^{-6}	30×10^{-5}
Psilomelane	Paramagnetic	270×10^{-6}	340×10^{-6}
Ilmenite	Paramagnetic	150×10^{-6}	190×10^{-5}
Hausmannite	Paramagnetic	60×10^{-6}	75×10^{-5}
Chromite	Paramagnetic	$225...580 \times 10^{-6}$	$280...730 \times 10^{-6}$

Spinel	Paramagnetic	2×10^{-6}	3×10^{-5}
Siderite	Paramagnetic	$210...810 \times 10^{-6}$	$260....1020 \times 10^{-5}$
Magnesite	Paramagnetic	5×10^{-6}	6×10^{-5}
Dolomite	Paramagnetic	1×10^{-6}	1.2×10^{-5}
Pyrite	Paramagnetic	3.4×10^{-6}	4.3×10^{-5}
Marcasite	Paramagnetic	$5...20 \times 10^{-6}$	$6...25 \times 10^{-5}$
Sphalerite	Paramagnetic	$0...160 \times 10^{-6}$	$0...200 \times 10^{-5}$
Chalcopyrite	Paramagnetic	$25...35 \times 10^{-6}$	$30...40 \times 10^{-5}$
Bornite	Paramagnetic	$45...70 \times 10^{-6}$	$55...90 \times 10^{-5}$
Arsenopyrite	Paramagnetic	$3...50 \times 10^{-6}$	$4...60 \times 10^{-5}$

* pure phases

TABLE 2.2. INTRINSIC MAGNETIC PROPERTIES OF FERROMAGNETIC MINERALS

Mineral	**Chemical Formula**	**Spontaneous Magnetisation (G)**	**Curie Temperature (°C)**
Iron*	Fe	1710	770
Awaruite*	Ni_3Fe	950	620
Magnetite*	Fe_3O_4	480	578
Ulvospinel*	Fe_2TiO_4	0	-153
Titanomagnetite	$Fe_{3-x}Ti_xO_4$	~ 480-600x (x < 0.8) 0 (x ≥ 0.8)	~ 578-580x-150x²
Maghaemite*	γFe_2O_3	440	>> 300 (750?)
Kenomagnetite (Cation-deficient magnetite)	$Fe_{3-y}O_4$ (0 < y < 1.3)	~460	~600...630
Titanomaghaemite	$Fe_{(3-x)R}Ti_{xR}O_4$ (0.89 < R < 1)	10...70 (not monotonic)	150...450 (common range)
Magnesioferrite*	$MgFe_2O_4$	≤ 220 (function of cation dist)	≤ 420 (function of cation dist)
Chromite*	$FeCr_2O_4$	0	-185
Ferrichromite/Cr-magnetite	$Fe_{3-x}Cr_xO_4$ e.g. Fe_2CrO_4	ferromag for 0 ≤ x ≤ 1.2 250	-185...578 200
Hercynite*	$FeAl_2O_4$	0	-265
Magnesian ulvospinel*	Mg_2TiO_4	0	diamagnetic
Picrochromite*	$MgCr_2O_4$	0	-258
Spinel*	$MgAl_2O_4$	0	diamagnetic
Jacobsite*	$MnFe_2O_4$	397	300
Jacobsite/Mn-magnetite	$Fe_{3-x}Mn_xO_4$	ferromag for 0 ≤ x ≤ 2.5	
Trevorite*	$NiFe_2O_4$	330	595
Coulsonite*	FeV_2O_4	0	-164
Haematite*	αFe_2O_3	2	680
Ilmenite*	$FeTiO_3$	0	-205
Titanohaematite	$Fe_{2-x}Ti_xO_3$	0 ≤ x < 0.5: antiferro 0.5 ≤ x ≤ 0.8: ferro 0.8 < x ≤ 1: para	~680-885x
Monoclinic pyrrhotite*	Fe_7S_8	90	320
Hexagonal pyrrhotite	Fe_9S_{10} ... $Fe_{11}S_{12}$	0	270...210
Smythite*	Fe_9S_{11}	~50	> 300 (~400?)
Greigite*	Fe_3S_4	~30	~350

* pure phases

$$1\ G = 1\ kAm^{-1}\ (SI)$$

TABLE 2.3. DENSITIES OF COMMON MINERALS

Mineral	Density (g/cm^3)	Mineral	Density (g/cm^3)
Quartz*	2.65	Pyrope	3.58
Orthoclase/ Microcline/Adularia	2.55-2.63	Almandine	4.32
Sanidine	2.53-2.56	Spessartine	
Albite	2.62*	Andradite	3.86
Plagioclase	2.62-2.76	Biotite	2.8-3.2
Calcite*	2.71	Phlogopite	2.86
Gypsum*	2.35	Muscovite	2.76-2.88
Anhydrite*	3.0	Cordierite	2.6-2.66
Halite*	2.1-2.2	Epidote	3.3-3.5
Galena*	7.2-7.6	Sphene	3.45
Sphalerite	3.9-4.2	Psilomelane	3.7-4.7
Apatite*	3.16-3.22	Ilmenite	4.5-5.0
Fayalite*		Hausmannite	4.7-4.8
Ferrosilite*		Chromite	4.5-4.8
Hedenbergite*	3.58-3.6	Spinel	3.5-4.1
Olivine	3.27-4.2	Siderite	3.7-3.9
Orthopyroxene	3.1-3.5	Magnesite	2.85-2.95
Clinopyroxene	3.2-3.6	Dolomite	2.85-2.95
Actinolite	3.1-3.3	Pyrite	5.0-5.2
Hornblende	3.0-3.4	Marcasite	4.8-4.9
Sodic amphiboles	3.0-3.5		
Magnetite	5.2	Chalcopyrite	4.2-4.3
Hematite	5.2-5.3	Bornite	5.7
Rutile	4.3	Arsenopyrite	5.9-6.2
Alunite	2.75	Kaolinite	2.58-2.6
Ferberite-Heubnerite	7.1-7.5	Serperntine	2.5-2.6
Sillimanite	3.2	Corundum	3.9-4.1
Andalusite	3.16-3.2	Spinel	3.5-4.1
Topaz	3.49	Molybdenite	4.7
Tourmaline	3.0-3.25	Covellite	4.59-4.76
Diopside	3.2-3.3	Pyrrhotite	4.6
Acmite (Aegerine)	3.55-3.6	Enargite	4.45
Augite	3.2-3.5	Tetrahedrite-tennantite	4.5-5.2
Enstatite	3.1-3.2	Chalcocite	5.5-5.8
Barite	4.48		
Scheelite	5.9-6.1		
Bronzite	3.2-3.5		
Tremolite	2.9		
Actinolite	3.1-3.3		

Hornblende	3.0-3.4		
Riebeckite	3.02-3.42		
Arvedsonite	3.5		
Wollastonite	2.8-3.09		
Prehnite	2.95		
Pumpellyite			
Astrophyllite	3.3-3.4		
Talc	2.58-2.83		
Nepheline	2.56-2.66		

3. MAGNETIC PETROLOGY OF IGNEOUS INTRUSIONS: IMPLICATIONS FOR EXPLORATION AND MAGNETIC INTERPRETATION

3.1 Introduction

The magnetic method has been widely used in mineral exploration for decades. Recent improvements in magnetic data acquisition, processing and presentation and reduced airborne acquisition costs have increased the utility and importance of magnetic surveys, particularly high resolution aeromagnetic surveys. Increasingly, high quality surveys of large areas are becoming available at reasonable cost. This has led to increasing emphasis on magnetic methods in area selection and regional mapping, as well as prospect-scale mapping and drill targetting.

The mineral exploration industry has now reached a stage where the ability to acquire, process and present magnetic survey data far outstrips capacity to interpret the surveys. There is often far more geological information in these very large data sets than can be presently extracted in the time available for interpretation. Better understanding of the relationships between magnetic signatures and geology can facilitate the interpretation process and produce more reliable geological interpretations.

A crucial limitation of interpretation of magnetic surveys arises from the fundamental non-uniqueness of potential field source distributions. This ambiguity in source geometry can only be addressed by constraining models. The most important control on the reliability of magnetic models is information on magnetic properties. Understanding of the factors that determine magnetisation intensities and directions for the geological units within the survey area is essential for resolving geological ambiguity in order to produce a reliable interpretation of subsurface geology.

Granitoids comprise a substantial portion of many geological provinces and intrusive-related mineralisation is a major exploration target. Information on the magnetic petrology of granitoids should therefore assist geological mapping and an understanding of the relationships between magnetic properties and metallogenic associations of granitoids is important in exploration for intrusive-related ore deposits. Extensive background material that cannot be included in this summary paper can be found in Clark *et al*. (1992a).

3.2 Principles Of Magnetic Petrology

3.2.1 What is Magnetic Petrology?

Magnetic petrology integrates rock magnetism and conventional petrology to characterise the composition, abundance, microstructure and paragenesis of magnetic minerals in order to define the processes that create, alter and destroy magnetic minerals in rocks. By relating magnetic mineralogy, bulk magnetic properties and petrology to observed magnetic anomalies an understanding of the geological factors that control magnetic signatures is obtained, which can be used to improve geological interpretation of magnetic surveys. Dunlop and Özdemir

(1997) have provided a comprehensive and up-to-date overview of rock magnetism. There is no corresponding textbook on magnetic petrology.

Useful reviews of magnetic petrological principles have been given by McIntyre (1980), Grant (1985) and Frost (1991a). Clark et al. (1992b) presented several magnetic petrological case studies. Clark and Emerson (1991) summarised magnetic properties of rocks and some principles of rock magnetism and magnetic petrology. Clark (1997) tabulated magnetic properties of rock-forming minerals, and reviewed general aspects of magnetic petrophysics and magnetic petrology.

Magnetic properties of rocks reflect the partitioning of iron in the rock between strongly magnetic oxides and/or sulphides and weakly magnetic phases (silicates, carbonates etc.). This partitioning depends on chemical composition, oxidation ratio of the iron, and petrogenetic conditions. Thus a host of geological factors influence magnetic properties and simplistic correlations between magnetic properties and lithotype are generally unreliable. It is dangerous to extrapolate empirical correlations between mapped geology and magnetics in one area to another area, ignoring changes in depositional environment, metamorphic grade or structural setting.

For the purposes of subsequent discussion, an informal classification scheme, based on rock susceptibility (k) is used. Igneous rocks are classified as

- diamagnetic (DIA) if $k < 0$,
- paramagnetic (PM) if $0 < k < 1260\times10^{-6}$ SI (100 μG/Oe),
- weakly ferromagnetic (WFM) if 1260×10^{-6} SI $\leq k < 3770\times10^{-6}$ SI (300 μG/Oe),
- moderately ferromagnetic (MFM) if 3770×10^{-6} SI $\leq k < 37{,}700\times10^{-6}$ SI (3000 μG/Oe),
- strongly ferromagnetic (SFM) if $k \geq 37{,}700\times10^{-6}$ SI (3000 μG/Oe).

Diamagnetic granitoids are extremely rare. The approximate magnetite contents corresponding to the ferromagnetic classes are: 0.02 vol % to 0.1 vol % for WFM granitoids, 0.1 vol % to 1 vol % for MFM granitoids and greater than 1 vol % for SFM granitoids. Rocks that have susceptibilities low enough to fall into the paramagnetic class contain at most trace amounts of ferromagnetic (*sensu lato*) minerals, such as magnetite or monoclinic pyrrhotite. In these rocks the measured susceptibility is generally dominated by contributions from paramagnetic minerals. Because paramagnetic minerals do not carry any remanent magnetisation, the remanent magnetisation of PM granitoids is very weak. Ferromagnetic granitoids, on the other hand, may carry significant remanence.

3.2.2 The Concept of Oxygen Fugacity

Standard textbooks on petrology treat the concept of oxygen fugacity in a geological context. Oxygen fugacity (fO_2) is measured in units of pressure and is formally defined as the chemical activity of oxygen. Apart from a small correction due to departures from ideal gas behaviour,
fO_2 is equal to the partial pressure of oxygen gas. It should be noted that the abundance of free oxygen is vanishingly small in magmas and hydrothermal fluids. Nevertheless, fO_2 is a well-defined thermodynamic variable that can be controlled in the laboratory and can be deduced from mineral assemblages. Frost (1991b) has recently clarified some common

misconceptions about oxygen fugacity and given an unusually clear and succinct treatment of the subject.

Iron, which is the fourth most abundant element in the Earth's crust, exists in three oxidation states: metallic (Fe°), ferrous (Fe^{2+}) and ferric (Fe^{3+}) iron. Oxygen fugacity is a variable that strongly influences the propensity for iron to occur in a particular oxidation state. At very low oxygen fugacities, such as in the Earth's core, in some serpentinised ultramafic rocks, and in a few exceptionally reduced lavas that have reacted with carbonaceous material, iron occurs as the native metal. Iron occurs in the divalent ferrous state at higher oxygen fugacities. In silica-bearing systems the ferrous iron is incorporated mainly into silicate minerals. With increasing oxygen fugacity, iron occurs in both the divalent and trivalent states and is incorporated into magnetite as well as silicates. At still higher oxygen fugacities, iron occurs in the ferric state and is incorporated into haematite. Note that the relative terms “low” and “high” $f\,O_2$ depend strongly on temperature (T). At 500°C an oxygen fugacity of 10^{-15} bar is strongly oxidising for most minerals, but at 1000°C the same $f\,O_2$ would correspond to very reducing conditions.

In the system $FeOSiO_2$, the fayalitemagnetitequartz (FMQ) buffer marks the lower oxygen fugacity limit for the stability of magnetite and the haematite-magnetite (HM) buffer marks the upper oxygen fugacity limit (Figure 3.1). The corresponding reactions are:

$$Fe_2SiO_4 + O_2 = Fe_3O_4 + SiO_2 \qquad \text{(FMQ)}$$
fayalite magnetite quartz

$$4Fe_3O_4 + O_2 = 6Fe_2O_3 \qquad \text{(HM)}$$
magnetite haematite

Whether or not magnetite is precipitated from an igneous melt that is cooling along a particular T-$f\,O_2$ path depends on the overall composition of the melt. For example, substitution of Mg for Fe in silicate minerals stabilises them to higher oxygen fugacity (Frost and Lindsley, 1991). In particular, addition of Mg reduces the activity of fayalite in olivine, thereby shifting the equilibrium in the FMQ reaction to the left. As a result, small amounts of magnetite and quartz react to produce fayalite, thereby partially restoring the fayalite activity, plus oxygen, which increases the oxygen fugacity. Thus the olivine-magnetite-quartz buffer is displaced upwards from FMQ and the stability field of magnetite is restricted. At higher Mg contents, this simple picture is complicated by reaction of Mg-rich olivine with quartz to produce orthopyroxene + magnetite. Thus, as shown in Figure 3.2, at high temperatures the oxygen fugacity of the Mg-rich $FeOSiO_2MgO$ system is defined by either a quartz-orthopyroxene-magnetite buffer curve (if the melt is saturated in quartz) or an olivine-orthopyroxene-magnetite buffer curve (if the melt is olivine-saturated). It is evident from Figure 3.2 that higher Mg content of a melt tends to restrict the occurrence of magnetite to higher oxygen fugacities.

On the other hand, substitution of ferrous iron + titanium for ferric iron in titanomagnetite reduces the activity of magnetite and displaces the fayalite-titanomagnetite-quartz equilibrium downwards with respect to FMQ. Thus titanomagnetite is stable in igneous rocks at lower

oxygen fugacities than is end-member magnetite. Similarly, because Ti substitutes even more readily into haematite than into magnetite, addition of Ti to the system displaces the HM buffer to lower fO_2.

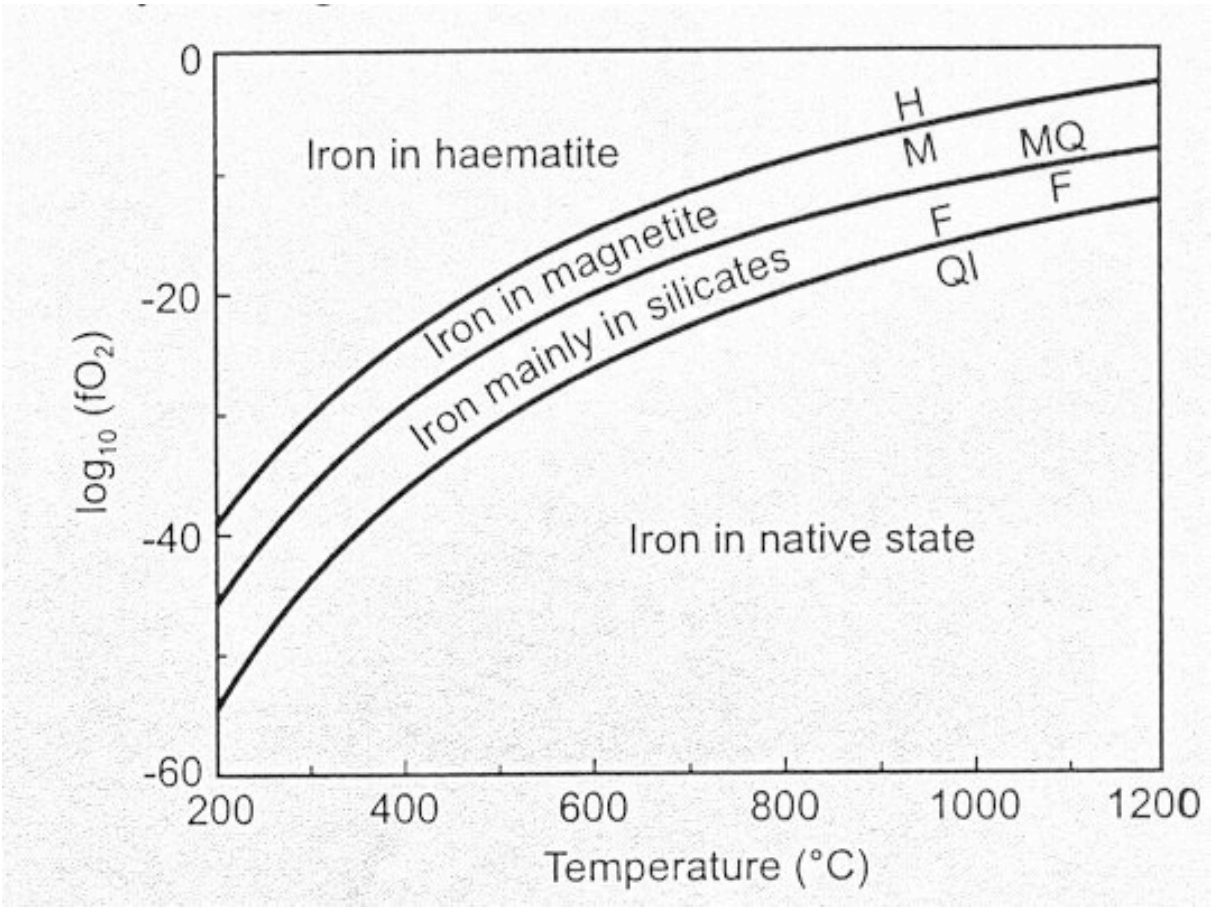

Figure 3.1. Plot of oxygen fugacity, expressed as $\log_{10}(fO_2)$, versus temperature showing the relative stabilities of the various oxidation states of iron in the system Fe-Si-O (after Frost, 1991b). Below the quartz-iron-fayalite (QIF) buffer iron is present as Fe°; between IQF and the fayalite-magnetite-quartz (FMQ) buffer iron occurs in the ferrous (Fe^{2+}) oxidation state; between FMQ and the haematite-magnetite (HM) buffer iron occurs in both ferrous and ferric (Fe^{3+}) oxidation states; and above HM iron is in the ferric state.

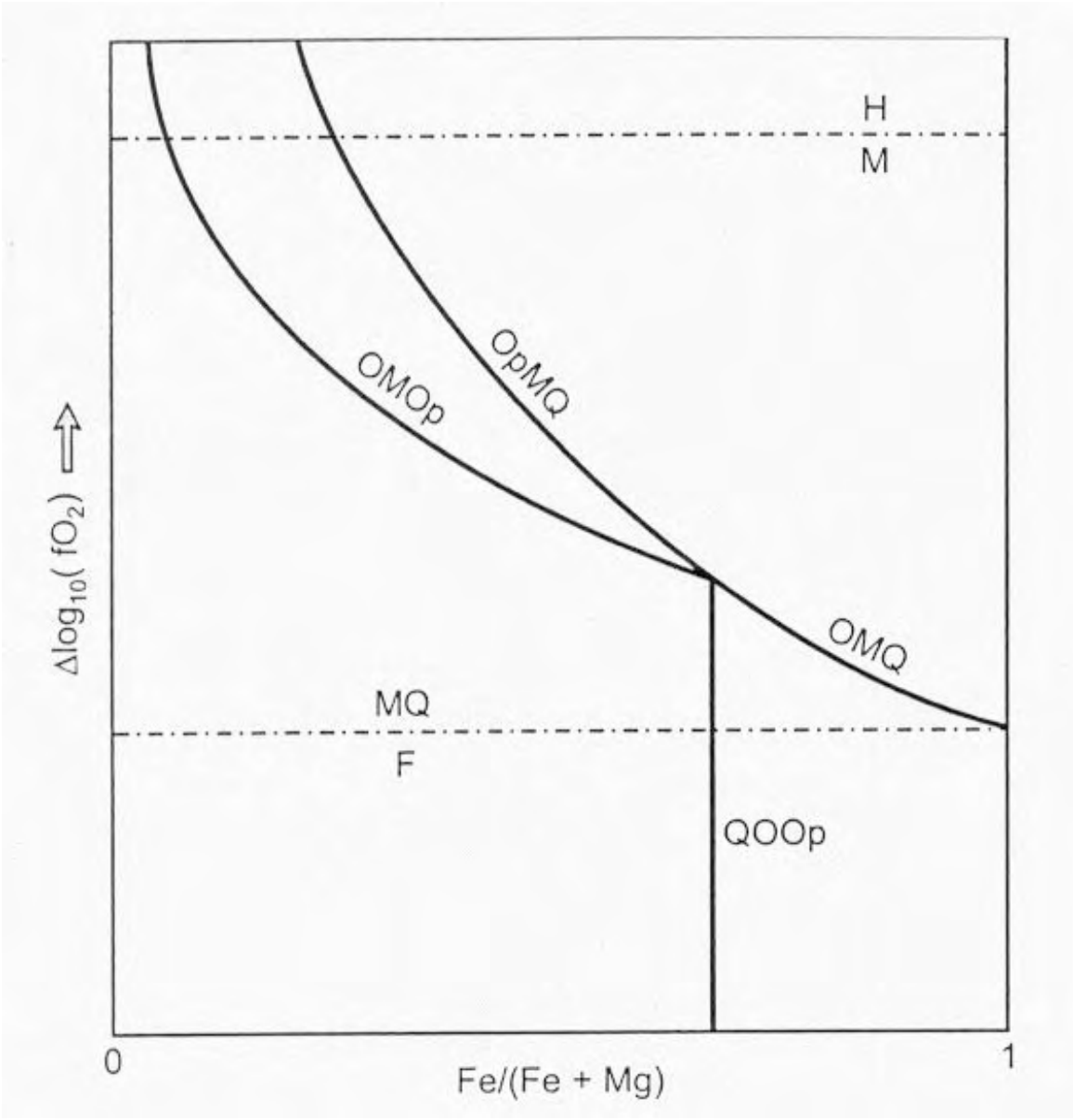

Figure 3.2. Schematic $\Delta\log_{10}(f\,O_2)$ versus Mg/(Fe+Mg) diagram showing effects of adding MgO to the Fe-Si-O system at a fixed temperature (after Frost and Lindsley, 1991). OMQ = olivine-magnetite-quartz, QOOp = quartz-olivine-orthpyroxene, OpMQ = orthopyroxene-magnetite-quartz, OMOp = olivine-magnetite-orthopyroxene, OHQ = olivine-haematite-quartz, OHOp = olivine-haematite-orthopyroxene. The parameter $\Delta\log f\,O_2$ is defined as $\log_{10}(f\,O_2) - \log_{10}(f\,O_2$: FMQ). The values of $\Delta\log_{10}(f\,O_2)$ for the FMQ and MH buffers are shown for reference. Note that these equilibria become displaced towards higher absolute $f\,O_2$ as Mg/(Mg+Fe) increases, because Mg preferentially enters olivine over magnetite and magnetite over haematite.

For many plutonic rocks that behave essentially as closed systems during their history, in particular many tholeiitic rocks, the Fe/Mg ratio of the silicates, plus the Ti content and the ferrous/ferric ratio of the oxides, monitor and, in effect, control the oxygen fugacity. In this case the cooling history of the rock is characterised by a path in fO_2 - T space that is approximately parallel to the standard mineral-buffered curves. In turn the oxygen fugacity influences the composition of the fluid phase and the stability of graphite and sulphides in such igneous rocks.

Fluid-buffering, rather than mineral buffering, of oxygen fugacity is evidently important during hydrothermal processes that have large fluid-rock ratios. Fluid buffering may also play a role in some magmatic processes. If the initial volatile content of the magma is sufficiently high the oxygen fugacity may be largely controlled by the fluid phase, rather than by the ferric and ferrous iron contents of the melt and the crystallising minerals. Takagi and Tsukimura (1997) suggest that the SO_2 - H_2S buffer may be important in the evolution of oxidised granitic rocks, provided the initial SO_2 content of the magma is greater than 250 ppm. Because this buffer curve lies below the FMQ buffer at high temperatures, but intersects FMQ at ~ 850°C and lies well above FMQ at lower temperatures, it represents a relatively oxidising cooling trend that in principle can oxidise ferrous iron in silicates to magnetite via the reaction:

$$\underset{\text{in silicates}}{9FeO} + SO_2 + H_2O \rightarrow 3Fe_3O_4 + H_2S.$$

Takagi and Tsukimura (1997) calculate that initial SO_2 contents of 250-1900 ppm by weight as the dominant sulphurous species are required to precipitate 0.2-1.5 vol % magnetite from granitic melts and show that other fluid buffers, e.g. H_2 - H_2O, CO_2 - CH_4, or CO_2 - CO, cannot produce the oxidising trends that are inferred for many calc-alkaline granitic rocks. The general relevance of sulphur dioxide buffering of melts is still an open question, however, because the primary contents of sulphur species and other volatile phases in magmas is poorly known (P. Blevin, pers. comm). Reported sulphur contents in granitoids are lower than the values that are required to produce substantial magnetite, but this may reflect significant late-stage loss of sulphur carried away by hydrothermal fluids, which sometimes produce related sulphide ore deposits.

Frost (1991b) points out that there can be no *unique* correlation between fO_2 during rock formation and Fe^{3+}/Fe^{2+} of the rock. For example, rocks that contain the same mineral assemblages must have formed at similar fO_2, but if they have very different abundances of the iron-bearing minerals, they may have very different absolute and relative abundances of ferrous and ferric iron. However, oxygen fugacity of melts and glasses is simply dependent on chemical composition, in particular the relative abundance of ferrous and ferric iron. Similarly, in the case of volcanic rocks that are relatively free of cumulate minerals fO_2 can be calculated at a given temperature and pressure, corresponding to crystallisation conditions midway between the liquidus and solidus for the rock, from the whole rock chemical composition, including ferrous and ferric iron. Kress and Carmichael (1991) show that the Fe^{3+}/Fe^{2+} ratio is by far the most important term in the relationship between fO_2 and chemical composition of volcanic rocks.

Blevin (1994) has shown that ferric/ferrous iron ratios in granitoid rocks are also very highly correlated with oxygen fugacity as calculated from the chemical composition (and confirmed by mineral assemblages that are dependent on oxygen fugacity). Thus Fe^{3+}/Fe^{2+}, often measured as $Fe_2O_3/(FeO + Fe_2O_3)$, can in practice be used as a proxy for oxygen fugacity in granitoids, in spite of the theoretical possibility that the nexus between oxidation state and fO_2 might be broken for rocks that formed under very different conditions or that have exotic compositions.

Figure 3.3(a) plots isopleths in fO_2 - T space for various titanomagnetite and ilmenite compositions, with the FMQ and HM buffers shown for comparison. Titanomagnetites are solid solutions of magnetite, i.e. $Fe^{3+}[Fe^{2+}Fe^{3+}]O_4$, and ulvospinel, $Fe^{2+}[Fe^{2+}Ti^{4+}]O_4$, whereas natural ilmenites invariably incorporate some haematite, $Fe^{3+}{}_2O_3$, in solid solution with ilmenite, $Fe^{2+}Ti^{4+}O_3$. The square brackets indicate octahedral cations in the spinel phases. Note that the titanomagnetite isopleths are quite oblique to the oxygen buffer curves, whereas the ilmenite isopleths are subparallel to the buffers. This implies that as an igneous melt cools and solidifies along a trajectory that is approximately parallel to FMQ, the stable titanomagnetite composition evolves from very ulvospinel-rich at high temperatures to magnetite-rich at subsolidus temperatures. Corresponding changes in ilmenite composition are less pronounced. For example, a relatively oxidised melt at ~1000°C (point A in Figure 3.3(a)) may be in equilibrium with Fe-Ti oxide compositions of 50 mole % magnetite-50 mole % ulvospinel (Mt50) and 85 mole % ilmenite-15 mole % haematite (Ilm85). If this magma cools slowly along the Ilm85 isopleth, which almost parallels FMQ, the ilmenite composition remains unchanged, but the equilibrium titanomagnetite composition at ~600°C (point B) evolves to Mt90.

The final titanomagnetite composition found in the rock depends on the initial redox state of the magma (relatively oxidised magmas initially crystallise titanomagnetites with lower Ti than more reduced magmas) and the temperature at which the titanomagnetite composition is "frozen in", which depends on cooling rate. Rapidly cooled volcanic rocks quench in relatively titaniferous compositions that are metastable at low temperatures. On the other hand, in slowly cooled intrusions oxide mineral compositions continue to re-equilibrate well below the solidus, producing titanomagnetites with progressively lower Ti, until the increasingly sluggish kinetics of Fe and Ti exchange between oxide phases inhibits further change. Furthermore, slowly cooled titanomagnetites tend to exsolve into intergrowths of magnetite-rich and ulvospinel-rich phases.

The magnetic properties of titanomagnetites depend on composition. Titanomagnetites with more than 80 mole % ulvospinel are paramagnetic at ambient temperatures and have very low susceptibility. Compositions with less Ti are ferromagnetic *sensu lato*. Consider a reduced ($\log_{10}[fO_2]$ = FMQ - 1), high temperature magma that is in equilibrium with Mt15 and Ilm99. If this magma were cooled very rapidly by being extruded onto the ocean floor, for example, the quenched titanomagnetite would be paramagnetic. However, if the magma is emplaced at depth and cools slowly, following a typical tholeiitic fO_2 - T cooling trend as shown in Figure 3.3(b), the Fe-Ti oxides re-equilibrate attaining compositions of Mt80 and Ilm97 by ~

600°C. If this titanomagnetite composition is metastably stranded upon further cooling, the titanomagnetite is ferromagnetic at ambient temperature and greatly enhances the

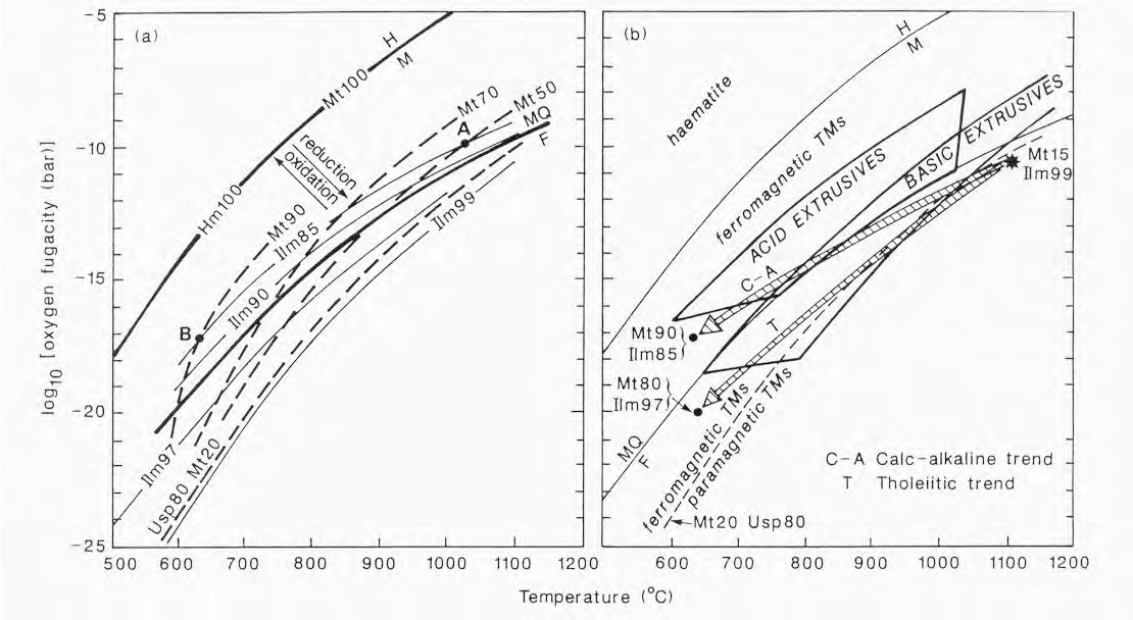

Fig.3.3(a) Isopleths for various titanomagnetite and ilmenite compositions, plotted in $f O_2$ - T space. The FMQ and HM buffers are shown for comparison. (b) Contrasting tholeiitic and calc-alkaline cooling trends in $f O_2$ - T space for an initially reduced ($\log_{10}[f O_2]$ = FMQ - 1), high temperature magma that is in equilibrium with Mt15 and Ilm99. The re-equilibrated Fe-Ti oxide compositions at ~600°C for the two cooling trends are indicated. The dashed line indicates the boundary between the stability fields of ferromagnetic (*sensu lato*) and paramagnetic titanomagnetites. The fields representing $f O_2$ - T conditions recorded by Fe-Ti oxides in basic and acid extrusive rocks (Haggerty, 1976) are also shown.

susceptibility of the rock. Thus ferromagnetic titanomagnetites may form even under relatively reducing conditions, provided the cooling is sufficiently slow. Figure 3.3(b) also shows an alternative, more oxidised, cooling trend that is characteristic of calc-alkaline magmas. Even though fO_2 decreases strongly with falling T, the calc-alkaline path falls more slowly than the FMQ buffer, so the system evolves to a relatively oxidised state that is in equilibrium with more oxidised mineral assemblages. In particular, the equilibrium Fe-Ti oxide compositions at ~ 600°C are Mt90 and Ilm85 for the calc-alkaline trend. Figure 3.3(b) is schematic, because initial magmatic conditions and cooling paths can vary substantially, but it serves to illustrate qualitative trends. Initial conditions of calc-alkaline magmas are generally more oxidising than those of tholeiitic magmas, so the final Fe-Ti oxide compositions may be even more oxidised than indicated in Figure 3.3(b). The fields representing fO_2 - T conditions recorded by Fe-Ti oxides in basic and acid extrusive rocks (Haggerty, 1976) are also shown in Figure 3.3(b).

Figure 3.4 plots the range of titanomagnetite compositions found in the major types of igneous rock. Note the tendency for decreasing Ti content of titanomagnetite, i.e. more magnetite-rich compositions, for more felsic compositions. There is also a clear tendency for lower Ti contents in titanomagnetites from intrusive rocks than for their extrusive analogues, reflecting greter re-equilibration during cooling for intrusive rocks. Paramagnetic titanomagnetite compositions are rare and are only found in a few mafic extrusive rocks with primitive compositions. The inferred primary magnetite composition of the Skaergaard gabbros, derived by reconstituting magnetite-ulvospinel intergrowths within single grains, is very Ti-rich and is close to a paramagnetic composition. However exsolution of primary titanomagnetite into relatively Ti-poor magnetite, which is ferromagnetic, and paramagnetic ulvospinel (or ilmenite, if oxidation-exsolution occurs) during slow cooling produces grains that are ferromagnetic overall. Although the saturation magnetisation of titanomagnetites depends strongly on composition, decreasing almost linearly from 480 kAm^{-1} for pure magnetite to zero for Usp80, the susceptibility is only weakly dependent on Ti content for ulvospinel contents of less than ~70% (Clark, 1997). Thus the titanomagnetites carried by igneous rocks, ranging from gabbroic to granitic compositions, are almost invariably ferromagnetic and the susceptibility of the rock is essentially proportional to the modal titanomagnetite (allowing for intergrown paramagnetic phases in composite grains) and only weakly dependent on titanomagnetite composition. This conclusion differs from that of Grant(1985), who assumed that titaniferous magnetites have much lower susceptibilities than Ti-poor magnetite.

3.2.3 Relationship between Lithology and Magnetic Properties

The data of Figures 3.5 and 3.6 are based on magnetic property measurements at the CSIRO Division of Exploration and Mining over the last 18 years and published studies and compilations. The systematic collection of petrophysical data by the geological surveys of Scandinavian countries, in particular, has greatly expanded the quantity and scope of the information available. It is evident from Figure 3.5 that each rock type exhibits a wide range

of susceptibilities and that susceptibility values are not generally diagnostic of lithology. Classical rock names are in fact much too broad to be useful for classification of magnetic

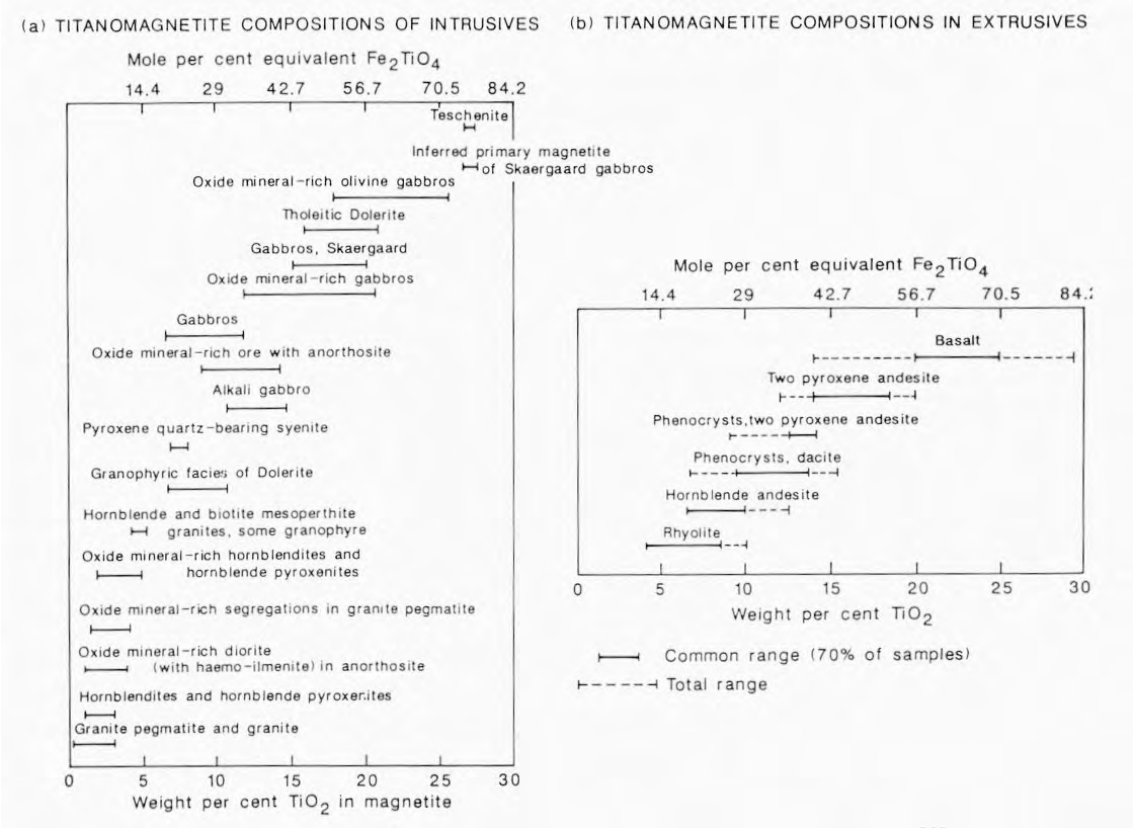

Figure 3.4. Range of titanomagnetite compositions found in the major types of igneous rock (after Buddington and Lindlsey, 1964).

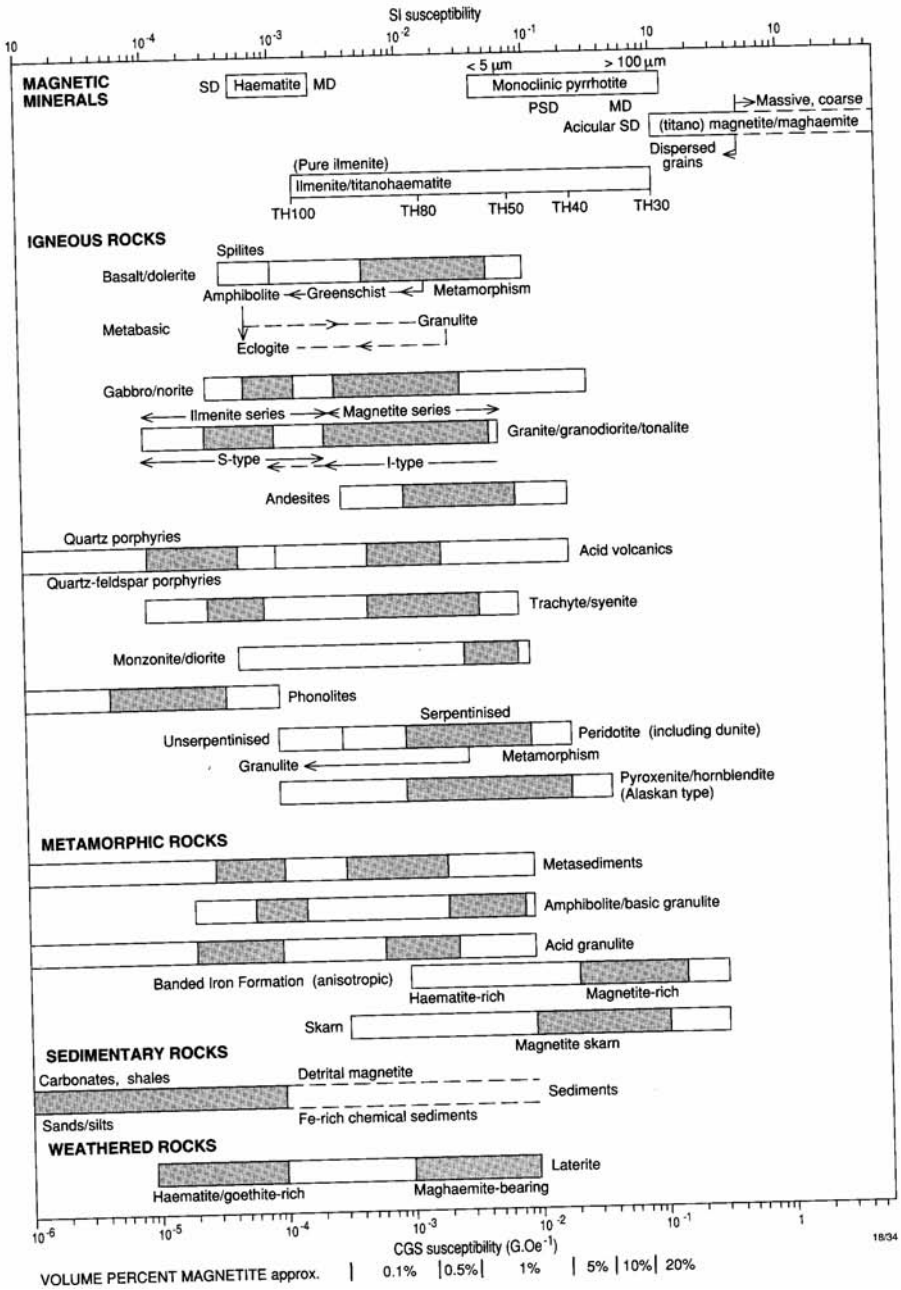

Figure 3.5. Range of magnetic susceptibilities for important magnetic minerals and major rock types. Stippled portions of bars indicate common susceptibility ranges for various lithologies. Note the bimodal susceptibility distributions for many rock types.

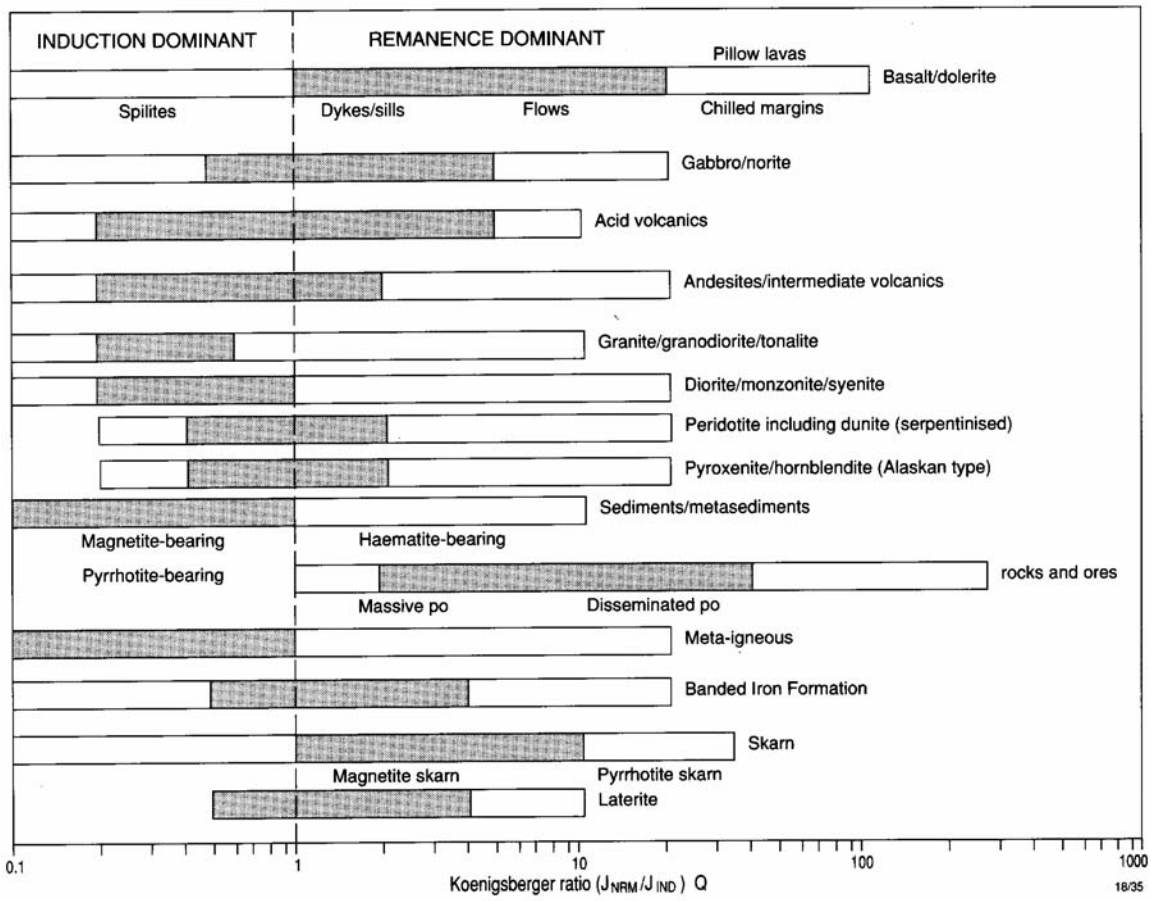

Figure 3.6. Range of Koenigsberger ratios for common rock types. Stippled portions of bars indicate common ranges.

properties. This is because the susceptibility of most rocks reflects the abundance of accessory minerals, particularly magnetite (*sensu lato*), which are generally ignored in petrological classification.

Koenigsberger ratios (Q) can also vary quite widely (see Figure 3.6), but useful rules-of-thumb can be stated. Ferromagnetic intermediate to felsic granitoid rocks contain multidomain magnetite, which is associated with Koenigsberger ratios less than unity (usually $Q < 0.5$, typically $Q \sim 0.2$). Furthermore, the remanence carried by such grains is generally unstable and is dominated by viscous remanence acquired in the recent field. However some, but not all, gabbros, norites and mafic diorites contain ultrafine pseudosingle domain to single domain magnetite hosted within silicate minerals, such as pyroxenes, olivine or plagioclase, as well as discrete multidomain grains. The ultrafine (<10 μm) grains are capable of carrying intense remanence and these rocks may accordingly exhibit Q values substantially greater than unity. Thus magnetisation by induction can be assumed as a first approximation for the more felsic granitoids, whereas remanent magnetisation, possibly oblique to the present field, may be significant for mafic plutonic rocks.

3.2.4 Bimodal Susceptibility Distributions Reflect Ferromagnetic and Paramagnetic Populations

A notable feature of Figure 3.5 is that the magnetic susceptibilities of a number of rock types have distinctly bimodal distributions. Puranen (1989) presented results from very large petrophysical sampling programs in Finland. His data confirmed that all broad field names, such as "granite", "gabbro", "mica schist", "amphibolite" etc., exhibit distinctly bimodal susceptibility distributions. Figure 3.7 shows frequency distributions of susceptibility for major intrusive rock types, based on Puranen's data. The two modes of the frequency distribution correspond to distinct paramagnetic and ferromagnetic populations, with a pronounced intervening gap. Iron in the weakly magnetic subpopulation is incorporated into paramagnetic silicate minerals, predominantly as Fe^{2+}, whereas similar rocks that are moderately to strongly magnetic contain significant Fe^{3+}, which is incorporated into magnetite.

Very highly oxidised rocks, however, tend to contain haematite rather than magnetite and are therefore also weakly magnetic. Within each of the subpopulations, the modal and mean values of susceptibility are much more closely related to rock type than for the total suceptibility distribution. For the paramagnetic subpopulation, in particular, the susceptibility is directly related to the chemical composition, which tends to have a restricted range for each lithology. Clark and Emerson (1991) give the relationship between iron content and susceptibility for paramagnetic rocks and between magnetite content and susceptibility for rocks that contain more than ~ 0.1% magnetite by volume.

When varietal mineralogy is incorporated into a refined rock classification, the bimodal susceptibility distribution tends to resolve into a paramagnetic subpopulation and a ferromagnetic subpopulation, each associated with a distinct mineralogy. Bimodality often also reflects the fact that important geological factors, such as geochemical affinity, alteration

and metamorphic grade are not considered in the simple classification schemes used for most petrophysical summaries. A truly meaningful magnetic petrological classification scheme

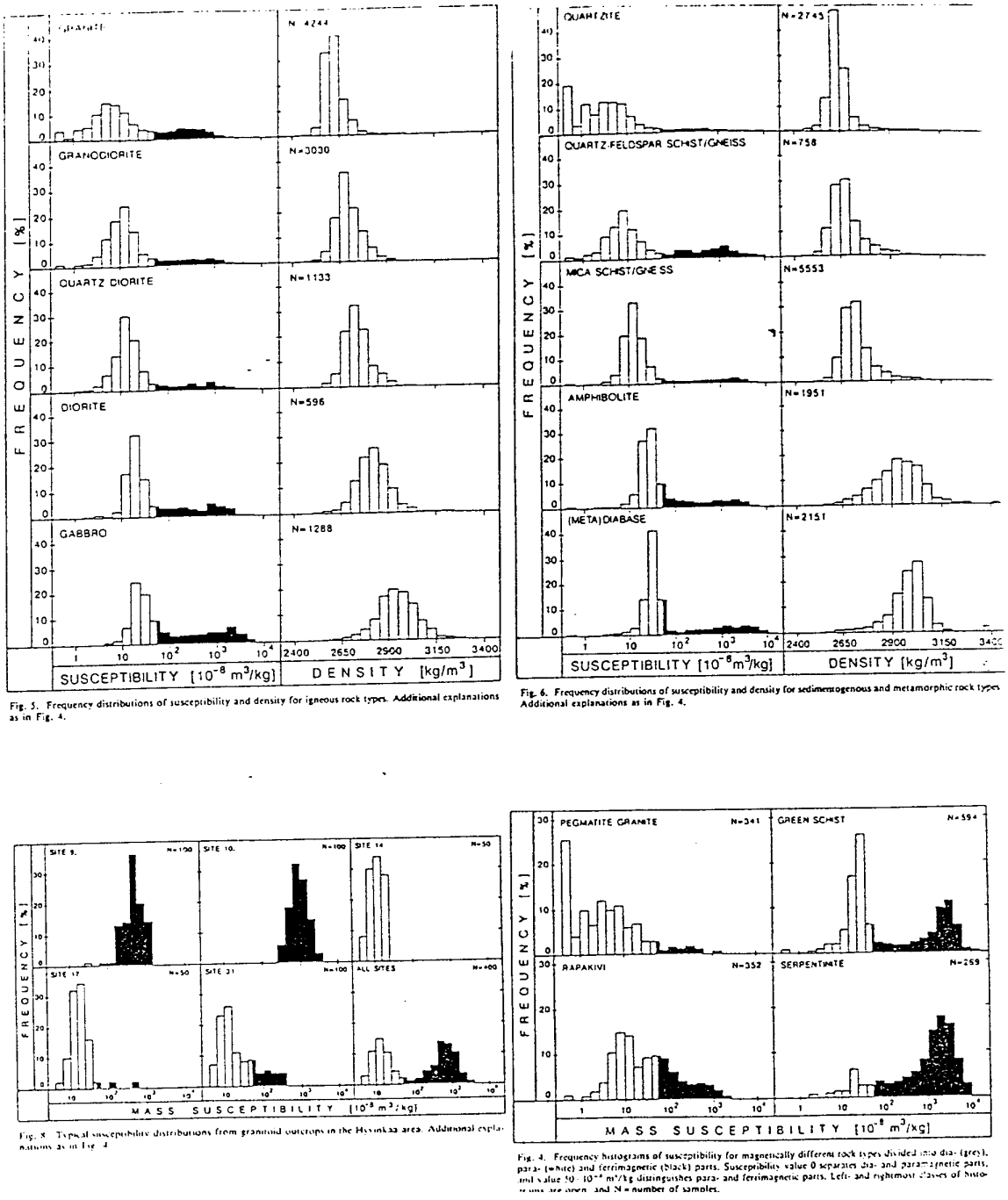

Fig. 5. Frequency distributions of susceptibility and density for igneous rock types. Additional explanations as in Fig. 4.

Fig. 6. Frequency distributions of susceptibility and density for sedimentogenous and metamorphic rock types. Additional explanations as in Fig. 4.

Fig. 8. Typical susceptibility distributions from granitoid outcrops in the Hyvinkää area. Additional explanations as in Fig. 4.

Fig. 4. Frequency histograms of susceptibility for magnetically different rock types divided into dia- (grey), para- (white) and ferrimagnetic (black) parts. Susceptibility value 0 separates dia- and paramagnetic parts, and value $50 \cdot 10^{-4}$ m³/kg distinguishes para- and ferrimagnetic parts. Left- and rightmost classes of histograms are open, and N = number of samples.

Figure 3.7. Histograms of SI mass susceptibility and density for plutonic rock types from Finland (after Puranen, 1989). Note the unimodal density distribution contrasting with the bimodal susceptibility distribution. The ferromagnetic subpopulation is shown as black; the small proportion of diamagnetic samples is shown hatched. To convert mass susceptibility to SI volume susceptibility, multiply by the density in kg/m^3.

must include chemical and/or mineralogical data for protoliths, plus information on metamorphic grade and environment, and/or alteration.

Similarly, when susceptibility distributions are considered on progressively smaller scales, the range of susceptibilities becomes more restricted. Within different geological provinces the relative proportions of paramagnetic and ferromagnetic subpopulations differ from those of other provinces. It is often found that within sufficiently small areas, e.g. within a particular geological environment or simply within a single outcrop, all susceptibilities fall exclusively within one of the subpopulations. Thus the distinct susceptibility subpopulations tend to reflect differing geological conditions, which are not considered in the primary rock classification schemes.

3.3 Classification Of Granitoids

3.3.1 IUGS Classification of Plutonic Rocks

The internationally accepted IUGS classification of mafic to felsic plutonic rocks (Le Bas and Streckeisen, 1991) is simply based upon the relative proportions of three major rock forming minerals: plagioclase (> An5); alkali feldspar (K-feldspar and albite); and either quartz (in oversaturated rocks) or a feldspathoid mineral, most commonly nepheline, in the case of an undersaturated rock. Figure 3.8 shows the fields and rock names on the QAPF double triangle. Ultramafic rocks, for which mafic minerals constitute 90% to 100% of the rock, are classified separately.

Given the fact that, in extreme cases, up to 90% of the mineral content of the rock may be ignored in the first-order classification, it is little wonder that magnetite abundance, for instance, is weakly correlated with rock name. It is also clear that there can be no unique correlation between rock name and bulk chemistry, given the wide range and variety of minor minerals that can be present within any one of the rock type fields. Of course, the classification is so useful and widely accepted because there are coherent patterns of mineralogical and chemical variation among plutonic rocks. Figure 3.9 illustrates some aspects of this coherency. A generalised plot of mineral composition for the full range of plutonic rock types is shown in Figure 3.9(a). Figure 3.9(b) shows average trends in plagioclase composition, mafic mineral contents and hornblende/biotite ratio in granitoid rocks, showing systematic variation with position in the QAP diagram.

Spatially related plutonic rock series show clear mineralogical and chemical correlations with tectonic environment and relative time of emplacement, as shown in Figure 3.10. These various rock associations are characterised by different metallogeny and can be related to magnetic petrology much more reliably than to the broad IUGS rock names. This has implications for exploration, as use of magnetic methods for locating granitoid-hosted or granitoid-related mineralisation requires better understanding of the relationship between rock magnetisation and the geological factors that influence mineralisation.

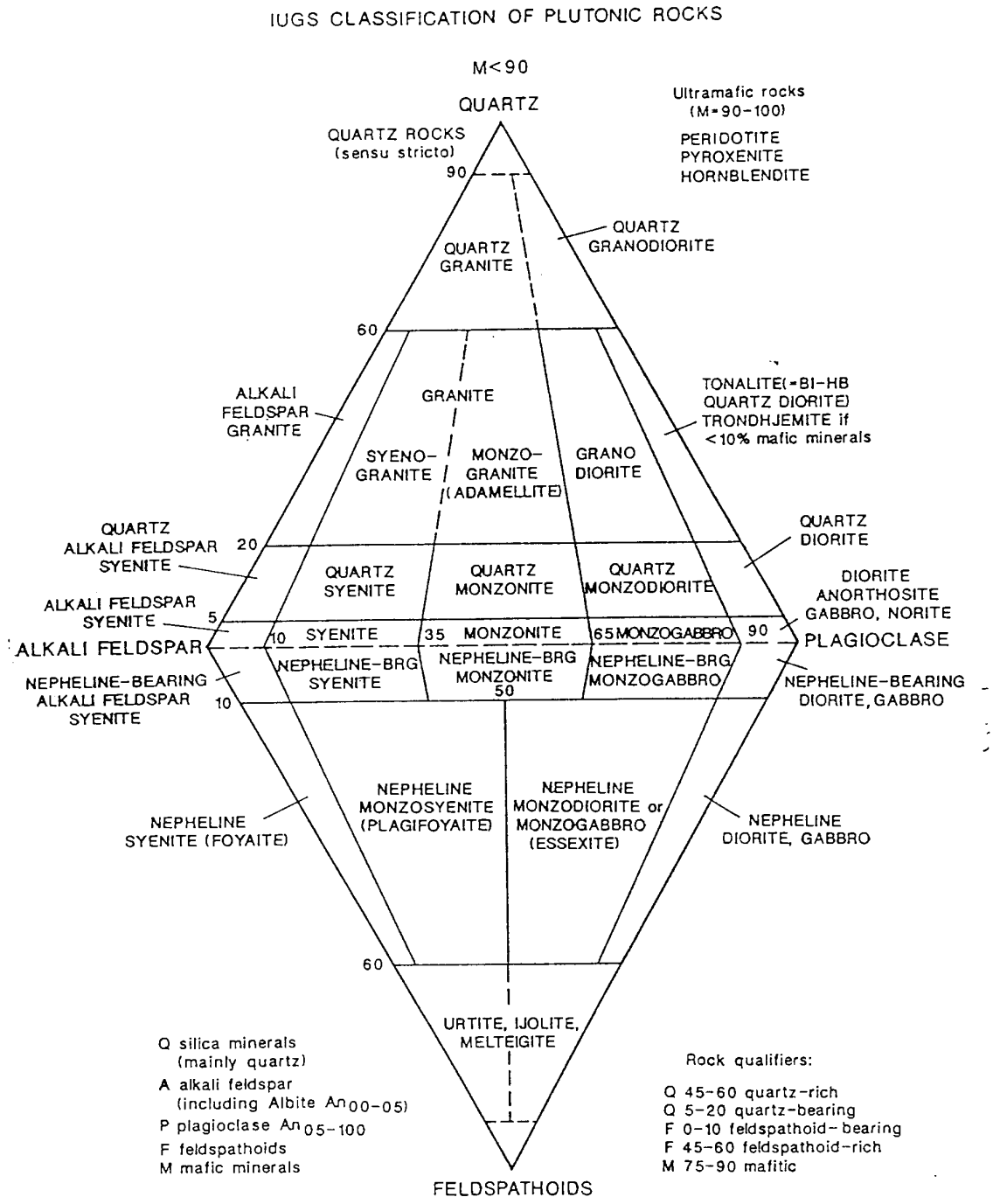

Figure 3.8. IUGS classification of plutonic rocks, based on the QAPF double triangle (Le Bas and Streckeisen, 1991). Q = quartz , A = alkali feldspar, P = plagioclase, F = feldspathoid (foid), M = mafic minerals, BI = biotite, HB = hornblende.

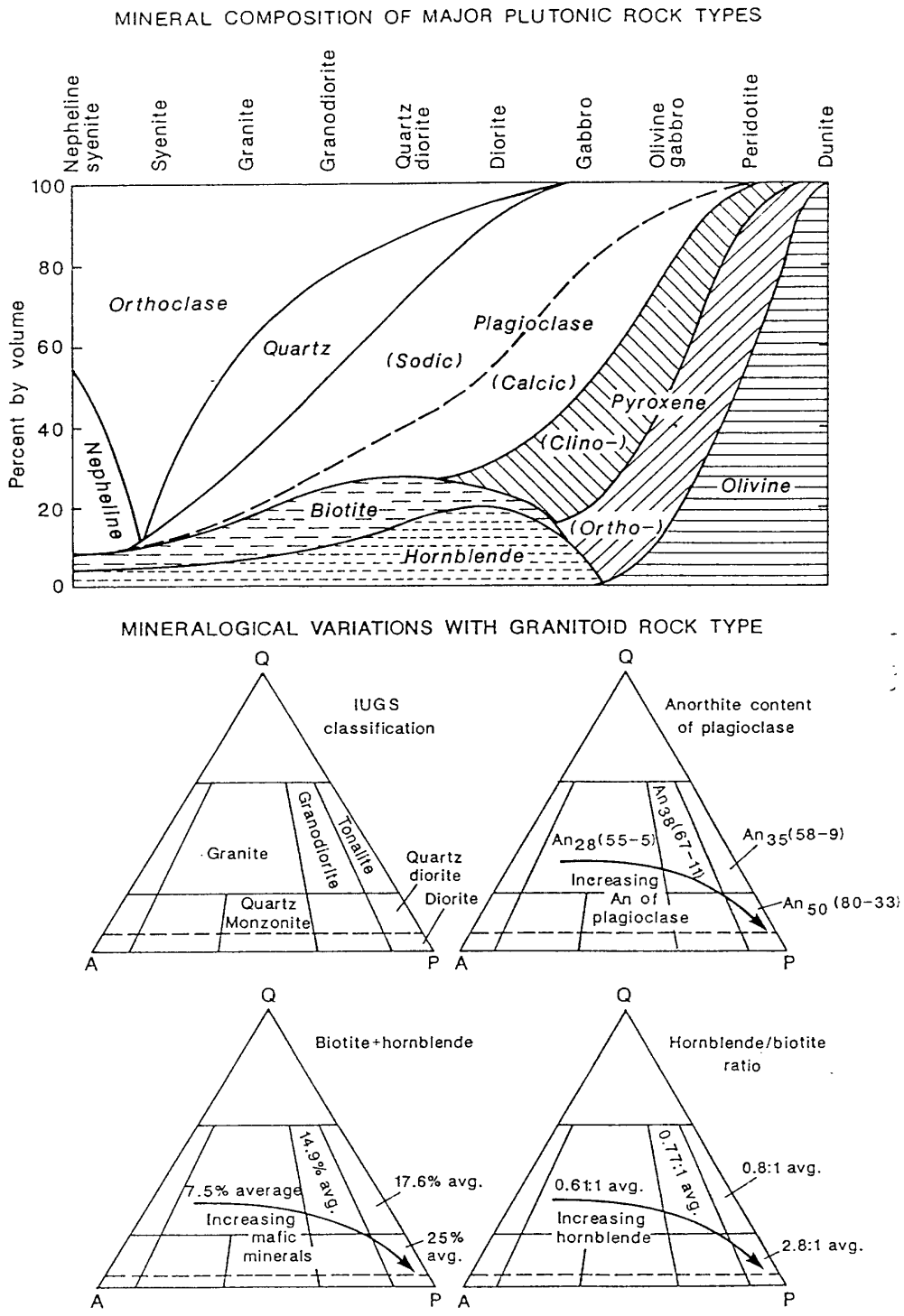

Figure 3.9. (a) Generalised plot of mineral composition for the full range of plutonic rock types (after Washington and Adams, 1951). (b) Average trends in plagioclase composition (expressed as average and range of anorthite contents (%)), mafic mineral contents and hornblende/biotite ratio in granitoid rocks, showing systematic variation with position in the QAP diagram (after Hyndman, 1972).

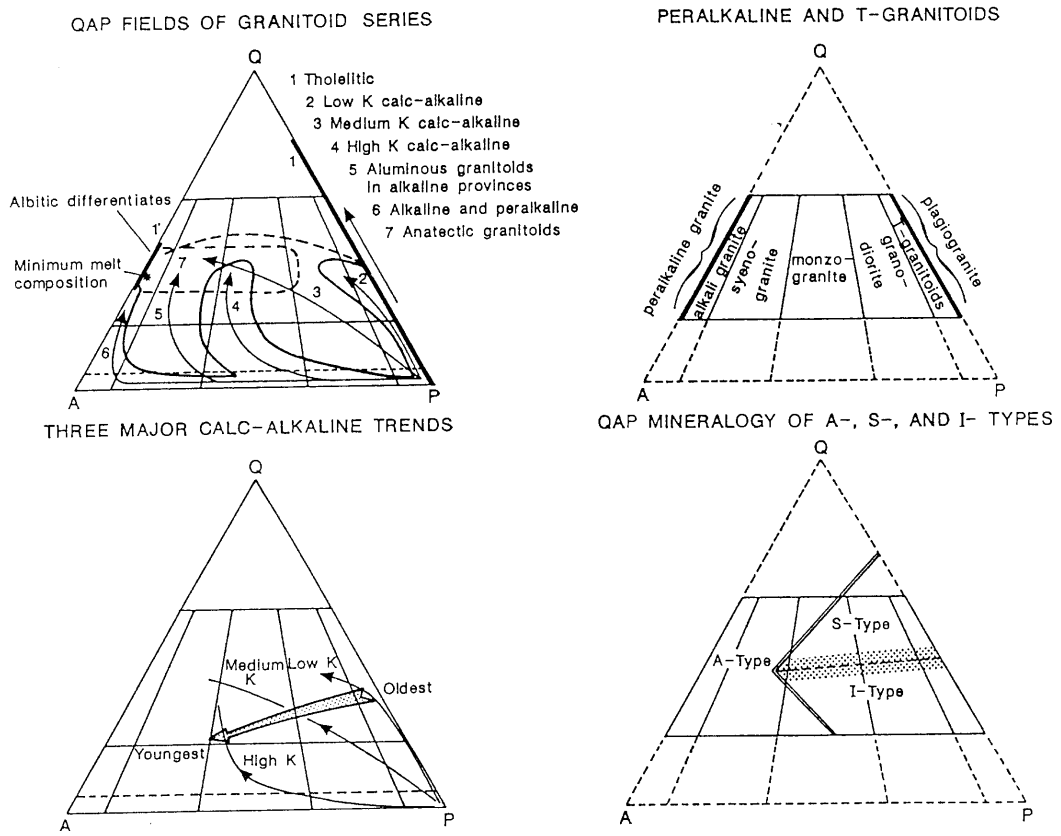

Figure 3.10. (a) QAP fields and differentiation trends for seven distinctive plutonic rock series. (b) QAP fields of peralkaline granites, plagiogranite and T-granitoids (tonalite/ trondhjemite). (c) Spatially related plutonic rock series show clear mineralogical and chemical correlations with tectonic environment and relative time of emplacement e.g. evolution of calc-alkaline series in orogenic belts from the oldest (low-K tonalitic series) through the medium-K granodioritic series to the youngest (high-K monzonitic series). (d) Fields of the QAP plot typically occupied by I-, S- and A-type granitoids (after Bowden *et al*., 1984).

3.3.2 Chemical Classification of Plutonic Rocks

The following summary of chemical classification schemes for plutonic rocks is largely based on the excellent textbook by Hughes (1982).

Feldspars are the commonest minerals in igneous rocks, for which they constitute more than 50%, on average. Alumina occurs in a 1:1 ratio with oxides of the alkali metals or alkaline earth elements in feldspars. Thus departures from this ratio cannot be accomodated by varying the feldspar compositions or relative proportions, but must be expressed in the varietal mineralogy. *Peraluminous* rocks are oversaturated with respect to alumina, i.e. molar Al_2O_3 (A) exceeds the sum of $Na_2O + K_2O + CaO$ (denoted A/CNK > 1), and are characterised by aluminous minerals, such as corundum (rarely), andalusite, sillimanite or kyanite, almandine garnet or, most commonly, muscovite. *Peralkaline* rocks, on the other hand, contain insufficient alumina to consume all of the sodium and potassium in feldspars, i.e. molecular Al_2O_3 is less than $Na_2O + K_2O$ (A/NK < 1). Such rocks are characterised by minerals of the aegirine, riebeckite, arfvedsonite or aenigmatite classes. *Metaluminous* rocks are intermediate in alumina saturation, such that all the alumina, soda and potash can be accomodated in feldspars, with excess calcium appearing in the norm as diopside and in the mode as calcium-bearing pyroxene, amphibole etc. Peraluminous chemistry may result either from high Al content, or from low levels of Na, K or Ca. For example, mature sedimentary rocks, their metamorphic equivalents, and granitic rocks derived from partial melting of the metasediments are peraluminous because of the severing of the nexus between alumina and Na+Ca during the sedimentary cycle. Sodium is partitioned strongly into seawater and calcium into carbonates, leaving sedimentary rocks with excess alumina.

Quartz is a major constituent of many igneous rocks, and its presence or absence is a very significant petrological characteristic. Many minerals exhibit a clear sympathetic or antipathetic association with quartz. *Oversaturated* rocks contain free quartz, together with oversaturated (compatible) minerals (e.g. Al- and Ti-poor pyroxenes, feldspars, amphiboles, micas, fayalitic olivine). *Undersaturated* rocks contain undersaturated minerals that are antipathetic to quartz (e.g. nepheline, magnesian olivine, sodalite, leucite, Al- and Ti-rich augite).

The abundance of Na and K exerts a strong influence on the silica saturation state. In feldspars every molecule of soda or potash in feldspars consumes six molecules of silica, whereas CaO only consumes two. Thus alkaline rocks, with relatively high Na and/or K for their silica content, have no excess silica to form a free silica phase and are undersaturated. The thermodynamic parameter, silica activity, is strongly dependent on the alkali content for this reason. As an example, alkali basalts are silica undersaturated and are characterised chemically by normative nepheline. Undersaturated magnesian olivine is relatively abundant in these basalts, whereas tholeiitic basalts are silica saturated, with hypersthene in the norm. Olivine, if present, is in a reaction relationship to ferromagnesian pyroxene and was therefore out of equilibrium with the tholeiitic magma.

An important geochemical classification of igneous rock series is based upon Peacock's (1931) alkali-lime index (ALI), which is a measure of the relative alkalinity of a rock series derived by igneous differentiation from a parental magma. With increasing differentiation, accompanied by increasing silica content, CaO decreases while Na_2O and K_2O increase. There is a value of silica content, therefore, where the trend of CaO plotted against SiO_2 intersects the trend of Na_2O+K_2O versus SiO_2. This SiO_2 value (in weight per cent) is the alkali-lime index, and is lower for more alkaline rock series. Rock series are classified on the basis of their alkali-lime index into one of four categories: alkalic (ALI < 51), alkali-calcic (ALI = 51-56), calc-alkalic or calc-alkaline (ALI = 56-61) and calcic (ALI > 61), as shown in Fig.3.11(a).

Examples of igneous rock series representing each of the ALI categories include: tholeiitic basalts (calcic); basalt-andesite-rhyolite series (calc-alkalic); alkali basalt-phonolite series (alkali calcic); and alkali syenite complexes (alkalic). The ALI provides a measure of the maturity of volcanic arcs, with igneous rock series tending to evolve from early mantle-derived, calcic magmatism, through calc-alkalic orogenic magmatism, reflecting crust-mantle interactions, to post-orogenic alkali-calcic or anorogenic alkalic magmatism.

Figure 3.11(b) shows a major difference in the behaviour of iron during differentiation of tholeiitic and calc-alkaline magmas. On a ternary plot of MgO, total iron and alkalis (AFM diagram) tholeiitic magmas show a pronounced initial iron enrichment trend, reflecting early crystallisation of Mg-rich olivine and pyroxenes. This trend is typical of many layered mafic complexes (e.g. the Skaergaard, Stillwater and Bushveld Complexes), for which the parental mantle-derived magma is anhydrous and relatively reduced. The initial oxygen fugacity in such magmas is too low to precipitate magnetite. The early-crystallising spinel phase in these intrusions is chromite. As fractional crystallisation proceeds, ferrous iron is increasingly sequestered in silicates and removed from the residual melt, whereas nearly all the ferric iron remains in the melt as the magma composition evolves along the iron-enrichment trend. Thus the Fe^{3+}/Fe^{2+}ratio steadily increases in the melt until the point is reached when magnetite can precipitate. The differentiation trend then turns towards the alkali apex of the AFM diagram as iron is removed from the melt in magnetite. In layered complexes, therefore, the primary ultramafic rocks near the base and the overlying lower gabbros are magnetite-free and have susceptibilities in the paramagnetic range. Overlying, more differentiated, gabbros, norites and anorthosites have higher susceptibilities, increasing upwards, due to the presence of intercumulus magnetic and the upper ferrogabbros and ferrodiorites are very strongly ferromagnetic due to copious amounts of cumulus magnetite.

Although the unaltered ultramafic cumulates are paramagnetic, serpentinisation, particularly of olivine-rich layers, frequently produces secondary magnetite and produces susceptibilities in the MFM range.

Calc-alkaline series, typified by orogenic andesites and their plutonic eqivalents, and minor related mafic and silicic rocks, show a quite different trend, with early depletion in iron and pronounced silica enrichment. This is thought to reflect more hydrous magmas associated with crust-mantle interactions in a subduction zone, with more oxidised parental magma and early, and continuing, crystallisation of Fe-Ti oxides and hydrous phases, such as hornblende.

This leads to a pronounced depletion in iron in the more evolved members of a calc-alkaline series, whereas fractionated rocks derived from tholeiitic magma are relatively iron-rich.

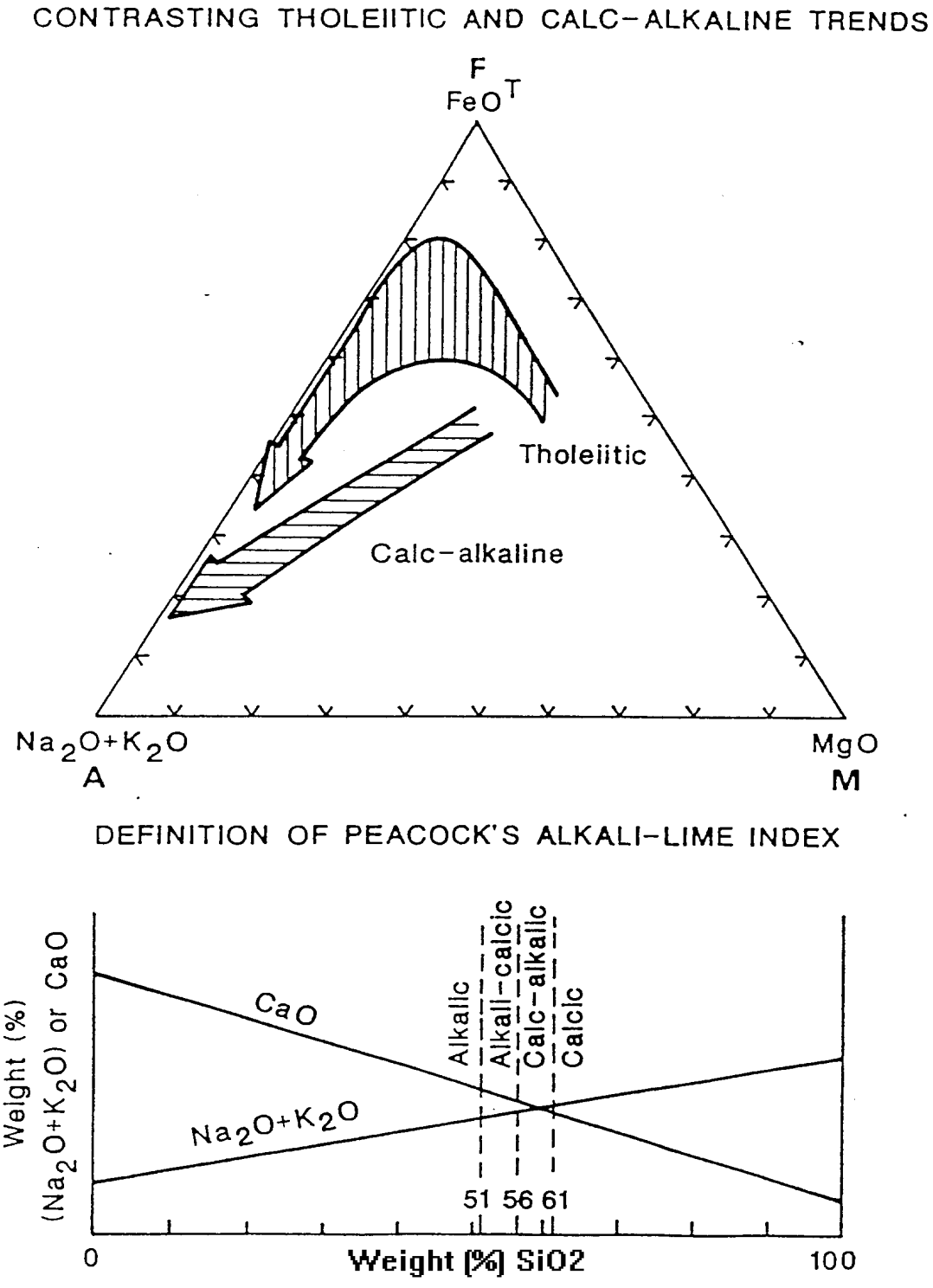

Figure 3.11. (a) Classification of comagmatic igneous rock series as alkalic, alkali-calcic, calc-alkalic and calcic on the basis of the alkali-lime index (Peacock, 1931). (b) Contrasting trends on the ternary plot of alkalis, total iron and MgO (AFM diagram) for differentiating tholeiitic and calc-alkaline magmas.

While calc-alkaline volcanics are subduction-related, calk-alkaline granitoids are not necessarily directly associated with subduction, but are often derived from partial melting of calc-alkaline source rocks produced during an earlier tectonic cycle. Tholeiitic magmas are associated with a variety of tectonic settings. These mainly, but not always, correspond to tensional regimes and include: mid-ocean ridges; mantle plume-related intraplate oceanic islands; and anorogenic continental settings, including flood basalts, major dolerite dyke or sill swarms and layered gabbroic complexes.

3.3.3 Source Rock Classification of Granitoids

Chappell and White (1974) recognised two categories of calc-alkaline granitoids with very distinctive mineralogical, chemical and geological features, which were interpreted as reflecting different source rocks. S-type granitoids are derived from partial melting of (meta)sedimentary rocks, and I-type granitoids from igneous source material. S may also stand for "Supracrustal" and I may represent "Infracrustal". S-type granitoids are characterised by metasedimentary inclusions (microgranitoid enclaves), whereas I-types contain hornblende-rich, mafic inclusions of igneous appearence. These inclusions are interpreted by Chappell and White as "restite", residual source material. Linear inter-element variation trends are regarded as due to restite unmixing. Alternative interpretations involving magma mixing have been suggested, but are not relevant to the present topic. This first order classification based on source rock has been extended to include M-type (mantle-derived) granitoids and A-type (anorogenic, alkaline, anhydrous and, somewhat cynically, “ambiguous”) granitoids, with distinctive characteristics. A-type granitoids are inferred to be derived by partial melting of F and/or Cl-enriched dry granulitic residue remaining in the lower crust after earlier extraction of an orogenic granitic melt (Whalen *et al*., 1987).

Selected characteristic features of these four granitoid types can be drawn from Pitcher (1983) and Bowden *et al.* (1984). They include:

I-type: metaluminous; calc-alkaline to alkali-calcic, relatively quartz-poor monzogranites, granodiorites and tonalites; 53% to 76% SiO_2; high Na/K, high Ca for mafic varieties; hornblende-bearing (except most felsic members).

S-type: strongly peraluminous; alkali-calcic to calc-alkaline, relatively quartz-rich monzogranites, granodiorites and tonalites; 65% to 74% SiO_2; low Na/K, Ca and Sr; with peraluminous minerals (muscovite, cordierite, garnet or andalusite); often biotite-rich.

A-type: peralkaline to metaluminous; alkalic to alkali-calcic syenogranites, alkali granites and quartz syenites; mostly 70% to 78% SiO_2; high Na+K, Fe/Mg, F+Cl and low Ca, Sr; accessory minerals such as fayalite, hedenbergite, ferrohastingsite, annite, fluorite, sodic pyroxenes, perthitic or rapakivi-textured feldspars.

M-type: metaluminous; calcic gabbros, diorites, quartz diorites, tonalites and plagiogranites; 45% to 78% SiO_2; little or no K-feldspar.

Refinements of the I-S classification have been suggested. Pitcher (1983) recognised I-Cordilleran and I-Caledonian granitoids, each with distinctive composition and mineralogy, on the basis of their tectonic setting. His data suggest that the tonalite-dominant I-Cordilleran granitoids tend to be relatively magnetite-rich, whereas the granodiorite-dominant I-Caledonian type granitoids tend to have less magnetite. Chappell and Stephens (1988) proposed that progressively more felsic and chemically evolved I-type granitoids result from successive remeltings of older mafic rocks that have underplated the crust. M-types comprise gabbros to mafic granites derived directly from the mantle or mantle wedge, I-tonalite types are derived from fusion of M-type material and I-granodiorite types represent remagmatised products of I-tonalite rocks. This classification allows for both I-tonalite and I-granodiorite types to occur in the one tectonic setting, although typically one subtype will predominate.

3.3.4 Granitoid Classification Based on Tectonic Setting

Pitcher (1983) has related other granite classification schemes to tectonic environment. Maniar and Piccoli (1989) have proposed an independent granitoid classification scheme, based on tectonic setting. A first order orogenic category is subdivided into island arc granitoids (IAG), continental arc granitoids (CAG), continental collision granitoids (CCG) and post-orogenic granitoids (POG). Anorogenic granitoids fall into three categories: Rift-Related Granitoids (RRG); Continental Epeirogenic Uplift Granitoids (CEUG); and Oceanic Plagiogranites (OP). Although the occurrence and abundance of magnetite was not noted by these authors, the detailed information on chemistry and mineralogy allows broad conclusions on likely magnetite contents to be inferred by comparison with other studies.

3.3.5 Granitoid Classification Based on Fe-Ti Oxide Mineralogy

Ishihara (1977) instigated a descriptive classification of calc-alkaline granitoids into a magnetite-series and an ilmenite-series, based on their characteristic iron-titanium oxide mineralogy. This classification can be directly related to magnetic properties and has important exploration implications, because of the association between metallogeny and the magnetite-series/ilmenite-series classification (Ishihara, 1981). The characteristic accessory mineralogies of the two categories of granitoid are:

magnetite-series — 0.1-2 vol % magnetite ± ilmenite; plus haematite, pyrite, sphene, oxidised Mg-rich biotite; and

ilmenite series — magnetite absent, ilmenite (< 0.1 vol %) + pyrrhotite, graphite, muscovite, reduced Fe-rich biotite.

Thus magnetite-series granitoids are ferromagnetic (MFM to SFM), with susceptibilities in the approximate range 3800-75,000 $\times 10^{-6}$ SI (300-6000 μG/Oe), whereas ilmenite-series granitoids are paramagnetic. Pyrrhotite is present in ilmenite-series granitoids in very minor amounts and cannot contribute significantly to the susceptibility, particularly since much of the pyrrhotite present in ilmenite-series granitoids is the hexagonal variety (Whalen and Chappell, 1988), which is weakly magnetic. Magnetite-series granitoids are significantly more oxidised than ilmenite-series granitoids. This is thought to reflect upper mantle/lower

crustal generation of the magnetite-series, involving minimal interaction with carbonaceous material, whereas the ilmenite-series is interpreted to have been generated in the middle to lower crust and to be significantly contaminated by C-bearing crustal rocks.

Fershtater *et al*. (1978) and Fershtater and Chashchukhina (1979) have devised a "Ferrofacies Classification" of granitoids. The ferrofacies concept has been applied to a wide range of granitoids from the former USSR and can be regarded as an extension of the magnetite-series and ilmenite-series classification. The categories in that classification are: the magnetite ferrofacies; the magnetite-bearing ferrofacies; the magnetite-"free" ferrofacies; and the titanomagnetite ferrofacies — each with distinctive mineralogical characteristics. This classification does not appear to have been used by other workers, but may form the basis for a refined magnetic petrological classification with metallogenic implications.

3.3.6 Suites, Supersuites and Basement Terranes

Hine *et al*. (1978) showed that granitoids of the Lachlan Fold Belt can be grouped into suites using petrographic, chemical and isotopic criteria. Members of a suite are interpreted to be derived from similar source rocks. Suites with similar character can be grouped into supersuites. Chappell *et al*. (1988) demonstrated that granitoids within specific provinces tend to exhibit common geochemical character. Since the compositions of the granitoids largely reflect compositions of their source regions, the distribution of granitoid suites and supersuites can be used to define terranes, within each of which the lower crust has distinctive geochemical characteristics. These basement terranes are often poorly correlated with the tectonostratigraphic terranes that are defined from the surface geology.

3.4 Geological factors that control magnetisation of granitoids

3.4.1 Iron Content and Oxidation Ratio

Many petrological studies of granitoids have been made that are relevant to the problem of defining the geological controls on magnetic properties in these rocks. To a good approximation, the magnetic susceptibility of granitoid rocks is simply proportional to their magnetite content. The directly relevant chemical parameters are the total iron content of the rock, which constrains the theoretical maximum attainable susceptibility, and the oxidation ratio (ferric/total iron), which essentially determines the partitioning of iron between silicates and oxides (mainly magnetite, in fresh igneous rocks). Figure 3.12(a) shows the typical trend for major elements with increasing silica for a series of igneous rocks derived from a basic parental magma. Total iron tends to decrease steadily, but it is important to note that even the most felsic members of common igneous rock series would contain sufficient iron to make them at least moderately to strongly ferromagnetic, provided that all the iron was contained in magnetite. Figure 3.12(b) gives an example of a total iron versus differentiation index trend for a comagmatic suite of granitoids, showing that even the most evolved members of this suite have at least 0.5 wt %, and generally more than 1 wt %, total iron.

Much of the iron, however, is always sequestered within paramagnetic silicate minerals. If the rocks are paramagnetic, the susceptibility decreases monotonically with increasing silica content. This occurs if the iron oxidation ratio of the rocks is low, particularly in the more evolved rocks. In that case the predominantly ferrous iron is taken up by silicates and the relatively small amounts of ferric iron can also be accomodated in silicates, mainly in hydrous phases. As the Fe oxidation ratio of the rocks increases, the silicates are obliged initially to take up more ferric iron. Once the oxidation ratio exceeds the maximum amount of ferric iron that can be accommodated in silicates, the excess ferric iron is forced to appear as magnetite.

Figure 3.12(c) shows, for the same suite of granitoids considered in Figure 3.12(b), how the Fe oxidation ratios of hornblende and biotite are correlated with oxidation ratio of the whole rock, indicating that these phases start to become saturated with ferric iron at rock oxidation ratios above ~20%. Maximum ferric iron contents in these silicates are attained when the oxidation ratio of the rock is ~30%. When this ratio is exceeded, there is a steady increase in magnetite content, until it constitutes ~20% of the mafic minerals, as the oxidatio ratio increases up to ~70%. Above this value, the whole rock ferric iron would be in surplus for forming magnetite, especially when the large proportion of ferrous iron in silicates is considered, and haematite or maghemite would be present in addition to magnetite.

In mafic anhydrous rocks without amphibole or mica, however, the anhydrous silicates can accommodate much less ferric iron than hornblende and biotite, and magnetite appears in such rocks at lower oxidation ratios. This explains why many gabbros and norites are strongly magnetic, in spite of lower oxidation ratios than for the granitoids considered in Figure 3.12(b)-(d).

Data on intrusive rocks from Finland, taken from Puranen (1989), are plotted in Figure 3.13. Figure 3.13(a) shows the average total iron, oxidation ratio, and percentage of ferromagnetic rocks for compositions ranging from gabbro to granite. There is a systematic increase in oxidation ratio with silica content, offsetting the effect on susceptibility of the decrease in total iron. This produces an increased proportion of ferromagnetic rocks at the felsic end of the spectrum, with a slight increase in average susceptibility for granites, compared to granodiorites, as a result (see Figure 3.13(b)). Note that these data, which are derived from a very large petrophysical sampling programme by the Finnish Geological Survey, refer to all sampled units within the appropriate QAP field, irrespective of geological setting, metamorphic grade, varietal mineralogy etc. Although systematic trends tend to be smoothed out by this geological and petrological variability, a clear correlation between chemistry and magnetic petrology is still evident. This indicates that there are strong underlying trends, when specific geological provinces, tectonic settings, geochemical characteristics or mineralogical varieties are considered.

Blevin (1994, 1996) has analysed a large collection of samples for relationships between susceptibility, oxidation state, granitoid type and composition. There is a distinct susceptibility gap between two main trends in the susceptibility-SiO_2 plot. The ferromagnetic trend, representing magnetite-bearing granitoids, exhibits a gradual decrease in susceptibility in both the maximum and average susceptibility values with increasing SiO_2, up to ~72 wt % SiO_2, and then plunges rapidly at higher silica contents.

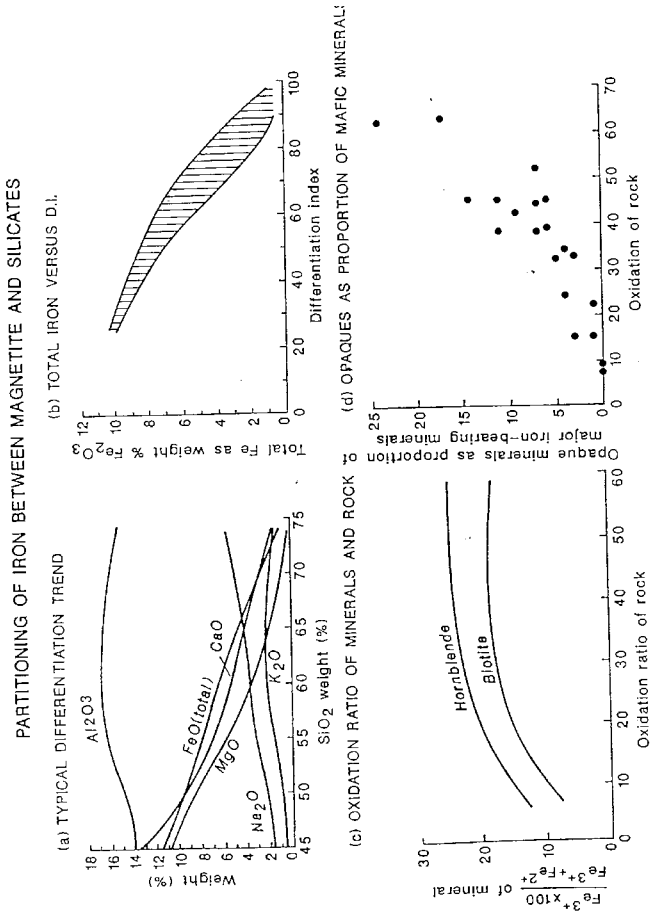

Figure 3.12.(a) Harker diagram showing typical differentiation trends for major elements in a comagmatic igneous rock suite. (b) Total iron versus differentiation index for a suite of granitoids from the Sierra Nevada Batholith (after Dodge, 1972). (c) Oxidation ratio (%) for hornblende and biotite from the Sierra Nevada granitoids versus oxidation ratio (%) of whole rock. (d) Opaque mineral (essentially magnetite) contents as proportion of total iron-bearing mineral assemblage of the Sierra Nevada granitoids versus oxidation ratio of rock.

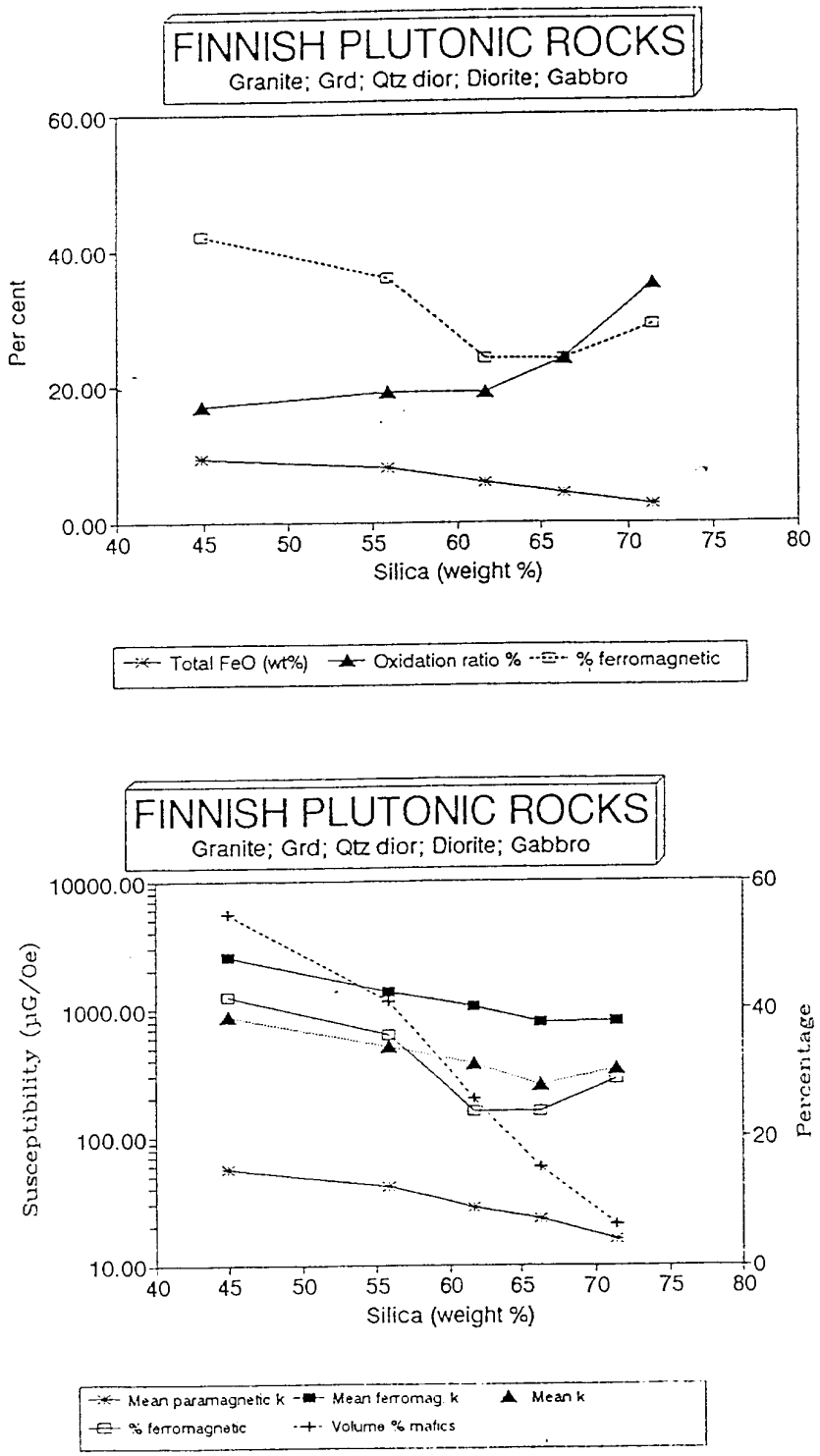

Figure 3.13.(a) Total iron as FeO (wt %), oxidation ratio (%), and percentage of the total sample for each rock type that is ferromagnetic versus SiO_2 for Finnish gabbros, diorites, granodiorites and granites. (b) Mean susceptibility of paramagnetic subpopulations, mean susceptibility of ferromagnetic subpopulations, mean susceptibility of total population, and colour index (volume % mafic minerals) versus SiO_2 for Finnish gabbros, diorites, granodiorites and granites (data from Puranen, 1989).

The paramagnetic trend lies two to three orders of magnitude below the ferromagnetic trend and also exhibits a gentle systematic decrease in susceptibility with increasing SiO_2. Oxidised granitoids generally have susceptibilities greater than 2000×10^{-6} SI (160 μG/Oe), with a maximum of $80{,}000 \times 10^{-6}$ SI (~ 6000 μG/Oe), whereas reduced granitoids have susceptibilities ranging from ~ 500×10^{-6} SI (~ 40 μG/Oe) at the low silica end to ~ 130×10^{-6} SI (~ 10 μG/Oe) at the highest silica contents.

For a given silica content, which generally implies similar total iron contents, there is pronounced increase in susceptibility with increasing oxidation ratio. Granitoids that plot in the gap between the main ferromagnetic and paramagnetic trends are either so felsic (SiO_2 > 72 weight %) that the iron content is too low to crystallise significant magnetite, irrespective of oxidation state, or show evidence of alteration of magnetite. There is little correlation between susceptibility, SiO_2 and Fe_2O_3/FeO for the latter group of granitoids, indicating that the processes of magnetite alteration are not systematically related to granitoid composition.

3.4.2 Geochemical and Mineralogical Associations with Magnetite

The clearest correlations between geochemical or mineralogical factors in granitoids and magnetite content are the general increase in magnetite abundance with increasing oxidation ratio (except for the most oxidised haematite-bearing rocks), for a given iron content, and the increase in maximum magnetite content with increasing total iron, for a given oxidation ratio. However, the occurrence and abundance of magnetite is clearly correlated with other geochemical characteristics. Metaluminous granitoids are much more likely to be ferromagnetic than peraluminous or peralkaline granitoids, and igneous rocks with extreme alumina saturation are almost always paramagnetic. Within each Ishihara series, there is a general correlation of decreasing susceptibility with increasing silica content.

Hornblende + pyroxene or olivine (except fayalite) in mafic varieties is favourable for the presence of magnetite, as is hornblende + biotite in more felsic rocks. Fayalitic olivine, however, indicates reducing conditions and is found only in magnetite-poor granitoids. Mg-rich hornblende and biotite indicate relatively oxidising conditions, with removal of iron into magnetite and consequent enrichment of the mafic silicates in magnesium, particularly when the Mg/Fe ratio increases with increasing rock SiO_2. When ilmenite is present, its composition is correlated with magnetite content. Granitoids without magnetite have relatively reduced ilmenite (< 8 mol % Fe_2O_3), whereas magnetite-bearing granitoids have either more oxidised ilmenite, or Mn-rich ilmenite. High Mn-ilmenite is favoured by oxidising conditions because Fe is preferentially incorporated into magnetite rather than ilmenite.

Figure 3.14(a) shows the correlation between opaque mineral content and susceptibility for Japanese granitoids and gabbroic rocks, showing an essentially proportional relationship (Ishihara, 1981). This reflects the dominance of magnetite over other opaque phases in magnetite-series plutons and the proportionality of susceptibility and magnetite content for normal ferromagnetic rocks. Figure 3.14(b) indicates that there is a wide range of

susceptibilities for mafic magnetite-series granitoids, with many strongly ferromagnetic examples, but the maximum magnetite content, and hence the maximum susceptibility, Figure 3.14(c) shows the relationships between susceptibility, lithology and varietal mineralogy for granitoids from central Australia (Mutton and Shaw, 1979). This confirms the decrease in maximum susceptibility for more felsic rocks, and the association of magnetite with pyroxene and hornblende (indicative of M- or I-type affinities) and the apparent antipathetic relationship of magnetite with muscovite, which is a mineral characteristic of peraluminous, usually S-type, granitoids. Susceptibility decreases steadily with increasing quartz + K-feldspar, so that the most felsic members of the series (syenogranites) are only weakly to moderately ferromagnetic. Ilmenite-series granitoids have very low opaque mineral contents (< 0.1 vol %) and there is still a distinctly lower average susceptibility for the ilmenite-series syenogranites than for their magnetite-series equivalents. There is also a general trend to decreasing paramagnetic susceptibility in more felsic ilmenite-series granitoids, as expected.

Blevin (1994, 1996) has established a useful relationship between feldspar colour and susceptibility for calc-alkaline granitoids. For granitoids with white plagioclase there is a distinct increase in average oxidation ratio and susceptibility with increasing pinkness of K-feldspar. Salmon pink K-feldspars tend to be most oxidised and have the highest susceptibilities. White K-feldspar indicates a reduced rock with low susceptibility. Brick red K-feldspars, on the other hand, which are most common in very felsic rocks, indicate hydrothermal alteration and are generally associated with lower susceptibilities than pink K-feldspars. Green plagioclase is generally indicative of alteration that tends to be magnetite-destructive and is correlated with variable, generally lower, susceptibilities that are poorly correlated with rock composition and oxidation state. Yellowish feldspars usually indicate weathering and such samples are not representative of the fresh rock. Overall, there is a reasonably predictable relationship between susceptibility and the field-observable features: colour index (percentage of mafic minerals), which provides a proxy estimate of silica and iron contents, and K-feldspar colour (provided the plagioclase is white).

3.4.3 Source Rock

Whalen and Chappell (1988) showed that most I-type granitoids of the Lachlan Fold Belt are magnetite-series and most S-types are ilmenite-series, although exceptions to the rule are found. Blevin (1994, 1996) has shown that ~80% of I-type granitoids from the Lachlan and New England Fold Belts have susceptibilities greater than 1000×10^{-6} SI (80 μG/Oe), mostly greater than 2000×10^{-6} SI (160 μG/Oe), whereas nearly all S-types have susceptibilities less than 1000×10^{-6} SI (80 μG/Oe). Exceptions to these generalisations occur within specific suites or supersuites and are confined to particular basement terranes.

Blevin (1994, 1996) has also shown that within each granitoid suite there is generally a systematic decrease in susceptibility with increasing SiO_2. This decrease becomes very rapid above ~74 wt % SiO_2. M-types from the southwest Pacific have the highest susceptibilities in this extensive collection of granitoid rocks from eastern Australia and Oceania, unless they

are altered. Both carbonate and pyrite-pyrrhotite-chalcopyrite alteration are magnetite-destructive in the M-type rocks.

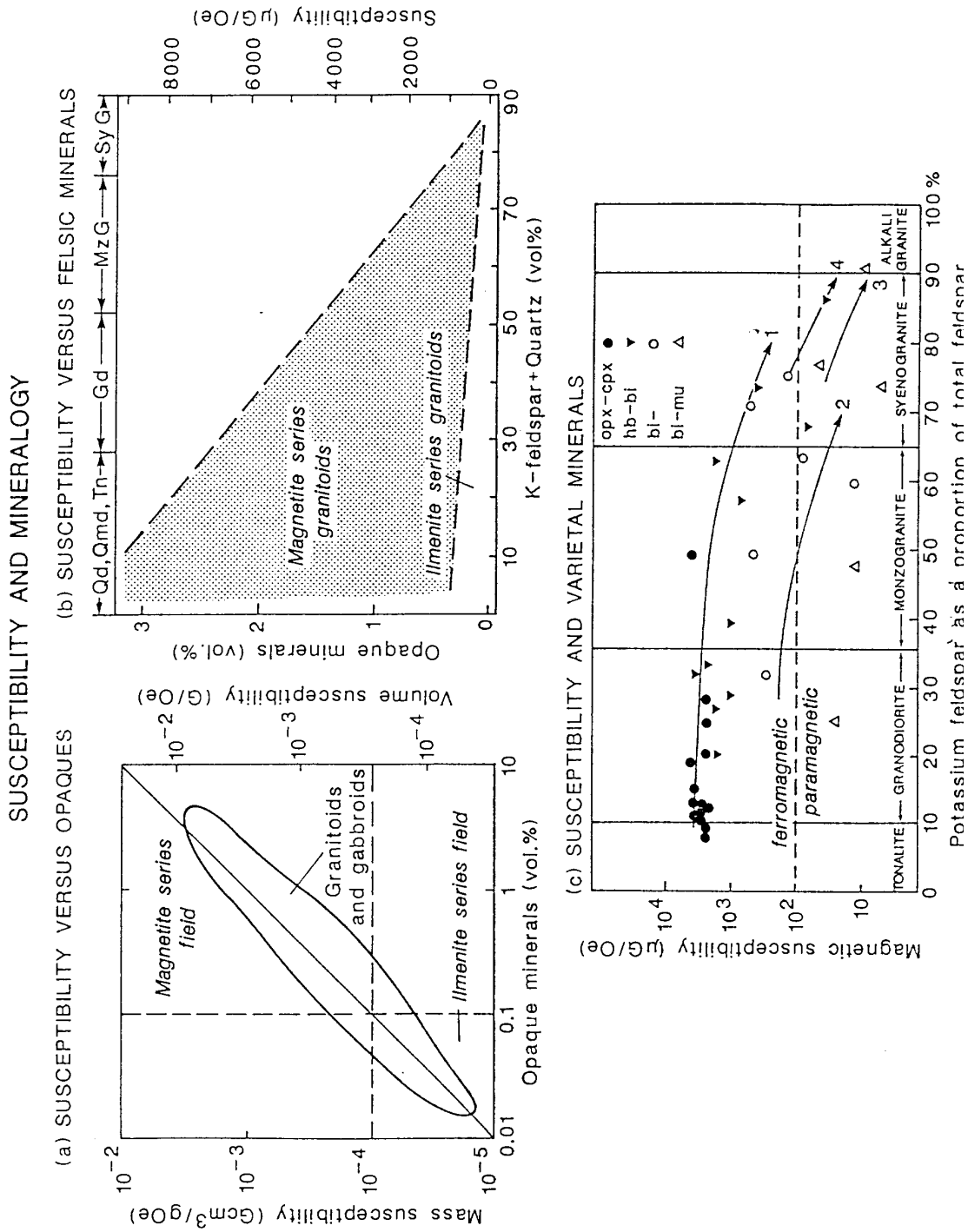

FigFigure 3.14. (a) Correlation between opaque mineral content and susceptibility for Japanese granitoids and gabbroids, showing an essentially proportional relationship (after Ishihara, 1981). Ilmenite series granitoids have very low opaque mineral contents (< 0.1 vol %), (b) range of susceptibilities for magnetite-series and ilmenite-series granitoids versus quartz + K-feldspar (after Ishihara, 1981), (c) relationships between susceptibility, lithology and varietal mineralogy for granitoids from central Australia (after Mutton and Shaw, 1979).

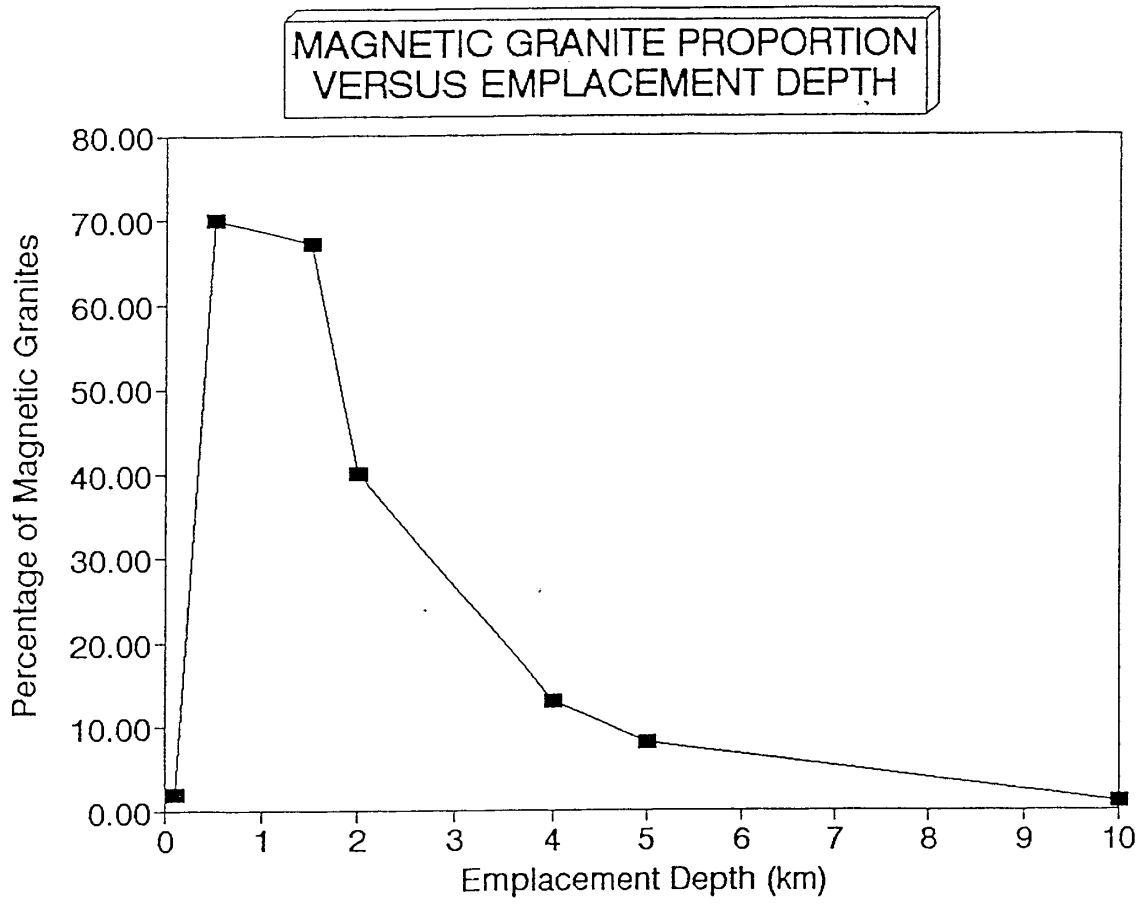

FigFigure 3.15. Proportion of ferromagnetic granitoids versus estimated emplacement depth for granitoids from NE Russia (data from Pecherskiy, 1965). The point at 200 m depth represents a single occurrence of felsic sills (possibly hypabyssal equivalents of S-type volcanics).

For silica contents of 70% to 74% by weight, A-type granitoids exhibit a bimodal distribution of susceptibilities, similar to those of oxidised and reduced I-types with equivalent SiO_2. Above ~74 wt % SiO_2 the A-types exhibit a broad unimodal susceptibility distribution, reflecting a rapid decrease from WFM to PM levels as SiO_2 increases from 74 wt % to 78 wt %.

Average susceptibilities for M-, I- and S-type granitoids are $40{,}000\times10^{-6}$, 8900×10^{-6} and 410×10^{-6} SI (3200 μG/Oe, 700 μG/Oe and 30 μG/Oe) respectively. The corresponding medians are $32{,}500\times10^{-6}$, 5600×10^{-6} and 270×10^{-6} SI (2600 μG/Oe, 450 μG/Oe and 20 μG/Oe). The median susceptibility of the limited set of A-type granitoids studied by Blevin (1994) is $\sim1000\times10^{-6}$ SI (~ 80 μG/Oe). For the ferromagnetic subpopulation of the slightly less felsic (70 wt % to 74 wt % SiO_2) varieties of A-type, the median susceptibility is an order of magnitude greater.

Magnetite contents of granitoids show distinct provinciality, along with other mineralogical and chemical characteristics, reflecting distinctive compositions of lower crustal source regions (Chappell *et al*., 1988; Blevin, 1994). For example, in most basement terranes I-type granitoids are relatively oxidised magnetite-series rocks. In the Melbourne Basement terrane, however, the I-type granitoids are reduced and belong to the ilmenite-series. The infracrustal protolith from which these rocks have been derived is therefore inferred to be more reduced than elsewhere in the Lachlan Fold Belt. Granitoids belonging to individual suites, which are derived from fairly homogeneous source rocks, exhibit a systematic correlation between magnetic susceptibility and composition that is much better defined than global relationships between these variables.

Overall, mantle-derived granitoids, I-types derived from mafic crustal underplates and second-generation I-types derived from oxidised I-type source rocks are magnetite-series, whereas I-types derived from reduced igneous rocks are ilmenite-series. A-types resemble felsic I-types and have subequal magnetite-series and ilmenite-series populations. Most S-types are reduced ilmenite series granitoids, probably reflecting presence of carbon in their lower to middle crustal source material.

3.4.4 Lithology

The overall proportion of ferromagnetic rocks within a given geological province or within a particular igneous rock series decreases from gabbro through to granite. This trend is apparent from Figure 3.13(a), which combines data from a wide range of areas and rock series, but is more clearly expressed within particular provinces or rock series. Mafic to felsic and intermediate to felsic associations are much more likely to be magnetite-series throughout, than compositionally restricted felsic associations. Alkaline intrusive rocks are often magnetite-series, with the exception of extreme compositions, such as peralkaline granites and agpaitic (peralkaline, undersaturated) nepheline syenites. In tholeiitic layered complexes, less evolved lower gabbros are paramagnetic to weakly ferromagnetic, whereas sufficiently evolved upper ferrogabbros and ferrodiorites, and associated granophyres, are usually strongly ferromagnetic.

3.4.5 Emplacement Depth

Pecherskiy (1965) noted a strong correlation between shallow emplacement depth and occurrence of magnetite for a wide variety of granitoids in northeastern Russia. Figure 3.15 shows the percentage of moderately and strongly ferromagnetic granitoids versus estimated depth of emplacement for a large number of plutons. There is a systematic increase in ferromagnetic proportion with decreasing depth of emplacement. The ferromagnetic proportion rises to 70% for subvolcanic/epizonal granitoids. This interesting observation does not appear to have attracted much attention, but other studies lend some indirect support. Czamanske *et al*. (1981) explain a similar correlation in Japan by invoking onset of second boiling in the residual melt in epizonal plutons. Dissociation of water and preferential diffusion of hydrogen out of the pluton into fractured country rock is the oxidation process that is postulated to produce the high magnetite contents of these plutons. However Candela (1986) has shown that dissociation of water can only be an important oxidising process for iron-poor (<<1 wt % FeO^T) granitoids. This mechanism may operate in Climax-type Mo porphyries, which are very felsic, but interaction with oxygenated meteoric waters is a more probable explanation for the relatively oxidised nature of at least some epizonal granitoids.

There is also a general correlation between the source rock, depth of generation and depth of emplacement of granitoids, which probably explains much of the empirical trend shown in Figure 3.15. Deep-seated, high temperature, anhydrous magmas rise to shallow crustal levels, whereas lower temperature, hydrous magmas (produced by partial melting of muscovite-rich pelitic metasediments, for example) do not rise very far from their source regions, producing catazonal granitoids. The former type of magma is more likely to produce magnetite-series granitoids, whereas the latter generally produces ilmenite-series granitoids, for reasons already explained.

3.4.6 Tectonic Setting

Referring to Maniar and Piccoli's (1989) classification, most island arc and oceanic plagiogranites, and more mafic continental arc granitoids, are ferromagnetic. Nearly all continental collision and post-orogenic granitoids are paramagnetic. Rift-related granitoids and continental epeirogenic uplift granitoids have an inferred bimodal distribution of susceptibilities, with the mafic compositions tending to be ferromagnetic and the felsic compositions generally paramagnetic.

3.4.7 Crustal Contamination and Contact Aureoles

Ishihara *et al.* (1987) presented evidence that local contamination of a I-type tonalitic pluton by sulphur and carbon derived from sedimentary country rocks produced a vertical zonation from low magnetic susceptibility ilmenite-series tonalite at lower levels to magnetite-series tonalite at higher levels. There was less contamination at higher levels. Similar effects have also been observed in the Lachlan Fold Belt, but only within a few metres of the granitoid margin (Blevin, 1994). More generally, Blevin (1994) argues that crustal contamination effects on oxidation state of Lachlan Fold Belt granitoids are negligible and that in the vast majority of cases the oxidation state of these granitoids is inherited from the source region.

On the other hand, Ague and Brimhall (1988) suggest that substantial contamination of granitoid magmas by country rocks has occurred in Californian batholiths. Where strongly contaminated by graphitic pelites, the I-type tonalites are reduced ilmenite-series, otherwise they are magnetite-series. Pecherskiy (1965) estimates that the nature of the country rocks has significant effects on the magnetic properties of granitoids in NE Russia in at most 20% of cases (probably much less).

As well as the country rocks affecting the magnetic properties of the granitoid, emplacement of granitoids frequently has a pronounced effect on the magnetic properties of country rocks that are metamorphosed and metasomatised by the intrusion. Often the magnetic signature of the contact aureole is more pronounced than that of the granitoid itself. Speer (1981) studied the mineralogical changes, including production of secondary magnetite, within the contact aureole of the Liberty Hill pluton, South Carolina. For that granitoid there is a very clear relationship between the detailed magnetic signature of the aureole and changes in metamorphic grade of the metapelitic country rocks, as shown in Figure 3.16. There are smooth variations in magnetite content, correlated with changes in mineral modes and mineral chemistry, within metamorphic zones, with inflections at metamorphic isograds. The susceptibility of the metamorphic magnetite zone is substantially greater than that of the magnetite-series pluton. Outside the aureole the susceptibility of the country rocks is very low. The magnetic signature of the granite and aureole comprises a relative magnetic high (~ 200 nT above regional background) over the granite, rimmed by a strong, narrow high (~ 500 nT above background) centred on the magnetite-rich middle to outer aureole, dropping to the regional background level outside the aureole.

Contact aureoles around granitoids that intrude pyritic sediments may exhibit substantial magnetic anomalies due to breakdown of pyrite to monoclinic pyrrhotite (the ferromagnetic variety of pyrrhotite). Monoclinic pyrrhotite generally carries a relatively strong remanent magnetisation, characterised by $Q >> 1$.

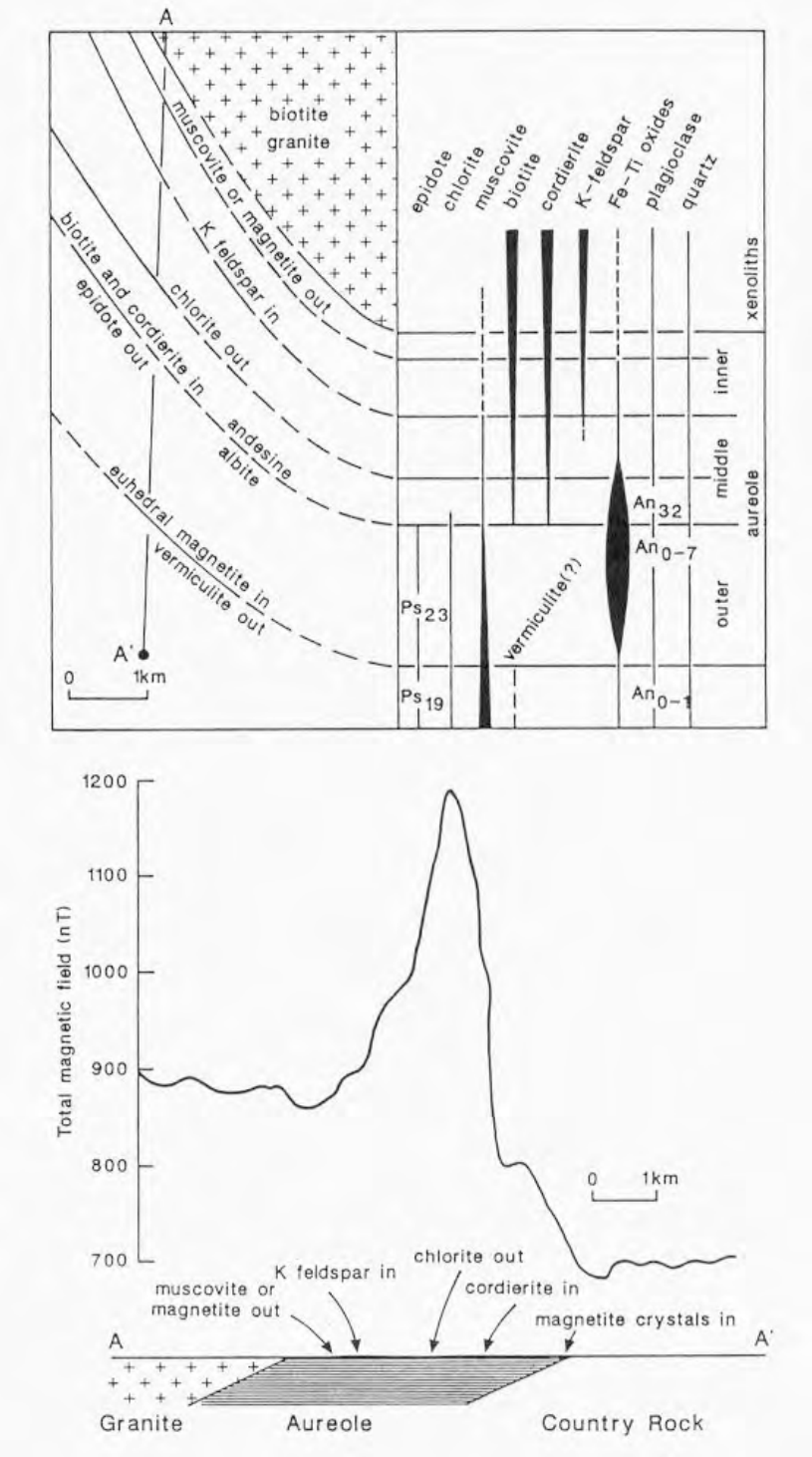

Figure 3.16. Magnetic expression of metamorphic magnetite formation in the contact aureole of the Liberty Hill pluton, South Carolina (after Speer, 1981).

3.5 Magnetic petrology and metallogeny of granitoids

3.5.1 Mineralisation in Layered Mafic/Ultramafic Complexes

Differentiation of reduced mafic magmas within large, essentially closed system, slowly cooled magma chambers proceeds according the tholeiitic trend discussed above, with initial iron-enrichment and late iron-depletion, producing zoned complexes with basal ultramafic layers, overlain by paramagnetic mafic rocks, then by increasingly more magnetic mafic rocks, grading finally to MFM granophyres. Cr-mineralisation occurs as chromite bands towards the top of the ultramafic zone, which contains no primary magnetite, but may be MFM due to secondary magnetite produced by serpentinisation of olivine. The paramagnetic mafic rocks that overly the ultramafic zone may host platinum group element and Cu-Ni mineralisation. In the upper portions of the zoned complex, the SFM upper ferrogabbro and ferrodiorite zones host bands of titanium- and vanadium-bearing cumulus magnetite, which may constitute economic ore deposits of Ti and V. The Bushveld Complex, which hosts the world's greatest repository of magmatic ore deposits, may be regarded as the type example of such mineralised layered mafic/ultramafic intrusions. An idealised model of the magnetic stratigraphy can be developed from this generalised picture of layered mafic/ultramafic complexes. This model has been used by Clark *et al*. (1992a; 1992b) to predict magnetic anomalies over tilted Bushveld-type complexes.

3.5.2 Oxidation State and Metallogenic Associations

More than 30 years ago Pecherskiy (1965) noted an empirical association of granitoid-related gold deposits with ferromagnetic granitoids and tin deposits with paramagnetic granitoids. Ishihara (1981) established the important correlation between his magnetite- and ilmenite-series granitoid classification and granitoid-related mineralisation. For example, copper and molybdenum porphyries are almost always magnetite-series, whereas tin granites are invariably ilmenite-series. It has become apparent in recent times that this relationship is not just empirically based, but can be related to redox conditions in the magma. Ishihara's data on metallogenic associations with granitoid series and with susceptibility are reproduced in Figure 3.17.

The compatible or incompatible behaviour of multivalent metals such as Cu, Mo, W and Sn in the melt depends on their valency, which is a function of redox conditions. For example, tin occurs in two oxidation states in magmas: stannous (Sn^{2+}) and stannic (Sn^{4+}). The oxidised stannic species fits easily into the structures of minerals such as magnetite and sphene, which are diagnostic of oxidising conditions in the magma, and is therefore dispersed throughout an oxidised granitoid. On the other hand, the reduced stannous ion is too large to be accomodated readily within mineral structures and is accordingly concentrated in the residual melt. Thus reduced, and therefore paramagnetic, granitoids are potential sources of tin mineralisation, whereas magnetite-bearing granitoids are too oxidised to be associated with tin deposits. Development of an exsolved fluid and partitioning of ore elements into hydrothermal liquids or vapour phases also depends strongly on the nature and concentrations of volatile species. The ratios SO_2/H_2S and CO_2/CH_4 depend on oxygen fugacity and

therefore oxygen fugacity exerts a major influence on hydrothermal evolution, concentration of ore elements into mineralising fluids, and transport and deposition of ore elements.

Khitrunov (1985) has attempted a general explanation of the empirical relationships between oxidation state of granitoids and associated Cu, Mo, W or Sn mineralisation, concluding that magmatic conditions are progressively more reduced for Mo, Cu, W and Sn mineralisation. Cameron and Carrigan (1987) and Hattori (1987) have pointed out the association between oxidised felsic magmas, magnetic granitoids and Archaean gold deposits. They have given a detailed discussion of the factors favouring incorporation of gold from sulphide minerals in source rocks, concentration into a CO_2-rich melt at mesothermal levels and deposition after development of an immiscible fluid phase. Sillitoe (1979) pointed out the association between gold-rich porphyry copper deposits and oxidised, magnetite-rich plutons with a magnetite-rich potassic alteration zone. Kwak and White (1982) distinguished between reduced porphyry tin and W-Sn-F skarn deposits and more oxidised W-Mo-Cu skarn deposits and Cu porphyries (Figure 3.18).

Blevin and Chappell (1992, 1995) have published thorough analyses of the metallogenic implications of granitoid chemistry, oxidation state and magmatic differentiation, based mainly on studies of the Lachlan Fold Belt. Sn mineralisation is associated with both S- and I-type granites that are reduced and have undergone fractional crystallisation. Such granites contain negligible magnetite and are paramagnetic. On the other hand Cu and Au mineralisation is associated with oxidised, magnetite- and/or sphene-bearing, intermediate I-type suites. Mo is associated with similar granites that are more fractionated and oxidised. W does not appear to show a close relationship to granitoid type and is an opportunistic ore element, occurring in association with a number of other metals. Within mineralised granitoid suites ore element ratios are simply related to relative oxidation state and degree of fractionation.

3.5.3 The Importance of Fractional Crystallisation

Blevin and Chappell (1992, 1995) point out that fractional crystallisation of magmas is a powerful mechanism for concentration of ore elements into the residual melt, which is a prerequisite for formation of intrusive-related mineralisation. Late stage fractional crystallisation leads to quasi-exponential increases of concentration for incompatible elements in the residual melt, which may then partition the ore elements into late stage fluids and ultimately deposit them in a suitable trap to form economic mineralisation. Fractionated granitoids can be recognised, for example, by high Rb content and high Rb/Sr, which are sensitive indicators of fractional crystallisation. Other causes of chemical variation within granitoid suites, such as restite unmixing, magma mingling or crustal contamination cannot produce the enormous concentration factors required to form an ore deposit. Magmatic differentiation by fractional crystallisation is characteristic of melt-rich magmas. Thus mineralisation is associated with granitoids that are derived from hot magmas (very hot magmas if the source region is relatively anhydrous) or with felsic granitoids that have undergone extensive fractionation after all restite has separated from the melt.

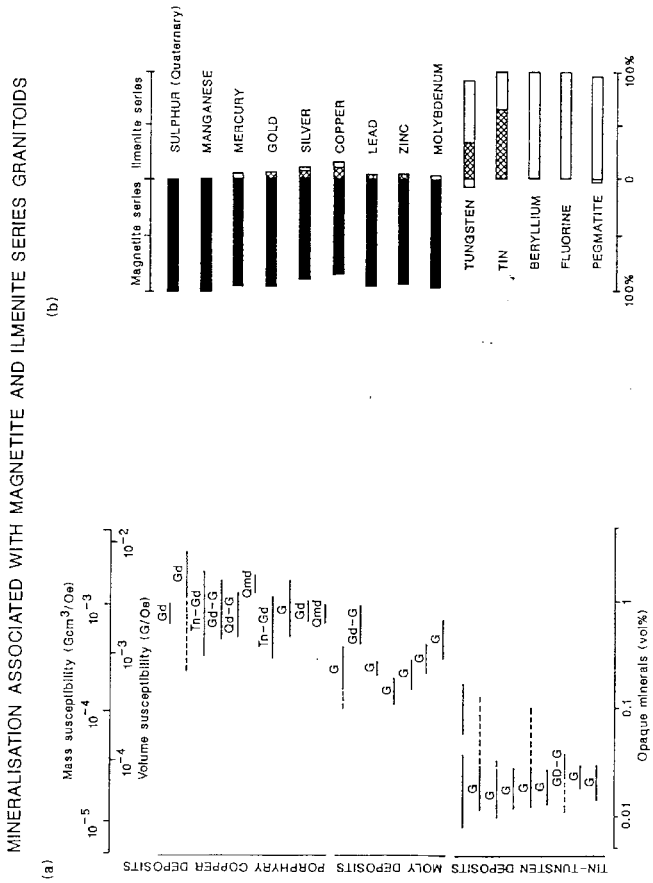

Figure 3.17. (a) Range of CGS mass and volume susceptibities and opaque mineral contents for granitoids associated with porphyry Cu, granitoid-related Mo deposits and granitoid-related Sn-W deposits (Gd = granodiorite, Tn = tonalite, G = granite, Qmd = quartz monzodiorite). (b) Proportions of mineral deposits, of a variety of commodities, that occur within magnetite-series and ilmenite-series granitoid belts. Hatched regions represent WFM magnetite-series granitoids. The mineral deposits are inferred to be genetically related to granitoids or to their associated volcanics. Pegmatite refers to stanniferous pegamtite deposits. SI volume susceptibility = CGS volume susceptibility (G/Oe) × 4π; mass susceptibility = volume susceptibility/density (after Ishihara, 1981).

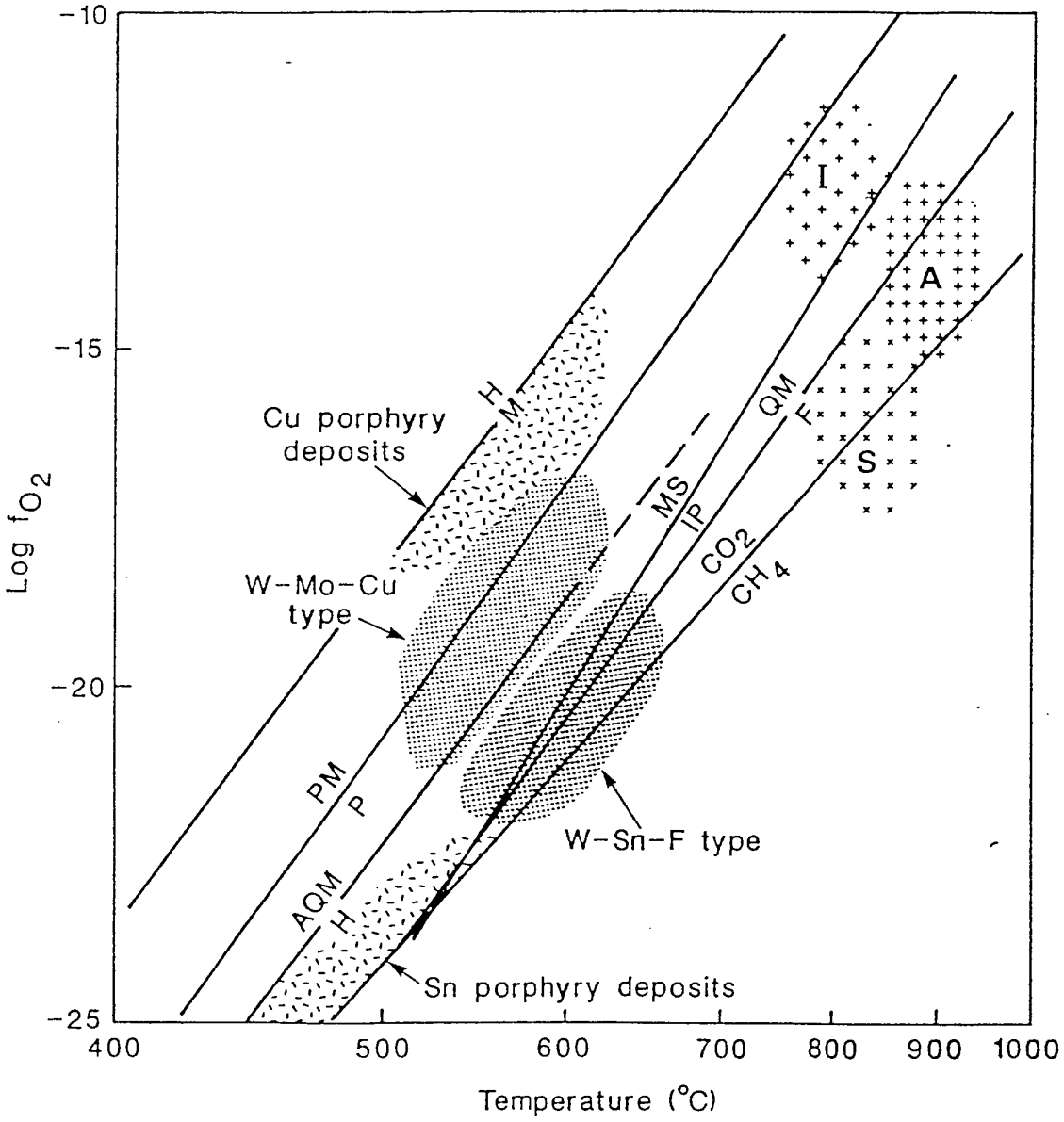

Figure 3.18. Oxygen fugacity versus temperature fields for typical I-, S- and A-type granitoids and for porphyry Cu, W-Mo-Cu skarn, W-Sn-F skarn and porphyry Sn mineralisation, together with a number of standard oxygen fugacity buffers (after Kwak and White, 1982). Mineral and fluid oxygen fugacity buffers that may be important controls on the magnetic mineralogy of the igneous intrusions and their associated mineralisation include (CO_2-CH_4; PMP = pyrite-magnetite-pyrrhotite; AQMH = andradite-quartz-magnetite-hedenbergite; MSIP = magnetite-sphene-ilmenite-pyroxene) as well as the FMQ and HM buffers.

The Tuolumne intrusion, California, represents a classic zoned pluton that grades from quartz diorite at the margin through progressively more felsic hornblende- and biotite-bearing granodiorite phases, to a core of biotite monzogranite porphyry (Bateman and Chappell, 1979). The normal zoning pattern, from mafic margin to felsic core, represents fractional crystallisation within the magma body as it cooled from the outside in. Figure 3.19 shows the compositional variations across the Tuolumne intrusion. Note the general slow decrease in opaque mineral (mainly magnetite) content from the margins towards the centre, with a pronounced dip in modal magnetite within the felsic core.

The expected magnetic signature of fractional crystallisation is gradation or zoning of susceptibility, where the most fractionated phase, which is most likely to be intimately associated with the mineralisation, has the lowest susceptibility. Figure 3.19 provides an example of this pattern. In the case of an oxidised comagmatic suite the susceptibility contrast between less evolved and more evolved phases should be large, whereas the effect will be subtle for a reduced paramagnetic suite. Large increases in radioelement concentrations and changes in radioelement ratios in the most fractionated rocks may also be detectable radiometrically. Airborne radiometric data can complement magnetic survey data in this environment, because the radiometric signal is best developed over the most felsic and fractionated intrusive phases, which are the phases that have the most subdued magnetic signature.

The Tuolumne pluton is unmineralised, probably because this intrusion, at least at the current level of exposure, was a sealed system during emplacement and cooling, precluding escape of late metal-bearing hydrothermal fluids, and because fractionation of the magma did not quite proceed to the stage required to concentrate metals into an ore-bearing fluid. However, a slightly more evolved variant of the Tuolumne intrusion, emplaced at a shallower depth or in a more favourable structural setting for tapping off hydrothermal fluids should be quite favourable for development of C-Au mineralisation.

3.5.4 Effects of Sulphur Saturation and Halogen Contents of Magmas

Wyborn and Sun (1994) suggested that most magma types are generally sulphur-saturated and are unlikely to produce gold or copper-rich fluids after fractional crystallisation. Au and Cu partition strongly to sulphide phases and sulphur saturation leads to precipitation of sulphides and early removal of these metals from the melt. For development of a magmatic Cu-Au deposit, the magma must remain sulphur-undersaturated throughout most or all of its magmatic evolution. Oxygen fugacity has a large effect on sulphur saturation. Under oxidising conditions sulphur becomes more soluble in the magma, dissolving as an anhydrite component. Thus oxidised magmas are more likely to be sulphur-undersaturated and are more likely to generate Cu-Au mineralisation.

The most favourable magma source for formation of high-gold sulphur-undersaturated magmas is lithospheric mantle that has already been depleted in sulphur by removal of sulphur-saturated basaltic melt, leaving behind small amounts of sulphide enriched in Cu, Au and other precious metals. If this refractory mantle is metasomatised, its liquidus temperature is lowered and it can subsequently undergo partial melting more readily, in appropriate

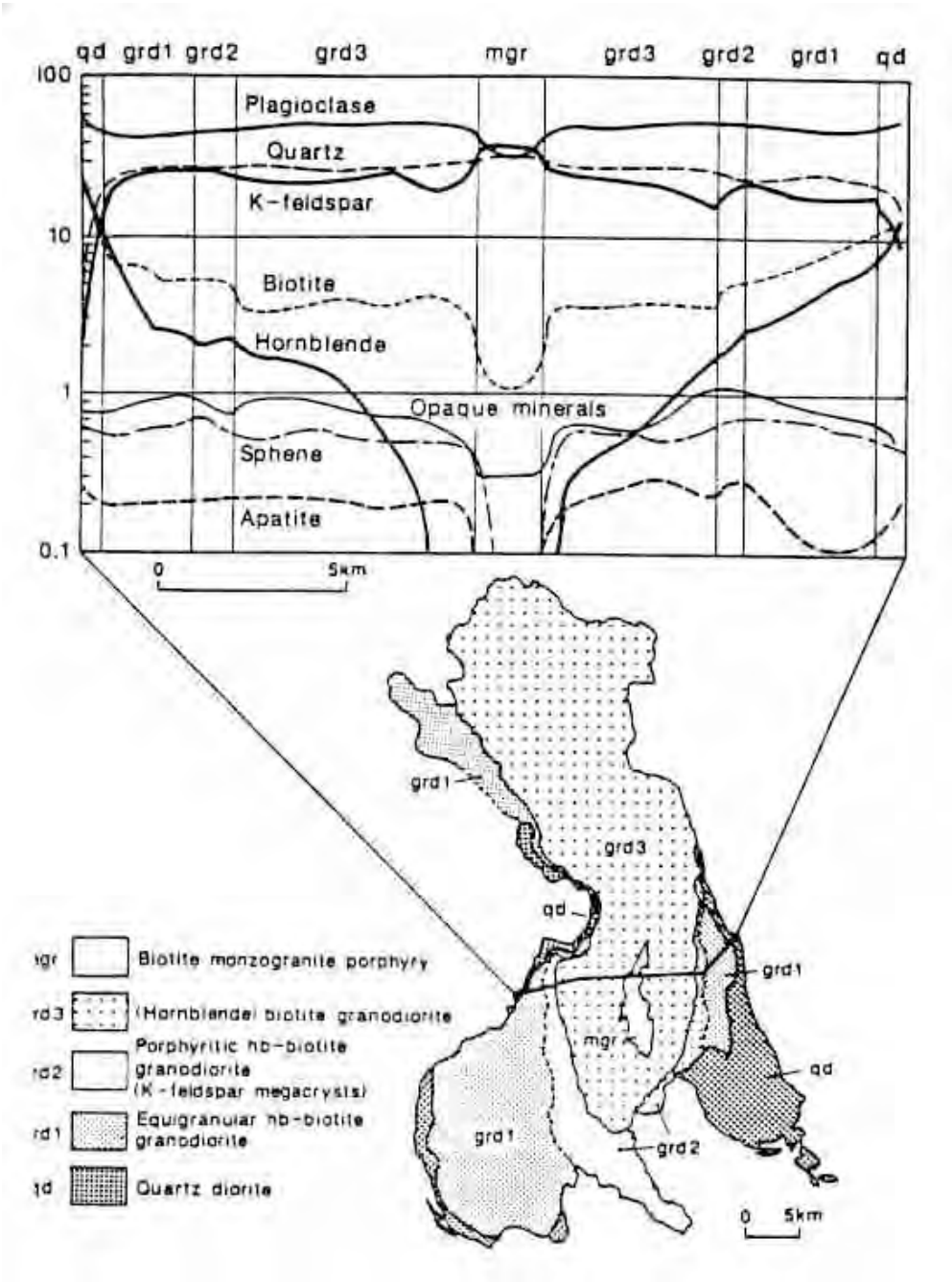

Figure 3.19. Compositional variations across the oxidised I-type Tuolumne intrusion, California, which shows a classic normal zonation from relatively mafic margin to felsic core, produced by fractional crystallisation (after Bateman and Chappell, 1979). Modal amounts of major, varietal and accessory minerals are plotted as a function of position along the profile indicated, which passes through all mapped phases of the pluton. Magnetite is the dominant opaque mineral.

tectonic conditions. The magmas generated often have shoshonitic affinities and have characteristics that are favourable for generation of magmatic-hydrothermal mineralisation. Less potassic magmas (i.e. those within the normal K-SiO_2 field for calc-alkaline magmas) that are derived from less metasomatised mantle can also give rise to large Cu-Au deposits, provided the mantle source is sulphur-undersaturated. Relatively low water and sulphur contents of these mantle-derived magmas produce rather inconspicuous alteration halos with restricted potassic zones and little iron sulphide. However, the oxidised nature of the magmas and high K^+, which boosts Fe^{3+} content, encourages formation of both magmatic and hydrothermal magnetite.

Halogens are important complexing agents for metals in hydrothermal fluids and Cl and F contents of magmas influence development of intrusive-related mineralisation. Cl decreases and F increases with fractional crystallisation in both I- and S-type granitoids (Blevin and Chappell, 1992). Cl contents of I-type granitoids are higher than for S-types. When a hydrothermal fluid exsolves from a silicate melt Cl partitions strongly to the aqueous phase, accompanied by chloride-complexed metals such as Fe, Mn, Cu, Mo, Pb, Sn and S. However, if a sulphur-enriched magmatic vapour phase forms, sulphide-complexed Cu and Au preferentially partition into the low viscosity vapour, which can travel considerable distances before deposition, whereas Fe, Mn, Pb and Zn preferentially partition into the brine and tend to be deposited closer to the intrusion from which they emanate.

3.5.5 Effects of Hydrothermal Alteration

Studemeister (1983) pointed out that the redox state of iron in rocks is a useful indicator of hydrothermal alteration. Large volumes of fluid or high concentrations of exotic reactants, such as hydrogen or oxygen, are required to shift Fe^{3+}/Fe^{2+} ratios. When reactions associated with large water/rock ratios occur, the change in redox state of the rocks produces large changes in magnetic properties due to creation or destruction of ferromagnetic minerals.

Criss and Champion (1984) studied the southern Idaho batholith. They showed that intense hydrothermal alteration around Tertiary plutons generally reduced the susceptibility of magnetite-series Mesozoic tonalites and granodiorites over substantial areas. However, hydrothermal alteration with a lower water/rock ratio locally produced secondary magnetite within ilmenite-series granitoids, enhancing their susceptibility.

Hollister (1975) distinguished between the Lowell and Guilbert (1970) quartz monzonite model of porphyry copper deposits and a diorite model. The Lowell-Guilbert model incorporates a core potassic zone, surrounded successively by phyllic, argillic and propylitic zones arranged in concentric but incomplete shells. This model is typically most applicable to calc-alkaline granodiorite-quartz monzonite porphyries (often associated with quartz diorite intrusions) with copper and molybdenum mineralisation, but negligible gold. In the diorite model the phyllic and argillic zones are absent and the propylitic zone adjoins the core potassic zone. Sulphides are less developed in the diorite model and lower pyrite contents in the altered host rocks allow some of their magnetite to survive alteration. The diorite model is applicable usually to syenite-monzonite porphyries associated with diorites and often contain gold, as well as copper, but no economic molybdenum mineralisation.

Phyllic alteration, argillic alteration and intense propylitic alteration associated with porphyry intrusions tend to destroy magnetite within the intrusion and in surrounding rocks. Weak to moderate, but pervasive, propylitic alteration may leave most of the magnetite in host rocks relatively unaffected. On the other hand, the potassic alteration zone associated with oxidised, magnetic felsic intrusions is often magnetite-rich. This is commonly observed for Au-rich porphyry copper systems (Sillitoe, 1979). It is evident from the above descriptions of the Lowell-Guilbert and Hollister's diorite models that the magnetic signatures of the two types of system should differ substantially. Clark *et al*. (1992a; 1992b) presented a theoretical magnetic signature of an idealised gold-rich porphyry copper deposit, based on the Sillitoe (1979) model and magnetic petrological concepts.

Early potassic (biotite-rich) alteration around the gold-mineralised Mount Leyshon Complex (Queensland), which is comprised of intrusive breccias and trachytic to rhyolitic porphyry plugs and dykes, produced abundant magnetite in metasedimentary and doleritic host rocks that adjoin the southern half of the Mount Leyshon Complex. That alteration is therefore largely responsible for the Mount Leyshon magnetic anomaly (Sexton *et al*., 1995). However, the equivalent alteration within felsic, iron-poor, granitic host rocks, around the northern portion of the complex, produces K-feldspar alteration with little or no secondary magnetite. Thus the Mount Leyshon magnetic anomaly is centred over the southern portion of the complex and its adjoining metasomatised aureole, rather than being symmetrically distributed around the complex.

In most porphyry systems both primary magmatic magnetite and hydrothermal magnetite are generally in the multidomain size range. Multidomain magnetite boosts susceptibility but is not an efficient or stable carrier of remanent magnetisation. Thus most of the magnetic signature of such porphyry systems is attributable to induced magnetisation, perhaps slightly enhanced by viscous remanence. However alteration of certain country rocks can produce substantial quantities of fine-grained magnetite that is capable of carrying intense and stable remanence.

The magnetic anomaly at Mount Leyshon is a pronounced low that arises from reversed remanent magnetisation ($Q >> 1$) of the biotite-magnetite altered metasediments and dolerites. Magnetite-bearing skarns with reversed remanence are also responsible for negative anomalies at the Red Dome Au deposit in NE Queensland (Collins, 1987). Monoclinic pyrrhotite may also carry intense remanence and produce large magnetic anomalies. Therefore pyrrhotite skarns may produce strong magnetic anomalies that are dominated by remanent magnetisation.

Magnetite-rich alteration zones around calc-alkaline porphyry copper deposits have been extensively discussed by Clark and Arancibia (1995). These authors argue that magnetite-rich vein systems in and around some porphyry systems are often early (pre-mineralisation) and are distinct from magnetite-biotite potassic alteration that is associated with sulphides and Cu-Au mineralisation. The magnetite ± amphibole ± plagioclase alteration, with very little sulphide, represents the initial stage in the evolution of a subclan of porphyry copper deposits. Deposition of this assemblage is favoured by host rocks of mafic-intermediate composition.

Host rocks influence deposition of magnetite around these systems, but iron metasomatism effected by magmatic conditions is also demonstrably important. The early strongly magnetic alteration appears to be associated with strongly oxidised intrusions that contain magnetite + sphene rather than the less oxidised assemblage magnetite + ilmenite.

Wall and Gow (1996) recognise a magnetite-rich Cu-Au class and a haematite-rich Cu-Au (U, REE) class of deposits associated with Proterozoic felsic plutons. Magnetite precipitation may be an important chemical control on sulphide precipitation in granitoid roof zones. The haematite association overprints the magnetite-rich bodies and results from highly oxidised lower temperature fluids with major meteoric component. La Candelaria-type magnetite mineralisation in Chile and Peru has some similarities and may be related to Mesozoic granitoids. The granitoids associated with these types of mineralisation are oxidised, high temperature, magnetite-series plutons.

3.5.6 Influence of Country Rocks

The nature of the country rock is crucial in the case of magmatic-hydrothermal skarn deposits, which develop in carbonate rocks that have been metamorphosed and metasomatised by the mineralising intrusion. In most cases emplacement of the intrusion into non-carbonate rocks would not have resulted in economic mineralisation. The review of Einaudi *et al*. (1981) contains much useful information relevant to magnetic petrology of skarn deposits. Magnetite contents of magnesian skarns developed in dolomite are generally higher than those of calcic skarns developed in limestone, because Fe-rich calc-silicates are not stable in a high-Mg system. However both island arc-type calcic skarns (associated with gabbros and diorites in volcano-sedimentary sequences) and Cordilleran-type magnesian skarns (associated with quartz monzonites or granodiorites intruding dolomites) have been mined for magnetite. Such deposits are evidently associated with very large magnetic anomalies.

Cu skarns (mostly associated with epizonal quartz monzonite and granodiorite stocks in continental settings) are associated with oxidised assemblages, including magnetite + haematite, with the less common magnesian skarns exhibiting higher magnetite and lower sulphide contents than calcic skarns. Tungsten-bearing skarns (associated with mesozonal calc-alkaline quartz monzonite to granodiorite intrusions) have a more reduced calc-silicate and opaque mineralogy than Cu-skarns, but typically contain minor magnetite and/or pyrrhotite and would therefore be expected to exhibit a relatively weak, but nevertheless detectable, magnetic signature in most cases. Calcic Zn-Pb skarn deposits associated with granodioritic to granitic magmatism and Mo skarns associated with felsic granites appear to contain relatively little magnetite. Sn skarns are associated with reduced ilmenite-series granites and have relatively low sulphide contents. The skarns themselves contain magnetite ± pyrrhotite and exhibit a substantially larger susceptibility than the paramagnetic granite and unaltered host rocks. Massive sulphide replacement tin orebodies in dolomite (e.g. Renison and Cleveland deposits, Tasmania) are rich in monoclinic pyrrhotite and have high susceptibilities, with substantial remanent magnetisation. This type of orebody may represent the low temperature distal analogue of magnesian Sn skarns.

Webster (1984) analysed magnetic patterns over a number of granitoids associated with tin mineralisation in the Lachlan Fold Belt and contrasted these with unmineralised and Cu-Mo-W mineralised granitoids. The characteristic magnetic signature of granitoid-associated tin mineralisation is: a granitoid with low magnetic relief, surrounded by a more magnetic aureole, with significant magnetic anomalies associated with the mineralisation.

Wyborn and Heinrich (1993) and Wyborn and Stuart-Smith (1993) have suggested that particular host rocks favour deposition of Au mineralisation from oxidised fluids that emanate from felsic granitoids and move up to 5 km from the granitoid contact. Graphite-, sulphide- and magnetite-bearing lithologies are capable of reducing the fluids and depositing Au and Cu, whereas Pb and Zn are preferentially deposited in carbonate rocks. Au-only mineralisation will preferentially be deposited within graphite-bearing but magnetite- and sulphide-poor rocks, whereas magnetite and or iron sulphide-rich rocks tend to precipitate Cu and Au together. These relationships appear to have been observed in the eastern Mount Isa Inlier and the Pine Creek Inlier. Thus a rock unit that is strongly magnetic, indicative of high magnetite content, may be a favourable site for deposition of Au-Cu mineralisation sourced from a nearby granitoid.

3.6 Conclusions

Relationships between magnetic properties of granitoids and their mineralogy, chemical composition, geological setting and history are complex. However, clear patterns can be discerned and much progress has been made in recent years in understanding the geological factors that control their magnetic properties. Although magnetic properties are not predictable with any reliability from first-order rock names, a more detailed classification of granitoids does correlate well with magnetic properties, because there are many correlations between magnetic properties of igneous intrusions and their geological, chemical and mineralogical characteristics. These patterns arise directly in some cases, e.g. the correlation between oxidation ratio and magnetite content, but in many cases they are indirect.

One example of an indirect relationship is the strong association between paramagnetic ilmenite-series granitoids and S-type granitoids. The magnetite-poor nature of most S-type granitoids arises from their reduced character, which reflects incorporation of crustal carbon. Carbon content is an incidental, rather than a defining, characteristic of an S-type granitoid. Data on geological, geochemical and mineralogical associations with magnetite in granitoids are summarised in Tables 3.1-3.4.

Of particular importance to exploration is the clear, albeit indirect, relationships between a number of important types of intrusive-related mineralisation and the magnetic properties of the associated granitoids and their alteration systems (Table 3.5). A more detailed discussion of magmatic and hydrothermal evolution of porphyry systems and exploration models for porphyry-related mineralisation follows in section 3.

There is now sufficient knowledge to develop and test improved magnetic exploration models for intrusive-related mineralisation. Clark *et al*. (1992b) showed some examples of basic

models. This topic is developed further in sections 7-8. Although such models are necessarily simplistic, because they are based on petrophysical data and magnetic petrological principles they should improve the utility of magnetic surveys in exploration.

Table 3.1. Geological Characteristics of Ferromagnetic and Paramagnetic Igneous Intrusions

FERROMAGNETIC INTRUSIONS	PARAMAGNETIC INTRUSIONS
Source Rock	
Mantle	Metasediments (particularly pelites)
Mafic crustal underplate	Reduced igneous rocks
Oxidised intermediate-felsic igneous rocks	
Lithology	
Gabbro>diorite>tonalite>granodiorite>granite	Predominantly granite and granodiorite
Hornblende ± biotite granitoids and biotite granites with high Mg, low Al biotite	Muscovite and two mica granitoids, most leucogranites, biotite-rich granitoids
Pyroxene ± hornblende granitoids	Cordierite, corundum or aluminosilicate-bearing granitoids
Many monzonites, quartz monzonites, syenites, quartz syenites and miaskitic nepheline syenites	Peralkaline granites, syenites or nepheline syenites
Most alkali gabbros, essexites, ijolites etc.	
Ferrogabbros, ferrodiorites and granophyres, within upper levels of layered mafic complexes	Lower gabbros in layered mafic complexes
Emplacement depth	
Predominantly epizonal, particularly subvolcanic, some mesozonal and catazonal	Predominantly mesozonal or catazonal, some epizonal
Associated rocks	
Associated volcanics common	Associated volcanics uncommon
Gabbro-diorite-trondhjemite associations	Syenogranite-monzongranite-granodiorite associations
(Gabbro)-diorite-granodiorite-monzogranite associations	Quartz syenite-syenogranite associations
Diorite-monzonite-quartz monzonite-monzogranite associations	

Syenite-alkali syenite-alkali granite associations	

Table 3.2. Tectonic Settings of Ferromagnetic and Paramagnetic Igneous Intrusions

FERROMAGNETIC INTRUSIONS	PARAMAGNETIC INTRUSIONS
Andinotype (subduction of oceanic plate beneath continental margin, generating Cordilleran I-type batholiths)	Hercynotype (continental collision, e.g. Himalayan and Hercynian leucogranites)
Island arc plagiogranites, gabbros and quartz diorites	Encratonic ductile shear belts with thickened continental crust
Alpinotype (tectonically emplaced serpentinised peridotites, gabbros and plagiogranites)	Late tectonic/post tectonic catazonal migmatites and mesozonal granitoids associated with regional metamorphism
Caledonian-type post-closure uplift and tensional regimes with major faulting	Compressional regimes
Anorogenic, rifting-associated moderately evolved granitoids	Anorogenic, rifting-associated highly evolved granitoids

Table 3.3. Chemical Characteristics of Ferromagnetic and Paramagnetic Igneous Intrusions

FERROMAGNETIC INTRUSIONS	PARAMAGNETIC INTRUSIONS
Predominantly metaluminous, but also weakly peraluminous or weakly peralkaline granitoids ($0.9 \leq A/NK < A/CNK \leq 1.1$)	Strongly peraluminous ($A/CNK > 1.1$) and strongly peralkaline ($A/NK < 0.9$) granitoids, some metaluminous granitoids
Moderate-high ferric iron ($Fe_2O_3 > 0.8$ wt %, typically 1-3 wt%) and moderate-high total iron (> 2 wt% FeO^T)	Low ferric iron ($Fe_2O_3 < 0.8$ wt %) *or* very low total iron (< 1 wt % FeO^T)
Moderate oxidation ratio (mean Fe^{3+}/Fe^{2+} ~ 0.6 at 60% SiO_2, Fe^{3+}/Fe^{2+} ~ 0.9 at 75% SiO_2, i.e. molar $Fe_2O_3/(FeO+ Fe_2O_3)$ ~ 0.2-0.3)	Low oxidation ratio (mean Fe^{3+}/Fe^{2+} ~ 0.1 at 60% SiO_2, Fe^{3+}/Fe^{2+} ~ 0.4 at 75% SiO_2, molar $Fe_2O_3/(FeO+ Fe_2O_3)$ = 0.05.-0.2) *or* very high oxidation ratio
Normative (diopside ± olivine ± acmite) plus > 1 wt % normative magnetite ± haematite	Normative corundum *or* normative acmite +sodium metasilicate
Relatively anhydrous	Relatively hydrous

A/NK = atomic Al/(Na + K); A/CNK = atomic Al/(Ca + Na + K)

Table 3.4. Mineralogical Characteristics of Ferromagnetic and Paramagnetic Igneous Intrusions

FERROMAGNETIC INTRUSIONS	PARAMAGNETIC INTRUSIONS
Generally higher colour index	Generally lower colour index
Biotite ± hornblende in felsic calc-alkaline granitoids; hornblende ± pyroxene ± olivine (except fayalite) in more mafic varieties	Biotite + muscovite, cordierite, garnet or aluminosilicate in calc-alkaline granitoids.
Fe^{3+} and Mg-rich biotite and hornblende; biotite colour is brown, black or olive green	Fe^{2+} and Al-rich (annite/siderophyllite-rich) biotite, often with "foxy red" colour; occasionally Fe^{2+}-rich hornblende or fayalite
Sphene (> 0.1 vol %) ± hemoilmenite (8 mole % to 20 mole % Fe_2O_3) *or* Mn-rich ilmenite (up to 30 mole % $MnTiO_3$) ± epidote ± allanite ± pyrite as accessories	"Reduced" ilmenite (< 8 mole % Fe_2O_3, usually Mn-poor) ± pyrrhotite (predominantly hex po) ± spinel ± graphite as accessories, primary sphene absent
White plagioclase + pink K-feldspar	White plagioclase + white K-feldspar *or* sometimes brick red K-feldspar; sometimes green plagioclase + pink K-feldspar
Intermediate to Fe-rich olivine and pyroxenes + intermediate to sodic plagioclase ± hornblende ± apatite in upper ± middle levels of tholeiitic layered intrusions	Mg-rich olivine and pyroxenes, calcic plagioclase ± chromite in lower to middle zones of tholeiitic layered intrusions
Zoned plagioclase (> 60 %) + quartz + biotite and/or hornblende in M-type oceanic/ ophiolitic plagiogranites	
Nepheline + alkali feldspar + plagioclase + calcic pyroxene + hastingsite + biotite in silica-undersaturated metaluminous (miaskitic) rocks	Quartz + alkali feldspar + sodic pyroxene and/ or sodic amphibole ± aenigmatite ± astrophyllite ± biotite in oversaturated peralkaline (ekeritic) rocks
Nepheline + alkali feldspar + sodic pyroxene and amphibole ± biotite without aenigmatite or astrophyllite in mildly peralkaline undersaturated rocks	Nepheline + sodic pyroxene + aenigmatite ± astrophyllite in silica-undersaturated peralkaline (agpaitic) rocks

Table 3.5. Magnetic Petrophysical Classes of Intrusive Rocks and Alteration Zones Associated with Mineralisation

TYPE OF MINERALISATION	MAGNETIC PETROPHYSICAL CLASSIFICATION
Au-rich (> 0.4 g/t) porphyry Cu within MFM mafic-intermediate igneous host rocks	SFM granitoid (M- or I-type) + SFM potassic alteration zone ± PM phyllic zone + WFM to MFM propylitic zone
Porphyry Cu within MFM mafic-intermediate igneous host rocks	MFM to SFM granitoid ± SFM potassic alteration zone + PM phyllic zone + PM argillic zone + WFM to MFM propylitic zone
Porphyry Mo	WFM granitoid directly associated with mineralisation, zoned to MFM less fractionated granitoid phase
Au-scheelite-quartz exogranitic plutonic vein (scheelite contains Mo)	WFM to MFM granitoid
W-Mo-Cu skarn	MFM to SFM granitoid + SFM skarn
W-Cu-Sn veins. Tungsten mineral is wolframite or Mo-free scheelite	PM granitoid
W-Sn-F skarn	PM granitoid + WFM to SFM skarn
Sn-W greisen	PM granitoid
Cr, PGEs, Ni-Cu in lower levels of layered mafic complex	PM to WFM gabbros overlying PM unserpentinised ultramafics *or*, more commonly, MFM to SFM serpentinised ultramafics
Ti, V in upper levels of layered mafic complex	SFM gabbros
Sn-W, Be, Li and U associated with peraluminous two-mica granites	PM granitoid
Nb-Ta, REE mineralisation associated with peralkaline anorogenic ring complexes	PM granitoid ± MFM to SFM carbonatite

PM = paramagnetic; WFM = weakly ferromagnetic; MFM = moderately ferromagnetic; SFM = strongly ferromagnetic; VSFM = very strongly ferromagnetic (see text).

4. METHODS OF DETERMINING MAGNETIC PROPERTIES WITHIN MINERALISED SYSTEMS

4.1 Laboratory Measurement of Susceptibility and Remanence

Figure 4.1 illustrates the principles of laboratory and field instruments that measure magnetic susceptibility and remanence of rock samples. Susceptibility meters use alternating fields to discriminate the induced response to the applied field from the static fields produced by remanent magnetisation of the specimen. The sensitivity of such instruments increases with operating frequency, but the apparent susceptibility is affected by specimen conductivity at high frequencies. Fig.4.2 shows errors in magnetic susceptibility for conductive ore specimens measured in frequencies of 1kHz, 5 kHz and 10 kHz. The “true” susceptibility of the specimens was determined by measuring in the CSIRO low frequency (211 Hz) susceptibility transformer bridge. It can be seen that the errors are negligible for an operating frequency of 1 kHz, but are significant for the higher frequencies. Most commercial susceptibility meters operate at ~ 1 kHz, so their readings should be relatively unaffected by conductivity, except for extremely conductive samples.

Measurements of the magnetic properties of strongly magnetic samples are affected by self-demagnetisation. Therefore it is important to correct for self-demagnetisation when measuring the properties of magnetite-rich samples, for example. The effect on susceptibility is dependent on the geometry of the sample/measuring instrument system, not just the sample shape. The intrinsic susceptibility of the specimen is given by:

$$k = k'/(1 - N_1 k'), \quad (1)$$

and the intrinsic remanence is given by:

$$J = J'(1 + N_2 k), \quad (2)$$

Where k is the intrinsic susceptibility, k' is the apparent susceptibility as measured by the instrument, N_1 is the demagnetising factor for the susceptibility instrument/sample configuration, J is the true remanence, J' is the apparent remanence and N_2 is the demagnetising factor of the isolated specimen.

For standard palaeomagnetic specimens the SI demagnetising factor N_2 is 1/3.

$$\therefore J = J' (1+k/3), \quad (3)$$

where k is determined from (1). In a transformer bridge the SI demagnetising factor N_1 is approximately equal to the total residual gap between the specimen and the poles of the magnetic core, divided by the total gap length. Therefore, if the specimen fills the entire gap, the demagnetising factor is effectively zero (neglecting leakage flux) and if the specimen is a very thin disc the demagnetising factor approaches its maximum value of 1.

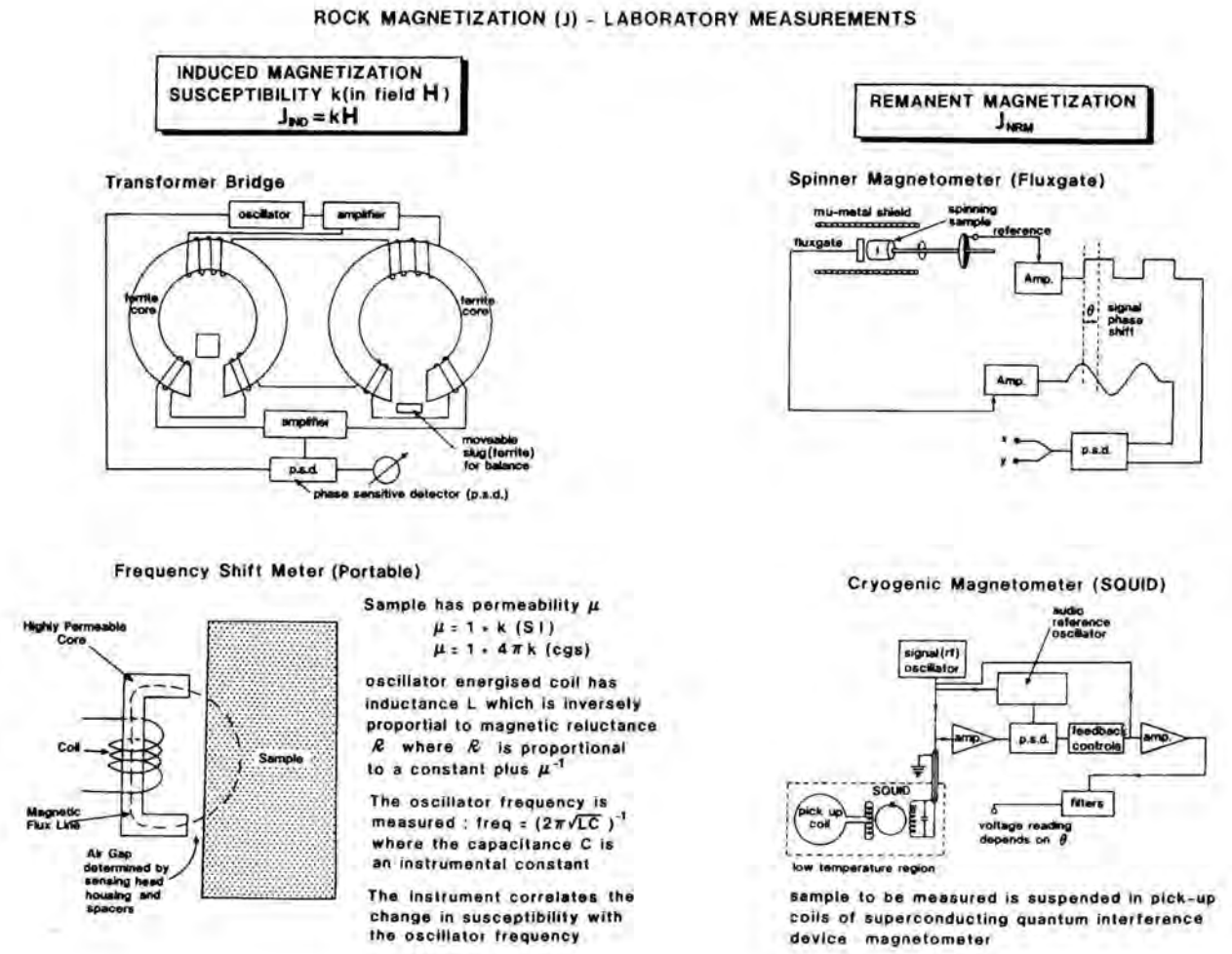

Fig.4.1. Principles of measurement of susceptibility and remanence of rock samples

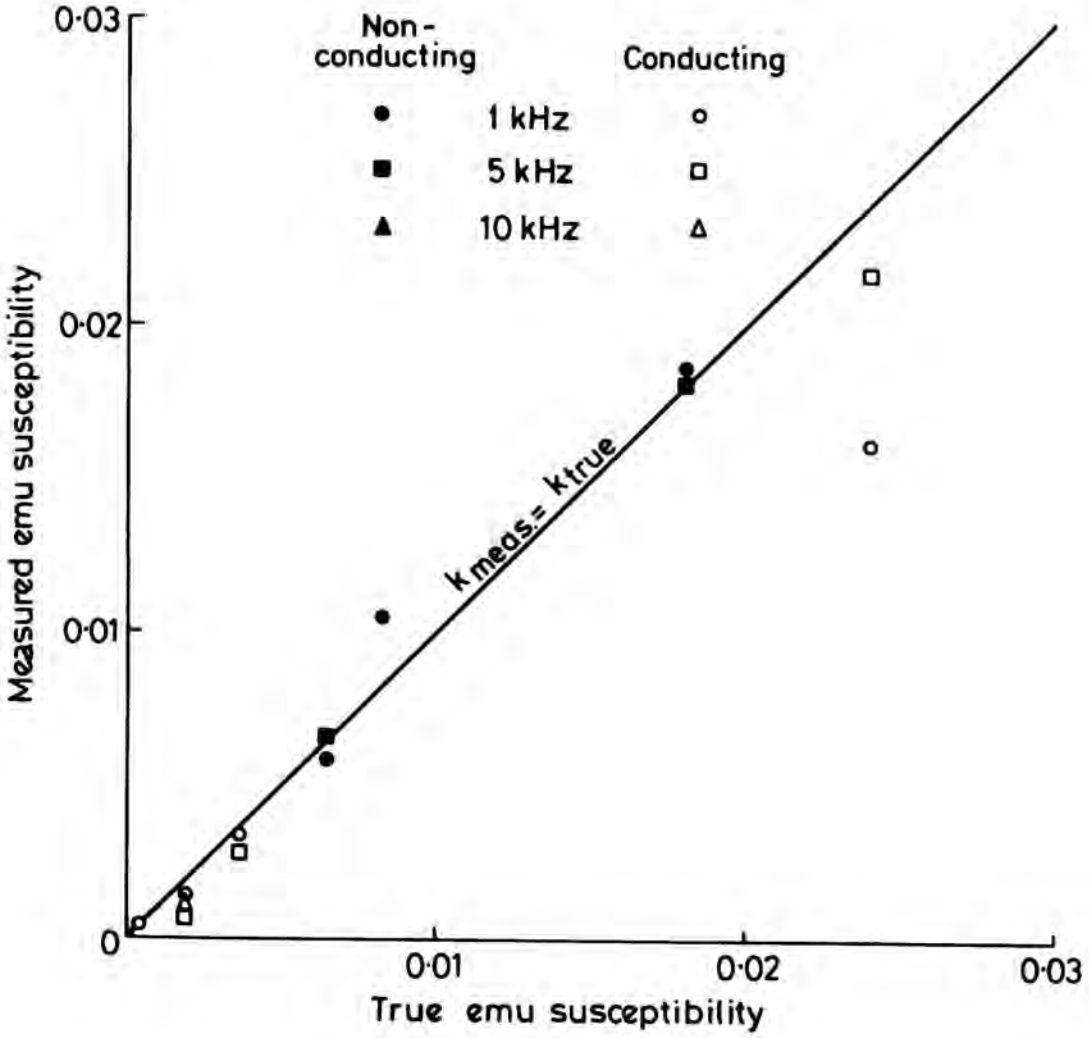

Fig.4.2. Effects of operating frequency on susceptibility measurement. Note the systematically lower apparent susceptibility for conductive massive sulphide specimens at high frquencies, compared to almost frequency-independent susceptibilities for non-conducting samples. Scatter in results also reflects some inhomogeneity of samples and different geometries of measuring instruments, requiring different sample shapes and sizes.

4.2 Field Measurement of Magnetic Properties

Hand-held susceptibility instruments that are used in the field are calibrated for large flat slabs of magnetic material (effectively a half-space). For this case the SI demagnetising factor is ½, irrespective of the operating principle of the instrument or the geometry of the flux lines. Assuming that the instrument reading has a linear calibration, the true susceptibility can be obtained from the meter reading as:

$$k = k'/(1 - k'/2) \text{ [hand-held meter; flat slab measurement].} \quad (4)$$

For measurements on drill core, split drill core, or small hand samples a geometric calibration factor also has to be taken into account.

Self-demagnetisation corrections are significant for susceptibilities greater than ~0.1 SI, corresponding to about 3 vol % magnetite, and are crucial for susceptibilities ≥ 0.5 SI, or more than ~13 vol % magnetite.

4.3 Determination of Properties from Magnetic Surveys

Figure 4.3 compares the principles of conventional magnetic surveys, which measure the static magnetic anomaly produced by a subsurface source over the survey area, and two types of unconventional survey that in principle can give more direct information on source properties. In conventional magnetic surveys the background field must be removed from the measured field in order to determine the anomalous field due to subsurface variations in magnetisation. Geomagnetic variations (time-varying fields) are a source of noise in this context.

The differential vector magnetometer or the combined vector magnetometer/gradiometer systems allow the direct determination of the direction of magnetisation, direction of remanence and the Koenigsberger ratio of the source of an individual anomaly, by using geomagnetic variations as a driving field to discriminate induced and remanent contributions to the anomaly (Clark et al., 1998). Although the current state of development of this technique restricts its application to very strong anomalies, future development of high-temperature SQUID-based magnetometer/gradiometer systems may allow its broader application.

Active source magnetics is technique that can potentially be applied to mapping subsurface magnetisation distributions using the inhomogeneous time-varying primary field of a loop or dipole source (e.g. a superconducting magnet) and a roving receiver. The inhomogeneity of the primary field provides a spatial resolution that overcomes much of the non-uniqueness of interpreted sources in conventional surveys and the time-varying field discriminates between induced and remanent contributions to the anomaly field. Given the rapid fall-off of the primary and secondary fields, this technique is only practicable for fairly shallow sources.

Determination of source properties from conventional magnetic surveys can be achieved in two main ways:

(i) modelling of magnetic anomalies,
(ii) indirect inference of magnetic properties from magnetic surveys.

Modelling of magnetic anomalies without independent geological information is afflicted with ambiguity. For example, the magnetisation direction of a dipping sheet cannot be uniquely determined from its anomaly, unless the dip is known. If the sheet also produces a well-defined gravity anomaly, however, the magnetisation direction can be determined by applying Poisson's theorem. For compact sources, the magnetic moment and direction of magnetisation can be modelled accurately. If the geometry of the source is known (e.g. defined by drilling or other geophysical methods) the magnetisation of the source can also be determined by modelling – most efficiently by inversion of the observed anomaly.

The magnetic moment and magnetisation direction of compact sources can also be determined from the observed anomaly directly by Fourier-based methods (Schmidt and Clark, 1998).

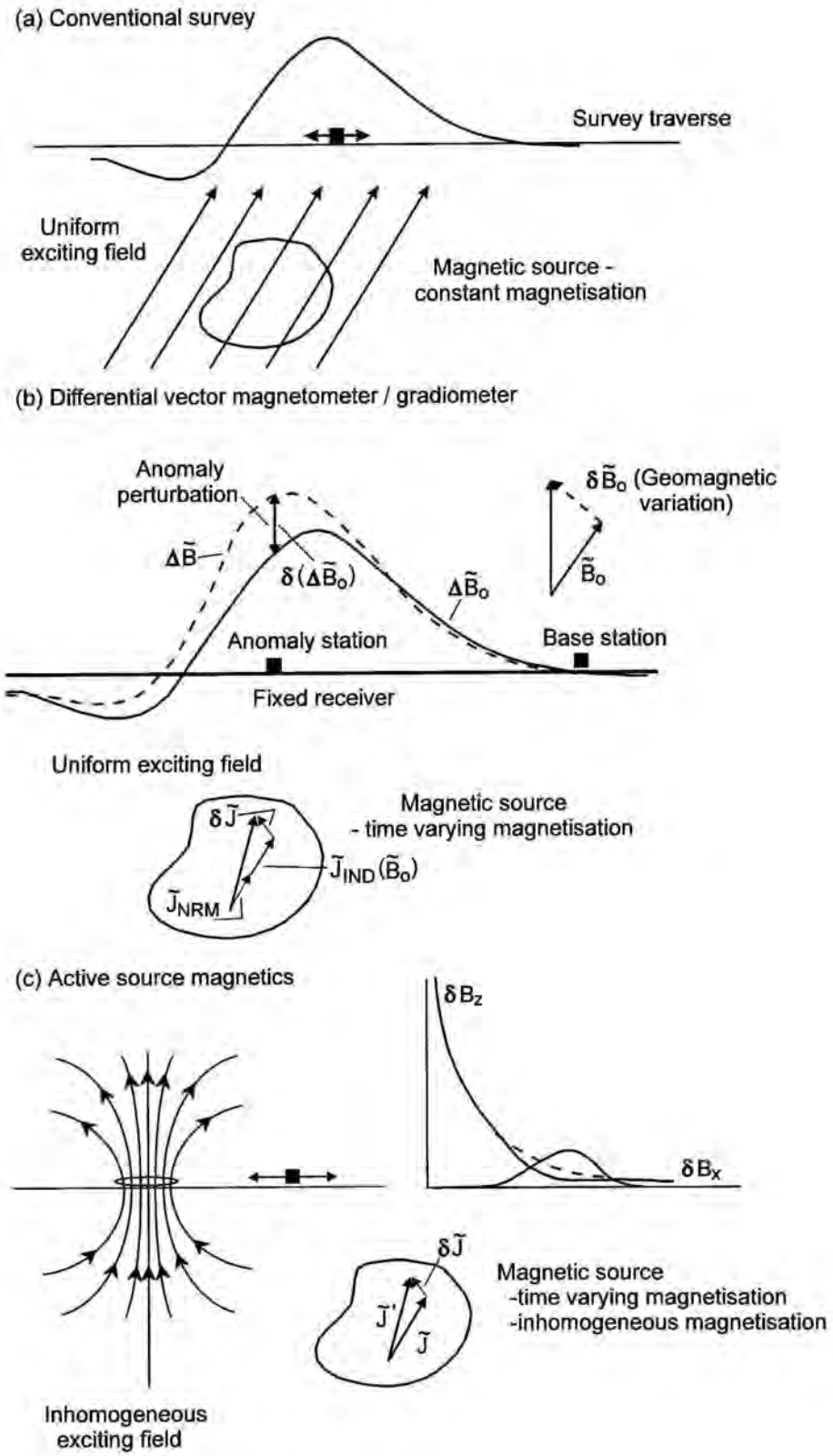

Fig.4.3. Comparison of conventional and unconventional magnetic surveys

4.6 Inference of Susceptibility and Remanent Intensity from Petrographic Information

Estimating Susceptibility from Modal Magnetite and Pyrrhotite

Section 2 gave formulae for susceptibility as a function of magnetite and monoclinic pyrrhotite contents. These relationships are plotted in Fig.4.4. An Excel spreadsheet that calculates susceptibility from magnetic mineral content (SUSCEPTIBILITY READY RECKONER.XLS) is supplied to sponsors.

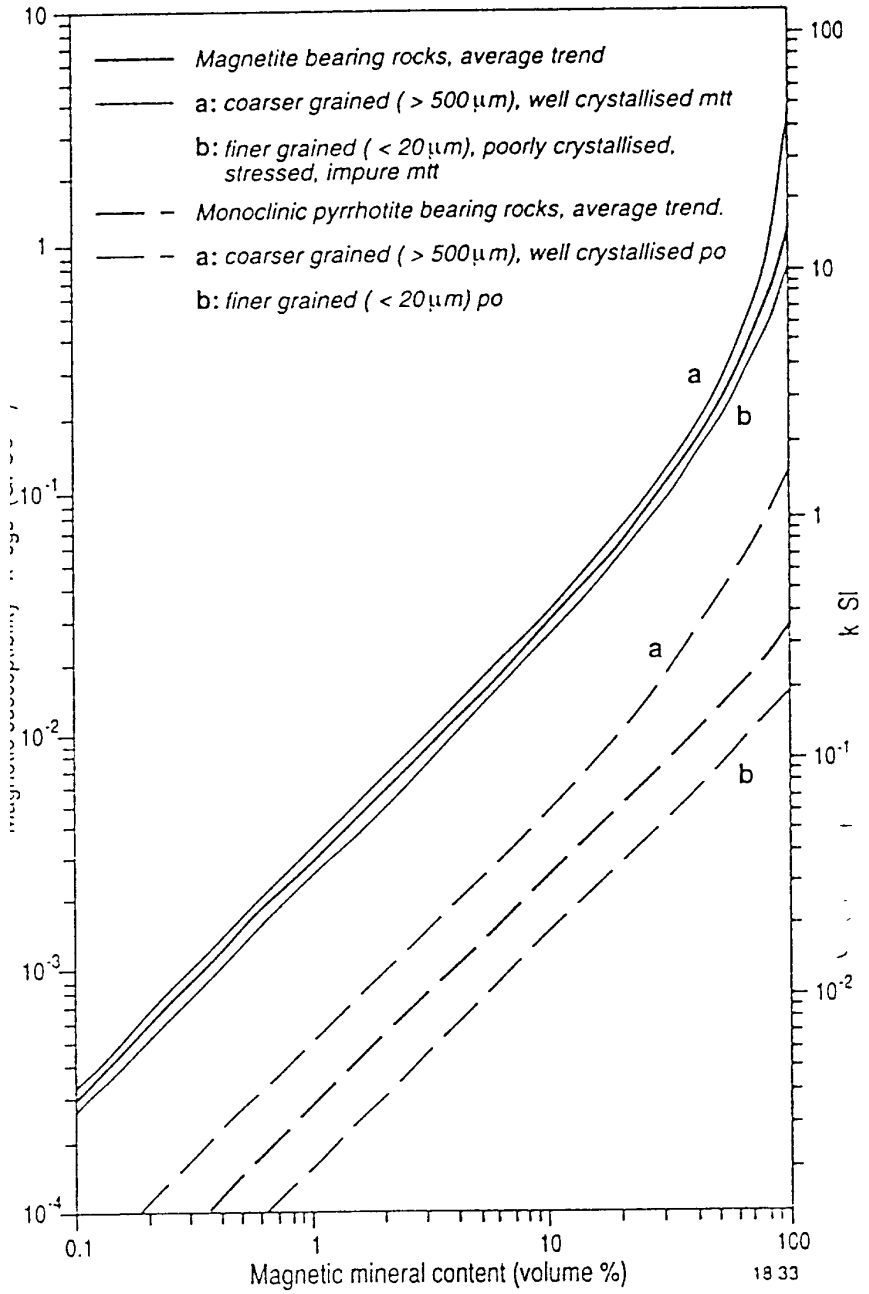

Fig.4.4. Magnetic susceptibility as a function of magnetite or monoclinic pyrrhotite content.

When is Remanence Important?

Koenisberger ratio Q reflects composition and microstructure of magnetic carriers. High Q and strong specific NRM intensity is associated with:

- Ultrafine (< 10 µm) (titano)magnetite and deuterically oxidised titanomagnetite with ilmenite lamellae
- Monoclinic pyrrhotite
- PSD-MD (> 15 µm) hematite *carrying thermoremanence*, particularly martite with relict magnetite and/or maghemite. Maximum TRM intensity is acquired by hematite grains that are 100 µm in size, or larger. Note that the remanence intensity – size relationship is opposite for magnetite and hematite
- Hemo-ilmenite (ferrian ilmenite with fine exsolution lamellae of titanohematite)

Figure 4.5 plots the remanence intensities for the common magnetic minerals, as a function of grain size and acquisition mechanism. Although this figure in its original form dates back to 1983, it has stood the test of time, with the exception of CRM carried by MD hematite. No experimental data have ever been published on the acquisition of chemical remanence by hydrothermally grown hematite. The estimate of CRM for MD hematite in Fig.4.5 was attained by applying theory developed for CRM of MD magnetite (Stacey and Banerjee, 1974), but this theory makes the assumption that the coercive force of the grains is smaller than the self-demagnetising field of the grain – an assumption that is inappropriate for hematite.

Figure 4.6 shows the Koenigsberger ratios for various types of magnetisation carried by common magnetic minerals, as a function of domain structure.

Recent work has confirmed the intense TRM carried by MD hematite and provided a theoretical basis for the quasi-saturation magnetisation acquired by this mineral when cooled from above the Curie temperature (680°C) in field strengths comparable to that of the geomagnetic field (Dunlop and Kletetschka, 2001). Figure 4.7 compares TRM acquisition curves for SD and MD hematite with those of SD and MD magnetite. Note that the TRM acquired by MD hematite in the Earth's field is over 50% of the saturation magnetisation and is much more intense than TRM of either SD hematite or MD magnetite.

Estimation of remanence intensities from petrographic information and geological history is more complex, and subject to much greater uncertainties, than estimation of susceptibilities. However, in principle the remanence intensity for a simple NRM (e.g. a thermoremanence of an igneous intrusion unaffected by subsequent metamorphism or metasomatism) can be estimated by multiplying the specific remanence intensities for each of the magnetic minerals in the rock by their volume proportions, normalising for the palaeofield intensity (if known). The palaeofield intensity reflects the palaeolatitude of the site, which can be estimated from palaeomagnetic data and the geomagnetic dipole moment at the time of remanence acquisition (see next section). Remanence is particularly strong when acquired at high latitudes at a time of geomagnetic dipole moment. The inclination dependence of the time-averaged field accounts for a factor of two between the poles and the equator. Thus the Koenigsberger ratio corresponding to a particular mineral and type of remanence can vary by a factor of up to four, if the terrane has moved far with respect to the pole since acquisition (Q is doubled for movement from the pole to the equator and halved for the opposite migration).

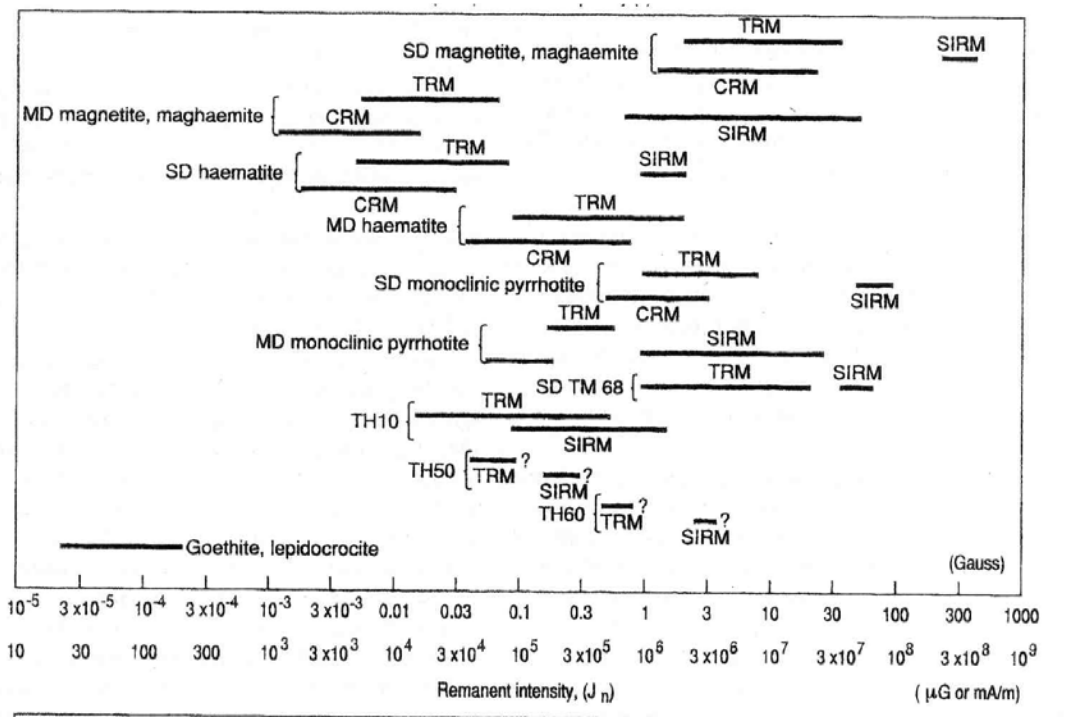

Fig.4.5. Remanence intensities for the common magnetic minerals, as a function of grain size and acquisition mechanism. Assumed field intensity is 0.5 Oe (50,000 nT).

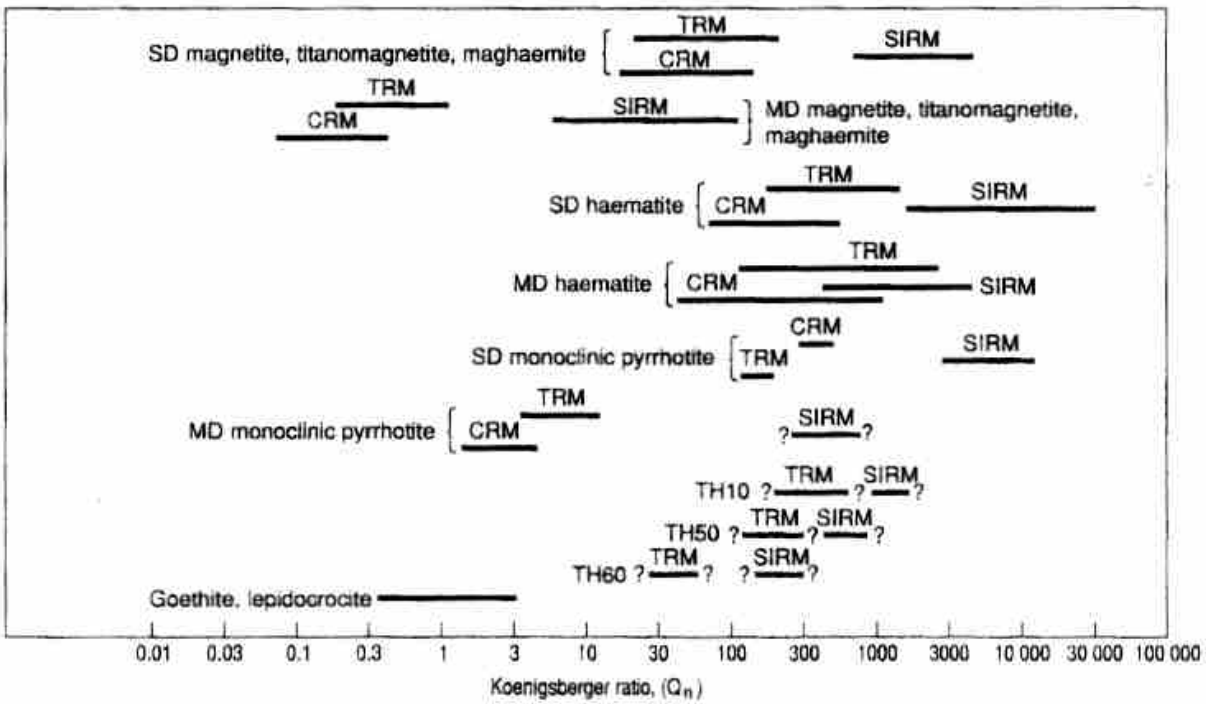

Fig.4.6. Koenigsberger ratios for the common magnetic minerals, as a function of grain size and acquisition mechanism.

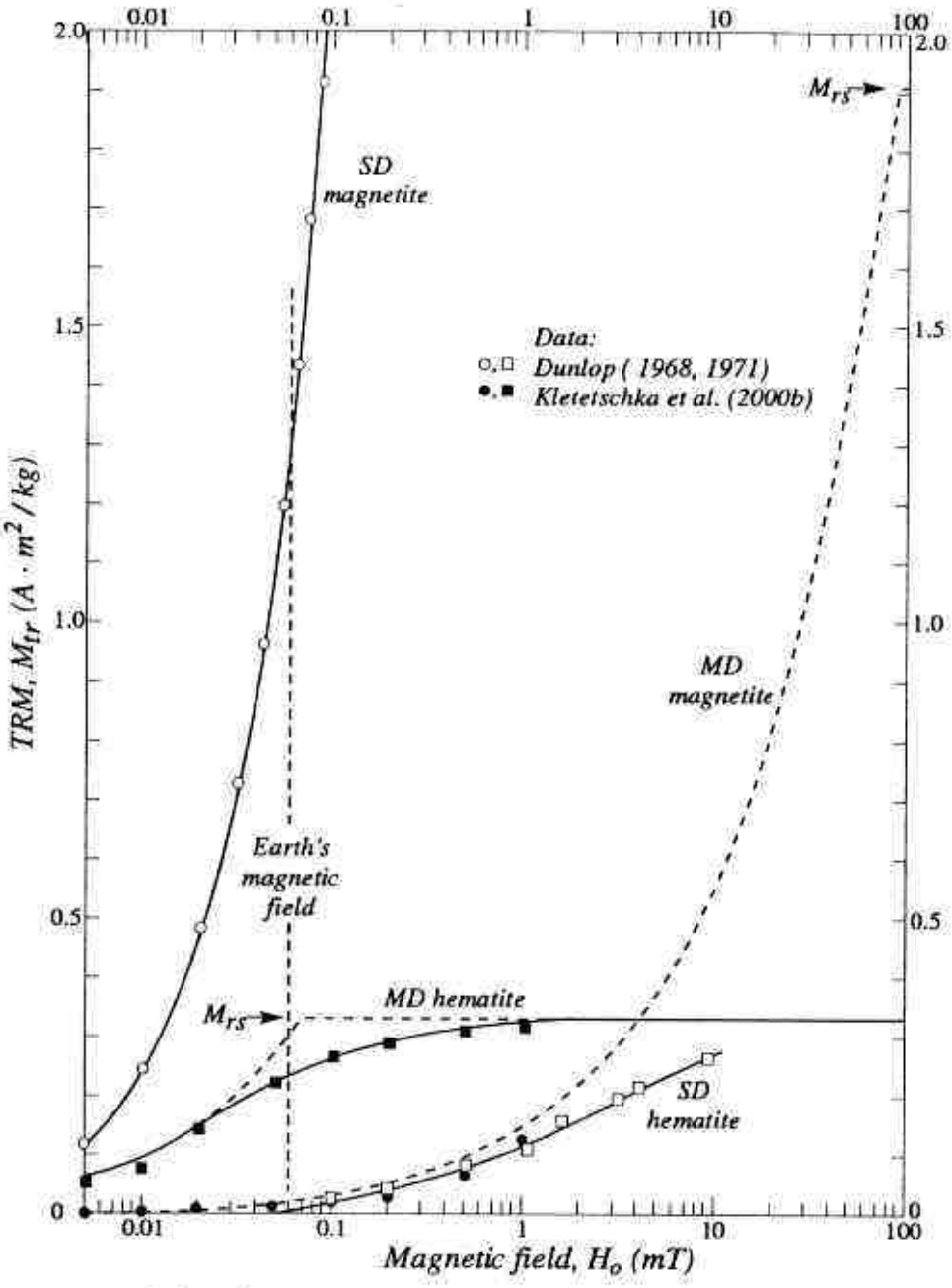

Experimental (points and solid curves) and theoretical (dashed curves) TRM values over an extended field range. Very different demagnetizing fields H_d cause hematite and magnetite to reach TRM saturation ($M_{tr} = M_{rs}$) in fields differing by 3 orders of magnitude.

Fig.4.7. TRM acquisition curves for SD magnetite, MD magnetite, SD hematite and MD hematite (Dunlop and Kletetschka, 2001).

4.7 Inferring Remanence Direction and Polarity from the Palaeomagnetic Database

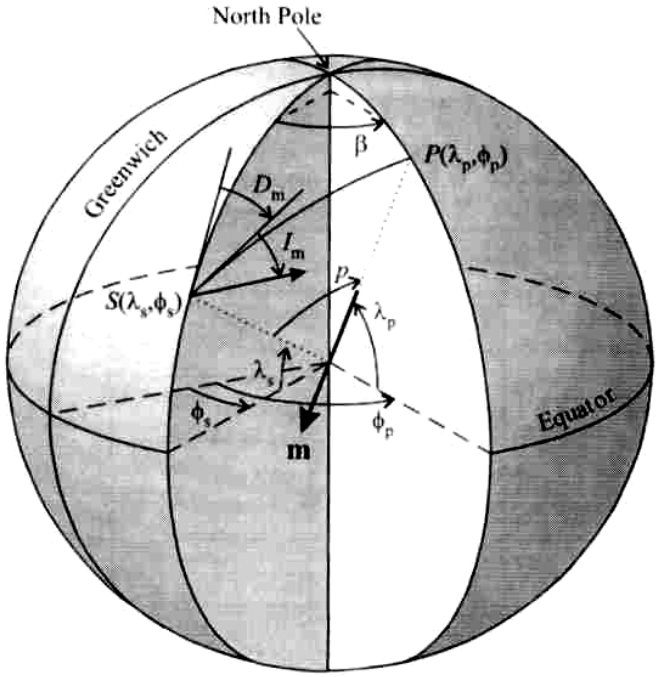

Relationship to calculate the position (λ_p, ϕ_p) of the paleomagnetic pole P relative to the sampling site S at (λ_s, ϕ_s) with mean magnetic direction (D_m, I_m).

Fig.4.8. Use of the axial geocentric dipole model to calculate palaeopole positions is an invertible process.

Determination of palaeomagnetic poles uses the axial geocentric dipole model to calculate palaeopole positions from measured palaeofield directions (Fig.4.8). Once palaeopole positions for various ages are established for a given terrane, this process can be inverted to predict the palaeofield direction for a specific locality from the corresponding palaeopole position. The sense of the palaeofield direction (normal or reversed) can be determined, with varying degrees of probability, from the geomagnetic polarity time scale (see Figs.4.9-4.12). Summary palaeopoles for major crustal blocks that host many important porphyry and Fe oxide Cu-Au deposits are given in Tables 4.1 – 4.6.

If the palaeopoles for the terrane of interest are not known directly, they can be determined using the Euler pole for its reconstruction to another terrane for which the palaeopoles are known. The program PALAEO provided to sponsors allows calculation of palaeofield directions at any site from the palaeopoles and also allows rotations of palaeopole positions about Euler poles to be calculated.

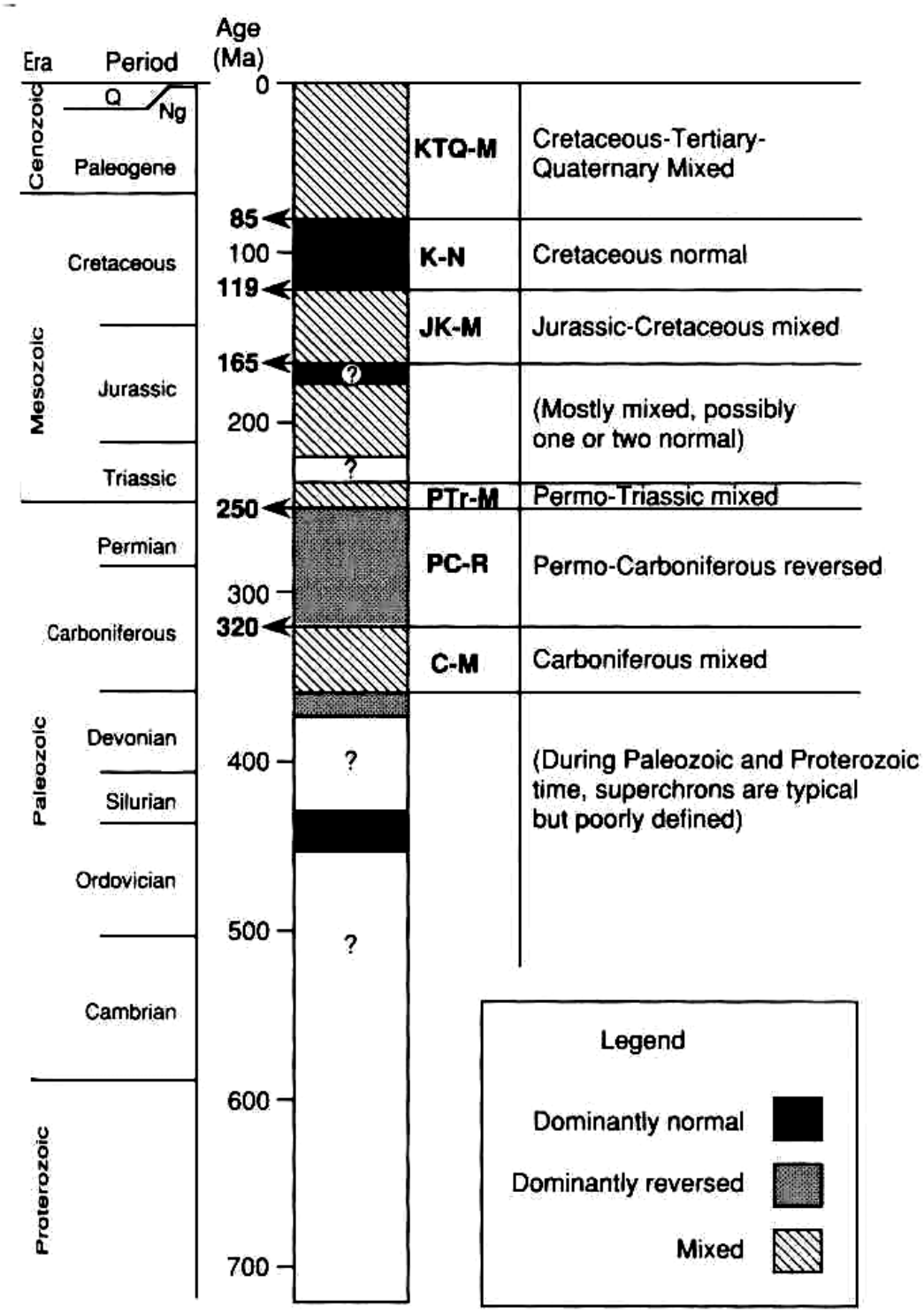

Fig.4.9. Phanerozoic geomagnetic polarity time scale (Butler, 1992)

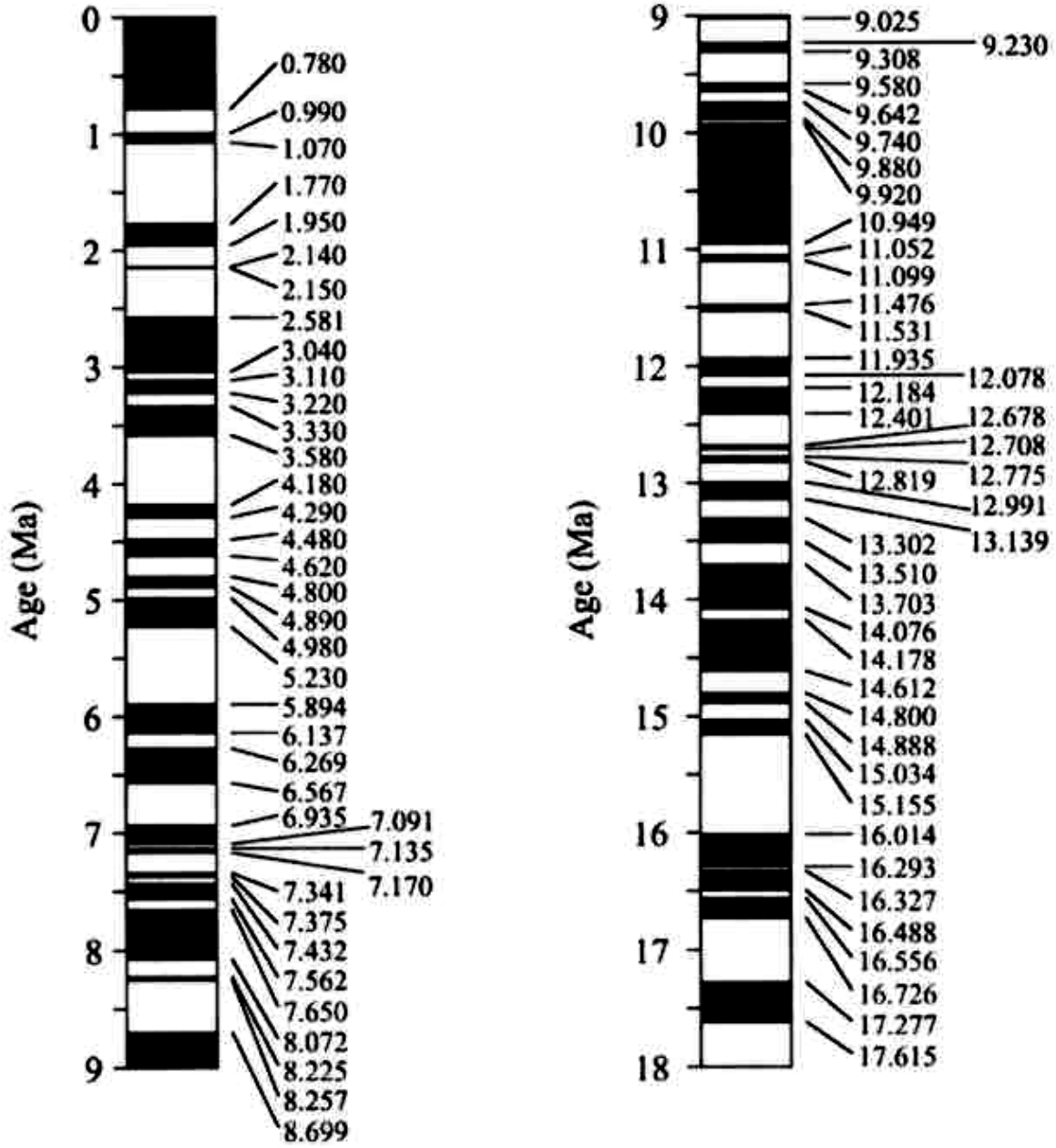

Fig.4.10. Late Tertiary detailed geomagnetic polarity time scale (normal polarity = black; reverse polarity = white) (McElhinny and McFadden, 2000)

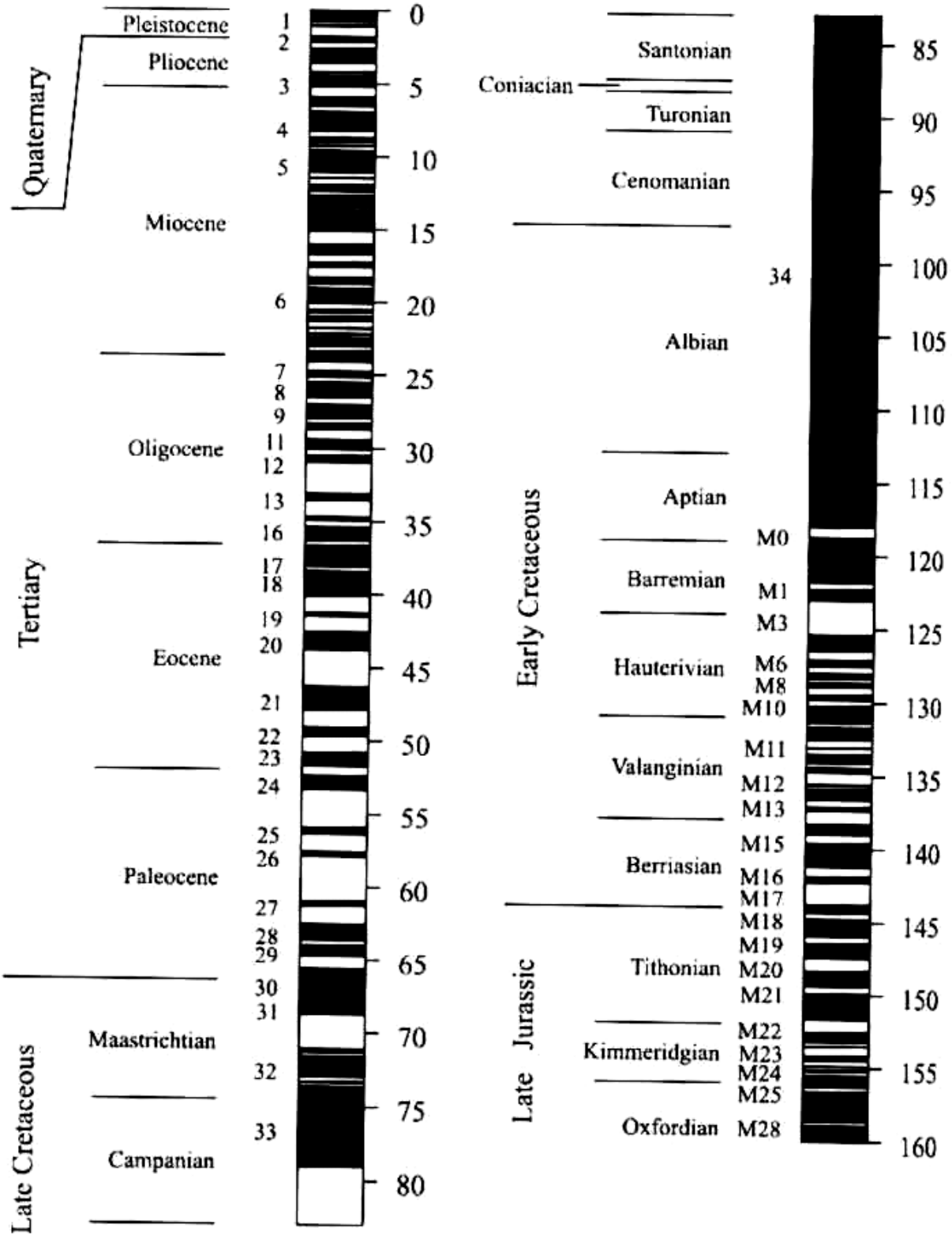

Fig.4.11. Tertiary – Late Jurassic geomagnetic polarity time scale (normal polarity = black; reverse polarity = white) (McElhinny and McFadden, 2000)

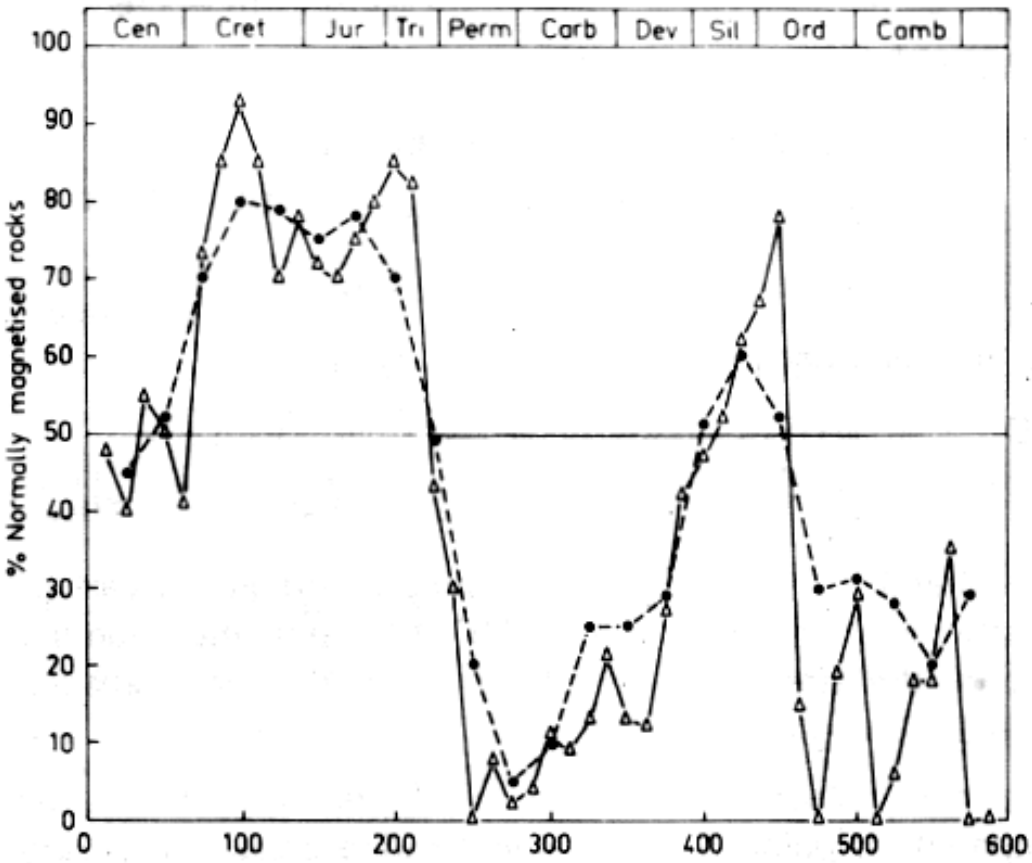

Geomagnetic polarity ratios (expressed as percentage of normally magnetised rocks) as a function of rock age for the Phanerozoic. Both 25 M.yr and 50 M.yr overlapping averages are shown. Some data used in the 50 M.yr averages are excluded from the 25 M.yr averages due to insufficient age precision: (△) 25 M.yr overlapping averages; (●) 50 M.yr overlapping averages.

Fig.4.12. Percentage of normally magnetised rocks as a function of age (Irving and Pulliah, 1974)

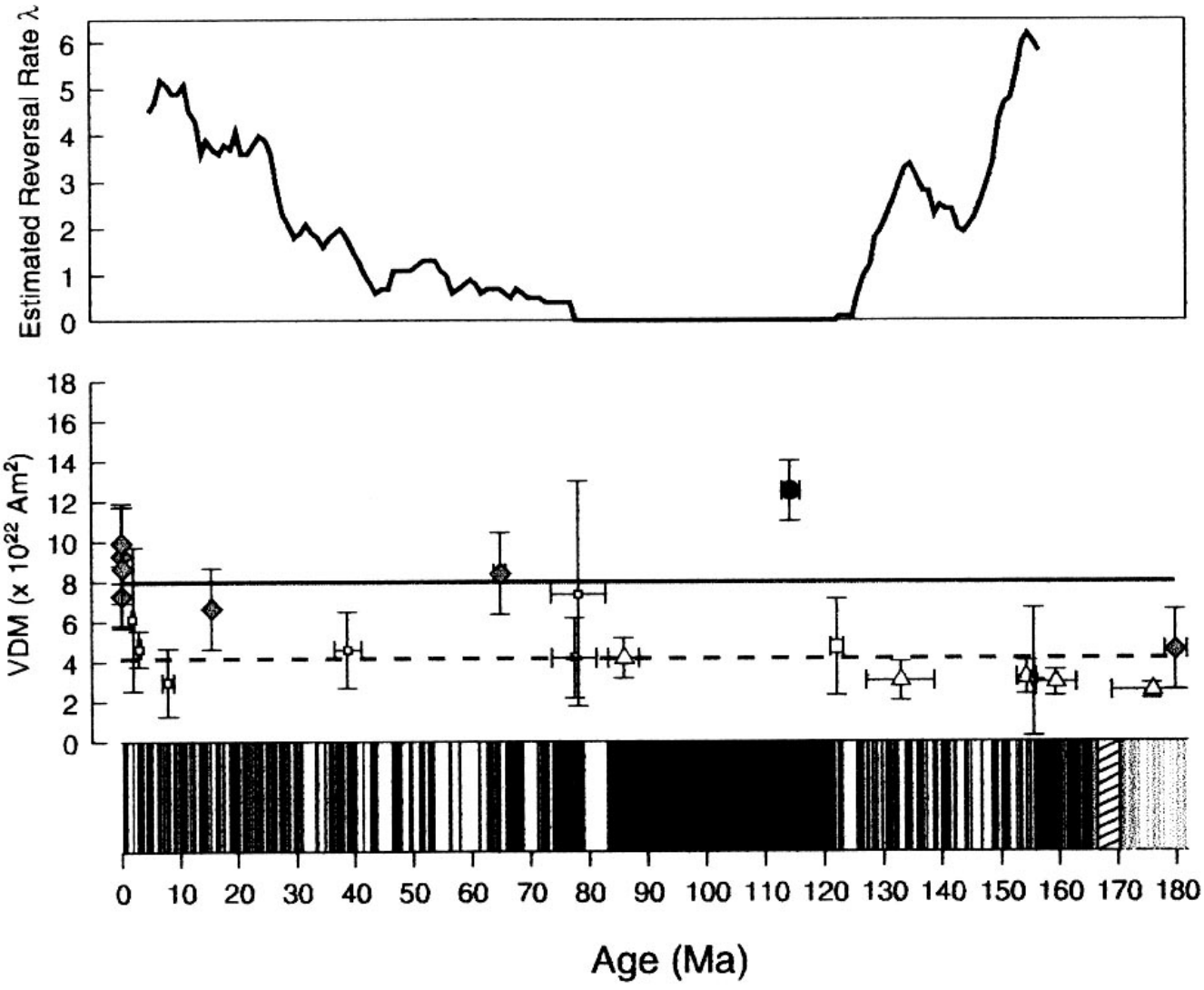

Fig.4.13. Tertiary – Late Jurassic geomagnetic polarity time scale with estimated reversal rate and virtual dipole moment corresponding to measured palaeofield intensities.

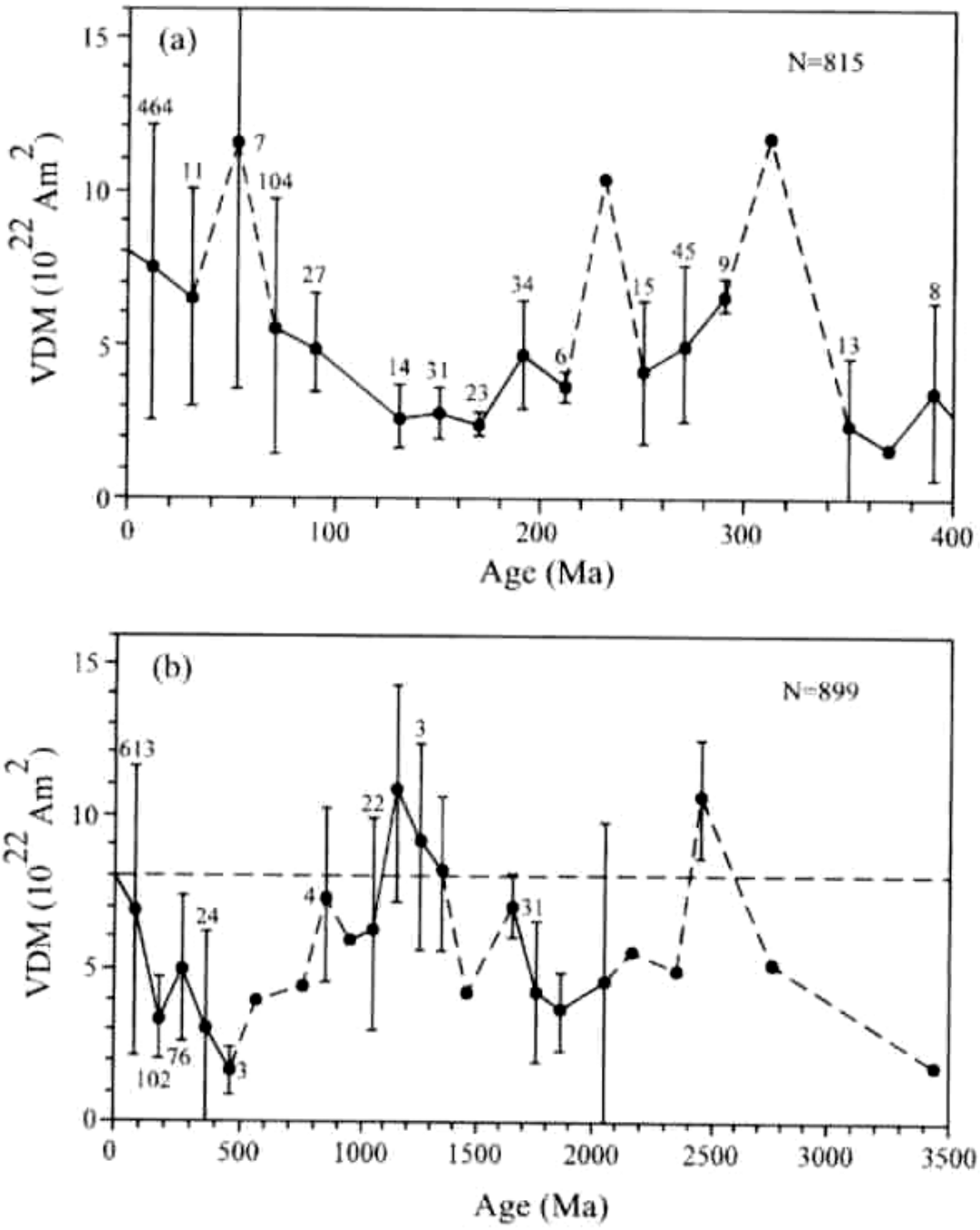

Fig.4.14. Estimated virtual dipole moment of geomagnetic field through geological time (McElhinny and McFadden, 2000).

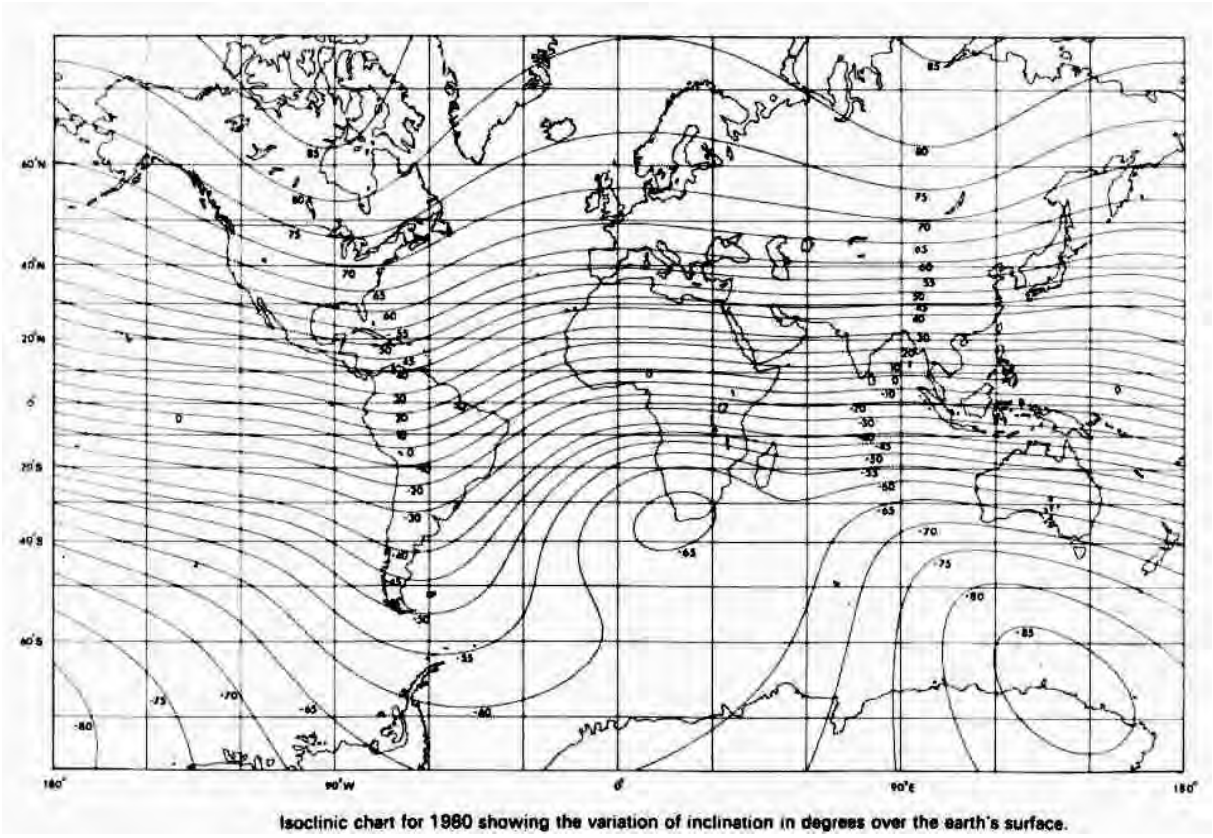

Fig.4.15. Global isoclinic chart (present geomagnetic inclination contours) (McElhinny and McFadden, 2000).

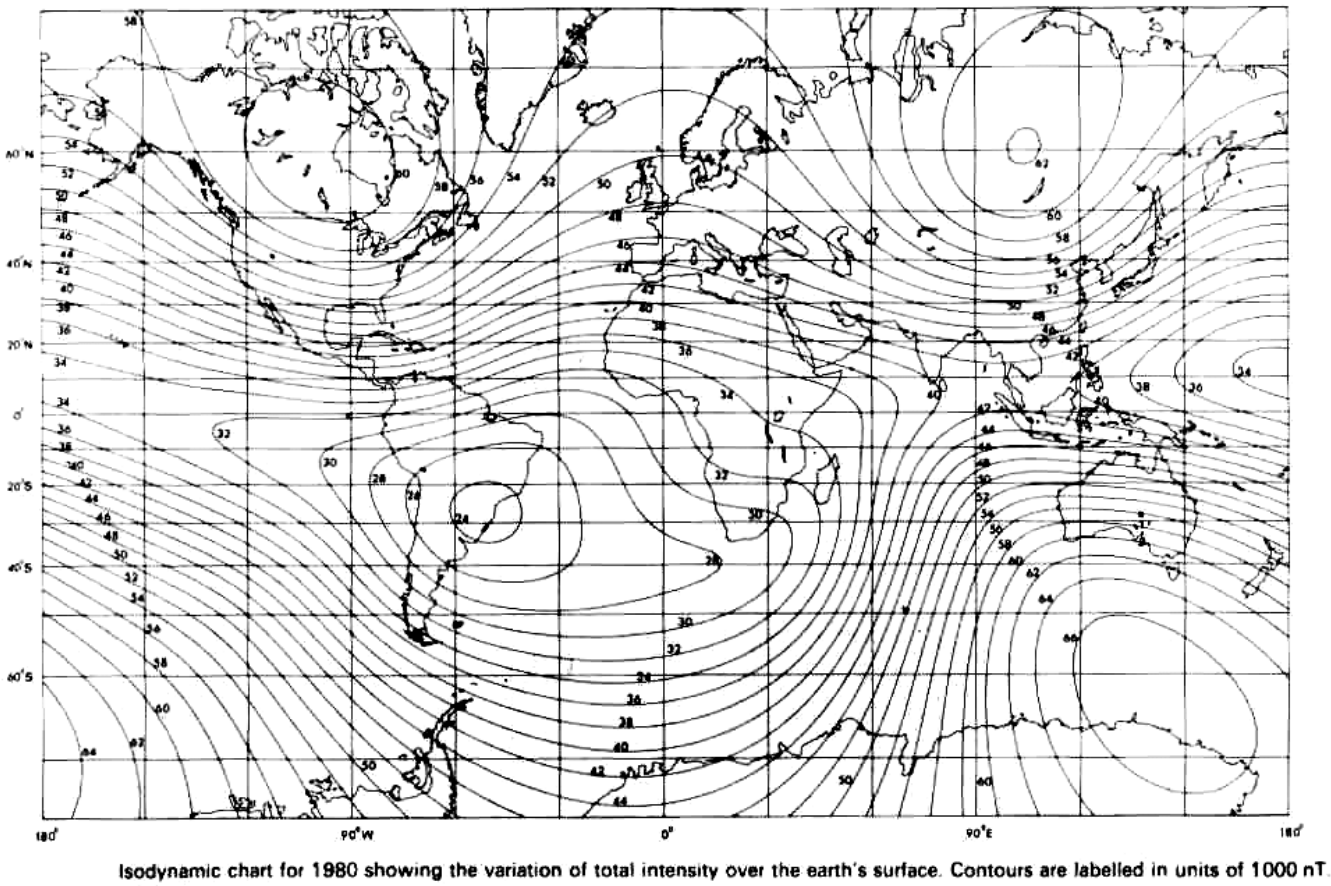

Fig.4.16. Global isodynamic chart (present geomagnetic field intensity contours) (McElhinny and McFadden, 2000).

Changes of the geomagnetic dipole moment with time are plotted in Figs.4.13-14. This information is useful for estimating palaeofield intensities, which affect the estimated remanence intensity. For a given remanence intensity, the Koenigsberger ratio depends on the present field intensity, as well as the susceptibility. To first order the present field intensity reflects latitude. Large areas of interest to explorers for porphyry, epithermal and Fe oxide Cu-Au deposits are in low latitudes (Fig.4.15), with correspondingly low geomagnetic inclinations that present problems for magnetic interpretation. Furthermore some substantial areas in South America and southern Africa have anomalously low field intensities (Fig.4.16), which tends to increase the relative importance of remanence acquired when the local field was stronger (either acquired in higher latitudes or when the dipole moment was stronger). This effect probably explains the substantially higher Q values for southern African kimberlites compared to Siberian kimberlites. Mesozoic kimberlites in Africa acquired remanence in relatively high latitudes, but now sit in an anomalously low field, whereas Devonian kimberlites in Siberia acquired remanence in low latitudes at a time of relatively low dipole moment, but now sit in high latitudes with a particularly strong field.

Application of the principles discussed above to determining palaeofield directions from Australian palaeomagnetic data is shown in Figs.4.17-4.18.

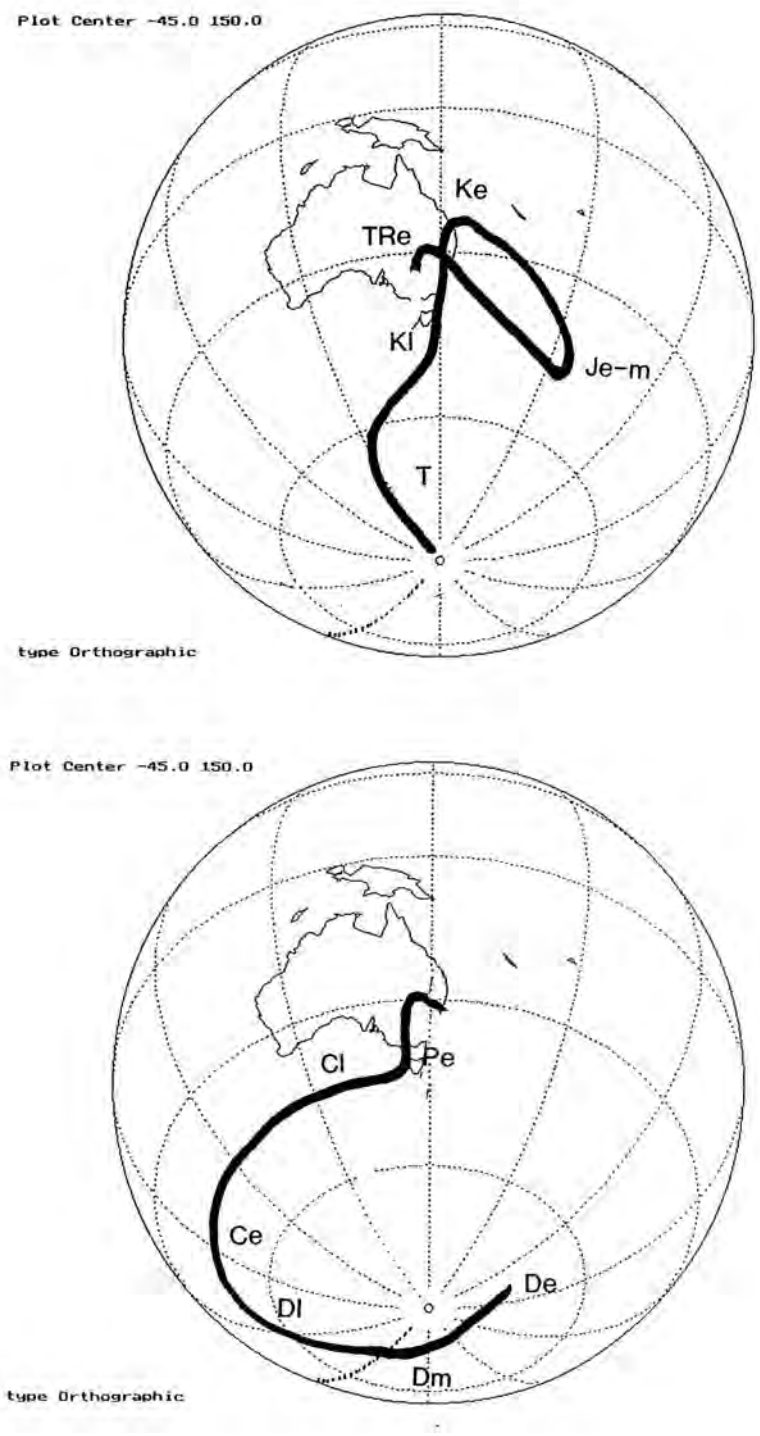

Fig.4.17. Apparent polar wander path (APWP) for Australia from the early Devonian to the present.

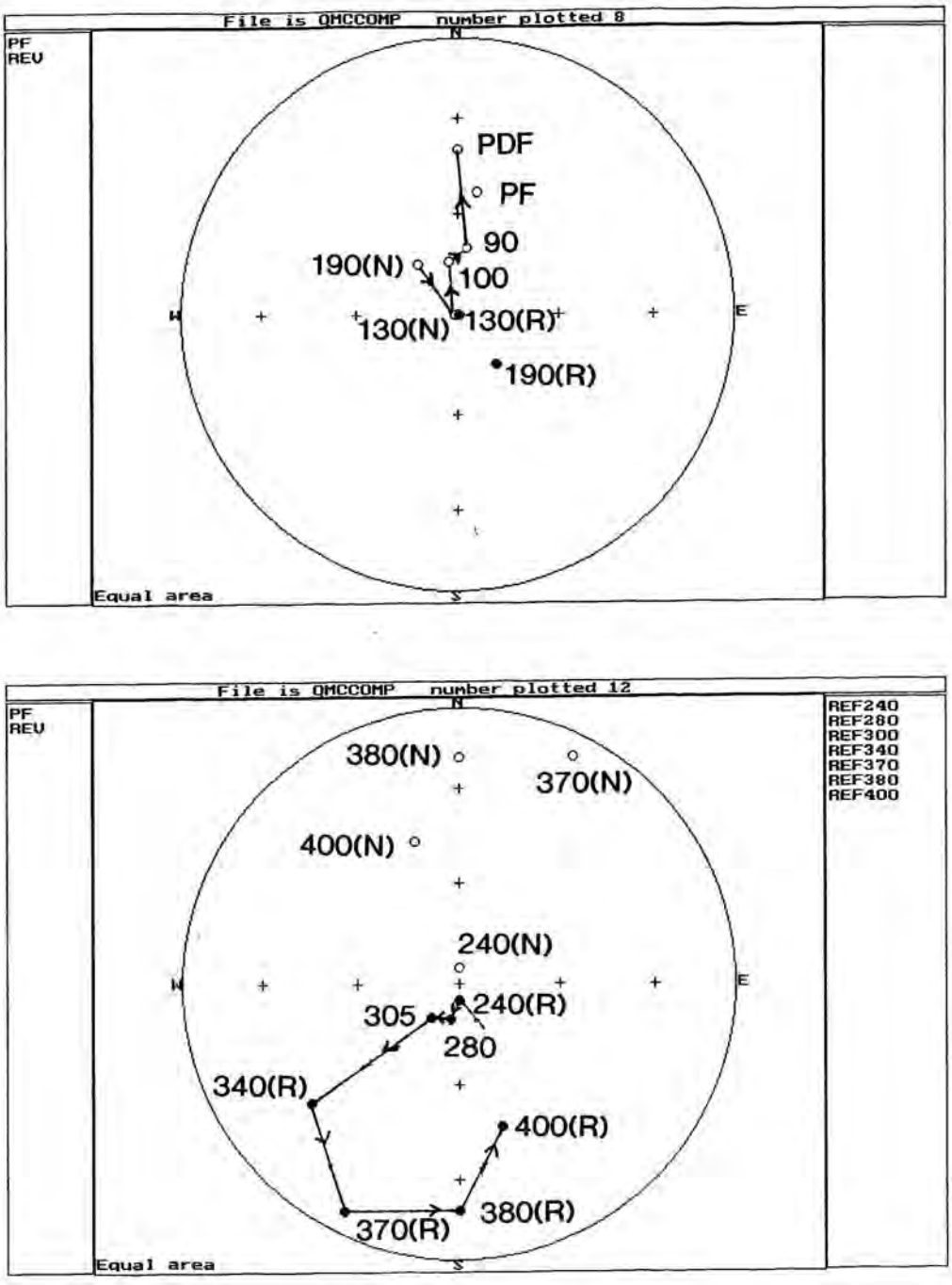

Fig.4.18. Palaeofield directions corresponding to palaeopoles shown in Fig.4.17, calculated for a site in central Queensland.

Table 4.1 Phanerozoic Palaeopoles for South America
(after McElhinny and McFadden, 2000)

Geological period/ epoch	Age range (Ma)	Mean (Ma)	Mean pole position		A_{95} (°)
			Lat (°N)	Long (°E)	
Late Cretaceous	65-97	80	84.6	196.9	7.2
Early Cretaceous	97-146	120	84.7	253.6	2.5
Middle/Late Jurassic	146-185	165	85.4	41.6	3.6
Early Jurassic	185-208	200	70.7	74.0	9.4
Late Triassic	225-235	230	79.4	1.7	5.4
Early/Middle Triassic	235-245	240	83.7	126.1	2.8
Late Permian	245-256	250	72.6	71.8	9.5
Early Permian	256-290	275	77.7	137.8	5.8
Late Carboniferous	290-323	305	55.2	168.6	3.6
Early Carboniferous	323-363	340	31.5	136.7	4.0
Middle Devonian	377-391	385	30.0	133.0	-
Ordovician	443-495	470	-11.0	153.3	-
Cambrian	495-545	520	-47.7	191.1	22.6

Table 4.2 Phanerozoic Palaeopoles for Laurentia (after McElhinny and McFadden, 2000)

Geological period/ epoch	Age range (Ma)	Mean (Ma)	Mean pole position		A_{95} (°)
			Lat (°N)	Long (°E)	
Eocene	35-56	45	80	158.0	3.7
Palaeocene	56-65	60	75.2	168.4	3.9
Late Cretaceous	65-97	80	72.3	194.8	3.7
Early Cretaceous 2	97-130	115	72.7	191.1	2.1
Early Cretaceous 1	130-146	135	64.0	203.4	3.9
Late Jurassic	146-160	155	66.5	155.1	8.3
Middle Jurassic	160-180	170	64.5	111.9	6.6
Early Jurassic	180-208	195	62.9	90.3	2.8
Late Triassic	208-225	215	55.9	93.9	2.1
Middle Triassic	225-240	235	54.4	104.4	1.7
Late Permian/Early Triassic	240-256	250	48.9	117.5	2.9
Early Permian	256-280	270	43.6	124.9	2.0
Late Carboniferous/ Early Permian	280-300	290	37.3	132.3	3.5
Late Carboniferous	300-330	315	32.8	128.9	4.1
Early Carboniferous	330-363	345	29.9	130.1	4.7
Late Devonian	363-377	370	29.1	121.4	3.6
Middle Devonian	377-391	385	21.6	117.3	7.6
Late Silurian/ Early Devonian	391-423	405	2.8	97.5	6.3
Early/Middle Silurian	423-443	435	21.3	131.6	10.4
Late Ordovician	443-458	450	22.2	129.1	6.4
Early/Middle Ordovician	458-495	475	17.7	154.2	9.0
Late Cambrian	495-505	500	-1.9	165.0	8.6
Early Cambrian	525-545	535	4…3	154.7	10.1

Table 4.3 Phanerozoic Palaeopoles for Australia (after McElhinny and McFadden, 2000)

Geological period/ epoch	Age range (Ma)	Mean (Ma)	Mean pole position		A_{95} (°)
			Lat (°N)	Long (°E)	
Eocene	35-56	45	69.1	295.7	5.2
Palaeocene	56-65	60	56.1	302.3	11.9
Late Cretaceous	65-97	85	55.6	318.6	3.1
Early Cretaceous	97-146	120	47.2	334.8	9.6
Middle/Late Jurassic	146-178	160	48.2	352.6	8.4
Early/Middle Jurassic	178-208	195	48.7	355.5	4.0
Late Triassic	208-235	220	33.0	0.3	11.4
Late Permian/ Early Triassic	245-256	250	33.4	326.1	11.8
Early Permian	256-290	275	34.3	292.8	23.0
Late Carboniferous A	290-315	305	51.4	321.0	2.6
Late Carboniferous B	315-323	320	85.7	331.7	22.1
Early Carboniferous	323-363	345	37.6	232.6	-
Late Devonian	363-377	370	58.0	211.3	8.0
Middle Devonian	377-391	385	73.2	159.1	11.0
Early Devonian	391-417	405	74.3	42.7	-
Late Ordovician/ Silurian	417-458	440	-15.7	242.7	-
Early/Middle Ordovician	458-495	475	15.5	216.7	15.0
Middle/Late Cambrian	495-518	510	31.1	201.6	6.0
Early/Middle Cambrian	518-530	525	-15.6	207.6	15.3
Early Cambrian	530-545	535	19.3	175.9	25.3

Table 4.4 Phanerozoic Palaeopoles for Stable Europe (Separating North Britain and Baltica for >425 Ma) (after McElhinny and McFadden, 2000)

Geological period/ epoch	Age range (Ma)	Mean (Ma)	Mean pole position		A_{95} (°)
			Lat (°N)	Long (°E)	
Eocene	35-56	45	82	168.9	2.0
Palaeocene	56-65	60	77.3	164.4	3.1
Late Cretaceous	65-97	80	71.5	151.8	4.1
Early Cretaceous	97-146	120	70.5	206.5	7.3
Late/Middle Jurassic	146-176	160	73.8	144.0	3.8
Early/Middle Jurassic	176-208	195	66.1	128.0	8.6
Late Triassic	208-225	215	53.2	136.3	11.1
Early/Middle Triassic	225-245	235	50.7	150.0	5.7
Late Permian	245-270	255	46.9	163.2	1.6
Early Permian	270-290	280	44.9	165.5	1.9
Permian (Western Europe only)	(245-290)	(265)	46.6	163.0	1.8
Permian (Russian Platform only)	(245-290)	(265)	45.7	165.1	1.6
Late Carboniferous	290-323	305	36.3	168.1	4.8
Early Carboniferous	323-363	345	27.2	157.8	7.1
Late Devonian	363-377	370	23.0	161.4	4.9
Middle Devonian	377-391	385	20.1	157.1	7.5
Early Devonian	391-417	405	2.7	142.1	4.2
Late Silurian	417-425	420	2.6	164.0	4.9
North Britain					
	425-443	435	19.5	164.2	5.1
Late Ordovician	443-458	450	10.1	186.8	5.1
Early/Middle Ordovician	458-495	475	9.1	205.5	7.2
Baltica					
Early /Middle Silurian	425-443	435	16.7	177.2	9.3
Late Ordovician	443-458	450	2.9	174.4	13.6
Middle Ordovician	458-470	465	-8.5	231.6	9.1
Early Ordovician	470-495	480	-20.5	230.1	5.8
Middle/Late Cambrian	495-530	510	-31.0	266.0	-

Table 4.5 Phanerozoic Palaeopoles for North China (after McElhinny and McFadden, 2000)

Geological period/ epoch	Age range (Ma)	Mean (Ma)	Mean pole position		A_{95} (°)
			Lat (°N)	Long (°E)	
Palaeocene/Eocene	35-65	50	86.3	200.1	-
Late Cretaceous	65-97	80	79.0	192.0	9.5
Early Cretaceous	97-146	120	79.3	213.7	5.5
Late Jurassic	146-157	150	72.9	220.0	2.5
Middle Jurassic	157-178	170	74.6	238.4	4.8
Early Jurassic	178-208	195	82.4	286.0	-
Middle/Late Triassic	208-235	220	59.8	11.0	5.9
Early Triassic	235-245	240	58.6	353.1	3.7
Late Permian	245-256	250	48.1	3.8	7.4
Early Permian	256-290	275	40.9	353.7	11.0
Late Carboniferous	290-323	305	35.3	339.5	21.4
Middle/Late Devonian	363-391	375	-34.2	48.7	-
Middle/Late Silurian	417-428	420	-26.2	48.4	-
Late Cambrian/ Early Ordovician	470-505	485	-28.8	130.9	-
Early/Middle Cambrian	505-545	525	-21.2	155.2	-

Table 4.6 Phanerozoic Palaeopoles for South China (after McElhinny and McFadden, 2000)

Geological period/ epoch	Age range (Ma)	Mean (Ma)	Mean pole position		A_{95} (°)
			Lat (°N)	Long (°E)	
Palaeocene/Eocene	35-65	50	77.2	278.5	10.2
Late Cretaceous	65-97	80	74.0	199.7	7.3
Early Cretaceous	97-146	120	73.9	208.0	9.2
Late Jurassic	146-157	150	74.9	198.9	6.5
Middle Jurassic	157-178	165	64.4	186.4	5.2
Early Jurassic	178-208	195	64.8	190.0	3.4
Middle/Late Triassic	208-235	220	31.5	197.1	8.6
Early Triassic	235-245	240	46.8	216.5	4.9
Late Permian	245-256	250	51.5	238.8	5.0
Early Permian	256-290	275	31.4	224.1	-
Carboniferous	290-363	325	23.5	223.0	4.8
Devonian	363-417	390	-8.9	190.4	-
Silurian	417-443	430	4.9	194.7	-
Early Ordovician	470-495	480	-38.9	235.7	-
Early/Middle Cambrian	505-545	525	-4.3	204.6	14.5

Up to date information of published palaeopoles can be obtained from the online version of the IAGA global paleomagnetic database: http://www.ngu.no/dragon/Palmag/paleomag.htm .

5. GEOLOGICAL MODELS OF PORPHYRY COPPER (Mo, Au), VOLCANIC-HOSTED EPITHERMAL AND IRON OXIDE COPPER-GOLD SYSTEMS

5.1 General Features of Porphyry Deposits

Definition

Many definitions of porphyry deposits have been proposed. For present purposes we adopt the following simple definition:

Porphyry deposits are intrusion-related, large tonnage, low grade mineral deposits with metal assemblages that may include all or some of copper, molybdenum, gold and silver. Their genesis is related to the emplacement of intermediate to felsic subvolcanic porphyritic intrusions that are commonly generated above subduction zones.

According to Lang *et al*. (1995a) some general characteristics shared by porphyry copper deposits, irrespective of the chemical classification of their associated intrusions include:

- association of mineralisation with magmatism in a volcanic arc environment,
- a range in size of associated intrusions from batholiths to dyke swarms,
- potassic alteration in the cores of systems with surrounding and locally overprintin, penecontemporaneous propylitic alteration,
- early pervasive or microfracture-controlled alteration followed by planar dilatant fracture filling,
- formation at moderate to shallow depths,
- close correlation between copper and gold grades in the cores of systems, and
- presence of hydrothermal fluids with similar temperature and total salinity, but differing in overall composition, reflecting in part magma chemistry.

This section summarises various classifications of porphyry deposits. Detailed discussions of alteration and mineralisation in porphyry systems are given in following sections.

McMillan and Panteleyev (1995) discuss general aspects of the classification of porphyry copper deposits of the Canadian Cordillera, including morphological/depth-zoning models and a chemical classification based on alkalinity. Corbett and Leach (1998) have given a comprehensive recent review of porphyry and related deposits in the SW Pacific.

Morphological/Depth-Zoning Classification

Sutherland Brown (1976) suggested three morphological/depth-zoning models for porphyry deposits in the Canadian Cordillera. The three types are:
(i) Plutonic deposits, which occur within plutons and formed at relatively great depths, often with associated dykes and breccia bodies. These deposits have alteration patterns similar to those of the Lowell-Guilbert quartz-monzonite model (Lowell and Guilbert; 1970, 1974) that typifies many deposits in the southwestern USA (see below) and are generally Cu-Mo deposits with Au grades less than 0.1 g/t.
(ii) Volcanic deposit types, associated with subvolcanic stocks, plugs, sills and dyke swarms in the root zones of ancient calc-alkalic and alkalic volcanoes. The country rocks consist predominantly of volcanics host most of the ore. An early developed biotite hornfels zone

usually surrounds the intrusions and propylitic alteration extends a considerable distance into the country rock. Calc-alkalic phases often occur within suites of dominantly alkalic rocks with related volcanic-type porphyry deposits.
(iii) Phallic type deposits are related to multiple subvolcanic intrusions, commonly with dykes and breccias. Country rocks may be volcanic or sedimentary. Early developed biotite hornfels, surrounded by a propylitic zone is characteristic. A core of potassic (biotite) alteration is surrounded by a phyllic zone which overprints part of the biotite hornfels envelope.

Figure 5.1 shows idealised cross-sections and plans for each of these deposit types.

Alkalinity

One major distinction concerns the alkalinity of the intrusions related to the mineralisation (Lang *et al*., 1992; 1995a,b). The three alkalinity classes of porphyry are calc-alkalic, quartz-alkalic and nepheline-alkalic. Quartz-alkalic intrusions are silica-saturated, whereas nepheline-alkalic intrusions are silica-undersaturated.

Calc-alkalic porphyries are typically Cu-Mo-Ag ± Au deposits, whereas alkalic porphyries are generally associated with Cu-Au deposits. High-K calc-alkalic depsoits such as Bingham Canyon (Utah), Ely (Nevada) and Bajo de la Alumbrera (Argentina) with Cu-Mo-Au-Ag metal assemblages are transitional to, and share some characteristics with, quartz alkalic deposits. Other differences include:

- Alkalic deposits tend to be smaller than calc-alkalic deposits and rarely exceed 150 million tons.
- Cu and Au grades are often higher in alkalic than calc-alkalic deposits.
- Dilatant fractures are much less abundant and pervasive alteration and mineralisation more important in alkalic deposits.
- Alteration and mineralisation in alkalic deposits tends to occur earlier in the magmatic-hydrothermal evolution than in calc-alkalic deposits, for which mineralisation is usually associated with highly differentiated late-stage intrusions.
- Mo is deficient in alkalic, compared to calc-alkalic systems.
- Peripheral mineralisation is not well developed in alkalic deposits and, where present, has formed close to, or on top of, of main ore zones.
- Sericitic (phyllic), intermediate argillic and advanced argillic alteration are generally absent or poorly developed in alkalic porphyries.
- Albitic alteration and potassium-calc-silicate alteration are more common in alkalic than in calc-alkalic systems.
- Quartz is rare in alkalic alteration systems, but carbonate minerals are abundant in many vein and alteration types.
- Magnetite is ubiquitous and abundant in alkalic deposits and is usually closely associated, temporally and spatially, with ore-grade mineralisation.

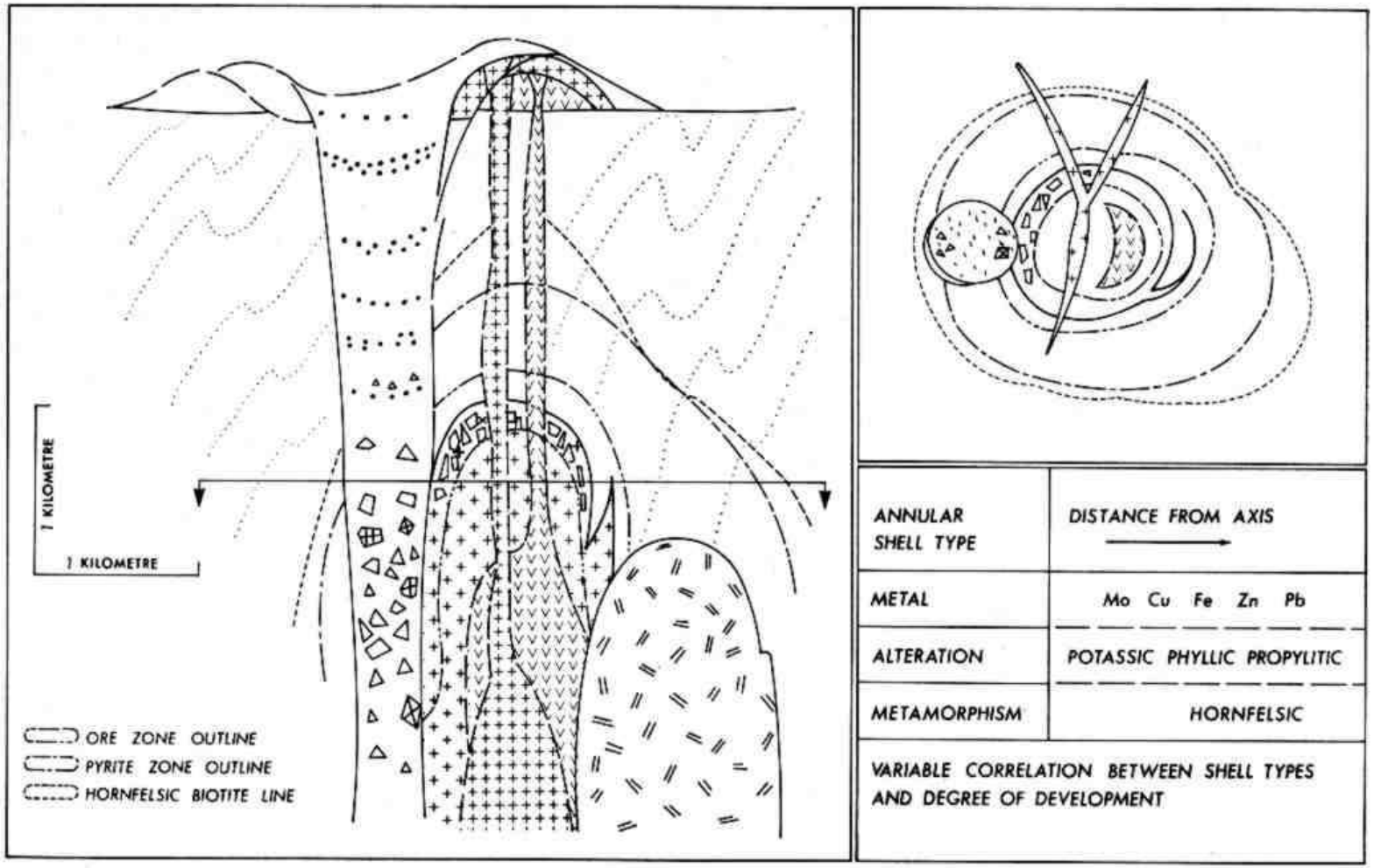

Phallic Porphyry Model in Plan and Section — showing four related intrusive phases, two pre-ore, a post-ore diatreme, and also shells of metamorphism, alteration and mineralization.

Fig.5.1a. Morphological/depth zoning classification of porphyry deposits (from Sutherland Brown, 1976). Phallic or classic model, showing four related intrusive phases, two pre-ore, a post-ore diatreme and shells of metamorphism, alteration and mineralisation.

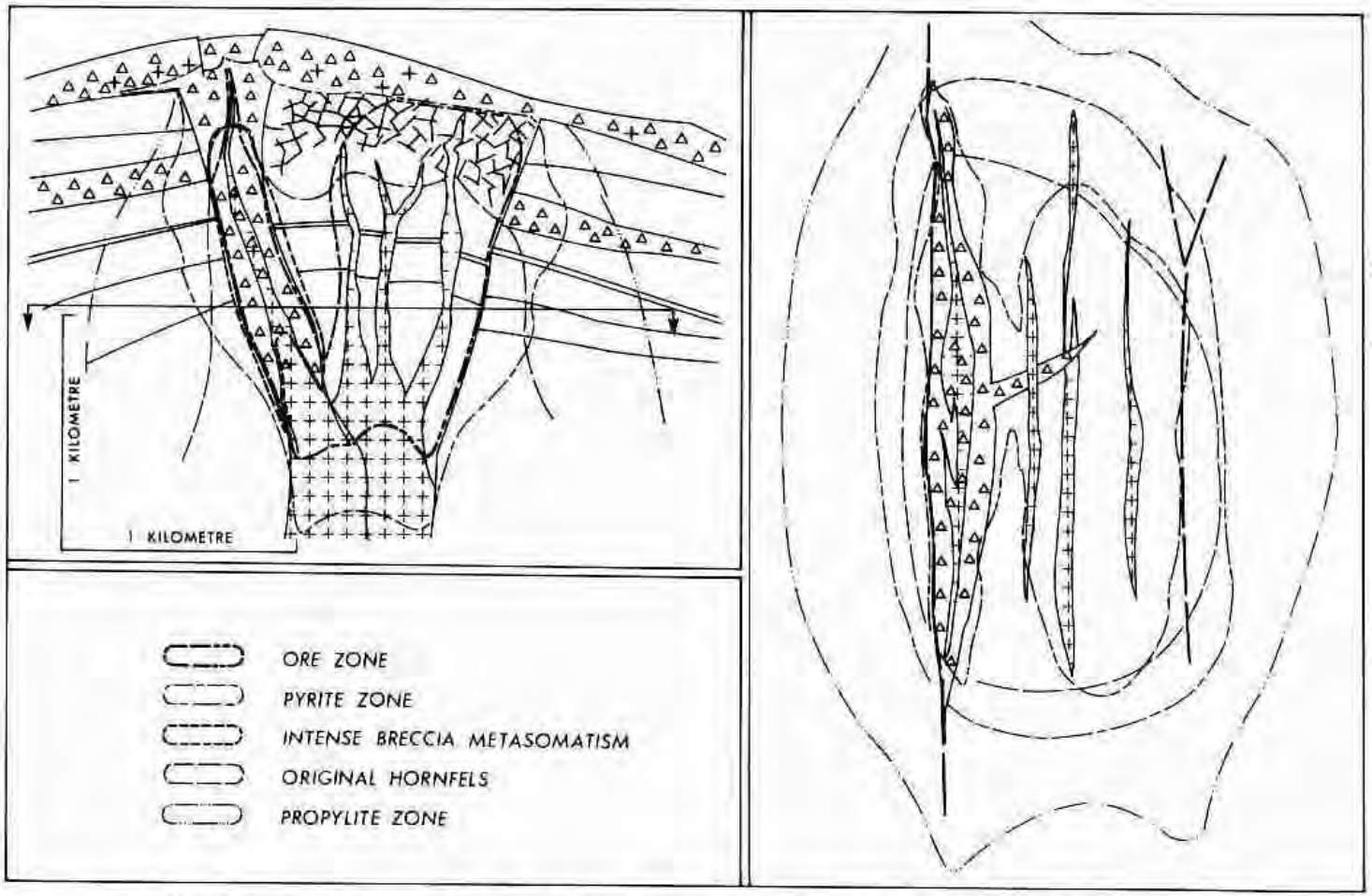

Volcanic Porphyry Model in Plan and Section — showing related intrusive porphyries, brecciated dyke and carapace breccia, all cutting related marine volcanic vent sequence.

Fig.5.1b. Morphological/depth zoning classification of porphyry deposits (from Sutherland Brown, 1976). Volcanic porphyry model, showing related intrusive porphyries, brecciated dyke and carapace breccia, all cutting related marine volcanic vent sequence.

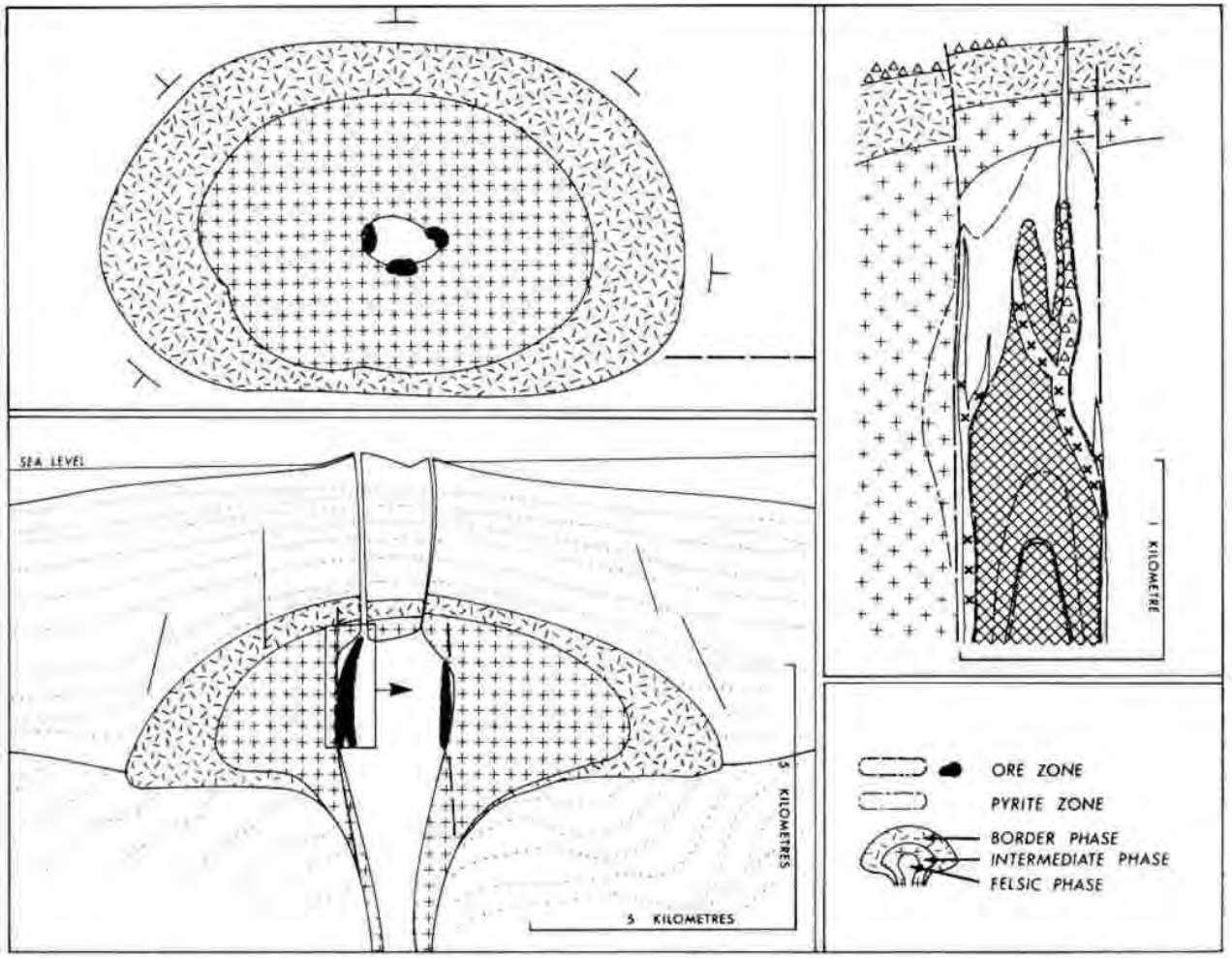

Plutonic Porphyry Model in Plan and Section — showing zoned pluton mushrooming at basal unconformity of quasi-coevel volcanic pile, internal orebodies of substantially simple nature controlled by faults that may be related to collapse, regular vein seas.

Fig.5.1c. Morphological/depth zoning classification of porphyry deposits (from Sutherland Brown, 1976). Plutonic porphyry model, showing zoned pluton mushrooming at basal unconformity of quasi-coeval volcanic pile, with internal orebodies of simple nature controlled by faults.

Diorites, monzodiorites and monzonites are the most common rock types in quartz-alkalic systems and true syenites are rare. Sphene is common and magnetite is abundant, locally attaining 15 vol %. Nepheline alkalic systems are dominated by silica-undersaturated syenite porphyries with lesser pyroxenite and monzonite. Magnetite is also abundant in nepheline-alkalic systems related to Cu-Au mineralisation. In British Columbia strongly undersaturated pyroxenite-syenite suite of alkaline intrusive complexes, characterised by melanite garnet, aegirine-augite and feldspathoids, contains two subgroups (Lang *et al*.,1995a):
(i) rocks with abundant augite, low magnetite and barren of Cu mineralisation,
(ii) rocks with abundant hornblende and magnetite, closely associated with Cu mineralisation.

Albitic alteration associated with mineralisation is common in quartz-alkalic systems and potassium-calcsilicate alteration is important in nepheline-alkalic systems.

Many alkalic deposits are associated with high-level stocks and dyke complexes, with zoned stocks, or with cumulates. Dykes are generally felsic and may be coeval with felsic breccia bodies. Stocks are zoned from gabbro or diorite margins to monzonite or syenite cores, late differentiates may be sodic and associated volcanic rocks may be shoshonitic.

High-sulphur versus Low-sulphur Deposits

Williams and Forrester (1995) distinguish high- and low-sulphur porphyries, noting that alteration patterns around porphyry intrusions differ greatly for the two types. Sulphur contents of porphyry copper intrusions range up to 8%. High sulphur content encourages development of broad magnetite-destructive alteration envelopes. Sulphur contents in the range 7-8% produce very large quartz-sericite aureoles, with extensive retrograde alteration relative to the size of the intrusion. Substantially lower sulphur contents result in the inner potassic and outer propylitic zones adjoining, with minimal development of intervening sericitic or argillic zones.

5.2 Igneous Petrogenesis

Burnham (1997) gives a recent review of the generation and emplacement of hydrous magmas that can be associated with intrusive-related mineralisation, building on earlier treatments by Burnham (1979) and Burnham and Ohmoto (1980). The magmas responsible for porphyry copper-gold and porphyry molybdenum mineralisation appear to be ultimately derived from partial melting of amphibolitised oceanic (i.e. tholeiitic) basalt, followed by crystal melt differentiation/fractionation. Burnham (1997) note that magmas generated under continental cratons produce mineralisation less frequently than those generated above subducting plates. However, mafic crustal underplates and metasomatised mantle beneath cratonic areas that inherit the character of an earlier subduction zone are also implicated in intrusive-related mineralisation.

Apart from mantle-derived magmas that produce M-type granitoids, I-type granitoid, representing second generation products of partial melting of mantle material, are implicated in Climax-type porphyry molybdenum deposits and in batholithic-type copper and gold deposits. S-type granitoids are often associated with tin and wolframite mineralisation, although reduced I-types can also produce Sn-W orebodies.

Spatially related plutonic series show clear mineralogical and chemical correlations with tectonic environment and relative time of emplacement, e.g. evolution of calc-alkaline series in orogenic belts from the oldest (low-K tonalitic series) through the medium-K granodioritic series to the youngest high-K monzonitic series). There appears to be no “magic” magma geochemistry for generation of economic ore deposits, as intrusive-related orebodies are associated with a wide range of geochemical types. For example, within the Ordovician volcanic/intrusive sequences of NSW, porphyry copper-gold mineralisation is associated with the very high-K Cadia intrusives and also with the nearby Copper Hill intrusives, which are members of a medium to low-K tonalitic suite (Blevin and Morrison, 1997).

The ascent of magmas is affected by several interrelated factors, including composition, density, viscosity and temperature. High-temperature melt-rich magmas rise much more readily than lower temperature restite-rich magmas. Thus high temperature melts are often emplaced at high levels in the crust. The density of granitic magmas is ~2.4 g/cm^3. Buoyancy assists ganitic magma to rise until the level of neutral buoyancy is reached, at which point ascent ceases and they tend to spread out. In the Andes, this occurred when the granitic magmas that formed the batholith reached the base of the volcanics. At Goonumbla (NSW) this occurred when the magma that formed the “mother intrusion” intruded its comagmatic volcanics deep in the caldera. When ascent ceases, progressive crystallisation of refractory minerals causes volatile-rich melt to accumulate in the roof zone, below the carapace. At this stage “second boiling” occurs as the magma exsolves all of its initial water content, except for minor amounts locked up in hydrous silicates, with a great increase in pressure and encourages fracturing of the carapace. development of second boiling is critically dependent on depth of emplacement and water content of the magma.

Fractional crystallisation is a prerequisite for concentration of ore metals to economic grades. Differentiation of magmas by fractional crystallisation manifests itself by compositional zoning (often concentric) of plutons, or by clusters of comagmatic intrusions, with a range of compositions, derived from an underlying magma chamber. Examples of intrusions, zoned over several kilometres from relatively mafic margins to felsic cores, centred on porphyry ore deposit districts include Bingham Canyon (Utah) and Ajo, Mineral Park and Sierrita (Arizona) (Guilbert and Lowell, 1974).

Wyborn (1988) introduced a classification of Proterozoic granitoids from Australia that has major metallogenic implications. The categories are:

Group I - restite-controlled granitoids; lowest temperature, melt generation by dehydration of muscovite; unmineralised; emplaced c.1860 Ma
Group II - intermediate temperature, melt-rich granitoids; derived by dehydation melting of biotite; associated with Au mineralisation; emplaced ~1840-1800 Ma
Group III - high temperature, melt-rich granitoids; melt generation by dehydration of hornblende; III_3 associated with Cu-Au mineralisation; emplaced c.1800 Ma ?

In Australia the Proterozoic granitoids were emplaced at ~1800 Ma and belong to the I-granodiorite type, as they are derived from older (~2400 Ma) felsic granitoids. They are associated with distal mineralisation (up to 5 km from the granitoid margin). By contrast, porphyry-style mineralisation is associated with M-type and I-tonalite granitoids. The source rocks for the Proterozoic granitoids are garnet-free. In restite-dominated suites there is no

fractionation between intrusives and associated volcanics. In melt-rich suites more metals dissolve from the source rock and differentiation is dominated by fractional crystallisation, which concentrates metals into residual melt that can bleed off the top of the intrusion. Melt-rich suites are characterised by zoned plutons, mixed plutons, felsic-and-fractionated plutons.

Thermal modelling has shown that rapid deposition of a thick sequence (~5 km) of volcanics or sediments during regional metamorphism causes temperature spike within crust, which can trigger generation of high temperature melts (e.g. Group III granitoids) within the lower crust (B. Hobbs and A. Ord, *pers. comm.*).. If extrusion of a thick volcanic pile follows a heat pulse at the base of the crust, generation of high temperature melts follows tens of Ma later. This scenario appears to be applicable to the gold ± base metal associated Proterozoic granitoids of Australia.

5.3 Tectonic Settings

Most porphyry deposits occur in orogenic belts and are associated with subduction-related plutonism and volcanism at consuming plate margins (island-arcs or continental margins). In island-arc settings, deposits are related to high level calc-alkalic or alkalic porphyritic intrusions of intermediate composition. These intrusions are oxidised, magnetite-series M-type granitoids and they tend to be gregarious or multiple. In continental arcs the intrusions are I-Cordilleran type or Andinotype (Pitcher, 1983), which are generally equivalent to the I-tonalite series of Chappell and Stephens (1988). These intrusions are also oxidised, magnetite-series granitoids, but tend to be somewhat less oxidised and magnetite-rich than the M-type island-arc intrusions (Blevin, 1994). Sillitoe (1990) states that 85% of intrusions associated with gold-rich porphyry copper deposits are at convergent plate margins above active subduction zones where mineralisation is often associated with extensional zones within the overriding plates.

Alkalic magmatism occurs in a range of complex tectonic settings, including rifted and rotated arcs, to remnant subduction zones and continental collision zones, but is only rarely associated with porphyry copper deposits (Lang *et al*., 1995a). However, within specific terranes, alkalic porphyries are economically important.

Some present-day continental settings comprise a mosaic of exotic accreted terranes, including terranes with oceanic affinities. The west coast of North America is a particularly well-studied example of this type of composite tectonic assemblage. Palaeomagnetic studies have played a crucial role defining the tectonic motions and timing of accretion of the terranes. In such areas, it is important to recognise terrane boundaries, which constrain the occurrence of particular styles of deposit. McMillan and Panteleyev (1995) discuss the tectonic setting of porphyry deposits in the composite terrane of the Canadian Cordillera and Lang *et al*. (1995a) describe the characteristic alkalic porphyry copper-gold deposits of the island-arc derived Quesnellia and Stikinia terranes of British Columbia. These deposits are of Triassic-Jurassic age and were emplaced in oceanic settings, prior to collision with the west coast of Canada.

The Lachlan Fold Belt of Eastern Australia also comprises numerous tectonostratigraphic terranes, which can be interpreteted in terms of differing plate tectonic settings and possible

successive eastward accretion (Scheibner and Basden, 1996). However, the basement terrane model of Chappell *et al*. (1988) suggests that the Lachlan Fold Belt is underlain by mostly Proterozoic lower crustal rocks that comprise a number of provinces, each with distinctive geochemical character. These basement terranes tend to be larger than, and to cut across, the tectonostratigraphic terranes that are defined by exposed supracrustal rocks. This suggests that the Lachlan Fold Belt has largely developed on a Proterozoic substrate, with little or no relative motion between overlying tectonostratigraphic terranes. It is possible that boundaries between basement terranes represent favourable sites for emplacement of magmas and movement of mineralising fluids. Resolution of the tectonic puzzle posed by accretionary versus *in situ* development models for the Lachlan Fold Belt may therefore have significant implications for exploration.

The basement terrane concept also explains why intrusions and porphyry deposits may have subduction-related signatures without contemporaneous subduction. Wyborn (1992a) has suggested that the Goonumbla porphyry copper-gold deposits of the central Lachlan Fold Belt, which are associated with Ordovician shoshonitic rocks, inherited a typical subduction geochemical signature from mantle rocks that were metasomatised during Cambrian subduction.

There is evidence that cessation of subduction, due to change in plate movement direction or seizing due to accreted terrane jamming the subduction zone, produces short-lived mantle plume, favourable for generation of magmas capable of producing porphyry mineralisation. Solomon (1990), for example, suggests that arc reversal is significant in the generation of many porphyry copper-gold deposits in island arcs. Gold-rich porphyry copper magmas may also be generated by deep-seated fracturing during late intra-arc extension or crustal slip faulting. In island arc settings, shoshonitic volcanic centres along structures that parallel the intra-arc transform faults are favourable sites for epithermal gold mineralisation.

Uplift rates in tectonically active zones may also be important for generation of mineralisation (Lum *et al*., 1992). Rapid uplift favours rapid vapour saturation, telescoping of mineralisation (e.g. porphyry and epithermal mineralisation at Porgera), and fault-controlled intrusion. At Chuquicamata rapid uplift (four times greater than uplift rates for the Sierra Nevada Batholith) appears to have assisted development of fault-controlled, late stage phyllic alteration that boosted copper grade to 1% from the “normal” 0.7% grade associated with potassically altered porphyry (B. McInnes, *pers. comm*.). Regional tectonics was also important in the generation of the giant Chuquicamata deposit, as a change of sense of strike-slip on a master fault controlled emplacement of porphyry magma.

Lum *et al*. (1992) also point out that porphyry and epithermal deposits in active tectonic belts, such as the southwest Pacific, are often disrupted and tilted by faulting soon after emplacement. Uplift rates of 2 km in a million years are common and rotation rates of 20° - 30° in 100,000 years are unexceptional. The Porgera Intrusive Complex appears to have suffered partial dismemberment and local block rotations, associated with rapid uplift, largely during its hydrothermal evolution from a porphyry to epithermal style of mineralisation (Clark and Schmidt, 1993; Schmidt *et al*., 1997).

It has been suggested that major episodes of magma generation and large scale fluid movements in the crust are associated with changes in intraplate stress fields that result from

changes in plate driving forces (Loutit *et* al., 1994). These events manifest themselves as bends and cusps in the apparent polar wander path of the plate, which indicate changes in plate motions.

5.4 Hydrothermal Evolution, Timing and Mechanism of Fluid Release

The critical phases in the generation of porphyry copper deposits have been summarised by Hunt (1991) as follows:

- generation of oxidised calc-alkaline to alkaline magma containing sufficient water, sulphur, metals and other volatiles,
- relatively rapid ascent of the magma to shallow levels, retaining metals and volatiles,
- emplacement of small to moderate-sized batholiths at depths less than 10 km, with coeval intermediate or intermediate-felsic volcanics,
- fractional crystallisation of the batholith and development of one or more cupolas with multiple phases of porphyritic dykes and stocks, usually within 1-5 km of the surface,
- simultaneous and intense fracturing of the cupolas and release of magmatic fluids with deposition of substantial amounts of sulphur, alkalis, copper and other metals, and hydrogen ions into the fractured cupolas and surrounding host rocks,
- interaction, to a varying degree, of ground water with the cooling mineralised cupolas, transition from alkali metasomatism to hydrolytic alteration and increasing sulphide ion activity, and reworking of earlier-formed magmatic mineralisation by dominantly pyritic mineralisation as cooling progresses.

The Goonumbla deposits in central NSW offer a type example of a mother intrusion with apophyses that attained shallow depths. The roof of the undelying magma chamber sat at the level of neutral buoyancy, with volatile-rich melt at top. Emplacement of narrow, volatile-rich apophyses was controlled by zones of weakness (particularly at intersections of lineaments) and was probably triggered by seismic activity.

As a general principle formation of vein systems reflects transient changes in the stress field. In porphyry systems, the local stress field is affected by overpressuring due to fluid exsolution beneath a carapace, which is then released by fracturing and release of fluid into cracks generated by the build up of pressure. Sealing of cracks by mineral deposition temporarily negates this avenue of pressure release. The process of carapace formation, build up of pressure, followed by fracturing is repeated, producing multiple episodes of veining and alteration. The process is strongly affected by changes in the regional stress field, reflecting uplift and fault movements, for example.

Chlorine and sulphur partition strongly into the aqueous phase developed during second boiling. Chlorine is mainly present as neutral complexes with alkalis, iron and other chalcophile metals, hydrogen and calcium. Sulphur is present as both hydrogen sulphide and sulphur dioxide, with their ratio dependent on (or, more likely, determining) the oxygen fugacity. The metal-carrying capacity of these aqueous fluids depends directly on their chloride and sulphide species contentsand ratios (Burnham and Ohmoto, 1980).

Escape of hot chloride- and sulphur-bearing fluids into cooler wall rocks causes mainly potassium and hydrogen ion metasomatism of aluminosilicates and Fe-silicate metasomatism of carbonates (skarn formation). Cooling of the fluids causes precipitation of metal sulphides and anhydrite from chloride complexes, mainly through hydrolysis of sulphur dioxide to hydrogen sulphide and sulphuric acid. This generates HCl, which promotes additional phyllic alteration.

The relatively low grades of most intrusive-related mineralisation reflect the fact that fluid-rock interaction is not very efficient mechanism for ore deposition. Mixing of oxidised and reduced fluids may be important factor in formation of giant ore deposits. Structural controls and timing of fluid generation and release are crucial factors for channelling different fluids into a site where mixing and deposition of metals can occur. There is evidence that such fluid mixing was important at the Porgera gold deposit, where early oxidised fluid was generated from the intrusive stocks, as evidenced by bleaching of bituminous shale wall rocks. Au was carried in reduced fluid, together with base metals, and is associated with phyllic alteration that was in equilibrium with reduced country rocks (Cameron *et al*., 1996).

5.5 Sources of Metals

The mantle is the direct or indirect source of most of the metals in porphyry copper and related deposits, which are associated either with M-type intrusions or I-type intrusions that are one step removed from mantle-derived melts. Fluid inclusions in olivine of mantle xenoliths have high Cu contents, indicating that Cu is transported within fluids in the mantle. Cu and other metals are derived from sulphide veins within mantle peridotites.

Wyborn and Sun (1994) point out that the most common magmas are generally sulphur-saturated and are unlikely to produce gold or copper-rich fluids after fractional crystallisation. Au and Cu partition strongly to sulphide phases and sulphur saturation leads to precipitation of sulphides and early removal of these metals from the melt. For development of a magmatic Cu-Au deposit, the magma must remain sulphur-undersaturated throughout its magmatic evolution. Oxygen fugacity has a large effect on sulphur saturation - under oxidising conditions sulphur dissolves as an anhydrite component.

The most favourable magma source for formation of high-gold sulphur-undersaturated magmas is lithospheric mantle that has already been depleted in sulphur by removal of sulphur-saturated basaltic melt, leaving behind small amounts of sulphide enriched in Cu, Au and other precious metals. If this refractory mantle is metasomatised, its liquidus temperature is lowered and it will undergo partial melting more readily in appropriate tectonic conditions. The magmas generated often have shoshonitic affinities and have characteristics that are favourable for generation of magmatic-hydrothermal mineralisation. Less potassic magmas derived from less metasomatised mantle can also give rise to large Cu-Au deposits, provided

the mantle source is sulphur-undersaturated. Relatively low water and sulphur contents of these mantle-derived magmas produce rather inconspicous alteration halos with restricted potassic zones and little iron sulphide. However the oxidised nature of the magmas and high K^+, which boosts Fe^{3+} content, encourages formation of both magmatic and hydrothermal magnetite.

Halogens are important complexing agents for metals in hydrothermal fluids and Cl and F contents of magmas influence development of intrusive-related mineralisation. Cl decreases and F increases with fractional crystallisation in both I- and S-type granitoids (Blevin and Chappell, 1992). Cl contents of I-type granitoids are higher than for S-types. When a hydrothermal fluid exsolves from a silicate melt Cl partitions strongly to the aqueous phase, accompanied by chloride-complexed metals such as Fe, Mn, Cu, Mo, Pb, Sn and S. However, if a sulphur-enriched magmatic vapour phase forms, sulphide-complexed Cu and Au preferentially partition into the low viscosity vapour, which can travel considerable distances before deposition, whereas Fe, Mn, Pb and Zn preferentially partition into the brine.

5.6 Types of Alteration

Reed (1997) gives a recent general treatment of hydrothermal alteration in the volume edited by Barnes (1997), building on reviews by Meyer and Hemley (1967) and Rose and Burt (1979) that appeared in earlier editions of that work. Other useful general references include Guilbert and Park (1986), Lentz (1994) and Thompson (1995).

The most important factors influencing identities and relative quantities of alteration minerals are:

- temperature
- pressure
- primary rock composition
- primary fluid composition, and
- fluid/rock ratio.

The somewhat nebulous, but qualitatively useful, concept of fluid/rock ratio determines whether the alteration is rock-buffered or fluid buffered. Figure 5.2 illustrates the concept of fluid/rock ratio (Giggenbach, 1997). Important differences between rock-buffered and fluid-buffered alteration include:

- At low fluid/rock ratios the system is rock-buffered and mineral assemblages tend to straddle stability field boundaries.
- On the other hand, in fluid-dominated systems alteration mineral assemblages tend to lie within stability fields, because the bulk composition of the altered rock is partially imposed by the fluid.
- The oxidation ratio tends to remain fixed during rock-buffered alteration. The oxidation ratio may change substantially if the system is dominated by a fluid that has a different redox state.

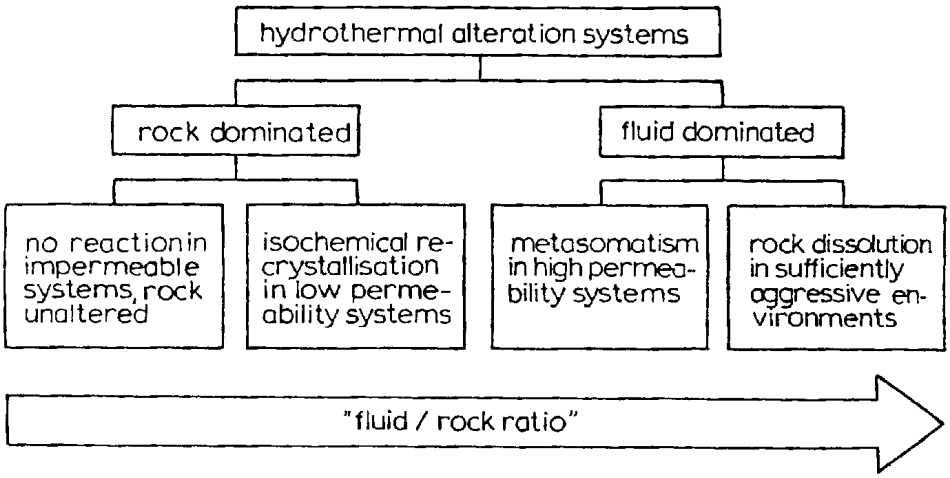

FIGURE 6.6a Classification of hydrothermal alteration systems as a function of effective fluid/rock ratio.

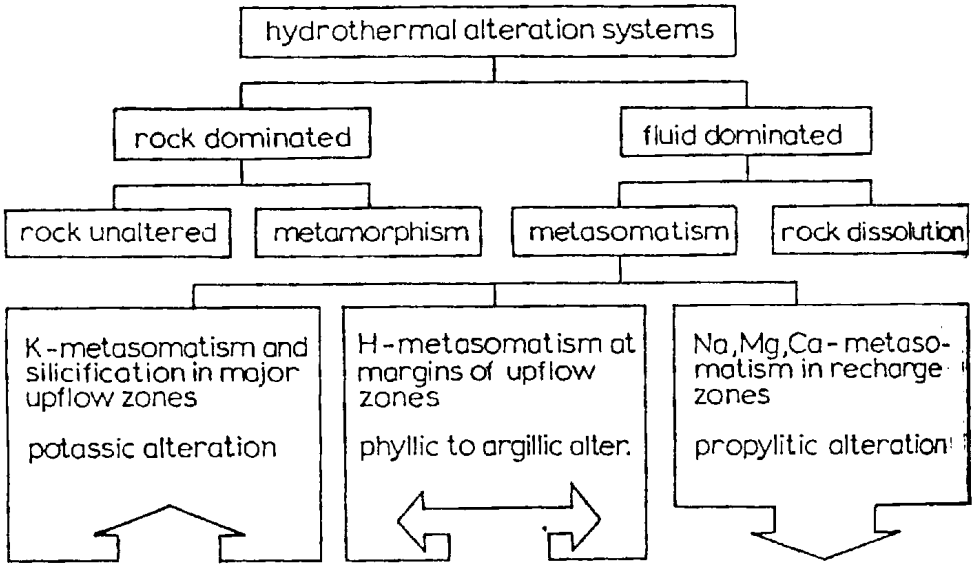

FIGURE 6.6b Classification of hydrothermal alteration systems with special emphasis on the three major types of metasomatic processes and alteration patterns.

Figure 5.2. Classification of hydrothermal alteration systems, with special emphasis on the three major types of metasomatic processes and alteration patterns (from Giggenbach, 1997). The fluid/rock ratio increases from left to right (unaltered rock ⇒ metamorphism ⇒ metasomatism ⇒ rock dissolution).

Relative solubilities of potassium-bearing aluminosilicate minerals decrease with decreasing temperature, whereas Na-, Mg- and Ca-containing minerals have increasing relative solubility as the temperature falls. Thus cooling hydrothermal solutions tend to deposit K-bearing minerals, such as K-feldspar, biotite and K-mica. On the other hand, Na-, Mg- and Ca-bearing minerals, typical of propylitic alteration, are stabilised by increasing temperatures experienced by descending recharge waters around a cooling pluton. K-metasomatism, accompanied by silicification in major upflow zones, produces potassic alteration. In more acid environments, K-rich clays and alunite, typical of phyllic to advanced argillic alteration form from rising hydrothermal solutions.

The main descriptive types of alteration that are important in intrusive-related mineralisation have the characteristic assemblages listed in Table 3-1. Effects of hydrothermal alteration on magnetic mineral assemblages are listed in Table 3-2. The main types of alteration will be discussed in turn.

Early Magnetite ± Amphibole ± Plagioclase Veins (M veins)

Clark and Arancibia (1995) recognise a preceding potassic alteration in a subclan of porphyry coppers associated with oxidised (magnetite + sphene)-bearing mafic to intermediate intrusions. The Island Copper Cu-Au-Mo deposit, British Columbia, provides the type example of this style of alteration (Arancibia and Clark, 1996). At this deposit the magnetite-rich alteration zone extends 500-700 m laterally and has an original depth extent of at least 450 m. It is zoned outwards from quartz-magnetite-albite-(amphibole)-(apatite) through quartz-magnetite- amphibole-albite or oligoclase/andesine-(apatite) to amphibole-magnetite-oligoclase or sodic andesine, and it is the earliest phase of hydrothermal alteration, clearly predating the main stage chalcopyrite-pyrite stockwork and associated potassic alteration. The magnetite-rich alteration involves intense Fe-metasomatism. Minor chalcopyrite and pyrite accompany the early Fe-metasomatism and Au may have been extensively introduced during the early stage magnetite-rich alteration.

These authors argue that magnetite-rich vein systems in and around some porphyry systems are often early (pre-mineralisation) and are distinct from magnetite-biotite potassic alteration that is associated with sulphides and Cu-Au mineralisation. The magnetite ± amphibole ± plagioclase alteration, with very little sulphide, represents the initial stage in the evolution of a subclan of porphyry copper deposits. Deposition of this assemblage is favoured by host rocks of mafic-intermediate composition. Host rocks influence deposition of magnetite around these systems, but iron metasomatism effected by magmatic conditions is also demonstrably important. The early strongly magnetite alteration appears to be associated with strongly oxidised intrusions that contain magnetite + sphene rather than the less oxidised assemblage magnetite + ilmenite.

This style of alteration is best developed in andesitic and basaltic country rocks. Where well-developed, magnetite concentrations are typically ~ 5 vol %, and are occasionally higher.

Table 5-1 Characteristic Mineral Assemblages of the Main Alteration Types in Porphyry Systems

ALTERATION TYPE (synonym)	CHARACTERISTIC ASSEMBLAGE
Early magnetite ± amphibole ± plagioclase veins	Quartz-magnetite ± amphibole ± plagioclase, sulphide-poor veins; Fe-metasomatism
Potassic (K-silicate)	K-feldspar and/or biotite, plus one or more of: sericite, chlorite and quartz (e.g. in the interior zone of porphyry copper deposits)
Sericitic (Phyllic)	Quartz-sericite-pyrite-chlorite (e.g. in large halos around porphyry copper deposits)
Intermediate Argillic	Smectite and kaolinite, commonly replacing plagioclase (e.g. variably developed zone outside sericitic zone in some porphyry coppers)
Propylitic	Albite (or K-feldspar in potassic rocks), chlorite and epidote group minerals; with only minor change in bulk composition (e.g. outermost alteration zone of porphyry copper deposits)
Albitic	Na-rich plagioclase + epidote and other propylitic minerals; with substantial addition of Na
Sodic-calcic	Sodic feldspar and epidote ± actinolite ± chlorite (e.g. adjacent to intrusion at depth, beneath certain porphyry copper deposits)
Advanced Argillic	Quartz plus one or more of: kaolinite, dickite, pyrophyllite, diaspore, pyrite, alunite, zunyite, topaz (e.g. in epithermal systems that may overlie porphyry systems)
Carbonate	Calcite, dolomite, ankerite, siderite plus sericite, pyrite and/or albite
Skarn	Ca and Mg silicates (limestone protolith: andradite and grossular, wollastonite, epidote, idocrase, chlorite, actinolite; dolostone protolith: forsterite, serpentine, talc, brucite, tremolite, chlorite)
Greisen	Granite protolith: coarse-grained muscovite, feldspars, quartz and topaz ± tourmaline (e.g. in some Sn and Mo deposits)
Hematite-sericite	Hematite-sericite-chlorite in iron oxide-Cu-Au-(U-REE) deposits (e.g. Olympic Dam)

Table 5-2 Effects of Hydrothermal Alteration on Magnetic Mineral Assemblages

ALTERATION TYPE (synonym)	EFFECTS ON MAGNETIC MINERALS
Potassic (~ K-silicate)	Usually magnetite-producing: up to 5 vol % in mafic/intermediate rocks (e.g. gold-rich porphyry copper deposits); minor magnetite addition in felsic rocks; often associated with early quartz-magnetite-(amphibole) veins. Sometimes magnetite-destructive in high sulphidation systems.
Sericitic (Phyllic)	Magnetite-destructive (pyrite + hematite produced)
Deep phyllic	Magnetite-destructive; pyrrhotite-producing (moderate susceptibility, relatively strong remanence)
Intermediate Argillic (Argillic)	Magnetite-destructive
Intense Propylitic	Partially to totally magnetite-destructive (Fe in pyrite, hematite, epidote, chlorite, actinolite)
Weak propylitic	Magnetite-stable
Albitic	Partially to totally magnetite-destructive
Sodic-calcic	Partially to totally magnetite-destructive
Advanced Argillic	Magnetite-destructive
Carbonate	Partially to totally magnetite-destructive
Skarn	Often magnetite-producing, particularly in magnesian skarn; sometimes pyrrhotitic
Greisen	Magnetite-destructive
Hematite-sericite	Partially magnetite-destructive; hematite (magnetite, maghemite) assemblage favourable for remanence
Supergene oxidation	Magnetite- and pyrrhotite-destructive; hematite and goethite produced

Potassic Alteration

Potassic alteration reflects K-metasomatism at high K^+ /H^+. Figure 5.3 shows alternative cooling paths during the magmatic-hydrothermal transition for fluid in equilibrium with granodiorite (Guilbert and Park, 1986, p. 176). It is evident that the potassic assemblage is stable at high temperatures, provided the initial K^+ /H^+ ratio is sufficiently high. Medium- and high-K granodioritic melts generate an initial hydrous fluid that passes through the K-feldspar + biotite field, whereas low-K melts may generate a fluid (point 1) that passes along path A, producing andalusite instead, unless hydrolysis or other reactions shift the K^+ /H^+ ratio towards point 2.

K-feldspar ranging in composition from nearly pure orthoclase to Or_{70}, sometimes accompanied by albite, is characteristic of potassic alteration related to intrusions, whereas in hot springs and epithermal systems, potassic alteration produces adularia. K-feldspar and/or biotite replace plagioclase or mafic minerals.

Porphyry-related potassic alteration of felsic rocks replaces plagioclase with K-rich orthoclase (typically Or_{85-90}), or occasionally microcline, and is accompanied by quartz and sulphides. Common associated minerals include biotite, greenish sericite, anhydrite and carbonates. In intermediate to mafic rocks, potassic alteration is characterised by biotitisation of mafic minerals (and sometimes plagioclase and other minerals). Chlorite, epidote, albite and actinolite (i.e. typical propylitic minerals) also occur in some potassically altered dioritic rocks.

Intrusion-related potassic alteration is characterised by high temperatures (300-600°C), and high oxygen and sulphur fugacities. Chlorite + orthoclase occurs at the lower temperature end of the spectrum, muscovite + biotite at higher temperatures and andalusite + K-feldspar at the highest temperatures. At the relatively high temperatures of potassic alteration acid-generating species, such as HCl, CO_2 and SO_2, are undissociated and the solutions are not strongly acidic. Chalcopyrite and molybdenite are generally accompanied by either pyrite or bornite, plus rutile and magnetite or hematite. Pyrrhotite is present in some higher temperature assemblages. In porphyry deposits that have sericite-bearing, pyrite-rich and magnetite-poor potassic zones at shallow levels, magnetite and chlorite increase at depth with respect to sericite and pyrite (e.g. the San Manuel-Kalamazoo, Arizona, system, which is the type area for the Lowell and Guilbert (1970) porphyry copper model). In such cases, the shallow zone may represent sericitic overprinting by circulating groundwaters of early magmatic-hydrothermal potassic alteration (Gustafson and Hunt, 1975). Where hematite is present in the assemblage, the feldspar is commonly very red. The colour reflects exsolution of ferric iron, substituting for Al^{3+} at high temperatures and trapped within the lattice, as hematite dust within the feldspar.

Vein assemblages accompanying early potassic alteration in and around intrusions generally contain quartz, K-feldspar, biotite, molybdenite, bornite and chalcopyrite. Magnetite is also frequently present.

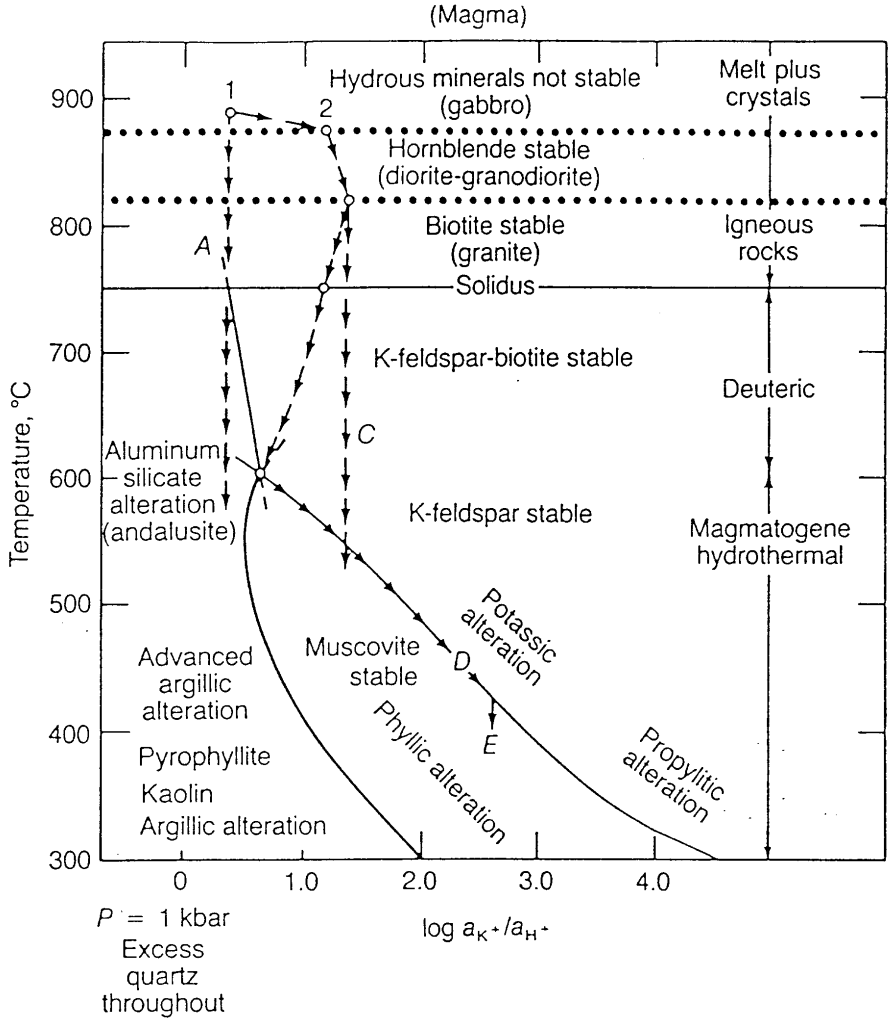

Figure 6.8: Aqueous fluid connection between igneous rocks (above), the deuteric late-stage orthomagmatic rocks and minerals (right center), and some common alteration assemblages (lower left), all as functions of temperature and the ratio of the chemical potentials of K^+ and H^+ at 1 kbar pressure—the pressure of approximately 3-to-4-km depth. A similar diagram using sodium would relate albite, the rare sodium mica paragonite and Na-montmorillonite, and the other rocks and minerals shown. Points 1 and 2 at the top represent aqueous chloride solutions in equilibrium with granodioritic magmas. 1 is low K, and the fluid never precipitates K-feldspar (path *A*): 1 can evolve toward 2 by any means that raises the K^+/H^+ ratio, such as reaction or hydrolysis. From 2, several paths are possible, depending on what happens to the fluid. They all pass through the potassic field to the potassic-phyllic boundary *D* and thence into the phyllic field *E*. (*After* Burnham and Ohmoto, 1980).

Figure 5.3. Alternative cooling paths during the magmatic-hydrothermal transition for fluid in equilibrium with granodiorite (Guilbert and Park, 1986, p. 176, after Burnham and Ohmoto, 1980). Point 1 represents a fluid initially in equilibrium with a low K granodioritic magma, which evolves along path A and never precipitates K-feldspar. 1 can evolve toward 2 by any means that raises the K^+/H^+ ratio, such as reaction or hydrolysis. Several paths are possible from point 2, depending on many factors, but all pass through the potassic field to the potassic-phyllic boundary, whence they cool along the K-feldspar + muscovite buffer (path D, marking the potassic-phyllic boundary) and thence into the phyllic field.

Sericitic (phyllic) Alteration

Figure 5.3 shows that fluids in equilibrium with a cooling medium- to high-K granodiorite intrusion reach the potassic-phyllic boundary at high temperatures (500-600°C) and thereafter cool along path D. The K^+/H^+ ratio along path D is buffered by the assemblage K-feldspar + muscovite. When all K-feldspar has been consumed, the fluid enters the phyllic field E and sericitic alteration develops.

Sericitic (phyllic) alteration commonly arises from hydrolyis (H^+ metasomatism) in rapidly cooled margins of upflow zones and along cross-cutting structures. Both K-feldspar and plagioclase are converted to sericite ± kaolinite. Pyrite is generally present and is often abundant (5-20 vol %). In deeper zones of porphyry and intrusive breccia systems, pyrrhotite may be present in addition to pyrite. Calcite and other carbonates, anhydrite, rutile and apatite may accompany the characteristic quartz-sericite-pyrite ± kaolinite assemblage. Chlorite and biotite may proxy for quartz-sericite when high Mg and Fe are inherited from the wall rock, e.g. for phyllic alteration of dioritic rocks.

Sericitic alteration often overprints earlier potassic alteration in intrusive-related systems. The spatial zonation of phyllic zones surrounding potassic cores in many intrusion-centred systems generally reflects retrograde collapse of thermal gradients and invasion of meteoric waters. Late veins at many porphyry deposits are pyrite-rich, with sericitic, grading outward into argillic, envelopes. Recently it has been pointed out that phyllic alteration can also be produced by magmatic fluids that evolve to lower (K^+/H^+) as they cool (Harris and Golding, 2001). Phyllic (quartz-sericite-anhydrite-bornite-chalcopyrite) mineralising alteration occurs in the core zones of the Goonumbla porphyry Cu-Au deposits of central NSW, Australia, and is caused by relatively high temperature, high salinity magmatically-derived fluids. Other deposits that apparently have phyllic alteration associated with magmatic fluids include Panguna (PNG), Porgera (PNG) and Far Southeast (Phillipines), suggesting that an island arc setting, or collision with an island arc, is more conducive to this type of alteration. Phyllic alteration due to magmatic fluids is also more likely to occur in batholithic deposits and deposits that conform to the plutonic model of Fig.5.1c.

More intense hydrolysis produces intermediate argillic, and eventually advanced argillic alteration. A low (K^+/H^+) fluid evolved from a low-K granodiorite magma may evolve from through the andalusite field to produce first advanced argillic alteration and finally intermediate argillic alteration at lower temperatures (path A).

Intermediate Argillic Alteration

Intermediate argillic, or simply “argillic”, alteration is produced at lower pH than sericitic alteration. The presence of substantial amounts of kaolinite, montmorillinite, or amorphous clay, mainly replacing plagioclase, characterises intermediate argillic alteration. Sericite may be present, K-feldspar may be unaltered or argillised, and there is substantial leaching of Ca, Na and Mg. Sulphides are usually not important.

Intermediate argillic alteration is developed at relatively low temperatures, where K-feldspar is metastable and only weakly affected. It is found commonly outboard of sericitic alteration envelopes around veins in granitic rocks. In porphyry systems, intermediate argillic zones are

commonly present between the inner potassic and outer propylitic zones. There is evidence that supergene processes are often involved in development of these argillic zones and that their importance decreases with depth.

Advanced Argillic

Advanced argillic alteration represents low (K^+/H^+) and (Na^+/H^+), due to both low alkali activities and high H^+. Under the highly acidic conditions of advanced argillic alteration, all feldspar is transformed to dickite, diaspore, alunite or other Al-rich phases. Common accompaniments are sericite, silica minerals, alunite, pyrite, tourmaline, topaz, zunyite and amorphous clays. It is found in some shallow precious-metal veins in volcanic areas and in acid hot-spring environments. In some intrusive-related systems, advanced argillic alteration occurs as envelopes around mineralised veins and in the upper parts of sericitic zones.

Propylitic Alteration

Moderate Na-Mg-Ca metasomatism, with possible addition of H_2O, CO_2 and S, produces the propylitic assemblage (albite, epidote (zoisite, clinozoisite), chlorite ± zeolites, smectites, prehnite, pumpellyite, actinolite, calcite, dolomite). This assemblage largely corresponds to the characteristic mineralogy of greenschist facies metamorphism, which is approximately isochemical. Because the term “propylitic” is restricted to rock-buffered (low fluid/rock) alteration, it is distinguished from chloritisation, albitisation and epidotisation, which involve extensive interaction with sea water or saline formation waters.

Propylitic alteration occurs under silicate-buffered, neutral and relatively reduced conditions, which allow galena, sphalerite and chalcopyrite to form, but not bornite, chalcocite or covellite, which form under acidic conditions for which feldspars, epidote, galena and sphalerite are not stable.

At relatively low temperatures (< 200°C), for example in upper and peripheral zones of active geothermal systems, propylitic assemblages may include the sub-greenschist minerals, zeolites and smectites. At greater depth and temperature, these minerals yield to chlorite+albite+epidote, followed by actinolite and biotite.

In K-rich rocks, K-feldspar may substitute for albite. In intermediate to mafic rocks, propylitic alteration may produce prehnite and pumpellyite or, at higher temperatures, actinolite, diopside and andraditic garnet. Calcite, dolomite, ankerite and siderite may occur in the propylitic assemblage if the altering fluids contain bicarbonate. In some porphyry systems, strong chlorite alteration of intermediate composition rocks, with abundant pyrite, appears to proxy for sericite-pyrite zones.

Propylitic zones around intrusions can be very extensive, often several kilometres in width. They tend to be zoned, with stronger development of chlorite and epidote in the inner zone and gradual changes in composition of minerals such as chlorite, grading gradually into background deuteric, metamorphic or diagenetic effects.

Albitic Alteration

The term “albitic alteration” is reserved for Na-metasomatism with replacement of aluminous minerals by Na-rich plagioclase (albite-sodic oligoclase) ± Na-rich amphibole. The associated minerals are generally members of the propylitic assemblage, particularly epidote. Minor sulphides and oxides are usually present. Magnetite is usually destroyed by intense albitic alteration.

Albitic alteration tends to be developed locally within propylitic zones of intrusion-centred systems. It also occurs patchily with potassic alteration in cores of alkalic porphyry copper deposits, particularly where alteration is intense, and in deeper portions of the systems.

Sodic-calcic Alteration

Sodic-calcic alteration at deep levels in porphyry systems of the Yerington district has been described by Carten (1986) and Dilles and Einaudi (1992). In quartz monzonitic host rock primary K-feldspar is replaced by sodic plagioclase (albite-oligoclase) and/or epidote, and hornblende and biotite are replaced by actinolite. The alteration involves addition of substantial Na and Ca, accompanied by lesser Al, Mg and Ti.

This type of alteration has spilitic affinities and appears to be restricted to geological settings with abundant marine sediments or marine volcanics. Sodic-calcic alteration is attributed to influx and heating of saline formation waters derived from marine rocks (including marine evaporites).

However, in alkalic porphyry systems from a wide range of geologic settings albitic, sodic-calcic and potassium-calc-silicate alteration are common. This suggests that, in this porphyry clan, magmatic fluid with high Ca+Na is evolved from related intrusions and produces these types of alteration (Lang *et al*., 1995).

Skarn

Formation of skarns proceeds through several stages. Contact metamorphism at 700-500°C as the magma crystallises is followed by metasomatism and iron-rich skarn formation at 600-400°C. The initial skarn forming fluid is mainly magmatic, with later contributions from meteoric waters. As the fluid evolves sulphur and metal contents tend to increase. Formation of exoskarn proceeds outwards from the edge of the intrusion, while calcium derived from reaction of the fluid with the carbonate wall rock migrates into the intrusion, producing endoskarn. Deposition of oxides and sulphides occurs mainly between 500°C and 300°C, largely during late hydrothermal alteration, which replaces early skarn. Scheelite and magnetite precede sulphides. Overall anhydrous calc-silicate minerals of the early zoned skarn stage are replaced by hydrous silicates, sulphides, oxides and carbonates. Andradite is replaced by quartz, calcite, magnetite and pyrite; diposide by actinolite, quartz and calcite; and wollastinite by calcite and quartz.

Oxygen fugacity exerts a strong influence on assemblages developed during skarn formation (Kwak, 1994). In calcic (low F and B) ore skarns, early prograde assemblages contain andraditic garnet and/or magnetite-bearing skarns with Mg-rich pyroxene in oxidised environments, whereas hedenbergitic pyroxene + grossularitic garnet occurs in reduced skarns. Pyrrhotite is common, sometimes abundant, in reduced skarns. Although the ore minerals in most skarns are deposited during retrograde skarn formation, Mo-rich scheelite forms in oxidised W-skarns instead of molybdenite in reduced skarns. Retrograde assemblages in calcic skarns progress from amphibole-epidote-quartz (± magnetite); through biotite-quartz; muscovite-chlorite-quartz; sulphides; and carbonates.

In magnesian skarns the prograde assemblage is garnet (andraditic and grossularitic) + salitic pyroxene + pyroxene (diopside > hedenbergite) + forsterite + calcite, commonly with spinel and magnetite where silica is deficient. Retrograde assemblages progress from tremolite + calcite (± sulphides or magnetite); through talc, phlogopite, serpentine, chlorite, sulphides without silicates, and carbonates.

Supergene Processes

Supergene alteration has profound effects on the economics of many intrusive-related ore deposits, particularly by supergene enrichment of grades and modification of metallurgical characteristics. Primary mineralogy, gangue minerals and ore assemblages are all affected. Iron oxides, oxyhydroxides and sulphates derive from decomposition of Fe-bearing sulphides. Acid derived from oxidation of pyrite reacts with K-silicate minerals to produce jarosite at low pH, whereas hematite and goethite are produced at higher pH. Acid attack on K-silicate minerals produces an assemblage that mimics advanced argillic alteration. Weathering of rocks with more than ~5% sulphide generally produces an assemblage with alunite, allophane and jarosite. Magnetite and pyrrhotite are never preserved in intensely weathered zones of intrusive-related systems, although magnetite is relatively resistant to moderate weathering of otherwise unaltered intrusive rocks.

5.7 Stability of Magnetic Minerals

Reaction of Acidic Fluid with Mafic to Felsic Wall Rocks

Reed (1997) considers the reaction of an initially highly acidic fluid at 300°C with mafic, intermediate and felsic protoliths. Such a fluid could be generated, for example, by condensation into groundwater of SO_2 and HCl that have separated from a magmatic brine. Figure 5.4 shows the changes in mineralogy associated with evolution of the acidic fluid, as it reacts with andesite. As the fluid/rock ratio decreases the alteration assemblages evolve from intense advanced argillic, through advanced argillic, and sericitic, to propylitic. It can be seen from Fig.5.4 that at this temperature magnetite is only stable over part of the propylitic field. Pyrite is precipitated throughout, except for weak propylitic alteration at very low fluid/rock ratios, where pyrrhotite may be produced. However, at very low fluid/rock values, reactions may not proceed to completion and a disequilibrium assemblage may result. Hematite is the stable iron oxide throughout the advanced argillic and sericitic stages.

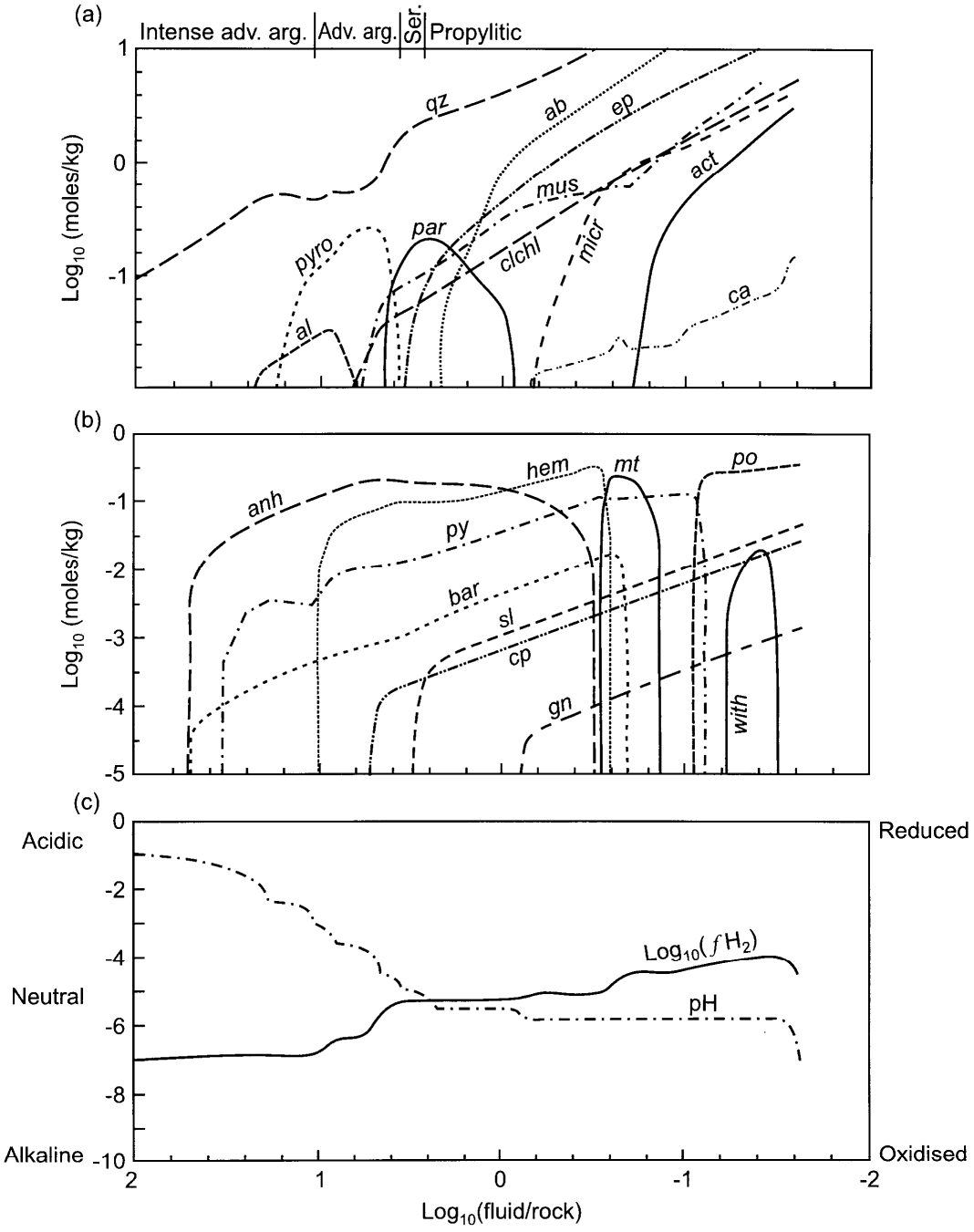

Figure 6.9: Progressive reaction of andesite with diluted acidic magnetic gas condensate at 300°C. (a) Principal alteration minerals. (b) Alteration sulphides, sulphates and oxides. (c) pH and hydrogen fugacity. *(after Reed, 1997)*

Figure 5.4. Changes in mineralogy associated with evolution of the acidic fluid at 300°C, as it reacts with andesite. As the fluid/rock ratio decreases the alteration assemblages evolve from intense advanced argillic, through advanced argillic, and sericitic, to propylitic. The fluid composition becomes progressively less acidic and more reduced (after Reed, 1997).

Quite similar patterns are also predicted for reaction of the fluid with basaltic and dacitic protoliths. The mineral assemblages at each alteration stage remain essentially the same for the mafic and felsic rocks, with minor changes in the range of fluid/rock ratios corresponding to each alteration type. The main effect of protolith composition is to change the relative quantities of the alteration minerals. Similar results also apply at lower temperatures, for example the alteration zoning around acid-sulphate epithermal deposits. Potassic alteration is not produced under the T-pH conditions considered in this example.

From Fig.5.4 we can infer that at temperatures ≤ 300°C, interaction between a range of igneous country rocks and an acidic fluid of mixed magmatic-meteoric origin is magnetite-destructive in the advanced argillic and sericitic zones and essentially magnetite-stable, possibly with minor magnetite production, in the weak propylitic zone (fluid/rock < 0.4). Pyrite + hematite is deposited, at the expense of magnetite at all higher fluid/rock ratios.

Magnetite is not stable under the conditions of sericitic alteration and has been destroyed wherever this alteration is strongly developed. Partial pyritisation of magnetite is commonly seen in zones of weak sericitic alteration. Ferric iron occurs mainly as hematite in these zones.

Although up to ~2 wt % magnetite is predicted to be present in the weak propylitic zone, possibly representing a substantial increase over the primary magnetite content of the protolith, much of the ferric iron that is allocated to magnetite in the calculation is probably sequestered in epidote, chlorite and actinolite. Thus the true amount of magnetite precipitated is likely to be lower than that calculated.

There is good evidence that greenschist grade metamorphism of magnetite-bearing basaltic and andesitic rocks tends to break down magnetite, with iron partitioning into hydrous mafic silicates, plus some hematite. This explains why most metabasalts in greenstone belts are weakly magnetic, whereas unmetamorphosed equivalents are strongly magnetic (Clark *et al*., 1992a,b). By analogy, we can infer that well-developed propylitic alteration is also magnetite-destructive, a conclusion that is borne out by empirical data from intrusive-related mineralised systems (see section 8). Experience has also shown that less intense propylitic alteration largely preserves magnetite, but little or no extra magnetite appears to be produced during propylitic alteration. The extensive, pyrite-rich propylitic zones that are commonly developed around some high sulphur porphyry copper deposits (e.g. many deposits in southwestern North America), are apparently magnetite-destructive.

Clark *et al*., 1992b also noted that magnetite-rich protoliths tend to retain their magnetite through greenschist facies metamorphism, presumably because the oxygen fugacity is largely buffered by the oxide assemblage and the metamorphic silicates are saturated in ferric iron. This observation suggests that protoliths containing several per cent magnetite, or more, should exhibit little reduction in susceptibility in response to propylitic alteration.

Magnetic Minerals in Skarns

Magnesian skarns (forsterite, serpentine, talc, brucite, tremolite etc.), produced by metasomatism of dolomite, often contain abundant magnetite and are sometimes magnetite orebodies. On the other hand calcic skarns (andradite and grossular, wollastonite, epidote, idocrase, chlorite, actinolite) replacing pure limestone, generally contain much less magnetite, as iron enters calcium-iron or calcium-manganese silicates. However, calcic Fe skarns associated with mafic (typically dioritic) intrusions in island arc and rifted continental margin settings are exceptional because they contain abundant magnetite (Einaudi et al., 1981). In this case the iron-rich igneous association imposes strong Fe metasomatism on the rocks. Dolomitic and argillic limestones yield more complex skarn mineralogies. Magnetite often accompanies amphibole, pyroxene and garnet in skarns, but does not occur with wollastinite.

Oxidised skarns, produced by magmatic (± oxidised) meteoric fluids derived from oxidised intrusions intrusions or by reaction with relatively oxidised host rock sequences (e.g. packages containing redbeds or oxidised volcanics) often contain hematite as well as magnetite. Reduced skarns, associated with reduced ilmenite-series intrusions or with reduced host rock sequences (e.g. containing carbonaceous shales) often contain pyrrhotite.

Stability and Composition of Pyrrhotite

Figure 5.5 shows phase diagrams for the iron-sulphur and Fe-S-O systems. Pyrite is a ubiquitous mineral in porphyry systems, whereas pyrrhotite is less common. The occurrence and composition of pyrrhotite in association with pyrite reflect sulphur activity and temperature. Pyrite is almost non-magnetic. The composition of pyrrhotite is of crucial importance for its magnetic properties. Monoclinic pyrrhotite (4C superstructure; ~ Fe_7S_8; 46.7 atomic % Fe; N_{FeS} = 0.934) has fairly high susceptibility and can carry strong and stable remanence. On the other hand, intermediate or “hexagonal” pyrrhotite, ranging in composition from ~ Fe_9S_{10} (5C superstructure; 47.4 at. % Fe; N_{FeS} = 0.948) through ~ $Fe_{10}S_{11}$ (11C superstructure; 47.6 at. % Fe; N_{FeS} = 0.952), to ~ $Fe_{11}S_{12}$ (6C superstructure; 47.8 at. % Fe; N_{FeS} = 0.956) is weakly magnetic at ambient temperatures.

Assemblages re-equilibrate readily to quite low temperatures and the actual composition and content of pyrrhotite depends critically on cooling rate. Pyrrhotite is more characteristic of high temperature assemblages that have been quenched. Above ~250°C monoclinic pyrrhotite is unstable with respect to high-temperature hexagonal pyrrhotite + pyrite. The Fe content of the 1C pyrrhotite in equilibrium with pyrite is a function of sulphur fugacity and temperature. Lower Fe/S is favoured by higher sulphur fugacity and higher temperature. Note that the pyrite-pyrrhotite buffer curve is oblique to the pyrrhotite composition contours, so that pyrrhotite compositions tend to become more Fe-rich on cooling in the presence of pyrite.

At a given sulphur fugacity the composition of the pyrrhotite produced by cooling the 1C + pyrite mixture depends on the cooling rate, as this determines the temperature at which the pyrrhotite composition becomes metastably stranded. Compositions that correspond to ~ Fe_7S_8 will produce monoclinic pyrrhotite on cooling through 250°C, whereas higher Fe contents will develop intermediate pyrrhotite on cooling to low temperatures. Monoclinic pyrrhotite, without intermediate pyrrhotite, results when the pyrite-pyrrhotite assemblage equilibrates above ~500°C and is quenched. Equilibration temperatures between 400°C and

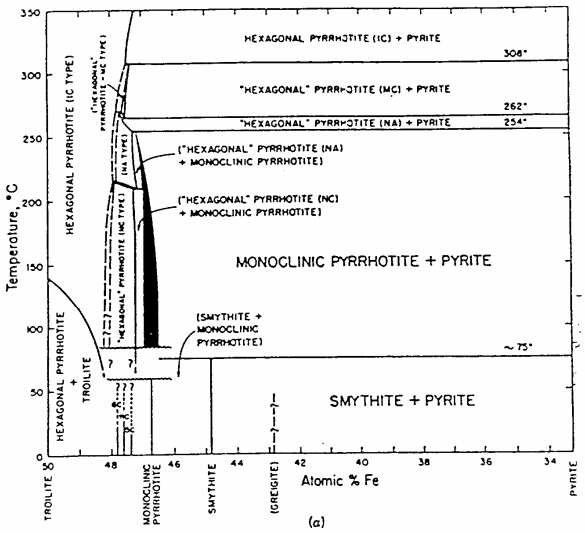

FIGURE 6.10: (a) Phase relations in the central portion of the Fe–S system below 350°C, based on Kissin and Scott (1982) and references therein. (b) Diagrams to show the ordered distribution of vacancies in three pyrrhotites (i) the 4C structure of Fe_7S_8, (ii) the 5C structure of Fe_9S_{10}, and (iii) the 6C structure of $Fe_{11}S_{12}$. Only cation layers (parallel to basal planes) are shown. (c) Schematic, isothermal free energy–composition diagram for the iron sulfide minerals. Here the gain in free energy involved in forming the various sulfides from the elements in standard states (ΔG_f°) in kilojoules per mole (of Fe) is plotted against composition. Stable phases fall on the dashed line (adapted from Vaughan and Lennie, 1991). (d) Revised phase diagram for the region FeS to Fe_7S_8 (adapted from Grönvold and Stolen, 1992). Phase designations are used in this diagram: alpha-iron (Fe); $Fe_{1-x}S$ (1C); intermediate temperature FeS (2A, C); unknown superstructures for $Fe_{1-x}S$ (NA, NC); troilite FeS (3A, 2C); $Fe_{11}S_{12}$ (6C); $Fe_{10}S_{11}$ (11C); Fe_9S_{10} (5C); noncommensurate phase $Fe_{0.89}S$ (M); Fe_7S_8 (4C); pyrite FeS_2 (py). Solid lines are macroscopic phase boundaries; lines broken by dots are suggested extensions of phase boundaries. Dashed lines are tentative phase boundaries for Fe_9S_{10} and Fe_7S_8; dotted lines are possible existence ranges for 6C and 11C. Crosses separated by two dashes show the antiferro- to paramagnetic transitions. Dots separated by two dashes indicate the spin–flip transition.

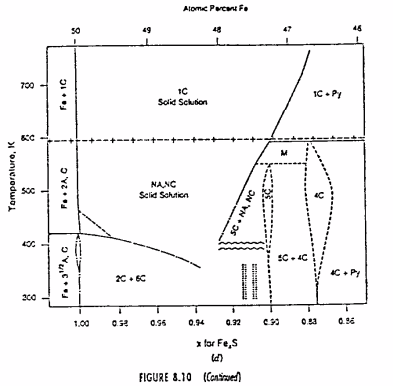

FIGURE 8.10 (Continued)

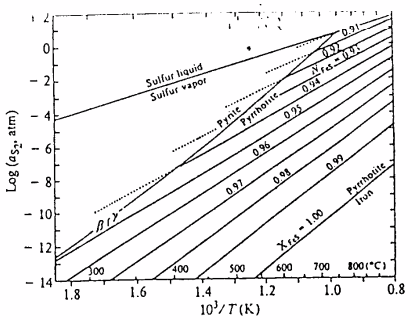

Fig.5.5. Phase diagrams for the Fe-S system (after Vaughn and Craig, 1997): (Top) composition of pyrrhotite in equilibrium with pyrite as a function of temperature and sulphur activity; (Bottom) phase relations in the pyrite-pyrrhotite-troilite portion of the iron-sulphur system below 350°C.

500°C produce monoclinic + intermediate pyrrhotite and lower temperatures produce only intermediate pyrrhotite. Very slow cooling rates, which result in re-equilibration to relatively low temperatures, should therefore result in intermediate pyrrhotite + pyrite assemblages that are essentially non-magnetic. The phase diagrams discussed above only consider the pure iron-sulphur system. When oxygen activity and pH are taken into account, it is found that pyrrhotite is stable under relatively reduced and alkaline conditions compared to pyrite.

Pyrrhotite is very rare in unmetamorphosed sedimentary rocks, but quite common in regionally metamorphosed sediments. Metamorphism of carbonaceous, pyritic shales produces reducing conditions that favour pyrrhotite at the expense of pyrite. Pyrrhotite is also commonly developed in the contact aureoles of igneous intrusions, where pyrite loses sulphur to the alteration fluids.

Pyrrhotite appears in addition to pyrite in the deeper, higher temperature, portions of some porphyry and other intrusive-related systems. At the Kidston (Queensland) gold mine, for example, pyrrhotite, associated with phyllic alteration, is present at depth in the breccia pipe and the pyrrhotite/pyrite ratio increases with depth. Pyrrhotite is more common in batholithic ore deposits, e.g. the Middle Fork (Washington) prospect (Patton *et al*., 1973) and the Quartz Creek (Washington) Cu prospect (Cheney and Trammell, 1996), than in shallow-level porphyry deposits. Princehouse and Dilles (1996) report pyrrhotite at the Wheeler Mine (Nevada) porphyry Cu-Au deposit, but this is possibly a product of the regional metamorphism that this deposit has undergone.

Many skarn and replacement deposits, associated with a wide range of ore metals, also contain pyrrhotite, e.g. the Lower Fortitude Au skarn deposit (Paterson and Hallof, 1993) and the Renison and Cleveland (Tasmania) tin deposits.

5.8 Alteration Zoning in Porphyry Systems

Introduction

Idealised zoning models of alteration/mineralisation in and around porphyry deposits have been widely applied in exploration. Although they have proved their worth many times, in other cases adherence to a preconceived model has seriously misled interpretation. No two deposits are exactly alike, so judgement must be exercised and simplistic models used with caution. Proper application of these models requires understanding of the geological factors that cause the wide range of variations observed. It is important to recognise that observed spatial patterns reflect a complex sequence of prograde and retrograde events, each with dynamic development of spatial zonation.

The classic porphyry copper model of Lowell and Guilbert (1970) neatly summarised the characteristics of an important class of porphyry copper deposits. However the model was based predominantly on Laramide porphyry deposits of the North American southwest. Hollister (1975) introduced a “diorite model” for another important class of deposits, based largely on examples from the Canadian Cordillera, supplementing the “quartz-monzonite model” of Lowell and Guilbert. The distinguishing characteristics of the two models are listed below:

Quartz-monzonite Porphyry Copper Model (Fig.5.6)

- Alteration comprises a core potassic (K-feldspar ± biotite) zone with phyllic, argillic and propylitic zones arranged in concentric but incomplete shells around it,
- the potassic zone is mainly developed within and adjacent to the intrusion and propylitic alteration is developed as a broad aureole at the outer edge of hydrothermal effects in either the intrusion or silicate wall rocks.
- generally developed in and around calc-alkaline granodiorite-quartz monzonite porphyries (often associated with quartz diorite intrusions),
- with copper and molybdenum mineralisation, but negligible gold,
- sulphide species are zoned from chalcopyrite-molybdenite-pyrite outwards through successive assemblages to distal galena and sphalerite with minor gold and silver in the propylitic zone,
- mineralisation is zoned from a barren core, surrounded by an ore shell that straddles the potassic/phyllic boundary, passing outwards into a pyrite halo and ultimately to a low pyrite shell,
- sulphides and oxides are also zoned vertically, with magnetite increasing at the expense of pyrite at deeper levels,
- sulphide-occurrence is also zoned, from a disseminated + microveinlet core, to predominatly disseminated plus lesser veinlet mineralisation in the ore shell, predominantly veinlet plus lesser disseminated sulphides in the pyrite shell, and veinlets only in the outer zone.

Guilbert and Lowell (1974) elaborate on the “typical” porphyry copper deposit from southwestern North America, which can be considered the type area for the quartz-monzonite model, before discussing variations on the theme and the geological causes of these variations. The typical features are:

- the deposit is hosted by a quartz-monzonite porphyry stock of elongate-irregular form, controlled by regional-scale faulting, intruding sediments and metasediments,
- the stock has approximate outcrop dimensions of 1200 m × 1800 m,
- the host stock is progressively differentiated from quartz diorite to quartz monzonite,
- the orebody is oval to pipelike, with plan dimensions of ~ 1000 m × 1800 m and gradational boundaries,
- 70% of the 140 Mt of ore occurs in the igneous host rocks, 30% in the country rocks,
- metal values include 0.45% hypogene Cu, 0.015% Mo and 0.35% supergene Cu, and
- visible alteration extends ~ 800 m beyond the ore zone.

Diorite Porphyry Copper Model

- In the diorite model the phyllic and argillic zones are absent and the propylitic zone may adjoin the core potassic zone.
- The potassic core contains orthoclase-biotite, orthoclase-chlorite, or sometimes is biotite-rich, with little orthoclase.

- The place of the phyllic zone is taken by chlorite-rich alteration.
- Sulphides are less developed in the diorite model and lower pyrite contents in the altered host rocks allow some of their magnetite to survive alteration.
- Copper sulphides, commonly with high gold content occur in the potassic zone as disseminations and fracture-fillings and may extend into the adjacent propylitic zone.
- Mo/Cu ratios are low compared to quartz-monzonite types.
- The diorite model is applicable usually to syenite-monzonite porphyries associated with diorites and often contain gold, as well as copper, but no economic molybdenum mineralisation.
- Mineralised veins are quartz-poor and sometimes quartz-free.

It is evident from these criteria that the quartz-alkalic class of porphyry copper deposits generally conform to the diorite model, rather than the quartz-monzonite model.

Oxidised Gold-rich Porphyry Copper Model

Sillitoe (1979, 1990, 1993c, 1996) noted that Au-rich (> 0.4 g/t) porphyry copper systems are usually associated with oxidised, magnetic felsic intrusions and have magnetite-rich ± hematite potassic zones. These deposits often fit the diorite model, rather than the quartz-monzonite model.

At the Island Copper Cu-Au-Mo deposit the early magnetite alteration halo extends from the mineralising dacitic quartz-feldspar porphyry intrusion, which belongs to the low-K calc-alkaline clan, into the predominantly basaltic country rocks to distances of 500-700 m. The main-stage potassic alteration, with chalcopyrite-pyrite stockworks, overprints the early magnetite-amphibole-plagioclase halo and forms an annular zone, approximately 100-150 m in width (Arancibia and Clark, 1996). The ore zone has been interpreted as associated with biotite-magnetite alteration (Perello *et al*., 1996), but Arancibia and Clark (1996) argue that this zone represents a conflation of sulphide-poor, magnetite-amphibole-plagioclase and later chalcopyrite-rich biotite-(K-feldspar) alterations.

Other intrusions and zones of phyllic, intermediate argillic and advanced argillic alteration occur outside the mine area, along or parallel to the major WNW-trending structure that controlled emplacement of the QFP intrusions and the mineralisation.

The magnetite-rich alteration, which is estimated to contain ~ 85% of the total alteration magnetite in the deposit, passes outwards into chlorite-dominated and then epidote-dominated propylitic subfacies, which probably are penecontemporaneous with the magnetite-amphibole-plagioclase alteration and, to a lesser extent the slightly later potassic alteration.

Early magnetite-rich and main stage magnetite-bearing alteration are locally overprinted by magnetite-destructive hydrolytic alterations of varying intensity. These stages were followed by sericite-clay-chlorite (intermediate argillic) alteration, which partially hematised magnetite. This SCC alteration, which affected substantial portions of the upper and central portions of the porphyry system, persisted throughout the remaining evolution of the alteration system, punctuated by episodes of more acid alteration. Subsequent fracture-controlled phyllic (quartz-sericite-pyrite) alteration is concentrated in the porphyries and

contiguous volcanic wall rocks. Late stage advanced argillic alteration is confined to upper levels, affecting breccia zones and adjoining QFP and volcanic rocks. The terminal phase of hydrothermal activity corresponds to carbonate (ankerite-calcite) and carbonate ± zeolite veins.

The overall magnetite distribution at Island Copper is zoned across strike from a heterogeneous, but relatively magnetite-poor core, surrounded by a wide magnetite-rich zone, passing outwards into slightly magnetite-depleted volcanics and ultimately to background (moderate) magnetite levels in the volcanics. A substantial aeromagnetic anomaly, up to 4200 nT in amplitude, extending 6 km along strike and 1.5 km across strike, shows that the magnetite-rich alteration extends well beyond the mine area.

Clark and Arancibia (1996) suggest that the early magnetite-amphibole-plagioclase alteration at Island Copper is much more common than realised hitherto. They state: "...in most magnetite-rich porphyry systems for which adequate petrographic documentation exists, much of the magnetite was deposited prior to the development of the sulphide ores, although some later vein systems may contain unusual amounts of magnetite" and argue that other examples include Panguna (P.N.G.), Tanamá (Puerto Rico), Park Premier (Utah), Bajo de la Alumbrera (Argentina), some deposits from the central Andes and many Phillipine deposits. Ylöjärvi (Finland) and other Svecofennide Cu-Au deposits exhibit alteration with similar features.

Although best-developed in mafic wall rocks, high protolith Fe contents are not a prerequisite for development of magnetite-rich alteration, provided there is substantial Fe-metasomatism. At Island Copper, felsic dacite porphyry as well as mafic volcanics exhibit the magnetite-rich alteration. The enrichment in both total iron and magnetite in this class of gold-rich porpyry copper deposits reflects processes inherent in the calc-alkaline magmatic source and in the mechanism of extraction of Cu, Au and S from the magmas. Clark and Arancibia (1995) suggest that this style of alteration is produced by highly oxidised, low sulphur magmas.

Skarn Zonation around Porphyry Copper Systems

Einaudi (1982a) describes the general zonation of calcic skarns developed within limestone around oxidised porphyry copper intrusions. Overall magnetite contents of these calcic skarns range from trace amounts to 10% by volume, accompanied by 2-15% sulphides. A proximal garnet zone with pyrite > chalcopyrite passes outwards into a garnet-pyroxene zone with py ≈ cp, thence into garnet-wollastonite with bornite and chalcopyrite (±sphalerite), and finally into marble with sph, cp and minor pyrite. Magnetite ± hematite is concentrated near the intrusive contact, in the garnet-rich zone, and also near the marble contact. It is scarce within the wollastonite zone. Pyrrhotite may occur in the distal zones.

Magnesian (forsterite-talc-serpentine) skarns developed within dolomitic rocks, on the other hand, have lower sulphide contents (< 6%) and more abundant magnetite (20-35%), which is distributed throughout the zone of skarn alteration.

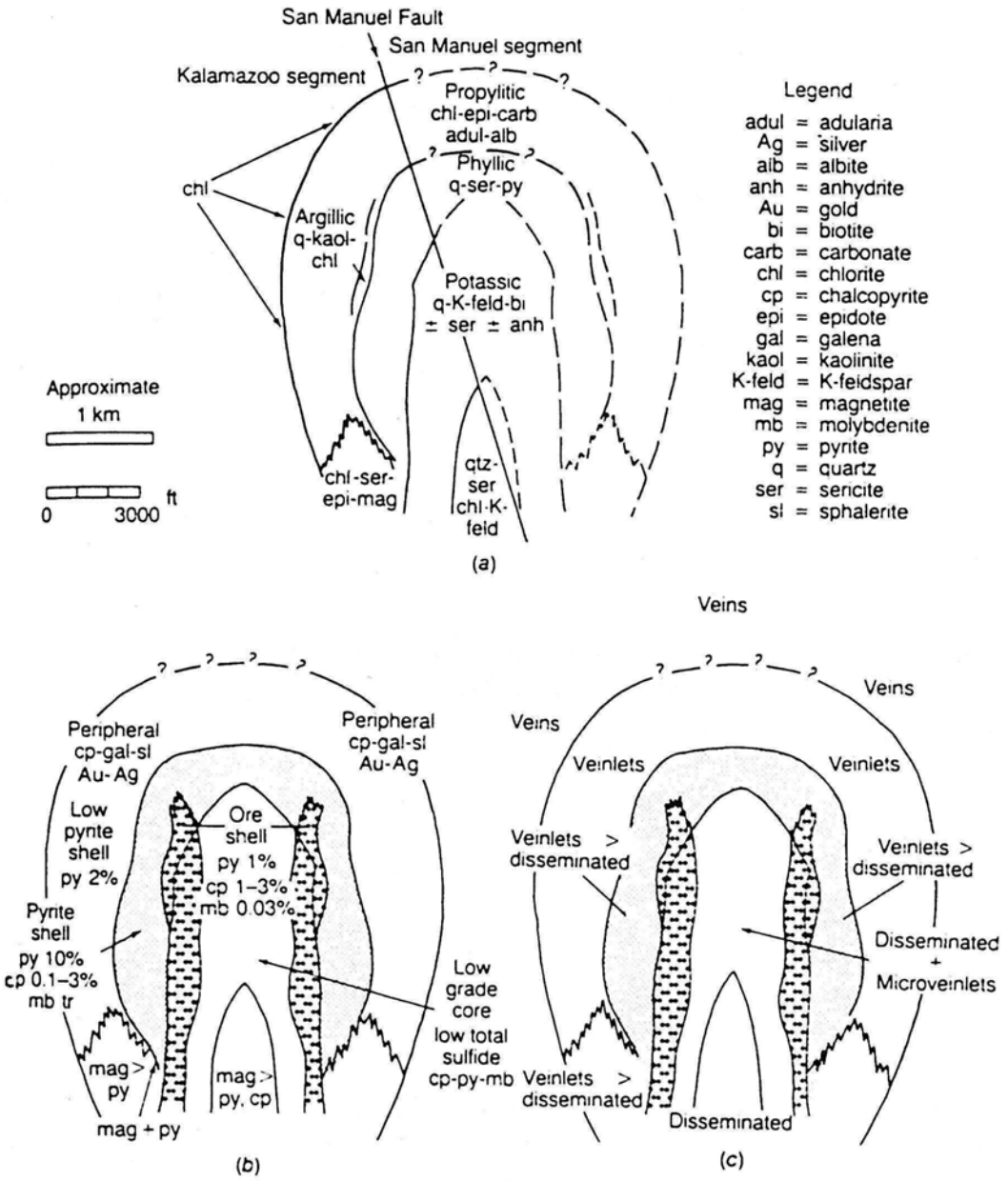

Fig.5.6. Zoning in a typical porphyry copper deposit (Guilbert and Park,1986; modified from Lowell and Guilbert (1970) and Guilbert and Lowell (1974)).

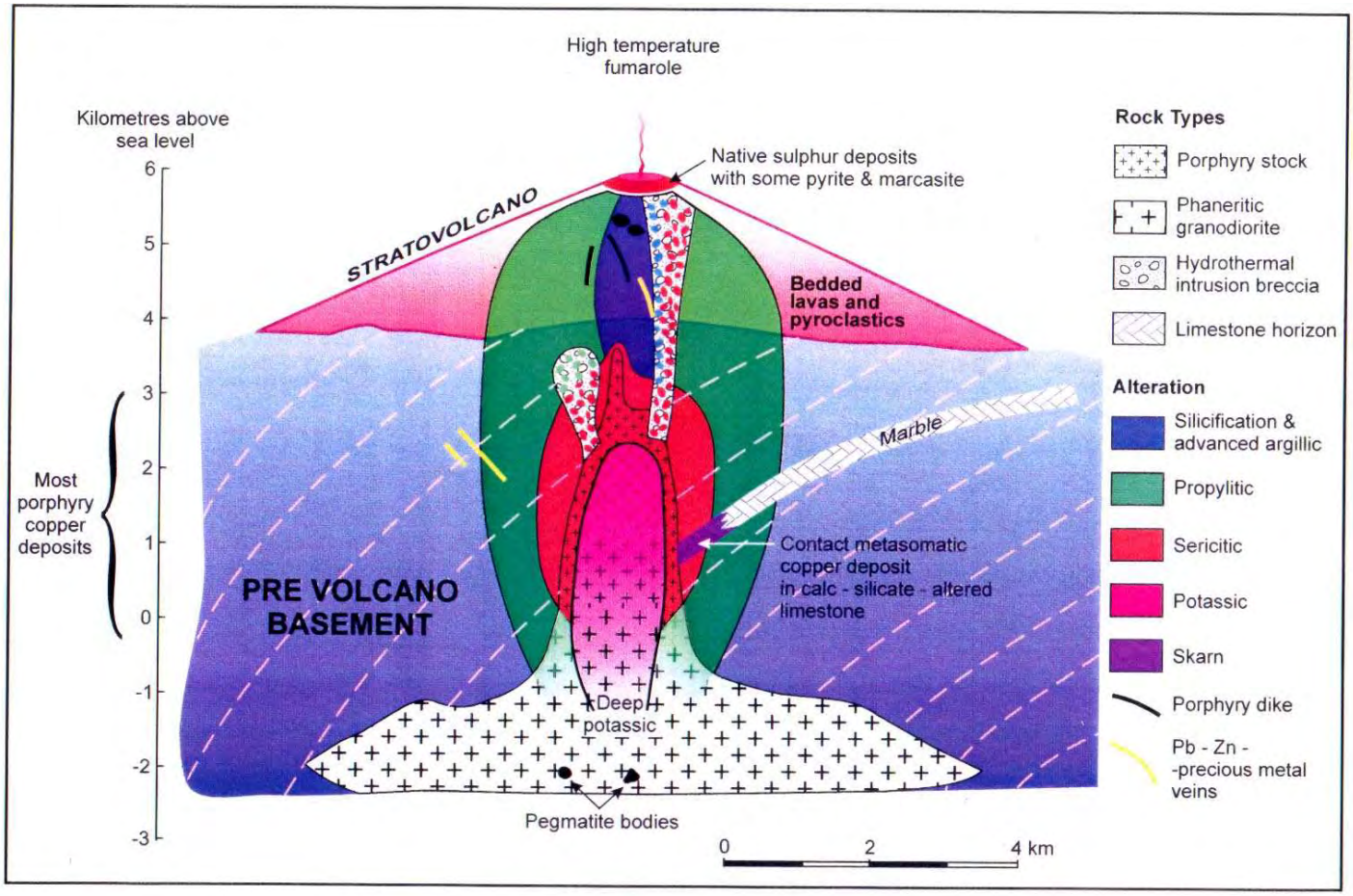

Idealised cross-section of porphyry copper system.

Fig.5.7. Idealised cross-section of a porphyry copper system (after Sillitoe, 1973a).

Deep Zones of Porphyry Systems

A number of authors have discussed zoning patterns at deep levels of, and beneath, porphyry copper systems (Lowell and Guilbert, 1970; Sillitoe, 1973; Yang and Bodnar, 1994; Gustafson and Quiroga, 1995). Sillitoe (1973) concluded that porphyry systems have vertical extensions of up to 8 km (see Fig.5.7). The reported data suggest a general tendency for magnetite to increase and sulphides to decrease at depth. The phyllic zone does not persist to great depths. Pyrrhotite may appear in the deeper portions of phyllic zones. Albite increases with respect to K-feldspar at greater depths. Sodic-calcic alteration is reported at great palaeodepths in the tilted porphyry systems of the Yerington district (Carten, 1986; Dilles and Einaudi, 1992).

Yang and Bodnar (1994) described phaneritic granites with anomalous, but subeconomic Cu, interpreted to have been emplaced at 10 km depths, beneath possible porphyry copper deposits that have since been removed by erosion. Saturation of the magmas with water occurred too late in the crystallisation history of these intrusions to form economic mineralisation, firstly by failing to concentrate copper sufficiently into the exsolving fluid and secondly failing to generate sufficent fracturing at the high ambient pressures.

"Inside-out" Alteration Zoning

Cheney and Trammell (1996) propose that batholithic copper deposits, such as the Quartz Creek (Washington) prospect, exhibit "inside-out" zoning with respect to the Lowell-Guilbert model (see Fig.5.8). These deposits are characterised by a batholithic setting and a lack of porphyritic rocks. The biotitic alteration zone in this style of deposit grades outwards into unaltered rock, but contains localised sericitic and chloritic alteration zones in its interior, centred on breccia pipes. The outer biotitic alteration generally has less than 1% sulphides and is accompanied by magnetite, but the inner biotitic zone contains more sulphides (py + po + cp + mb) and less magnetite. A zone of chloritic alteration (chlorite plus minor epidote replacing biotite) occurs between the biotite zone and the phyllic (quartz-sericite-pyrite) core. This QSP core hosts most of the high grade mineralisation, which occurs as lenses of massive pyrrhotite-chalcopyrite-pyrite.

Central phyllic zones overprinting broader potassic halos are also found in porphyry copper-gold systems, such as the E26N and E48 deposits at Goonumbla , NSW (Harris and Golding, 2001). This pattern is more consistent with the diorite model and is quite common in alkalic porphyry copper deposits. The Panguna deposit (Bougainville, PNG) also has phyllic alteration due to magmatic fluids and exhibits this zoning pattern. The Waruwari (Porgera) porphyry gold deposit in PNG has magmatic-derived Au mineralisation associated with base metal sulphides and phyllic alteration. At the present surface this phyllic alteration is surrounded by propylitic alteration, but deep drilling and geophysical evidence suggests that at depth there is a substantial zone of typical porphyry-style potassic alteration around the mineralised phyllic zone. The breccia-pipe hosted, porphyry-related gold deposits at Mount Leyshon and Kidston (Queensland) both exhibit extensive phyllic alteration in the central pipe, with major (Mount Leyshon) to minor (Kidston) potassic alteration developed in wall rocks. The phyllic alteration is later than the potassic alteration, but the time lag is small. A common theme in all these cases is that the phyllic alteration is associated predominantly with magmatic, rather than meteoric, fluids. It is plausible that phyllic overprinting associated with

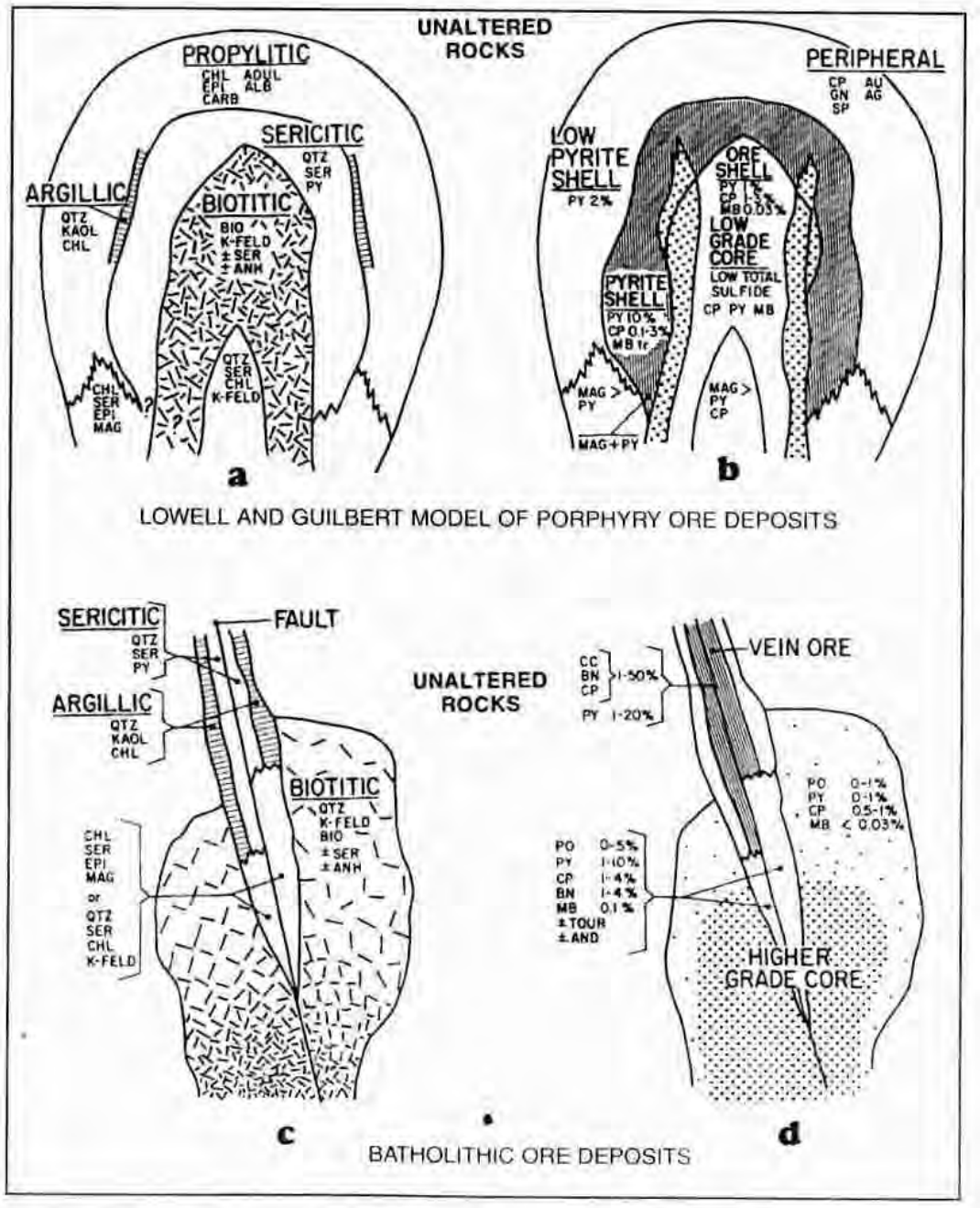

Fig.5.8. Comparison of Lowell-Guilbert model and Batholithic model with inside-out alteration zoning (Cheney and Trammell, 1996).

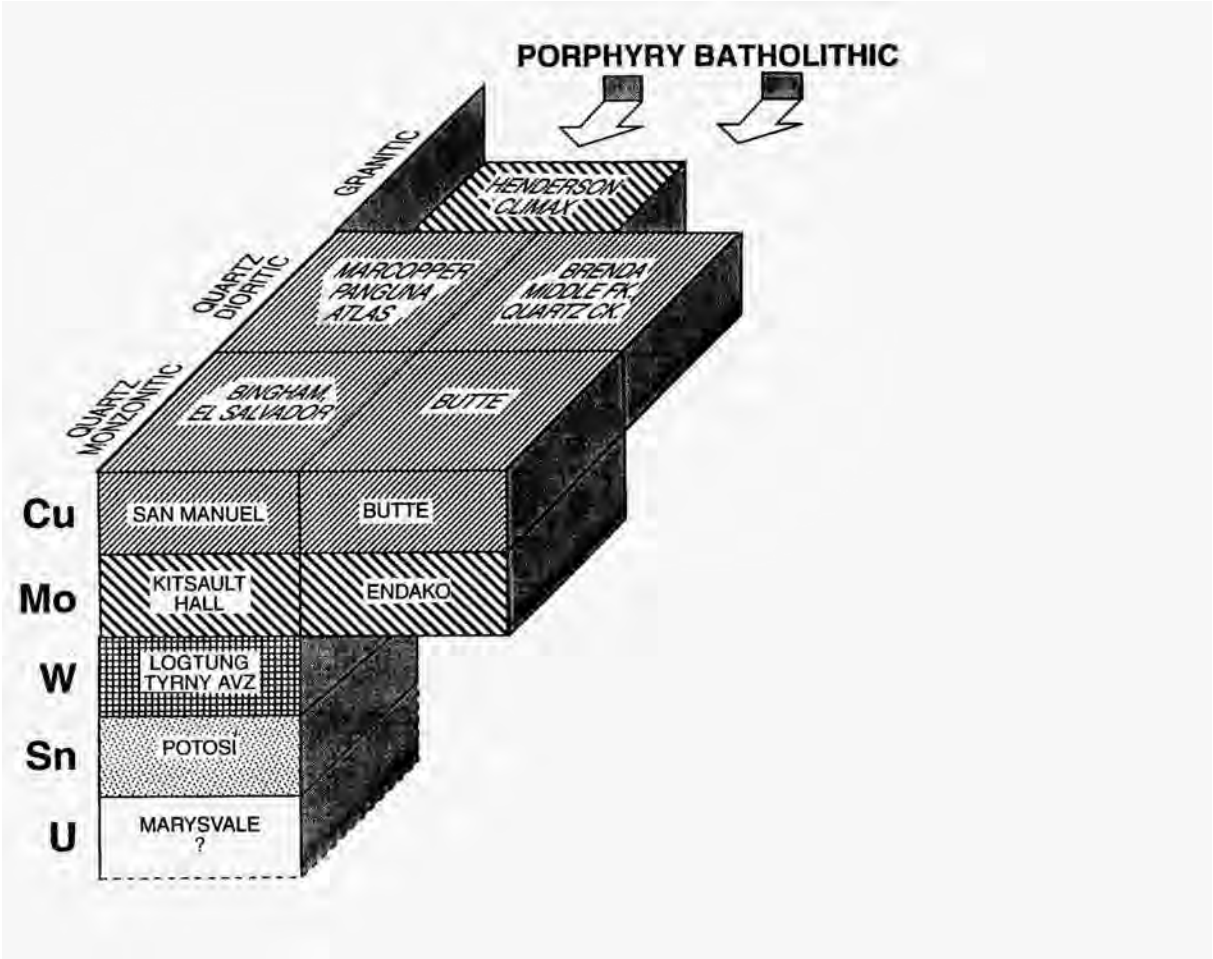

Fig.5.9. Classification of intrusive-related deposits into porphyry and batholithic classes (Cheney and Trammell, 1996).

evolving lower temperature magmatic fluids will tend to follow the conduits used by the early fluids associated with potassic alteration and overprint the potassic zone from the inside out, with intense overprinting restricted to the central zone and a substantial annular region of potassic alteration surviving.

Cheney and Trammell (1996) propose that the inside-out zoning of batholithic deposits represents restricted, structurally controlled, access of meteoric fluids at the emplacement depths of these deposits. Ingress of meteoric fluids into batholiths may be limited to major, discrete structures, such as breccia pipes (e.g. Quartz Creek) or faults (e.g. Butte, Montana). However, the possibility remains that some or all of the phyllic alteration in many batholithic deposits may be associated with magmatic fluids and the zoning pattern has a similar origin to that in the gold-rich porphyry deposits and the breccia-pipe hosted porphyry-related gold deposits mentioned above. Figure 5.9 shows the classification of various intrusive-related deposits into porphyry and batholithic classes, after Cheney and Trammell (1996).

Departures from Idealised Models - Geological Causes

Guilbert and Lowell (1974) discuss deviations from the standard quartz-monzonite model and the geological causes of these variations. These geological factors include:

- depth of exposure,
- composition of pre-mineral wall rocks,
- pre-ore structural controls on mineralisation,
- variations in composition of both igneous host rock and mineralising fluids,
- size of the mineralising system,
- variations in development of contemporaneous controls on mineralisation (veinlets, veins and brecciation, and
- the breadth of stability fields of important silicate alteration minerals such as sericite and K-feldspar.

“These factors all affect the size, shape, mineralogy, symmetry, intensiveness and extensiveness of porphyry copper alteration-mineralisation.” However they conclude that: “ ... variations are generally predictable on the basis of local geological variables”.

Gustafson (1978) pointed out that evolution of geological factors through time exerts critical influences on the observed features of porphyry deposits and that most descriptions and idealised models do not consider timing relationships sufficiently.

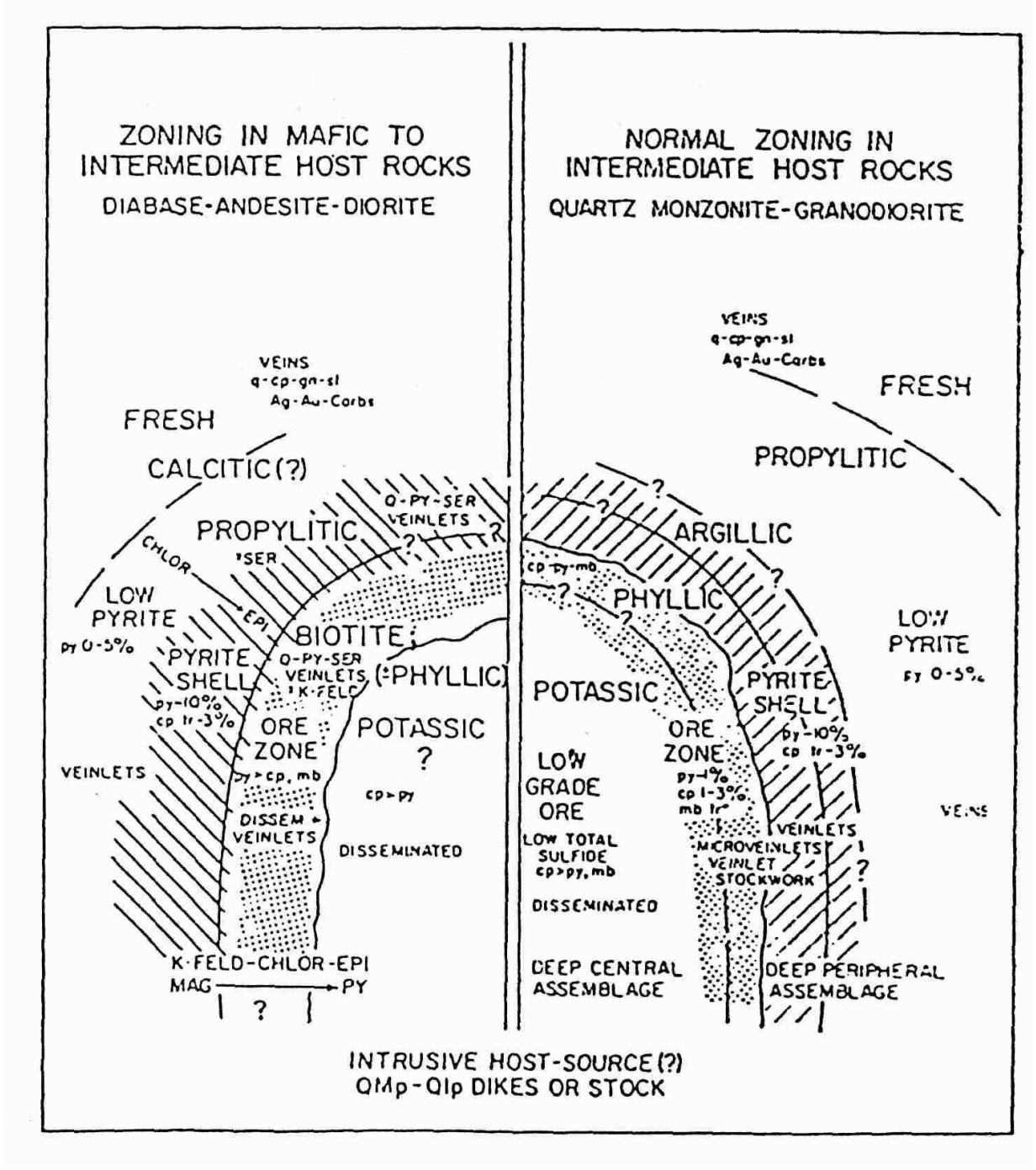

Fig.5.10 Comparison of porphryry-associated alteration assemblages in mafic host rocks versus quartz monzonitic - granodioritic host rocks

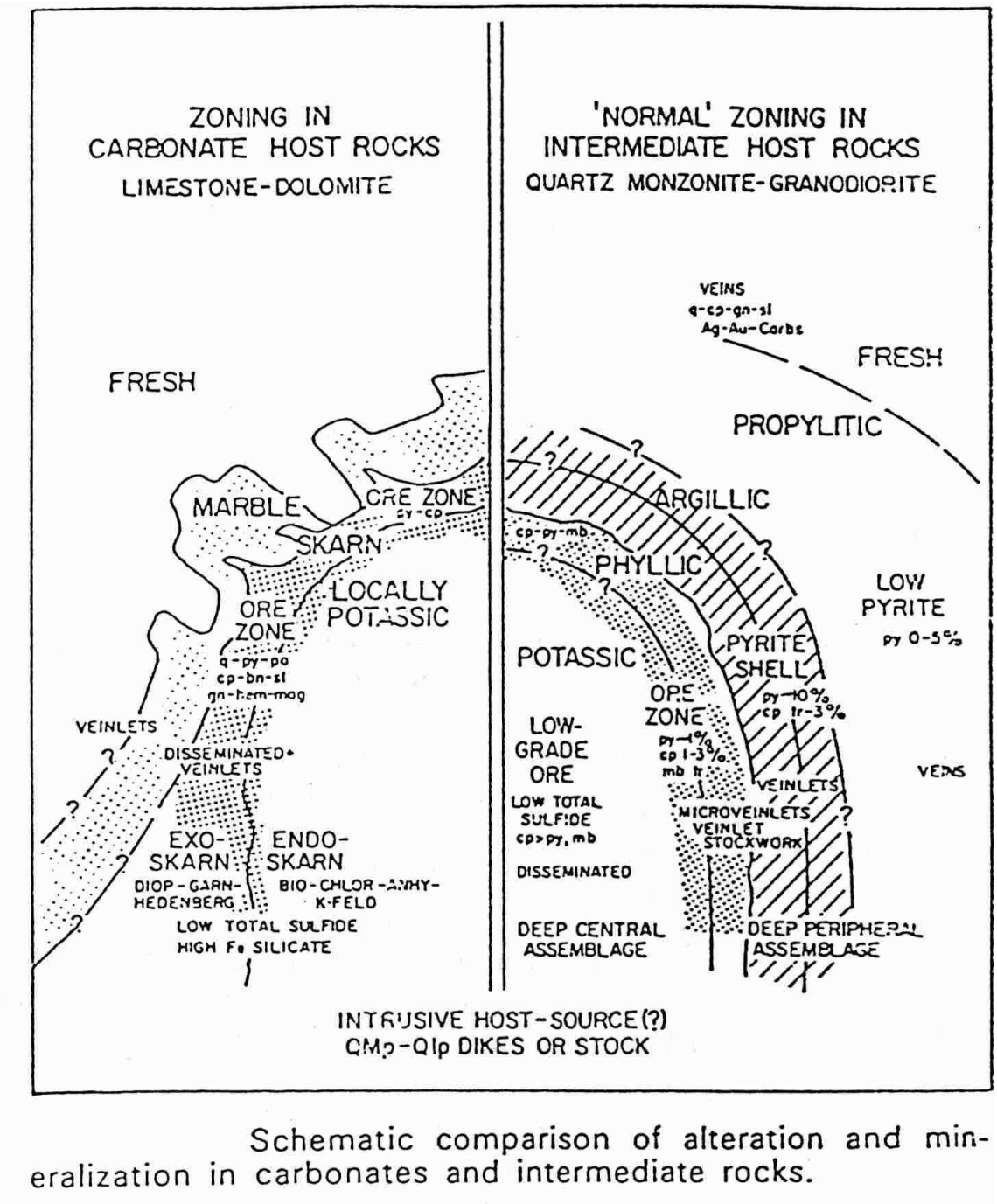

Schematic comparison of alteration and mineralization in carbonates and intermediate rocks.

Fig.5.11 Comparison of porphryry-associated alteration assemblages in carbonate host rocks versus quartz monzonitic - granodioritic host rocks

Effects of Protolith Composition

Beane (1994) showed differences in alteration assemblages as a function of protolith composition, which are summarised in Table 5-3 below,

TABLE 5-3. PORPHYRY COPPERS: EQUIVALENT ALTERATION STAGES/ DIFFERING HOST ROCKS

Stage	Quartz Monzonite	Diorite	Limestone
Early	K-feldspar + biotite + pyrite + magnetite or hematite	Biotite + KF + albite + epidote + magnetite	Garnet + pyroxene
Copper mineralisation	KF + chlorite + sericite + pyrite ± hematite	Chlorite + epidote + pyrite + magnetite	Actinolite + epidote + pyrite + magnetite
Late	Sericite + pyrite	Chlorite + anhydrite + pyrite + hematite + ?zeolite	Quartz + pyrite

Arkosic sedimentary rocks develop potassic, phyllic and propylitic alteration assemblages that resemble those developed in granitic wall rocks, although they may less perfectly developed, possibly due to the planar fabric (Guilbert and Lowell, 1974). On the other hand, quartzites are relatively poor indicators of alteration zoning, because quartz is essentially non-reactive. Mafic and intermediate igneous rocks contain high Mg, Fe and moderate calcium. Where these are the dominant wall rocks, wide zones of propylitic alteration are favoured, potassic alteration is dominated by biotite and biotite and chlorite tend to proxy for sericite in intervening zones, reducing or eliminating the phyllic zone.

The most spectacular difference in alteration zoning occurs with carbonate wall rocks, which are highly reactive and acid-neutralising. Skarn assemblages produced by alteration of carbonates are discussed above. Figures 5.10-5.11 illustrate the differences in alteration assemblages for mafic, intermediate and carbonate host rocks around mineralised porphryries.

Effects of Pre-ore Structures

Pre-existing structural grain and major structures clearly influence the shapes of both host intrusions and ore zones in many deposits. Local ore-controlling structures are more likely to be obliterated by magmatic-hydrothermal events than regional structures, particularly if the intrusions are large.

Fluid Chemistry and Volume

Acid-generating volatile phases, such as HCl, CO_2 and SO_2, clearly influence alteration assemblages and mineral deposition. These phases donate the radicals that form many accessory alteration minerals and form complexes with metal ions. Oxygen and sulphur fugacities exert an important control on the oxide, sulphide and silicate phases (e.g. Mg/Fe of biotite, chlorite and amphibole) deposited by the fluid. Large fluid volumes are required to generate large orebodies of adequate grade.

Scale of Intrusive-related System

Larger porphyry systems usually produce more regular and better developed alteration/mineralisation zoning. Small deposits, even of ore grade, tend to be associated with less regular alteration effects.

5.9 Other Intrusive-related Mineralisation

Wyborn (1988) and Wyborn and Stuart-Smith (1993) have described an important class of Australian Proterozoic granite-related deposits. These deposits all occur outside the granite, up to 5 km from the contact. The Proterozoic granitoids were emplaced at ~1800 Ma and belong to the I-granodiorite type, as they are derived from older (~2400 Ma) felsic granitoids. The earliest (~1860 Ma) granitoids belong to the restite-dominated Group I and are never mineralised. Between 1840 Ma and 1800 Ma, Group II granitoids, derived from fusion of biotite-bearing source rocks, were emplaced. The Group II granitoids are associated with Au mineralisation. Group III granitoids, derived from fusion of hornblende-bearing rocks, were emplaced last, beginning with Group III_1 A-type, F-rich granites associated with Sn and Mo mineralisation. Fluorine encourages incorporation of base metals into silicates. The youngest granitoids are Group III_3 granitoids, which are the highest temperature, most oxidised granitoids and are associated with Cu-Au mineralisation.

The Cullen Mineral Field (Northern Territory) affords an example of this type granite-related mineralisation. There is strong evidence of Proterozoic granite-related origin for ironstone-hosted Cu-Au deposits, such as Starra (Selwyn), Osborne and Ernest Henry in the Eastern Mount Isa Inlier, which are related to the Williams and Naraku Batholiths (Wyborn and Heinrich, 1993a,b) and appear to have affinities with the Olympic Dam class of Cu-Au-REE-U deposit (Wall and Gow, 1995).

5.10 Reduced intrusion-related Au and reduced porphyry Cu-Au deposits

In recent years the existence of a distinct association of Au and Cu-Au deposits related to relatively reduced intrusions has been recognised. This relationship is contrary to the general association of porphyry copper and Cu-Au deposits with oxidised intrusions. Thompson et al. (1999) and Lang and Baker (2001) nominate Fort Knox and other deposits in Alaska and the Yukon, Mokrsko (Czech Republic), Salave (Spain), Vasilkovskoe (Kazakhstan), Timbarra (NSW), Kori Kollo (Bolivia) and Kidston (Queensland) as examples of intrusion-related gold deposits associated with relatively reduced intrusions, often in Sn-W belts. The genetically associated plutons often straddle the ilmenite-series/magnetite-series boundary. Note, however, that AMIRA P425 established that Kidston is related to oxidised magmas that

generated the Lochaber granite and associated rocks, so that this deposit does not in fact fit into the reduced intrusion-related category.

The characteristics of intrusion-related gold deposits are (Thompson et al. (1999); Lang and Baker (2001)):

- metaluminous (I-type), subalkalic intrusions of intermediate to felsic composition that lie near the magnetite-series/ilmenite-series boundary
- carbonic hydrothermal fluids
- a metal assemblage that variably combines Au with elevated Bi, W, As, Mo, Te and/or Sb and low concentrations of base metals
- a low sulphide mineral content, mostly < 5% with a reduced ore assemblage that typically contains arsenopyrite, pyrrhotite, and pyrite, without magnetite or hematite
- areally restricted, commonly weak hydrothermal alteration, except in the shallowest systems
- a tectonic setting well inboard of convergent plate boundaries, where continental magmatism commonly contains intrusions of alkalic, metaluminous calc-alkalic, and peraluminous (e.g. S-type) compositions
- a location in magmatic provinces associated with W and/or Sn deposits
- intrusion-hosted Au deposits are most commonly of sheeted vein/veinlet type, although greisen-like, disseminated and breccia deposits also may occur
- Au may also be concentrated distally (1-3 km) with respect to the intrusions as skarn, disseminated replacement or vein types
- K feldspar, albite and/or sericitic alteration assemblages, commonly including carbonate, accompany the Au mineralisation.

Approximate synonyms for this type of deposit include “porphyry gold deposits” (Hollister, 1992; Bakke, 1995), “intrusion-related stockwork-disseminated deposits” (Sillitoe, 1991), “plutonic-related gold deposits” (Newberry et al., 1988; McCoy et al., 1997). These types of deposit explain the correlation between intrusive-related gold mineralisation and reduced intrusions in certain provinces that was reported by Keith and Swan (1987) and Leveille *et al*. (1988).

Rowins (1999, 2000) has also promoted a new class of deposit, “reduced porphyry Cu-Au type”, which appear to closely resemble the intrusion-related Au category described above. The characteristics of the reduced porphyries include:

- pyrrhotite-rich hypogene ore assemblages (massive pyrrhotite veins very common)
- no primary magnetite, hematite or sulphate minerals (e.g. anhydrite)
- ore fluids commonly CO_2-bearing, with a significant CH_4 component
- mineralisation associated with ilmenite-bearing, reduced I-type granitoids
- relatively low grades of Cu and Au in potassic and/or phyllic zones are common
- genesis of these deposits is attributed to the potential for reduced ore fluids in a “boiling” porphyry environment to transport large quantities of Au and, to a lesser extent Cu, as reduced S complexes, largely in a vapour phase, to distal sites relative to the causative porphyry
- mineralisation in this peripheral environment may take several forms, including structurally controlled, sheeted sulphide veins in hornfels and sulphide replacement bodies (mantos) in calcareous metasedimentary rocks

The result of this genesis is a low grade Cu-Au core, which gives the impression of a "failed" porphyry system and may discourage further exploration. Accordingly, the search for higher grades should concentrtae on distal sites that are favourable for focussing and precipitating Au- and Cu-rich vapours. Rowins (1999, 2000) suggests that Seventeen Mile Hill (Telfer District, Western Australia), Boddington (Western Australia), San Anton (Mexico), Copper Canyon (Nevada), Madeleine Cu deposit (Quebec) and some hitherto enigmatic deposits in Alaska and British Columbia. It should be noted that the mineralisation at Boddington has been dated recently and found to be substantially younger than the intrusion, thereby negating the inclusion of Boddington in this class of deposit. The San Jorge Porphyry Copper deposit (Argentina) is another example of this class of deposit (Williams et al., 1999).

Clearly, the magnetic signatures of this type of deposit should differ substantially from those of the classical oxidised porphyry copper clan. For example magnetic highs at San Jorge are associated with distal pyrrhotite-bearing mineralisation that is also conductive and chargeable, but not with the associated reduced intrusion (Williams et al., 1999; W.Williams, pers. Comm., 2002).

5.11 Volcanic-hosted Epithermal Au Mineralisation

Volcanic-hosted epithermal gold deposits form at shallow depths (1-2 km) and relatively low temperatures (<150°C to ~300°C) in volcano-plutonic arcs associated with subduction zones. Two end-member deposit styles occur: high-sulphidation (acid-sulphate) deposits hosted by leached silicic rock associated with oxidised acidic fluids and low sulphidation (adularia-sericite) deposits associated with reduced, neutral pH fluids. The terms "high- sulphidation" and "low-sulphidation" refer to the chemical activity of sulphur, expressed as $f(S_2)$ and do not simply reflect the sulphur content of the magma or fluid, although high-sulphidation mineralisation tends to have higher overall sulphur content than low-sulphidation mineralisation. The high-sulphidation state is characterised by oxidised sulphur species (S^{4+} and S^{6+}) and low-sulphidation by reduced sulphur species (S^{2-}), and can be identified by characteristic mineral assemblages (see Table 5-4). The fundamental division between high-sulphidation (HS) and low sulphidation (LS) types of volcanic-hosted epithermal gold deposit is discussed by many authors, including a thorough review by Heald *et al*. (1987) and extensive discussion in Corbett and Leach (1998). Some epithermal deposits are regarded as formed above related porphyry systems, as shown, for example, in the generic porphyry model in Fig.5.6 and in Fig.5.12. Einaudi (1994) has applied a sulphidation state classification to porphyry-related deposits (Table 5-6).

The general geological settings of the two types of deposit are illustrated in Fig.5.13-5.14. High-sulphidation systems are largely fluid-buffered, resulting from interaction of oxidised SO_2-rich magmatic vapours with meteoric waters. On the other hand, LS deposits are associated with geothermal waters that have largely equilibrated with country rocks, evolving to reduced (buffered by ferrous and ferric iron-bearing minerals), neutral pH conditions, analogous to the fluid evolution shown in Fig.5.4. Figures 5.12-5.14 put the two types of mineralising environment into geological context and Fig.5.15 plots the fluid evolution and conditions of formation of the two types of deposit.

The alteration types that occur in epithermal deposits are summarised in Table 5-5. Bonham (1988) has presented models for volcanic hosted epithermal deposits, including LS precious metal deposits related to granite/rhyolite magmatism, LS hot springs Au-Ag deposits, HS Nansatsu-type hot springs Au deposits and HS precious metal deposits related to granodiorite/dacite magmatism, and alkalic epithermal precious metal deposits, which are low sulphidation systems with distinctive mineralogy, genetically associated with alkaline igneous rocks. Figures 5.16-20 illustrate these models.

To our knowledge, no published descriptions of either HS or LS epithermal deposits report magnetite as part of the alteration assemblage or as a relict mineral. Furthermore, the conditions inferred for mineralisation and alteration in these deposits are incompatible with the existence of magnetite. Pyrrhotite, although a possible component of LS epithermal alteration systems is only occasionally reported and, if present, seems to be only a minor phase. The magnetic susceptibilities of the intensely altered central portions of epithermal systems are therefore very low.

Epithermal deposits exhibit a great variety of styles and geometries, reflecting varying influences of structural, hydrothermal and lithological factors on rock permeability. However, from the viewpoint of magnetic signatures the differences are much less significant. A near universal theme is intense magnetite-destructive alteration in the core of the system, surrounded by a relatively extensive zone of partial magnetite-destruction, grading into the background anomaly patterns of the unaltered host volcanics.

Table 5-4. S U LPH I D A T I O N S T A T E CHARACTERISTIC ASSEMBLAGES (Einaudi, 1994)

VERY LOW	LOW	INTERMEDIATE	HIGH	VERY HIGH
Löl + po + S_2 = asp	löl+ S_2=asp+As	po + S_2 = py mgt + S_2 = hem + py	ten + S_2 = enar cpy + py + S_2 = bor	Dig + S_2 = cov

SYSTEM	1	2	3	4	5	6	7
Fe-S	pyrrhotite (po)	pyrrhotite	pyrrhotite	pyrite (py)	pyrite	pyrite	pyrite, **S**
As-S	As	As	As	As	**realgar**, **orpiment**	**orpiment**, As-S glass	As-S glass
Fe-As-S	**löllingite+po, löllingite**	**löllingit,** arsenopyrite (asp)	arsenopyrite	aresenopyrit**py+asp, py+As**			
Cu-S	chalcocite	chalcocite	chalcocite, digenite	digenite	digenite	digenite	**covellite**
Cu-Fe-S	chalcopyrite (cpy) +pyrrhotite	chalcopyrite (cpy) +pyrrhotite	chalcopyrite +pyrrhotite	**chalcopy +pyrite**	**chalcopy +pyrite**	**bornite (bor)+py, digenite +pyrite**	**digenite +pyrite**
Cu-Fe-As-S	**löl+bor, löl + cpy**	**asp+cpy, löl+cpy**, asp+tennan	**asp+cpy,** asp + tennantite	asp+tennan, **asp+py**	enargite	enargite	enargite
Cu-Fe-S-O	magnetite (mgt) +bornite, mgt+cpy	mgt+bor, mgt+cpy	mgt+bor, mgt+cpy	mgt+bor, mgt+cpy, **mgt+py**	mgt+cpy, hematite (hm) +py	hem+py	hem+py
OTHER	Bi, Ag, Hg, Sb, **Sb+po**, galena(gal)+hematite	Bi, Ag, Hg, Sb, **Sb+po**, galena(gal)+hematite	Bi, Ag, Hg, Sb, bismuthinit, stibnite, gal+hem, argentite, berthierite	bismuthinit (bis), argentite, berthierite, cinnabar, stibnite(stb), gal+hem, stb+py	bis, arg, cin, stb, gal+hem, anglesite +py, stb+py, famatinite	bis, arg, cin, stb, stb+py, anglesite +py, famatinite	bis, arg, cin, stb, stb+py, anglsite+py, famatinite
mol% FeS in sphalerite coexisting with Fe-sulf	**>40**	**40-35**	**35-20**	**20-5**	**5-0.1**	**0.1-0.01**	**<0.01**

Table 5-5. Characteristic Mineral Assemblages of the Main Alteration Types in Epithermal Systems (Hedenquist et al., 1996; Bonham, 1988)

ALTERATION TYPE (synonym)	CHARACTERISTIC ASSEMBLAGE [stability of magnetite]
Advanced Argillic (high T)	Quartz, dickite, pyrophyllite, alunite (typical of HS epithermal systems, proximal to ore zones) [magnetite-destructive]
Advanced Argillic (low T)	Quartz, cristobalite, kaolinite, alunite (typical of steam-heated overprint of LS or HS epithermal systems) [magnetite-destructive]
Quartz-Sericite	Quartz-sericite-illite-pyrite (e.g. as halos around AA zones or below argillic alteration) [magnetite-destructive]
Silicification and residual silica	Quartz, rutile or anatase [magnetite-destructive]
Argillic (high T)	Quartz, illite, illite/smectite (e.g. peripheral to AA zone in HS deposits; adjacent to ore veins at depth in LS deposits) [magnetite-destructive]
Argillic (low T)	Quartz, cristobalite, smectite, kaolinite (e.g. peripheral to or above AA zone in HS deposits; adjacent to ore veins at shallow levels in LS deposits) [magnetite-destructive]
Propylitic (high T)	Albite, chlorite, epidote, calcite, pyrite (extensive envelopes around LS and HS epithermal systems and deeper associated intrusions) [partially magnetite-destructive]
Propylitic (low T)	Smectite, igneous plagioclase (extensive areas at shallow levels around LS and HS epithermal systems) [partially magnetite-destructive]
Ore (HS deposit) [*ore*, gangue] (a) = abundant, (m) = minor, (vm) = very minor, (±) = variable	*Pyrite(a)*, *enargite-luzonite* (±), quartz (a), *Au* (vm), *tellurides* (vm), *covellite* (m), *tennantite* (±), *tetrahedrite* (±), *chalcopyrite* (m), *sphalerite* (±), *galena* (±), barite (m), alunite (±), kaolinite (m), pyrophyllite (±), illite (m) [magnetite-destructive]
Ore (LS deposit) [*ore*, gangue] (a) = abundant, (m) = minor, (vm) = very minor, (±) = variable	*Pyrite(a)*, quartz (a), *Au* (vm), *electrum* (±), *tellurides* (vm), *chalcopyrite* (vm), *sphalerite* (±), *galena* (±), *arsenopyrite* (m), *tetrahedrite* (vm), *pyrargerite* (vm), chalcedony (±), adularia (±), calcite (±), illite (a), smectite (m) [magnetite-destructive]
Ore (LS alkalic deposit) [*ore*, gangue] (a) = abundant, (m) = minor, (vm) = very minor, (±) = variable	*Pyrite(a)*, quartz (a), *Au-Ag tellurides* (vm), *arsenopyrite* (±), *Mo-Cu-Zn-Pb sulphides* (m), fluorite (±), adularia (±), roscoelite (±), carbonate (±), hematite (±) [magnetite-destructive]

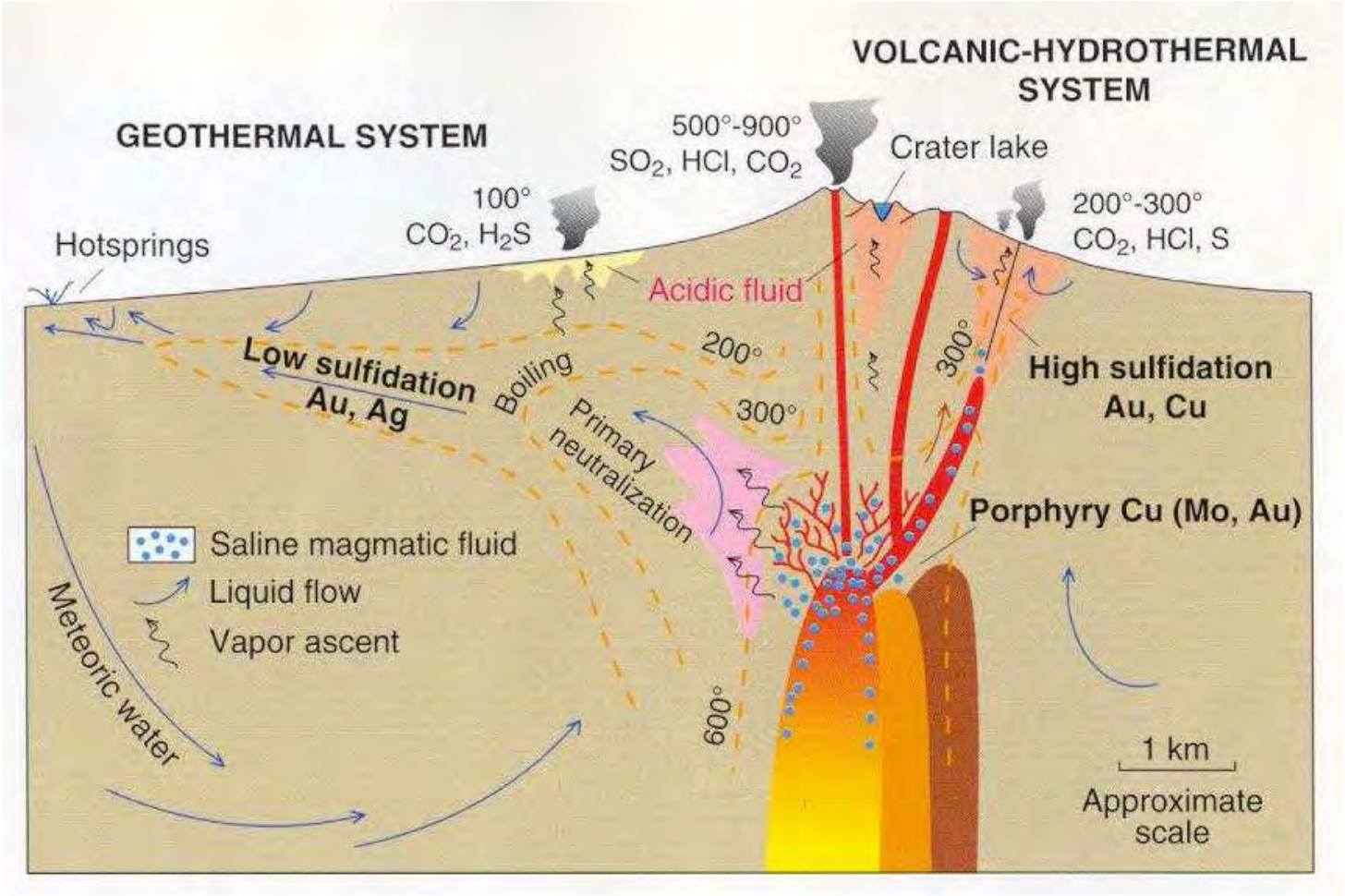

Fig.5.12. Generalised geological setting for HS epithermal, LS epithermal and related porphyry Cu (Mo, Au) deposits (Hedenquist et al., 1996).

Table 5-6. CHARACTERISTICS OF LOW- AND HIGH-SULFIDATION PORPHYRY-RELATED COPPER DEPOSITS (based on Einaudi, 1982)

Feature	**Low-sulfidation Disseminated Copper Deposits**	**High-sulfidation Lode Copper Deposits**
morphology of **plutonic rocks**	multiple stocks and dikes associated with small batholiths; post-ore dikes common.	small, isolated plugs and dikes; post-ore dikes absent
post-ore porphyry dikes	common	absent
igneous and hydrothermal **breccias**	not common and post-date ore	common and temporally associated with ore
ore textures	sulfides finely disseminated & in veinlets; conducive to bulk mining	sulfides are massive in open-space fillings in breccia matrices, veins; less conducive to bulk mining
metals	Mo common; average 0.35 to 1.0% Cu, 0.1 oz/t Ag, <0.03 oz/t Au; rarely contain significant Pb-Zn-Ag but, if present, only in limestone	Mo rare; average 2 to 6% Cu, 2-4 oz/t Ag, Au data incomplete but high Au present in some examples; contain major Pb-Zn-Ag in both igneous and sedimentary rocks
major **ore-mineral assemblages** in copper ore	bornite-chalcopyrite with or without magnetite, chalcopyrite with or without magnetite, chalcopyrite-pyrite; late hematite may be present	pyrite-enargite, pyrite-covellite, pyrite-digenite, pyrite-bornite, locally hematite is abundant
timing of **pyrite introduction** in copper ore	pyrite is late	pyrite is early
timing of **sphalerite introduction** in copper ore	sphalerite is uncommon in copper zone and is late relative to copper sulfides	sphalerite is common in copper zone, is early, and is replaced by copper sulfides (like Kuroko!)
lateral zoning of sulfidation state	zoned outward from low to high sulfidation states	zoned outward from very high to intermed and low sulfidation states
wall-rock alteration in copper zone of **quartz-feldspathic wall rocks**	potassic (biotite-orthoclase-anhydrite) with late sericitic (quartz-sericite-pyrite)	Advanced argillic (including acid sulfate) with peripheral sericitic and intermediate argillic
wall-rock alteration in copper zone of **carbonate wall rocks**	andradite-salite skarn locally retrograded to chlorite-clay-carbonate	silica-pyrite replacement bodies and breccias
"endmember" examples (note that tops of low-sulfidation districts may have been eroded, and bottoms of high-sulfidation districts may be at depth below present drilling	Twin Buttes, Christmas, Silver Bell, and Mission, Arizona; Santa Rita, New Mexico; Yerington and Copper Canyon, Nevada; El Salvador, Chile	Magma (Superior) and Bisbee, Arizona; Cerro de Pasco, Peru; Yauricocha, Peru; Tintic, Utah; Nena, Papua New Guinea
Examples dominated by low-intermediate sulfidation (diss'd) but with some high-sulfidation lodes	Ely, Nevada; Red Mountain, Arizona; Bingham, Utah; Cananea, Mexico	
Examples dominated by high-sulfidation lodes but with some low-intermediate disseminated ores		Butte, Montana; Chuquicamata and Collahuasi, Chile; Morococha, Peru; Lepanto, Philippines; Recsk, Hungary; Bor, Serbia

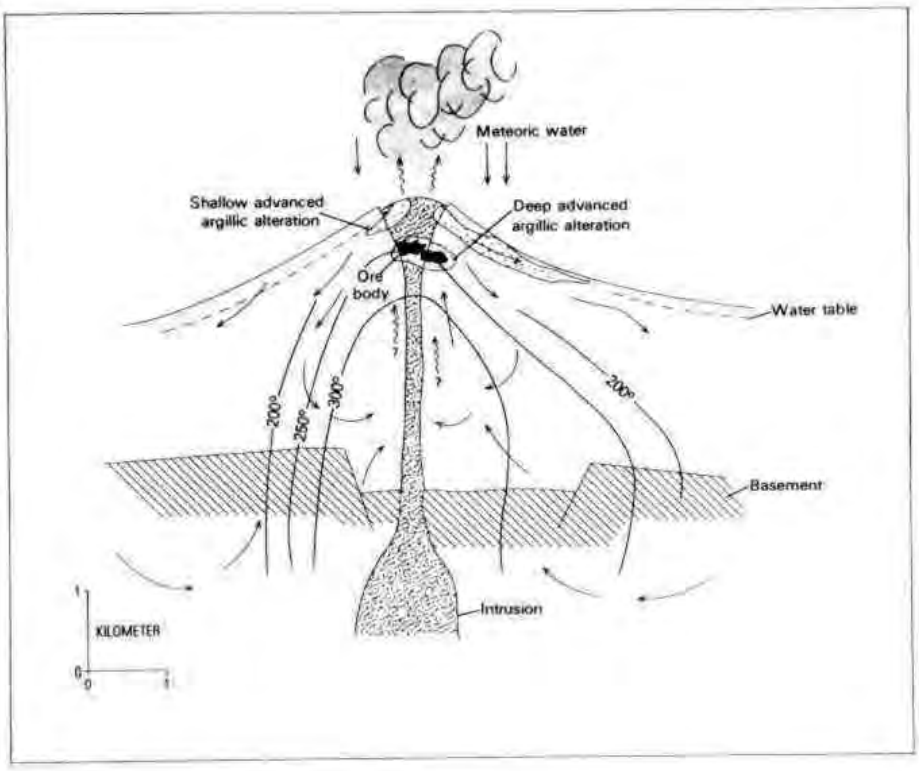

Fig.5.13. Geological setting of HS epithermal deposits

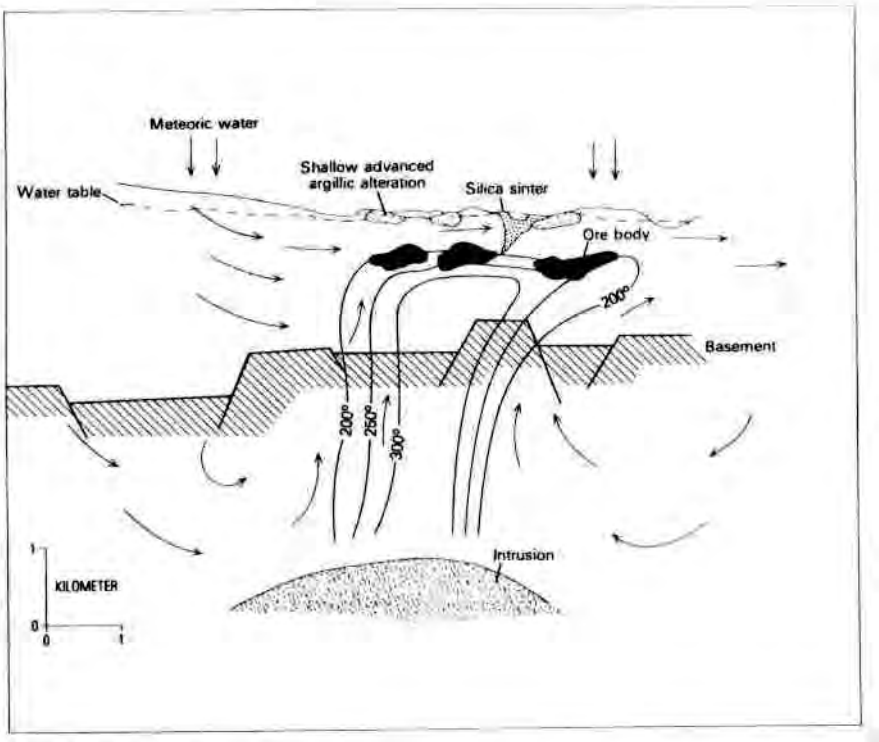

Fig.5.14. Geological setting of LS epithermal deposits

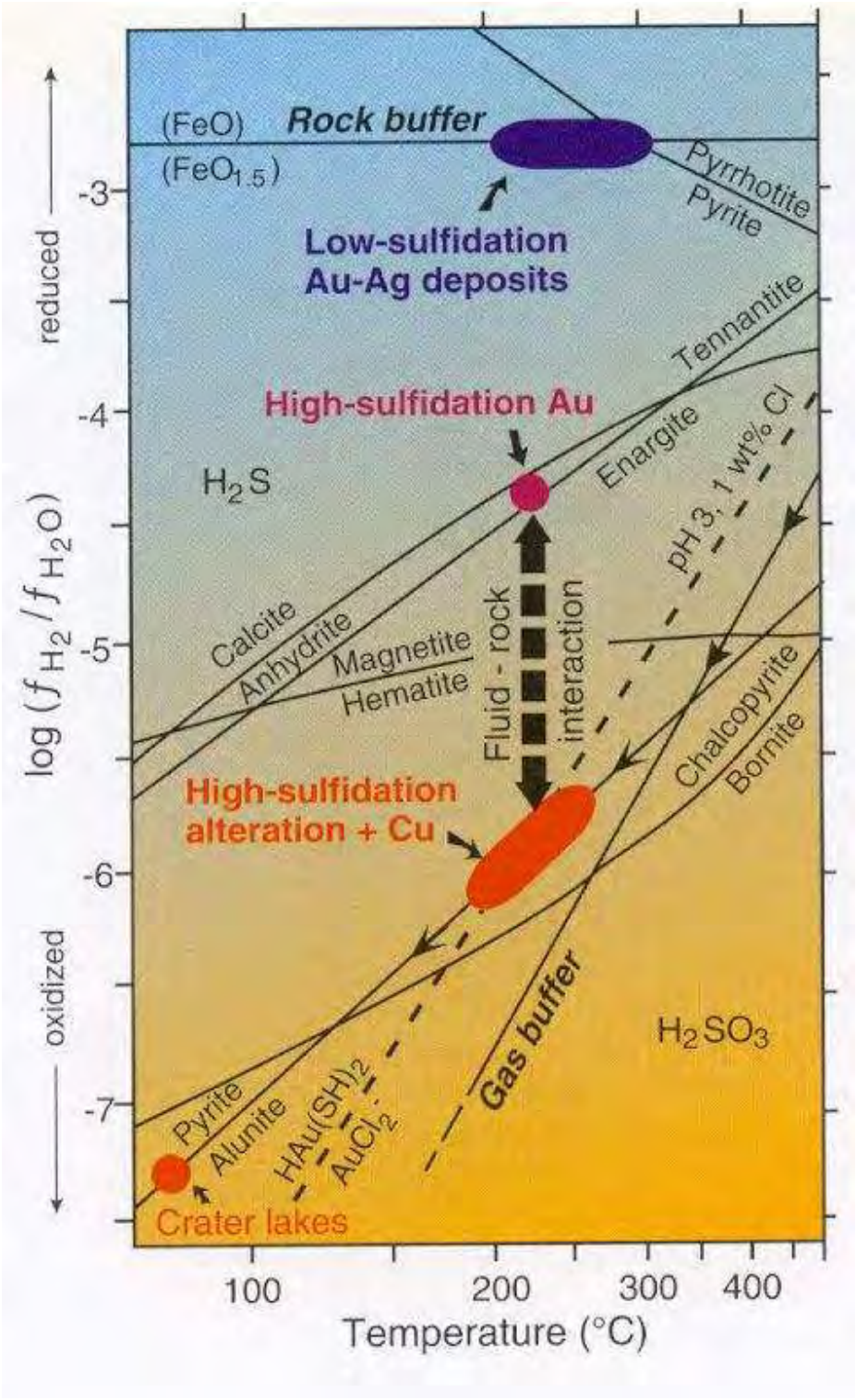

Fig.5.15 Fluid evolution and conditions of deposition for HS and LS epithermal systems (Hedenquist et al., 1996)

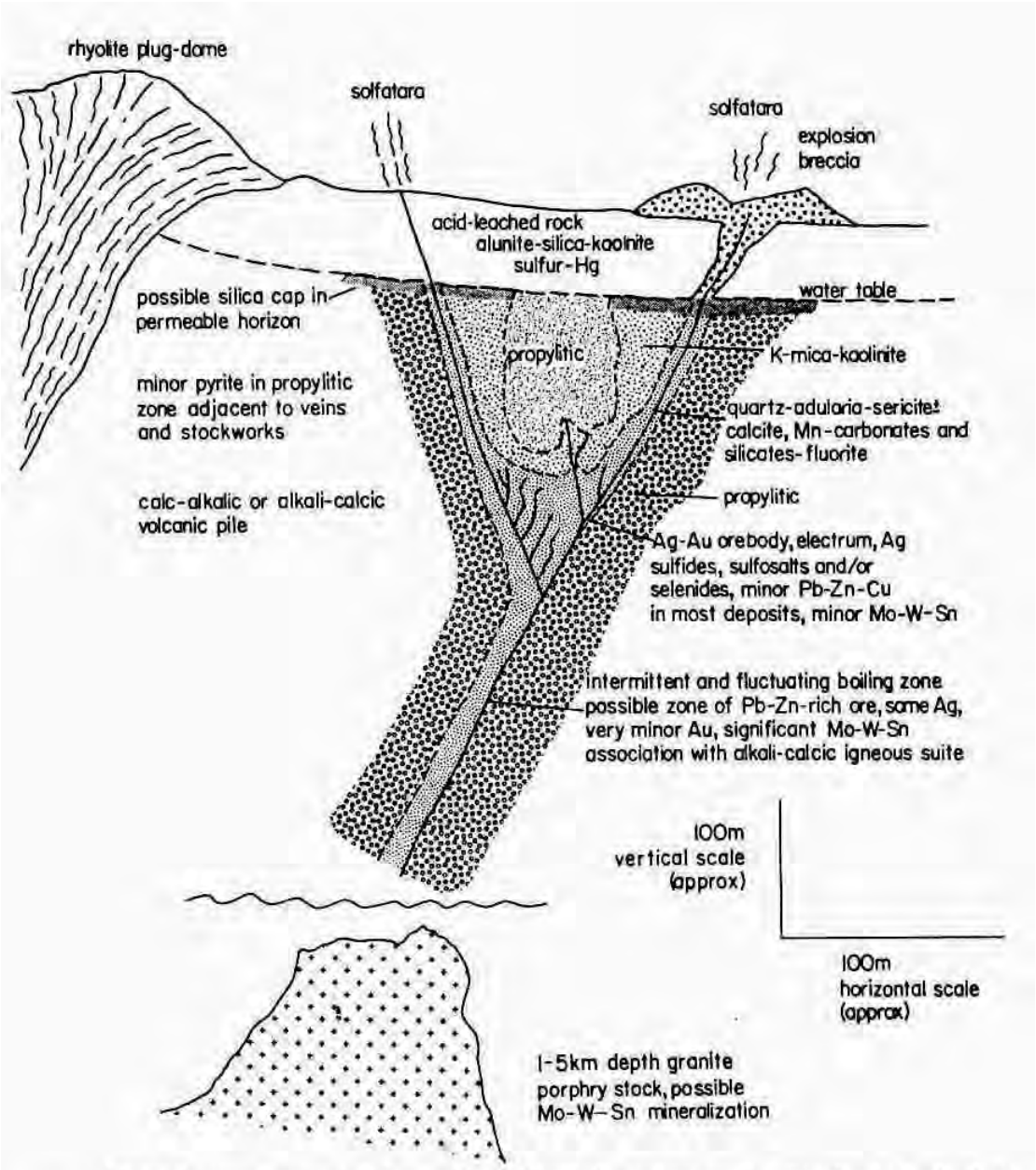

Schematic cross section of low sulfur epithermal precious-metal mineralization related to granite/rhyolite magmatism, in part modified from: Giles and Nelson, 1983, Buchanan, 1981.

Fig.5.16. LS epithermal (rhyolitic) precious metal model of Bonham (1988)

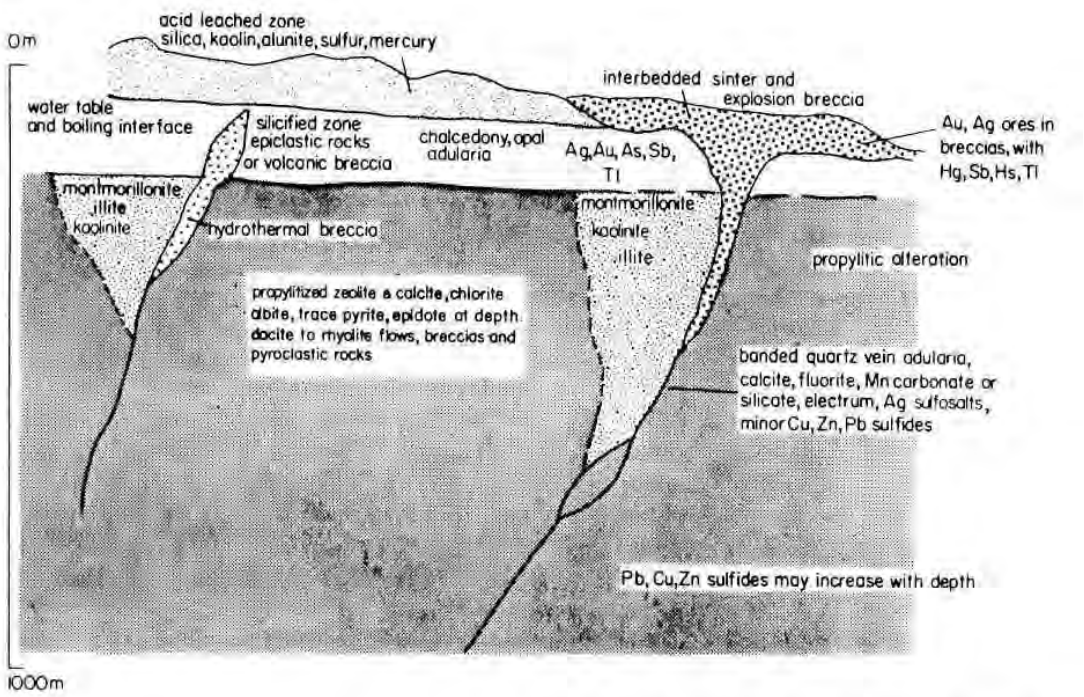

Schematic model, low sulfur hot springs type Au, Ag deposits, modified after Silberman, 1982, Giles and Nelson, 1985

Fig.5.17. LS epithermal precious metal model (hot springs type) of Bonham (1988).

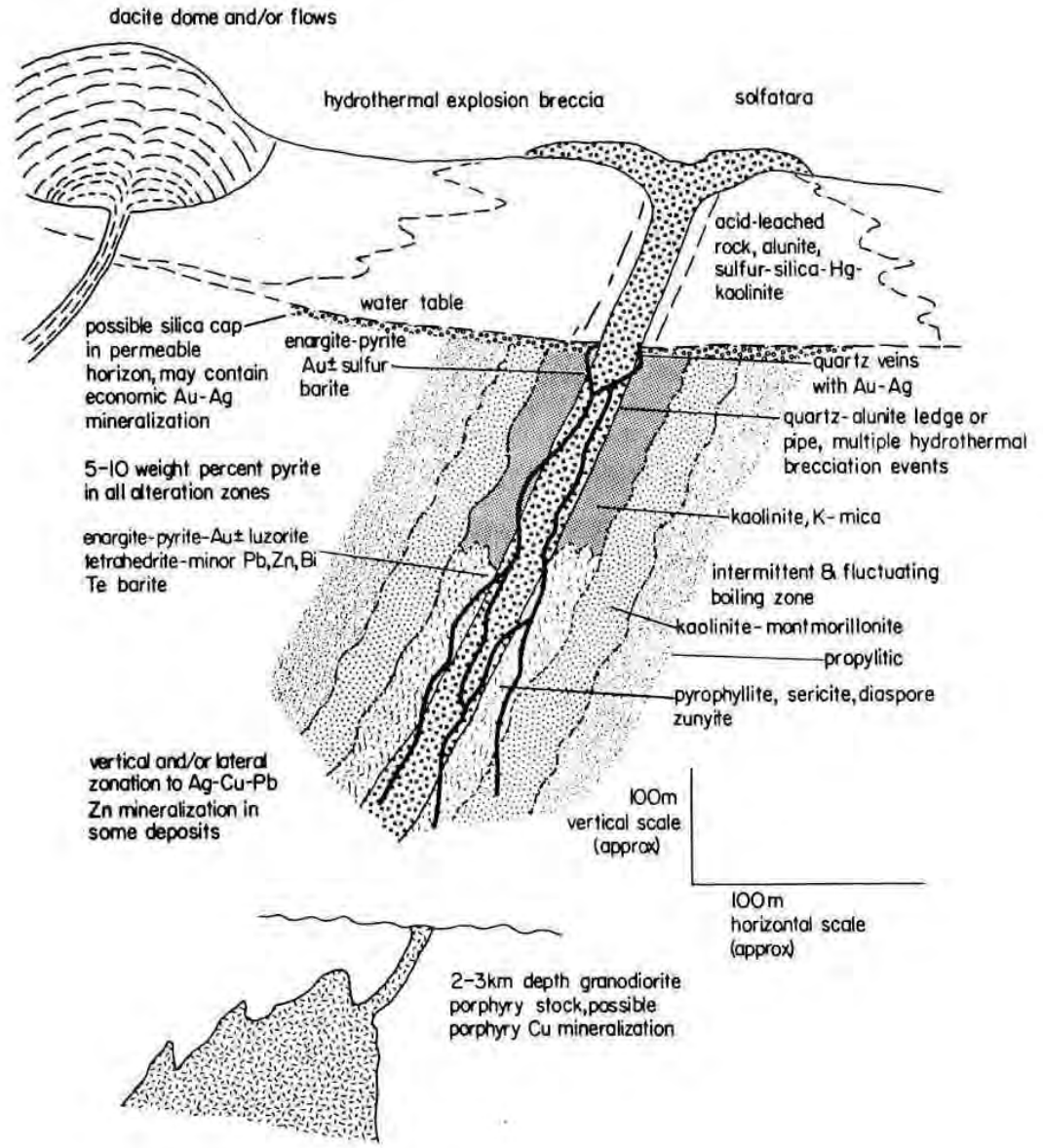

Schematic cross section, epithermal enargite/precious metal or high-sulfur-type deposits associated with granodiorite-dacite magmatism.

Fig.5.18. HS epithermal (dacitic) precious metal model of Bonham (1988).

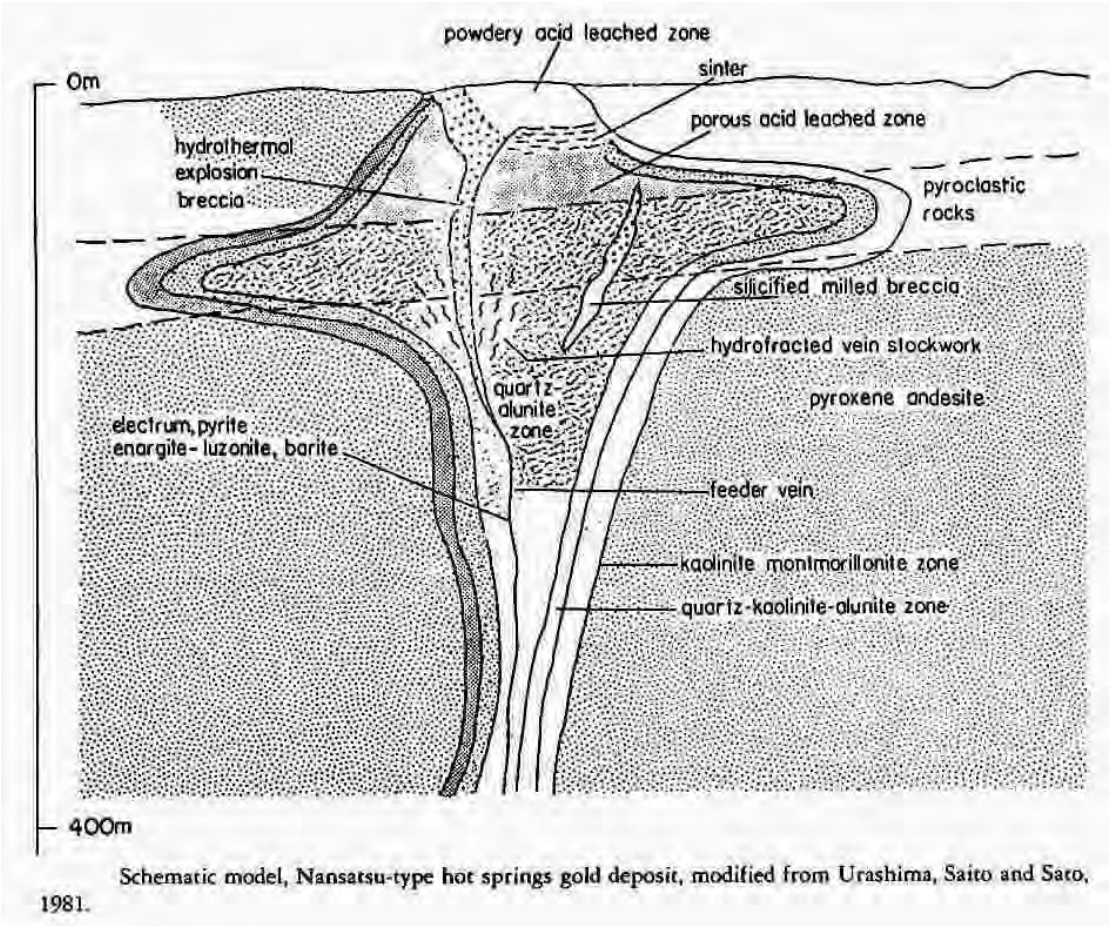

Fig.5.19. HS epithermal Au model (Nansatsu-type hot springs) of Bonham (1988).

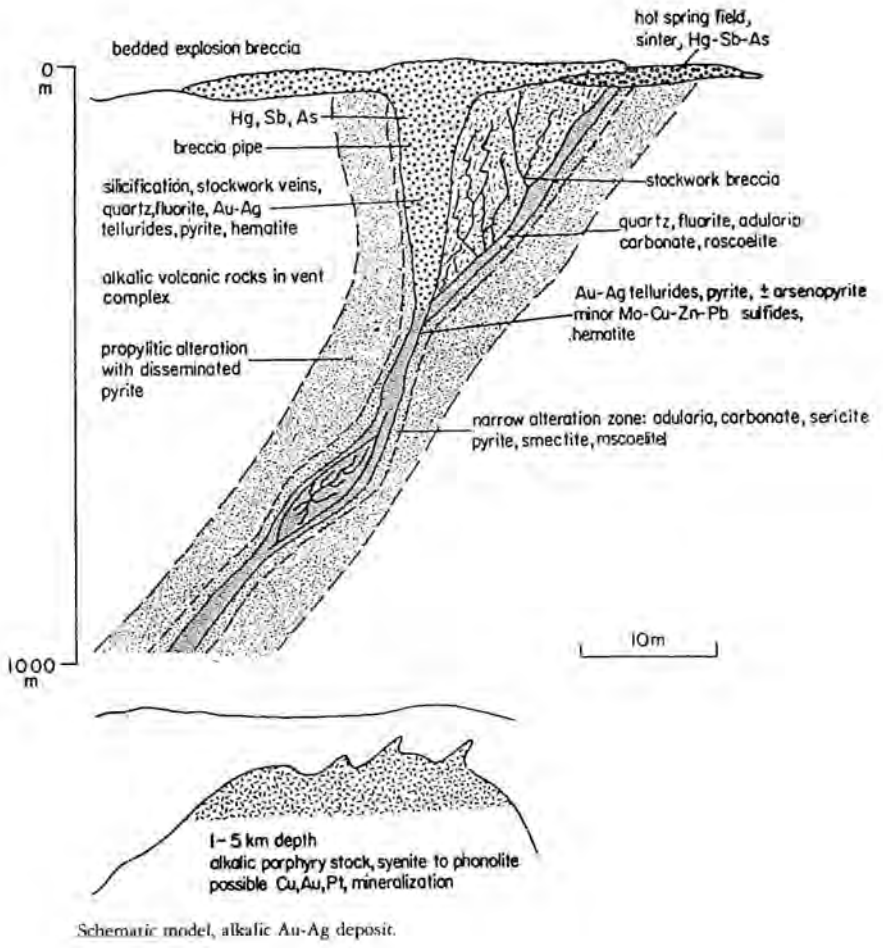

Schematic model, alkalic Au-Ag deposit.

Fig.5.20. Alkalic LS epithermal precious metal model of Bonham (1988).

5.12 Effects of Metamorphism

Contact Metamorphism

Contact metamorphism of a porphyry system by a later, large intrusion could greatly modify magnetic properties of the rocks within the system. Outside the altered zone, felsic country rocks may be little affected, whereas more mafic igneous rocks may develop secondary magnetite in the baked zone. The Tuckers Igneous Complex (Queensland) affords a good example of this lithological control on magnetic properties of the hornfels zone (Clark, 1996). This igneous complex comprises several intrusive phases, ranging from early gabbro and quartz diorite through quartz monzonite and late granodiorite, emplaced into comagmatic andesites. The intrusions are coeval with and geochemically related to the nearby Mount Leyshon Intrusive Complex, which hosted a major gold orebody (now mined out). The Tuckers Complex represents a somewhat less evolved equivalent of the Mount Leyshon system whose hydrothermal system did not develop sufficiently to generate large volumes of mineralising fluids and for which ground preparation via brecciation was insufficient to provide suitable loci for mineralisation. The high temperature, relatively mafic, melts produced pyroxene hornfels in the host igneous rocks adjacent to the Tuckers Complex, passing out through a broad biotite hornfels zone and finally into heated, but essentially unaltered rock. The susceptibility of moderately magnetic tonalitic wall rocks is substantially enhanced within the pyroxene and biotite hornfels zones, but the susceptibility of weakly ferromagnetic felsic granites is only slightly increased.

Intensely propylitised rocks may generate secondary magnetite in the baked zone, and pyrite-rich rocks (e.g. in the phyllic zone) may develop pyrrhotite by the breakdown of pyrite.

Regional Metamorphism of Intrusive-related Deposits

Published studies of regionally metamorphosed intrusive-related deposits are few. Princehouse and Dilles (1996) describe the Wheeler Mine (Nevada) porphyry Cu-Au deposit, which has been metamorphosed, probably to upper greenschist grade. Compositions of silicate assemblages have been modified by the metamorphism, but sulphide assemblages still reflect original alteration zoning and overprinting relationships. Pyrrhotite is interpreted as part of the hydrothermal assemblage, with magnetite and pyrite, in gold-bearing veins of the transitional stage between early potassic/albitic alteration and later sericitic alteration. However, it is possible that the pyrrhotite was produced by the metamorphism.

Magnetic petrological studies of metamorphosed terrains (e.g. Clark *et al*., 1992a,b) suggest the following predictions for behaviour of magnetic minerals in metamorphosed porphyry deposits:

- Magnetite-bearing intrusives, alteration zones and country rocks with moderate magnetite contents (up to 1-2 vol %) will tend to be progressively demagnetised by lower greenschist to mid-amphibolite grade metamorphism, as Fe partitions into metamorphic phases, particularly hydrous mafic silicates.

- At uppermost amphibolite or granulite grade metamorphic magnetite will be produced as anhydrous silicates replace hydrous phases. Thus originally magnetic rocks, demagnetised during medium grade metamorphism, will have their magnetite contents approximately restored.
- At very high pressures, during high pressure granulite or eclogite grade metamorphism, metamorphic magnetite will break down, with ferric iron accomodated in garnet and clinopyroxene.
- Magnetite-rich zones, with several per cent magnetite or more, tend to resist metamorphic breakdown of magnetite through greenschist and amphibolite grade metamorphism, as the silicate minerals cannot accomodate all the Fe, particularly the ferric iron.
- Hydrothermal pyrite may generate pyrrhotite during metamorphism to greenschist grade or higher. Based on studies of pyrrhotite-bearing metasediments, the pyrrhotite produced is likely to be dominantly the monoclinic variety. This suggest that originally non-magnetic pyrite-rich zones of intrusive-related systems may develop substantial magnetisation during metamorphism. Sulphur driven off during breakdown of pyrite may react with surrounding magnetite-bearing rocks, reducing their magnetisation.
- Metamorphic magnetite is associated with low Koenigsberger ratios and unstable, predominantly viscous, NRM.
- On the other hand, pyrrhotite is usually associated with high Koenigsberger ratios and stable, NRM that dates from the final cooling event experienced by the rocks.

5.13 Some Key Findings of AMIRA P425/426

Investigations carried out during P425, coupled with earlier work by the principal investigators of that project, allow a number of conclusions to be drawn about intrusive-related gold deposits: (Blevin, Morrison and Chappell, 1997):

- Au is associated with high level oxidised fractionating intermediate to felsic magmas.
- These magmatic suites are M- or I-type.
- The magmas have widely varying potassium contents: low- to high-K calc-alkaline or shoshonitic.
- Au is part of several *polymetallic* associations, whose cores (Cu, Mo-W, Sn etc.) are controlled by magmatic redox state and composition.
- There is an association with Mo in all systems (even over Cu), and with Bi in the felsic systems.

Experimental studies on Au partitioning in felsic magmas, which have been carried out in P. Candela's laboratory and made available to P425 sponsors, have concluded:

- The solubility of Au in a water-saturated, moderately oxidised (log [fO_2] = NNO + 0.5) rhyolite melt at 800°C is tens of ppm, whereas in the aqueous fluid (3 wt % NaCl equiv.) it is hundreds of ppm.
- For Au the MVP/melt partitioning coefficient is 24 ± 12 (1σ).

- Fe-free rhyolite with *iss* and pyrrhotite at 850°C develops Fe, S and Cu concentrations of 0.7 wt %, 200 ppm and 20 ppm. For high SiO_2 melts, S >> Cu.
- Au partitions strongly into S-poor, oxidised, Cl-bearing vapours. Au-S complexing at high temperatures may be a red herring.

These findings have important geophysical, as well as geological and geochemical, implications. Magmas with oxygen fugacity between the Ni-NiO and hematite-magnetite buffers precipitate magnetite as they cool, subject to availability of iron. Only the most felsic differentiates of such magmas fail to contain at least some magnetite. Previous work by Cygan and Candela (1995) has refuted earlier suggestions (Keith and Swan, 1987; Leveille *et al*., 1988) that Au is readily incorporated into the lattice of magnetite and therefore behaves compatibly in oxidised melts. In fact high oxygen fugacity suppresses precipitation of sulphides, delaying removal of Au from the melt. Thus there is no reason to suppose that Au behaves compatibly in an oxidised melt.

Substantial solubilities of Au and Cu in oxidised melts favour incorporation of these ore elements from oxidised source regions, incompatible behaviour in fractionating oxidised melts builds up concentration, and strong partitioning into fluids exsolving from oxidised melts favours further concentration and possible attainment of ore grades.

5.15 Iron Oxide Cu-Au (IOCG) Deposits

Since the discovery of a hitherto unrecognised style of mineralisation at the giant Olympic Dam Cu-U-Au-Ag-REE deposit in South Australia, much has been written on genesis of Olympic Dam-type deposits and on relationships to a wide variety of other Fe oxide hydrothermal deposit types. A comprehensive set of reviews and deposit descriptions has been compiled by Porter (2002). These deposits are characterised by:

- an abundance of hydrothermal magnetite and/or hematite, with relatively low iron sulphide contents
- a chemically distinctive suite of elements (REE-Cu-Co-Au-Ag-U), often with elevated Ba, P, F
- a mineralogical assemblage of iron oxides with one or more copper sulphides and pyrite, with associated K feldspar or sericite or albite or biotite and chlorite within the host rocks. Carbonate is also common.

but they exhibit a wide variety of geological settings, have very variable distributions and volumes of associated alteration and are associated, directly or indirectly, with a wide range of magmas.

Locations of major IOCG deposits are shown in Fig.5.21. Deposits that have been assigned to this category range in age from Archaean to Tertiary. A range of tectonic settings, including orogenic basin collapse, anorogenic continental rifting, and extensional environments within a subduction-related continental margin has been inferred for these deposits, as shown in Fig.5.22 (Hitzman, 2000). Magmatism related to mantle underplating, high heat flow, and relatively oxidised source rocks (subaerial basalts, oxidised sediments and/or oxidised igneous rocks) are features

common to these tectonic settings. Hitzman (2000) argues that IOCG deposits generally do not appear to have a direct spatial relationship with specific intrusions, but are localised along high- to low-angle faults that are usually splays off major, crustal-scale faults.

The origins of the ore-forming fluids are still controversial. Barton and Johnson suggest that two end members occur. The first type, which has relatively high-temperature mineralisation and high K/Na and Si/Fe, is related to magmatic fluids. This type overlaps with porphyry Cu-Au and related deposits. The second end-member corresponds to more oxide-rich, sulphide-poor mineralisation, low Si/Fe ratios and voluminous alkali-rich metasomatism, generally with sodic dominating over potassic alteration. This latter type is related to non-magmatic fluids, such as basinal brines. Some IOCGs represent hybrids between the two end-members.

An association between sedimentary sequences with evaporitic rocks and the occurrence of IOCG deposits has been suggested, but Pollard (2000) points out that many host rock sequences lack evaporites and suggests that the coexisting hypersaline and CO_2-rich fluid inclusions that are typical of these deposits may have resulted from unmixing of an original H_2O-CO_2-salts fluid of magmatic origin. Syn- to post-mineralisation Na-Ca-rich fluids that are present in many deposits may represent meteoric and/or connate fluids that mixed with hypersaline magmatic fluids.

Pollard (2002) also points out a general association with magnetite-series, high-K, mildy alkaline intrusive rocks, ranging from diorite to granite in composition. These types of intrusives resemble those associated with porphyry Cu-Au mineralisation. In the intracratonic environments that typify the older deposits, magmas are generally derived by high-temperature partial melting of older igneous rocks, triggered by injection of mantle-derived magmas into the crust. Thus the intrusive rocks are mainly I-granodiorite type, with the possibility of mixing with some M-type magmas. Pollard (2002) suggests that this promotes enrichment of the magmas in U, F, Mo and REE, which may be enhanced by further fractionation and ultimately transferred to associated IOCG deposits. Incorporation of components derived from host rocks and/or non-magmatic fluids is common in IOCG and porphyry Cu-Au deposits. In particular, sodic-calcic alteration of magmatic or non-magmatic origin can extract Fe, K and Cu from country rocks. These components may then be deposited within the zones of mineralisation.

Haynes (2000) states that IOCG deposits universally occur within host successions that have little or no elemental carbon, reduced carbon compounds, or reduced sulphur minerals, i.e. the successions are relatively oxidised. Within such successions, magnetite is invariably present and variably abundant, producing a magnetically active environment.

On the other hand, Haynes (2000) recognises an iron sulphide copper-(gold) (ISCG) class of deposit that typically occurs near the boundaries between discrete reduced and oxidised domains. The Mount Isa Inlier is an example of an area that hosts both types of deposit. The reduced domains have an abundance of carbonaceous rocks or reduced carbon minerals and have relatively subdued magnetic patterns.

Alteration Associated with IOCG Deposits

Extensive sodic and/or sodic-calcic alteration, often of regional extent, is associated with all IOCG deposits and most ISCG deposits (Haynes, 2000). This alteration produces an albite-magnetite-chlorite or actinolite assemblage, usually with scapolite, hematite, epidote, calcite and sphene. Alteration zones are typically tens to hundreds of km² in area. These types of alteration have a different character to sodic and sodic-calcic alteration developed around deep levels of some porphyry systems, which are produced by convecting meteoric or connate waters and are magnetite-destructive. The sodic and sodic-calcic alteration types associated with IOCGs involve substantial iron metsomatism, i.e. the fluids are Na-Ca-Fe rich. Another fundamental difference in the alteration fluids of IOCG and porphyry systems appears to be that IOCG-related fluids are rich in CO_2, whereas porphyry-related fluids are usually very low in CO_2.

The main types of alteration recognised in IOCG systems are:

- sodic (extensive albitisation of host rocks, accompanied by magnetite ± scapolite ± chlorite ± actinolite ± hematite),
- sodic-calcic (plagioclase-magnetite-epidote-calcite-sphene ± scapolite ±chlorite ± actinolite ± garnet ± hematite),
- sodic-potassic (albite-K feldspar-magnetite-quartz ± sericite ± biotite ± hematite ± chlorite ± actinolite),
- potassic-calcic (K feldspar-biotite-magnetite-epidote-calcite-sphene ± chlorite ± actinolite ± garnet ± hematite),
- potassic (Kfeldspar-sericite-magnetite-quartz ± biotite ± hematite ± chlorite ± actinolite),
- sericite-hematite (sericite-hematite-chlorite-carbonate ± quartz).

The sericite-hematite type of alteration has also been termed “argillic” or “hydrolytic”. The acronym HSCC (hematite-sericite-chlorite-carbonate) is also used for this alteration type. Sodic and sodic-calcic alteration styles tend to be early (pre-mineralisation) and particularly extensive. Potassic alteration is more restricted in area, more closely associated with mineralisation, and occurs at higher levels in the system. Sericite-hematite alteration is magnetite-destructive and occurs at upper levels of the system. Sodic-potassic, potassic, potassic-calcic or sericite-hematite alteration may all be associated with mineralisation, depending on the degree of interaction with meteoric or connate fluids (Hitzman, 2000).

As always, actual assemblages reflect host rock influence as well as the alteration fluids. Examples of some of the main types of alteration are shown in Figs.5.23-26. The CAM (calc-silicate-albite-magnetite) assemblage represents sodic-calcic alteration and the biotite-magnetite-albite (BM) assemblage represents sodic-potassic alteration. The magnetite-destructive alteration illustrated in Fig.5.25 is a mineralising alteration that is a transitional potassic-sericitic overprint of earlier CAM alteration. Chalcopyrite and pyrite were deposited as biotite and actinolite were converted to chlorite, albite was replaced by chlorite and K feldspar, and magnetite was oxidised to hematite.

Haynes (2000) suggests that, in general, copper precipitation in IOCG deposits results from reduction of oxidised, copper and sulphate-bearing fluids, precipitating copper sulphides, ferric iron-bearing minerals and producing acid. The reducing agent is ferrous iron, either in solution (in the case of mixing of with a reduced fluid), or in iron-rich rocks. A generalised reaction is:

$$2Cu^{+} + SO^{4-} + 8\ H_2O + 8Fe^{2+} \rightarrow\ 4Fe_2O_3 + 16\ H^{+} + Cu_2S.$$

The hydrogen ions produce a strongly acidic fluid, which is neutralised by hydrolysis of feldspars. In the case of fluid mixing or reaction with rocks rich in ferrous iron-bearing silicates, this process produces magnetite and/or hematite. Reaction of the oxidised fluid with magnetite-rich rocks precipitates copper sulphides by coupling reduction of the sulphate with oxidation of magnetite to hematite. Thus magnetite-rich rocks represent favourable sites for precipitation of copper sulphides, with some or all of the magnetite being converted to hematite during the mineralising process.

Zoning models of alteration in IOCG systems are not as well developed as those for porphry systems. Figure 5.28 shows alteration zoning around an intrusion-centred Cu-Au system at Arizaro (Argentina). This deposit appears to represent a transitional type between a porphyry copper-gold system and and IOCG system. The alteration at Arizaro is zoned from distal propylitic (calcite-epidote-chlorite) alteration inwards through potassic-calcic alteration (actinolite-K feldspar-magnetite-biotite ± diopside ± albite) to a central core of intense potassic alteration with a K feldspar-magnetite-biotite assemblage. Weak hydrolytic alteration (quartz-sericite-clay) that overprints other alteration types occurs on the periphery of the system. This zoning pattern may be typical of similar hybrid porphyry Cu-Au/IOCG deposits.

The Olympic Dam deposit is inferred to have formed at very shallow depths and is dominated by sericite-hematite ± quartz ± chlorite ± siderite ± fluorite ± barite alteration. Magnetite has been totally replaced by hematite in the central and upper portions of the deposit, but is present in deeper and peripheral zones. Figure 5.29 shows the distribution of alteration and ore minerals in the Olympic Dam deposit.

The general zoning pattern inferred for IOCG deposits is shown shematically in Fig.5.30. It is clear that IOCG systems tend to be zoned vertically from magnetite-dominant at depth to hematite-dominant at upper levels. Magnetite is also abundant peripheral to the ore zones. This pattern may be altered by tectonic tilting of the system or by faulting. Therefore the magnetic and gravity signatures of IOCG deposits should generally reflect *superposed* or *juxtaposed* gravity and magnetic anomalies. Positive gravity anomalies arise from both magnetite-rich and hematite-rich zones, whereas the deeper, peripheral, or adjacent magnetic sources correspond to the magnetite-rich zones.

The simplistic notion of *coincident* magnetic and gravity anomalies is misleading, as the sources of the anomalies are spatially separated. This is why the term "superposed" is preferable. Detailed modelling of the gravity and magnetic sources should usually resolve vertical zonation of iron oxides by inferring a deeper source for the magnetic anomaly than for the gravity source. An exception to this expectation could occur when hematite-rich bodies have been heated above 680°C by contact or

regional metamorphosism and have thereby acquired sufficient remanence to produce substantial magnetic anomalies.

The total mass of iron oxide minerals within typical IOCG systems is very large, which raises questions about sources of Fe, transportation of Fe in solution and deposition mechanisms of the iron oxides. Iron may be derived from magmaa or leaching of iron-bearing rocks by metamorphic fluids or basinal brines. Ferrous iron is much more soluble than ferric iron, so it is transported as Fe^{2+}. IOCG deposits and their alteration envelopes often exhibit evidence of replacement of magnetite by hematite (martitisation), or vice versa, forming "mushketovite". Similar replacements of one iron oxide by another are also common in skarns. These transformations are often assumed to be redox reactions (i.e. oxidation of magnetite to hematite or reduction of hematite to magnetite). However, Ohmoto (2003) points out that this is not necessarily the case. In particular the acid-base reaction,

$$Fe_2O_3 + H_2O + Fe^{2+} \leftrightarrow Fe_3O_4 + 2H^+,$$

represents transformation of hematite to magnetite by reaction with Fe^{2+}-bearing hydrothermal fluid, generating acidity in the process, or the reverse transformation of magnetite by acidic solutions to hematite, with excess ferrous iron passing into solution. This is *not* a redox reaction, because the ferric and ferrous ion contents are unchanged. The forward reaction represents Fe-metasomatism, whereas the reverse reaction describes leaching of ferrous iron from the rock.

Figure 5.31 illustrates how reaction of an Fe^{2+}-rich hydrothermal fluid with hematite-bearing rocks at temperatures of 150-250°C can produce magnetite at the expense of hematite. The hydrogen ions produced during this forward reaction can be consumed by feldspars to produce sericite, muscovite or clay minerals. A cooler (50-200°C) fluid that is deficient in Fe^{2+} (e.g. a normal hot spring water), on the other hand, will produce the reverse reaction, with magnetite replaced by hematite, accompanied by an increase in dissolved Fe^{2+} and an increased pH.

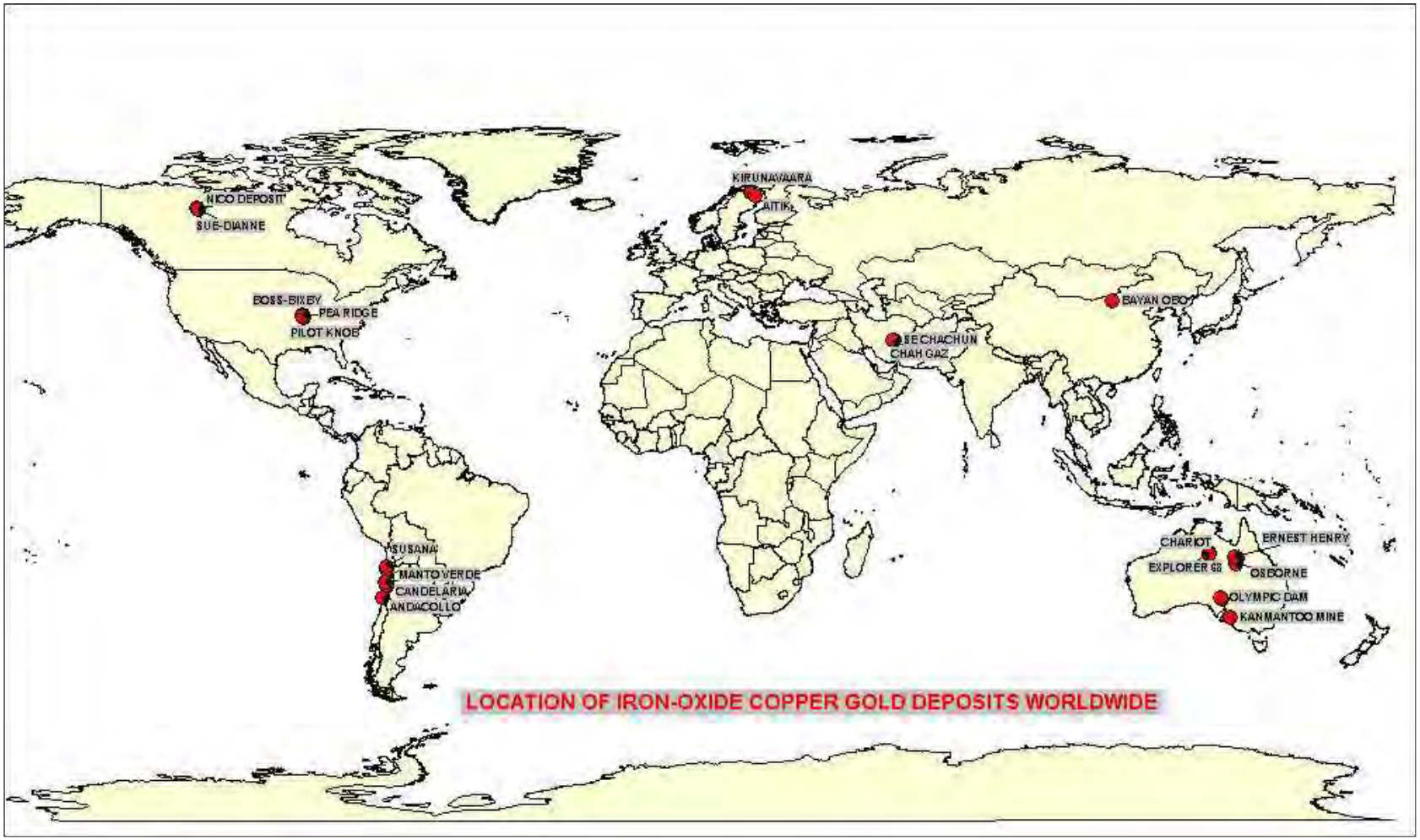

Fig.5.21. Locations of Fe oxide Cu-Au deposits worldwide

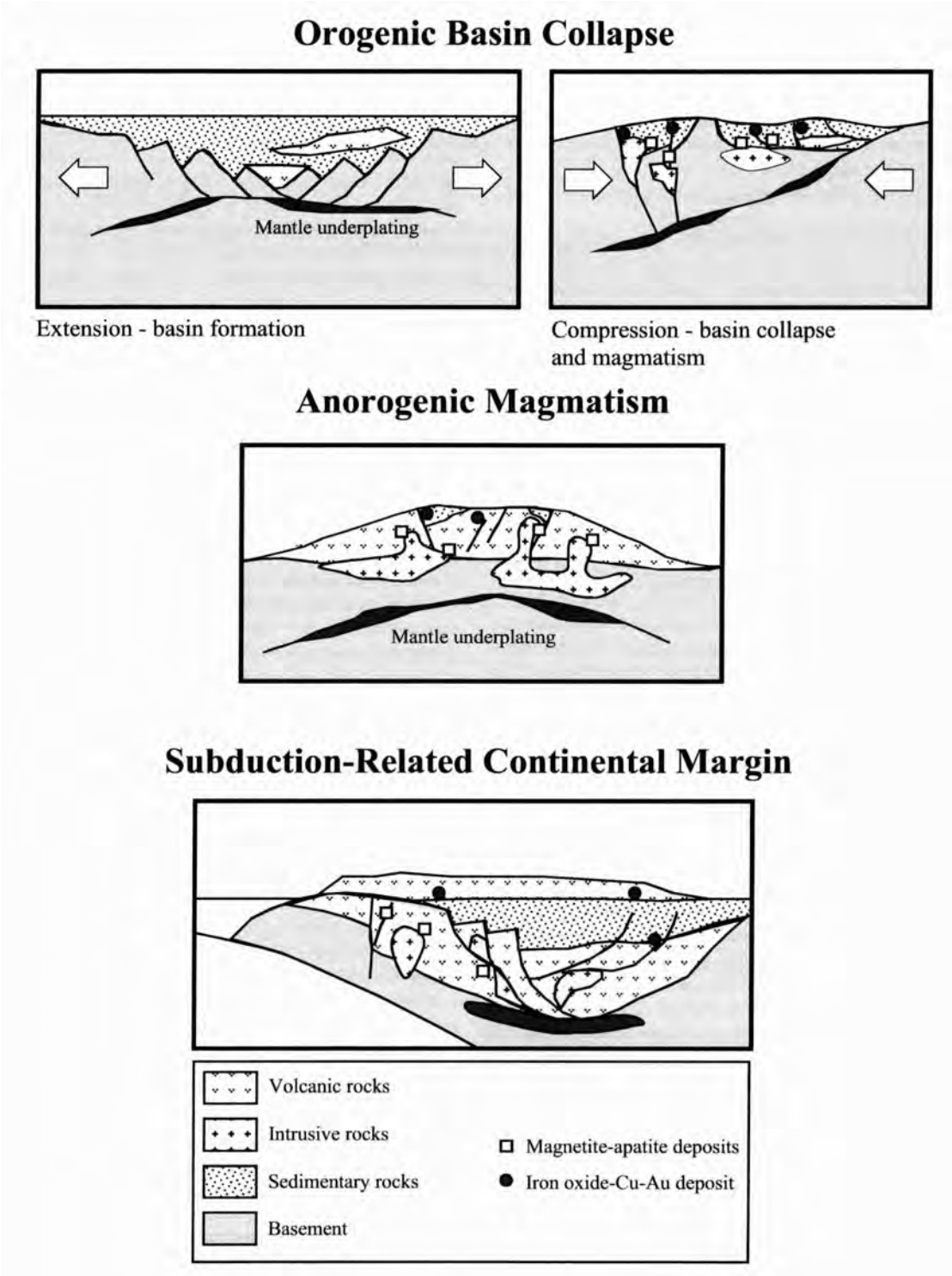

Fig.5.22. Inferred tectonic settings for Fe oxide Cu-Au deposits (Hitzman, 2000)

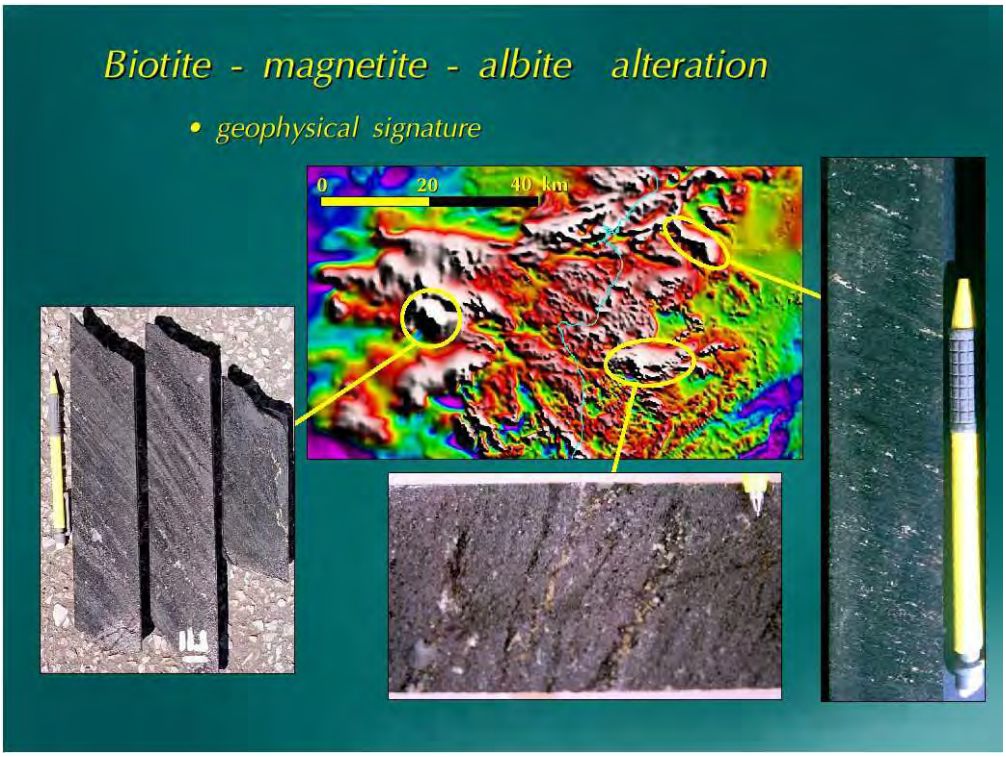

Fig.5.23. Biotite-magnetite-albite alteration typical of the Moonta area, South Australia, and similar to alteration associated with many IOCG deposits (Raymond et al. 2002)

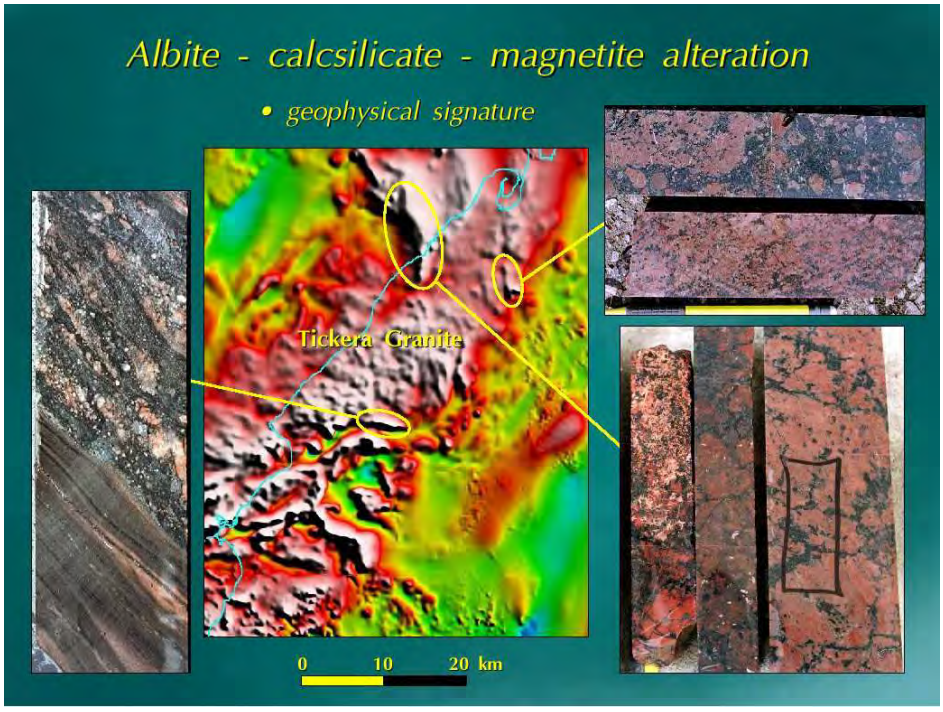

Fig.5.24. Calcsilicate-albite-magnetite (CAM) alteration typical of the Moonta area, South Australia, and similar to alteration associated with many IOCG deposits (Raymond et al. 2002)

Fig.5.25. Magnetite-destructive chlorite-quartz ± hematite ± K feldspar ± pyrite ± chalcopyrite alteration typical of the Moonta area, South Australia, and similar to alteration associated with many IOCG deposits (Raymond et al. 2002)

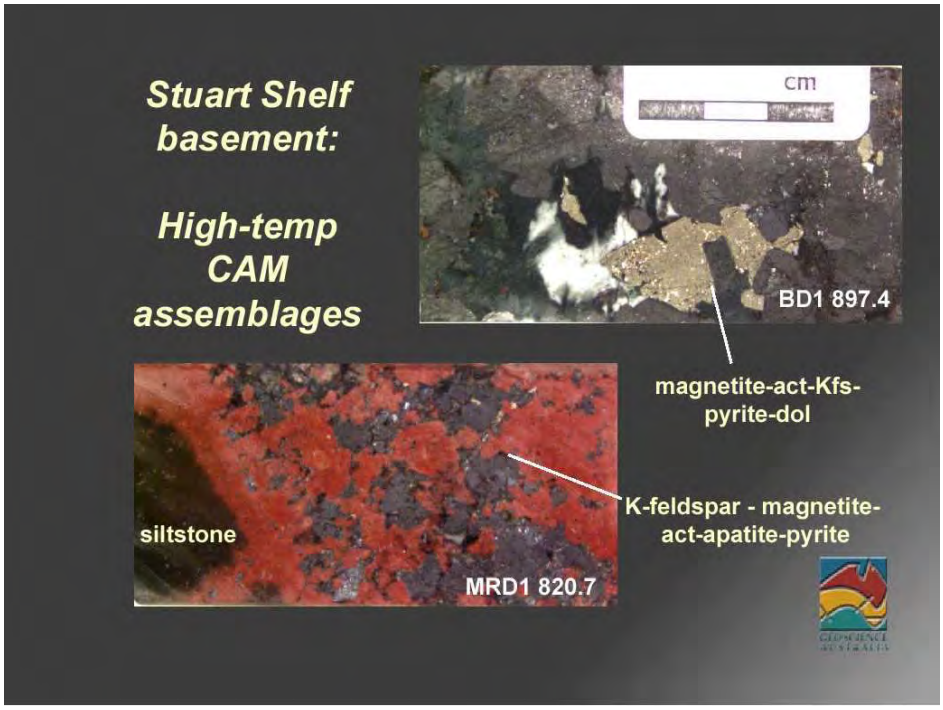

Fig.5.26 Typical high-temperature CAM alteration associated with IOCG deposits of the Stuart Shelf, South Australia (Skirrow et al. 2003).

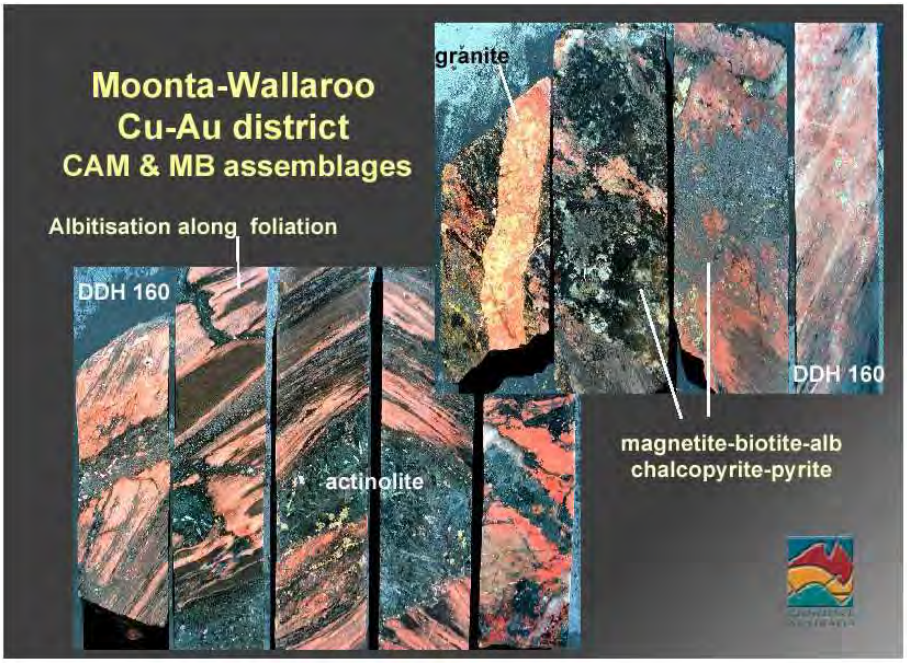

Fig.5.27 Typical high-temperature CAM and BM alteration associated with IOCG deposits of the Moonta-Wallaroo area, South Australia (Skirrow et al. 2003).

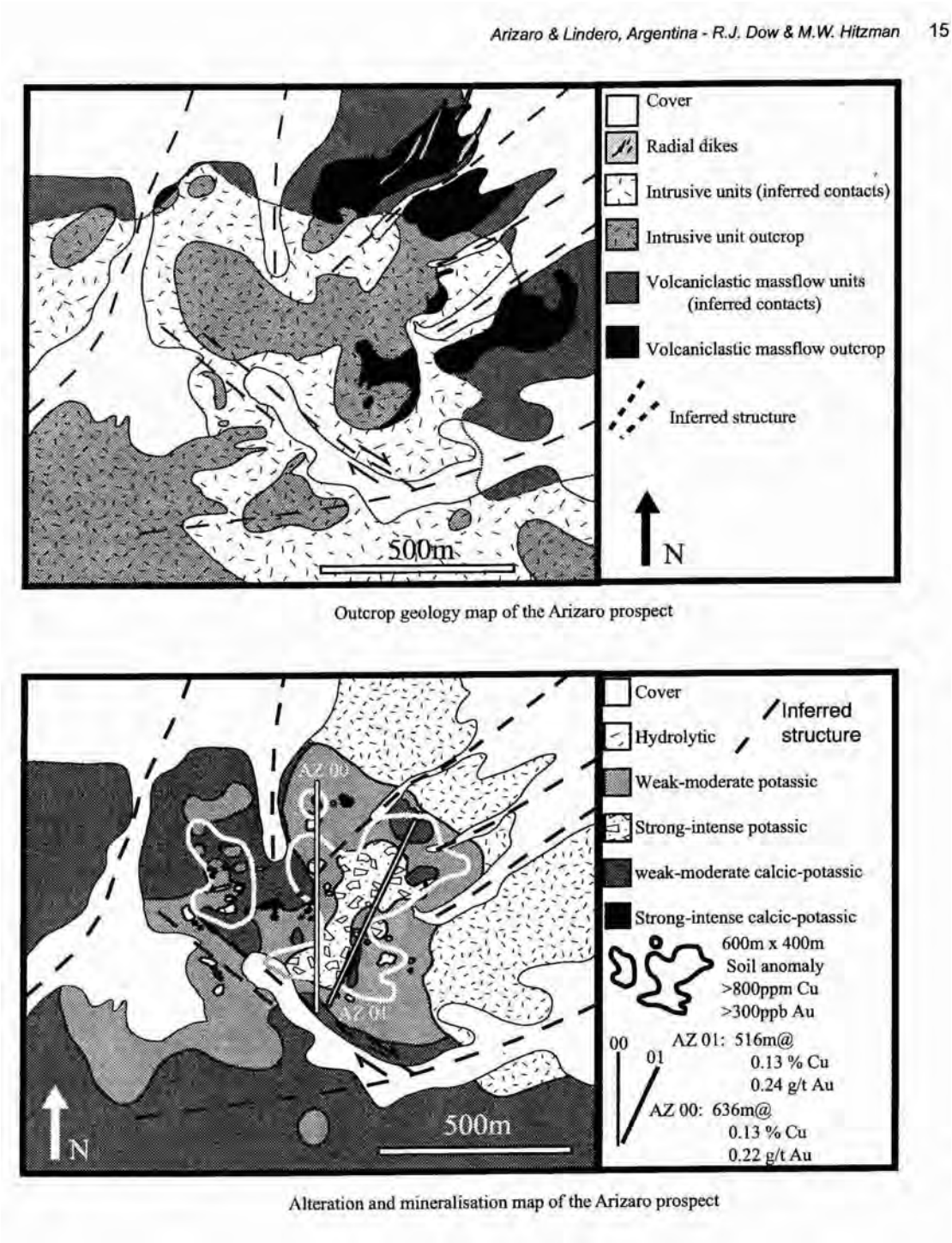

Fig.5.28. Geology and alteration maps of the Arizaro prosect, Argentina (Dow and Hitzman, 2002)

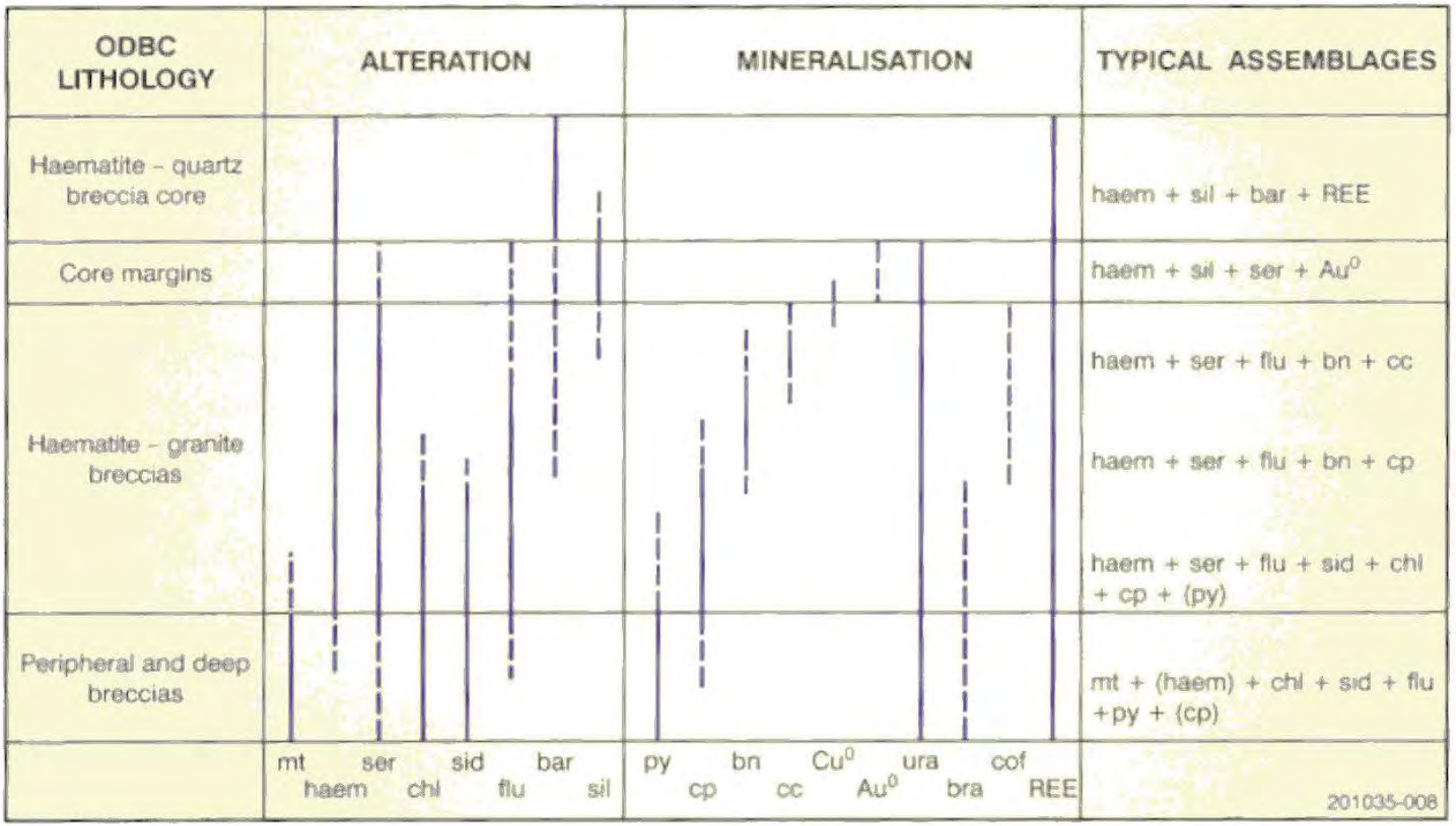

Fig.5.29. Alteration/mineralisation mineralogy at Olympic Dam. Note the peripheral and deep distribution of magnetite relative to hematite.

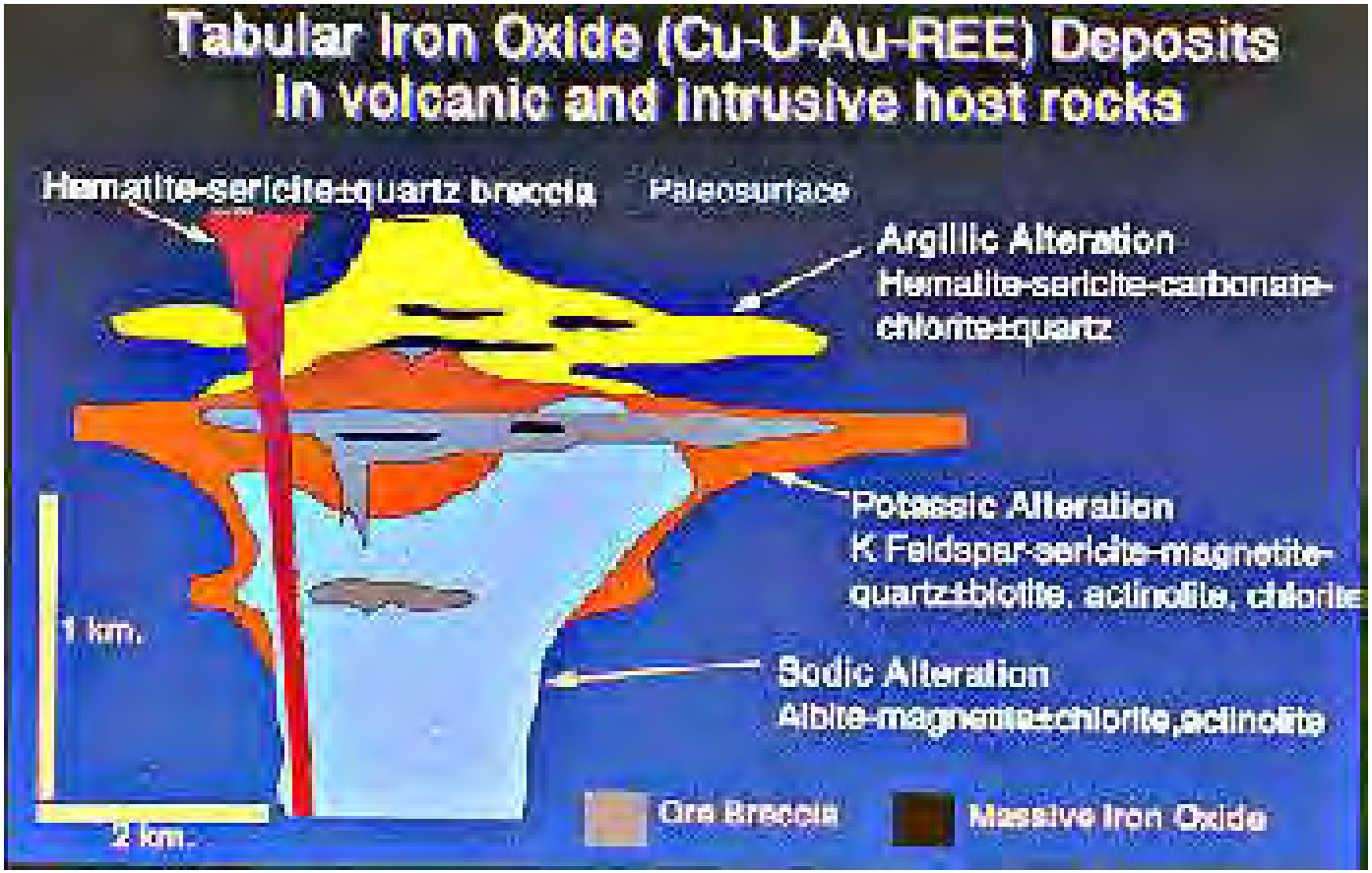

Fig.5.30. Generalised IOCG model (Hitzman, 1992)

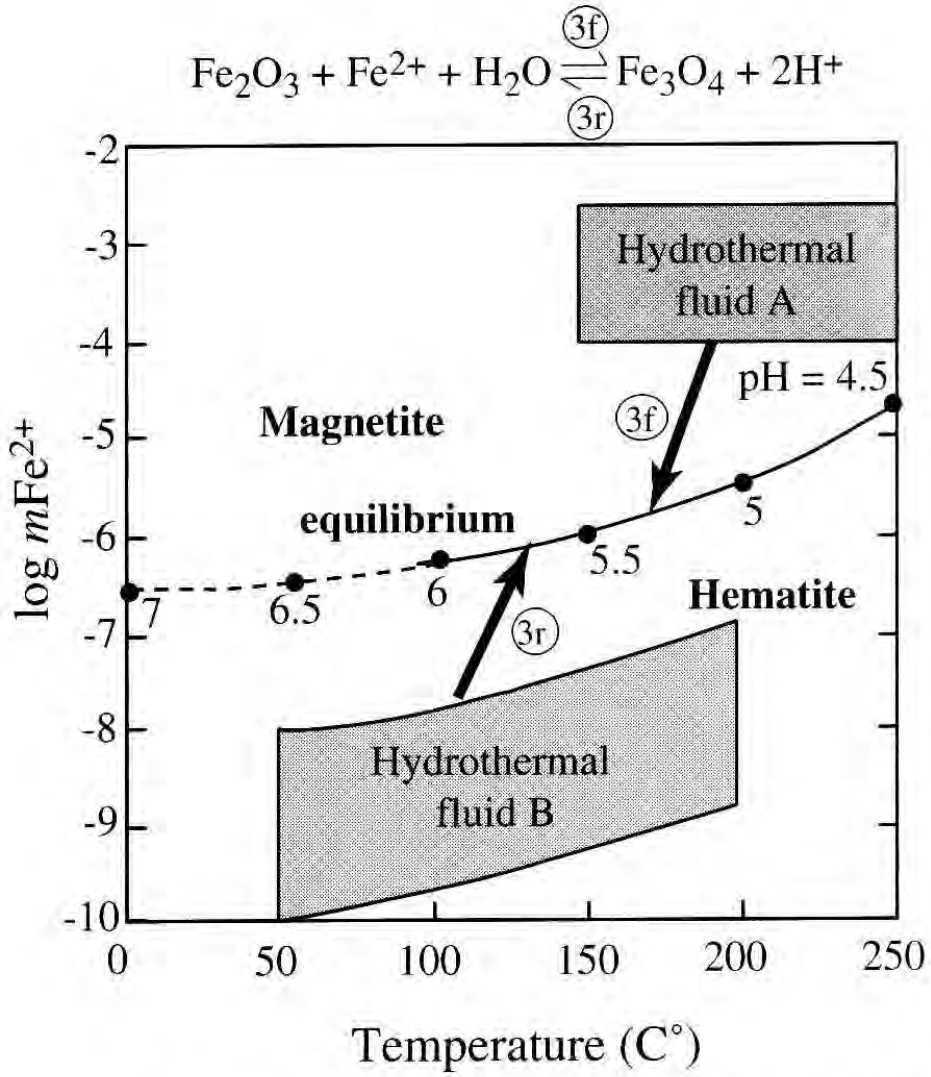

Comparisons of the Fe^{2+} contents of typical submarine hydrothermal fluids (A), typical subaerial geothermal fluids (B), and the fluids in equilibrium with the magnetite-hematite assemblage (solid and dashed line). The equilibrium Fe^{2+} values are estimated for the most common pH value of hydrothermal fluid at each temperature (cf. Ohmoto and Goldhaber, 1997). Note the reaction between hematite and hydrothermal fluid A will transform the hematite to magnetite (path 3f), whereas the reaction between magnetite and hydrothermal fluid B will transform the magnetite to hematite (path 3r

Figure 5.31 Non-redox mechanism for transformations between magnetite and hematite (Ohmoto, 2003).

6. GEOLOGICAL AND GEOMAGNETIC FACTORS THAT CONTROL MAGNETIC SIGNATURES OF PORPHYRY, EPITHERMAL AND IRON OXIDE COPPER-GOLD DEPOSITS

6.1 General Principles

A number of well-known geological models of porphyry and epithermal deposits are routinely used in exploration, even though most deposits fail to match the idealised models closely, due to post-emplacement tectonic disruption and rotations, asymmetric alteration zoning due to emplacement along a contact between contrasting country rock types, and so on. These complications are taken into account by exploration geologists as geological information about a prospect accumulates. Geological models of porphyry and epithermal deposits have been developed and refined as more deposits, in a wide range of geological settings, have been intensively studied and documented and experimental studies and theoretical modelling of alteration-mineralisation processes have progressed (e.g. Lowell and Guilbert, 1970; Hollister, 1976; Sutherland-Brown, 1976; Sillitoe, 1979; Heald *et al*., 1987; Bonham, 1988; McMillan and Panteleyev, 1988; Panteleyev, 1988; Cox and Singer, 1992; White, 1991; Sillitoe, 1993a,b; Lang *et al*., 1995; Richards, 1995; Sillitoe, 1995, 1996, 1999; Cooke *et al*., 1998). Interpretations of alteration patterns and ore genesis have been refined and validated by actualistic studies of geothermal systems that represent modern analogues of ancient ore forming systems. For example, Simmons and Browne (2000) have recently presented data that provide a 3D picture of fluid types, temperature gradients and flow paths in the Broadlands-Ohaaki hydrothermal system, which can elucidate patterns of alteration zonation and precious metal deposition in low-sulphidation epithermal precious metal deposits.

In practice, when deposits conform closely to an idealised geological model, their magnetic signatures correspond well to the expected patterns. Figure 6. 1 shows the predicted magnetic signature for a subcropping gold-rich porphyry copper deposit emplaced into mafic to intermediate volcanic rocks. Figure 6. 2 is an example of such a deposit, undisrupted by tectonic movements since emplacement, which exhibits a well-defined magnetic signature that conforms closely to the predicted signature. This example confirms that idealised geophysical exploration models for porphyry and epithermal mineralisation can be useful, *if geological factors such as tectonic setting, exploration target type, country rock composition, level of exposure, and structural and metamorphic modification are considered.*

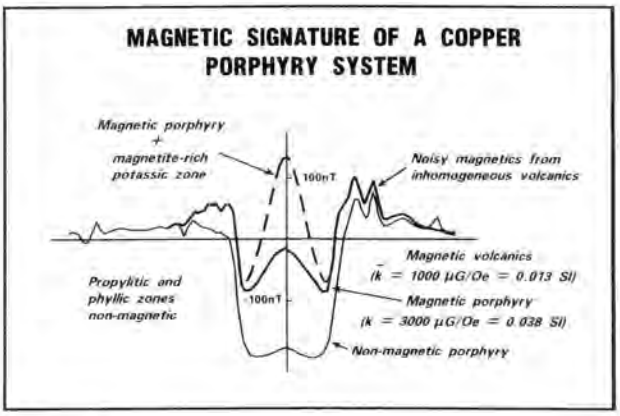

FIGURE 4
Idealised magnetic anomaly associated with a porphyry copper system, showing the noisy background associated with magnetic volcanics, the 'alteration low' associated with the propylitic and phyllic alteration zones, the high arising from the magnetic porphyry plus, in the case of gold-rich copper mineralisation, the magnetite-bearing potassic alteration zone.

Fig.6.1. Idealised magnetic signature of Au-rich porphyry copper deposit emplaced within magnetic volcanic host rocks (Clark et al., 1992).

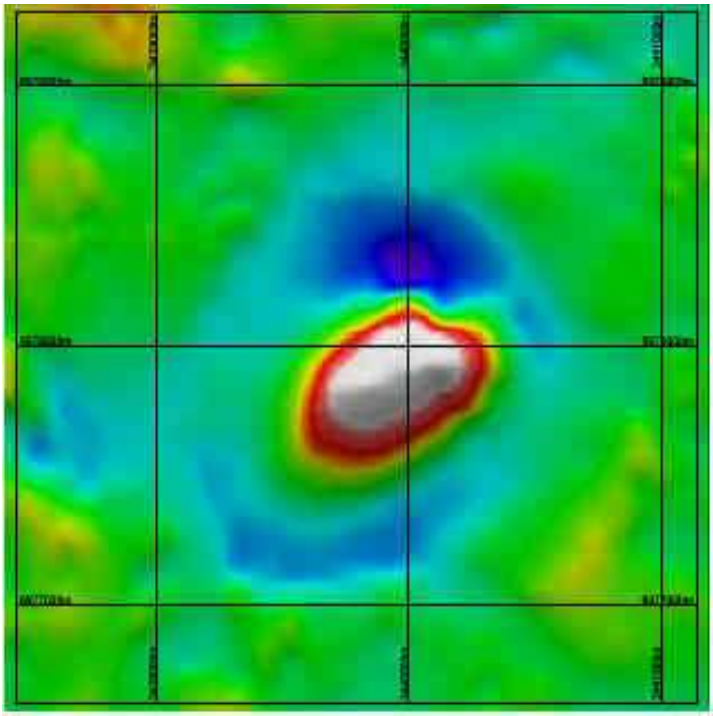

Fig.6.2. RTP magnetic signature of an Au-rich porphyry copper deposit that conforms to the idealised model of Fig.6.1. The central magnetic high is due to the potassic (biotite-magnetite) core zone and the annular magnetic low is due to magnetite destruction within the surrounding phyllic zone. In the outer propylitic zone the magnetic response gradually returns to the background level and the busy texture of the andesitic host rocks. This "type" magnetic signature occurs because the mineralising intrusion was emplaced into relatively homogeneous host rocks and the deposit has not been subsequently tilted or disrupted by faulting.

6.2 Tectonic Setting/Magma type

Porphyry and epithermal deposits form in a range of tectonic settings. Not only do the geological models depend on the tectonic setting, but the magnetic properties differ for different igneous rock associations found in different tectonic settings. Thus predictive magnetic exploration models need to take the tectonic environment into account. For example, the widely applied quartz-monzonite porphyry copper model of Lowell and Guilbert (1970) is appropriate to Cordilleran settings with thick continental crust, whereas the Hollister (1975) diorite model is more applicable to island arc settings. Alkalic porphyry models are relevant to tensional environments in a range of complex tectonic settings, including rifted and rotated arcs, marginal basins, and remnant subduction zones. Many such deposits occur within terranes that are exotic to their present setting (e.g. island arc derived terranes of the Canadian Cordillera).

The magnetic signatures of these distinct types or porphyry copper deposit differ markedly. Overall, both the geological models and the corresponding predicted magnetic signatures reflect factors such as shallowly versus steeply dipping subducting slabs, depth of magma generation, presence of metasomatised mantle associated with palaeosubduction, arc reversal and nature and thickness of the crust.

The magnetic petrology of igneous intrusions, and implications for exploration for intrusive-related mineralisation, have been recently reviewed by Clark (1999). The oxidation state of the magma has a crucial influence on the primary magnetic mineralogy and also influences the style and extent of alteration and associated mineralisation during the magmatic-hydrothermal evolution of intrusions. A general association between relatively oxidised, magnetite-series granitoids and porphyry copper, copper-molybdenum and molybdenum deposits has long been noted (Ishihara, 1981; Fig.6.3). By contrast, Sn and W-Sn deposits are invariably associated with reduced, ilmenite-series granitoids. Oxidation states of magmas affect the redox states of exsolving late-stage mineralising fluids and associated alteration assemblages, including skarn deposits (Kwak and White, 1982; Fig.6.4).

Significant differences in magnetic susceptibility, at equivalent degrees of differentiation, are found for mantle-derived (M-type) intrusions, found typically in island arcs, and I-type granitoids in continental arcs. Intrusions associated with gold-rich porphyry copper deposits are more oxidised than those associated with gold-poor porphyry copper deposits, and accordingly contain more abundant igneous (titano) magnetite and produce greater quantities of hydrothermal magnetite during early potassic alteration. An empirical association between Au-rich (> 0.4 g/t) porphryry copper deposits and abundant magnetite in the potassic core has been documented by Sillitoe (1979, 1990, 1996) and confirmed by many other workers.

Williams and Forrester (1995) distinguish high- and low-sulphur porphyries, noting that alteration patterns around porphyry intrusions differ greatly for the two types. The corresponding magnetic signatures also differ profoundly. For development of a magmatic Cu-Au deposit, the magma must remain sulphur undersaturated throughout most or all of its evolution (Wyborn and Sun, 1994). Sulphur saturation of the magma is strongly affected by oxidation state, as well as by sulphur content. At high oxygen

fugacities, sulphur becomes more soluble in the magma, dissolving as an anhydrite component. Early precipitation of sulphides is suppressed and ore metals are retained in the melt and concentrated during fractional crystallisation, greatly enhancing the chances of producing economic mineralisation when late stage fluids are evolved. The magnetite content of the unaltered intrusive rocks, and the generation of early hydrothermal magnetite, are both boosted by high oxygen fugacity in the magma, particularly for relatively K-rich magmas.

6.3 Composition and Disposition of Host Rocks

Host rock compositions control magnetic signatures of mineralised systems in two important ways:

- magnetic anomalies arise from magnetisation *contrasts* – thus the magnetic properties of the unaltered country rocks inherently influence the magnetic signature of the mineralised system. For example, a moderately magnetic intrusion emplaced into weakly magnetic, unreactive country rocks, such as quartzites or silicic volcanics, will have an associated RTP magnetic high. On the other hand, a similar intrusion emplaced into strongly magnetic rocks, e.g. fresh basalts, will have a RTP magnetic low.
- Alteration assemblages, including magnetic minerals, that are associated with a particular alteration phase around a mineralising system are strongly controlled by the protolith composition, as well as the chemical and physical state of the hydrothermal fluid.

The magnetic mineralogy of the altered rock depends on the abundance and composition of primary magnetic minerals and on the ability of the protolith to create secondary magnetic minerals during reaction of the hydrothermal fluid with the pre-existing mineralogy. For example, mafic wall rocks have greater capacity to form secondary magnetite during potassic alteration than do relatively iron-poor felsic rocks.

Skarn deposits constitute an important class of intrusive-related mineralisation. The magnetic properties of prograde and retrograde skarns are sensitive to the composition of the carbonate host rock. Substantial differences in the magnetic mineralogy and magnetic signatures occur between magnesian skarns produced within dolomitic country rocks and calcic skarns within impure limestones.

Because the magnetic signature of intrusions and alteration zones depends strongly on host rock composition, signatures of deposits and alteration systems that straddle geological contacts can be distorted with respect to equivalent systems that occur wholly within one host rock type. Many mineralising intrusions are emplaced along contacts between contrasting rock types. Faulted boundaries, in particular, represent zones of structural weakness that are often exploited by ascending magmas. Asymmetric alteration zoning around such intrusions produces asymmetric magnetic signatures. Unless the effect of host rock composition is taken into account, the magnetic signature of a prospective system may be overlooked, because it departs from the idealised concentrically zoned model. Figure 6. 5 shows an example of asymmetric alteration zoning around a mineralising porphyry emplaced into a geological contact. Early pervasive alteration is zoned from proximal orthoclase to distal epidote in the volcanic wall rocks, The corresponding zones in

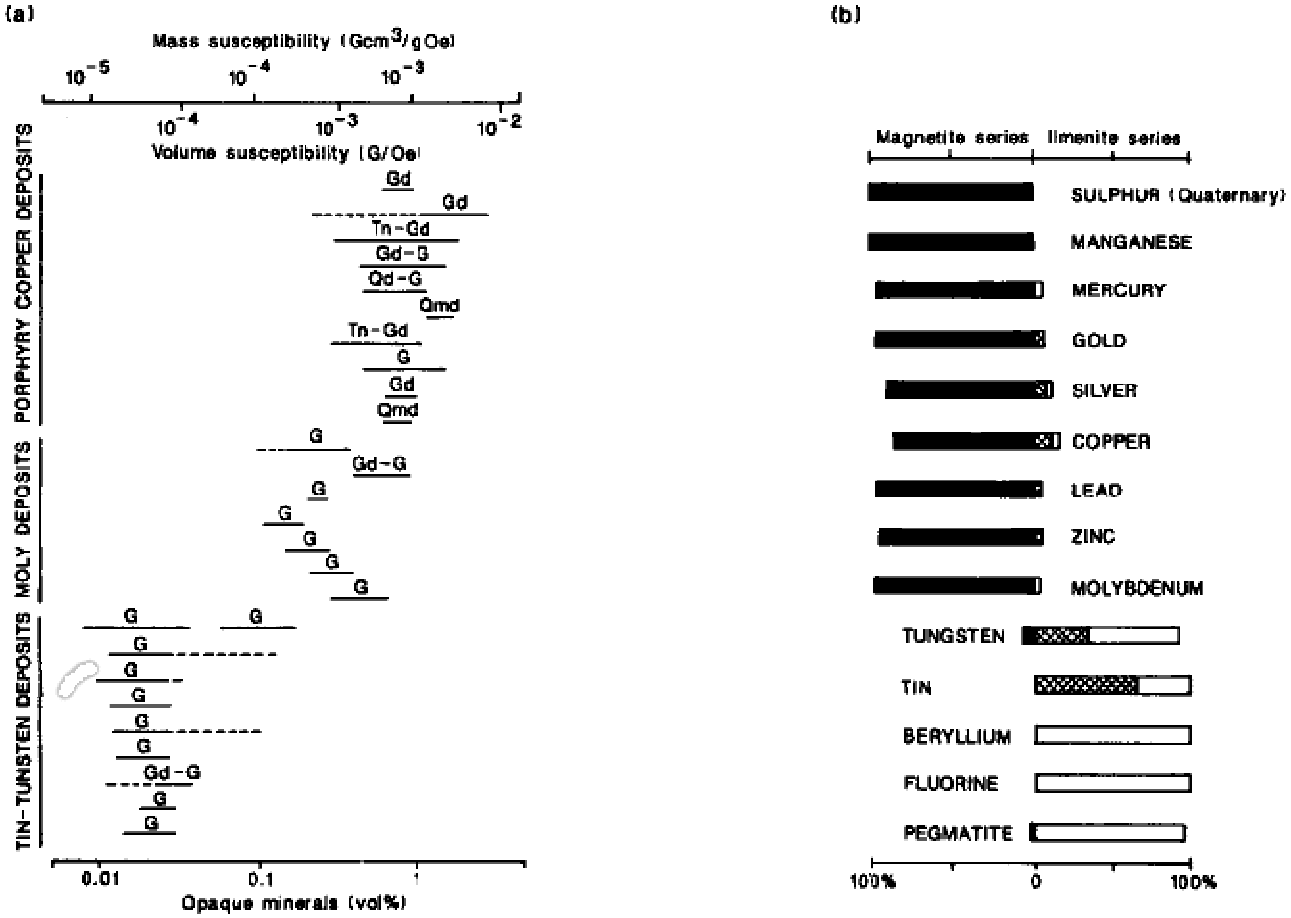

Figure 17. (a) Range of CGS mass and volume susceptibilities and opaque mineral contents for granitoids associated with porphyry Cu, granitoid-related Mo deposits and granitoid-related Sn-W deposits (Gd = granodiorite, To = tonalite, G = granite, Qmd = quartz monzodiorite). (b) Proportions of mineral deposits, of a variety of commodities that occur within magnetite-series and ilmenite-series granitoid belts. Hatched regions represent WFM magnetite-series granitoids. The mineral deposits are inferred to be genetically related to granitoids or to their associated volcanics. Pegmatite refers to stanniferous pegmatite deposits. SI volume susceptibility = CGS volume susceptibility (G/Oe) × 4π; mass susceptibility = volume susceptibility/density (after Ishihara, 1981).

Fig.6.3. Relationships between Ishihara (1981) granitoid class, magnetic susceptibility and type of intrusive-related mineralisation (Clark, 1999).

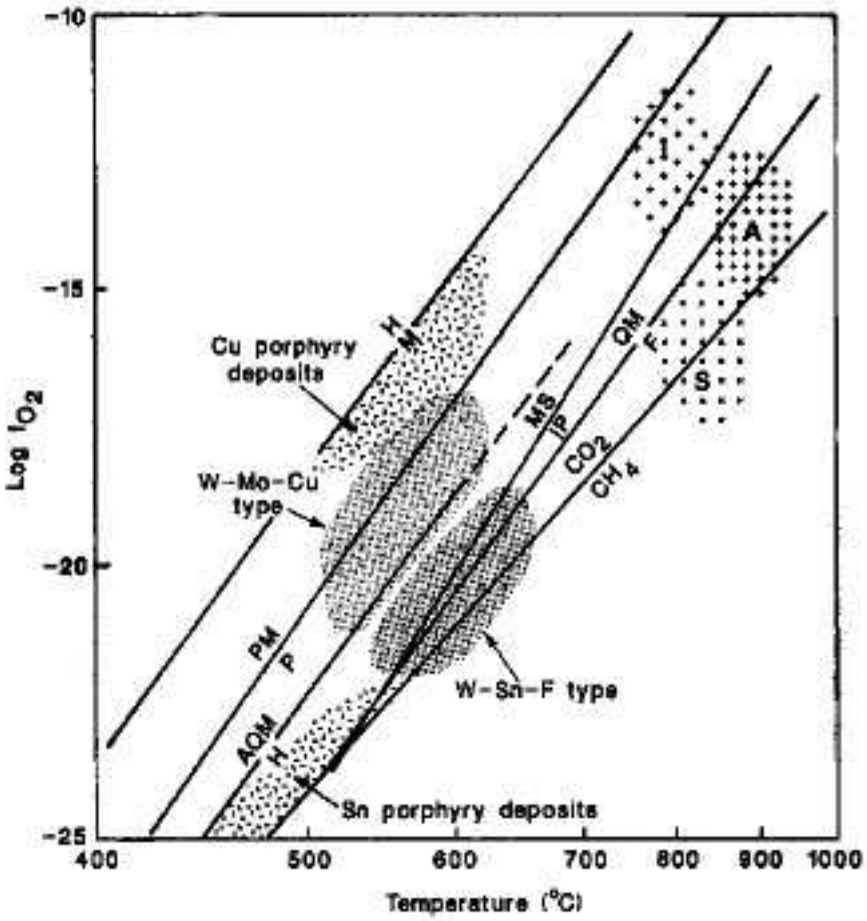

Figure 18. Oxygen fugacity versus temperature fields for typical I-, S- and A-type granitoids and for porphyry Cu, W-Mo-Cu skarn, W-Sn-F skarn and porphyry Sn mineralisation, together with a number of standard oxygen fugacity buffers (after Kwak and White, 1982). Mineral and fluid oxygen fugacity buffers that may be important controls on the magnetic mineralogy of the igneous intrusions and their associated mineralisation include (CO_2-CH_4; PMP = pyrite-magnetite-pyrrhotite; AQMH = andradite-quartz-magnetite-hedenbergite; MSIP = magnetite-sphene-ilmenite-pyroxene) as well as the FMQ and HM buffers.

Fig.6.4. Oxygen fugacity and temperature conditions prevailing during crystallisation of typical I-, S- and A-type granitoids and during formation of associated mineralisation (Clark, 1999; after Kwak and White, 1982).

wall rocks are diopside or garnetites proximally, passing outwards to marble. Intermediate vein alteration assemblages of quartz-orthoclase-biotite; quartz-chalcopyrite and quartz-orthoclase- chlorite-chalcopyrite within volcanic wall rocks have counterparts in the carbonate rocks in veins of quartz-(chrysotile or tremolite)-chalcopyrite. Late quartz-sericite-pyrite alteration in the volcanics is equivalent to pyrite-jasperoid in the limestone. Most of the copper mineralisation occurs in skarn adjacent to the porphyry stock. In cases such as these, the magnetic signature is distinctly asymmetric, reflecting the asymmetric alteration zoning.

Depth of Emplacement/Erosion Level/ Depth of Burial

Depth of emplacement is an important control on style of mineralisation, which directly affects the magnetic properties of the mineralised system. The observed magnetic signature depends strongly on the current depth of the system beneath the survey level. This in turn reflects the current level of exposure (in areas that have undergone significant erosion) or the depth of burial beneath younger sedimentary or volcanic rocks. For airborne surveys the flying height adds to the effective depth of the deposit. Figure 6. 6 illustrates a simple case of epithermal systems that are exposed at different levels in different parts of an extensive volcanic terrain.

Significant differences in magnetic susceptibility, at equivalent degrees of differentiation, are found for mantle-derived (M-type) intrusions, found typically in island arcs, and I-type granitoids in continental arcs. Intrusions associated with gold-rich porphyry copper deposits are more oxidised than those associated with gold-poor porphyry copper deposits, and accordingly contain more abundant igneous (titano)magnetite and produce greater quantities of hydrothermal magnetite during early potassic alteration. An empirical association between Au-rich (> 0.4 g/t) porphryry copper deposits and abundant magnetite in the potassic core has been documented by Sillitoe (1979, 1990, 1996) and confirmed by many other workers.

Lum *et al*. (1991) note that uplift rates may be important for generation of mineralisation. In active tectonic belts, such as the SW Pacific, uplift rates of 2 km per million years are common. Rapid uplift favours rapid vapour saturation, telescoping of mineralisation (e.g. porphyry and epithermal mineralisation at Porgera), and fault-controlled intrusion. At Chuquicamata rapid uplift (four times greater than uplift rates for the Sierra Nevada batholith) appears to have assisted development of fault-controlled late stage phyllic alteration that boosted copper grade to 1% from the "normal" 0.7% grade associated with potassically altered porphyry (B. McInnes, *pers. comm*.). Clearly, such rapid uplift rates exert a major influence on exposure level as a function of age and on development of supergene mineralisation.

The maximum depth of burial for which the magnetic signature of mineralisation is detectable can be predicted, for a given magnetic exploration model and regional magnetic environment. This can be useful for evaluating the utility of magnetics at the area selection stage and for airborne survey design.

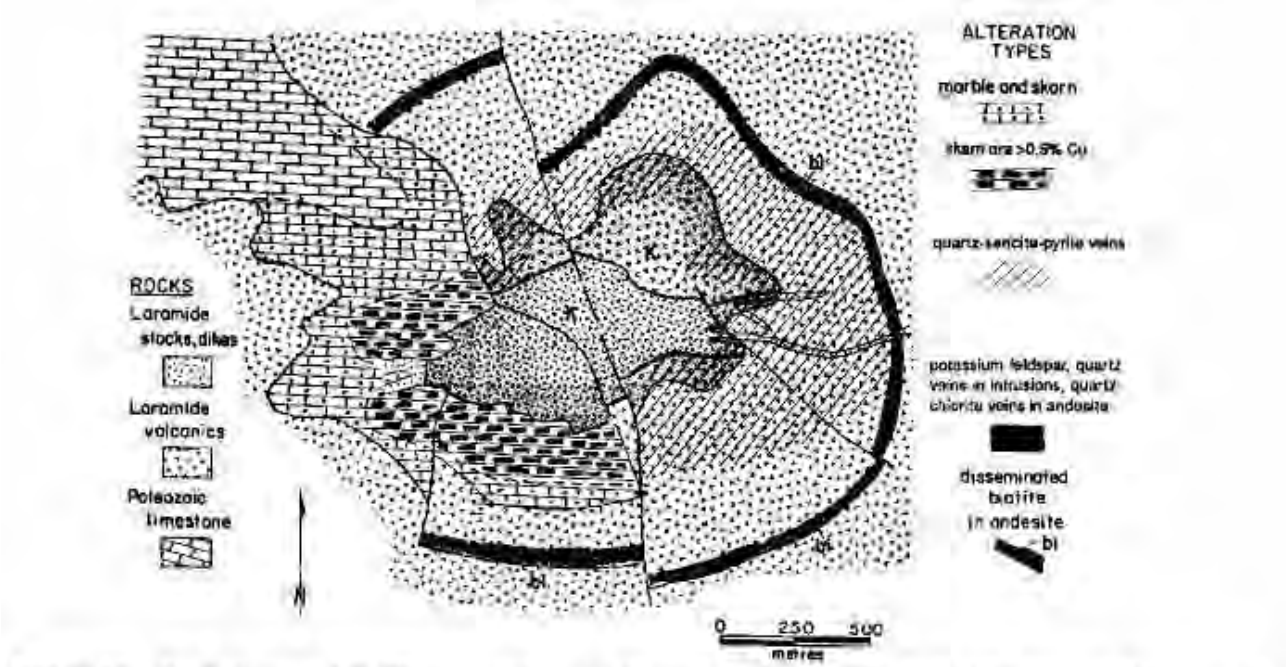

Figure 14. *Geologic map of the Christmas, Arizona, deposit, adapted from Koski and Cook (1982). Ores mined from this deposit have been from calc-silicate-altered Paleozoic carbonates on one side of a small intrusion. The deposit manifests alteration of both kinds of wall rock (carbonate and calc-silicate). Note that Koski and Cook have mapped an envelope of biotite alteration; most deposits of the southwest Arizona districts occur in such envelopes.*

Fig.6.5. Example of asymmetric alteration zoning around a mineralising porphyry emplaced along a contact between contrasting rock types (from Titley, 1994). Alteration assemblages are very different in carbonate wall rocks, on the western side of the porphyry, and silicate rocks (volcanics) on the eastern side. In such cases the magnetic signature is also predictably asymmetric. “Type” signatures can be generated for porphyries emplaced entirely into each rock type, or along a contact between different rock types (for each pair of contrasting lithologies).

Post-emplacement Faulting and Tilting

The Lowell-Guilbert (1970) porphyry copper model has been highly influential in exploration programs and has been successfully applied in many different areas. It may not always be remembered, however, that the model is based on a reconstruction of the San Manuel and Kalamazoo porphyry deposits in Arizona, which originally formed a single intrusion-centred orebody with concentric zoning, before being tilted and disrupted by faulting (Lowell, 1968; Force *et al*., 1995; see Fig.6.7). The present disposition of intrusive rocks and alteration zones in and around these orebodies differs greatly from the idealised model, but when the displacement along the San Manuel fault is removed and the intact porphyry system restored to the vertical, it is apparent that the system originally conformed closely to the model.

Such post-emplacement disruption of porphyry systems is common. Wilkins and Heidrick (1995) report that ~45% of the deposits of the southwestern North American porphyry copper province have been significantly faulted, extended and rotated during Oligocene and Miocene time. Tilting through more than 50° is common. Geissman *et al*. (1982) have quantified rotations in the Yerington district using palaeomagnetism. A palaeomagnetic study of the Porgera Intrusive Complex by Schmidt et al. (1997) showed that the upper levels of this complex have been disrupted by thin-skinned tectonics. The exposed intrusions have undergone substantial, but varying, degrees of tilting and rotation about vertical axes (Fig.6.8). Lum *et al*. (1991) point out the prevalence of local block rotations that distort outcrop patterns of high level intrusions and porphyry and epithermal alteration systems in the tectonically very active SW Pacific (Fig.6.9). Rotation rates of 20°-30° in 100,000 years are unexceptional.

A more straightforward modification of a zoned alteration system is afforded by the Chuquicamata Cu deposit, which has been bisected by a major fault, leaving a mineralized system with zoned alteration juxtaposed against unaltered intrusive rocks (Fig.6.10). Mineralised systems are susceptible to dismemberment, because major faults that controlled emplacement of intrusions and flow of hydrothermal fluids, as at Chuquicamata, are often reactivated during or after deposition of mineralisation.

It is evident that the magnetic and other geophysical signatures of tilted and dismembered porphyry systems differ substantially from those of the intact, upright equivalents. Detailed model studies of tectonically disrupted systems are required to facilitate recognition of such systems from their magnetic signatures. Figure 6. 11 demonstrates the profound change in magnetic signature when an analogue of the Kidston Breccia Pipe is tilted through a large angle.

Remanence Effects/Ages of Intrusion and Alteration

The magmatic-hydrothermal evolution of a porphyry deposit is often recorded faithfully by magnetic remanence carried by both primary and secondary magnetic minerals. Analysis of palaeomagnetic data from various intrusive phases of the Porgera Intrusive Complex showed that primary thermoremanences of the intrusions were highly rotated from the Miocene reference field directions, indicating post-emplacement structural disruption (Schmidt et al., 1997). Overprint magnetisations associated with hydrothermal alteration were less rotated (Fig.6.8), but still

moderately discordant to the Miocene field, indicating that the alteration occurred while tectonic rotation of the intrusions was continuing and allowing the sequence of rotation events to be constrained. At least two reversals of the geomagnetic field were recorded by the altered intrusive rocks of the Porgera Intrusive Complex, allowing some magnetostratigraphic constraints on relative timing of multiple intrusive and alteration events.

In some cases the remanent magnetisation is sufficiently intense that it can substantially influence the magnetic anomalies associated with porphyry systems. The importance of remanence depends on a number of factors, including the composition of the intrusions and the country rocks and on the behaviour of the geomagnetic field at the time the porphyry system was forming. The geomagnetic field was reversing rapidly during the Tertiary and porphyry systems of Tertiary age are generally characterised by dual polarity remanences, with substantial cancellation of the effective contribution of remanence to the magnetic anomaly. Porphyry systems emplaced in the Cretaceous normal Polarity Superchron or the Permo-Carboniferous Reverse Polarity Superchron, on the other hand, have much more consistent remanence directions throughout the deposit and their magnetic anomalies are therefore are more likely to be influenced by remanence.

A recent study of the Candelaria Cu-Au deposit in Chile suggested that the associated magnetic anomaly is dominantly due to remanent magnetisation, carried by hydrothermal magnetite, which has reversed polarity, was probably acquired during an Early Tertiary remagnetisation event and has been rotated clockwise from the reference field direction by regional crustal rotations (Taylor, 2000). Figure 6. 12 shows a local magnetic anomaly map, which has a low to the NE and a high to the SW. Viewed in isolation this signature suggests a source magnetisation that is dominated by remanence of reversed polarity, with azimuth rotated clockwise from south (the reference field direction for reversed polarity Late Cretaceous-Recent magnetisations in cratonic South America).

Our magnetic property measurements of samples from the Candelaria mine and nearby batholithic rocks, and a reassessment of the regional magnetic anomaly patterns, show that this apparent reversed magnetisation is an artefact of ignoring the magnetic context of the anomaly. In fact RTP magnetic highs correspond well to the two main Candelaria orebodies (Mathews and Jenkins, 1997), the northernmost of which is off the map in Fig.6.12.

Sexton et al. (1995) and Clark (1996) have discussed the magnetic properties of the Mount Leyshon Au deposit, Queensland, which is associated with a pronounced magnetic low due to reverse polarity remanence acquired by hydrothermal magnetite in the Permian. Figure 6. 13 shows the disposition of the magnetic anomaly with respect to the intrusive breccia and porphyry complex and the gold mineralisation. It is noteworthy that the zone of palaeomagnetic overprinting extends well beyond the visible alteration and the magnetic anomaly, providing a larger exploration target. Furthermore, the palaeomagnetic carriers are zoned from distal hematite to proximal magnetite, providing a vector to the core of the system.

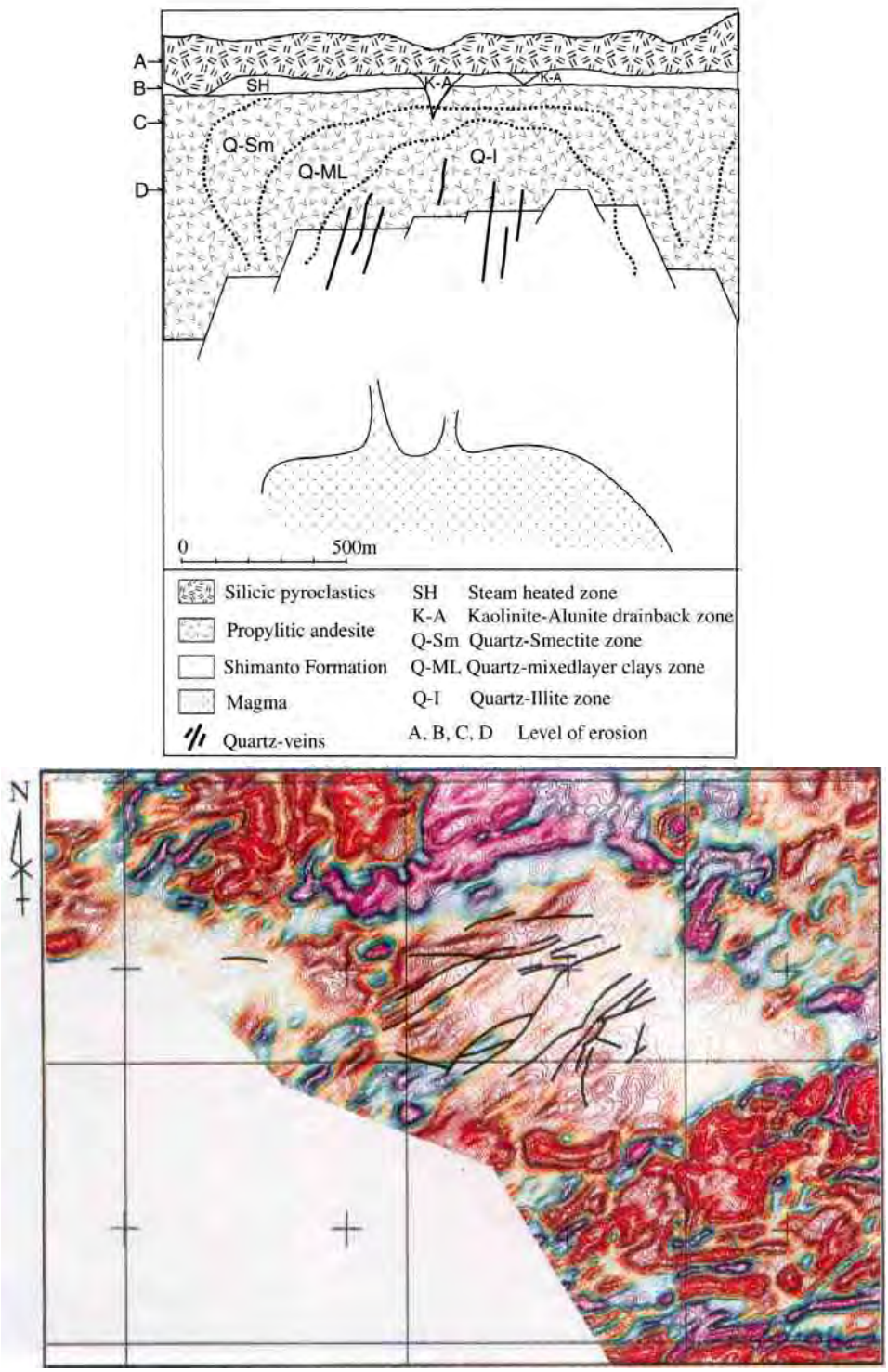

Fig.6.6. In detailed aeromagnetic data over the Hokusatsu area a flat smooth texture is associated with low-sulphidation epithermal mineralised zones for a wide range of erosion levels. However, the amplitude of the base level shift and the textural contrast with the surrounding , variably magnetised, volcanics varies with the current level of exposure. Alteration mapping, geochemistry and airborne radiometrics are ineffective in Case A, but are increasingly useful with increasing erosion. From Feebrey *et al*. (1998).

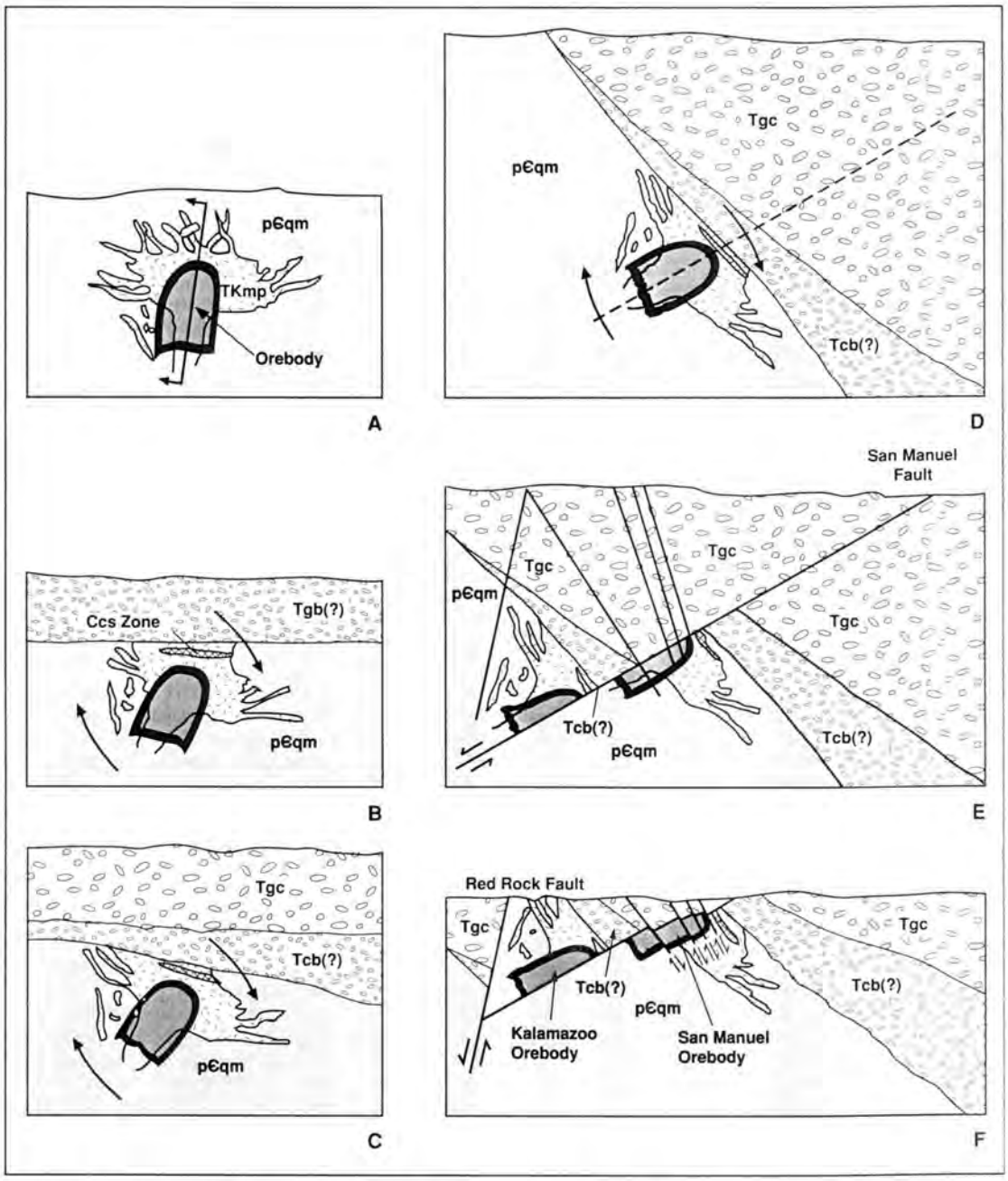

Figure 7. Schematic east-northeast to west-southwest-oriented cross section showing the sequential tectogenetic development of the San Manuel-Kalamazoo Orebody. (A) Precambrian quartz monzonite (pЄqm) intruded by Laramide age monzonite porphyry (TKmp) dike swarm with the near hollow, cylindrical 1 by 2.5 km San Manuel-Kalamazoo Orebody formed nearly vertical and centered on the dike swarm. (B) Top-to-the-east tilting of the orebody followed by erosion, deposition of upper Oligocene Cloudburst volcanics and conglomerates (Tcb?) and chalcocite blanket development (Ccs). (C) and (D) Progressive erosion, tilting, synorogenic deposition of the lower Miocene Gila Conglomerate (Tgc), and initiation of movement along the San Manuel Fault. (E) Upper portion of orebody displaced 2.5 km west-southwest downdip along the San Manuel Fault. (F) Late Miocene uplift, erosion, and conjugate high-angle Basin and Range normal faults offset orebody and San Manuel Fault. See Lowell (1968) for details.

Fig.6.7. Tectonic rotation and disruption of the San Manuel – Kalamazoo porphyry copper system, which serves (after restoration) as a “type” example of the Lowell-Guilbert (1970) quartz-monzonite porphyry copper model (from Wilkins and Heidrick, 1995).

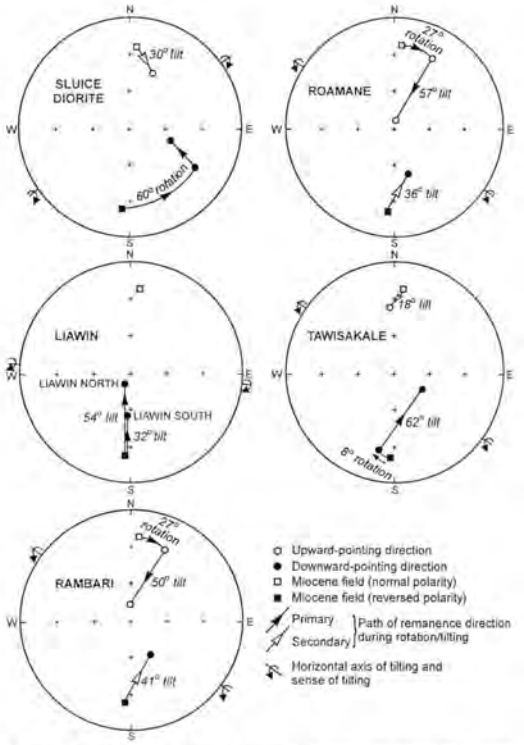

Figure 3. Hypothetical rotations of Porgera intrusions with respect to the Late Miocene reference field direction. The relationships allow the relative timing of the rotations and alteration to be determined (open symbols plot on upper hemisphere, closed symbols on lower hemisphere).

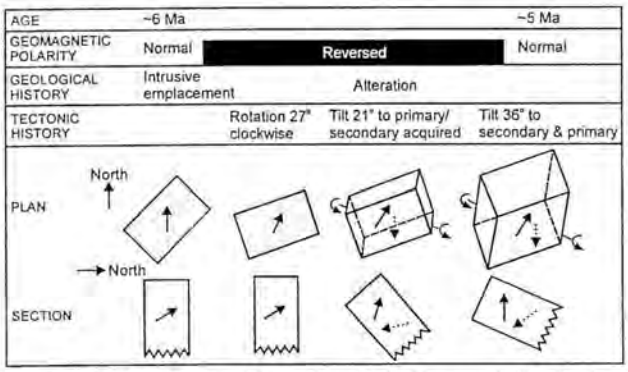

Figure 4. A model of the tectonic history keyed to the Geomagnetic Polarity Time

Fig.6.8. Local rotations of fault-bounded blocks within the upper levels of the Porgera Intrusive Complex, which hosts telescoped quartz-roscoelite epithermal Au and porphyry Au-base metal deposits, occurred during the magmatic-hydrothermal evolution of the complex, in response to thin-skinned tectonic processes. The upper diagram shows primary remanence directions, which are highly rotated with respect to the Miocene reference field axis, and less-rotated secondary remanence components that record emplacement and hydrothermal alteration respectively. For each block the total rotation can be resolved into tilting and azimuthal rotation. The inferred rotation history is illustrated for the Roamane intrusion, which hosts the high-grade epithermal Au deposit. The complex records at least two geomagnetic reversals during the evolution of the system (from Schmidt *et al*., 1997).

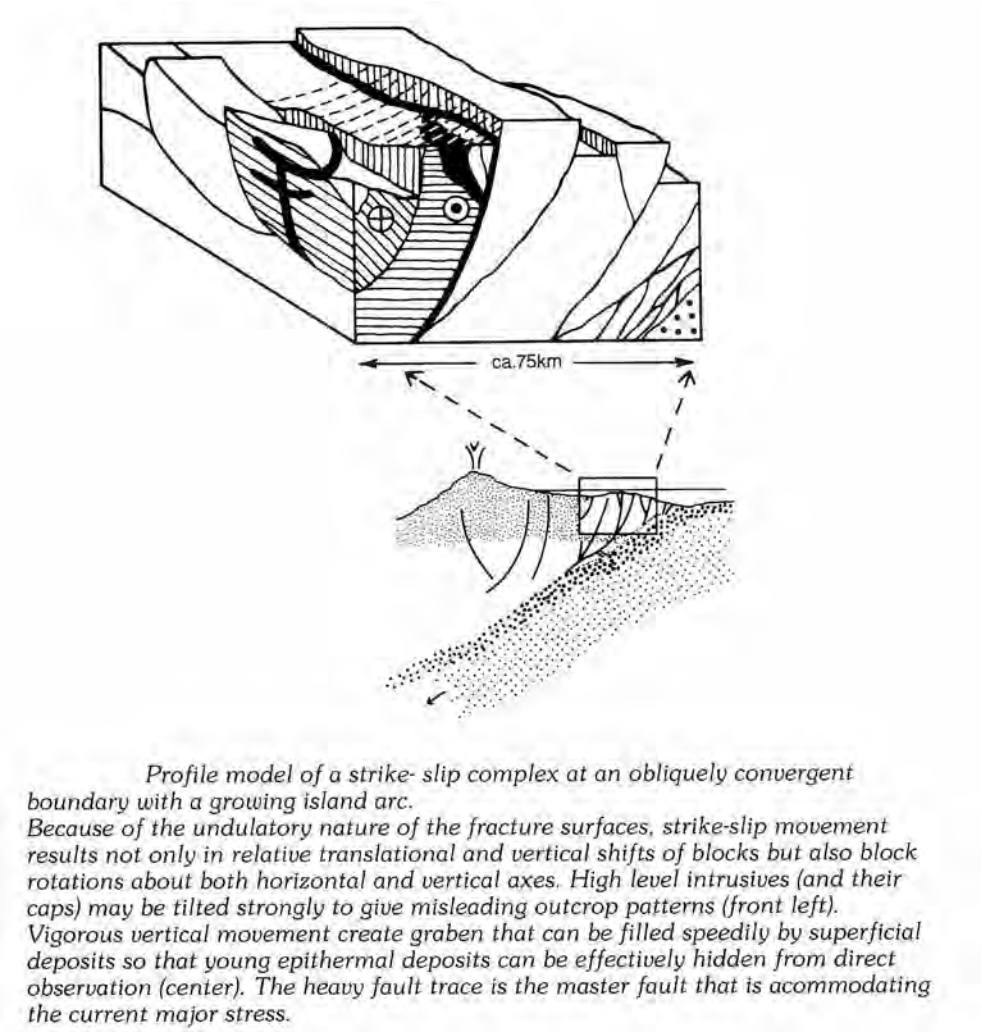

Fig.6.9. Rapid differential uplift and rotations of fault-bounded blocks in active fold-and-thrust belts affect the level of exposure and distort outcrop patterns and, by implication, the geophysical signatures of epithermal and porphyry deposits (from Lum *et al*., 1994)

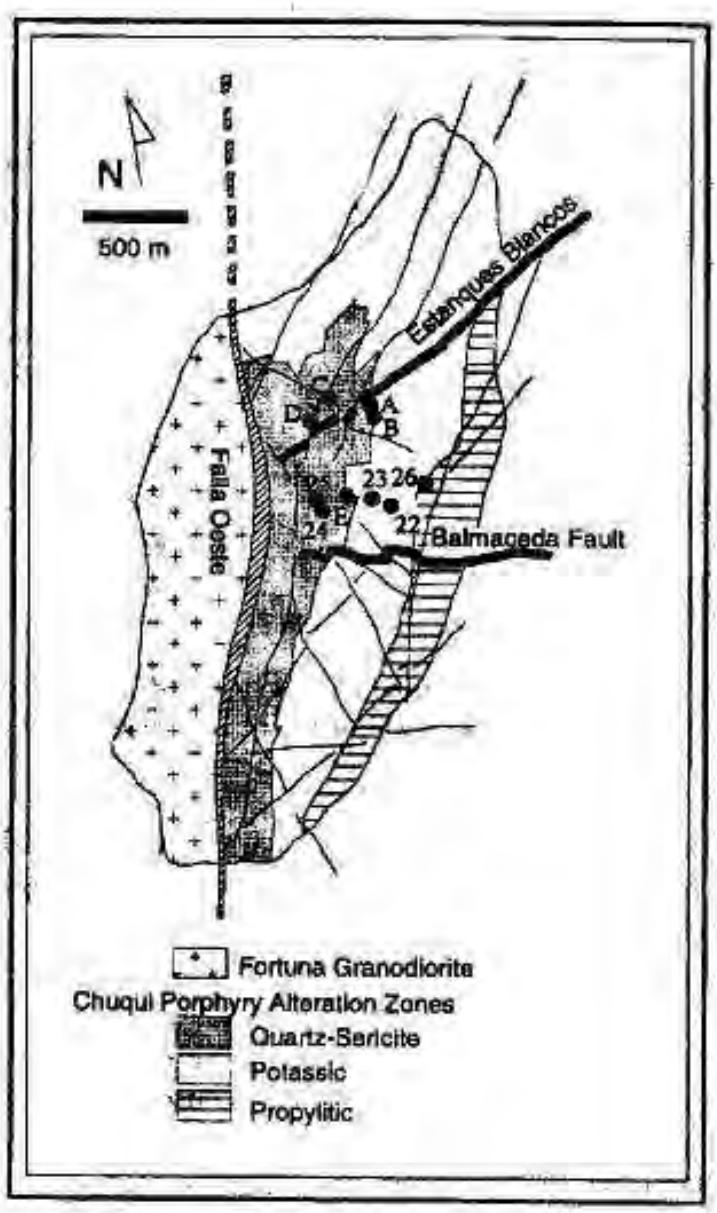

FIG. 6. Structural systems found at Chuquicamata as interpreted by Martin et al. (1993). Estanques Blancos (R) and Balmaceda (R') faults are emphasized. These faults had been interpreted as a Riedel-type strike-slip system, with the Falla Oeste being the master fault (cf. Fig. 5). Structural sampling sites discussed in the text are shown.

Fig.6.10. Example of an mineralised system truncated by a post-mineralisation fault, producing a highly asymmetric alteration zoning pattern and provoking a search for the missing half of the orebody (from Lindsay *et al*., 1995).

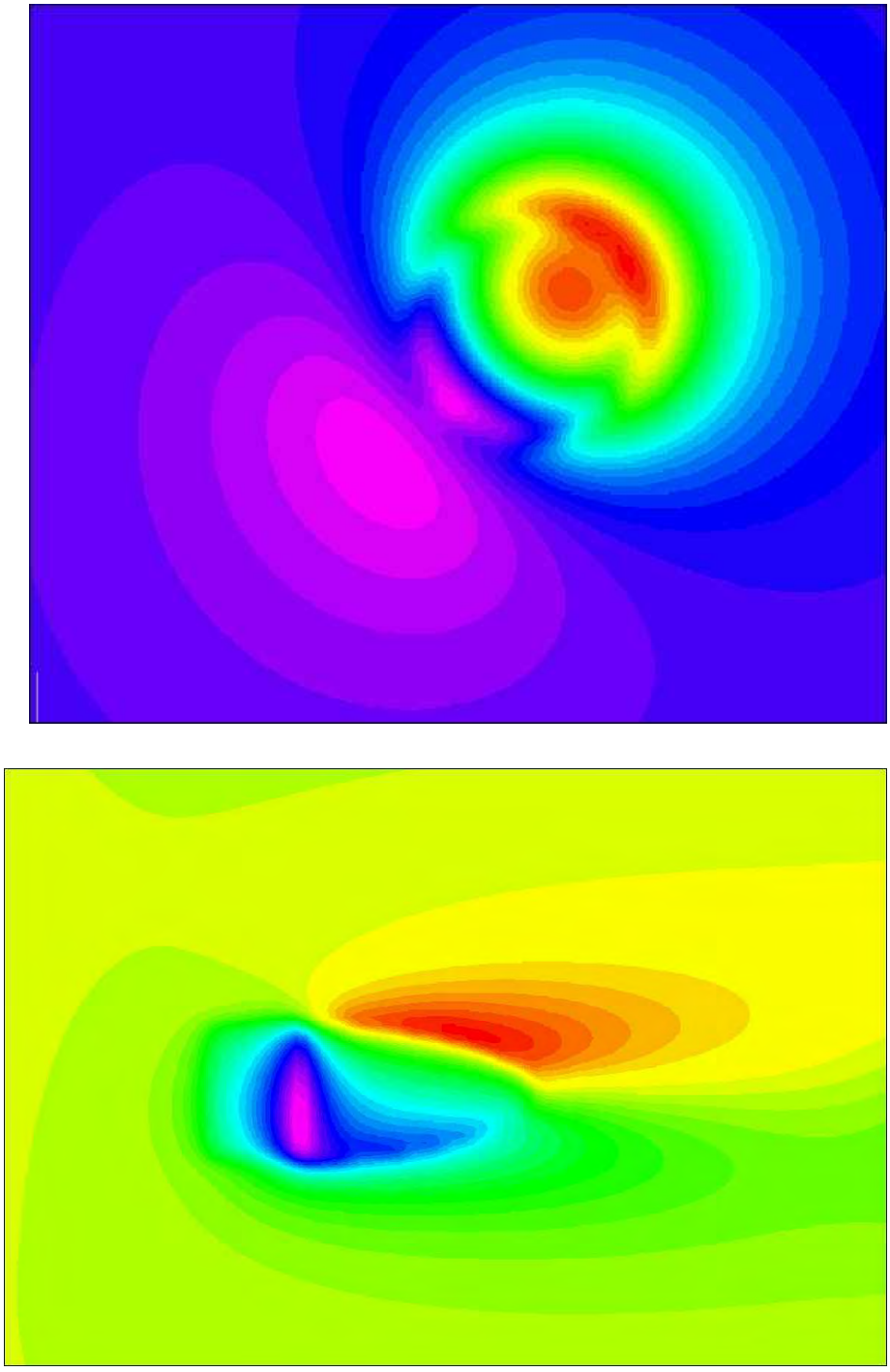

Fig.6.11. Predicted RTP magnetic anomalies over an analogue of the Kidston Breccia Pipe, North Queensland. The magnetic anomaly reflects a shallow non-magnetic zone of pyrite-rich phyllic alteration, which produces a negative magnetisation contrast with the moderately magnetic country rocks, plus the magnetic response from the deep phyllic zone, which has pyrrhotite as well as pyrite. The magnetisation of the pyrrhotite is dominated by remanence, acquired in the Early Carboniferous during the phyllic alteration event. Top: Magnetic signature of the untilted system; Bottom: signature assuming system was subsequently tilted 70°, producing a plunge of 20° to the east (Clark and Dickson, 1997).

The aeromagnetic anomaly is asymmetrically disposed with respect to the gold deposit, because the mineralised intrusive breccia and porphyry complex was emplaced along a geological contact, with much more significant development of secondary magnetite during early potassic (biotite) alteration of the metasiltstones and dolerites to the south than in the equivalent (K-feldspar) alteration in the very felsic granite to the north. However, the palaeomagnetic overprinting is detectable within the granite several kilometres from the complex, although the magnetisation is too weak to produce a detectable aeromagnetic anomaly.

Metamorphism

In older deposits, metamorphism can substantially modify the magnetic mineralogy of the deposits and host rocks, with concomitant changes in the magnetic anomaly pattern. Although the majority of porphyry and epithermal deposits are relatively young and, at most, weakly metamorphosed, some relatively ancient deposits are known. There is a strong possibility that some older porphyry and epithermal deposits occur that have not been recognised, because effects of metamorphism and deformation have obscured their true nature.

Metamorphism alters the partitioning of iron between magnetic oxides and silicate minerals, and can drastically change the magnetic properties of intrusions and host rocks. Pyrite/pyrrhotite ratios are also modified by metamorphism, with important effects on magnetic properties of mineralised zones and their associated magnetic signatures.

Magnetic Environment

When the *geological* model of a mineralised system is well defined and the magnetic petrology is well understood, it is possible to predict a type magnetic signature, for any assumed subsequent geological history. However, the expected signature will still depend on the local *magnetic environment*. In some areas strong regional gradients, or overlapping anomalies, distort the observed signature and can make it difficult to recognise, as shown in Fig.6.14. In areas with rugged topography, magnetic signatures can be distorted by topographic effects.

These problems can be ameliorated by using the grid of values for the type magnetic signature as a template that can be moved over a “regional field” map (a suitably smoothed version of the observed magnetic survey data). At each location the predicted signature, including the distortion produced by the magnetic environment can be calculated by adding the undistorted type signature to the interpolated “regional” field. The location-sensitive predicted signatures be then be compared with observed local anomaly patterns, to recognise prospective targets. Once such targets are recognised, subtraction of a sensibly interpolated regional field from the observed field, should yield a residual anomaly that can be compared with the type signature and interpreted in more detail.

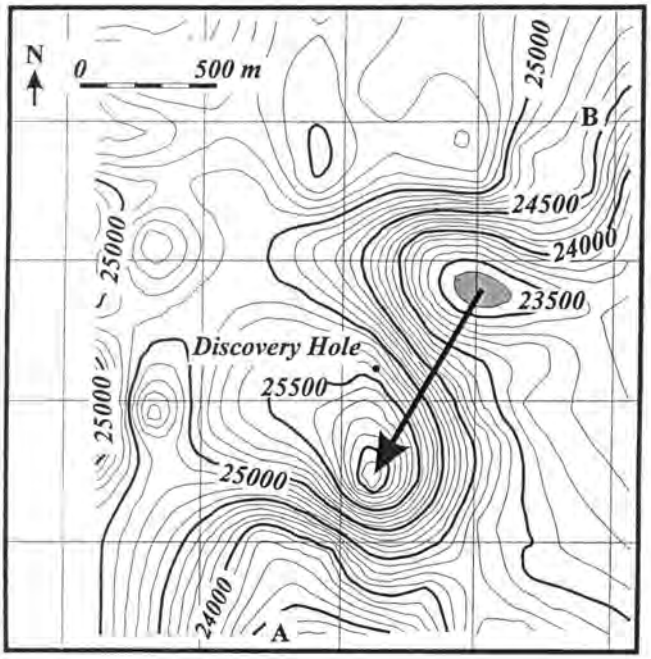

Total field ground magnetic anomaly map of the Candelaria area (after Ryan et al. 1995). The original discovery hole is located close to the NE-SW trending axis of the anomaly (marked by the *arrow*). Note that the low and high parts of the anomaly are located to the NE and SW respectively, with a subsidiary low to the south marked by the open contours. Grid lines are every 500 m, magnetic anomaly values are in nT, contour intervals are 100 nT and closed magnetic lows *shaded*. *A-B* marks the line of profile modelled in Fig. 6

Fig.6.12. Magnetic anomaly of the Candelaria Cu-Au deposit, apparently exhibiting a remanence-dominated signature. The dipolar anomaly has reverse polarity and the anomaly axis is rotated clockwise, reflecting tectonic rotation of the remanence, together with the crustal block that hosts the Candelaria deposit (Taylor, 2000). Viewed in its magnetic context, however, this local anomaly is only part of a larger anomaly associated with magnetite-rich alteration/mineralisation to the NE. Anomaly patterns are also complicated by the low field inclination in this area.

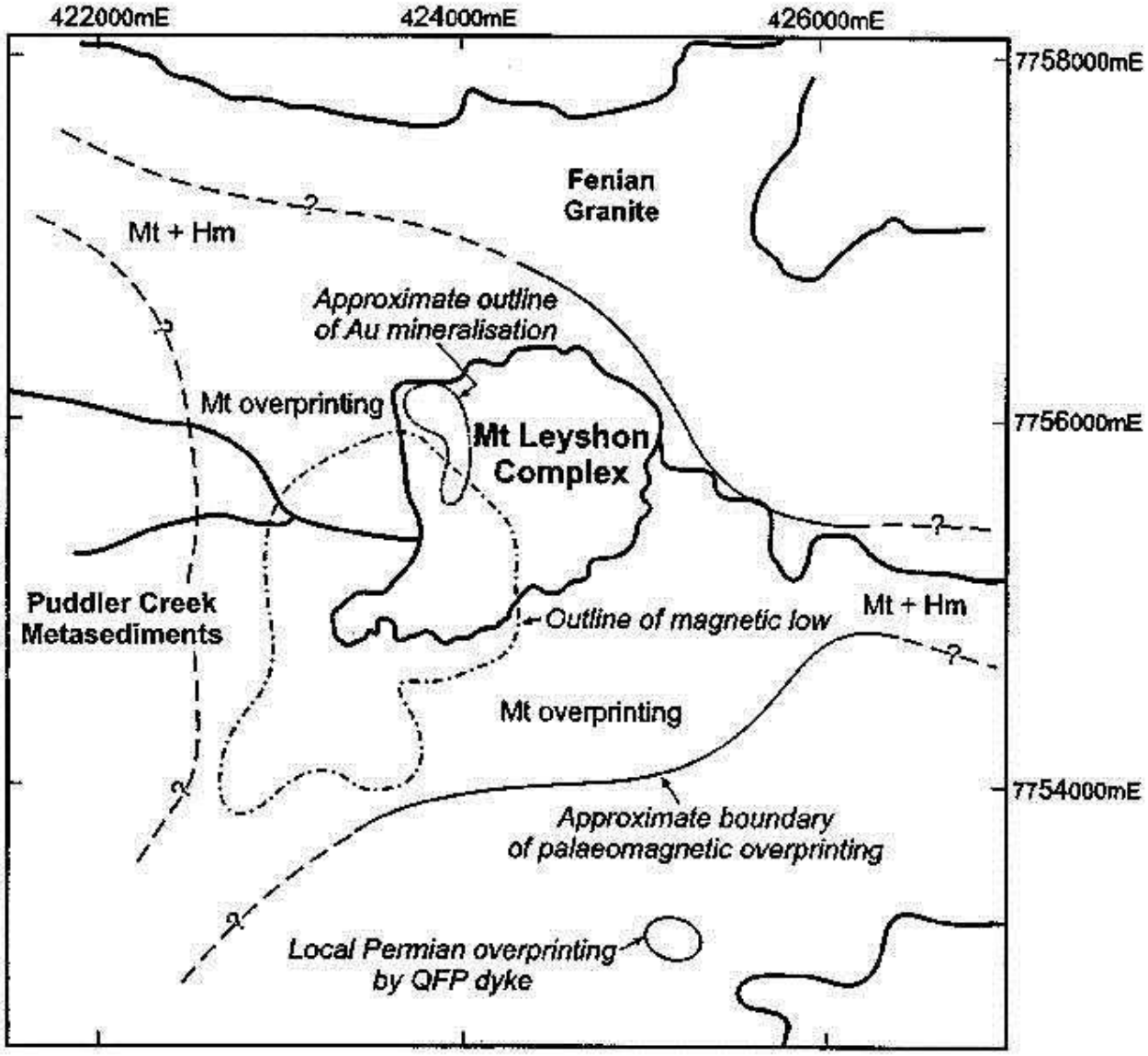

Fig.6.13. The Mount Leyshon Intrusive Complex, North Queensland, exhibits a broad zone of palaeomagnetic overprinting (Clark, 1996). The reverse polarity, Early Permian palaeomagnetic overprint can be detected well beyond the zone of visible alteration and the associated magnetic anomaly. The palaeomagnetic signature can therefore provide a larger target zone, in favourable circumstances, and allows fluid pathways to be traced (along an ESE trending fracture zone and to the SW, along the Mount Leyshon corridor). Palaeomagnetic zoning at Mount Leyshon is magnetite-dominant proximally and hematite-dominant distally.

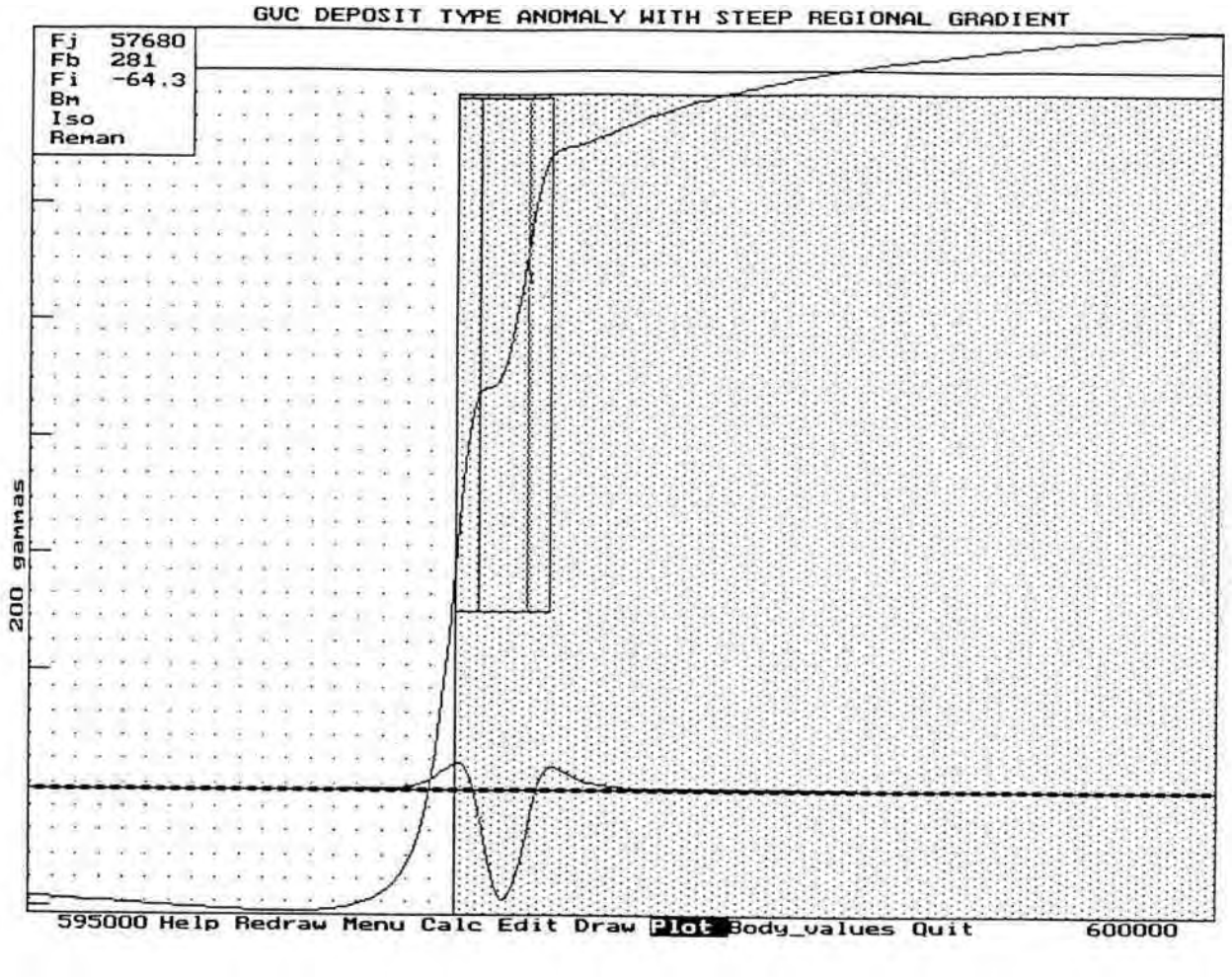

Fig.6.14. Distortion of “type” magnetic signature by strong magnetic field gradient. The lower profile shows a symmetric RTP TMI profile over a Goonumbla-type Cu-Au deposit, with an early broad halo of biotite-magnetite alteration, centred on the narrow mineralising intrusion, which is subsequently overprinted by phyllic alteration, in and around the porphyry spine. However, mineralising intrusions in the Goonumbla Volcanic Complex are tapped off larger, zoned intrusions that produce strong anomalies. The strong magnetic field gradient associated with a large intrusion distorts the signature of the deposit, which degenerates to the subtle inflections shown on the steep “regional” field caused by the large neighbouring intrusion (upper curve).

7. PETROPHYSICAL PROPERTIES OF VOLCANO-PLUTONIC TERRAINS, PORPHYRY SYSTEMS, IRON OXIDE COPPER-GOLD SYSTEMS AND VOLCANIC-HOSTED EPITHERMAL SYSTEMS – P700 CASE STUDIES

7.1 Magnetic properties of the Candelaria Fe oxide Cu-Au deposit, Chile

Sampling

Oriented blocks were collected from exposures in the north pit of the Candelaria mine. Three localities represent the magnetite and/or hematite-rich mineralisation within the Lower Andesite unit, and other two represent skarns located within the Upper Andesites. Diorite samples belonging to the Mid-Cretaceous batholith were collected at two additional sites. In addition, representative samples of oriented drill cores from holes SO-009, SO-010 and SO-011 were taken. Each sample was redrilled to obtain cylindrical specimens of 2.5 cm diameter and 2.2 cm height, for palaeomagnetic measurements.

Basic magnetic properties

Some of the samples have very high susceptibilities, and therefore the measured magnetic properties of the specimens are affected by self-demagnetisation. The results given below have been corrected for self-demagnetisation, to give representative values that the rock units would exhibit *in situ*.

A natural remanent magnetisation (NRM) more representative of the *in situ* remanence carried by multidomain magnetite-bearing rocks was obtained after applying low temperature demagnetisation using liquid nitrogen. This palaeomagnetic cleaning technique largely removes the contamination induced by drilling, exposure to pencil magnets or other causes, which often affects the remanence of multidomain magnetite (i.e. magnetite with grain size greater than ~20 μm).

The bulk susceptibilities, remanence vectors and Koenigsberger ratios are given in Table 7-1. The combined NRM (J) for each sample is calculated as the vector sum of the individual specimen NRMs, divided by the number of specimens. The Koenigsberger ratio (Q) was calculated as J/kF, where k is the susceptibility and F is the geomagnetic field strength in equivalent units to J (B= 22,300 nT, F= 17,750 mA/m). Alternating field (AF) and thermal demagnetisation were applied to selected specimens from every site. Demagnetisation behaviour for representative samples is illustrated in the composite plots (demagnetisation curves, stereonets and vector plots).

Most of the samples have high bulk susceptibilities due to the presence of magnetite. The maximum values (2-8 SI) were observed in semi-massive magnetite sampled in pit exposures and in hole SO-011. A substantial part of the remanence of these rocks (60-80%) was removed by low temperature demagnetisation, which indicates multidomain magnetite is the main carrier of the NRM.

Although scattered, NRM directions plot broadly in the NE quadrant of a stereonet, with moderate negative (upward) inclination; some samples, however, have positive

(downward) inclination. The scatter is higher for more strongly magnetic samples, which contain abundant multidomain magnetite that is not capable of carrying a very stable remanence. Because raw NRMs are often contaminated by spurious components, acquired during mining or diamond drilling, or induced by exposure to pencil magnets or other sources of magnetic fields, "cleaned" remanence directions are less scattered and more representative of the undisturbed *in situ* NRM directions. AF cleaning in 10 mT removes most sources of palaeomagnetic noise in these samples, revealing two main clusters of directions: a dominant group in the NE up octant and a subordinate, antipodal, cluster in the SW down octant (Fig.7.1). This implies that both polarities of remanent magnetisation are observed, although normal polarities predominate. The remanence directions overall are rotated clockwise with respect to the expected directions for mid-Cretaceous/Early Tertiary fields, which for an unrotated terrane at this latitude are north with moderate negative inclination (normal polarity) or south with moderate positive inclination (reverse polarity).

The Koenigsberger ratios (Q) of the samples are typically much less than one, indicating that remanence is subordinate to induced magnetisation for these samples. This conclusion is reinforced by the partial cancellation of remanent magnetisations within the orebody due to the presence of opposite polarities. Thus there is no evidence from this collection of samples for the intense reversed remanence inferred for the Candelaria orebody by Taylor (2000), based on modelling of a portion of the associated magnetic anomaly. However, the remanence directions do support the inferred clockwise rotation of the terrane that hosts La Candelaria with respect to cratonic South America.

Stability of remanence

Demagnetisation behaviour for representative specimens of all rock types is shown in Figs.7.2-11. AF demagnetisation almost completely removes the remanence of strongly magnetic rocks in applied peak fields of 30-50 mT (e.g. Figs.7.2-3). Thermal demagnetisation produced noisy results, however remanence was erased with temperatures of 550-580^{o}C (Fig.4). This behaviour characterizes all the orebody samples and most of the remaining highly magnetic specimens.

On the other hand, some samples from the Lower Andesite unit are moderately magnetic and show very stable behaviour. The sigmoid shape of the AF demagnetisation curve and the discrete unblocking temperature around 570^{o}C point to the presence of single domain magnetite, which is submicron in size (Fig.7.10). An intermediate behaviour between the two described above was observed in a few sites, suggesting the presence of pseudosingle domain magnetite grains in the size range 1-20 µm.

By contrast, weakly magnetic skarn specimens have a very stable magnetisation (Figs.7.5-6), which could not be removed with peak fields as high as 100 mT. The unblocking temperature of 300-350°C suggests that monoclinic pyrrhotite is the mineral carrying the remanence.

Samples from dioritic rocks of the batholith carry remanence with moderate to high stability to AF (Fig.7.7), which thermal demagnetisation unblocks predominantly

between 500°C and 580°C, indicating that the main magnetic carrier is pseudosingle domain magnetite.

Palaeomagnetic directions

The main intrusive and hydrothermal events in the Candelaria area are mid-Cretaceous in age, during the Cretaceous normal polarity superchron, which lasted from 118 Ma to 83 Ma. Thus remanence directions recorded at Candelaria should have normal polarity. Figure 7.1 shows that remanence directions from the magnetite-rich orebody are somewhat scattered, even after AF cleaning to 10 mT. This may reflect local deflections of the geomagnetic field within the highly magnetic orebody, similar to the deflections of compass needles observed within the Candelaria pit and in bore holes. However, the NE dominant grouping and the subordinate SW cluster are still apparent in the stereogram (Fig.7.1(a)). The two antipodal clusters are much better defined for samples from holes SO9 and SO11. Skarn samples from the pit, within the Upper Andesites, all exhibit normal polarity cleaned directions, as do samples from the batholith (see Fig.7.1(e-f)). Directions from hole SO10 are quite scattered. Overall the cleaned remanence directions suggest a clockwise rotation of the Candelaria area, including the adjacent batholith, of at least 45° since the acquisition of the normal and reversed remanence components.

Detailed analysis of remanence components isolated by AF and thermal demagnetisation reveals a complex history of overprinting in these rocks and ores. Figures 7.2-11 illustrate the variety of behaviour exhibited by these samples. Figure 7.2 shows that the remanence of a semi-massive magnetite ore sample from site 1 in the pit is dominated by a NE up (normal) component of moderate coercivity that is removed steadily up to 50 mT, revealing a much less intense, but more stable, reversed component at higher demagnetising fields. This is shown by the directions on the stereonet moving steadily towards, and then into, the SW down octant as the vector endpoints trend past, rather than directly towards, the origin. By contrast, a similar specimen from site 2 shows only the normal polarity, NE up component (Fig.7.3), whereas another ore sample from site 3 shows only a reversed component that is stable to ~570°C (Fig.7.4).

Figure 7.5 shows that a skarn specimen from site 4 has a single NE up component that is barely changed by 10 mT AF, but is totally demagnetised by heating to 350°C. Judging from its demagnetisation characteristics and the NRM intensity, this component appears to be carried by trace amounts of fine-grained monoclinic pyrrhotite.

Figures 7.6-7 illustrate a diorite sample that carries a single normal polarity component of high coercivity, stable to 100 mT, and another sample for which AF demagnetisation reveals a subordinate reversed component, removed in fields between 2 mT and 20 mT, superimposed on a NE up component that is stable up to 100 mT. Thus even the batholith records a subtle overprinting event with reversed polarity, presumably acquired post 83 Ma. The stable normal polarity remanence is interpreted as primary, dating from initial cooling of the mid-Cretaceous diorite intrusion.

The skarns and hornfelses that enclose the Candelaria orebody also show clear evidence of a post 83 Ma overprint magnetisation with reverse polarity, although the dominant component is a normal polarity remanence of moderate to high stability which is interpreted as acquired during the alteration event(s) that have created the magnetic minerals (predominantly magnetite). Figure 7.8 shows a sample with only the normal polarity component, whereas Figs.7.9-10 show samples that are completely overprinted, so that they carry only the reverse polarity component. Figure 7.11 shows that a specimen of typical biotite-albite-quartz altered "hornfels" of the Lower Andesites carries both normal and reverse polarity components, with the normal component initially removed by AF demagnetisation to 9 mT, revealing a reversed component that is removed up to 350°C, after which the residual remanence is again normal. The most stable component is not very well resolved, because the demagnetisation behaviour is noisy, but is still present up to 580°C (the Curie temperature of magnetite). The normal polarity magnetisation appears to be carried by both magnetite and hematite, while the reverse polarity component is probably carried by pyrrhotite.

Conclusions

- The magnetisation of the Candelaria orebody is predominantly induced, refuting earlier suggestions (Taylor, 2000) that the associated magnetic anomaly is dominated by remanence. Modelling of the Candelaria anomaly in its regional context is required to reconcile the measured properties with the observed magnetic anomalies.
- The average susceptibility of the orebody samples is 3.4 SI, reflecting the high magnetite content of the Candelaria mineralisation. Altered host rock samples adjacent to the orebody have an average susceptibility of 0.12 SI and diorite samples from surface exposures of the batholith have much lower average susceptibility (~0.04 SI). Remanent magnetisation of the orebody is on average directed NE and up, but is only 10% of the induced magnetisation.
- Both polarities of remanence are recorded by the rocks and ores of the Candelaria area. The dominant normal polarity component is NE and up. This component is interpreted as mid-Cretaceous: primary in the case of the diorites; secondary, associated with magnetite (and minor pyrrhotite) alteration, in the Candelaria sequence. The subordinate reverse polarity direction is antipodal: SW down. This is interpreted as an overprint related to a low grade thermal event or weak alteration event that is considerably younger (< 83 Ma) than the mid-Cretaceous Candelaria mineralisation.
- Palaeomagnetic directions indicate clockwise rotation of the Candelaria area, including the nearby batholith, through at least 45° since the mid-late Cretaceous. This rotation is recorded by reverse polarity directions as well as normal polarity remanence, indicating that it occurred post 83 Ma. This conclusion confirms the suggestion of Taylor (2000) that the area had undergone clockwise rotation, based on the NE-SW orientation of the axis of a local dipolar magnetic anomaly at Candelaria.

Reference

Taylor, G.K. 2000. Palaeomagnetism applied to magnetic anomaly interpretation; a new twist to the search for mineralisation in northern Chile. Mineralium Deposita, **35**, 377-384.

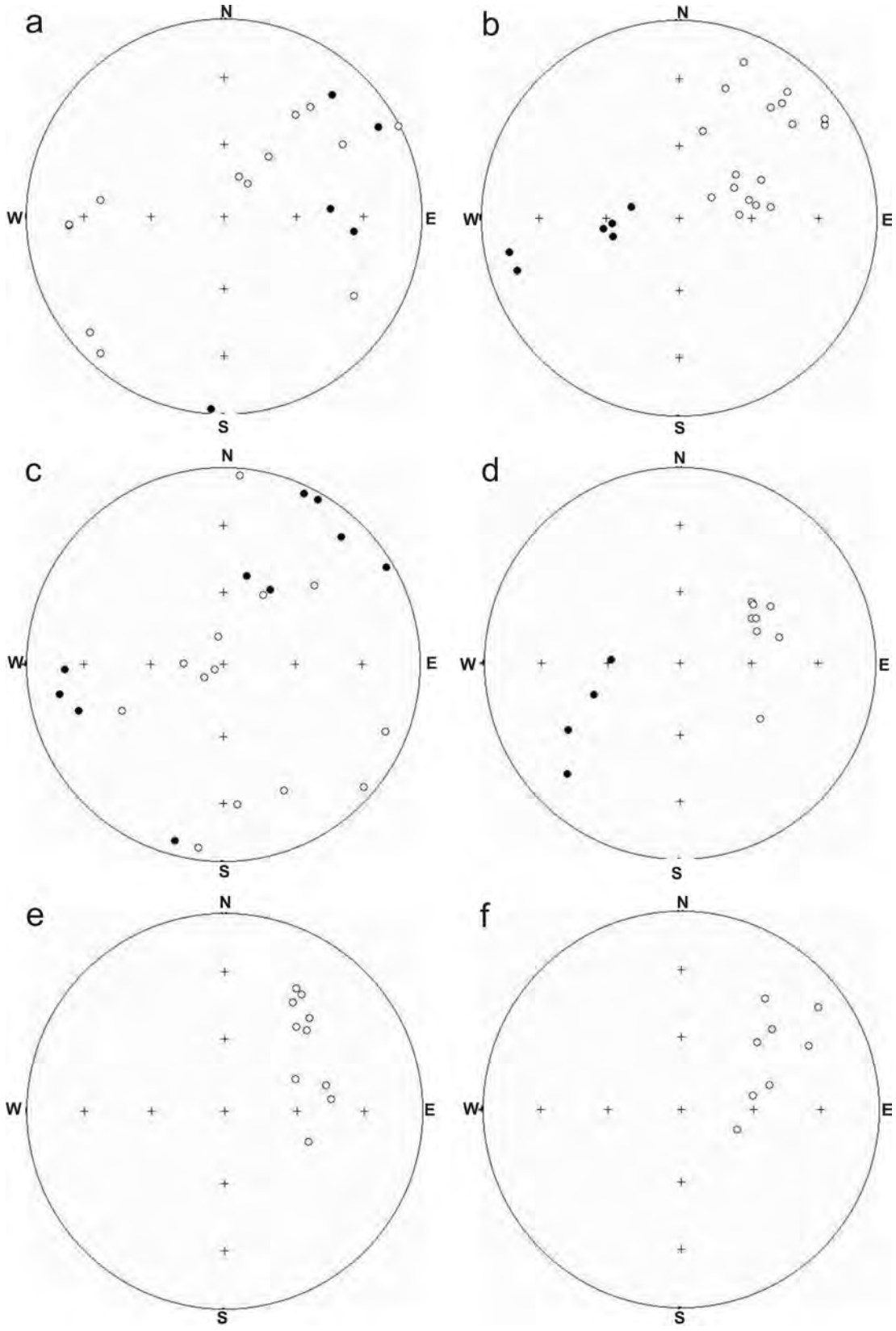

Fig.7.1. Stereograms of “cleaned” remanence directions (10 mT AF) from (a) the Candelaria orebody, (b) drill hole SO9, (c) hole SO 10, (d) hole SO11, (e) skarn samples from the Candelaria pit, (f) the batholith. Open symbols are on the upper hemisphere (negative inclinations), filled symbols are on the lower hemisphere (positive inclinations).

Table 7-1. Magnetic properties of Candelaria samples

Site/ sample	Rock unit	Alteration	Susceptibility (10^{-3} SI)	NRM Dec (°)	NRM Inc (°)	NRM Int (A/m)	Q
can01*	Lower andesite	Bio-qtz-amph-mt-cp (py, hm)	4949.0	249.2	-29.6	18.192	0.25
can02	Lower andesite	Bio-qtz-amph-mt-cp (py, hm)	2597.7	11.9	-60.8	5.809	0.18
can03	Lower andesite	Bio-qtz-amph-mt-cp (py, hm)	8153.5	49.6	-36.4	30.699	0.32
can04	Upper andesite	Pyx-scap-gar-(Kfsp) (skarn) ovp bio (hnfls)	0.3	37.6	-34.8	0.005	1.20
can05	Upper andesite	Pyx-scap-gar-(Kfsp) (skarn) ovp bio (hnfls)	87.5	345.4	-36.0	0.424	0.51
can06	Diorite	-	35.3	51.7	-45.8	0.557	0.65
can07	Diorite	-	39.4	48.3	-41.5	0.169	0.28
09-077m	Upper andesite	Pyx-scap (skarn) ovp bio-Kfsp-ep-amph	1.9	11.7	-24.7	0.019	0.58
09-135m	Upper andesite	Gar-pyx-scap-chl (skarn)	1.8	249.3	-5.7	0.001	0.02
09-142m	Upper andesite	Pyx-scap-amph-gar (skarn) ovp bio	1.2	52.2	-23.5	0.001	0.06
09-171m	Dacite sill*	amph-mt-py ovp pyx-scap (skarn)	702.3	333.8	-66.9	10.250	0.91
09-180m	Dacite sill*	Kfsp-amph-mt-(ep) ovp pyx-scap (skarn)	59.0	174.8	74.7	0.255	0.25
09-205m	Upper andesite	Pyx-scap-amph-(py) (skarn)	389.7	56.9	-10.5	1.542	0.25
09-214m	Upper andesite	Pyx-scap-(Kfsp-amph-chl-ep)	70.2	24.3	-53.5	0.246	0.21
10-051m	Upper andesite	Bio-plag	96.6	4.2	2.6	0.629	0.39
10-061m	Upper andesite	Bio-plag	59.8	43.0	-19.0	0.036	0.04
10-073m	Upper andesite	Bio-plag-qtz	1.0	183.2	1.3	0.008	0.46
10-250m	Tuff	Gar-bio	0.9	113.4	-14.6	0.002	0.10
10-279m	Tuff	Bio-plag-(Kfsp-qtz-mt)	125.7	142.6	50.6	0.351	0.20
10-296m	Lower andesite	Mt breccia (pyx-scap-mt-(chl-amph-cp-py))	184.9	68.6	-28.1	0.935	0.34
10-297m	Tuff	Pyx-scap-(cp, py, po)	62.0	109.2	-18.8	0.091	0.13
10-298m	Tuff	Pyx-scap	224.6	77.8	41.8	0.231	0.17
10-308m	Tuff	Amph-Kfsp-chl-sph-scap-(mt, cp,py)	46.3	12.2	-64.5	0.044	0.09
10-315m	Lower andesite	Bio-qtz-(mt,cp, py)	116.4	241.7	-78.6	0.151	0.11
10-322m	Lower andesite	Bio-qtz-(mt,cp, py)	2.9	250.8	25.3	0.079	1.52
11-275m	Lower andesite	Bio-plag-(qtz, mt, amph)	47.7	47.6	-26.2	0.215	0.29
11-303m	Lower andesite	Mt breccia (bio-pyx-scap-mt-cp-(py))	2275.4	221.8	44.7	10.623	0.28
11-311m	Lower andesite	Mt breccia (bio-pyx-scap-mt-cp-(py))	2054.8	55.6	-25.5	12.556	0.39
11-322m	Lower andesite	Bio-plag-qtz-(mt, amph)	343.4	55.8	-43.4	1.955	0.35
11-333m	Lower andesite	Bio-plag-qtz-(mt, amph)	258.6	65.0	-47.7	1.225	0.28
11-338m	Lower andesite	Bio-plag-qtz-(mt, amph)	156.4	315.9	72.0	0.049	0.02
COMBINED							
Orebody			3370	34.3	-60.6	5.86	0.10
Host rocks			124	16.1	-60.1	0.60	0.27
Diorite			37	50.9	-44.8	0.36	0.55

*magnetite is replacing hematite (i.e. identified as mushketovite in hand sample)

Figures 7.2-11 (following pages). Composite demagnetisation plots for samples from the Candelaria area. Top left diagrams show residual remanence intensity versus treatment step (LN = low temperature cleaning in liquid nitrogen; AF treatment steps are in mT; thermal steps in °C). The corresponding stability spectra are shown as histograms. Bottom left digrams are stereograms of successive remanence directions during demagnetisation. Open symbols are on the upper hemisphere (negative inclinations), filled symbols are on the lower hemisphere (positive inclinations). RHS gives orthogonal projections of successive remanence vector endpoints: horizontal symbols are the projection onto the horizontal (i.e. a plan view), open symbols are the projection onto a vertical plane (i.e. a section view). One horizontal axis, either N-S or E-W, is common to both projections. When corresponding segments on both projections are linear, a single remanence component is being removed; curved segments indicate multiple components with overlapped stability spectra. When the highest treatment steps produce a linear trend directly towards the origin, this defines the most stable remanence component, after removal of any overprint magnetisations.

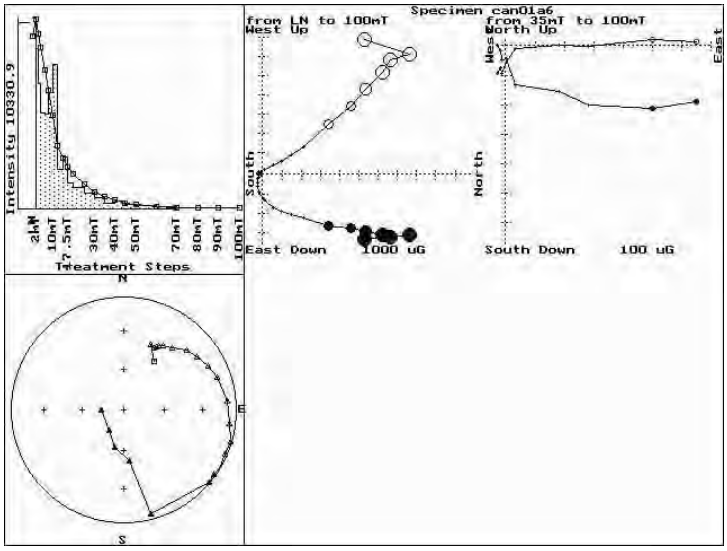

Fig.7.2. AF demagnetisation of an orebody specimen from site 1.

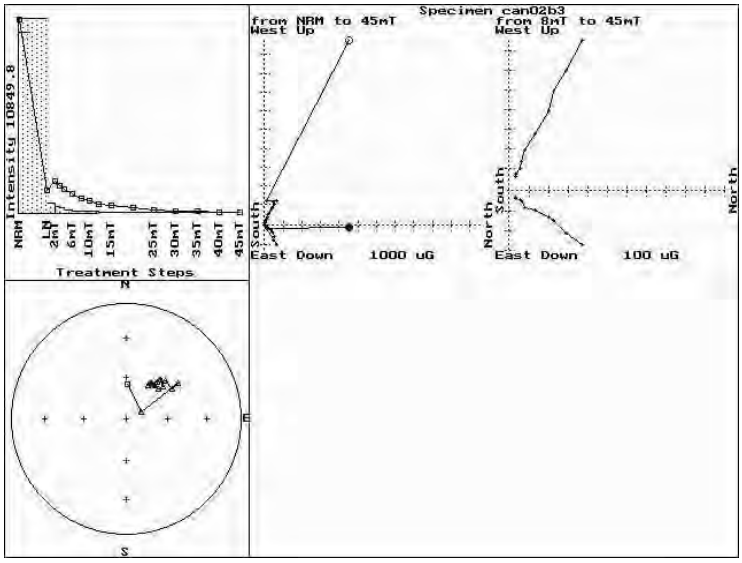

Fig.7.3. AF demagnetisation of an orebody specimen from site 2.

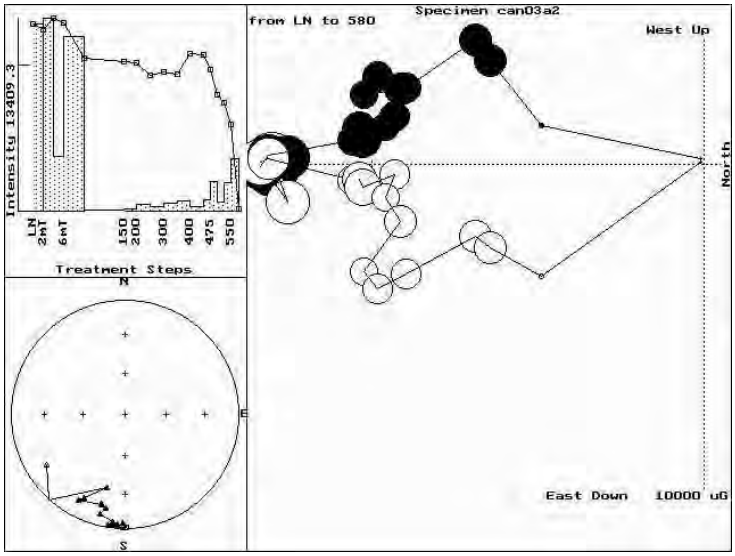

Fig.7.4. AF + thermal demagnetisation of an orebody specimen from site 3.

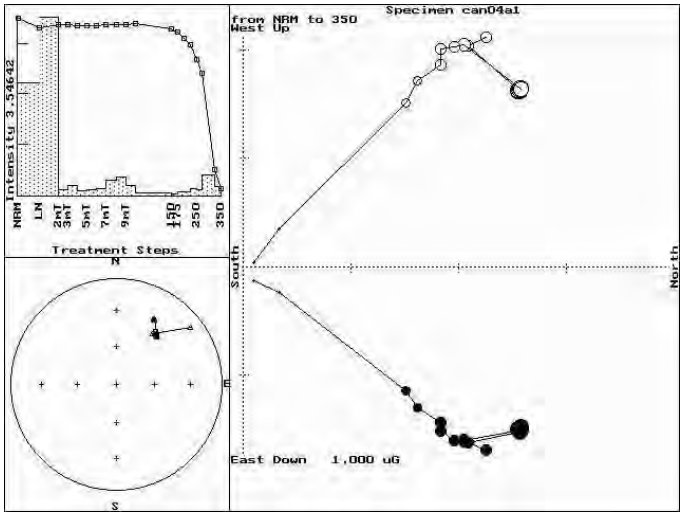

Fig.7.5. AF + thermal demagnetisation of a skarn specimen from site 4.

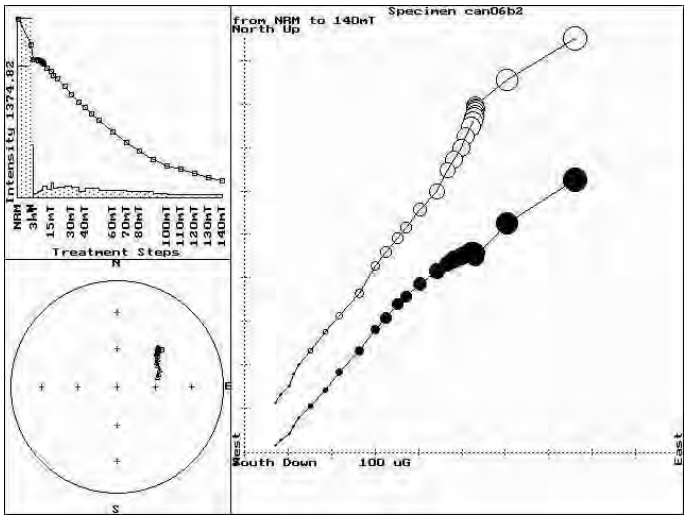

Fig.7.6. AF demagnetisation of a diorite specimen from site 6.

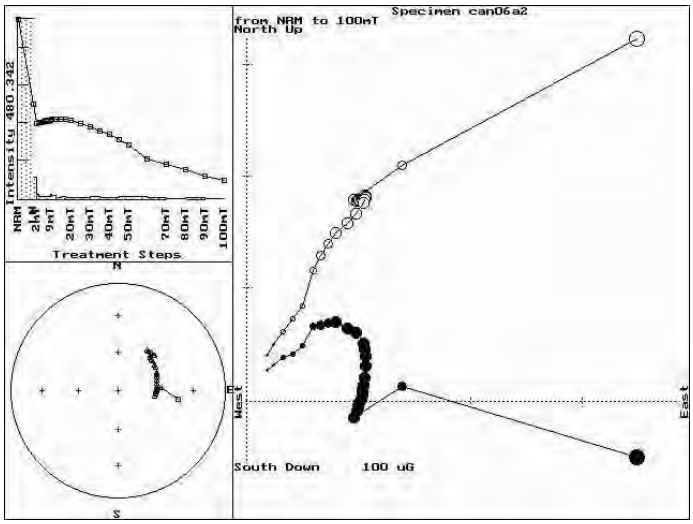

Fig.7.7. AF demagnetisation of a diorite specimen from site 6.

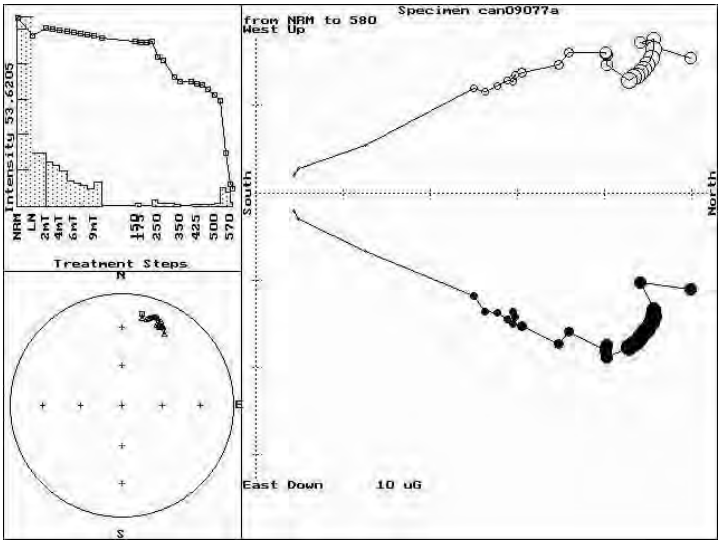

Fig.7.8. AF + thermal demagnetisation of a skarn specimen from SO9-77m.

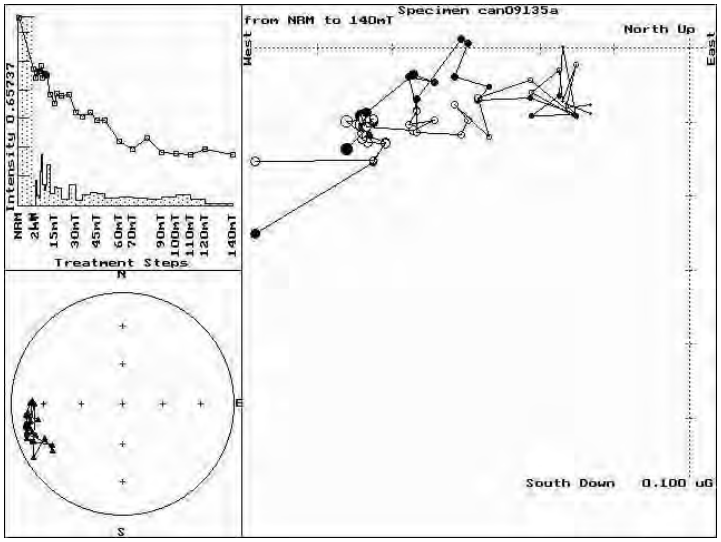

Fig.7.9. AF demagnetisation of a skarn specimen from SO9-135m.

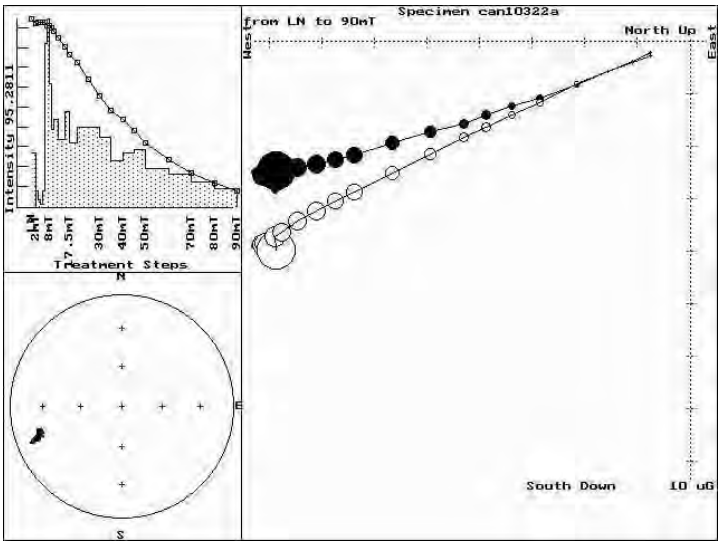

Fig.7.10. AF demagnetisation of a hornfels specimen from SO10-322m.

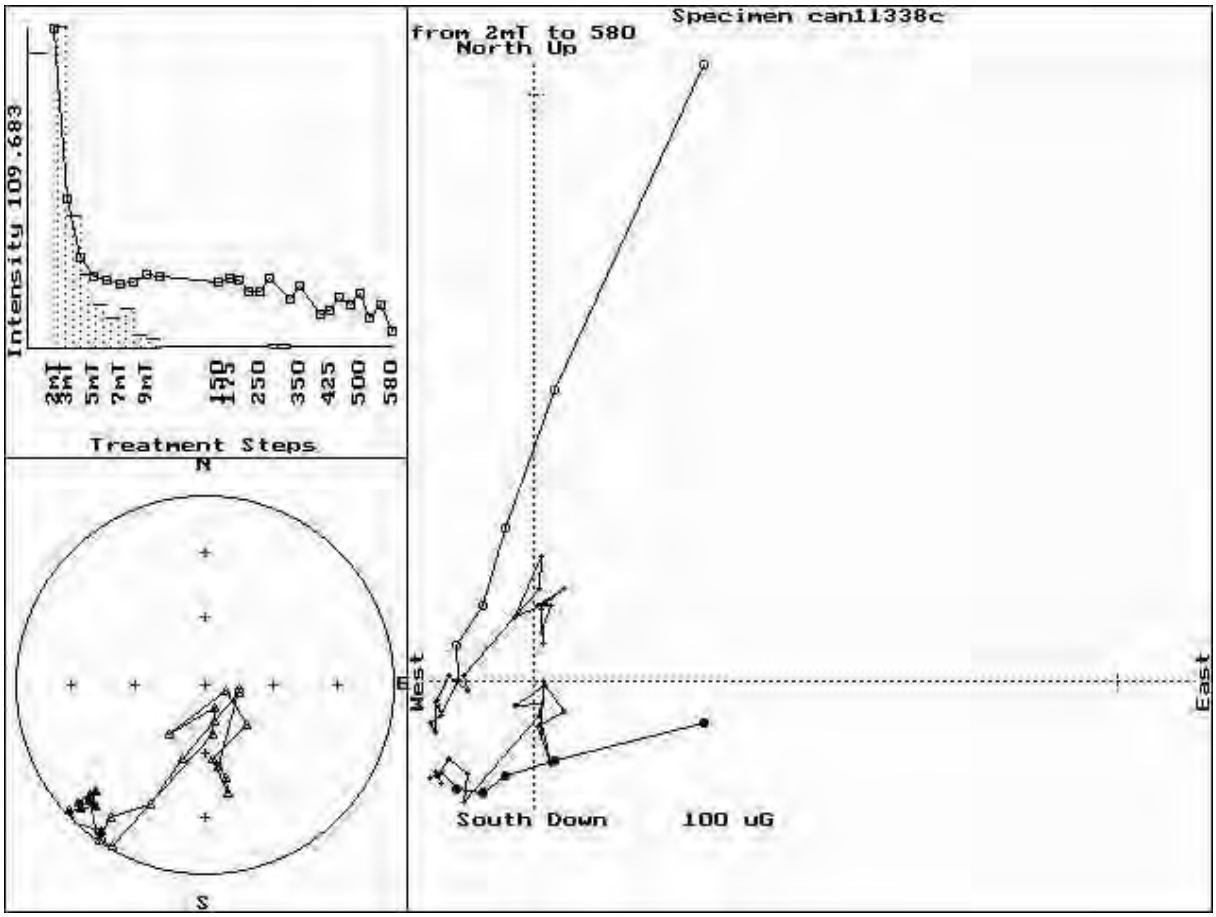

Fig. 7.11. AF and thermal demagnetisation of a biotite-altered Lower Andesite specimen from SO11- 338 m initially removes a NE up (normal) component, followed by a SW down (reversed) component, revealing a poorly resolved normal polarity component as the most stable. This behaviour indicates a complex history of overprinting in the wall rocks of the Candelaria deposit.

7.2 Magnetic properties of massive hematite bodies of the Mount Woods Inlier

The recent discovery of IOCG mineralisation, with close similarities to the Olympic Dam deposit, at Prominent Hill in the Mount Woods Inlier has renewed interest in this area. A number of mineralised and unmineralised massive hematite and massive magnetite-hematite bodies with prominent magnetic anomalies have been drilled around the White Hill Gabbro, a large mafic intrusion of probable Hiltaba Suite affinity, penecontemporaneous with the ~1590 Ma Gawler Range Volcanics magmatism and the Olympic Dam mineralisation. Figure 7.12 shows a TMI image of the White Hill Gabbro and surrounding prospects. The White Hill Gabbro is delineated by the zoned ovoidal magnetic high (white to pink), surrounded by strong magnetic highs in the contact aureole. The Balta Granite lies to the north and has a smooth magnetic low signature, with strong contact aureole effects. Peculiar Knob lies within the aureole of the Balta Granite and Manxman B is within the aureole of the gabbro. Both have remanence-dominated anomalies. Prominent Hill lies outside the aureole.The magnetic high at Prominent Hill represents a weakly mineralised massive magnetite body, separated from the mineralised hematite breccia and massive hematite zones by a fault. The hematite zones have little or no magnetic anomaly.

Our measurements of magnetic properties and modelling of the spectacular magnetic anomaly and associated gravity anomaly at Peculiar Knob have shown:

- Although semi-massive to massive hematite has relatively low susceptibility, coarse-grained specular hematite at Peculiar Knob and Manxman B is often strongly remanently magnetised and retains an ancient magnetisation, which is oblique to the present field. One implication is that a large magnetic anomaly may be associated with hematite-rich Olympic Dam-type deposits that have been through a similar thermal history, even though the susceptibility is far too low to account for the observed anomaly.
- Proterozoic Fe oxide bodies of the Gawler Craton tend to have remanence directed steeply upwards. Contact metamorphosed hematite-rich compositions have Koenigsberger ratios much greater than unity (up to several hundred) and the bulk magnetisations of large volumes of these hematite-(magnetite) bodies have effective Koenigsberger ratios greater than 10. At Peculiar Knob a ground magnetic anomaly of ~30,000 nT is associated with hematite-rich alteration with moderate susceptibility (~0.25 SI), but a remanent intensity (measured and modelled) of 120 A/m ($Q \approx 10$). These values of NRM and Q are effective values, averaged over the whole massive hematite occurrence. The effective Koenigsberger ratio for similar compositions at Manxman B, obtained by vectorial averaging, is ~60.
- The massive hematite bodies at Prominent Hill and Manxman B show clear textural evidence (e.g. triple junctions) of high-temperature recrystallisation and their NRM intensities are consistent with thermoremanent magnetisations acquired under laboratory conditions in a field of ~50,000 nT. Coupled with the geological evidence that these deposits lie within the contact aureoles of large high-temperature intrusions, the strong magnetic signatures of these deposits can be explained by intense TRMs carried by MD hematite, acquired during contact metamorphism.
- The magnetisation of unmetamorphosed hydrothermal hematite, e.g. at Prominent Hill and Olympic Dam is inferred to be a relatively weak chemical remanent magnetisation, accounting for their much less prominent magnetic anomalies.

Should an analogous deposit be heated above 680°C during upper amphibolite-granulite grade regional metamorphism or by contact metamorphism, however, a very large, remanence-dominated magnetic anomaly should result.

- Remanence effects are likely to be important for Precambrian deposits, because geomagnetic reversal frequency appears to have been lower than for most of the Phanerozoic. With the exception of the two geomagnetic superchrons, the Permo-Carboniferous (~317-260 Ma) Reverse Superchron and the Cretaceous Normal Superchron (118-83 Ma), the magnetic signatures of most deposits of Phanerozoic age should not show strong remanence effects. This is due to the high frequency of geomagnetic reversals and the prolonged magmatic-hydrothermal evolution of most deposits, which spans one or more reversals and produces substantial cancellation of remanence over large volumes of rock. At a local scale, most Tertiary porphyry deposits exhibit two or more palaeomagnetic components that record different events in the evolution of the deposit (e.g. emplacement of an intrusion and its subsequent alteration) and also reflect any tectonic rotations that have occurred after the remanence was acquired.
- When remanence effects are known or suspected to be important, remanence directions can be predicted from the deposit age and the apparent polar wander path for the crustal block that hosts the deposit. Polarity of remanence can be predicted from the geomagnetic polarity time scale. Sponsors will be supplied with pole lists for major crustal blocks and a Visual Basic program that enables palaeofield directions to be predicted.

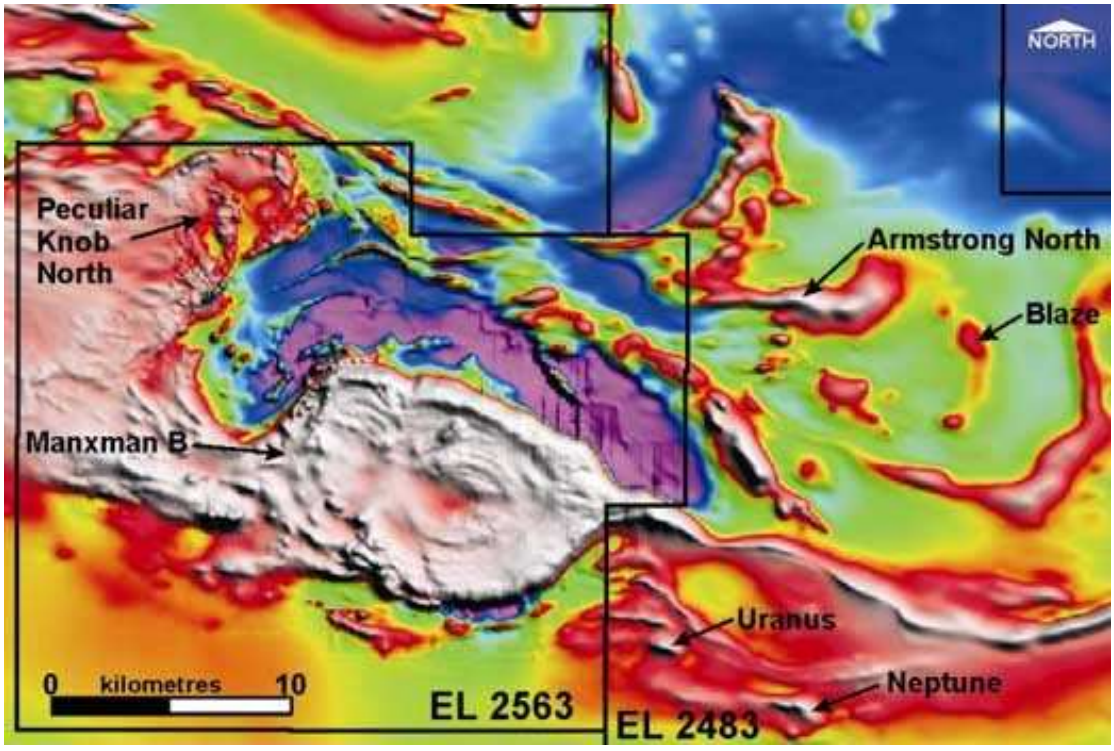

Fig.7.12. TMI image of part of the Mount Woods Inlier showing locations of the Peculiar Knob, Manxman B and Uranus (now Prominent Hill) prospects (see Minotaur website: http://www.minotaurresources.com.au/MtWoodsJV.html).

7.3. Magnetic properties of IOCG deposits from the Cloncurry Belt

The main conclusions obtained from this study were:

- By contrast with hematite-dominant IOCG systems (e.g. Olympic Dam), magnetite-rich members of the iron oxide Cu-Au class have very high susceptibilities (e.g. 1.8 SI for the primary zone and 0.7 SI for the secondary zone at Ernest Henry; ~6 SI for magnetite ironstones at Osborne and ~20 SI for massive magnetite at Selwyn/Starra) and subordinate remanence.
- The total magnetisations (induced + remanent) of magnetite-rich IOCGs are comparable to those of contact metamorphosed TRM-carrying hematite-rich examples. Koenigsberger ratios are typically 0.1 – 1, so remanence effects should not be neglected for detailed modeling and drill targetting. Raw NRMs are not representative of the *in situ* remanence, because they are usually contaminated by drilling-induced magnetisation and other palaeomagnetic noise, so palaeomagnetic cleaning is required to determine representive remanence vectors.
- Magnetite-rich mineralisation with pronounced banding is highly anisotropic (e.g. A ≈ 1.5 for banded magnetite alteration around Ernest Henry), so anisotropy effects can be important for modelling. Whether massive or banded, the effects of self-demagnetisation are important for interpreting magnetic anomalies associated with magnetite-rich deposits. For example, the early drilling at the Osborne Cu-Au deposit went down-dip because the interpreted dip of the magnetite-rich ironstones was out by 55°, due to neglect of self-demagnetisation and distortion of the geomagnetic field by the intense anomaly.
- Iron oxide Cu-Au deposits with intergrowths of hematite and magnetite or partial replacements of one by the other have properties intermediate between the hematite-dominated and magnetite-dominated end members. Remanence effects are often important for this mineralogy, probably because lattice mismatch between hematite and magnetite produces residual stresses within grains that stabilises and intensifies remanent magnetisation.

7.3. Magnetic properties of IOCG deposits from the Tennant Creek Block

Data from 14 Tennant Creek-type deposits are included in the database. The geological setting and genesis of Tennant Creek ironstones is unlike that of most other iron oxide Cu-Au deposits. The orebodies are small high- to very high-grade deposits that are not typical targets for major exploration companies, but they nevertheless provide excellent analogues for the magnetic properties of the larger iron oxide bodies that are attractive targets in the present exploration environment.

The Tennant Creek deposits for which data are available are: Warrego, Juno, Argo, West Gibbet, Gecko, Eldorado, Peko, West Peko, TC8, White Devil, Explorer 50, Rover 1, Rover 4 and Explorer 142. These deposits include representatives of oxidised (hematite > magnetite ± pyrite) Au-Bi(Cu) orebodies, intermediate (magnetite-chlorite ± pyrite) Cu-Au-Bi orebodies and reduced (magnetite-pyrrhotite) Cu-Au-Bi orebodies.

Apart from the hematite-dominant ironstones, the magnetic signatures of Tennant Creel ironstones are strongly influenced by self-demagnetisation, which suppresses magnetisation along the shortest axis of the body and deflects the induced

magnetisation away from the geomagnetic field direction, towards the long axis of the ironstone. This affects anomaly shape as well as amplitude, often rotating the TMI high-low axis from the normal N-S orientation, an effect normally diagnostic of remanent magnetisation, and changing the relative amplitudes of the high and low. Ignoring the latter effect produces errors in the interpreted dip/plunge of the ironstone.

Susceptibilities of magnetite-dominant ironstones (massive magnetite, quartz-magnetite, chlorite-magnetite) range from 2.5 SI to 10 SI, with an average of ~ 5.7 SI. Quartz-hematite ironstones have much lower susceptibilities (as low as 0.0025 SI). The ironstones are hosted by Palaeoproterozoic (~1860 Ma) Fe-rich, oxidised greywackes, siltstones and shales of the Warramunga Formation, which have moderate susceptibilities (0.006 – 0.04 SI). Ironstone bodies formed during regional greenschist grade metamorphism c. 1840-1850 Ma; Cu-Au-Bi mineralisation overprinted the ironstones around 1830 Ma.

Ironstones are usually surrounded by a halo of chloritic alteration with disseminated magnetite. In some cases the “magnetic sediments” make a substantial contribution to the magnetic anomaly, in spite of their lower magnetisation than the ironstone, because of their relatively large volume.

The NRMs of the ironstones are dominated by an ancient steep up component of magnetisation that is similar to a ubiquitous overprint component found in the sedimentary rocks that host the ironstones. Remanent magnetisation is subsidiary to induced magnetisation for the intermediate redox class (magnetite-dominant with pyrite as the main iron sulphide) of ironstone, although it is not negligible for detailed modelling. Effective Koenigsberger ratios (Q) range from ~0.2 to ~1 The reduced class (magnetite-pyrrhotite) ironstones carry strong remanence with Q ~ 2. The low susceptibility hematite-dominant ironstones can also produce detectable anomalies that arise predominantly from remanent magnetisation. Remanence is subordinate to induced magnetisation (Q ~ 0.2) for the sedimentary host rocks.

The host rocks and some of the ironstone bodies retain a stable, dual polarity remanence component that underlies the softer steep up component. The more stable component is directed WNW with moderate upward inclination, or ESE with moderate downward inclination. The ages of the most stable and the overprint remanent magnetisations are interpreted from the corresponding pole positions to be ~1800 Ma (related to cooling from peak metamorphic temperatures, attained c.1810 Ma) and ~1650 Ma (coincident with a thermal event recorded by Rb-Sr systems) respectively.

8. MAGNETIC PROPERTIES OF PORPHYRY, EPITHERMAL AND IRON OXIDE COPPER-GOLD SYSTEMS - SYNTHESIS

TABLE 8.1 MAGNETIC PROPERTIES OF WEAKLY ALTERED INTRUSIVE ROCKS RELATED TO MINERALISATION

LITHOLOGY	**Strongly Oxidised (NNO-HM)**				**Strongly Reduced (≤ QFM)**			
	k (10^{-3} SI)	ΔB_z (nT)	NRM	Associated mineralisation	k (10^{-3} SI)	ΔB_z (nT)	NRM	Associated mineralisation
Syenogranite, Alkali granite	1-30	25-750	Wk, VRM, Q<1	Mo, Mo-W, (Au)	0.1-0.3	3-6	V. wk, VRM, Q << 1	Sn, Sn-W
Monzogranite (Adamellite), Qtz monzonite	3-40	75-1000	VRM, Q < 1	Cu, Cu-Mo, Au	0.1-0.4	3-10	V. wk, VRM, Q << 1	
Granodiorite, Monzonite, Tonalite	20-70	500-1750	VRM, Q < 1	Cu, Cu-Mo, Cu-Mo-Au, Au	0.2-0.5	5-15	Wk; Q << 1	
Qtz diorite, Qtz monzodiorite	25-90	625-2250	VRM + TRM?; Q < 1	Cu-Au, Cu-Au-Mo, Au	0.4-0.6	10-15	Wk; Q << 1	
Monzodiorite, diorite	30-100	750-2500	TRM + (VRM); Q ~ 1 (Q < 1)	Cu-Au, Au	0.5-0.8	13-20	Wk; Q << 1	
Gabbro, Norite, Alkali gabbro	40-160	1000-4000	TRM + (VRM); 0.5 < Q < 10	Fe, Ti, V	0.6-1.3	15-30	Wk; Q << 1	Cr, PGEs

Rocks that have undergone deuteric alteration and/or minor rock-buffered hydrothermal alteration of normal type and intensity, as well as essentially unaltered rocks, are included here. ΔB_z is the maximum associated magnetic anomaly (steep field, non-magnetic country rocks, diameter >> depth below sensor, great depth extent). Susceptibilities of unaltered and unmetamorphosed volcanic rocks are similar to those of their corresponding intrusive rocks (e.g. k[andesite] ≈ k[diorite]).

TABLE 8.2 MAGNETIC PROPERTIES OF WEAKLY ALTERED METAMORPHIC ROCKS

LITHOLOGY	OXIDISED (NNO-HM)			REDUCED (≤ QFM)		
	k (10^{-3} SI)	**ΔB_z (nT)**	**NRM**	**k (10^{-3} SI)**	**ΔB_z (nT)**	**NRM**
Amphibolite/Mafic granulite/Mafic gneiss	13 ± 8	325 ± 200	Weak; Q < 1	0.9 (0.4 -1.3)	23 (10-33)	Very weak; Q < 1
Felsic granulite/Felsic gneiss	40 (1-60)	1000 (25-3000)	Weak-moderate; Q < 1	0.4 (0.05-1)	10 (1-25)	Very weak; Q < 1
Psammitic metasediments (amphibolite-granulite grade)	17 ± 7	425 ± 175	Weak; Q < 1	0.48 ± 0.08	12 ± 2	Very weak; Q < 1
Pelitic metasediments (amphibolite-granulite grade)	13 ± 4	325 ± 100	Weak; Q < 1	0.39 ± 0.04	10 ± 1	Very weak; Q < 1
Slate/phyllite/metasiltstone/quartzite/ marble (greenschist grade)	2.3 ± 1.4	60 ± 35	Very weak	4.0 ± 3.2 (±po)	100 ± 80	Weak-moderate; Q = 2-7
Mafic schist (greenschist grade)	15 ± 10	375 ± 250	Weak; Q < 1	1.3 ± 0.2	33 ± 5	Very weak; Q < 1

Rocks that have undergone deuteric alteration and/or minor rock-buffered hydrothermal alteration of normal type and intensity, as well as essentially unaltered rocks, are included here. ΔB_z is the maximum associated magnetic anomaly (steep field, non-magnetic country rocks, diameter >> depth below sensor, great depth extent).

TABLE 8.3 MAGNETIC PROPERTIES OF WEAKLY ALTERED SEDIMENTARY ROCKS

LITHOLOGY			
	k (10^{-3} SI)	**ΔB_z (nT)**	**NRM**
Red shales/siltstones/cherts	0.7 ± 0.1	15 to 20	Very weak
Black shales	-0.01 to 0.3	-0.3 to 8	Weak
Ferruginous shales (iron-formation)	1 to 10	25 to 250	Weak to moderate (0.05 – 10 A/m)
Carbonates	-0.01 to 1.5	-0.2	Very weak
Typical clastic sediments (undifferentiated)	0 to 0.5	-0.3 to 13	Very weak

Rocks that have undergone deuteric alteration and/or minor rock-buffered hydrothermal alteration of normal type and intensity, as well as essentially unaltered rocks, are included here. ΔB_z is the maximum associated magnetic anomaly (steep field, non-magnetic country rocks, diameter >> depth below sensor, great depth extent).

TABLE 8.4 TYPICAL MAGNETIC PROPERTIES OF SKARNS

LITHOLOGY			
	Av. k ± SE (10^{-3} SI) [Range]	**ΔB_z (nT)***	**Average NRM ± SE [Range] Average Q ± SE [Range]**
Oxidised Magnetite Skarn†	650 ± 160 [120 - 2000]	16,250 ± 4000 [3000 - 50,000]	J = 50 ± 20 [0.3 – 210] Q = 1.4 ± 0.4 [0.05 – 4.5]
Reduced Pyrrhotite Skarn†	5 ± 2 [1 - 8]	125 ± 50 [25 – 200]	J = 14 ± 8 [1 – 34] Q = 16 ± 4 [8 – 25]
Reduced pyroxene ± garnet† skarn (mt rare or absent)	1.1 ± 0.2 [0.1 - 2]	28 ± 5 [2.5 – 50]	J < 0.02 Q << 1
Calcic Fe (Cu, Co, Au) skarn‡ (mafic intrusion; island arc or rifted continental margin)	2000 [1200 - 3500]	50,000 [30,000 – 175,000]	J : [5 – 300] Q ~ 1 [0.1 – 5]
Magnesian Fe (Cu, Zn) skarn‡ (felsic intrusion; continental margin)	2000 [1200 – 2700]	100,000 [60,000 – 87,500]	J : [5 – 220] Q ~ 1 [0.1 – 5]
Calcic Cu (Mo, W, Zn) skarn - proximal‡ (Grd-Qmz; continental margin)	[30 - 400]	[750 – 10,000]	J: [1 – 50] Q ~ 1.5 [0.1 – 5]
Magnesian Cu (Mo, W, Zn) skarn‡ (Grd-Qmz; continental margin)	[800 -1700]	[20,000 – 42,500]	J: [5 – 100] Q ~ 1.5 [0.1 – 5]

*ΔB_z is the maximum associated magnetic anomaly (steep field, non-magnetic country rocks, diameter >> depth below sensor, great depth extent), calculated from total magnetisation for case where remanence is parallel to induced magnetisation. The effective susceptibility is therefore taken to be k(1 + Q). †Averages from P700 Database and from CSIRO Catalogue of Magnetic Properties (Clark, 1988). ‡Inferred values from data in Einaudi et al. (1981).

TABLE 8.5 ZONATION OF MINERALOGY AND MAGNETIC PROPERTIES OF A TYPICAL COPPER SKARN (DEEP SKARN, CARR FORK MINE, BINGHAM MINING DISTRICT, UTAH)

ZONE	Distance from intrusive contact (m)	GANGUE	SULPHIDES	Cu (wt %)	Magnetite (vol %)	k (10^{-3} SI)
Bingham stock (potassic zone)	> 100	qtz, Kfsp, bio	cp, bn, py	0.65 (shallow) < 0.1 (deep)	0.1 –1	3.5 - 35
Endoskarn (Bingham stock)	< 100	act, ep	(0.5 vol %) mb > cp	< 0.1	~ 0.1	~ 3.5
Proximal exoskarn	0-50	and > di, cal, qtz,	(1-2 vol %) cp, (bn)	~0.2	1-2	35 - 70
Exoskarn	50 – 100	and	(2-5 vol %) cp > py	~ 0.6	2 - 5	70 - 180
Exoskarn	100 – 300	and >> di	(15 vol %) cp ≥ py	~ 8	5 – 10	180 - 380
Exoskarn	300 - 350	and ≥ di	(5 vol %) cp:py = 0.2	~ 0.5	2	70
Exoskarn	350 – 400	wo (gar, di)	(1 vol %) bn, cp, sph, (py)	~ 0.5	< 0.1	< 3.5
Distal exoskarn	400 - 600	wo-di-qtz; wo-cal; marble	(0.5 vol %) bn, cp, sph, gal	< 0.5	< 0.1	< 3.5
Marble, limestone	> 600	cal, marble	(< 0.1 vol %) (sph, gal, py)	0	0	0

Ore zone (~120-600 m from contact) average grades: ~2.3 % Cu, 0.6 g/t Au, 12 g/t Ag, 0.03 % Mo. Data from Einaudi (1982a).

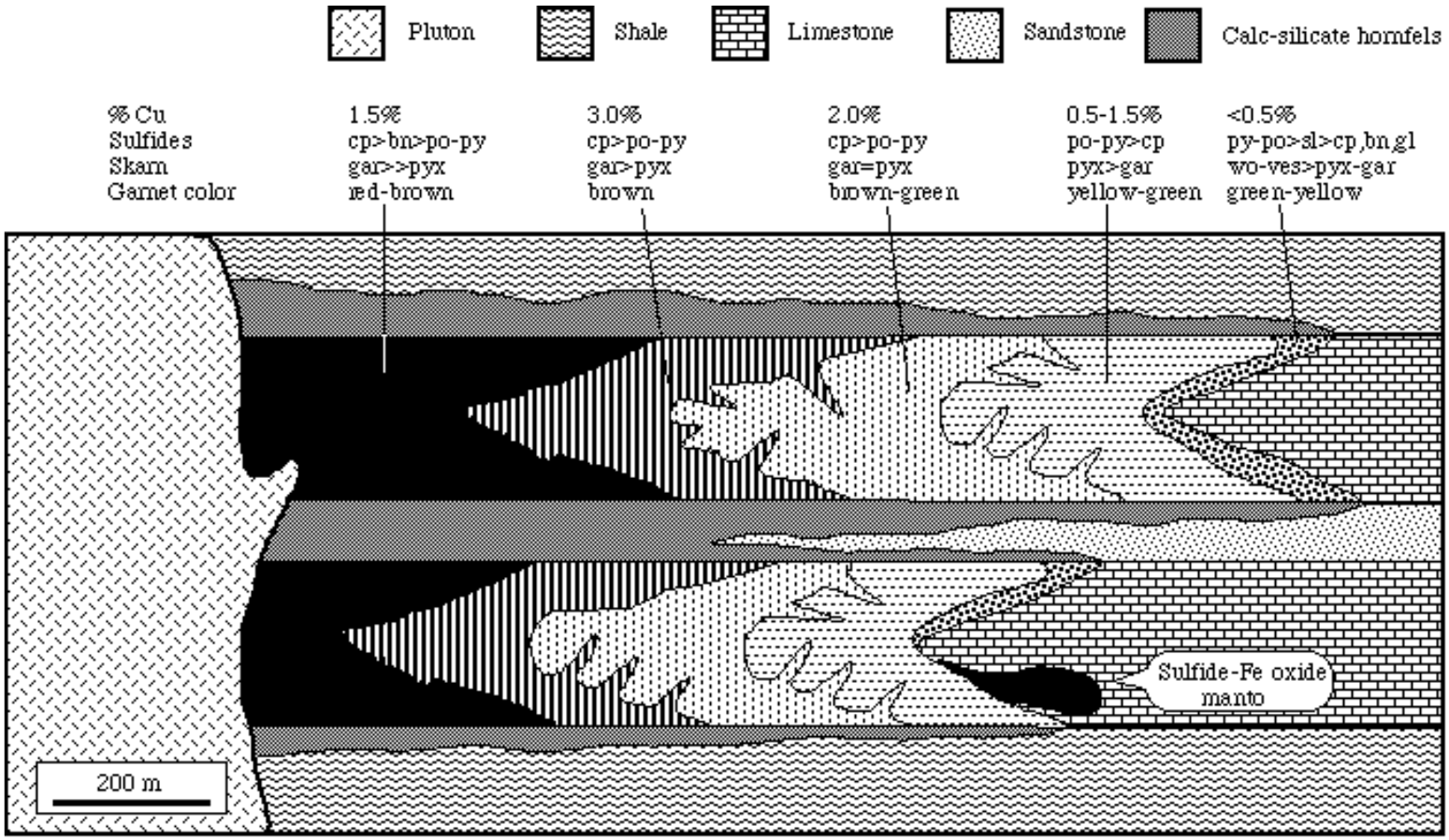

Fig.8.1 Typical zonation pattern of copper skarn (Meinert, 1992)

TABLE 8.6 TYPICAL EFFECTS OF PORPHYRY-STYLE ALTERATION ON MAGNETIC PROPERTIES OF INTRUSIVES AND HOST ROCKS (Δk in 10^{-3} SI, or percentage change)

	ALTERATION							
LITHOLOGY	**Hornfels** (bio;pyx)	**Magmatic Sodic-calcic (M-vein)***	**Potassic**	**Phyllic**	**Deep Phyllic (po)**	**Strong propylitic†**	**Inter. Arg./ Adv. Argillic**	**Sodic-calcic (meteroric/ connate)**
Felsic (meta)igneous rocks/Arkose	+(1-20) +(50-100%)	+(50-500)	+(0-50)	-(10-95%); k < 2	+(1-10); Q > 1	-(0-5) -(0-50%)	-(1-20) -(90-100%)	-(10-90%)
Intermediate-mafic (meta)igneous rocks/mafic schists	+20 (0-40); +50% (0-100%)	+(100-1000)	+(10-200)	-(80-95%)	+(5-30); Q >> 1	-(10-90%)	-(90-100%)	-(10-90%)
High grade psammites (ox/red)	Δk ~ 0	+(50-500)	+(0-50)/ Δk ~ 0	-(80-95%)/ -(10-95%)	~0/+(1-10); Q > 1	-(10-90%)/ Δk ~ 0	-(90-100%)/ -(10-90%)	-(10-90%)/ Δk ~ 0
High grade pelites (ox/red)	Δk ~ 0	+(50-500)	+(0-50)/ Δk ~ 0	-(80-95%)/ -(10-95%)	~0/+(1-10); Q > 1	-(10-90%)/ Δk ~ 0	-(90-100%)/ -(10-90%)	-(10-90%)/ Δk ~ 0
Int. redox shale/siltstone/slate/ phyllite	+(0-150): mt	+(50-500)	+(0-50)	-(10-95%)	+(1-10); Q > 1	Δk ~ 0	-(10-90%)	-(10-90%)
Carbonaceous shales/slates	+(5-30): po; Q >>1	+(50-500)	Δk ~ 0	Δk ~ 0	+(1-10): po Q > 1	Δk ~ 0	Δk ~ 0	Δk ~ 0
Red sediments	~0; J ~10-100 A/m; Q >> 1	+(50-500)	Δk ~ 0	Δk ~ 0	~0	Δk ~ 0	Δk ~ 0	Δk ~ 0
Quartzite	Δk ~ 0	+(50-500)	Δk ~ 0	Δk ~ 0	Δk ~ 0	Δk ~ 0	Δk ~ 0	Δk ~ 0

* Early quartz-magnetite-plagioclase-amphibole alteration associated with Fe metasomatism and M-veins; † Weak propylitic alteration leaves susceptibilities largely unchanged

TABLE 8.7 TYPICAL EFFECTS OF EPITHERMAL-STYLE ALTERATION ON MAGNETIC PROPERTIES OF INTRUSIVES AND HOST ROCKS (Δk in μG/Oe or percentage change)

	ALTERATION						
LITHOLOGY	**HS Ore**	**LS Ore**	**Weak/Low T propylitic**	**Strong/High T propylitic**	**Quartz-sericite**	**Argillic/ Advanced Argillic**	**Silicification**
Felsic (meta)igneous rocks/Arkose	k ~ 0	k ~ 0	Δk ~ 0	-(0-5) -(0-50%)	k ~ 0	k ~ 0	k ~ 0
Intermediate-mafic (meta) igneous rocks/ mafic schists	k ~ 0	k ~ 0	-(10-50%)/	-(10-90%)	k ~ 0	k ~ 0	k ~ 0
High grade psammites (ox/red)	k ~ 0	k ~ 0	-(10-50%)/ Δk ~ 0	-(10-90%)/ Δk ~ 0	k ~ 0	k ~ 0	k ~ 0
High grade pelites (ox/red)	k ~ 0	k ~ 0	-(10-50%)/ Δk ~ 0	-(10-90%)/ Δk ~ 0	k ~ 0	k ~ 0	k ~ 0
Int. redox shale/siltstone/ slate/phyllite	k ~ 0	k ~ 0	Δk ~ 0	Δk ~ 0	k ~ 0	k ~ 0	k ~ 0
Carbonaceous shales/slates	k ~ 0	k ~ 0	Δk ~ 0	Δk ~ 0	k ~ 0	k ~ 0	k ~ 0
Red sediments	k ~ 0	k ~ 0	k ~ 0	k ~ 0	k ~ 0	k ~ 0	k ~ 0
Quartzite	k ~ 0	k ~ 0	k ~ 0	k ~ 0	k ~ 0	k ~ 0	k ~ 0

TYPICAL MAGNETIC PROPERTIES AND DENSITIES OF IOCG-STYLE ALTERATION SYSTEMS

SUSCEPTIBILITY: $k\ (SI) = 20\ V_{MT}/[100 + 4.775(100 - V_{MT})] + 0.0002\ V_{HM}$

$= 20\ f_{MT}\ /[1 + 4.775(1- f_{MT})] + 0.02\ f_{HM}$

For dilute dispersions of magnetite ($f < 0.1$, $v < 10$):

$$k\ (SI) \approx 3.47\ f_{MT} + 0.02\ f_{HM} = 0.0347\ V_{MT} + 0.0002\ V_{HM}$$

CHEMICAL REMANENT MAGNETISATION [T << 580°C (MT); << 680°C (HM)]:

$$CRM \approx 18\ f_{MT} + 5\ f_{HM} = 0.18\ V_{MT} + 0.05\ V_{HM}\ (A/m)$$

THERMOREMANENT MAGNETISATION [T > 580°C (MT); > 680°C (HM)]:

$$TRM \approx 60\ f_{MT} + 1000\ f_{HM} = 0.6\ V_{MT} + 10\ V_{HM}\ (A/m)$$

KOENIGSBERGER RATIOS:

CRM: Q(magnetite) ≈ 0.13; Q(hematite) ≈ 6

TRM: Q(magnetite) ≈ 0.43; Q(hematite) ≈ 1250

DENSITY: $\rho = \rho_{GANGUE} + (\rho_{OXIDES} - \rho_{GANGUE})\ f_{MT+HM}$

f_{MT} = volume fraction of magnetite; f_{HM} = volume fraction of hematite; V_{MT} = volume per cent magnetite; V_{HM} = volume per cent hematite. Both minerals are assumed to be in their respective true multidomain size ranges (> 20 µm for magnetite; > 100 µm for hematite). $\rho_{OXIDES} = 5.2\ g/cm^3 = 5200\ kg/m^3$.

Susceptibility versus volume per cent magnetite. Conversion to weight per cent assumes a gangue density of 2800 kg/m^3. Assumed intrinsic susceptibility of pure magnetite is 20 SI, average grain demagnetising factor is 0.239 SI (= 3 Oe/G).

wt% mt [> 20 µm]	vol% mt [> 20 µm]	k (SI)	k (10^{-3} SI)
0.18	0.1	0.0035	3.47
0.37	0.2	0.0069	6.94
0.55	0.3	0.0104	10.42
0.92	0.5	0.0174	17.39
1.83	1	0.0349	34.92
2.74	1.5	0.0526	52.60
3.64	2	0.0704	70.43
4.53	2.5	0.0884	88.41
5.41	3	0.1065	106.54
7.16	4	0.1433	143.27
8.87	5	0.1806	180.63
10.56	6	0.2186	218.64
12.22	7	0.2573	257.32
13.86	8	0.2967	296.68
15.47	9	0.3367	336.75
17.05	10	0.3775	377.54
20.15	12	0.4614	461.36
24.61	15	0.5930	593.03
31.62	20	0.8299	829.88
38.14	25	1.0914	1091.41
44.22	30	1.3817	1381.69
49.90	35	1.7058	1705.76
55.22	40	2.0699	2069.86
64.91	50	2.9520	2952.03
69.34	55	3.4934	3493.45
73.51	60	4.1237	4123.71
77.46	65	4.8666	4866.64
81.19	70	5.7554	5755.40
84.73	75	6.8376	6837.61
88.10	80	8.1841	8184.14
91.29	85	9.9053	9905.32
94.33	90	12.1827	12182.74
97.23	95	15.3380	15338.04
100.00	100	20.0000	20000.00

TABLE 8.8. TYPICAL MAGNETIC PROPERTIES AND DENSITIES OF IOCG-STYLE ALTERATION SYSTEMS (LOW METAMORPHIC GRADE)

ZONE	Volume % magnetite	Volume % hematite	Effective susceptibility (10^{-3} SI)*	Density (kg/m^3)
Felsic Host	0.15	0	6	2650
Outer hematite halo - upper (HSCC) zone	0.2	2	10.7	2710
Inner hematite halo - upper (HSCC) zone	2	4	84	2800
Hematite breccia - upper (HSCC) zone	1	36	42 (random CRM)	3590
Hematite-quartz breccia - upper (HSCC) zone	0	37	7 (random CRM)	3590
Massive hematite lens	0	60	87 (CRM)	4180
Potassic/Potassic-calcic/sodic/sodic-calcic deep zones	3.5	0	137 (CRM) 174 (TRM)	2740
Massive magnetite lens	60	0	900 (CRM)† 1200 (TRM)†	4180
Mt-rich Mafic Host	5.2	0	181 (random NRM)	3000
Outer hematite halo - upper (HSCC) zone	2	5	86	3150
Inner hematite halo - upper (HSCC) zone	2	9	91	3240
Hematite breccia - upper (HSCC) zone	1	41	43 (random CRM)	3810 (ρ_G = 2800)
Hematite-quartz breccia - upper (HSCC) zone	0	42	8 (random CRM)	3810 (ρ_G = 2800)
Massive hematite lens	0	60	87 (CRM)	4240 (ρ_G = 2800)
Potassic/Potassic-calcic/sodic/sodic-calcic deep zones	8.5	0	333 (CRM) 422 (TRM)	3190
Massive magnetite lens	60	0	900 (CRM)† 1200 (TRM)†	4320

*includes contributions of remanence (if it is consistently oriented).
†Corrected for self-demagnetisation.

TABLE 8.9. TYPICAL MAGNETIC PROPERTIES AND DENSITIES OF IOCG-STYLE ALTERATION SYSTEMS (HIGH GRADE METAMORPHOSED‡)

ZONE	Volume % magnetite	Volume % hematite	Effective susceptibility (10^{-3} SI)*	Density (kg/m^3)
Felsic Host	0.15	0	6	2650
Outer hematite halo - upper (HSCC) zone	0.2	2	10.7	2710
Inner hematite halo - upper (HSCC) zone	2	4	84	2800
Hematite breccia - upper (HSCC) zone	1	36	91 (CRM)	3590
Hematite-quartz breccia - upper (HSCC) zone	0	37	54 (CRM)	3590
Massive hematite lens	0	60	15,000 (TRM)	4180
Potassic/Potassic-calcic/sodic/sodic-calcic deep zones	3.5	0	174 (TRM)	2740
Massive magnetite lens	60	0	1200 (TRM)†	4180
Mt-rich Mafic Host	5.2	0	204 (pTRM)	3000
Outer hematite halo - upper (HSCC) zone	2	5	86	3150
Inner hematite halo - upper (HSCC) zone	2	9	91	3240
Hematite breccia - upper (HSCC) zone	1	41	99 (CRM)	3810 (ρ_G = 2800)
Hematite-quartz breccia - upper (HSCC) zone	0	42	61 (CRM)	3810 (ρ_G = 2800)
Massive hematite lens	0	60	15,000 (TRM)	4240 (ρ_G = 2800)
Potassic/Potassic-calcic/sodic/sodic-calcic deep zones	8.5	0	422 (TRM)	3190
Massive magnetite lens	60	0	1200 (TRM)†	4320

*includes contributions of remanence (if it is consistently oriented).
†corrected for self-demagnetisation.
‡ Assumed metamorphic effects: (1) magnetite-rich mafic host retains equivalent magnetite content due to self-buffering and high grade of metamorphism, (2) upper levels of hematite-rich alteration acquire a CRM/partial TRM below 680°C, (3) massive hematite lens is remagnetised, acquiring TRM, due to contact metamorphism, (4) deeper magnetite-rich alteration acquires TRM above 580°C due to high heat flow.

9. MAGNETIC AND OTHER GEOPHYSICAL SIGNATURES OF P700 STUDY AREAS

9.1 Magnetic Signatures of IOCG deposits

- Although semi-massive to massive hematite has relatively low susceptibility, coarse-grained specular hematite that has formed at, or been remagnetised at, high tempertures is strongly remanently magnetised and can retain an ancient magnetisation, which may be quite oblique to the present field. One implication is that a large magnetic anomaly may be associated with hematite-rich Olympic Dam-type deposits that have been metamorphosed, even though the susceptibility is far too low to account for the observed anomaly.
- Examples of Olympic Dam analogues for which this is the case include the Peculiar Knob and Manxman B hematite bodies in the Mount Woods area of the Gawler Craton, which has been the subject of much interest following the recent Minotaur discovery at Prominent Hill. Proterozoic Fe oxide bodies of the Gawler Craton tend to have remanence directed steeply upwards. Peculiar Knob has been remagnetised due to contact metamorphism by the Balta Granite and Manxman B has been similarly affected by the White Hill Gabbro. Hematite-rich compositions within these deposits have Koenigsberger ratios much greater than unity (up to several hundred) and the bulk magnetisations of large volumes of these hematite-(magnetite) bodies have effective Koenigsberger ratios greater than 10. At Peculiar Knob a ground magnetic anomaly of ~30,000 nT is associated with hematite-rich alteration with moderate susceptibility (~0.25 SI), but a remanent intensity (measured and modelled) of 120 A/m (Q ≈ 10). The effective Koenigsberger ratio for similar compositions at Manxman B is ~60.
- The massive hematite body at Prominent Hill, on the other hand, lies outside the contact aureoles of the Hiltaba Suite intrusions that have affected Peculiar Knob and Manxman B. The magnetisation of the Prominent Hill massive hematite is weak, due to the low susceptibility of hematite and the absence of TRM.
- On the other hand, magnetite-rich members of the iron oxide Cu-Au class have very high susceptibilities (e.g. 1.8 SI for the primary zone and 0.7 SI for the secondary zone at Ernest Henry; ~6 SI for magnetite ironstones at Osborne and ~20 SI for massive magnetite at Selwyn/Starra) and subordinate remanence. The total magnetisations (induced + remanent) of magnetite-rich Olympic Dam analogues in the Gawler Province are comparable to those of and hematite-rich examples. Koenigsberger ratios are typically 0.1 – 1, so remanence effects should not be neglected for detailed modelling and drill targetting. Raw NRMs are not representative of the *in situ* remanence, because they are usually contaminated by drilling-induced magnetisation and other palaeomagnetic noise, so palaeomagnetic cleaning is required to determine representive remanence vectors.
- Magnetite-rich mineralisation with pronounced banding is highly anisotropic (e.g. A ≈ 1.5 for banded magnetite alteration around Ernest Henry), so anisotropy effects can be important for modelling. Whether massive or banded, the effects of self-demagnetisation are important for interpreting magnetic anomalies associated with magnetite-rich deposits. For example, the early drilling at the Osborne Cu-Au deposit went down-dip because the interpreted dip of the magnetite-rich ironstones was out by 55°, due to neglect of self-demagnetisation and distortion of the geomagnetic field by the intense anomaly.

- Iron oxide Cu-Au deposits with intergrowths of hematite and magnetite or partial replacements of one by the other have properties intermediate between the hematite-dominated and magnetite-dominated end members. Remanence effects may be important for this mineralogy, probably because lattice mismatch between hematite and magnetite produces residual stresses within grains that stabilises and intensifies remanent magnetisation. The ore at La Candelaria is hosted by semi-massive magnetite that appears in many cases to have partially to totally replaced earlier hematite (mushketovite). However, suggestions of important remanence effects at La Candelaria in Chile (Taylor, 2000) have been refuted by the petrophysical study carried out during this project.
- Remanence effects are likely to be important for Precambrian deposits, because geomagnetic reversal frequency appears to have been lower than for most of the Phanerozoic. With the exception of the two geomagnetic superchrons, the Permo-Carboniferous (~317-260 Ma) Reverse Superchron and the Cretaceous Normal Superchron (118-83 Ma), the magnetic signatures of most deposits of Phanerozoic age should not show strong remanence effects. This is due to the high frequency of geomagnetic reversals and the prolonged magmatic-hydrothermal evolution of most deposits, which spans one or more reversals and produces substantial cancellation of remanence over large volumes of rock. At a local scale, most Tertiary porphyry deposits exhibit two or more palaeomagnetic components that record different events in the evolution of the deposit (e.g. emplacement of an intrusion and its subsequent alteration) and also reflect any tectonic rotations that have occurred after the remanence was acquired.
- When remanence effects are known or suspected to be important, remanence directions can be predicted from the deposit age and the apparent polar wander path for the crustal block that hosts the deposit. Polarity of remanence can be predicted from the geomagnetic polarity time scale. Sponsors will be supplied with pole lists for major crustal blocks and a Visual Basic program that enables palaeofield directions to be predicted.

9.2 Magnetic Signatures of IOCG deposits of the Gawler Craton

Figure 9.1 shows the basement geology of the portions of South Australia underlain by the Gawler Craton and Fig.9.2 shows major domain boundaries superimposed on a TMI image. Figure 9.3 shows more detail of the basement geology of the Olympic Domain. The giant Olympic Dam Cu-U-Au-(REE) deposit is in the northern part of the Olympic Domain, with nearby hematite-rich and magnetite-rich IOCG occurrences at Acropolis, Wirrda Well, Oak Dam and Emmie Bluff. The recently discovered Prominent Hill mineralisation and other prospects, such as Peculiar Knob, White Hill and Manxman, occur within the Mount Woods Inlier. Cu-Au mineralisation at Moonta and Wallaroo occurs in the southern portion of the Olympic Domain.

The mineralisation appears to be related temporally and spatially with granitoids of the 1595-1570 Ma Hiltaba suite. The massive Gawler Range Volcanics magmatism represents the extrusive equivalent of the Hiltaba Suite. This major igneous event is anorogenic in character, with bimodal magmas generated during crustal extension associated with incipient continental rifting. The granitoids are oxidised I- and A-type, ranging in composition from gabbro to syenogranite.

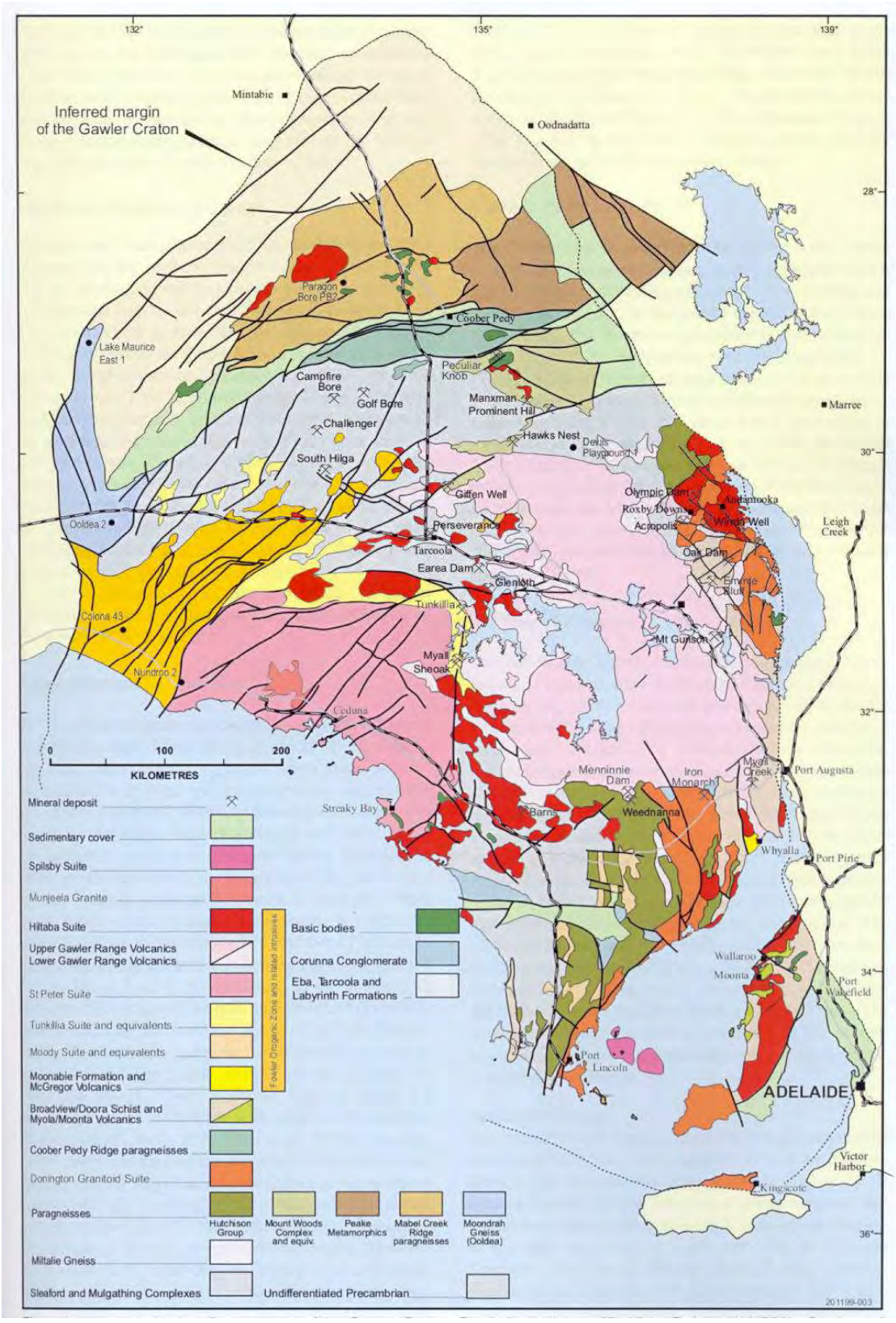

Fig.9.1. Interpreted subsurface geology of the Gawler Craton and Stuart Shelf (Ferris et al., 2002)

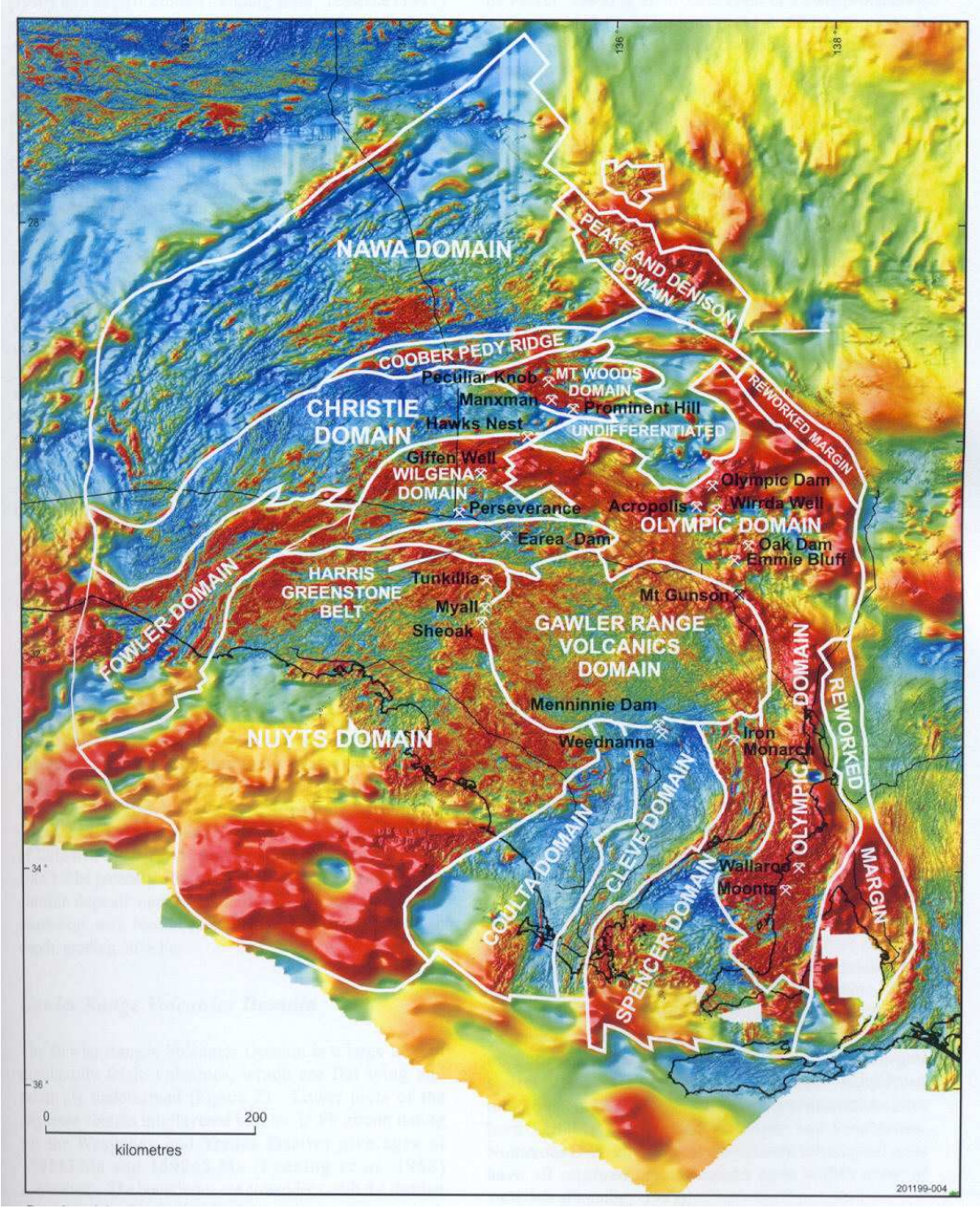

Fig.9.2. TMI image of the Gawler Craton, showing major domains and selected mineral deposits (Ferris et al., 2002).

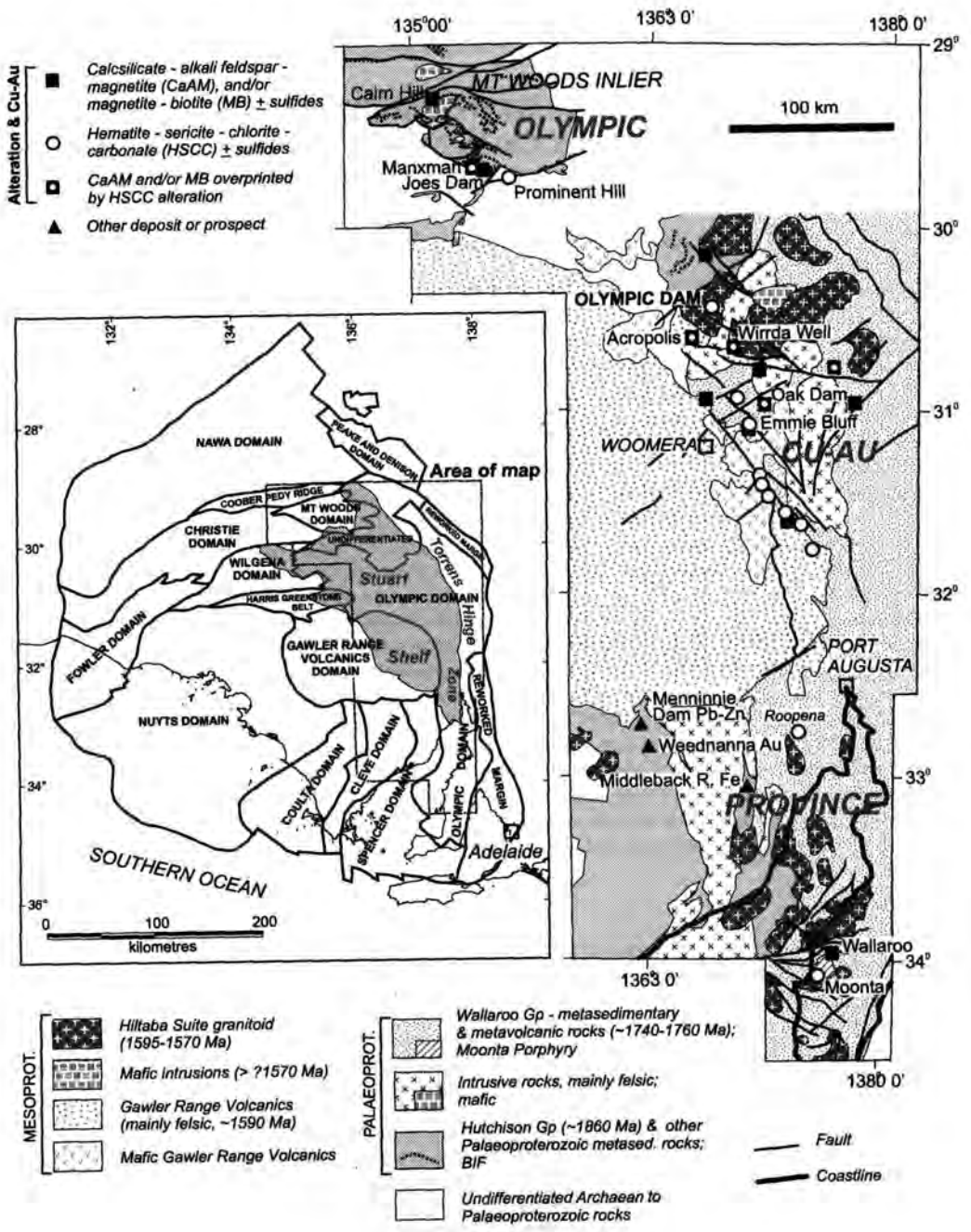

Fig.9.3. Basement geology interpretation and alteration in the Olympic Province (Skirrow et al., 2002).

On a regional scale it is evident that all these deposits occur within highly magnetic domains. This phenomenon seems to apply to IOCG provinces globally. Individual deposits represent significant accumulations of dense, often strongly magnetic, iron oxides and are therefore associated with positive gravity anomalies and, in many cases, positive magnetic anomalies. For example the Olympic Dam deposit represents a resource of greater than 2 billion tonnes containing an average of 26 wt% Fe (Reynolds, 2000). The deposit occurs within a broad magnetic high (~1000 nT, after removal of the regional gradient) and is associated with a 17 mgal gravity high.

Another important feature of IOCG deposits is that in some cases at least, their location appears to be controlled by regional lineaments that can be seen by suitable enhancements and stretches of regional potential field data sets, or in satellite imagery. These lineaments, some of which have been inferred to be related to continental-scale features, presumably represent major crustal structures that have controlled ascent of magmas and/or mineralising hydrothermal fluids, of magmatic or other origin. Figure 9.4 shows the location of Olympic Dam with respect to major lineaments within the Gawler Craton.

The geology of the Olympic Dam deposit is shown in Fig.9.5. Figure 9.6 shows an schematic model of Olympic Dam type deposits, based on known geology of Olympic Dam itself and on other nearby prospects that interpreted to be equivalents portions of the undrilled deeper portions of Olympic Dam. Figure 9.7 shows regional magnetic and gravity data from the northern Olympic Domain, covering Olympic Dam and nearby prospects, clearly showing the magnetic and gravity highs associated with the IOCG-type mineralisation. Figure 9.8 zooms in on the Olympic Dam deposit, showing an image of the first vertical derivative of regional TMI and superimposed gravity contours.

The geophysics of the Olympic Dam deposit has been discussed in detail by Rutter and Esdale (1985) and Esdale et al. (1987, 2003). Figure 9.9 shows detailed gravity contours and the petrophysically and geologically constrained density model developed to match the observed gravity data (Esdale et al., 2003). Although the gravity anomaly is clearly related to the mineralised hematite-rich alteration system, the situation with regard to the magnetics is more ambiguous. Olympic Dam lies within a broad magnetic high on a strong regional magnetic gradient (Figs.9.10-11). Within the broad high a narrower superimposed high is more closely related to the deposit. The first vertical derivative of the TMI focusses more clearly on the deposit itself (Fig.9.11). The broad magnetic feature was traditionally interpreted as a deep source, e.g. a large mafic intrusion, that may not necessarily be directly related to the Olympic Dam deposit. This interpretation is reasonable, given that the magnetic anomaly is considerably broader than the intensely hematite-altered zone and the relatively low susceptibility of the hematite alteration in the central part of the system.

Figure 9.12 demonstrates the equivalence of deep compact and shallow/broad sources of potential field anomalies. This is an example of the fundamental non-uniqueness of unconstrained potential field modelling. Its relevance to Olympic Dam consists in the observations that deeper and peripheral portions of the deposit contain some magnetite, as well as hematite, and that the zone of hematite ± magnetite alteration is now known to extend well beyond (about 7 km on average) the main hematite and hematite-granite breccias. If the hematite within this halo carries systematically

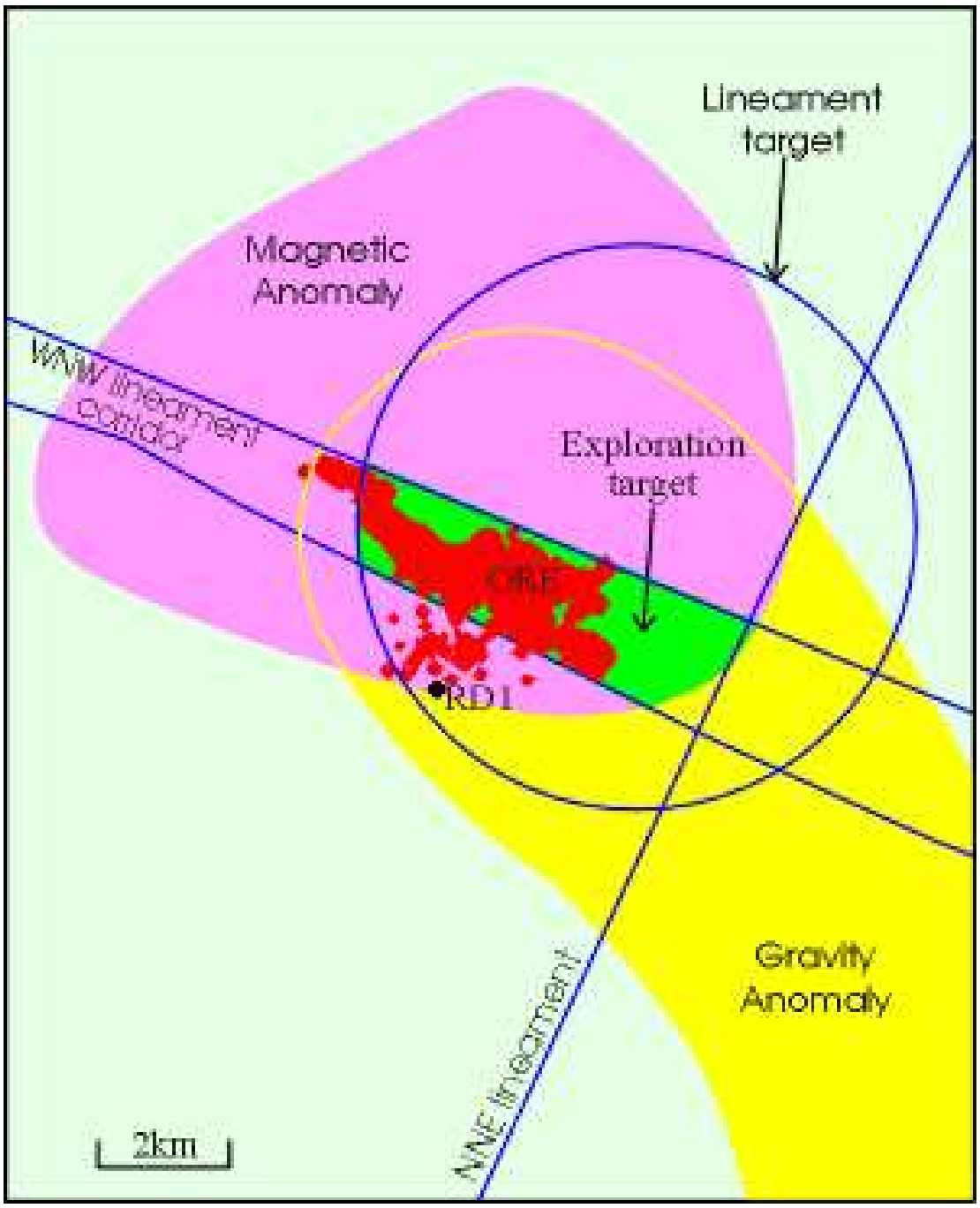

Fig.9.4 Relationships between potential field anomalies associated with the Olympic Dam deposit and major lineaments defined by regional potential field and remote sensing data sets.

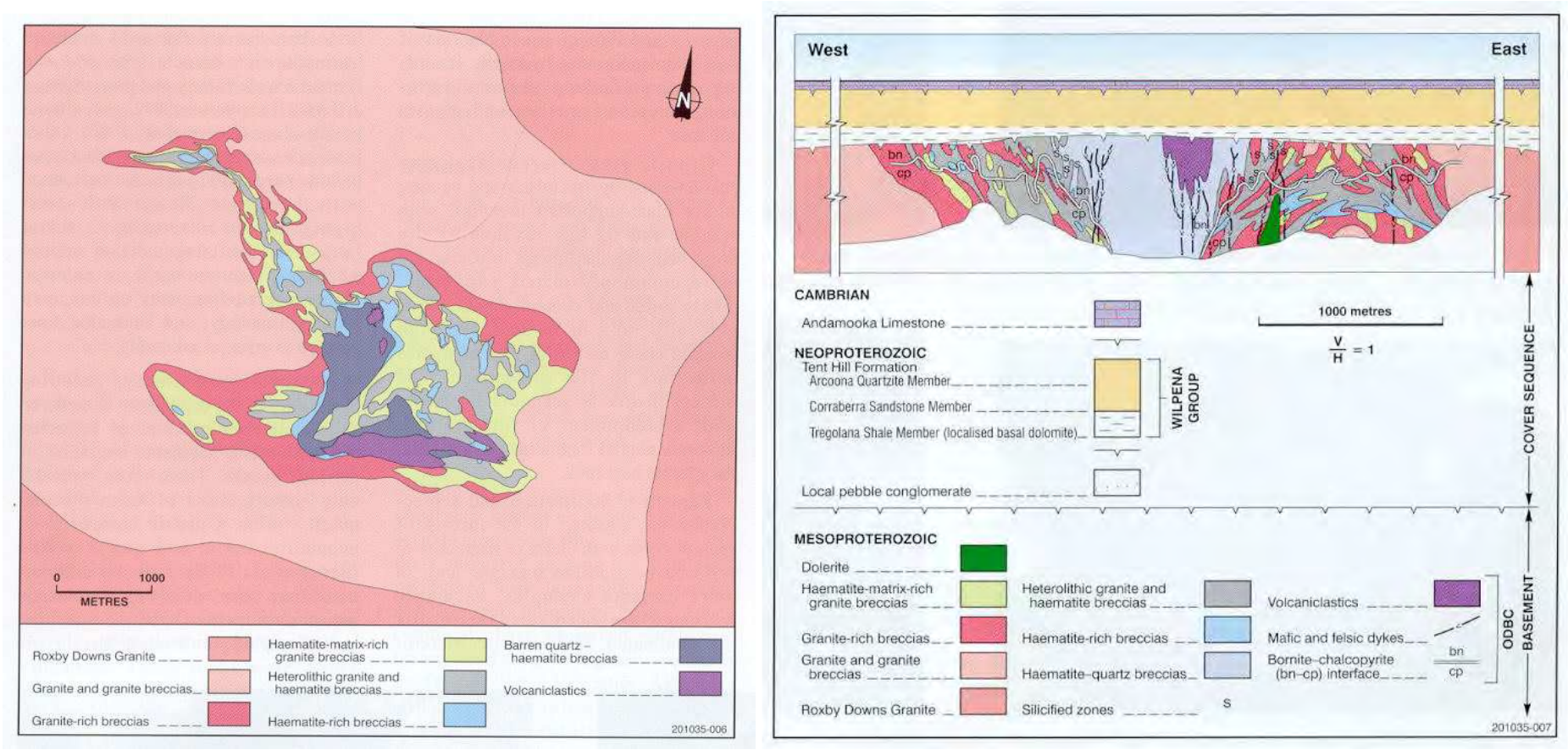

Fig.9.5 Geology of the Olympic Dam deposit (Reynolds, 2000)

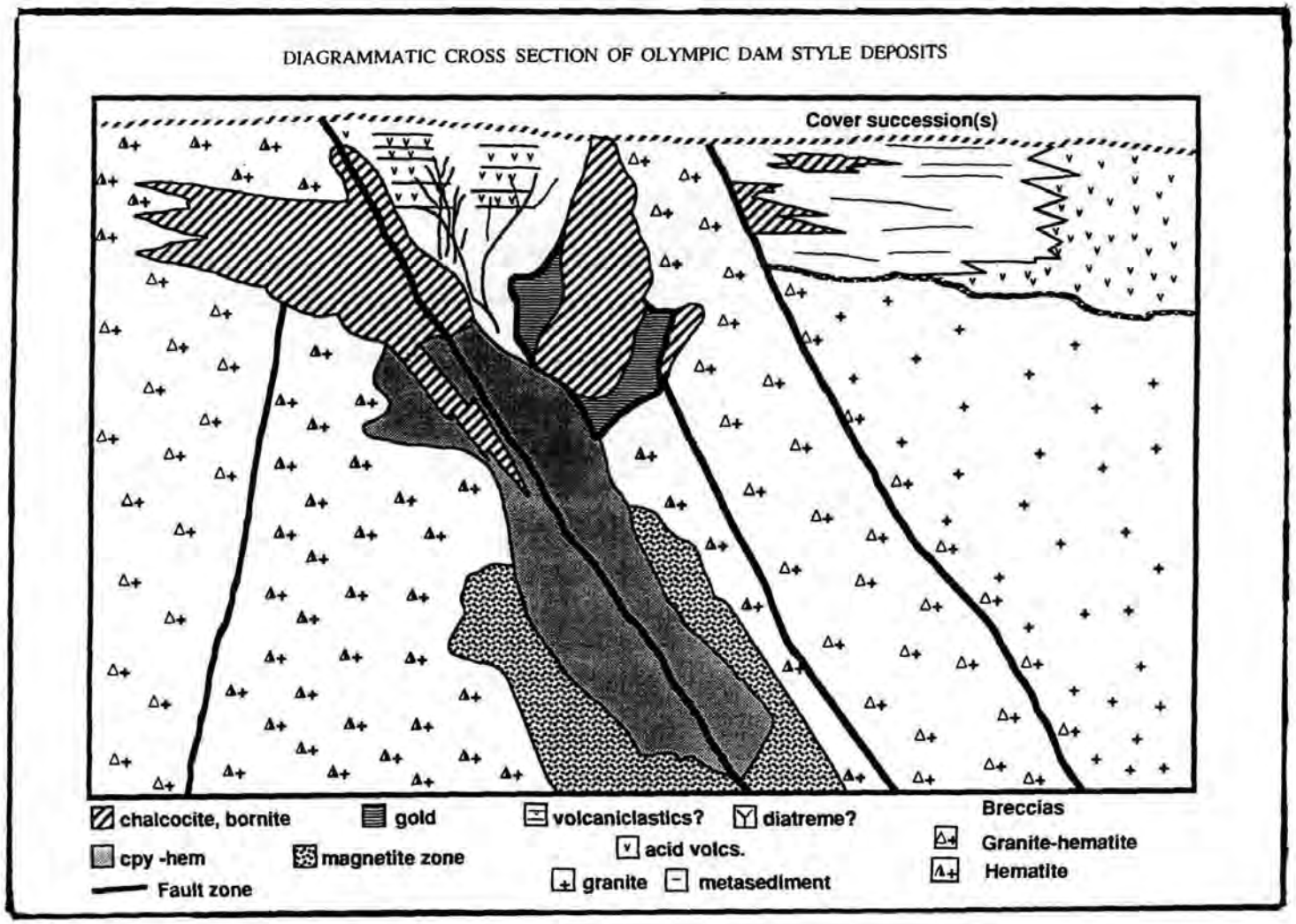

Fig.9.6 Schematic cross-section of Olympic Dam style deposits (Wall and Gow, 1996).

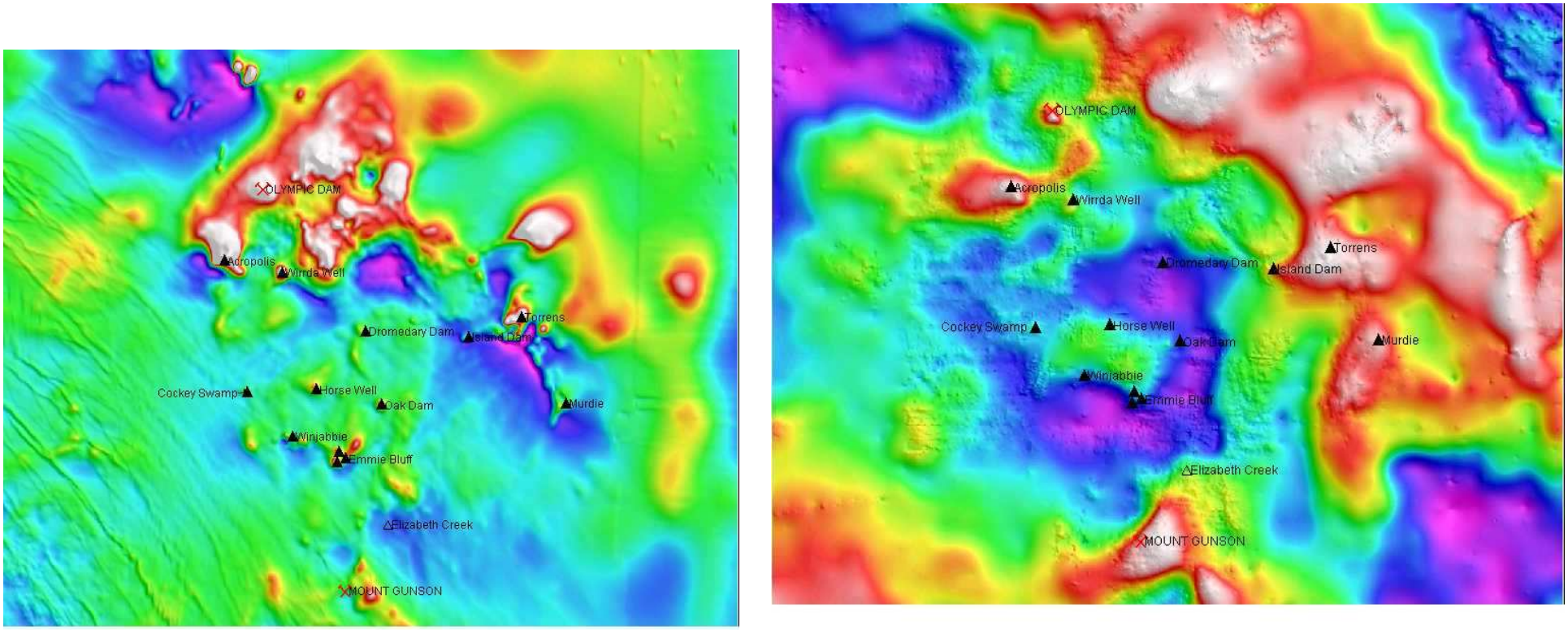

Fig.9.7 Regional TMI (left) and gravity (right) images over the northern Olympic Domain (Anderson and McConachy, 2003).

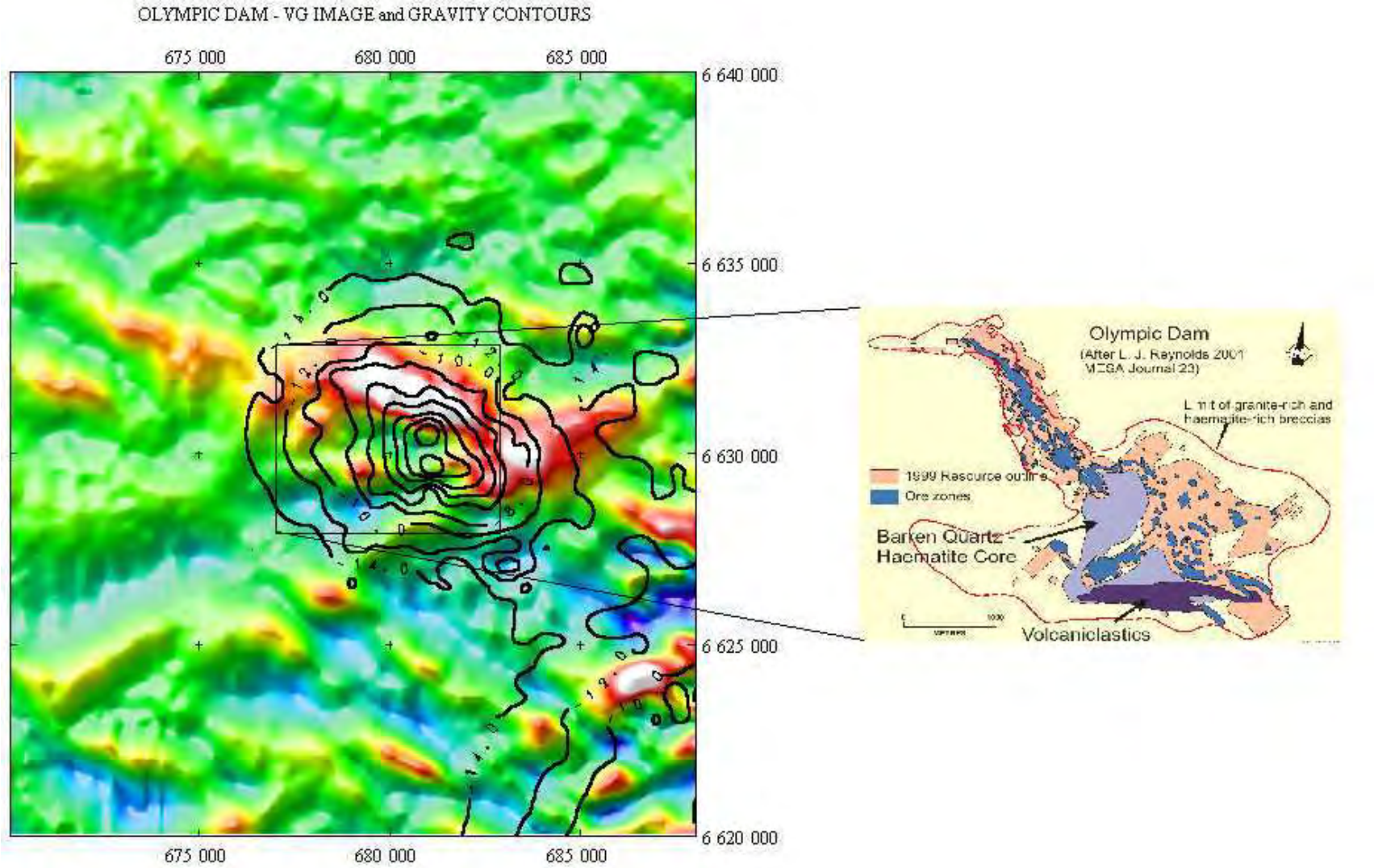

Fig.9.8. First vertical derivative of regional TMI and superimposed gravity contours over the Olympic Dam deposit (Anderson and McConachy, 2003).

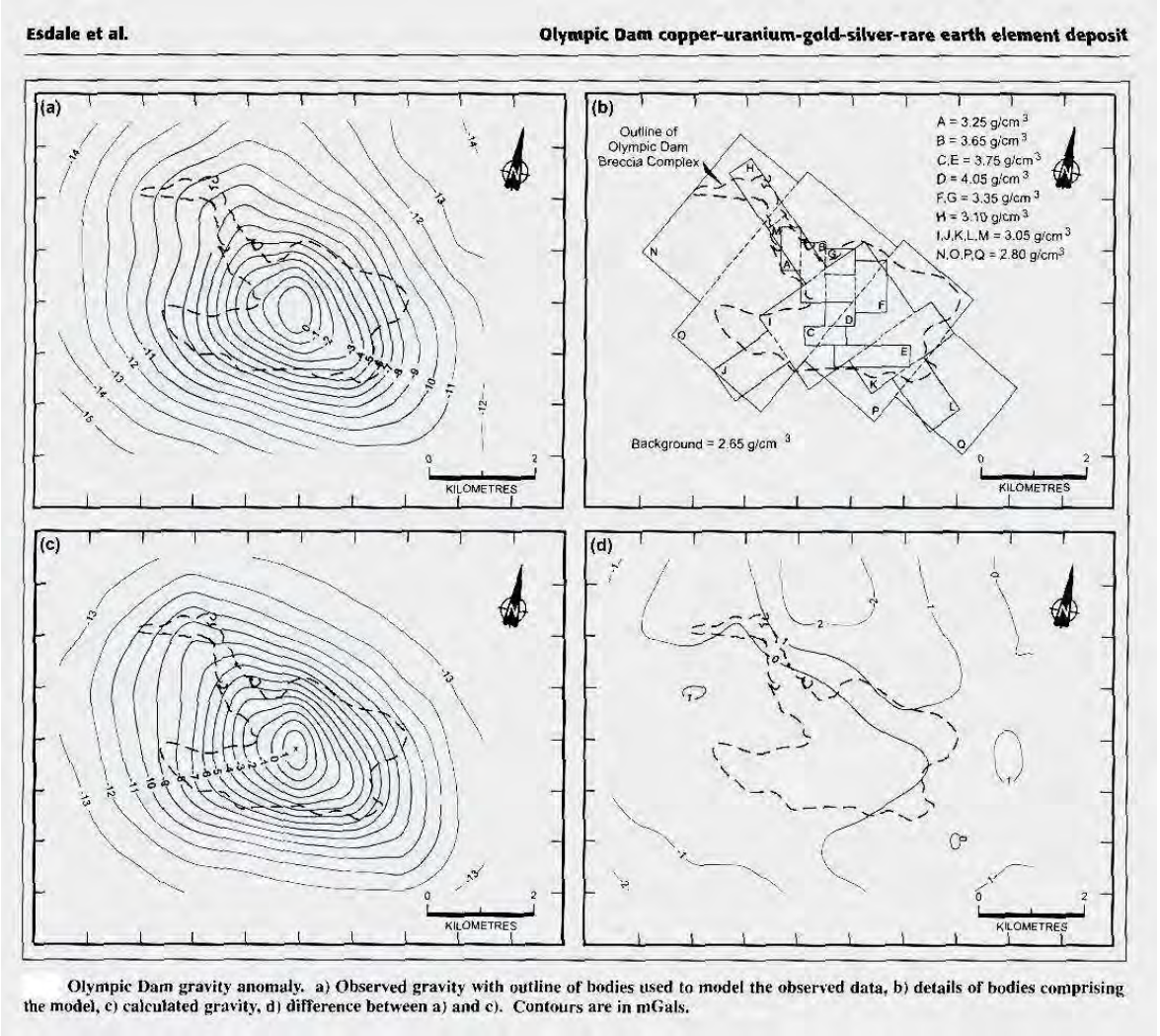

Fig.9.9. Gravity contours and density model for Olympic Dam deposit (Esdale et al., 2003)

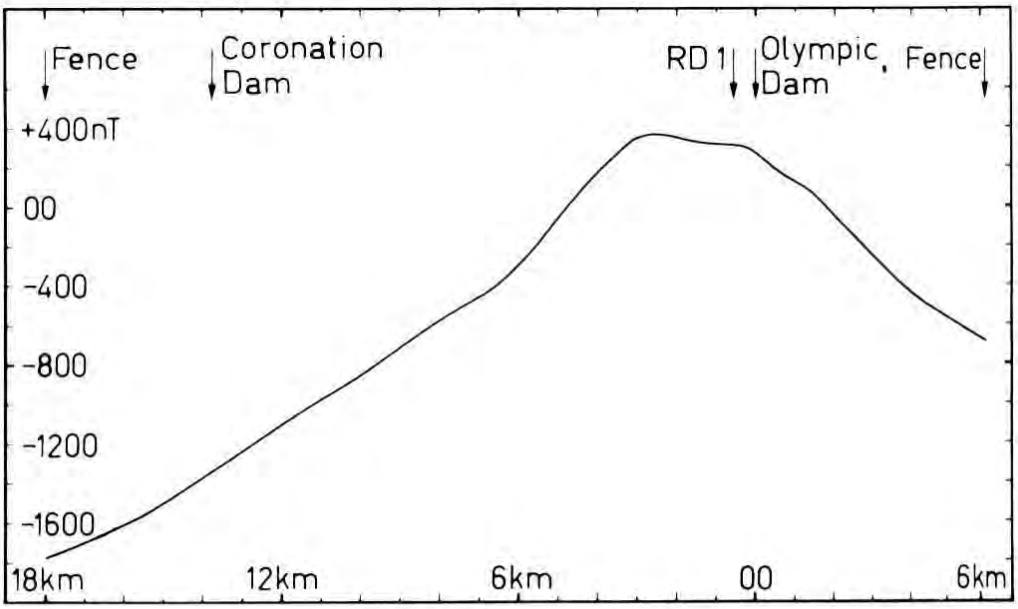

Ground magnetic traverse Coronation Dam–Olympic Dam relative values.

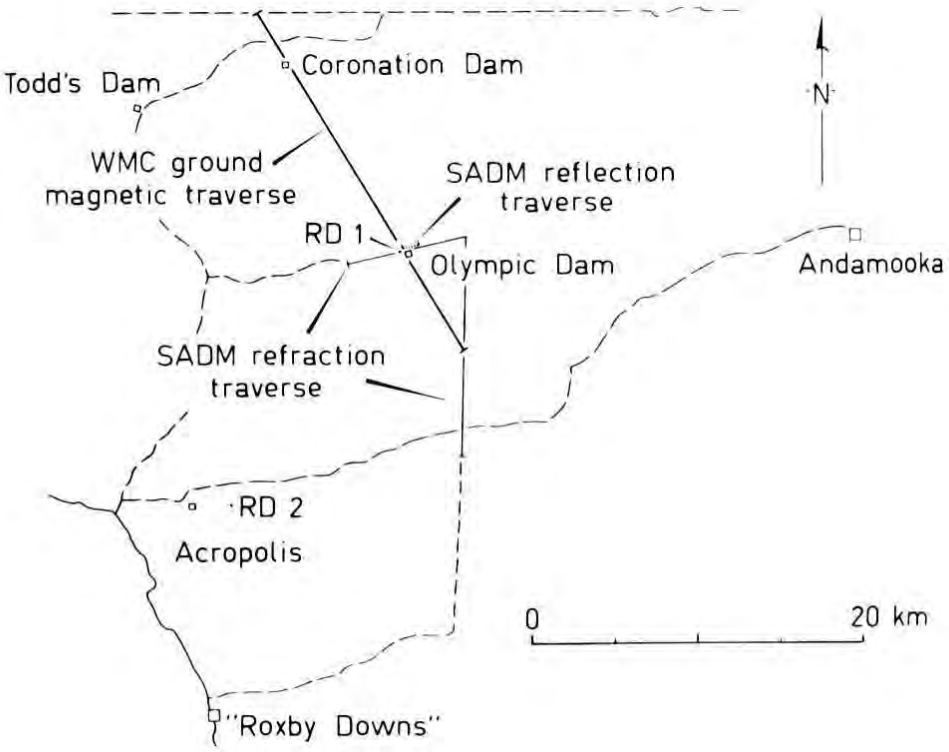

Geophysical ground surveys.

Fig.9.10. Ground magnetic profile over Olympic Dam (Rutter and Esdale, 1985).

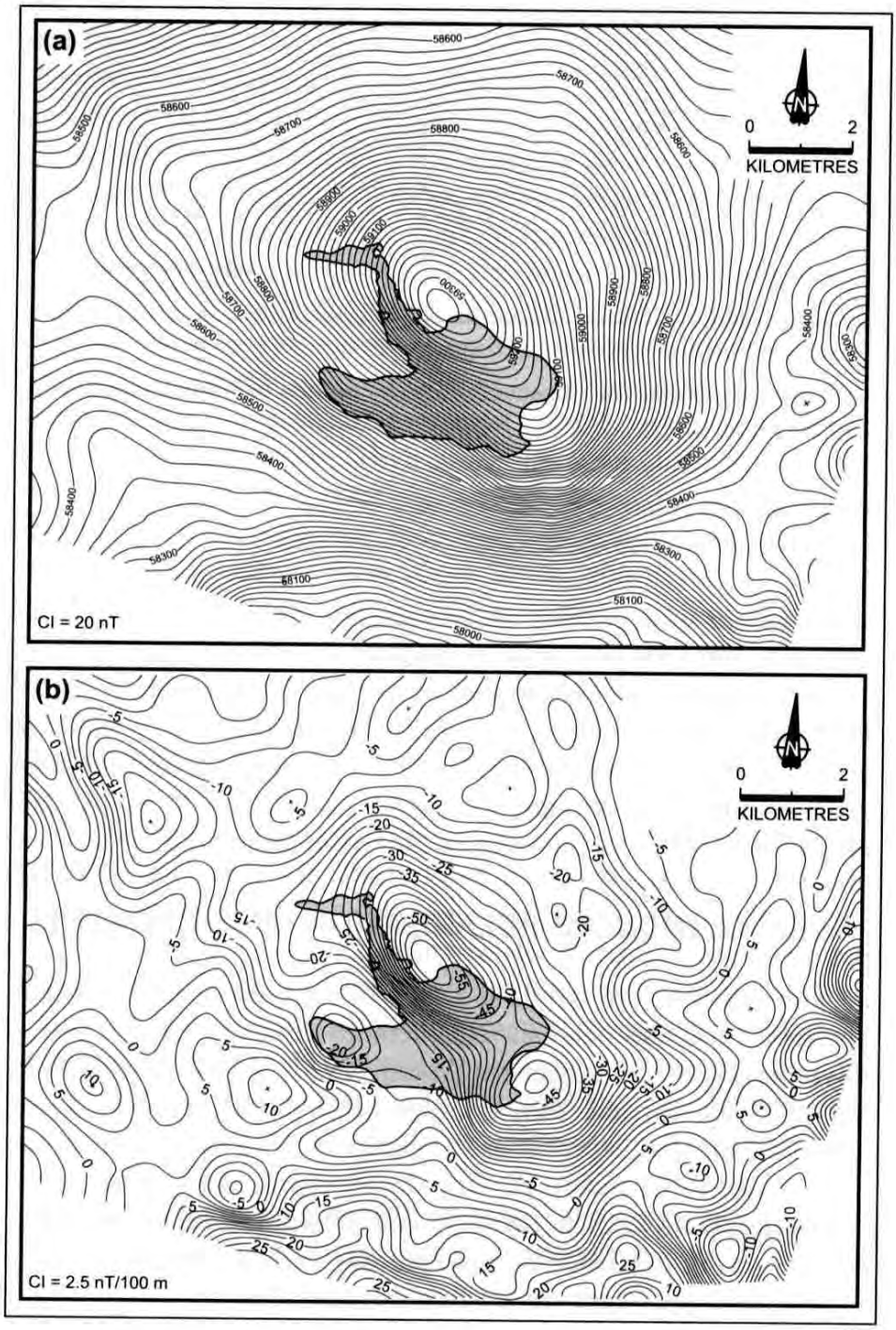

Aeromagnetic data from the Olympic Dam area. The shaded region is the extent of the ODBC. a) TMI, b) 1ST vertical derivative (negative vertical derivative anomalies correspond with shorter wave length TMI anomalies).

Fig.9.11. Detailed TMI contours (20 nT interval) and first vertical derivative of TMI over Olympic Dam (Esdale et al., 2003).

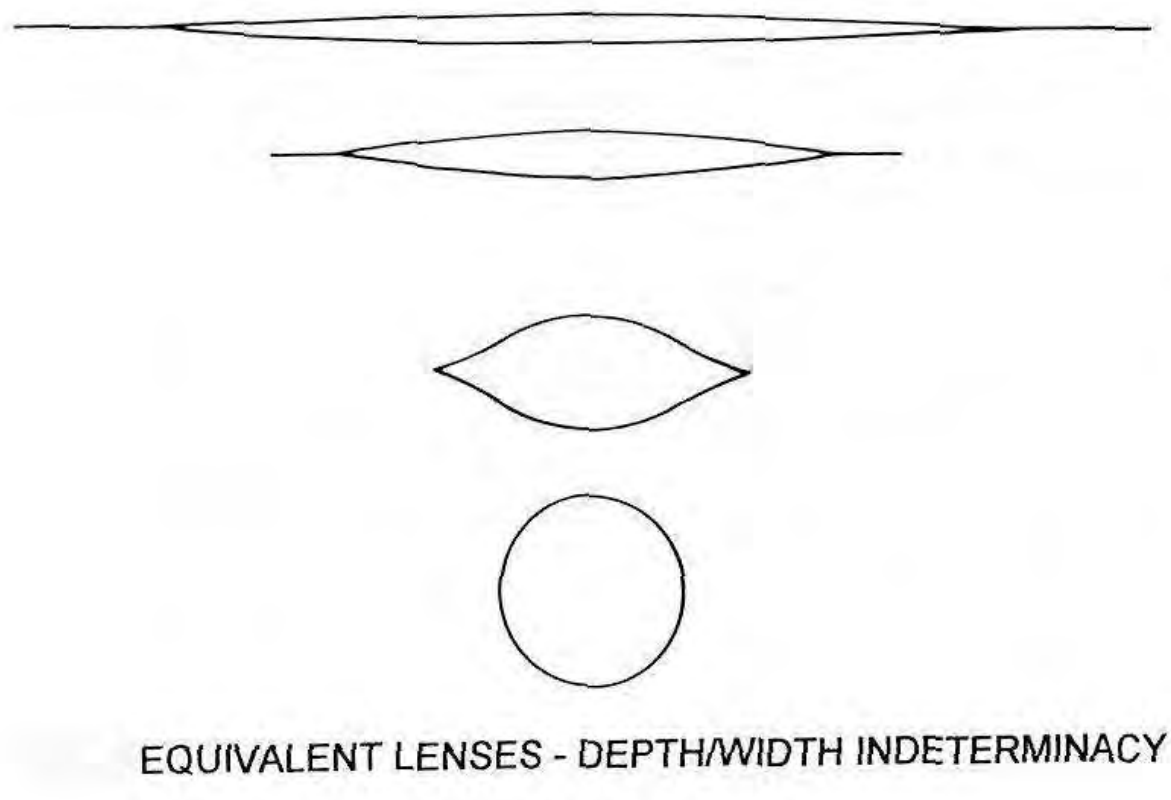

Fig.9.12. Equivalent lenses that produce identical magnetic anomalies, demonstrating the trade-off between depth and width that may explain the broad magnetic anomaly at Olympic Dam.

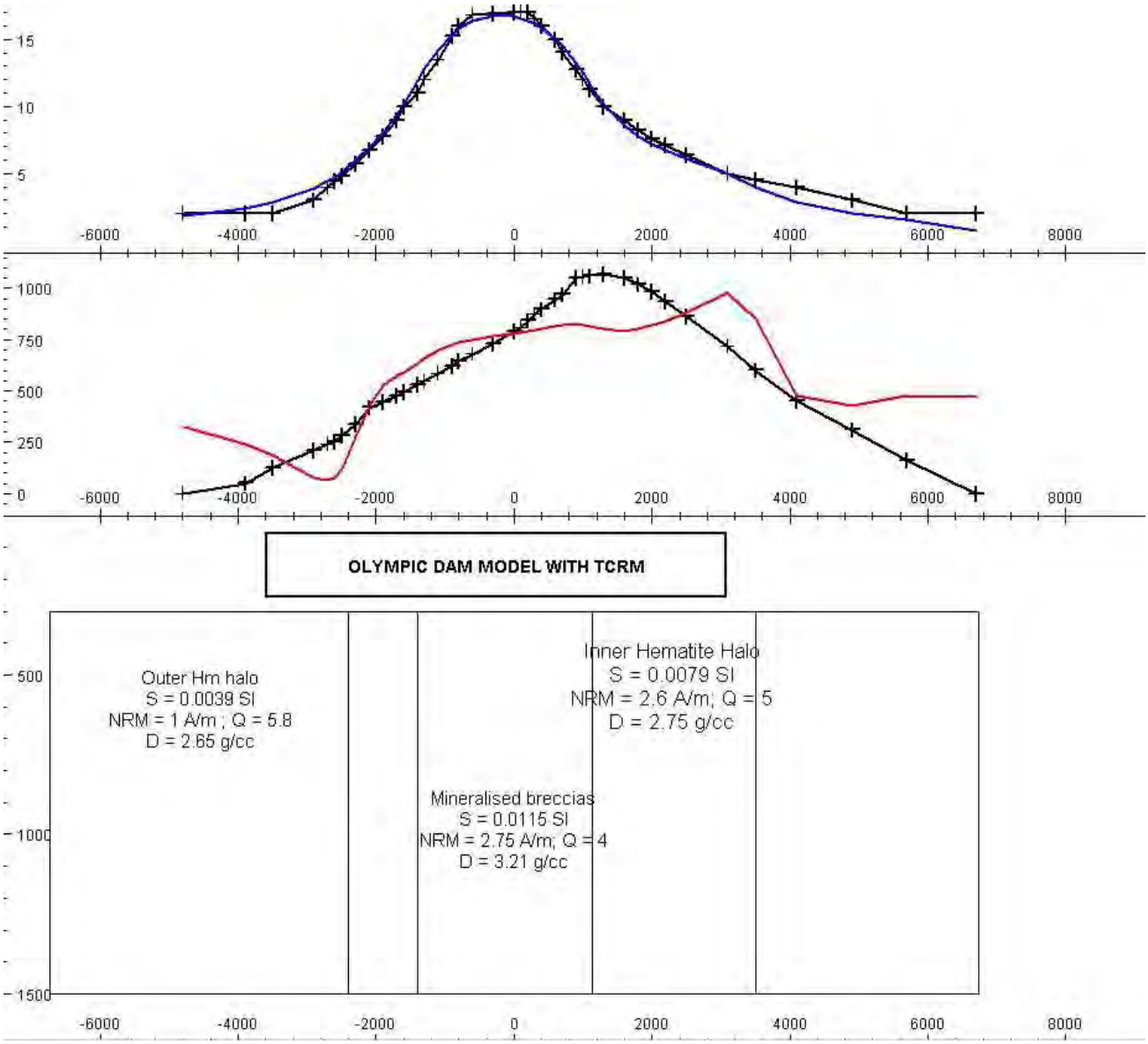

Fig.9.13. Crude magnetic and gravity model of the Olympic Dam deposit (section), with a broad hematite alteration halo carrying a moderate chemical remanent magnetisation acquired at hydrothermal temperatures. The width and amplitude of the Olympic Dam magnetic anomaly can be explained by such a model, although detailed matching of anomaly form requires refinement of the model, particularly to replace abrupt zone boundaries with gradual changes magnetisation intensity, reflecting gradual outward reduction in intensity of alteration.

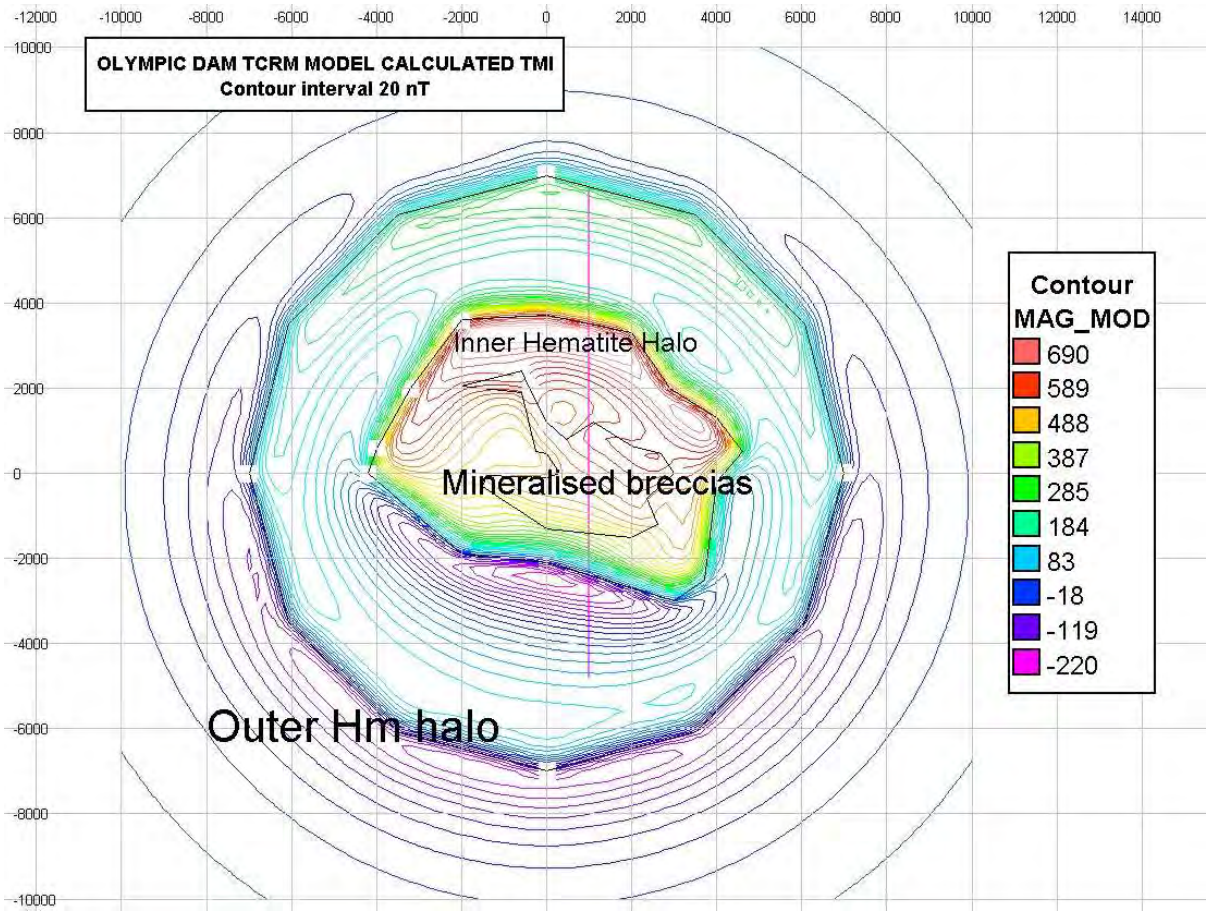

Fig.9.14. Crude magnetic and gravity model of the Olympic Dam deposit (plan view), with a broad hematite alteration halo carrying a moderate chemical remanent magnetisation acquired at hydrothermal temperatures. The width and amplitude of the Olympic Dam magnetic anomaly can be explained by such a model, although detailed matching of anomaly form requires refinement of the model, particularly to replace abrupt zone boundaries with gradual changes magnetisation intensity, reflecting gradual outward reduction in intensity of alteration.

directed remanence, the magnetisation of this hematite halo may contribute significantly to the observed magnetic anomaly. Wall and Gow (1996) have modelled the gravity and magnetic anomalies, using peripheral and deep disseminated magnetite zones around the hematite-rich core.

Figures 9.13-14 show that the broad ~1000 nT magnetic anomaly could in principle be explained by zoned hematite alteration carrying chemical remanent magnetisation of plausible intensity, given the known extent of the hematite halo around the deposit. These compementary approaches, therefore, show that it is not necessary to invoke a discrete deep source well beneath the deposit to account for the observed magnetic anomaly, although a contribution from such a body cannot be ruled out, given in the present incomplete state of knowledge about the distribution of magnetic minerals and their magnetic properties in and around the deposit.

Although the magnetic and gravity anomalies at Olympic Dam are traditionally described as *coincident*, the magnetic anomaly is broader and in appearance, and probably in reality, suggests a magnetic source that is deeper overall than the gravity source. This is consistent with the generalised picture of IOCG deposits as zoned vertically from hematite-rich HSCC zones to laterally extensive, deeper potassic zones with magnetite, underlain by magnetite-bearing sodic alteration. Thus the gravity and magnetic sources are, at least in part, spatially separated and are better described as *superposed*.

Esdale et al. (2003) also discuss the application of electrical methods to the Olympic Dam deposit. The most effective surface-based technique was found to be high powered, large separation dipole-dipole IP, which detected low resistivity, chargeable zones associated with porous hematite-rich breccias in the core of the deposit. Mineralisation occurs mainly in the outer part of the low resistivity, chargeable zone.

Typical magnetic signatures of various types of IOCG alteration (CAM: calcsilcate-alkali feldspar-magnetite; and BM: biotite-magnetite) in the southern Olympic Domain are shown in Figs.5.23-24). Other magnetic and gravity signatures of deposits from the Olympic Domain are included in the P700 Atlas of Geophysical Signatures.

Recent promising intersections of Cu-Au mineralisation at Prominent Hill have highlighted the prospectivity of the Mount Woods Inlier for Olympic Dam style mineralisation. Figure 7.12 shows a regional TMI image of this region, which clearly indicates zoned Hiltaba Suite plutons, including the magnetic White Hill Gabbro and the weakly magnetic Balta Granite, with prominent magnetic aureoles. Some major lineaments that may relate to structural controls of known occurrences of IOCG mineralisation are also prominent. Figures 9.15-16 compares TMI images with linear and equalised stretches, illustrating the different aspects of the data that are emphasised by each presentation. Figure 9.17 shows regional gravity over a similar area and detailed gravity data over the Prominent Hill and surrounding prospects.

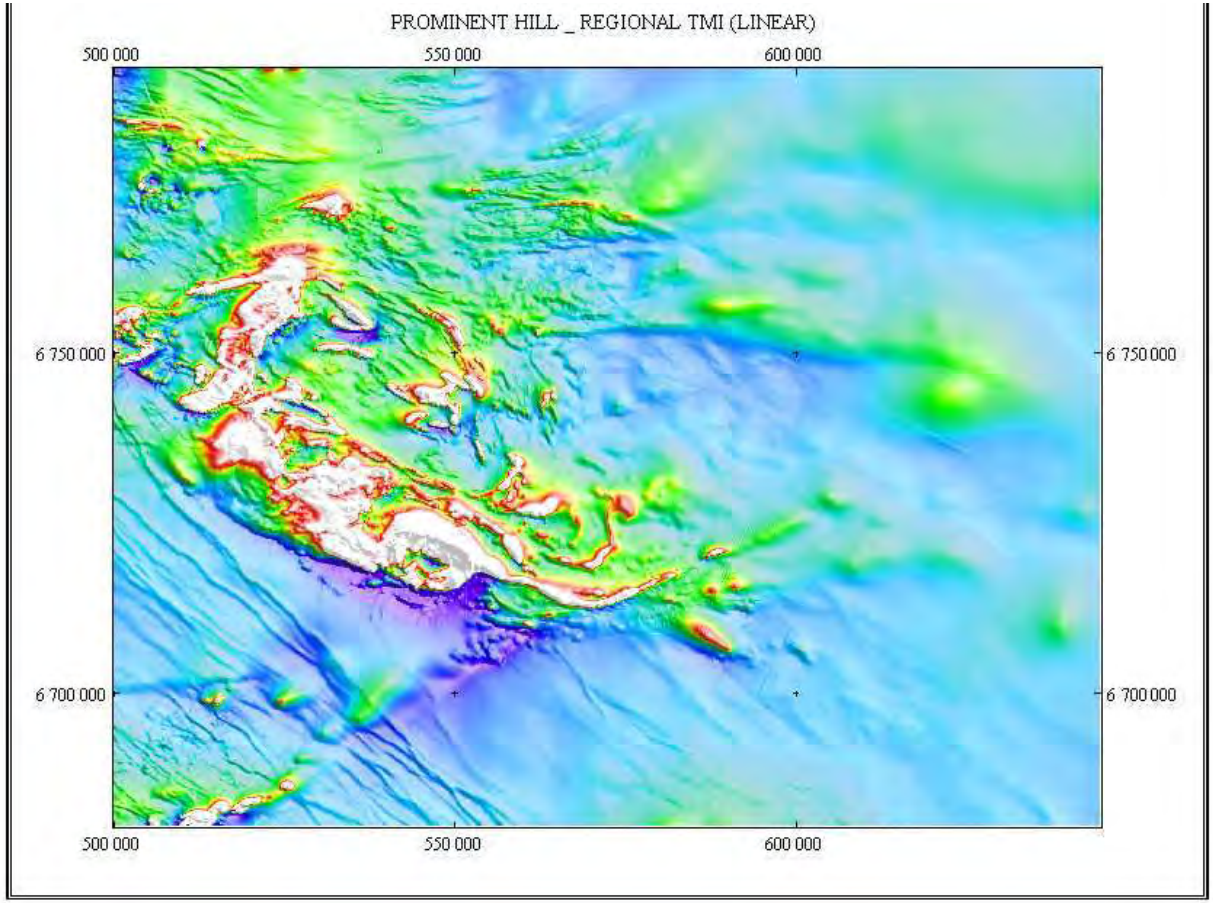

Fig.9.15. Regional TMI image of the Mount Woods Inlier with linear stretch, providing a realistic depiction of the relative amplitude of anomalies and identifying the strongest discrete sources in the region (Anderson and McConachy, 2003).

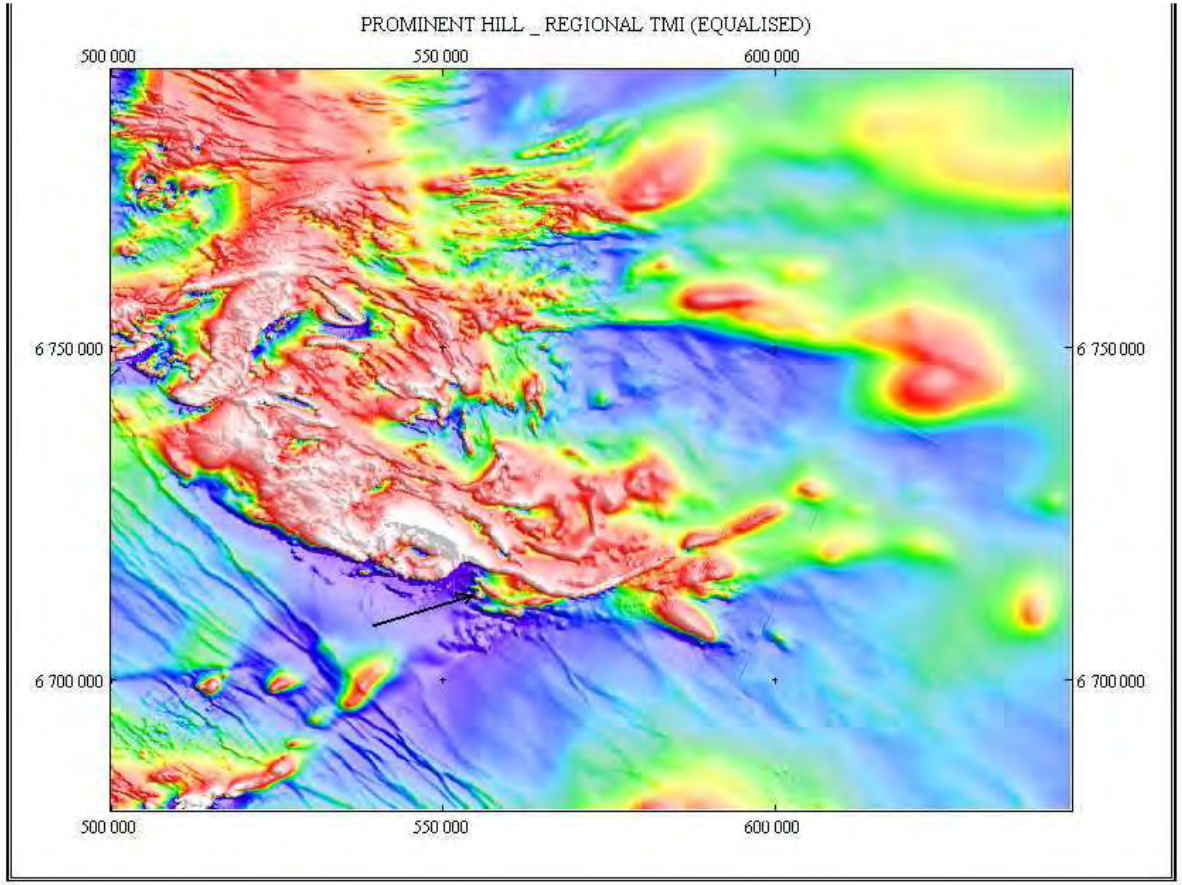

Fig.9.16. Regional TMI image of the Mount Woods Inlier with equalised stretch, improving the visibility of anomalies across the full dynamic range of the data and enhancing some structural detail (Anderson and McConachy, 2003). The arrow indicates Prominent Hill.

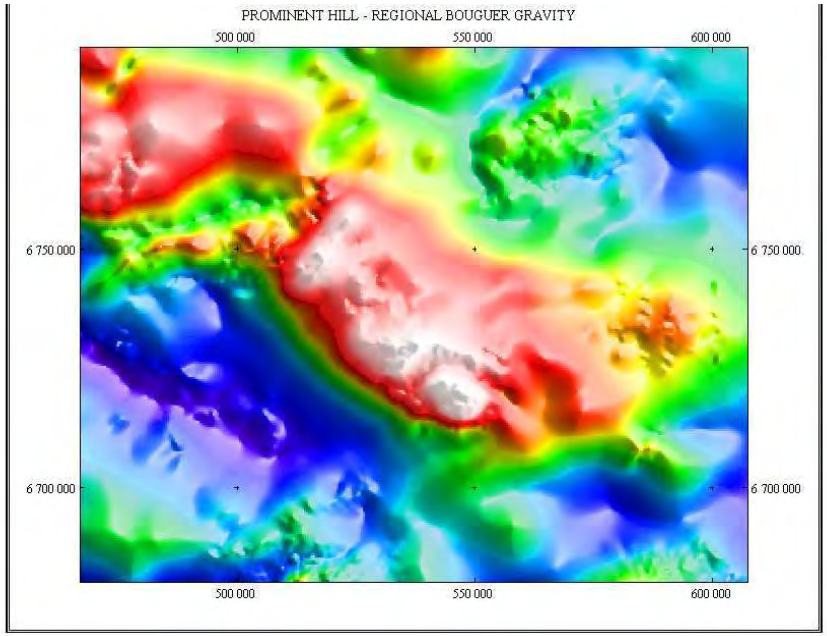

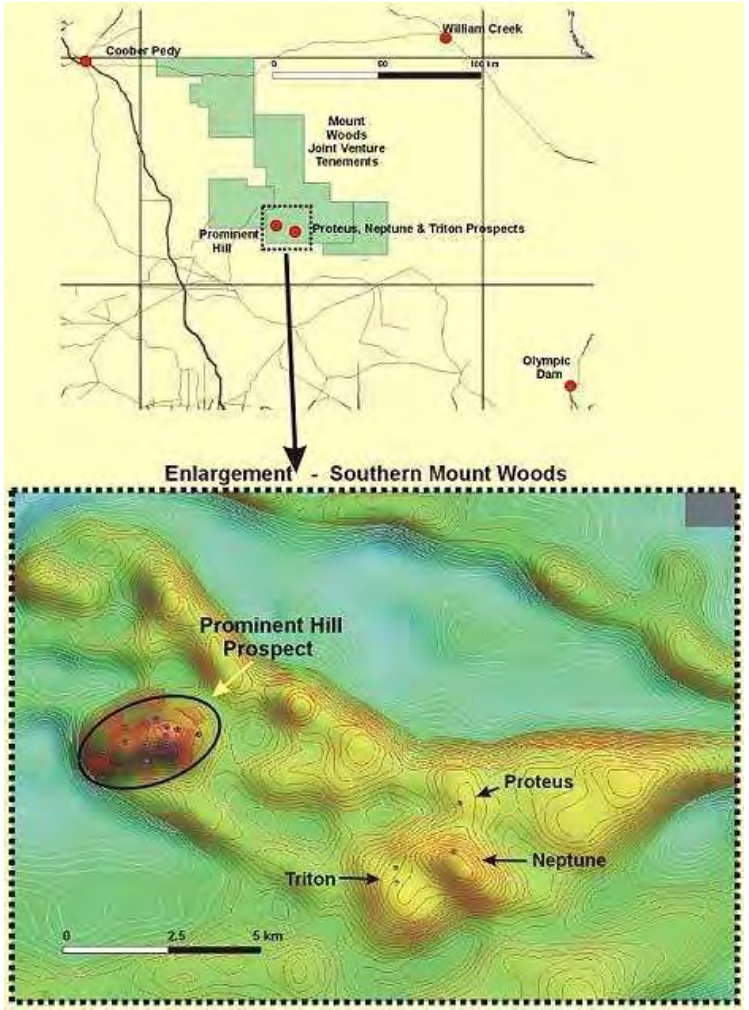

Fig.9.17. Regional Bouguer gravity image of the Mount Woods Inlier (left) and detailed gravity of the Prominent Hill and nearby prospects.

The geophysics of the Prominent Hill deposit has been described by Hart and Freeman (2003). The potential field signature of Prominent Hill consists of *juxtaposed* gravity and magnetic highs. Figure 9.18 shows contours of the second horizontal derivative of the Bouguer gravity on an image of the ground magnetics, clearly showing the lateral separation of the magnetic and gravity sources. The juxtaposition of the two types of anomaly is also shown in profile in Fig.9.19.

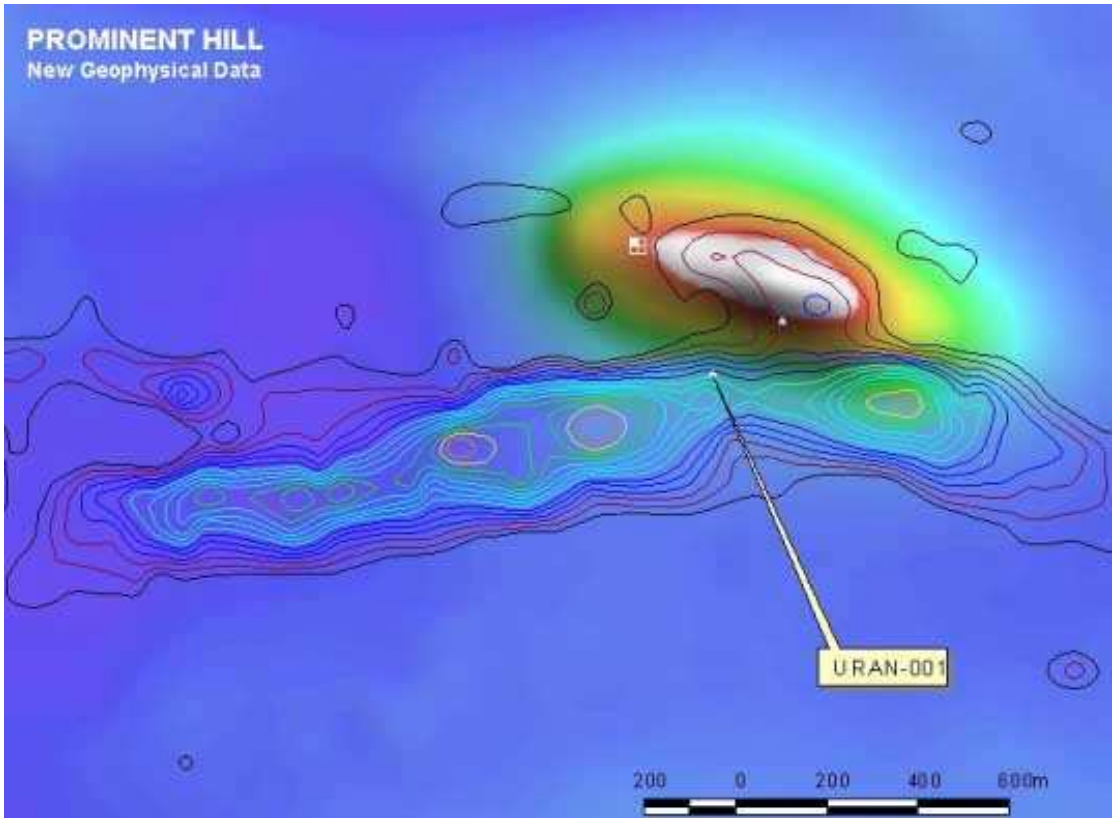

Fig.9.18. Contours of the second horizontal derivative of the Bouguer gravity on an image of the ground magnetics.URAN-001 is the “discovery” drill hole for the hematite-breccia hosted Cu-Au mineralisation.

Figure 9.20 shows the emerging geological picture of the Prominent Hill prospect. The magnetic domain in the north, which appears to have CAM (skarn-like) character is separated from the massive hematite and HSCC-altered mineralised hematite breccia zones by a fault. The magnetic zone probably represents an upfaulted block of the magnetite-rich deeper portions of a classically zoned IOCG system.

The White Hill prospect may represent such a deeper formed magnetite-rich portion of an IOCG system, now at relatively shallow depths (see Fig.9.21). The Peculiar Knob prospect represents massive hematite mineralisation that is associated with a very large magnetic anomaly, due to acquisition of thermoremanence during contact metamorphism (see section 7.2 and Figs.9.22-23).

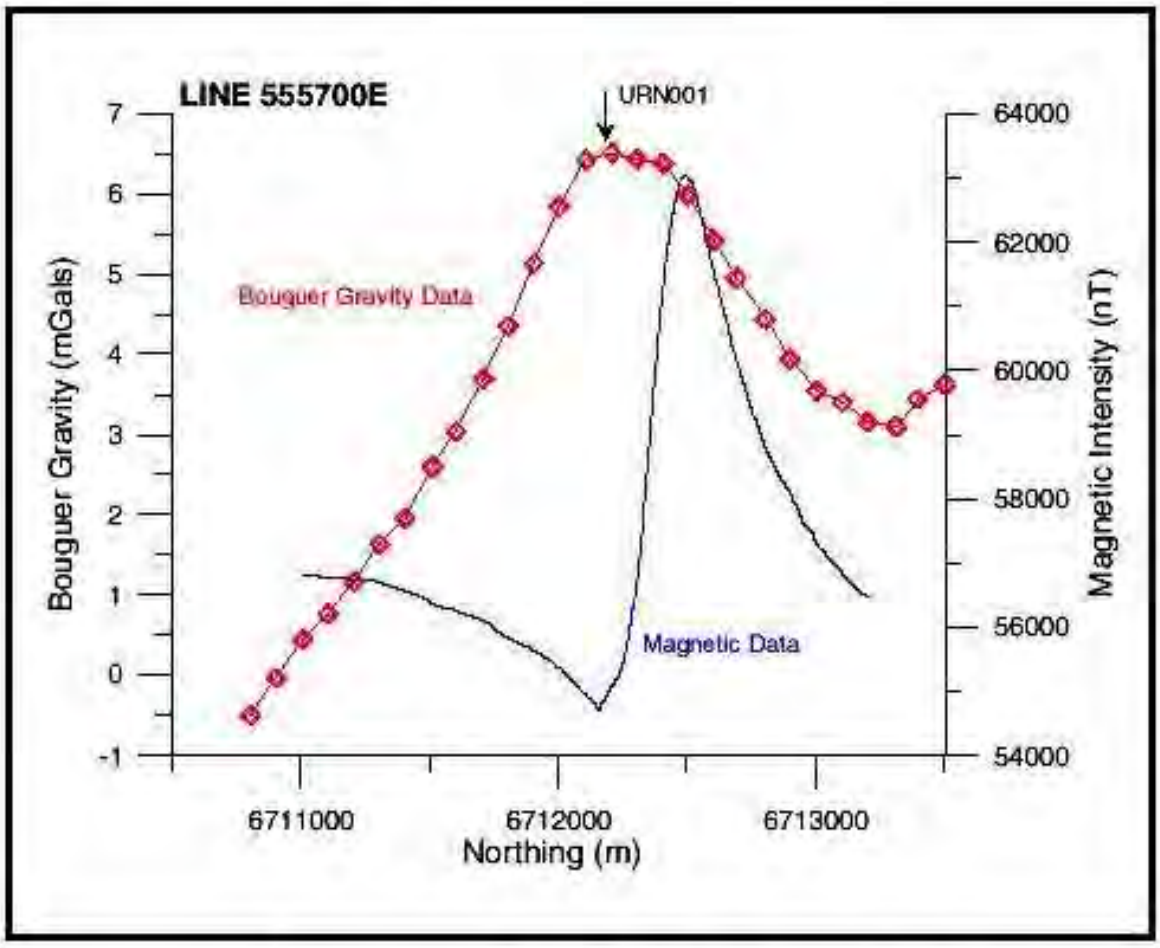

Bouguer Gravity Data and Ground Magnetic Data from Line 555700E, Prominent Hill Grid. Location of URN001 shown.

Fig.9.19. Gravity and magnetic profiles over Prominent Hill (Hart and Freeman, 2003).

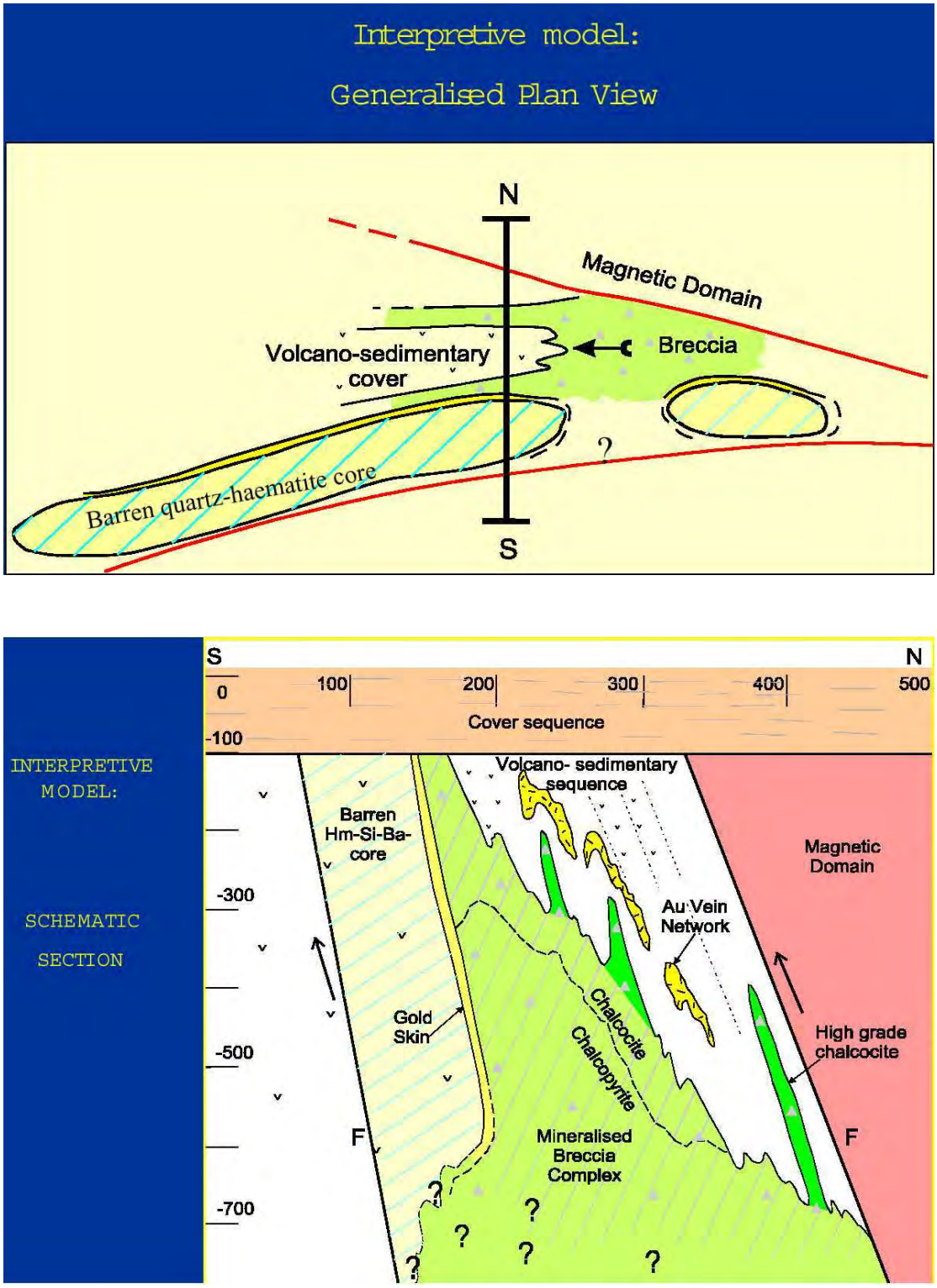

Fig.9.20. Schematic geology of the Prominent Hill prospect – an Olympic Dam analogue within the Mount Woods Domain of the Gawler Craton (Belperio, 2002).

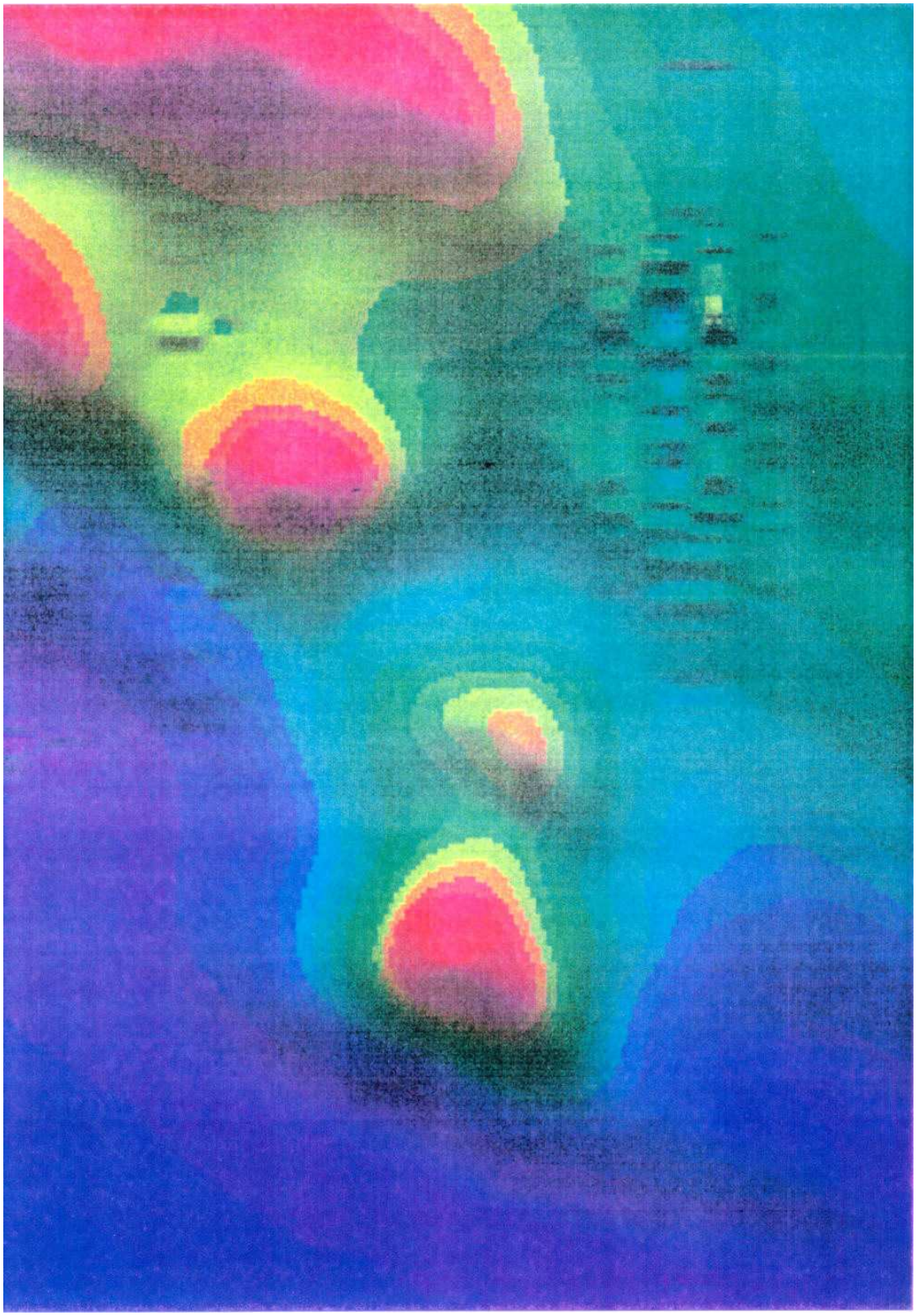

Fig.9.21. TMI image over the White Hill Prospect, Mount Woods area, Gawler Craton. Intense (up to 12,000 nT) magnetic highs are associated with magnetite-rich Cu-Au mineralised bodies ~100 m below the surface.

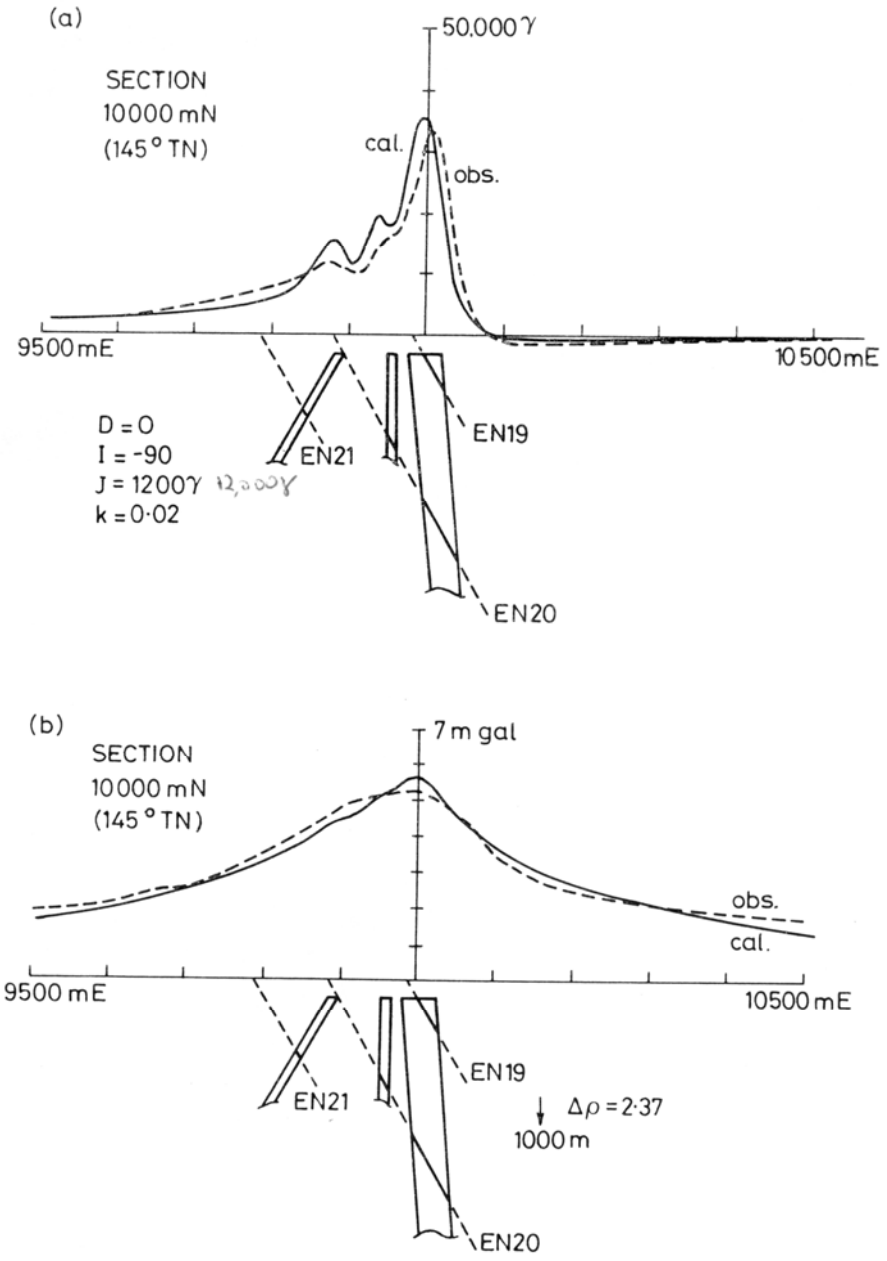

Fig.9.22. Magnetic and gravity models for the Peculiar Knob prospect, Mount Woods Inlier, Gawler Craton. Massive hematite mineralisation with minor magnetite and maghemite has a moderate susceptibility (< 0.3 SI) but carries an intense remanence (~120 A/m), directed very steeply upwards. The corresponding Koenigsberger ratio is ~10. The intersected bodies account for the observed gravity and magnetic anomalies when the measured properties, including remanence, are taken into account, but the observed susceptibility is an order of magnitude too low to produce the magnetic anomaly.

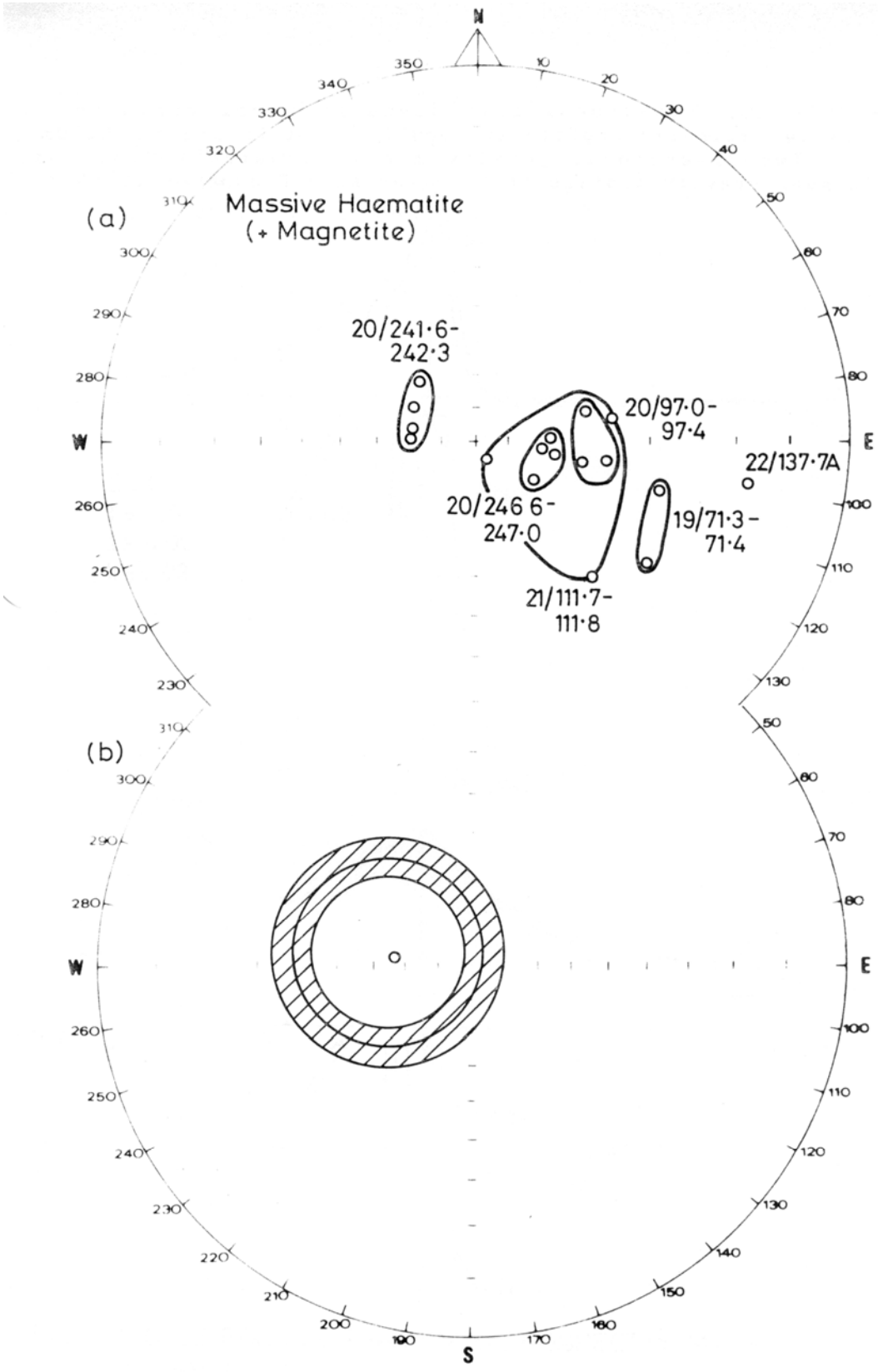

Fig.9.23. (a) Cleaned remanence directions of azimuthally unoriented drill core samples from Peculiar Knob, showing a consistently steep inclination. (b) Annular region of possible remanence directions for the Peculiar Knob massive hematite body.

9.3 A case study of self-demagnetisation in a magnetite-rich IOCG deposit

Fig.9.24. Osborne measured TMI from the 1994 ground survey

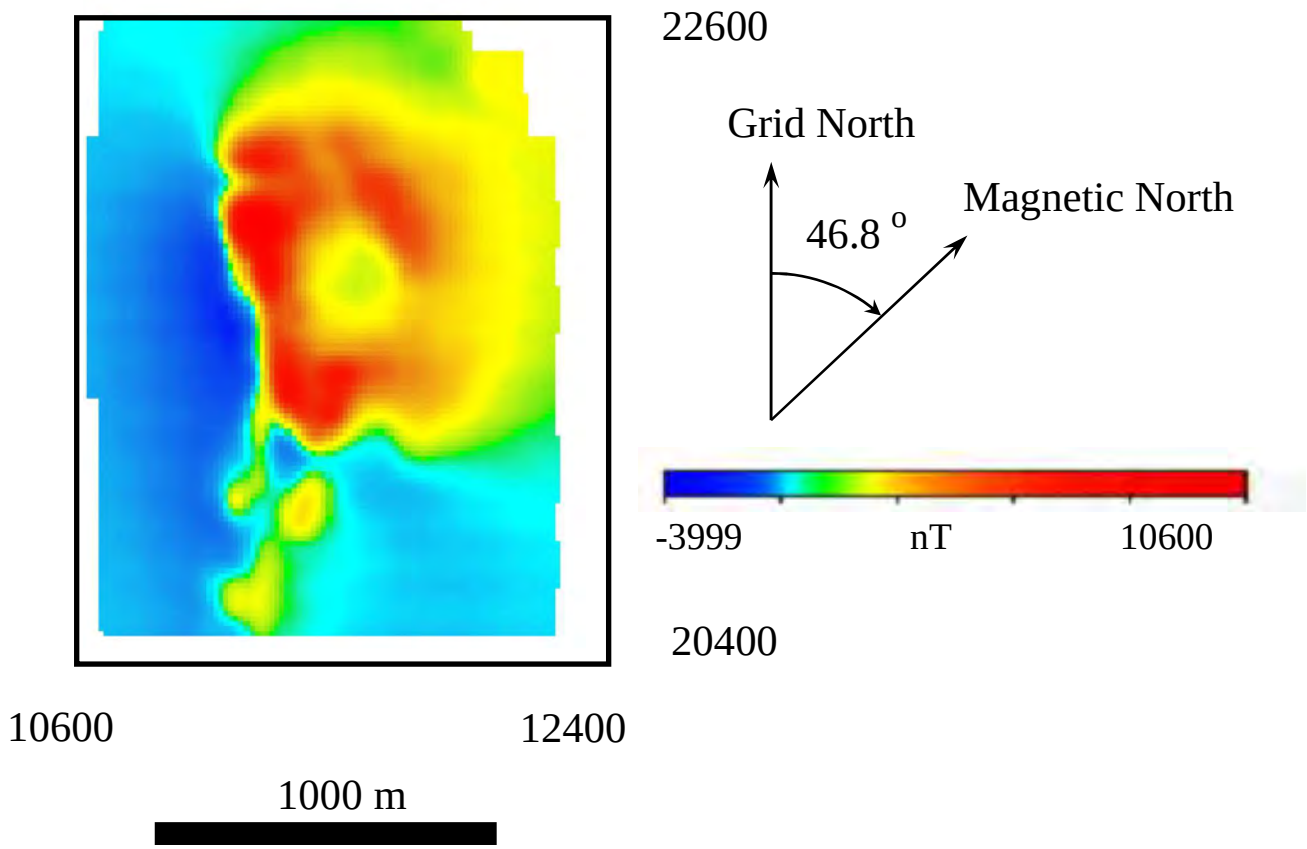

Survey specifications
Operators: Placer Dome Exploration.
Line spacing: 35m. Direction: grid east-west. Station spacing: 5m.
Magnetometers : Geometrics G856. Diurnally corrected.

Reference: Keiran Logan and Robert Angus,
"An iterative method to calculate self-demagnetisation for 3D magnetic bodies, with application to the Osborne copper gold deposit",
ASEG Conference, Sydney, February 1997.

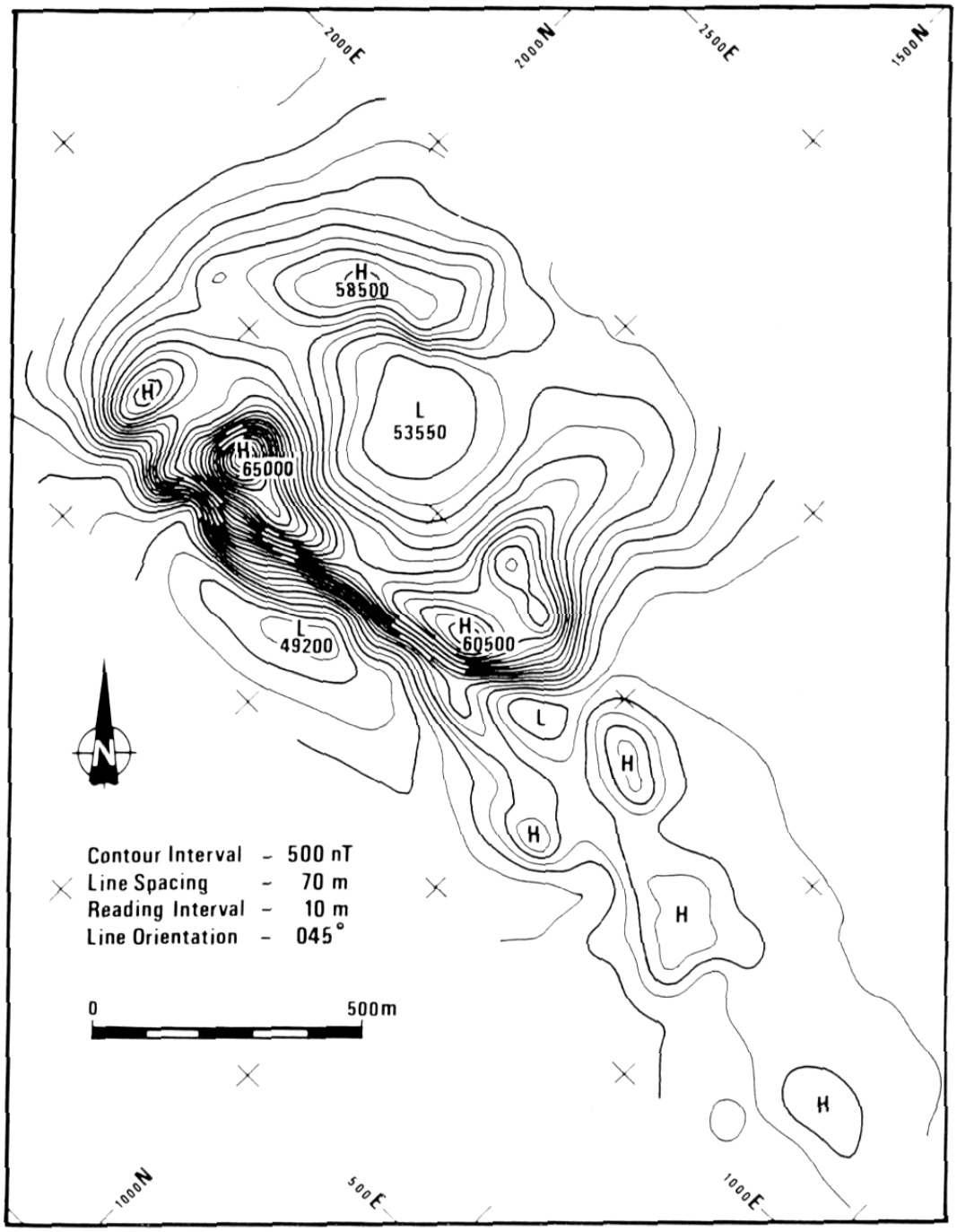

Fig.9.25. Ground magnetic contours for the Trough Tank Prospect (now the Osborne Mine) (Gidley, 1988)

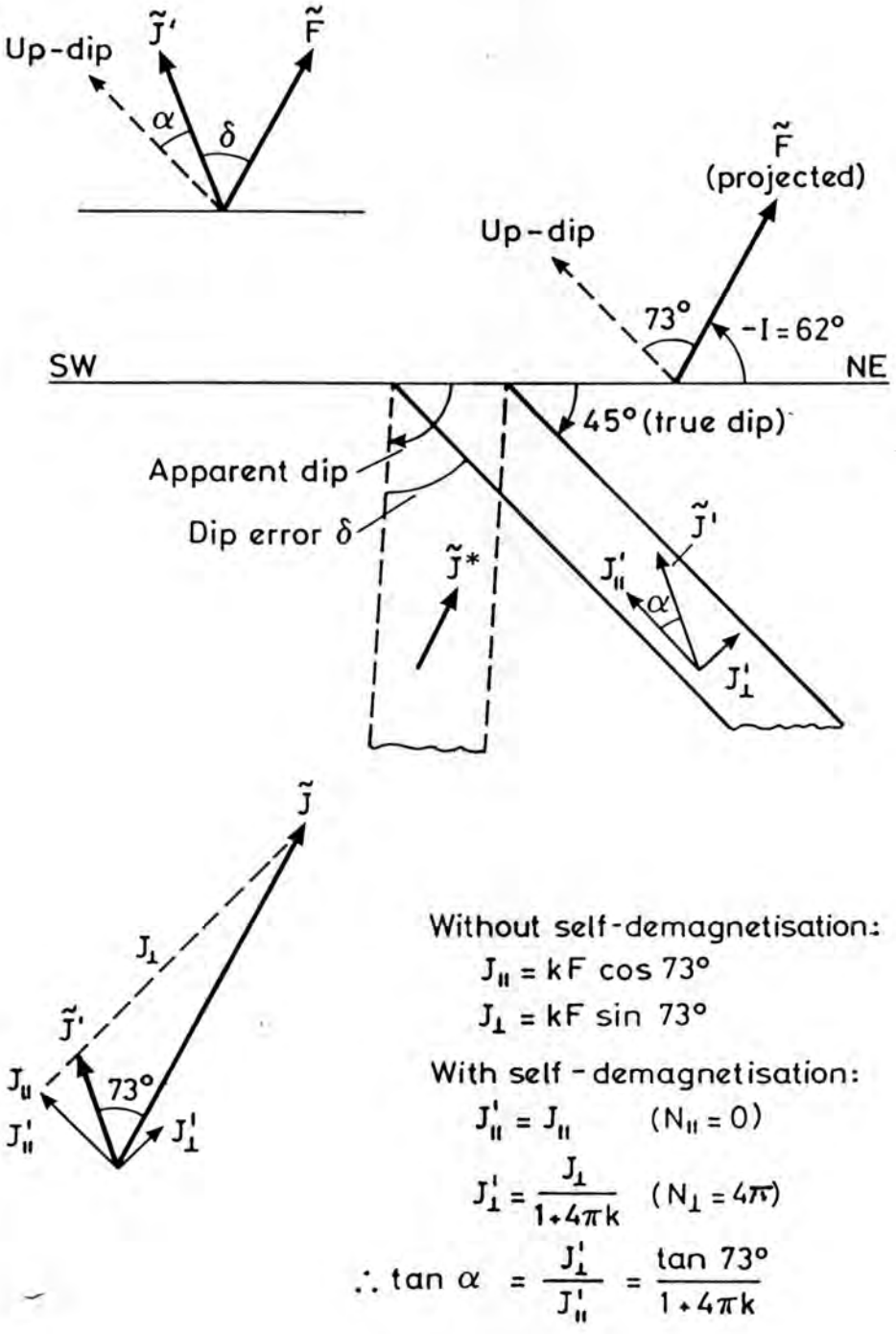

Fig.9.26. Deflection of induced magnetisation for an idealised Trough Tank ironstone unit, representing the ironstones intersected by TTNQ3, which produces an erroneous apparent dip. When self-demagnetisation is taken into account, the correct dip is obtained. Reference: D.A. Clark. Self-demagnetisation in practice: the Osborne Cu-Au deposit. Preview, April 2000, 31-36.

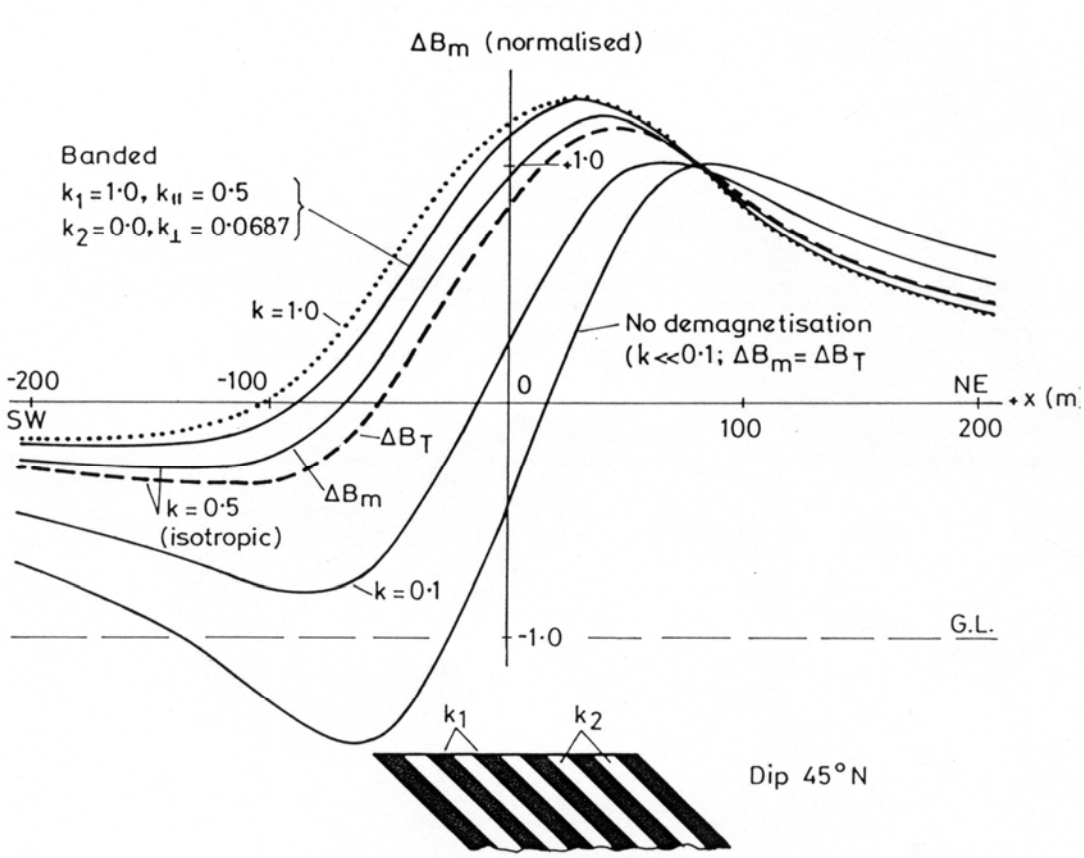

Fig.9.27. Effects of self-demagnetisation and mesoscopic anisotropy on anomaly shape for a dipping sheet with the approximate geometry of the Osborne ironstones. Susceptibilities are in G/Oe (CGS). SI susceptibilities are larger by a factor of 4π. In order to illustate effects on anomaly shape, all anomalies are normalised to unity at the point where the anomaly for the low susceptibility case is a maximum.

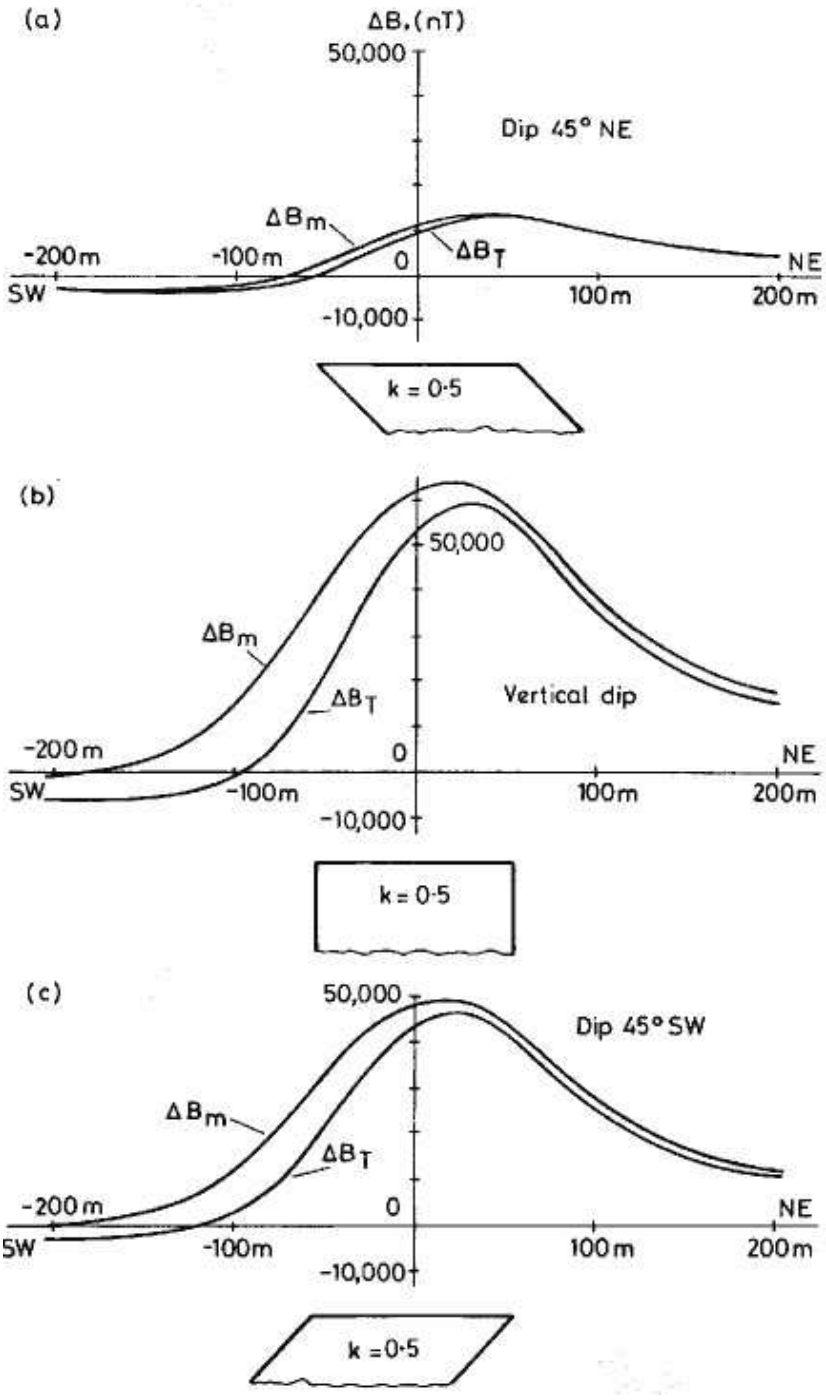

Fig.9.28. Dip dependence of ΔB_m and ΔB_T anomalies as a function of dip for analogues of the Osborne ironstones. (a) approximates the geometry at Osborne. Note that much larger anomalies, and a much larger discrepancy between the two anomaly types, would be observed for vertical or moderately SW-dipping ironstones, as shown in (b) and (c) respectively.

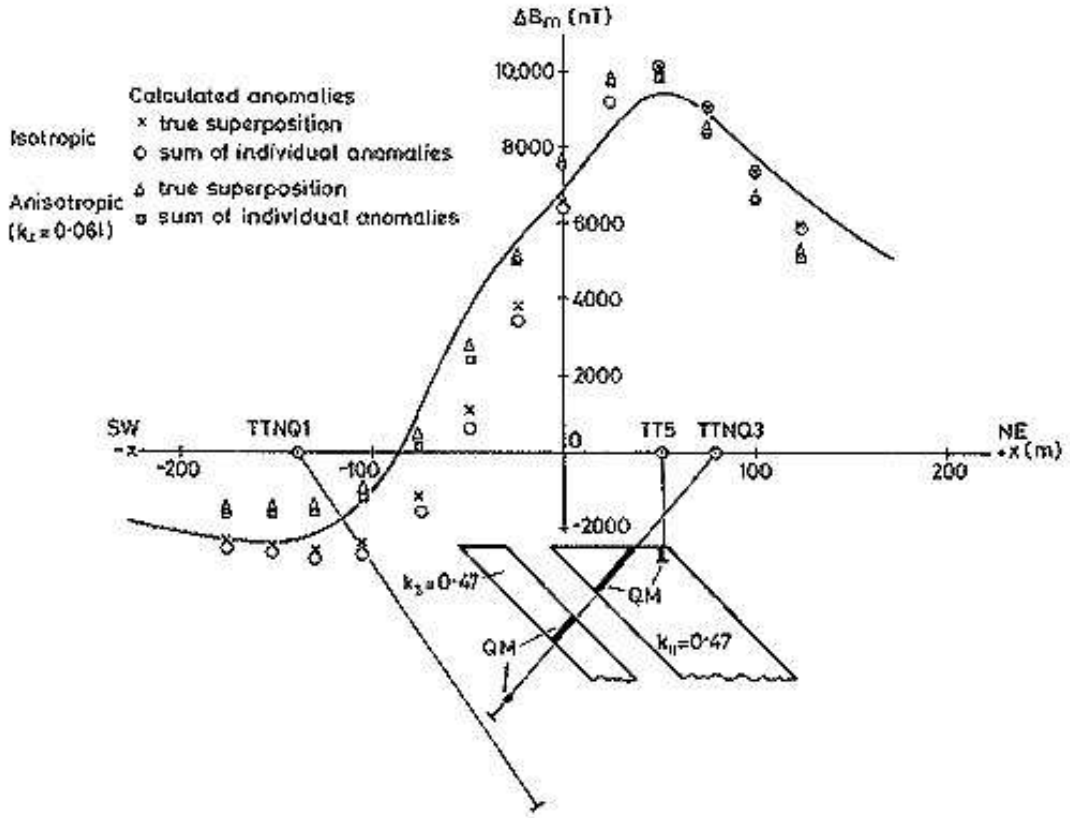

Fig.9.29. Observed (solid line) and calculated ground magnetic anomalies along line 1770N (Keel grid), showing a twin dipping sheet model, constrained by drill intersections. Note that the first diamond drill hole (TTNQ1) was sited to intersect an interpreted SW dipping target and failed to intersect ironstone. TTNQ3 was the first hole based on incorporation of self-demagnetisation into modelling, which indicated a NE dip.

9.4 Other Cu-Au deposits of the Cloncurry Belt

Figure 9.30 shows magnetic and airborne gravity signatures over the Proterozoic (c.1510 Ma) Ernest Henry IOCG deposit of the eastern Mount Isa Inlier, formed in an extensional rift basin or backarc extensional basin. The Cu-Au orebody is hosted by a hydrothermal breccia developed within K feldspar-altered plagioclase-phyric intermediate metavolcanic rocks. A magmatic contribution to mixed-source mineralising fluids comes from A-type, fractionated, oxidised granitoids of the Williams-Naraku Batholith. The alteration sequence is early regional sodic-calcic metasomatism, overprinted by early mineralisation-related potassic (biotite-magnetite and garnet-Kfsp-biotite) alteration, Kfsp-hematite veining and alteration, magnetite-calcite-pyrite-biotite-Kfsp-qtz-chalcopyrite Cu-Au mineralisation, and post-mineralisation calcite-dolomite-(quartz) alteration.

The ground magnetic anomaly associated with the deposit is a high of amplitude 10,000 nT. Other geophysical signatures include a 2.5 mgal ground gravity high; 50 Eo airborne Gzz anomaly; weak, localised surface TEM anomaly; downhole TEM response from supergene ore and pockets of hypogene ore; and IP response from the supergene zone (Webb and Rowston, 1995; Smith, 2002).

The regional TMI image shows that the deposit occurs in a very magnetically active environment, reflecting a generally oxidised package of rocks with extensive magnetite-rich sodic-calcic alteration systems. The potential field signature can be classified as juxtaposed magnetic and gravity anomalies, with the gravity anomaly focussed over the semi-massive to massive magnetite bodies that host the mineralisation. The magnetic anomaly is well developed over the orebody, but extends well beyond the main mineralised zone, reflecting the whole alteration system. This pattern is probably typical of deeper-formed magnetite-rich IOCG systems.

The Eloise deposit also occurs in the eastern Mount Isa Inlier, within a more reduced package of rocks. It is a Proterozoic (~1530 Ma) iron sulphide Cu-Au (ISCG) deposit hosted by Mesoproterozoic amphibolites and metasediments with regional sodic alteration. High grade pyrrhotite-chalcopyrite replacement lodes with chlorite-muscovite and minor pyrite, magnetite and calcite are localised by earlier formed quartz-biotite-hornblende ± albite alteration zones in meta-arkose and schist. Magnetite is concentrated in altered amphibolite 500 m to south of orebody.

Fig.9.31 shows magnetic contours for the Eloise area. The most prominent magnetic feature is an 1100 nT high over the magnetite-altered amphibolite. A magnetic ridge of amplitude ~500 nT is associated with the pyrrhotite-bearing Eloise mineralisation. Other geophysical responses include a surface TEM response to the conductive mineralised zone, a strong downhole TEM response, and a 1 mgal high from hb-bio-altered amphibolite + mineralisation (Brescianini, 1992). Again the magnetic zone is much larger than the mineralised zone. The gravity anomaly, whilst not large, is more focussed on the mineralisation.

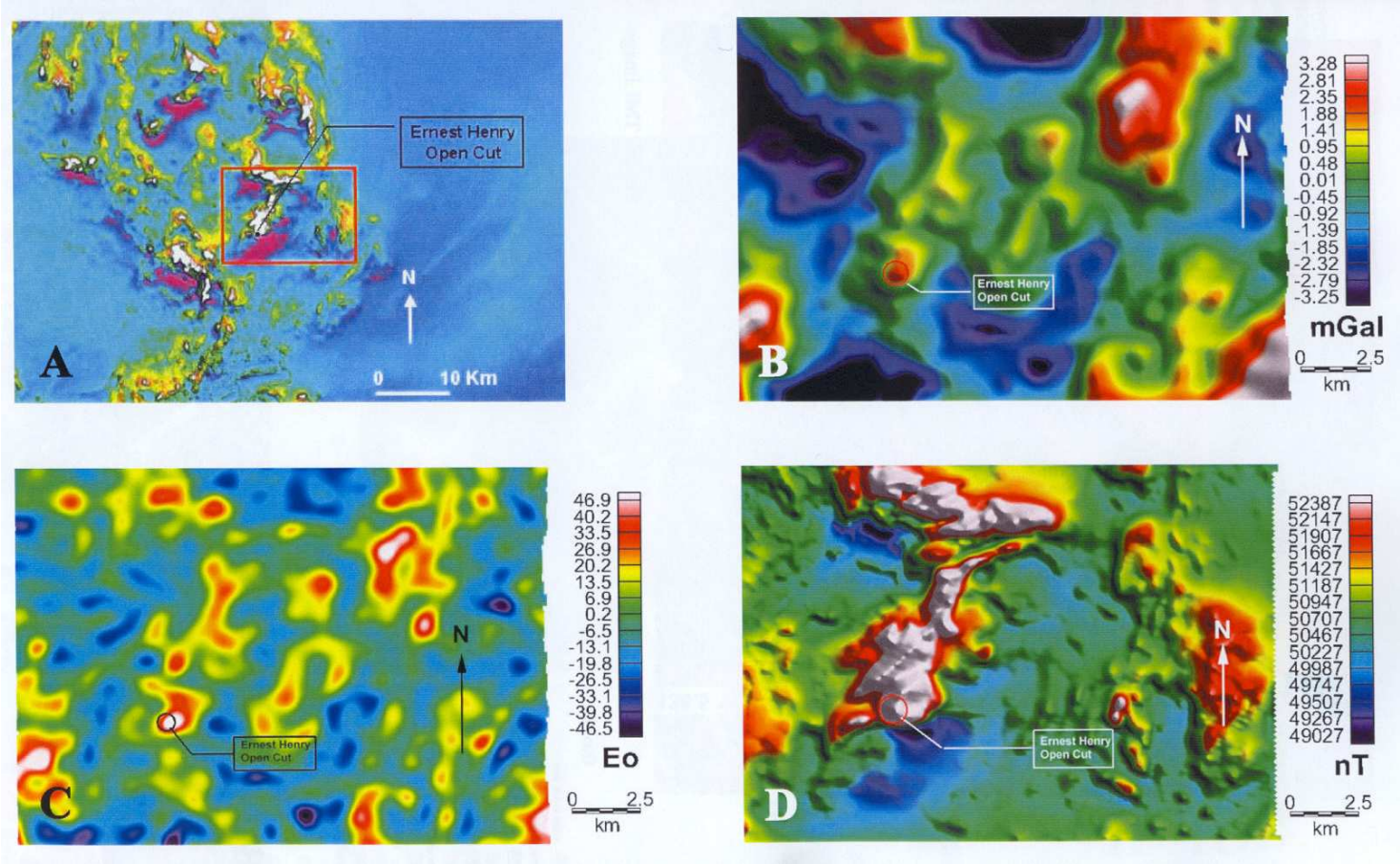

Fig.9.30. Magnetic and gravity signatures of the Ernest Henry deposit (Smith, 2002). A. Shaded TMI image of Ernest Henry District. B. Shaded G_z image over Ernest Henry. C. Shaded G_{zz} image over Ernest Henry. D. Detailed TMI over Ernest Henry (data and images produced by BHP-Billiton).

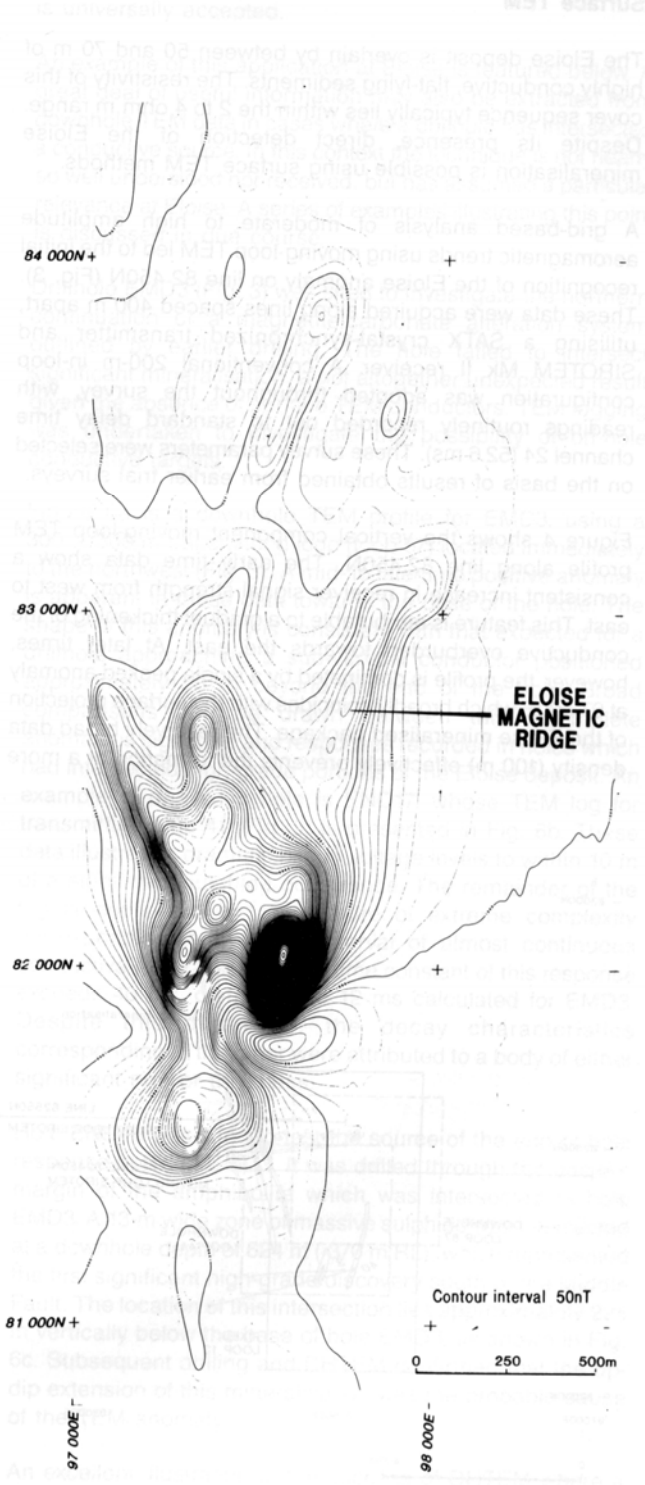

Fig.9.31. Ground magnetic contours for the Eloise area (Brescianini, 1992)

10. MAGNETIC SIGNATURES OF PORPHYRY, EPITHERMAL AND IRON OXIDE COPPER-GOLD MINERALISATION - REVIEW AND SYNTHESIS

10.1 Categories of Magnetic Response over Porphyry Systems

Jerome (1966) and Brant (1966) summarised magnetic patterns that could be expected over porphyry copper deposits. The earliest systematic attempt to classify the magnetic signatures of porphyry copper deposits in the open literature appears to be the synthesis of Gay and Mardirosian (1970), which summarised geological information and aeromagnetic anomalies for 34 porphyry copper and porphyry molybdenum deposits, mainly in the American southwest. The available aeromagnetic data were of poor quality by today's standards. Modern surveys provide much more detailed information on lithology, alteration and structure. Nevertheless, the magnetic surveys clearly reflected some broad geological features and provided some useful information in most of the case studies. They recognised four general classes of response:

- Intrusion Highs (35-50%)
- Alteration Lows (40-65%)
- Skarn Highs (~15%)
- Magnetic Lineaments that define structural controls (~ 15 %).

All but three of the 34 deposits analysed by Gay and Mardirosian had aeromagnetic signatures that reflected one or more of these features. Because some deposits showed more than one feature, the percentages given above give a total greater than 100%. It will be shown below that this classification, although undoubtedly a worthwhile first-pass analysis, is biased by the relatively restricted geological settings and limited geographical extent of the database. The magnetic interpretations were also compromised by the low resolution of the aeromagnetic data from the 1950s and 1960s and by the long history of mining at many of the deposits. Much better magnetic data are now available from many deposits, representing a range of geological settings, geographic areas and deposit types.

Intrusion highs arise from intrusions that are regarded as related to the mineralisation, directly or indirectly, and are more magnetic than the surrounding rocks. On the strictest interpretation of the genetic association, about one third of the deposits fell into this category; up to approximately one half, if intrusions of much greater extent than the mineralisation and less directly linked to mineralisation episode are included.

Alteration lows were the most prevalent responses in the sample examined by Gay and Mardirosian (41% interpreted as definite cases, up to 65% if "probable" alteration lows were included). The signatures represent magnetite-destructive alteration, associated with porphyry emplacement and subsequent hydrothermal activity, within magnetite-bearing host rocks. The presence of alteration lows is therefore contingent on the existence of magnetic country rocks. Where the porphyries intruded sediments or other weakly magnetic rocks, no alteration low is developed.

Approximately one sixth of the deposits lay on or adjacent to clearly defined long magnetic lineaments. These linear zones may represent structures that controlled emplacement of the porphyries and influenced development of the deposits. The lineaments were interpreted from contour maps and the low resolution of the data

probably prevented recognition of a number of other cases in this category. Modern data are much better suited to recognising structural controls on mineralisation, especially given the advances in image processing of high resolution data sets.

Skarn highs characterised four or five of the deposits, out of 34. Development of skarns requires the presence of carbonate host rocks, and therefore skarn high magnetic signatures are restricted to areas where such rocks are exposed or occur near the surface.

Since the 1970s, in the light of many new discoveries and improved quality of magnetic data, it has become apparent that the above classification requires considerable augmentation and refinement. The importance of magnetite-producing alteration in many deposits has been increasingly recognised. Detailed zoning of magnetite-generating, magnetite-stable and magnetite-destructive alteration; overprinting of pre-existing systems by later intrusions and their associated alteration; delineation of fine-scale structure; multiple intrusive phases and zoned intrusions are often evident in low level surveys with closely spaced flight lines. A substantial increase in geological, geochemical and geophysical information on deposits from many different areas and geological environments, plus improved understanding of magmatic and hydrothermal evolution of porphyry deposits, regional tectonic settings and magnetic petrology have laid the foundation for more geologically-based interpretation of magnetic surveys and other geophysical data over porphyry systems and improved targetting of potential mineralisation. It is now possible, at least in principle, to develop predictive geophysical models of mineralised porphyry systems that take into account a range of geological influences, including structural setting, nature of host rocks, degree of metamorphism etc.

10.2 Examples of Alteration ± Intrusion Highs

Sillitoe (1979) noted the common association between magnetite and biotite ± K-feldpsar in potassic alteration zones of gold-rich porphyry copper deposits. In these deposits the main mineralisation occurs in the potassic zone of an oxidised magnetite-bearing intermediate to felsic porphyry intrusion. According to Sillitoe's model of an idealised Au-rich porphry Cu deposit, abundant magnetite occurs in a central potassic zone near the top of the intrusion. This zone is surrounded by an extensive propylitic zone, which is magnetite-destructive where intense propylitisation is accompanied by abundant pyrite. A magnetite-destructive phyllic zone may be present between the potassic and propylitic zones. When emplaced into magnetic host rocks, e.g. volcanics that are comagmatic with the intrusion, the expected RTP magnetic signature of an exposed or shallowly buried Au-rich porphyry Cu deposit is a prominent, relatively narrow high, possibly characterised by internal complexity, centred on the mineralised zone, which is surrounded by a broader, relatively smooth low, corresponding to the phyllic and propylitic zones. This low is surrounded in turn by the typically "busy" signature of magnetic volcanics, with short wavelength fluctuations above and below regional base level (see Fig.10.1)

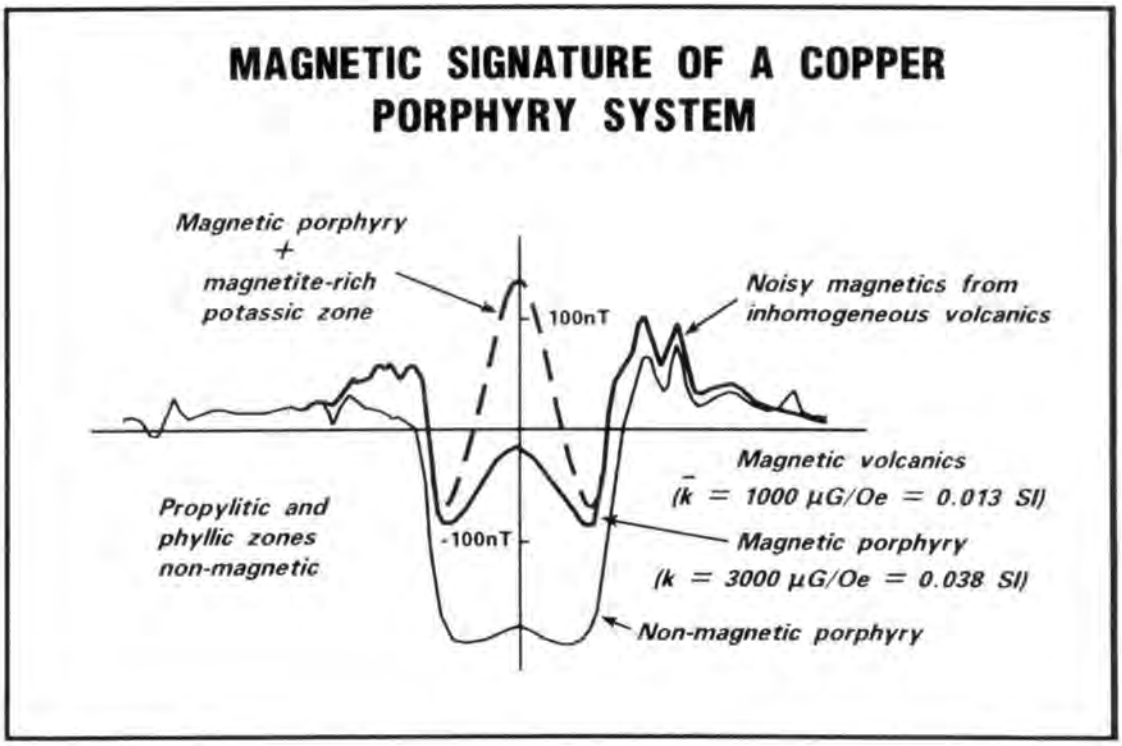

Idealised magnetic anomaly associated with a porphyry copper system, showing the noisy background associated with magnetic volcanics, the 'alteration low' associated with the propylitic and phyllic alteration zones, the high arising from the magnetic porphyry plus, in the case of gold-rich copper mineralisation, the magnetite-bearing potassic alteration zone.

Fig.10.1. Predicted RTP magnetic signature of an idealised gold-rich porphyry copper system (Clark *et al*., 1992b).

Sillitoe (1997) discusses the 11 largest gold-rich porphyry copper deposits of the circum-Pacific region and concludes that only two (Bingham and Ok Tedi) do not have appreciable magnetite associated with potassic alteration. At Bingham, the mineralisation is associated with pyrite-rich potassic (quartz-orthoclase-phlogopite) alteration, which is surrounded by a magnetite-stable actinolite-chlorite-(epidote) propylitic zone within a magnetite-bearing augite-actinolite-biotite monzonite stock (Lanier *et al*., 1978). The unaltered intrusive rocks contain about 2 vol.% magnetite, which is pyritised within the mineralised potassic zone. Gay and Mardirosian (1970) note that a broad +400 nT magnetic anomaly is centred on the genetically related, unaltered Last Chance Stock, which is adjacent to the Bingham deposit. The source of the anomaly is broader than the exposed magnetic intrusion and appears to extend beneath the mineralised zone, suggesting that the anomaly is associated with the "mother intrusion" representing the magma chamber from which the Last Chance and Bingham stocks were derived. In the low resolution survey available to those authors, there is, unsurprisingly, no indication of a magnetisation contrast between the mineralised Bingham stock and its sedimentary country rocks.

The Grasberg Cu-Au deposit (MacDonald and Arnold, 1994, 1996; McDowell et al., 1996; Potter, 1996) provides an excellent example of a mineralised central, magnetite-rich potassic zone, in the upper portions of a magnetite-bearing stock, that is associated with a bulls-eye magnetic high (see Figs.10.2-10.4). The magnetite content of the unaltered Main Grasberg intrusions is ~1-2 wt % (≈ 0.5-1 vol. %) and the potassic alteration is associated with 7-10 wt % (≈ 4-6 vol.%) magnetite. The corresponding susceptibilities are ~2000 μG/Oe (0.03 SI) for the unaltered intrusives and ~14,000 μG/Oe (0.17 SI) for the mineralised potassic zone. The amplitude of the magnetic anomaly at Grasberg is ~2125 nT (Potter, 1996).

The deposits in the Ordovician volcanics of NSW (Goonumbla, Cadia, Copper Hill) that were studied in P425/426 are all associated with intrusion highs. However, the magnetic signature differs in the case of Goonumbla, as the intrusions were emplaced into comagmatic volcanics with similar properties, whereas the Cadia intrusions were emplaced into much less magnetic rocks. At Copper Hill the strongly magnetic unmineralised mafic intrusion that is comagmatic with the relatively felsic mineralising intrusive phases is associated with a magnetic high, but the adjoining mineralised intrusions are less magnetic than host surrounding volcanics and are therefore characterised by a magnetic low.

The Tuckers Igneous Complex does not have a large magnetisation contrast with its surrounding tonalitic rocks, but does have a well developed alteration high associated with the pyroxene and biotite hornfels zones rimming it. The narrow high associated with the hornfels is surrounded by a magnetic low within the unaltered tonalite due to purely thermal resetting of remanent magnetisation in a reversed geomagnetic field.

Mount Milligan also exhibits an intrusion plus alteration high in the western portion of the complex (Paterson and Hallof, 1993). However the response of the MBX East deposit is different, reflecting a different alteration regime (see below).

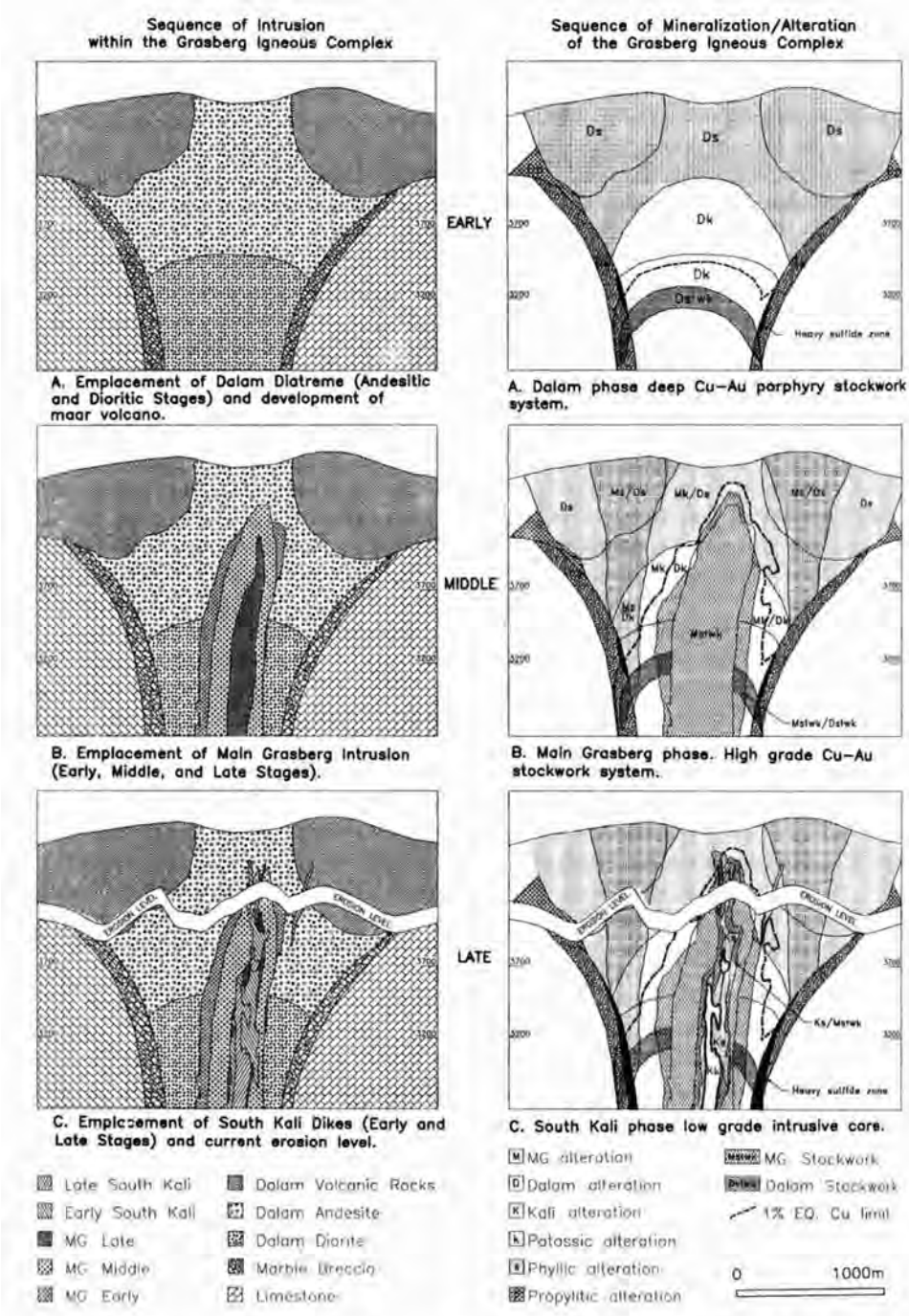

Geologic history of the Grasberg Igneous Complex (e.g., Ks/Mstwk = Kali phase phyllic alteration overprinting MG stockwork).

Fig.10.2. Geologic history of the Grasberg Igneous Complex (MacDonald and Arnold, 1994).

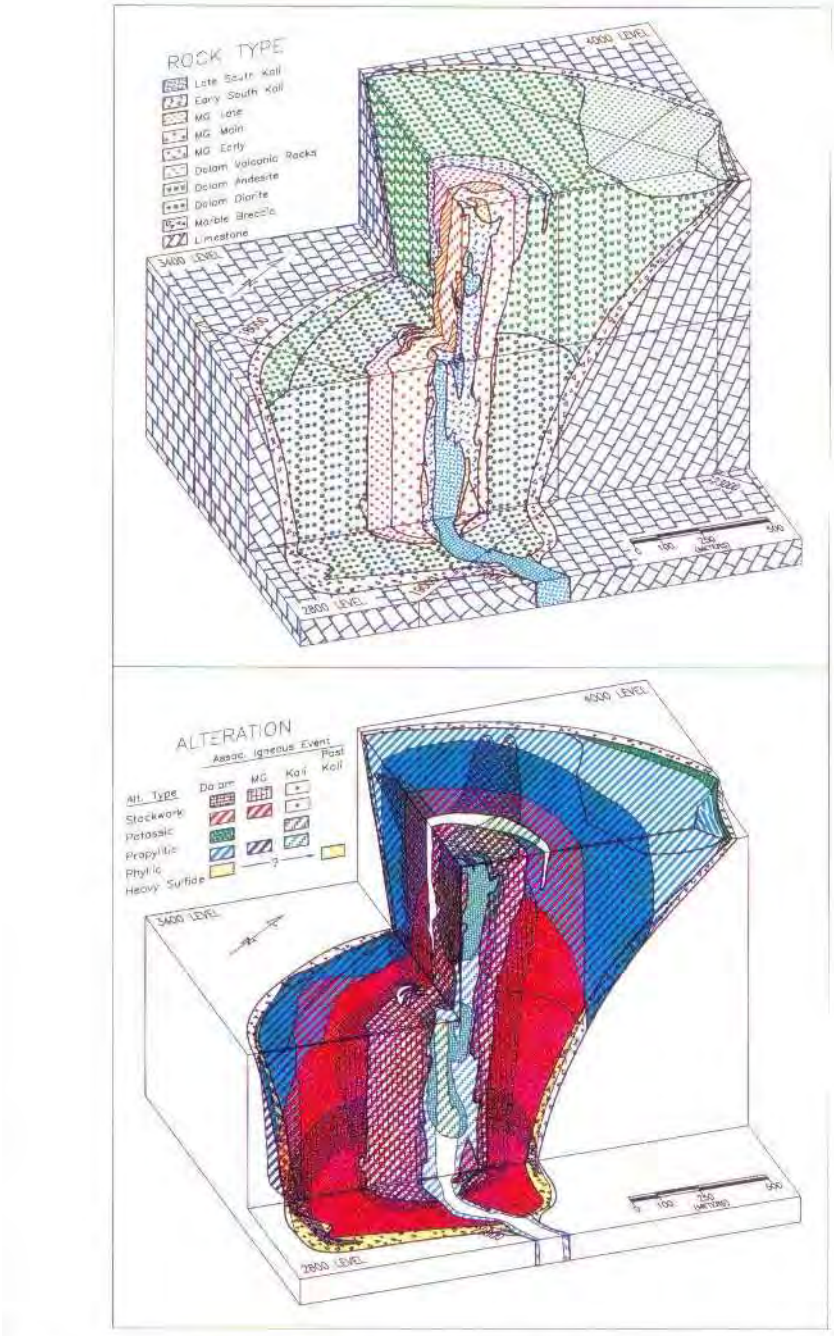

Block diagram showing the Grasberg Igneous Complex and zoned alteration. Weak stockwork and potassic alteration associated with South Kali Dikes are not shown.

Fig.10.3. Block diagram showing the Grasberg Igneous Complex and zoned alteration (MacDonald and Arnold, 1994).

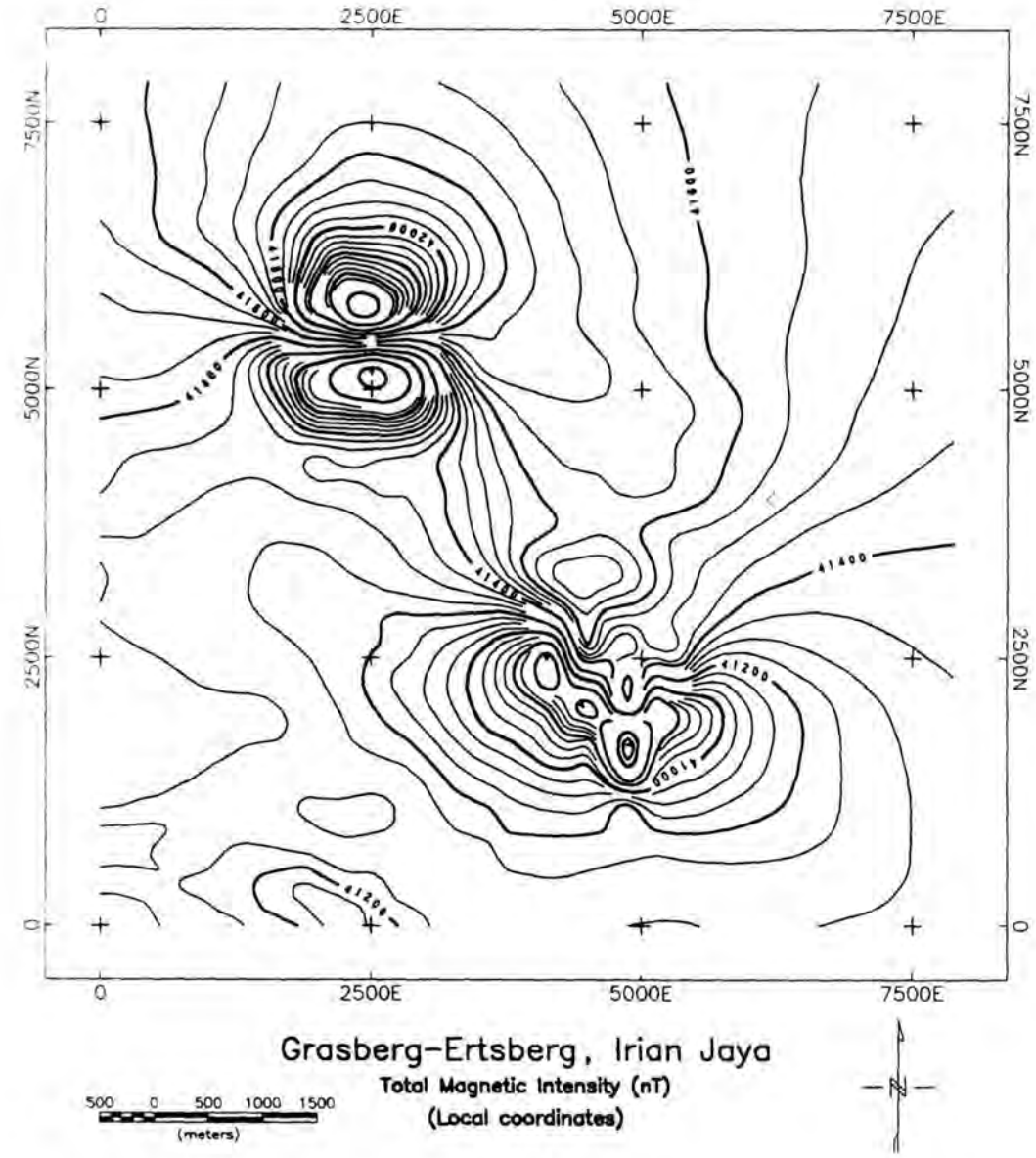

Fig.10.4. TMI anomalies (50 nT contours) associated with the Grasberg Igneous Complex and Ertsberg skarns (Potter, 1996).

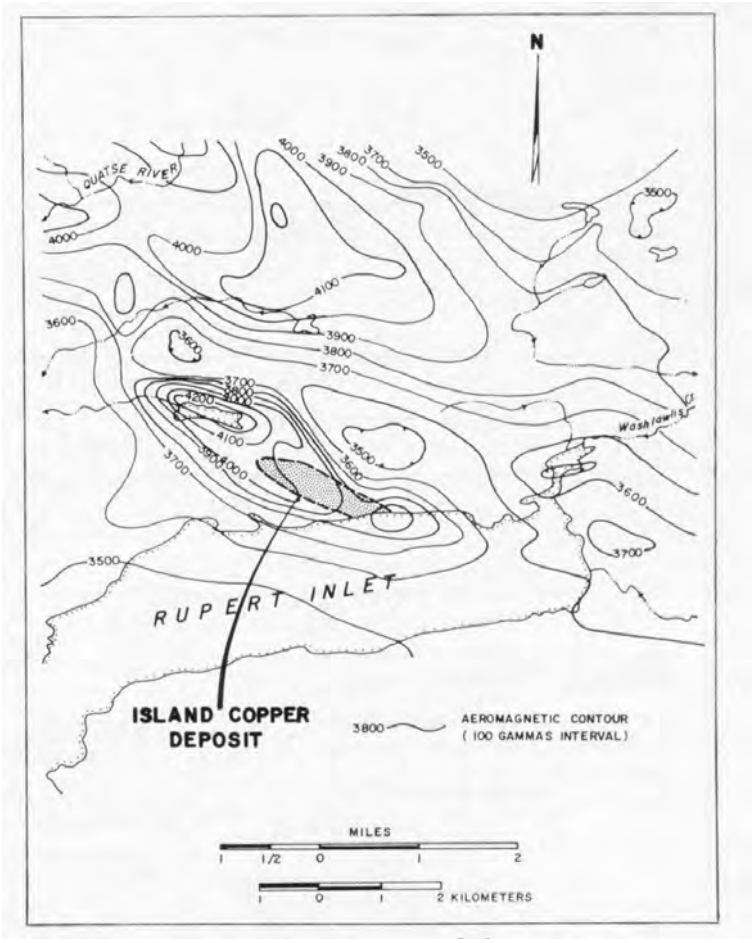

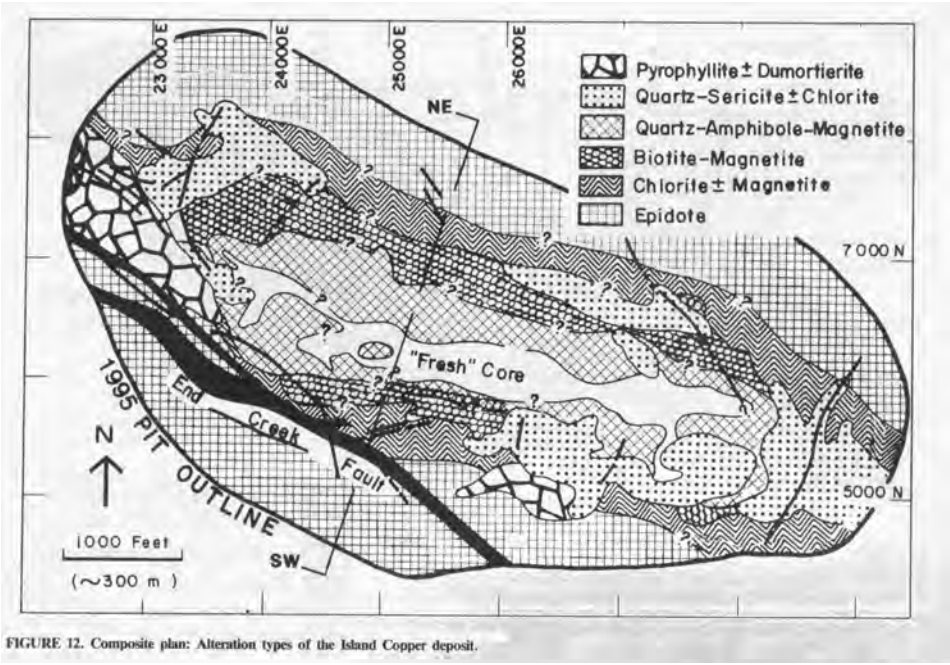

FIGURE 12. Composite plan: Alteration types of the Island Copper deposit.

Fig.10.5. (Top) Aeromagnetic anomaly associated with the Island Copper deposit (Cargill et al., 1976). (Bottom) Distribution of the magnetite-amphibole-plagioclase, potassic, and propylitic alteration zones in the upper part of the Island Copper deposit. All later alteration facies have been omitted (Arancibia and Clark, 1995).

Island Copper exhibits an extensive 700 nT magnetic high due to magnetite-rich alteration of the Bonanza Volcanics (Fig.10.5). The magnetisation contrast between the intrusion and the unaltered volcanics would produce a much more subdued anomaly, in the absence of the alteration.

10.3 Examples of Alteration Lows

Examples of alteration lows are common for epithermal deposits and also for many porphyry systems: Cripple Creek (Kleinkopf *et al*., 1970), Copper Canyon (Paterson and Hallof, 1993; see Fig.10.6), Conway-Bimurra (Lackie *et al*., 1992), Rotorua (Reed, 1987), the Boulder Batholith (Hanna, 1969)). Some examples with documented properties include:

Mount Milligan (MBX East deposit)

At Mount Milligan (British Columbia) potassic (K-feldspar + biotite + magnetite) alteration is accompanied by chalcopyrite-bornite mineralisation with Au. At the MBX West deposit, the mineralised zone has enhanced susceptibility and moderate chargeability. Codeposition of Au and Cu, transported as chloride complexes, due to cooling of the high temperature (> 350°C) fluid accounts for the relatively constant Cu/Au ratio of ~15,000 (Oldenburg *et al.*, 1997). The reactions involved are:

$$CuCl_2^- + Fe^{2+} + 2H_2S \rightarrow CuFeS_2 + 2Cl^- + H^+ + e^-,$$

$$AuCl_2^- + e^- \rightarrow Au° + 2Cl^-.$$

However, at the MBX East deposit, Oldenburg *et al.* (1997) showed that the Au mineralisation, which has a lower Cu/Au ratio than the MBX West deposit, is associated with a susceptibility low and chargeability high. This pattern is attributable to deposition of Au from a lower temperature fluid associated with propylitic alteration. At lower temperatures Au forms a strong bisulphide complex, unlike Cu. The postulated reaction for the deposition of gold consumes ferric iron in magnetite and sequesters it in epidote, and perhaps chlorite, which are characteristic propylitic minerals:

$$Au(HS)_2^- + Fe_3O_4 \rightarrow Au° + FeS_2 + Fe_2O_3 + H_2O + e^-.$$
(in epidote, chlorite)

Thus the magnetite is replaced by pyrite + epidote or chlorite. The magnetic signature associated with the MBX East depsoit is a local *alteration magnetic low*, adjacent to an *intrusion high*. Figure 10.7 shows a ground magnetic profile and resistivity and chargeability pseudosections for the MBX West and East deposits.

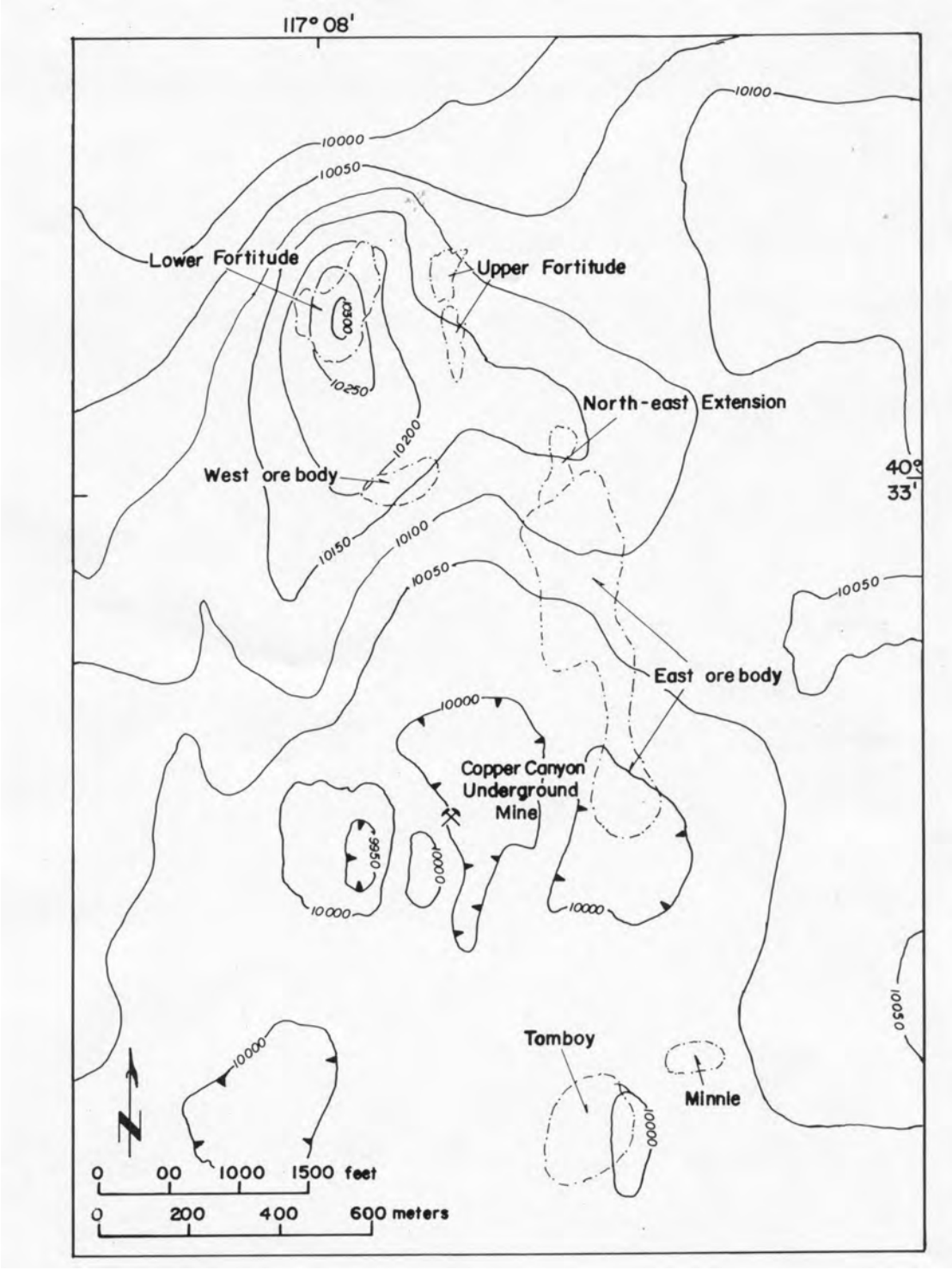

Fig.10.6. TMI anomalies over the Copper Canyon (alteration low) and Lower Fortitude (pyrrhotite-skarn high) deposits (Wotruba et al., 1988).

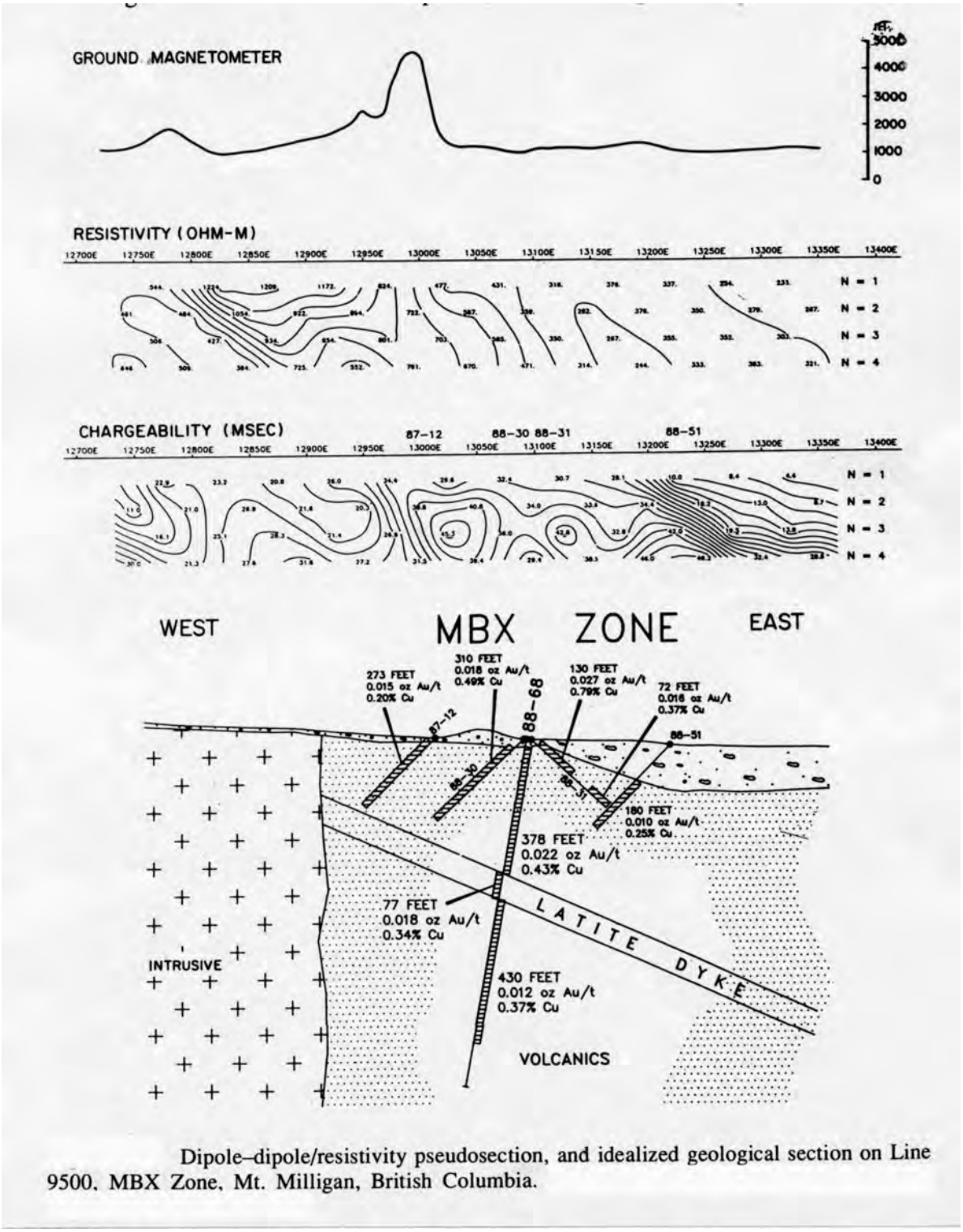

Dipole–dipole/resistivity pseudosection, and idealized geological section on Line 9500, MBX Zone, Mt. Milligan, British Columbia.

Figure 10.7. Ground magnetic profile and resistivity and chargeability pseudosections for the MBX West and East deposits (Paterson and Hallof, 1993).

Porgera

The magnetic signature of the Porgera deposit has been discussed by Schmidt *et al*. (1997; see Figs.10.7, 10.8). Unaltered intrusive stocks of the Porgera Intrusive Complex contain up to 2 vol % magnetite and produce local magnetic highs, superimposed on a broader high arising from the mother intrusion at depth. Widely developed weak-to-moderate propylitic alteration, which represents early, relatively high temperature alteration within the Porgera Intrusive Complex, appears to be magnetite-stable. The open pit Au deposit is associated with the intensely phyllically altered Waruwari intrusion, in which magnetite has been largely destroyed. The magnetic signature of the deposit is a very subdued magnetic high, reflecting a weak positive magnetisation contrast with the essentially non-magnetic shales that host the Porgera intrusions. If emplaced into volcanic rocks the Waruwari deposit would produce a classic alteration low. In its actual geological setting, however, the signature can be classified as a *relative alteration low* (compared to neighbouring, coeval and comagmatic, barren intrusions).

Conway-Bimurra (Irvine and Smith, 1990; Lackie *et al*., 1992b)

In the Conway-Bimurra, Queensland, area Late Devonian felsic volcanics, which are prospective for epithermal gold, are difficult to distinguish in the field from non-prospective Late Carboniferous felsic volcanics. The Carboniferous units are distinctly more magnetic and can therefore be mapped using aeromagnetics.

The oxide mineralogy is a function of primary rock composition and type and degree of alteration. Within each volcanic suite, susceptibility tends to decrease in the order andesite, dacite, rhyolite. The susceptibility of the Devonian volcanics is probably lower because of pervasive weak propylitic alteration, which has partially replaced titanomagnetite by carbonate and rutile, coupled with a greater proportion of rhyolitic rocks. Ubiquitous Carboniferous overprinting of remanence in these rocks suggests that the regional alteration is coeval with the eruption of the Carboniferous volcanics.

Within the Devonian volcanics adularia-sericite alteration centres, representing low sulphidation epithermal systems, show up as very smooth, flat magnetic zones, reflecting magnetite destruction. Titanomagnetite is replaced by sphene in the intense propylitic zone and by rutile in the sericitic zone. A specially designed “alteration filter”, based on a sawtooth stretch of high-pass filtered magnetics, emphasises these zones, giving them the appearance of “oil slicks” in grey scale images.

A busy magnetic pattern associated with the Carboniferous volcanics reflects variations in susceptibility, which mainly reflects magnetite content, and Q value, which is dependent on magnetite grain size. Major shifts in magnetic base level reflect varying Q values, with reversed remanence overwhelming induced magnetisation and producing magnetic lows when $Q > 1$.

Devonian volcanics can be distinguished palaeomagnetically from Carboniferous units by the retention of some primary Devonian remanence, which has a distinctly different direction from the characteristic Late Carboniferous magnetisation.

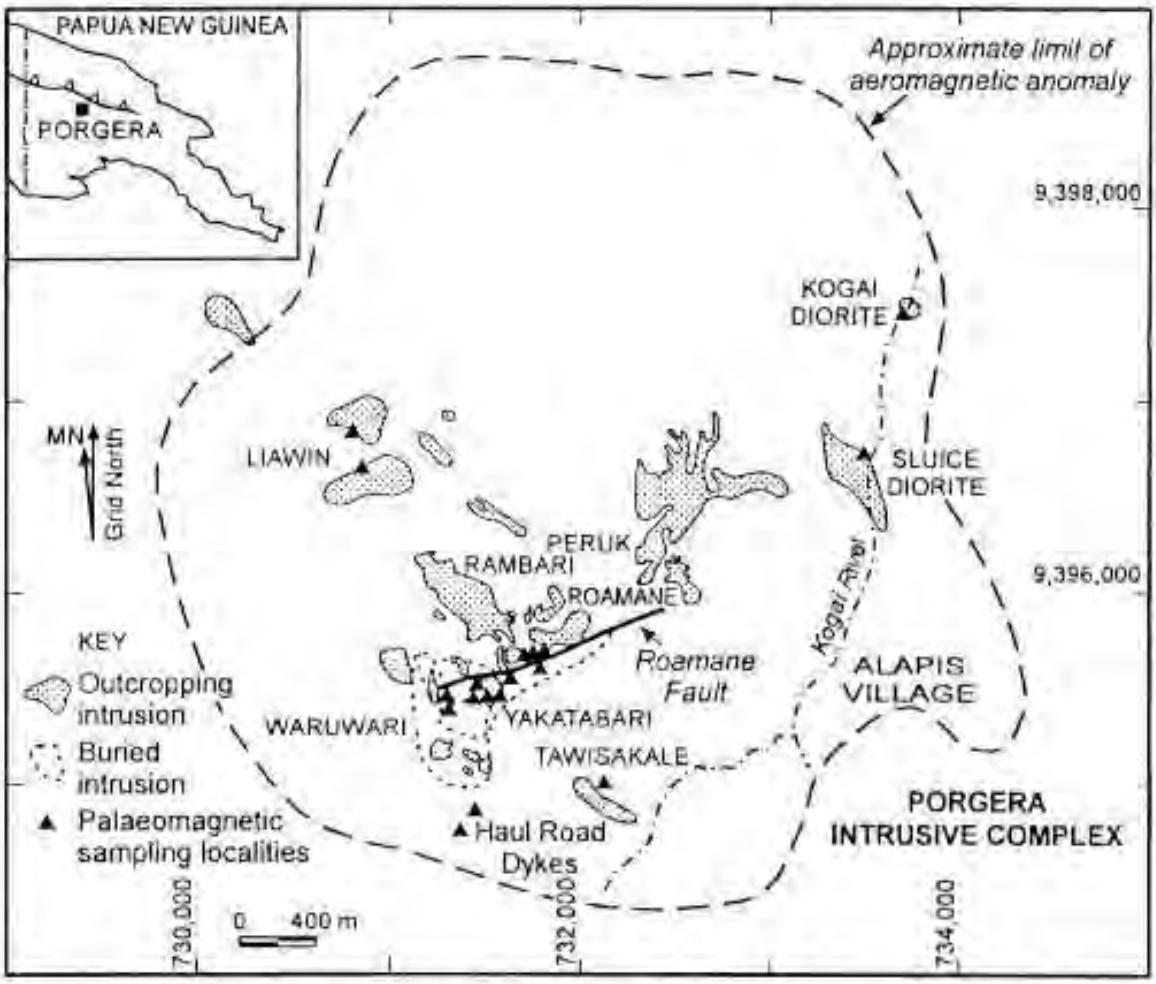

Locality and geological sketch map of the Porgera Intrusive Complex (AMG Zone 54).

Fig.10.8. Geology of the Porgera Intrusive Complex, showing the distribution of intrusive phases, including the phyllically altered Waruwari intrusion that hosts the open-pit gold deposit and location of the Roamane Fault that hosts the high-grade Zone VII epithermal-style mineralisation (Schmidt *et al*., 1997). The dashed line outlines the approximate extent of the broad magnetic high associated with the inferred mother intrusion at depth.

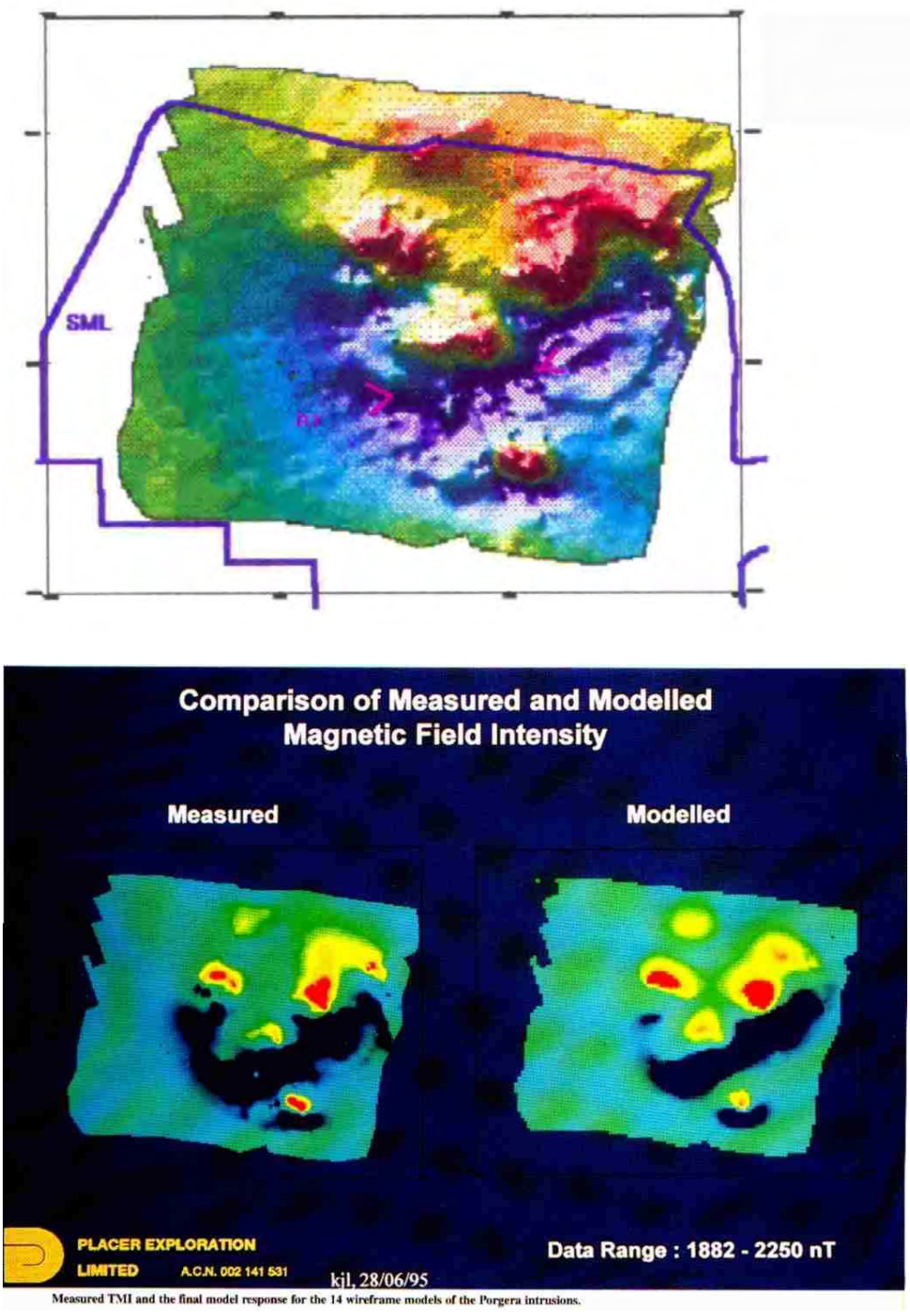

Fig.10.9. Top. TMI image for Porgera Intrusive Complex. Local magnetic highs correspond to unmineralised intrusive stocks. The response of the mineralised Waruwari intrusion is very subdued. The Roamane Fault, indicated by magneta arrows, is associated with a magnetic lineament. Bottom. Observed and calculated magnetic anomalies for the Porgera Igneous Complex. (Schmidt *et al*., 1997).

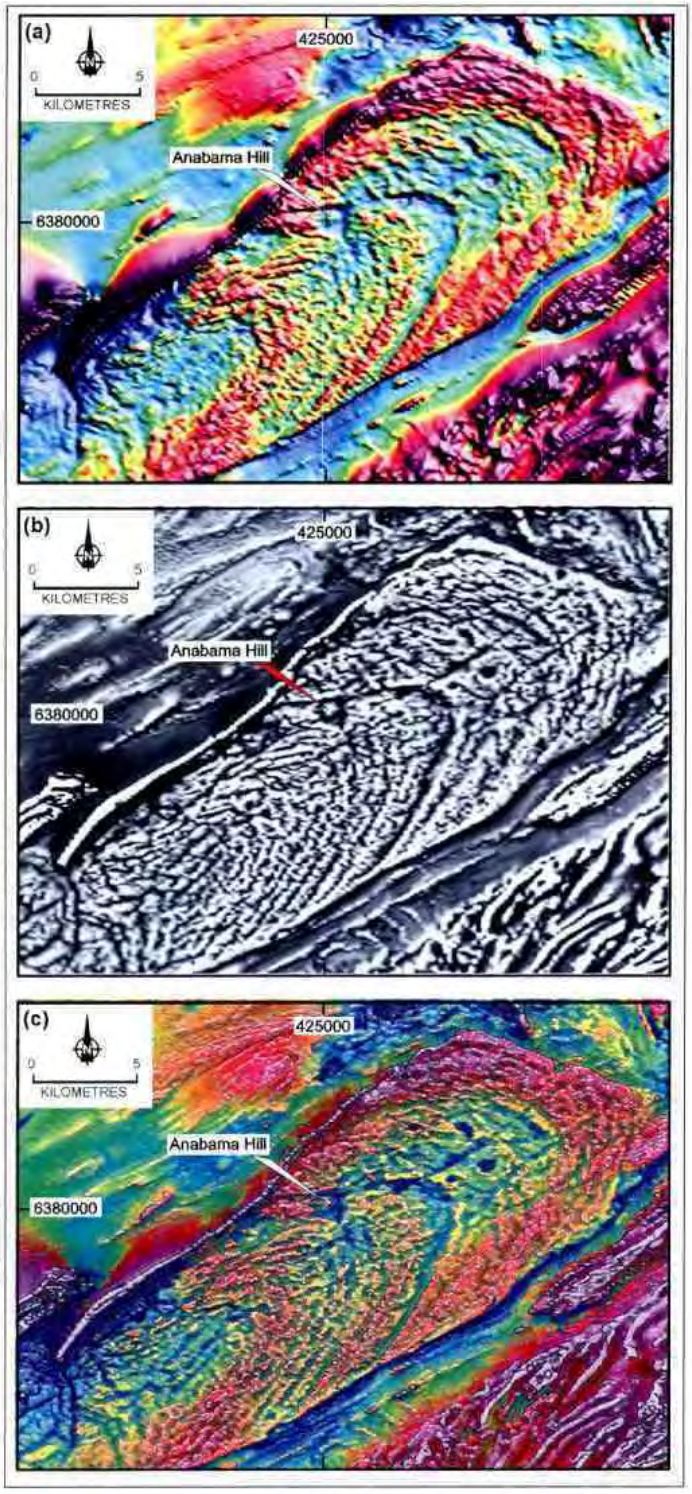

TEISA aeromagnetic data across the Anabama Granite. a) TMI, b) TMI with extended separation filter, c) TMI with terracing operator. Co-ordinates are AMG zone 54.

Fig.10.10. Anabama Hill porphyry Cu prospect – magnetics images (Dentith, 2003).

10.4 Examples of Skarn Highs

The Ertsberg (Irian Jaya) Cu-Au deposit (Mertig et al, 1994), is associated with prominent skarn highs, as well as intrusion high anomalies (see Fig.10.4). The amplitude of the combined anomalies is 1200-1500 nT. In the Lachlan Fold Belt, the Cadia Cu-Au deposit is adjacent to magnetite + hematite-rich skarn that produces a substantial magnetic high, as well as the high associated with the Cadia Monzonite Complex. In the SW USA examples of skarn highs include Santa Rita, Reward, Pima and Twin Buttes. Lower Fortitude is an example of a magnetic high associated with pyrrhotite-bearing skarn (Fig.10.6).

10.5 Examples of Structural Controls Associated with Magnetic Lineaments

Structural controls on intrusion and mineralisation are commonly apparent in suitably processed aeromagnetic data. At Porgera the high grade epithermal style Zone VII mineralisation is closely associated with a major deposit-scale structure, the Roamane Fault, which shows up clearly in magnetic images (Fig.10.9).

Regional structures that serve to locate the Mount Leyshon Intrusive Complex, mines in the Boori lineament zone (e.g. Rishton) within the Leyshon-Tuckers corridor, the Kidston Breccia Pipe (Clark and Dickson, 1997), the Endeavour Linear and other structures in the Goonumbla Volcanic Complex, are examples.

10.6 Examples of Zoned Alteration Signatures

At Santa Rita, New Mexico (Rose and Baltosser, 1966; Nielsen, 1968) a “doughnut” magnetic anomaly ringing mineralised zone (Gay and Mardisorian, 1970) arises from alteration magnetite in skarns and (?other host rocks) surrounding magnetite-destructive alteration in the deposit.

A better type example of zoned alteration in aluminosilicate rocks is afforded by several Goonumbla deposits (E48, E27, E26N) where magnetite-destructive overprinting in the core of an early magnetite halo produces doughnut anomalies.

Mount Milligan also exhibits zoned alteration signatures (Paterson and Hallof, 1993). Guilbert (1995) describes a spectacular “archery target” magnetic anomaly at Bajo de la Alumbrera, Argentina, reflecting a classic zoning pattern from an inner magnetite-rich potassic core, surrounded by a magnetite-destructive phyllic ring, through a magnetite-depleted propylitic zone, grading into unaltered magnetic country rocks. This pattern conforms to the idealised gold-rich porphyry copper signature of Fig.10.1.

10.7 Examples of Remanence-dominated Signatures

Relatively strong remanent magnetisation with high Koenigsberger ratios results from:

- fine-grained magnetite (< 20 µm),
- multidomain hematite, particularly with grain size *greater* than 100 µm, that carries a thermoremanence acquired during cooling from high temperatures (~650°C or higher).
- monoclinic pyrrhotite, over a wide range of grain sizes.

Mount Leyshon, the Tuckers Igneous Complex aureole and Red Dome (Collins, 1987) afford examples of remanence carried by fine-grained magnetite. The Peculiar Knob prospect, South Australia, is a hematite-rich body that is a possible contact metamorphosed analogue of hematite-rich IOCG deposits at Olympic Dam and Prominent Hill. This body exhibits a huge magnetic anomaly (~15,000 nT) that is predominantly due to intense thermoremanence carried by hematite-(magnetite-maghemite) grains (McEnroe et al., 2003). The mineralogy of the Olympic Dam deposit suggests that remanence may account for the "missing magnetisation" at Olympic Dam, which is currently attributed to an intrabasement source.

The pyrrhotite-bearing deep phyllic zone at Kidston carries a remanent magnetisation that, superimposed on an alteration low arising from the upper phyllic zone, accounts for the low amplitude annular magnetic high associated with the Kidston Breccia Pipe. Typical pyrite-rich porphyry systems metamorphosed to amphibolite grade may develop pyrrhotite at the expense of pyrite and could be expected to acquire relatively intense remanent magnetisation. At Kidston there is also a local magnetic low associated with reversely remanently magnetised potassically-altered wall rocks adjacent to the Macks Porphyry. This is analogous to Mount Leyshon, but on a much smaller scale.

10.8 Examples of Zoned Pluton Signatures

At a mining camp scale the Bingham Canyon (Utah) and Ajo, Mineral Park and Sierrita (Arizona) porphyry copper deposits exhibit pronounced zoning of intrusions, from relatively mafic margins to felsic cores centred on the mine districts (Guilbert and Lowell, 1974). Of the P425/426 study areas, the Lochaber and Bagstowe Granites, associated with the Kidston deposit, exhibit well-developed magnetic and radiometric zoning that are sensitive recorders of fractional crystallisation. In the Quesnel Belt, which hosts the Mount Milligan deposits, related plutons also show zoning (Paterson and Hallof, 1993). The Anabama Hill porphyry copper prospect, South Australia, is associated with a zoned pluton that is particularly well delineated in detailed aeromagnetic data (see Fig.10.10).

Zoning of intrusions at a variety of scales is evident at Mount Leyshon, Goonumbla and Cadia. However, primary zoning of small intrusions is often difficult to detect, because of masking effects of alteration and country rock lithology.

As a cautionary note, it is well to remember that fractional crystallisation is almost a *necessary* condition for development of economic mineralisation, but it is *not sufficient*. The Tuolumne intrusion exhibits a classic zoning pattern (see Fig.2.19), but is not associated with any mineralisation, because it crystallised at depth as a sealed system, with no opportunity for exsolution and escape of a mineralising fluid phase. Initial water contents also have a major influence on the capacity to develop porphyry type mineralisation and carbon dioxide content of the source magma also exerts a strong control on the depth at which a fluid phase develops.

10.9 Examples of Nested/Multiple Intrusion Pluton Signatures

In many cases the process of fractional crystallisation took place in magma chambers beneath intrusive-related deposits. The zoned intrusion is therefore not exposed and if it is at considerable depth may not be detectable in magnetic surveys. However, repeated tapping off of magma batches from various levels of a zoned magma chamber generates multiple intrusions, either nested to form a composite pluton or else a cluster of spatially and temporally-related intrusions. These intrusions represent differing stages of differentiation in the parent magma chamber and accordingly exhibit distinct magnetic and radiometric properties, which can be detected in high resolution surveys.

Examples of multiple comagmatic intrusions studied in this project include the Mount Leyshon Intrusive Complex, the Kidston Breccia Pipe and Goonumbla. Porgera is a classic example of variably fractionated multiple apophyses above a “mother intrusion”.

10.10 Examples of Contact Aureole Effects

Prominent contact metamorphic aureoles developed around the larger intrusions that are genetically related to porphyry systems are indicative of emplacement of high temperature magmas at upper crustal levels. Such magmas are candidates for prolonged fractional crystallisation, which encourages accumulation of incompatible metals in residual melt. Broad metasomatic halos around intrusions reflects development of a significant hydrothermal system and is also favourable.

The Tuckers Igneous Complex, near the Mount Leyshon Au deposit, the Cadia Monzonite Complex, associated with the Cadia and Ridgeway Cu-Au deposits, the deep intrusion beneath the Goonumbla Volcanic Complex and the Anabama Granite that hosts the Anabam Hill porphyry Cu prospect are examples of intrusions that have magnetically prominent aureoles. Reduced intrusion-related Au mineralisation within Sn provinces is also characterised by contact aureoles that show up well in aeromagnetic surveys (Webster, 2003). In this case quite subtle enhancements in susceptibility of intruded sedimentary rocks are visible, because of the weakly magnetisation of the ilmenite-series granites.

10.11 Examples of Magnetic Indicators of Lithological Control

Wyborn and Stuart-Smith (1993) and Wyborn and Heinrich (1993a) have emphasised the importance of lithological control of ore deposition in the distal zones of Proterozoic granite-related deposits of Australia. Magnetite and graphite act as reducing agents for oxidised metal-bearing fluids emanating from crystallising plutons. Examples of Cu-Au mineralisation (IOCG-type) apparently induced by reaction of fluids with magnetite-rich rocks include the Osborne, Starra (Selwyn) and Ernest Henry deposits in the Mount Isa Inlier and the Tennant Creek deposits, Northern Territory. Clearly magnetic surveys can be very effective in tracing favourable horizons in this environment.

10.11 Geophysical Signatures of Porphyry Copper Deposits – Summary

Combining the deposits considered by Gay and Mardosirian with porphyry deposits in the P700 database for which information on the magnetic signatures is available, we have 50 deposits with known magnetic signatures. The quality of the data is highly variable, making definitive statistical conclusions difficult. Taking the data at face value, however, we find the following empirical rates of occurrence for various types of anomaly:

- Intrusion highs (~50 %)
- Alteration highs (~70 %)
- Alteration lows (~70 %)
- Skarn highs (~20 %)
- Structural control lineaments (40 % - 60 %)

Recognition of structural controls, in particular, is very sensitive to the quality of the data. Many deposits show more than one of these features, accounting for the fact that the proportions add up to more than 100 %.

Of the deposits with high resolution data, 12 show well developed concentric zoning patterns. Ten of these, the majority from the Goonumbla cluster, have “doughnut” patterns – a central alteration low surrounded by an annular alteration high. Two, the Bajo de la Alumbrera Cu-Au deposit and the Anabama Hill Cu prospect, have “archery target” patterns, with central alteration highs surrounded by annular alteration lows.

Although the number of well-characterised empirical examples of these types of signature is low, the likely occurrence of similar signatures can be inferred from other information, e.g. the distribution of magnetite reported for some deposits. The predictive models developed for the P700 Atlas are designed to bridge the gap between purely geological models (both idealised models and detailed deposit descriptions) and empirical magnetic signatures. This process has suggested the following conclusions for deposits that have not been significantly modified by post-emplacement tectonism or metamorphism:

- The majority of gold-rich porphyry copper deposits (classic morphology, quartz-monzonite zoning) hosted by magnetic mafic-intermediate volcanics are predicted to have large (> 1000 nT) bullseye high RTP anomalies over the potassic core, with incipient to prominent development of the archery target signature, depending on the extent of the phyllic zone, *providing erosion has exposed or nearly exposed the potassic zone*. This signature should be easily detectable

beneath 100 m of sedimentary cover, and even beneath a similar thickness of magnetic volcanics.

- For a completely buried, uneroded or slightly eroded, gold-rich porphyry copper system the signature is basically an alteration low due to the large volume of magnetite-destructive alteration surrounding the deeply buried magnetic core. At intermediate levels of exposure a more complex pattern of a central high surrounded by an alteration low occurs, with the relative amplitude of the high and low dependent on the erosion level.
- Similar deposits emplaced into weakly magnetic felsic rocks or unreactive rocks, such as quartzites or shales, are characterised by a strong bullseye high, without a surrounding low.
- If emplaced into limestone the bullseye high associated with the potassically altered intrusion is likely to be supplemented by skarn anomalies (possibly remanently magnetised) associated with proximal magnetite-garnet skarn in favourable horizons, with discrete anomalies associated with distal skarn bodies, developed near the marble interface in structurally controlled zones. The skarn signature should be more strongly developed if the host rocks are dolomitic.
- Alkalic porphyry Cu-Au deposits typically exhibit diorite model zonation, with poorly developed phyllic zones, and produce strong bullseye highs over the potassic core.
- In areas of greater crustal influence on magmas (e.g. the Laramide province), magmas with relatively high sulphur content generate large volumes of magnetite-destructive alteration. Porphyry Cu and Cu-Au deposits of this type are associated with alteration lows, if emplaced into magnetic host rocks, or very weak signatures if emplaced into non-magnetic host rocks.
- Giant porphyry copper deposits of the Atacama desert are characterised by large volumes of magnetite-destructive alteration, with locally developed magnetite-bearing potassic alteration, and thick overlying supergene blankets. The signature of such deposits, when hosted by moderately magnetic rocks, is an areally extensive alteration low, with a typical amplitude of –100 nT. Such deposits will be visible to magnetics if they are covered by non-magnetic overburden, but cover by magnetic volcanics renders them difficult to see. When hosted by non-magnetic rocks the magnetic signature is inconspicuous, apart from local highs associated with remnant zones of potassic alteration within the broad zones of phyllic overprinting. These deposits are ringed by chargeable zones due to pyrite-bearing propylitic halos.
- Phyllic alteration produced by magmatic, rather than meteoric, fluids tends to be “inside-out” with respect to the potassic zone, producing a doughnut magnetic signature. Another source of this reverse zoning pattern may be structurally controlled access of meteoric fluids to deeper portions of a deposit. This type of signature is to be expected in two main settings: Volcanic morphological models, with small intrusive spines within comagnatic volcanics, tapped of a large mother magma chamber, and plutonic/batholithic porphyry deposits.
- Reduced porphyry Au-(Cu) and reduced intrusion-related gold deposits are characterised by incomplete doughnut signatures on a scale of kilometers, due to distal pyrrhotite-bearing mineralisation developed in favourable sites, around a weakly magnetic intrusion.

10.12 Geophysical Signatures of Volcanic-hosted Epithermal Deposits – Summary

Intense epithermal-style alteration, whether low- or high-sulphidation, is invariably magnetite-destructive. The magnetic signature is strongly dependent on the host rocks. Epithermal alteration systems hosted by magnetic volcanic rocks are characterised by smooth, flat magnetic low zones within the overall busy magnetic texture. Similar systems within non-magnetic sedimentary rocks have negligible magnetic expression. High sulphidation systems may have a diffuse intrusion + alteration high due to a deeper porphyry system within a few hundred meters to a few kilometres of the deposit. This may be more prominent if post-formation faulting has brought the intrusion closer to the surface, or the porphyry and epithermal systems are telescoped by rapid uplift during formation.

Magnetics can also be useful for detecting structural corridors and fluid pathways that are related to more localised epithermal systems. Radiometrics can detect K-rich alteration (e.g. adularia-sericite) asscoiated with some exposed or subcropping epithermal deposits.

Although in favourable circumstances magnetics is a useful tool for defining prospective hydrothermal systems, delineation of the ore zones is not possible. Electrical methods are generally more useful for detecting conductive mineralisation and defining resistive zones of silicification. Gravity methods are sometimes useful for defining lower density alteration, or in some cases enhanced density due to silicification of porous rocks.

10.13 Gravity and Magnetic Signatures of IOCG Deposits – Summary

Magnetite and hematite both have densities of ~5200 kg/m^3, which is very high compared to silicate minerals. Crustal average densities are about 2670 kg/m^3. Iron oxide Cu-Au deposits contain abundant Fe oxides, by definition, and are therefore considerably denser than silicate- or carbonate-dominated rocks. The large density contrast between IOCG deposits and their host rocks ensure that they have a substantial positive gravity anomaly, unless they are very small.

The density of a rock that contains significant iron oxides can be estimated from:

$$\rho = \rho_{GANGUE} + (\rho_{OXIDES} - \rho_{GANGUE})\, f_{MT+HM},$$

where f refers to the volume fraction of iron oxides and ρ_{GANGUE} is the average density of the gangue minerals. Weight fractions can be converted to volume fractions by:

$$f_{OXIDES} = (w_{OXIDES} \times \rho_{GANGUE})/[(\rho_{OXIDES}\,(1- w_{OXIDES}) + \rho_{GANGUE}\, w_{OXIDES}],$$

where w_{OXIDES} is the weight fraction of oxides. Weight per cent Fe can be converted to hematite weight per cent, assuming essentially all the iron occurs as hematite, by dividing by 0.7. If magnetite is the only significant iron mineral in the rock the corresponding factor is 0.724.

Of the IOCG deposits in the P700 database, nine have positive gravity anomalies of known amplitude. Two others have associated gravity highs, but the size of the anomaly is not reported. Reported gravity anomaly amplitudes range from 1 mgal, for the small (2.1 Mt) Tennant Creek-type deposit at White Devil, to 20 mGal for the Acroplis deposit, near Olympic Dam. The Olympic Dam deposit has a 17 mGal gravity high. The average amplitude is 7 ± 2 (1 S.E.) mGal. The gravity highs are centred on the zones of massive iron oxide alteration, but are not specifically related to mineralised zones within the iron oxide bodies. Some contribution to gravity highs is made by large envelopes of disseminated iron oxides in alteration envelopes around the semi-massive to massive iron oxide bodies.

The magnetic signatures of IOCG deposits, and their relationships to the gravity anomalies, depend on the geological history and are much more variable. Overall the magnetic sources tend be deeper and more laterally extensive than the gravity sources. The main factors affecting the magnetic signatures are:

Redox conditions during deposition and alteration overprinting

Magnetite, formed under relatively reducing conditions, has very high susceptibility compared to hematite. Hematite has low susceptibility and fairly weak remanence, unless it has formed at, or been taken to, very high temperatures. Monoclinic pyrrhotite, formed under reducing conditions with moderate sulphur fugacity, has moderate susceptibility, but tends to carry intense remanence. The oxidation state of the host sequence appears to influence the oxidation state of the IOCG deposits, as well as the redox state of the source (e.g. magmatic fluids) and the palaeodepth (more oxidised at shallow depths).

Level of exposure

In a typical vertically zoned IOCG system, magnetite-destructive, hematite-rich HSCC alteration dominates upper levels, whereas magnetite-rich alteration dominates at depth. Thus the current erosion level determines whether the exposed or near-surface portions of the system are hematite-rich or magnetite-rich.

Structural modification

Tilting of a vertically zoned system, or upfaulting of the deeper magnetite-rich portion, may juxtapose the magnetite and hematite zones, producing juxtaposed, rather than “coincident” gravity and magnetic anomalies.

Thermal History

High grade regional or contact metamorphism of hematite-rich zones can impart an intense thermoremanence to the hematite, which can cause large magnetic anomalies. This appears to explain the strong magnetic anomalies exhibited by massive hematite bodies of the Mount Woods Inlier that have been contact metamorphosed, whereas similar massive hematite at Prominent Hill produces no discernible magnetic anomaly.

Overall, exploration for IOCG deposits using potential field methods should be guided by the following principles:

- favourable tectonic settings for ancient deposits may be recognisable from regional potential field data sets, supplemented by seismic, magnetotelluric or other deep-penetrating methods. Ancient buried subduction zones are characterised by arc-parallel linear belts of magnetic highs, corresponding to magnetite-series granitoid provinces, and lows, corresponding to ilmenite-series granitoid provinces or sedimentary basins. Subduction-related magnetite-series belts are much more prospective for ICOG and porphyry copper-(gold) deposits. Continental rift settings, which are also prospective for ICOG deposits, may be associated with rift-parallel regional gravity and magnetic highs along the ancient continental margin, with a quiet magnetic zone outboard of the regional highs and relatively busy magnetic patterns inboard of the margin (see Figs.10.11-12).
- at a regional scale major structures that control the emplacement of mineralising or heat-engine magmas, or channel flow of crustal fluids, are often evident in suitably processed gravity and magnetic data sets. These features may also be visible in satellite imagery. Intersections of lineaments appear to be particularly favourable for ICOG mineralisation.
- Structural controls at a range of scales, from province to prospect scale, may be evident in detailed magnetic data.
- Large intrusions associated with bimodal magmatism, which is characteristic of anorogenic environments, including several ICOG provinces, can be seen in magnetic and gravity images, due to the contrasting physical properties of mafic and felsic intrusions. A large range of magma compositions within a comagmatic suite is indicative of fractional crystallisation and is favourable for development of intrusive-related mineralisation.
- Strongly zoned oxidised intrusions exhibit zoned magnetic signatures and, if exposed or subcropping, zoned radiometric patterns. These signatures are good indicators of fractional crystallisation and are therefore favourable.
- ICOG deposits seem to occur within relatively oxidised sequences, characterised by active magnetics. Within the regional magnetic variability, the deposits lie within or near relatively strong magnetic highs, associated with semi-regional magnetite-producing sodic and sodic-calcic alteration systems.
- If the level of exposure is sufficiently deep, overprinting magnetite-rich potassic alteration tends to be more focussed around the deposits, enhancing the magnetic highs.
- On the other hand, if upper levels of the system have been retained, magnetite-destructive hematite-rich alteration hosts the mineralisation. In this case the signature is a relatively smooth pattern, which can be a local magnetic low (depending on the host rock magnetisation) within the overall broad high associated with deeper and/or more laterally extensive magnetite-dominant alteration.
- ICOG deposits (unless they are small or too deeply buried) are associated with substantial positive local gravity anomalies (up to 20 mGal) that arise mainly from the semi-massive to massive iron oxide zones, in some cases possibly enhanced by large volumes of disseminated iron oxides in surrounding alteration halos.

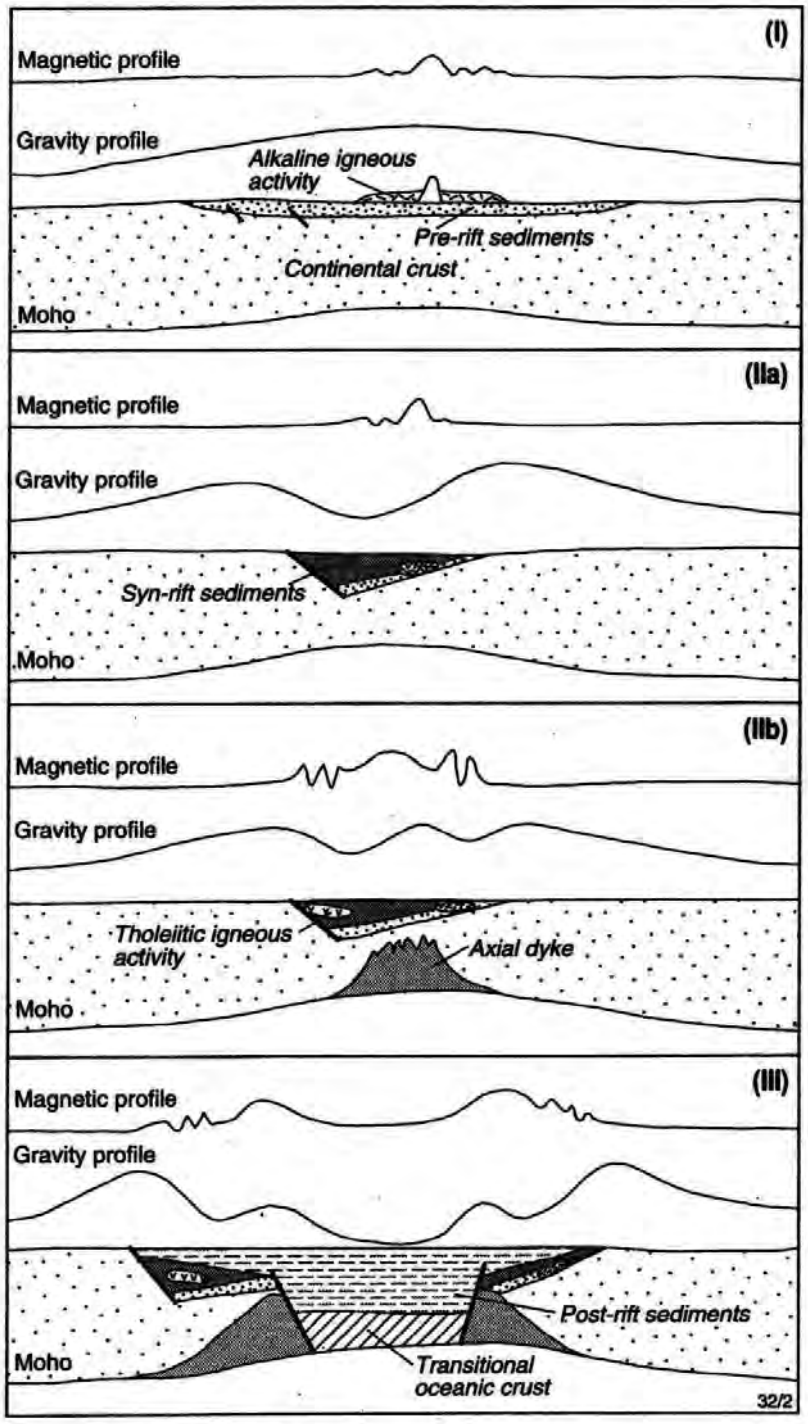

Magnetic and gravity expressions of the pre-rift and syn-rift stages.

Fig.10.11 Development of magnetic and gravity signatures during rifting (Gunn, 1997)

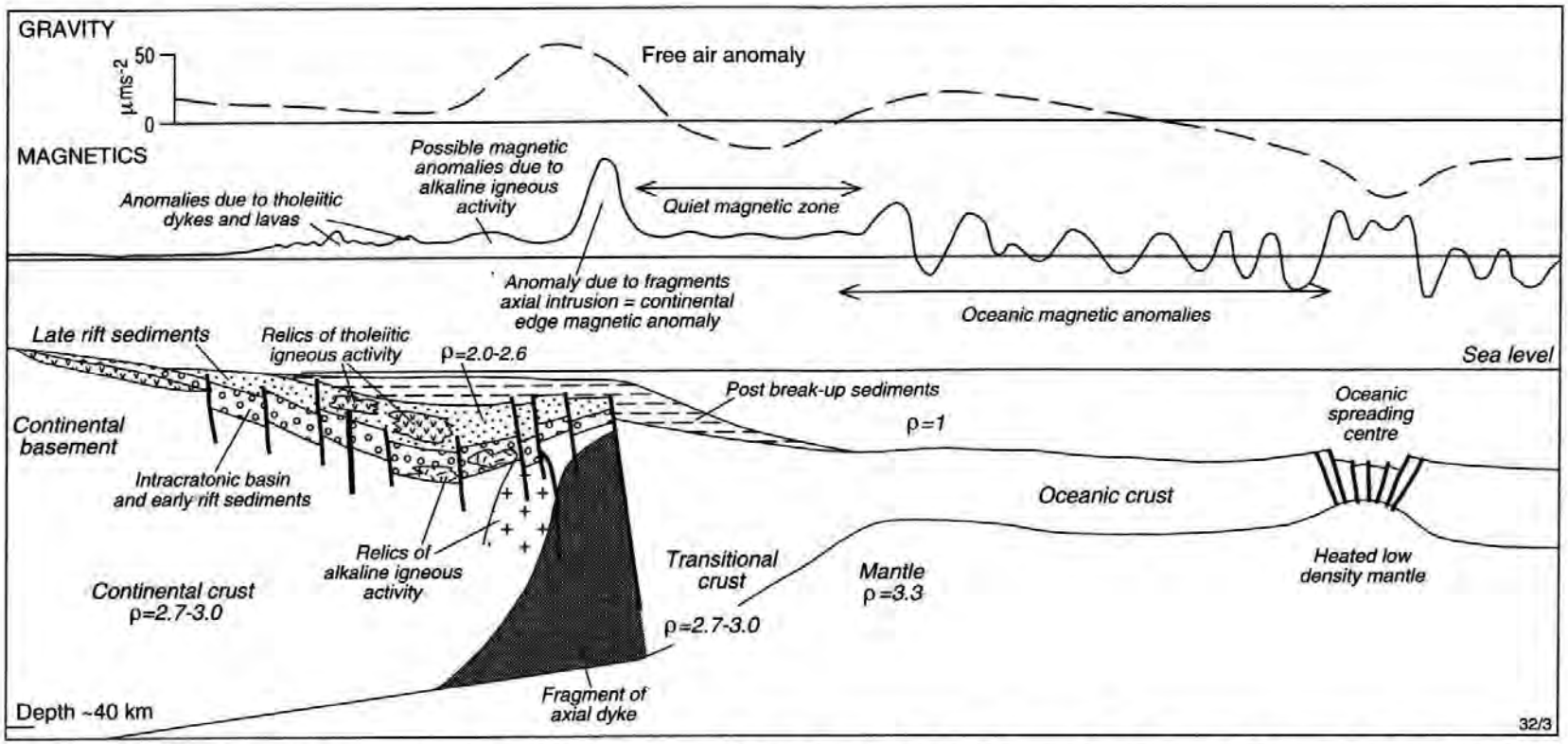

Idealised gravity and magnetic profiles over an 'Atlantic-type' continental margin where crustal splitting and sea-floor spreading have occurred.

Fig.10.12 Idealised magnetic and gravity signatures of a rifted margin (Gunn, 1997)

- Detailed modelling of nominally coincident magnetic and gravity anomalies of hematite-rich ICOG systems should indicate a deeper magnetic source than gravity source, due to vertical and lateral zonation of oxide mineralogy. The sources of the potential field anomalies are therefore superposed, rather than coincident. By contrast, other possible sources (such as a mafic intrusion) should be explainable by a single body.
- Regional zonation of alteration (extensive early magnetite-rich alteration with more localised hematite-rich overprinting), and faulting or tilting of originally vertically zoned alteration often produces juxtaposed, rather than coincident, gravity and magnetic anomalies. Combined interpretation of gravity and magnetic patterns should bear zonation models in mind.

Magnetic and gravity are the major tools for locating potential ICOG systems, but are ineffective at delineating Cu-Au mineralisation within these systems. Other geophysical techniques that may be useful in exploration for IOCG deposits include:

- IP methods, which may delineate mineralised zones with relatively low resistivity and high chargeability within the more extensive iron oxide-rich alteration,
- EM, which can in favourable circumstances detect higher conductivity chalcopyrite + iron sulphide zones within moderately conductive magnetite-rich hosts,
- Radiometrics, which can detect large potassic alteration zones (e.g. the NICO deposit, Canada) and enhanced uranium. It can also be a useful mapping tool at a regional scale, defining structures and defining compositional variations within large intrusive bodies (zonation or multiple, nested intrusions).

.

11. EXPLANATORY NOTES FOR THE P700 DATABASE

11.1 Structure of the Database

The Access database comprises four linked tables:

- the Deposit table, which contains geographic, geological, economic and geophysical information on individual deposits,
- the Rock Unit table, which lists rock units from each deposit in the Deposit Table, with relevant geological and geophysical information,
- the Alteration Table, which lists petrological and petrophysical data for individual alteration zones for each rock unit in the Rock Unit Table,
- the Reference Table, which gives citations for each deposit in the database.

Each deposit has a unique identifying number, as does each rock unit, allowing the tables to be linked.

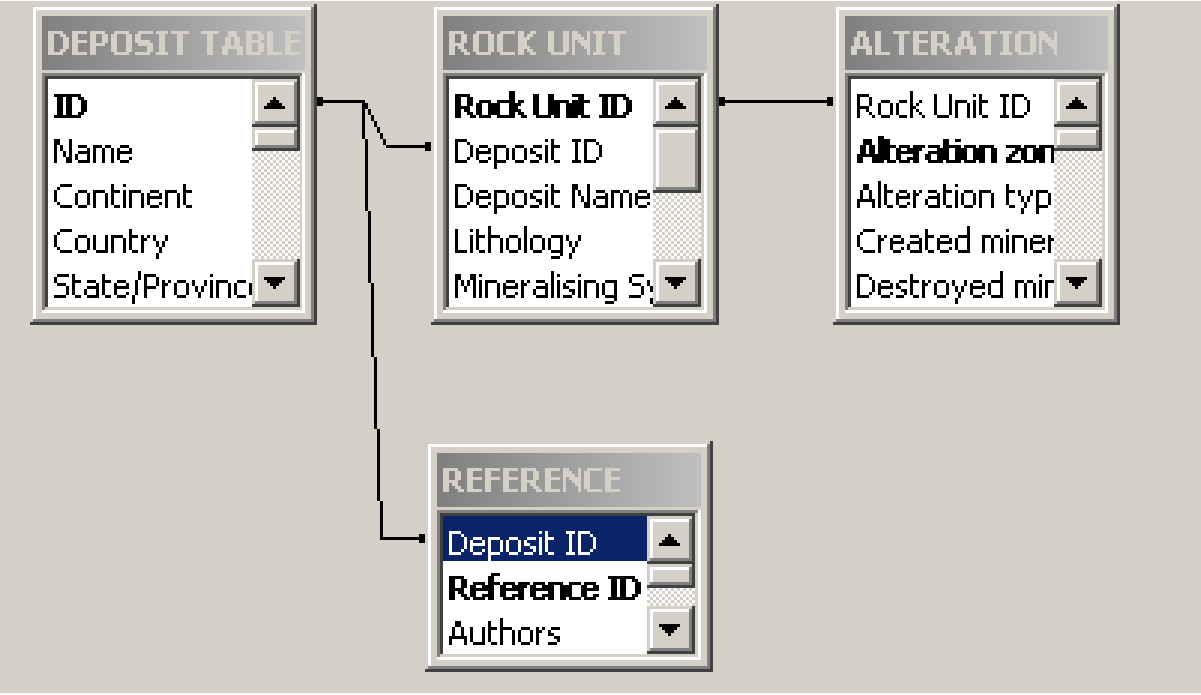

11.2 Interrogating the Database

1. After opening the database, click on the “Queries” button....

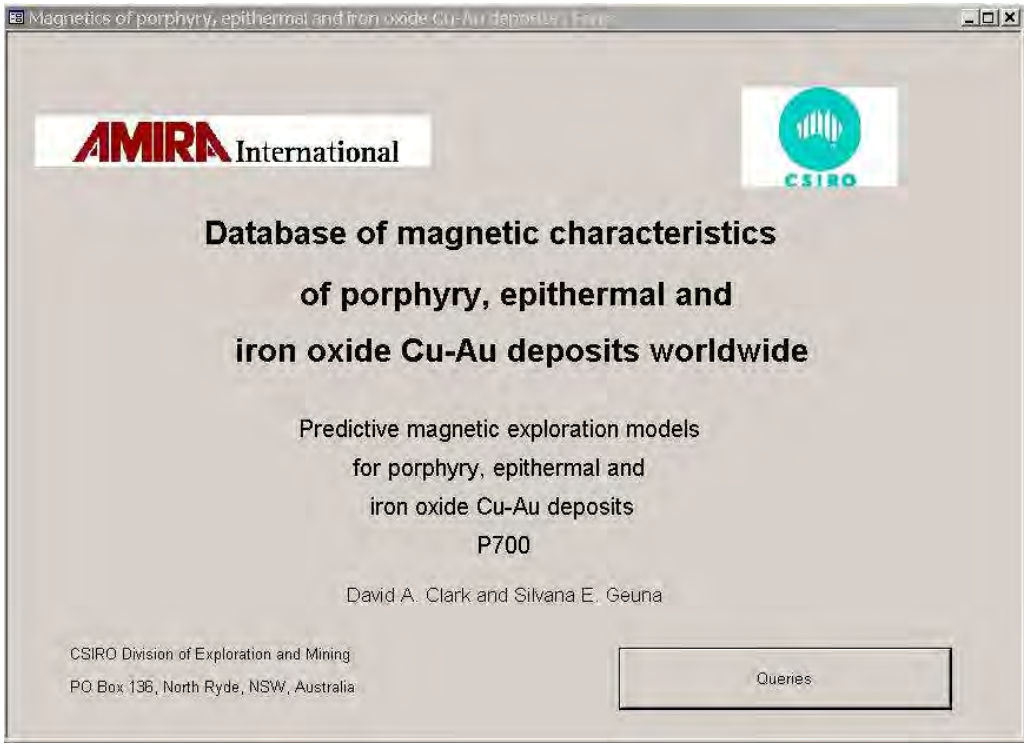

2. ...which brings up the “Deposits: General Characteristics” Form. Select the criteria for your search.

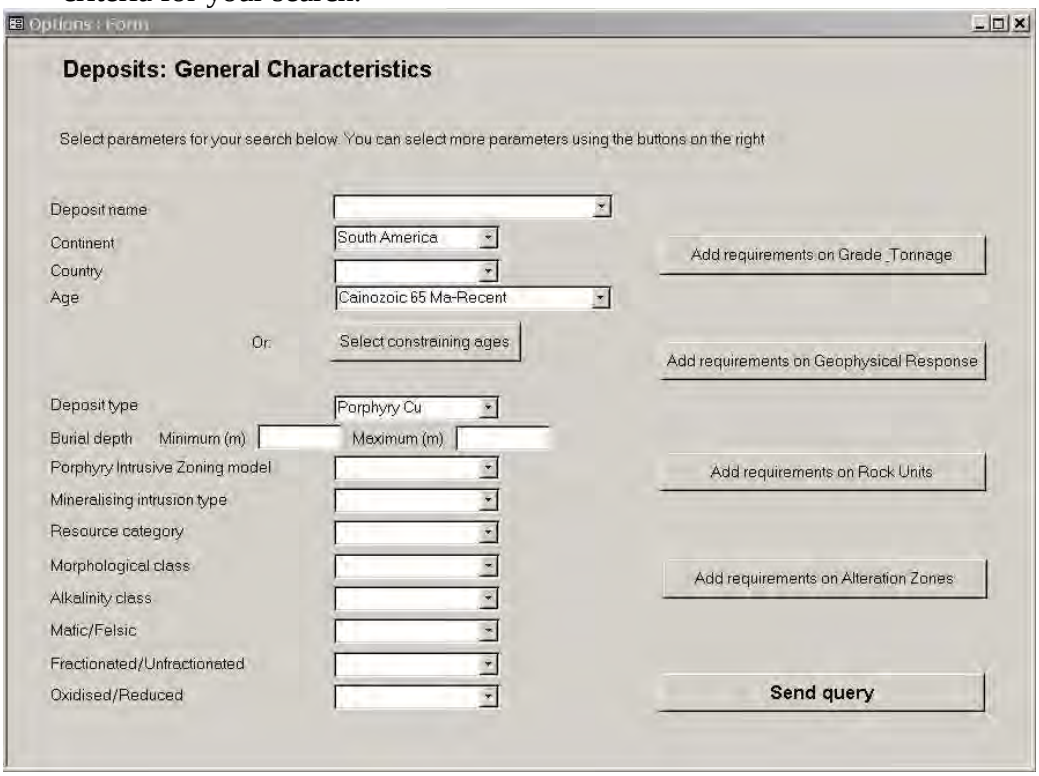

These may include a specific deposit name (leaving this field blank searches for all deposits that satisfy the other criteria); a continent or country; an age (either a geological period or a numerical range); deposit type (e.g. porphyry Cu); constraints on the deposit type or type of associated intrusion – all selectable from drop-down lists. Other criteria can be chosen by clicking on the buttons on the RHS of the form.

3. An example of the information available on individual deposits is shown below:

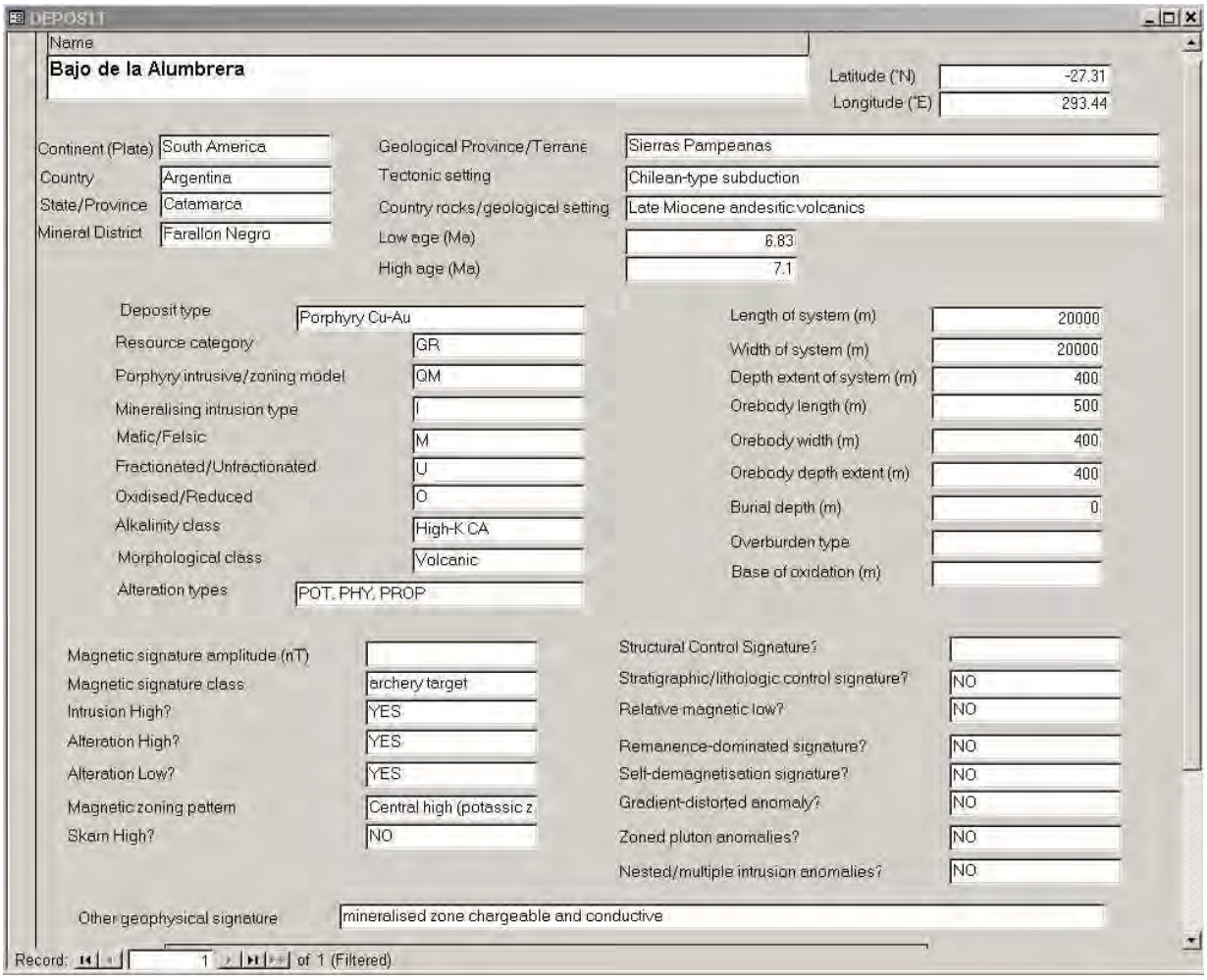

4. If results for specific rock types are needed, click on the “Rock Units” button to get:

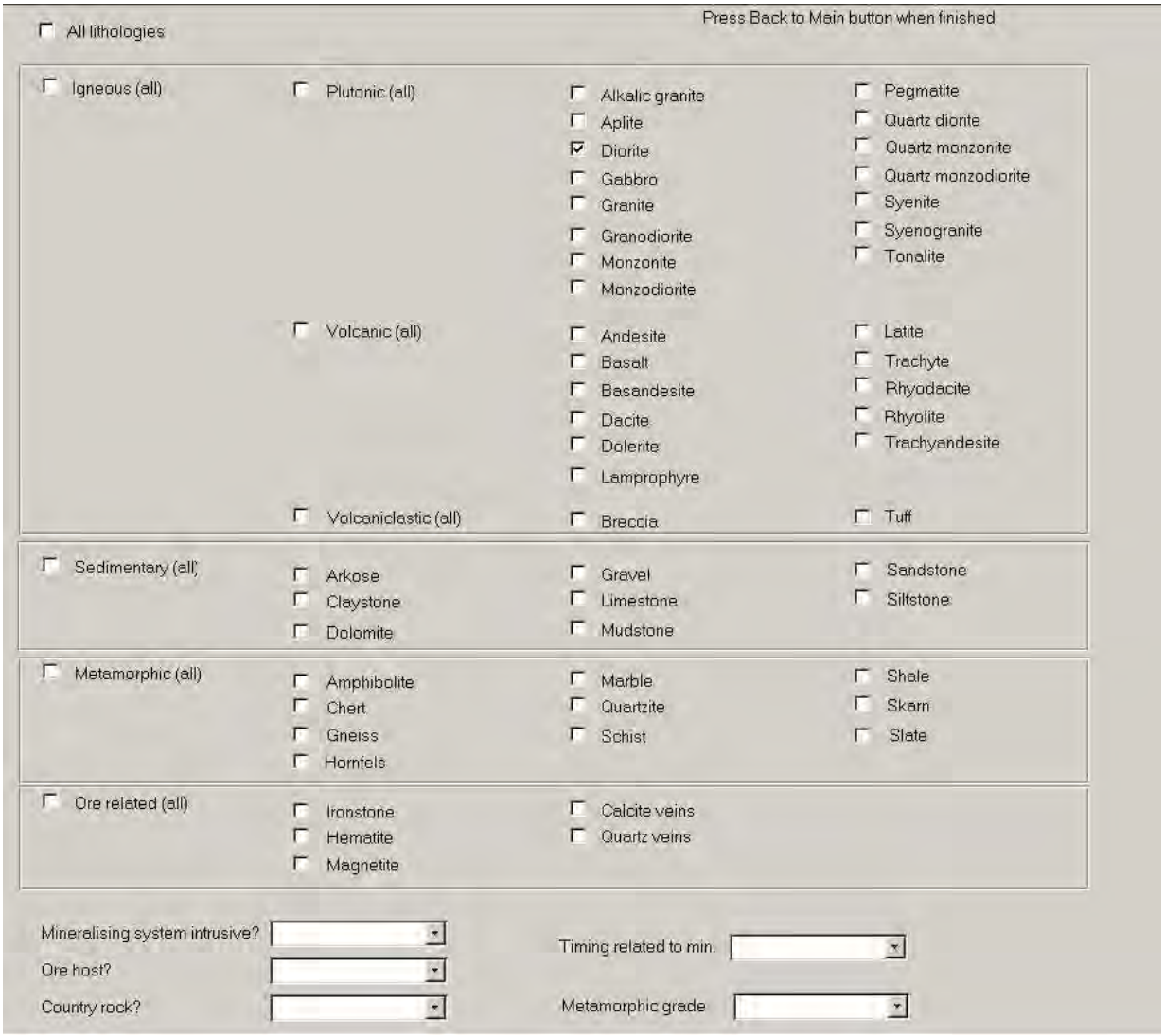

5. After checking boxes for all rock types of interest, click the “Return to Main” button at the bottom of the form, which returns to the “Deposits: General Characteristics” Form shown above after step 2.

6. Clicking on the Alterations button brings up the following form....

...the bottom half of which is:

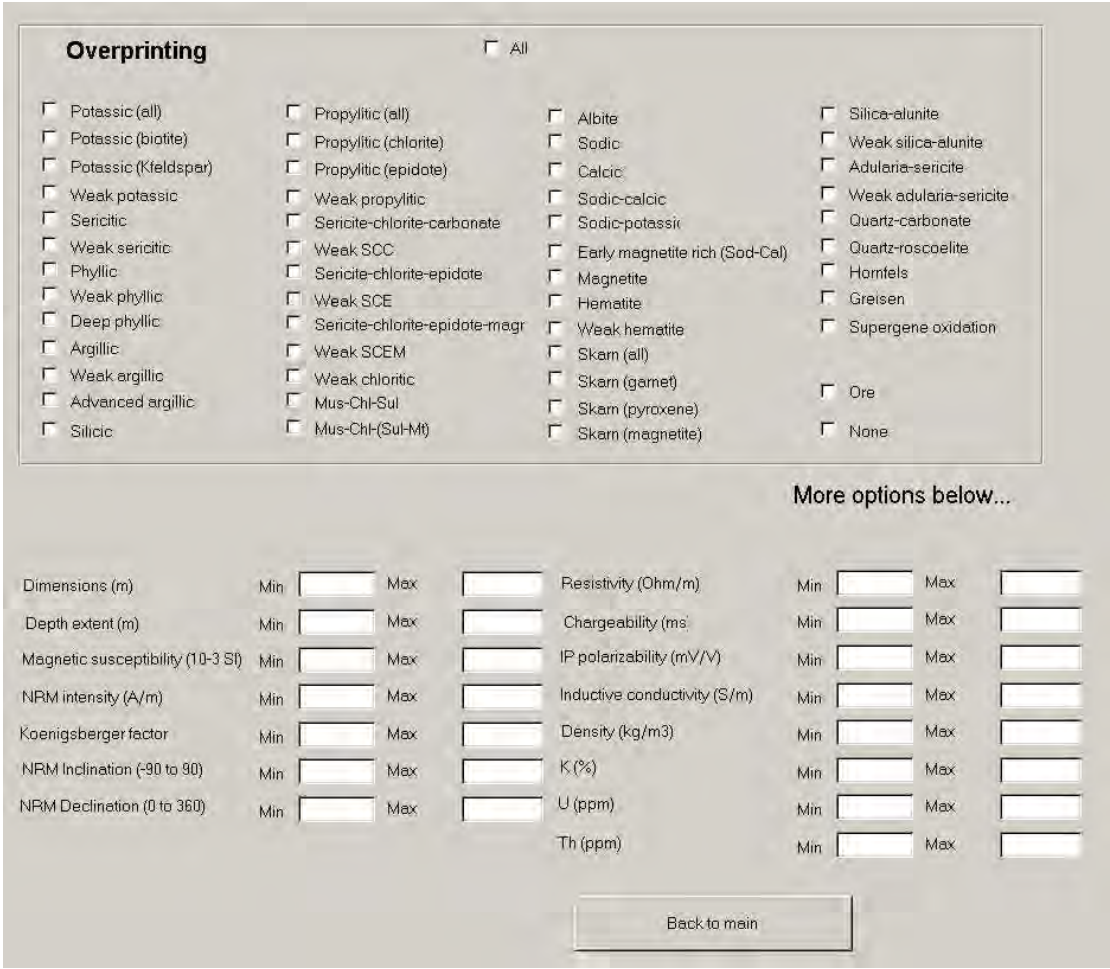

7. Check the boxes for the alteration type(s) of interest. As an example, if you are interested in phyllic alteration that overprints early potassic, check the boxes for potassic alteration in the top half and for phyllic alteration in the bottom (Overprinting) section, then click on “Back to Main”. If only one type of alteration, without overprinting, is required, check “None” in the Overprinting section. Other criteria on dimensions and physical properties can also be selected before returning to the Deposits Form.

8. When all desired criteria have been selected, click on the “Send Query” button. Results are returned in the following Form:

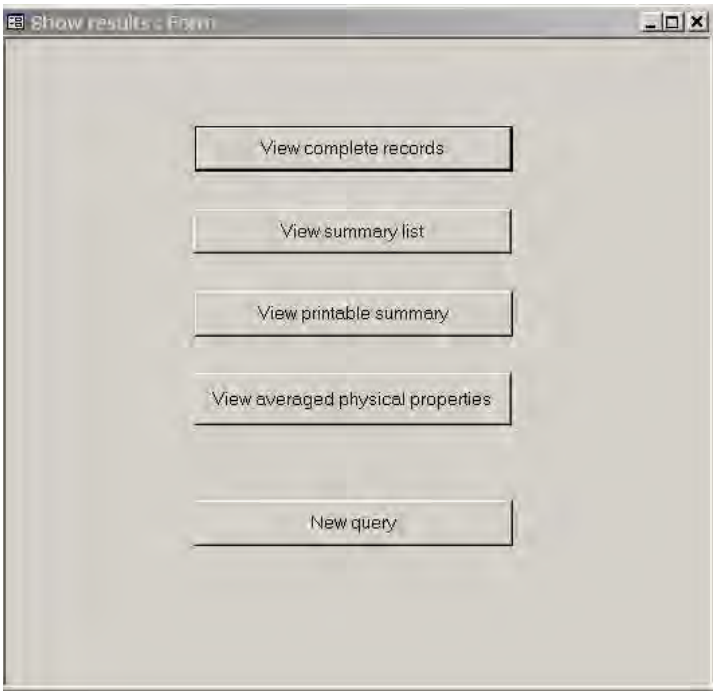

9. Clicking on “View summary list” button gives:

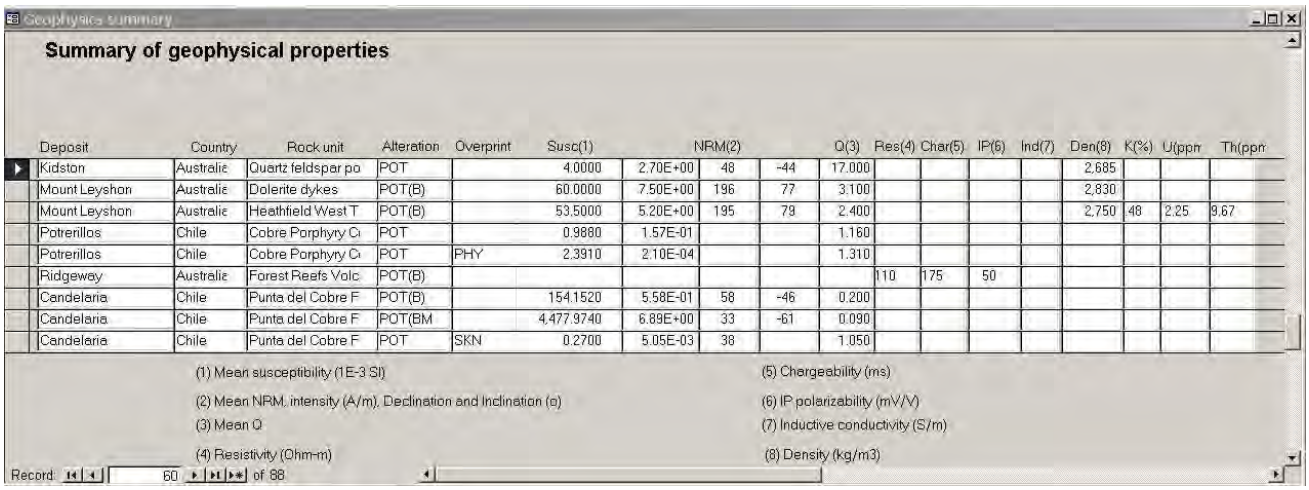

which lists deposits/rock units/alteration zones that have satisfied the selected criteria, with the corresponding physical properties. Closing this form returns to the Results Form (step 7 above). Clicking on “View printable summary” gives an easily printable version of the summary list.

10. Clicking on “View complete records” gives detailed results for each deposit in the summary list, in turn. Specific deposits are selected using the arrow buttons on the “Record xx of yy” box at the bottom:

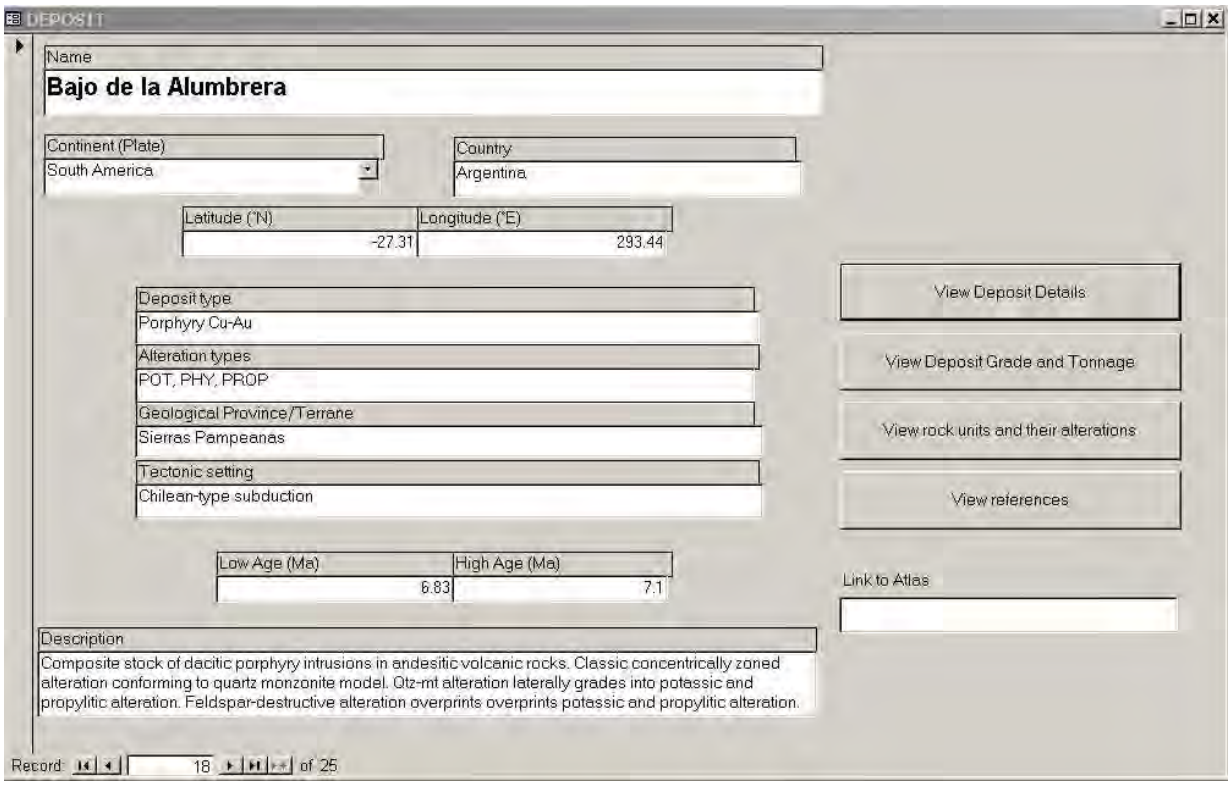

11. Deposit details, grade and tonnage information, or references can be viewed at this point by clicking on the corresponding buttons. Clicking on “View rock units and their alterations” gives details on each qualifying rock unit, in turn:

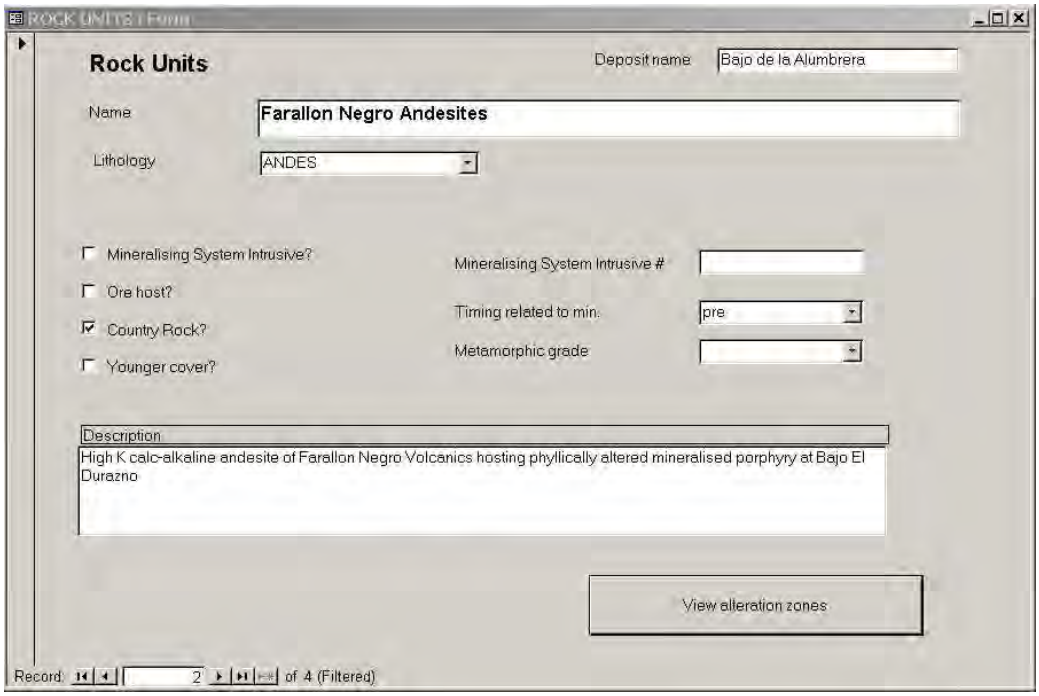

Specific rock units are selected using the arrow buttons on the “Record xx of yy” box at the bottom.

12. For each rock unit, clicking on the “View alteration zones” button gives details on each alteration zone for the rock unit:

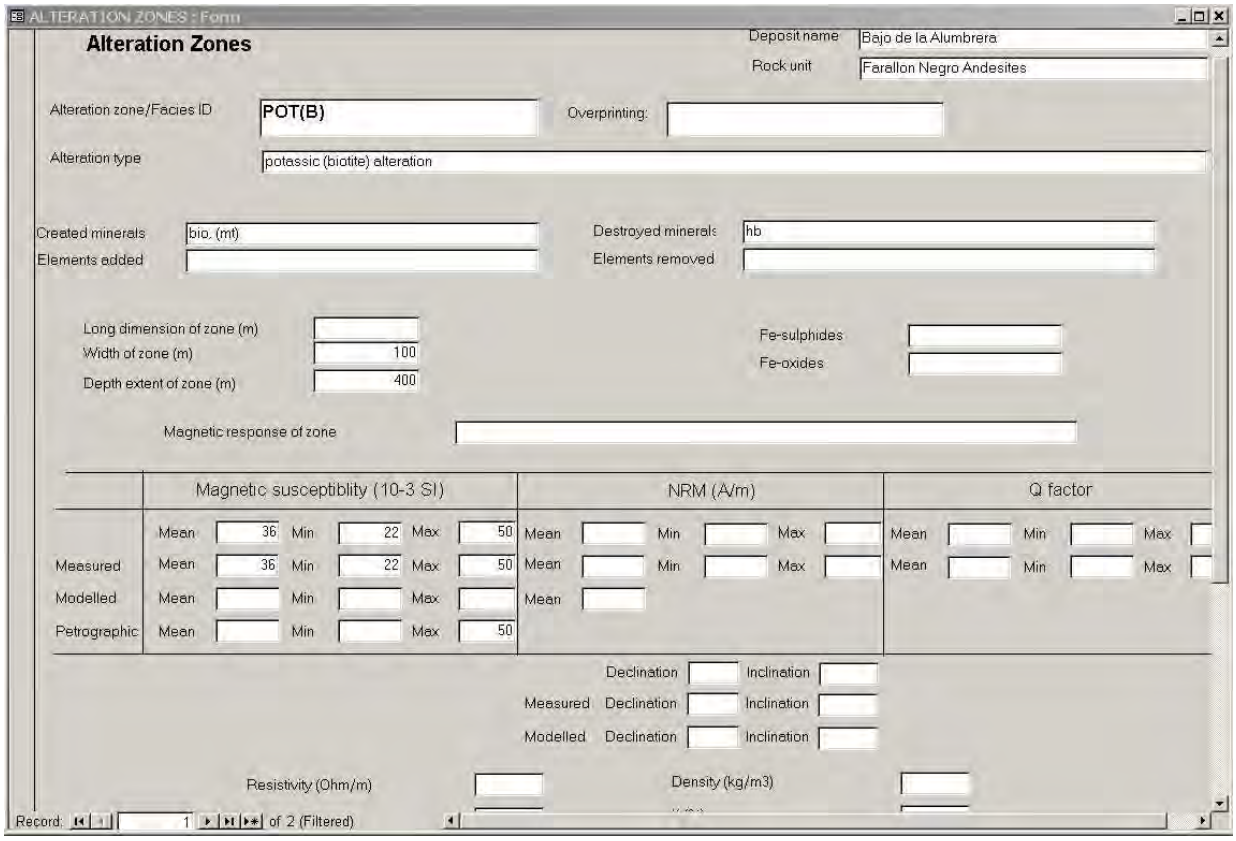

13. Closing these detailed results windows and returning to the main results panel (shown for step 7 above), clicking on “View averaged physical properties” returns averages and standard deviations for the physical properties:

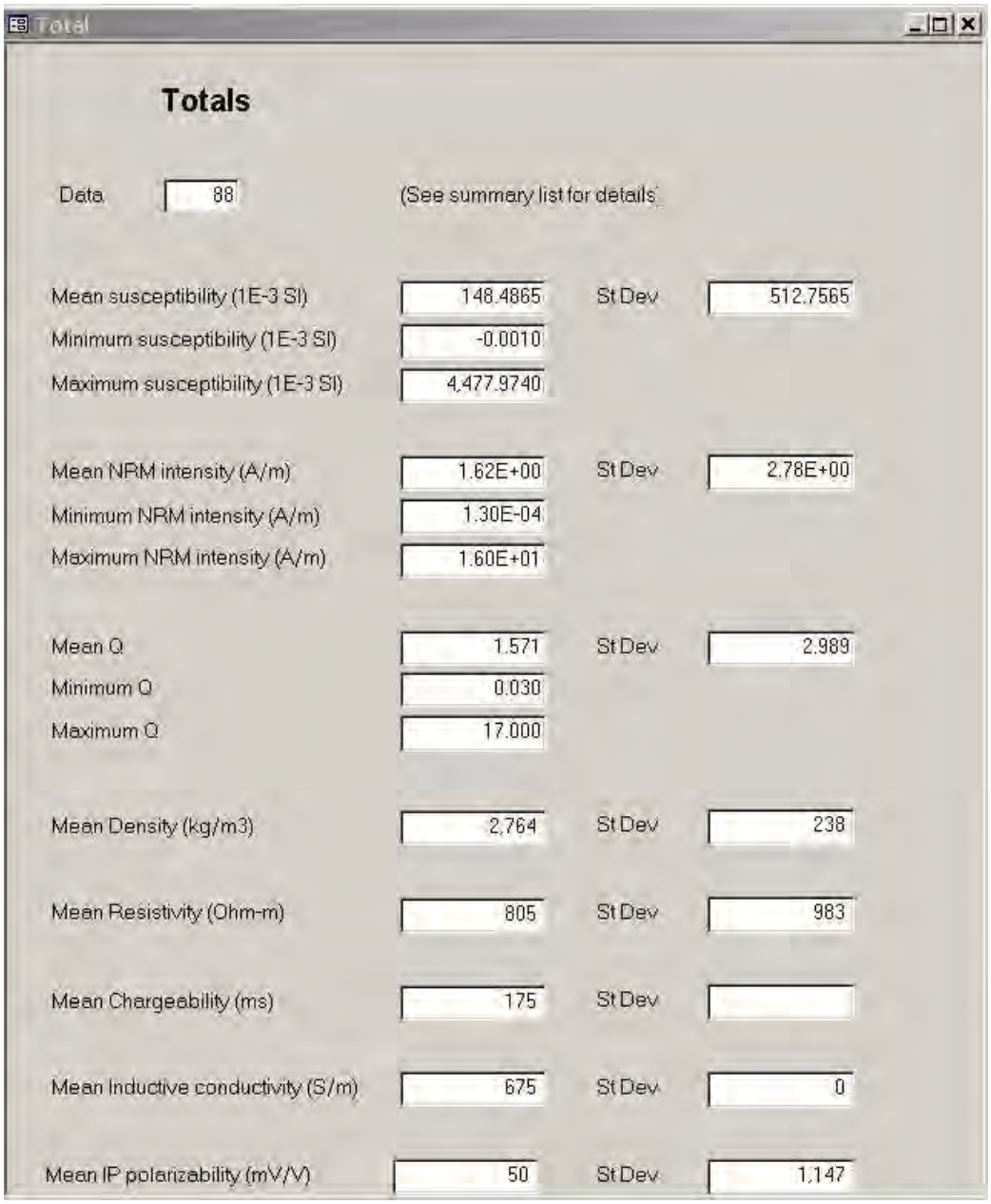

11.3 Classification of Igneous Rocks Associated with Mineralisation

Igneous Type

Where possible the igneous rocks associated with the mineralised system are placed within one of four possible classes: I-, S-, A-, or M-type. I-type granitoids may be further subdivided into I-tonalite or I-granodiorite series. Selected characteristic features of these four granitoid types can be drawn from Pitcher (1983) and Bowden *et al.* (1984). They include:

M-type (**M**antle-derived): metaluminous; calcic gabbros, diorites, quartz diorites, tonalites and plagiogranites; 45% to 78% SiO_2; little or no K-feldspar.

I-type (**I**gneous source rock/**I**nfracrustal): metaluminous; calc-alkaline to alkali-calcic, relatively quartz-poor monzogranites, granodiorites and tonalites; 53% to 76% SiO_2; high Na/K, high Ca for mafic varieties; hornblende-bearing (except most felsic members). Chappell and Stephens (1988) proposed that progressively more felsic and chemically evolved I-type granitoids result from successive remeltings of older mafic rocks that have underplated the crust. M-types comprise gabbros to mafic granites derived directly from the mantle or mantle wedge, I-tonalite (I-t) types are derived from fusion of M-type material and I-granodiorite (I-g) types represent remagmatised products of I-tonalite rocks.

S-type ([meta]**S**edimentary source rock/**S**upracrustal): strongly peraluminous; alkali-calcic to calc-alkaline, relatively quartz-rich monzogranites, granodiorites and tonalites; 65% to 74% SiO_2; low Na/K, Ca and Sr; with peraluminous minerals (muscovite, cordierite, garnet or andalusite); often biotite-rich.

A-type (**A**nhydrous, **A**norogenic, **A**lkaline): peralkaline to metaluminous; alkalic to alkali-calcic syenogranites, alkali granites and quartz syenites; mostly 70% to 78% SiO_2; high Na+K, Fe/Mg, F+Cl and low Ca, Sr; accessory minerals such as fayalite, hedenbergite, ferrohastingsite, annite, fluorite, sodic pyroxenes, perthitic or rapakivi-textured feldspars. A-type granitoids are inferred to be derived by partial melting of F and/or Cl-enriched dry granulitic residue remaining in the lower crust after earlier extraction of an orogenic granitic melt (Whalen *et al*., 1987).

Mafic/Felsic Categories

A silica content of 68% corresponds to the most mafic possible variants of granitic/rhyolitic compositions. Accordingly, the igneous rocks associated with the mineralised system are classified as mafic (M) if they have $SiO_2 < 68\%$ (corresponding to diorite/andesite to mafic granodiorite/dacite compositions) and felsic (F) if $SiO_2 > 68\%$ (felsic granodiorite/dacite and granite/rhyolite compositions).

Oxidation State

Igneous rocks associated with the mineralised system are classified on the basis of the oxidation state into four groups: strongly reduced, reduced, oxidised, or strongly oxidised. These categories can be determined on the basis of chemistry (if ferrous and ferric iron contents are known) or mineralogy. Figure 11.1 shows the fields for these categories on an Fe_2O_3/FeO versus FeO^T diagram. Characteristic mineral assemblages for each of the oxidation classes are:

Strongly reduced (SR): ilmenite (low Fe^{3+} and Mn) + pyrrhotite; magnetite absent

Reduced (R): ilmenite without magnetite

Oxidised (O): magnetite ± ilmenite (high Fe^{3+} or Mn)

Strongly oxidised (SO): magnetite + primary sphene ± hematite.

Fig.11.1. Classification of oxidation state on the basis of Fe_2O_3/FeO (Champion and Heinemann, 1994).

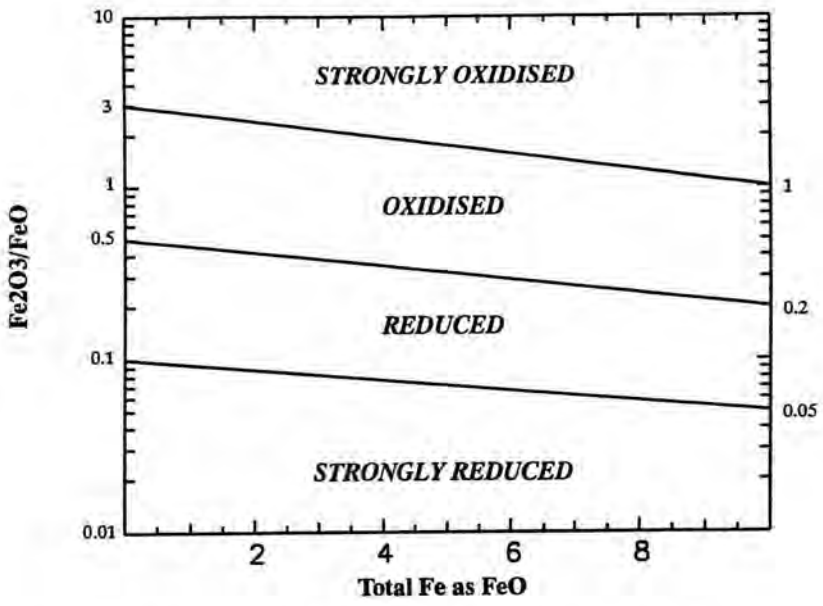

A plot of Fe_2O_3/FeO versus total Fe as FeO* (wt%) showing the fields for strongly reduced, reduced, oxidised and strongly oxidised. Boundary between reduced and oxidised modified from Ishihara & others (1979). Other field boundaries calculated from Blevin & Chappell (1992, their Fig. 2b).

Degree of Fractionation

Felsic igneous rocks (SiO_2 > 68%) are classified as fractionated (F) if they have evidently undergone removal of feldspars by fractionation processes such as crystal fractionation or convective fractionation. Conversely they are classified as unfractionated (U) if these processes have not occurred. Fractionation produces depletion of Sr and Ba and enrichment in Rb, resulting in moderate to high Rb(>200 ppm), moderate Rb/Sr ratios (≥ 1) and either low Ba (< 200 ppm) or evidence of Ba depletion. Figure 11.2 shows an Rb-Ba-Sr ternary plot that can be used to identify fractionated versus unfractionated units.

Fig.11.2. Rb-Ba-Sr ternary diagram distinguishing fractionated (strongly differentiated) from unfractionated (normal) granitic and rhyolitic rocks.

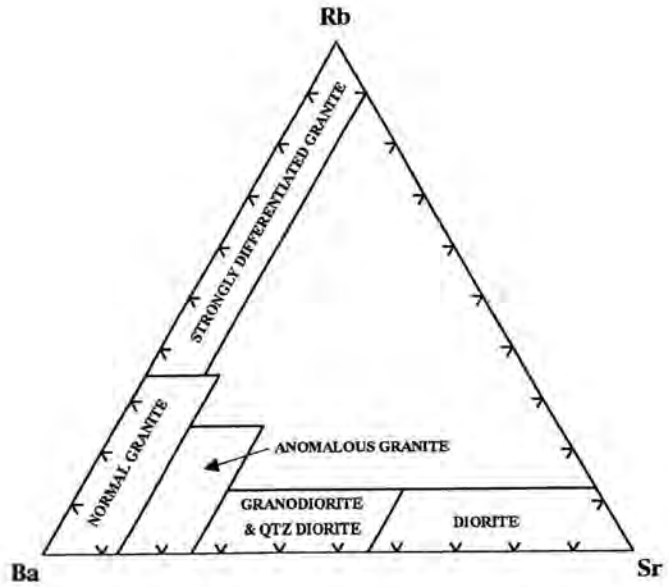

Rb-Ba-Sr triangular plot from El Bouseily & El Sokkary (1975) showing the fields for normal and fractionated granites.

Alkalinity Class

Igneous rocks related to mineralisation are classified in the database according to their alkalinity *sensu lato*, where sufficient geochemical information is available. They are classed as members of calcic (C), calc-alkaline (CA), alkali-calcic (AC) or alkalic (Alk) igneous series according to their alkali-lime index of Peacock (1931), which is defined in Fig.11.3.

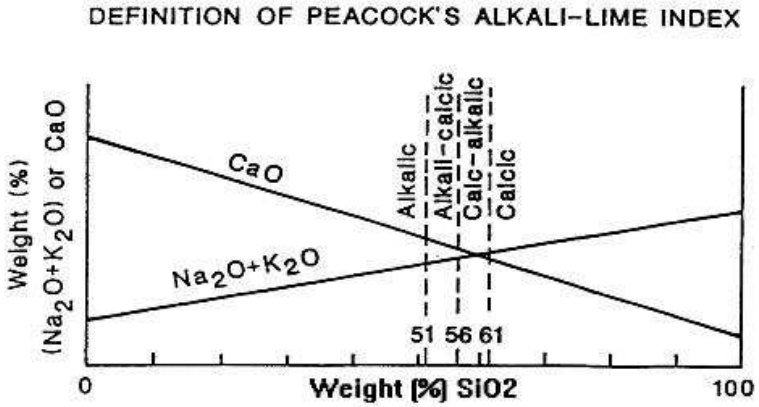

Figure 11.3 Classification of comagmatic igneous rock series as alkalic, alkali-calcic, calc-alkalic and calcic on the basis of the alkali-lime index (Peacock, 1931).

Alkalic rocks can be further grouped into silica-saturated quartz-alkalic (QA) or silica-undersaturated nepheline-alkalic (NA).

The igneous rocks can be further subdivided into low-K, medium-K, high-K or very high-K (shoshonitic) groups according to a K2O-SiO2 plot (Fig.11.4).

Fig.11.4. Definitions of low-, medium-, high- and very high-K igneous rocks.

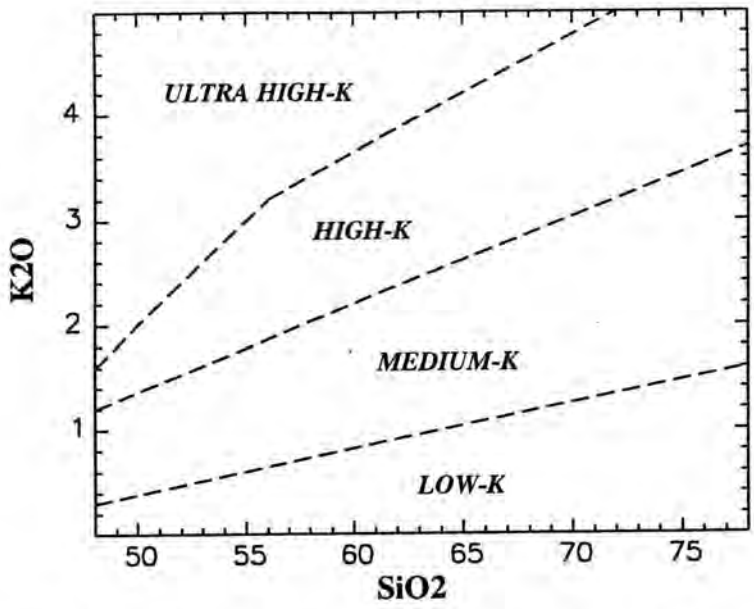

Plot of K_2O versus SiO_2 (wt%) showing the fields for low-K, medium-K and high-K igneous rocks (from Peccerillo & Taylor, 1976).

12. EXPLANATORY NOTES FOR THE P700 ATLAS OF PREDICTIVE MAGNETIC EXPLORATION MODELS

The Atlas of Magnetic Signatures contains illustrative examples of actual signatures of deposits and prospects, together with explanatory material such as geological maps and sections, as well as suites of synthetic models and their calculated responses. Magnetic properties of the rock units/alteration zones in the synthetic models were derived from information in the Database.

12.1 Gold-rich Porphyry Copper Models

The gold-rich porphyry copper models conform to general geological models of this type of deposit (e.g. Sillitoe 1979, 2000), but are closely based on deposits that may be regarded as archetypes for particular settings. In particular, the model adopted for mafic-intermediate host rocks is based upon the Bajo de la Alumbrera deposit in Argentina, and the model for carbonate host rocks is based upon Grasberg/Ertsberg (Papua New Guinea).The assumed zoning is concentric and conforms to the quartz-monzonite model, i.e. a magnetite-rich potassic core surrounded by a shell of phyllic alteration passing outwards into propylitic alteration (in silicate host rocks) or zoned skarn alteration (in a carbonate host).

The geometry of the gold-rich porphyry copper model hosted by intermediate-mafic oxidised igneous rocks (nominally “andesite”) is shown below. In this case there has been insufficient erosion to expose the deposit. The top of the mineralisation lies 500m below the surface and the only sign of the mineralised system at the surface is a patch of propylitic alteration that could easily be overlooked or, if observed, assumed to be of little significance.

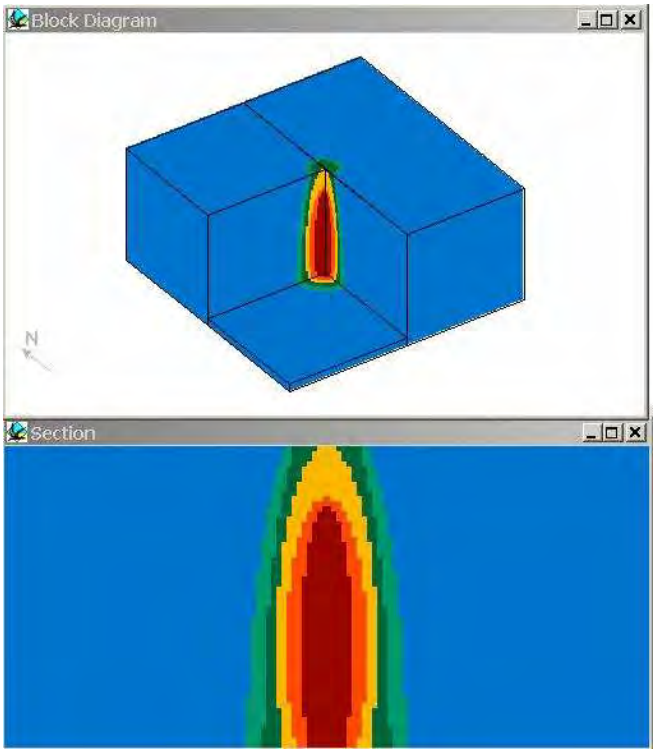

Gold-rich porphyry copper model, unexposed by erosion. Dark red is inner potassic zone, orange is outer potassic, yellow is phyllic (argillic), dark green is strong propylitic and light green is weak propylitic alteration. Host andesite is blue.

The inner potassic zone is strongly mineralised and magnetite-rich. It is surrounded by an outer potassic zone that contains less abundant, but still significant, magnetite. The inner potassic zone represents relatively intense development of quartz-magnetite-K feldspar veins, whereas the outer potassic zone corresponds to biotite- K feldspar-quartz-magnetite alteration. A shell of magnetite-destructive phyllic alteration with very low susceptibility envelops the potassic zones. At upper levels this alteration may grade into intermediate argillic and shallow advanced argillic alteration, but the magnetic properties are equivalent for these alteration types and a single shell is sufficient to model the effects. The phyllic zone is surrounded by a zone of intense propylitic alteration, which is partially magnetite-destructive, which passes out into weak propylitic alteration and then into unaltered andesite.

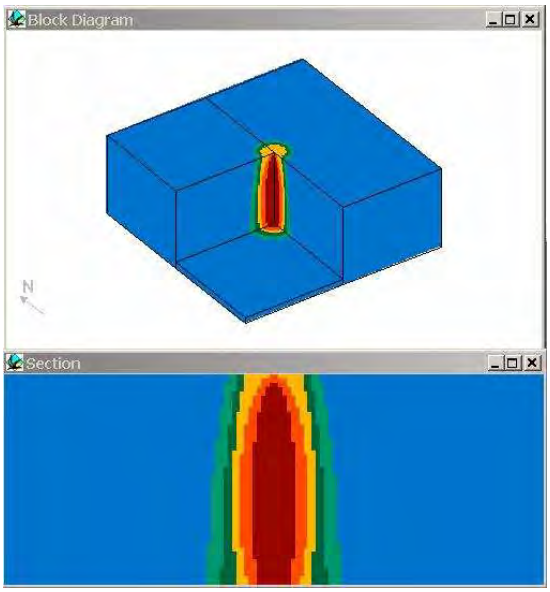

Gold-rich porphyry copper deposit after 500 m of erosion

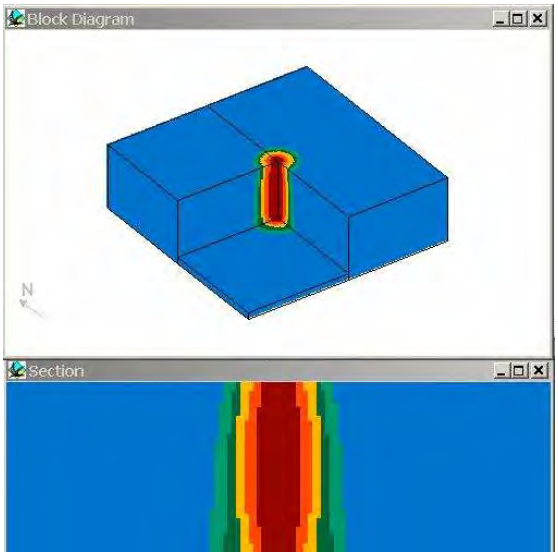

Gold-rich porphyry copper deposit exposed by 1000 m of erosion

After 500m of erosion a patch of phyllic, surrounded by propylitic, alteration is exposed, but the mineralisation is only subcropping. Removal of a 1 km thickness of rock exposes the mineralised core of the system and its surrounding alteration zones, as at Bajo de la Alumbrera.

The dimensions and susceptibilities of the zones are given below:

Zone	Diameter* (m)	Width* (m)	Depth extent (m)	Susceptibility (SI)
Inner potassic	360	360	2400	0.351
Outer potassic	600	120	2500	0.173
Phyllic	1000	200	3000	0.003
Strong propylitic	1200	100	3000	0.007
Weak propylitic	1500	150	3000	0.027
Andesite/Basalt/ Diorite/Gabbro	Very large	Very large	3000	0.043

* Diameters and widths of zones are maxima (at a depth 2000 m below the top of the phyllic zone for the propylitic and phyllic zones, and 1000 m below the top of the phyllic zone for the potassic zones).

Alternative models include deposits hosted by different country rocks, including unreactive sedimentary rocks (e.g. quartzites), and carbonates. Quartzites (unaltered and within the propylitic and phyllic zones) and unaltered carbonates have zero susceptibility. Magnetite-skarn, developed distally within a carbonate host, near the marble contact 700 m from the intrusion, is 100 m wide and has k = 0.2. The potassically altered intrusion has susceptibility 0.18, surrounded by phyllically altered intrusive with zero susceptibility.

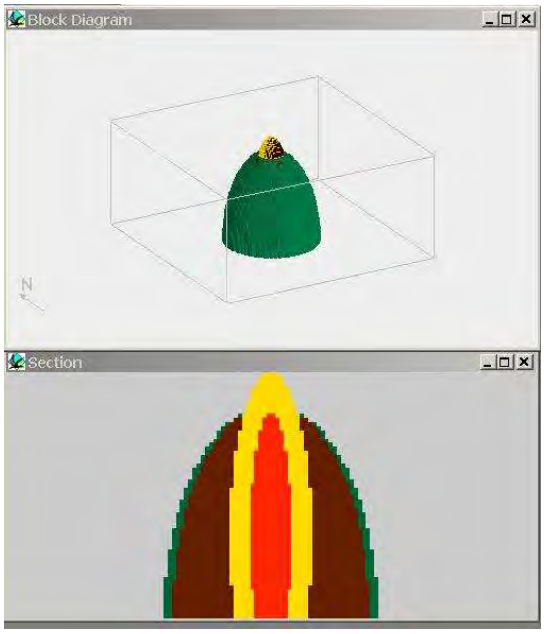

Carbonate host and marble (light grey); distal mt-skarn (green); proximal garnet skarn (brown); phyllic zone (yellow); potassic zone (red)

The RTP magnetic signatures for this type of model depend strongly on the level of exposure. For exposed systems within magnetic intermediate-mafic igneous host rocks, a strong central high is surrounded by a relatively weak annular low over the phyllic zone, gradually returning to background levels over the propylitic zone. For a completely buried system, however, the signature is basically an alteration low due to the large volume of magnetite-destructive alteration surrounding the deeply buried magnetic core. At intermediate levels of exposure a more complex pattern of a central high surrounded by an alteration low occurs, with the relative amplitude of the high and low dependent on the erosion level.

For quartzites and similar host rocks, on the other hand, the signature is a simple high over the mineralised, potassically altered intrusion, for all levels of exposure. The anomaly amplitude falls off with increasing depth of burial of the magnetic core.

The signature for felsic host rocks is intermediate between the signatures for mafic hosts and unreactive sedimentary host rocks, but the annular low around the central high is poorly developed, due to the relatively low magnetisation contrast between the magnetite-destructive alteration zones (phyllic and strong propylitic) and the unaltered felsic rocks. Carbonate host rocks have the central high, with highs also developed over magnetite-rich skarn zones.

The models above correspond to Au-rich porphyry Cu deposits with particularly well developed magnetite-rich potassic zones. Such deposits tend to be either relatively mafic systems in island arc environments or associated with alkaline (e.g. high-K calc-alkaline to shoshonitic) magmatism in continental settings. An alternative suite of models with lesser secondary magnetite was also produced. These models are more generally applicable to less strongly oxidised or relatively felsic systems, or low-medium K calc-alkaline associations, typically in areas with thick continental crust. The geometry of this type of model is illustrated below:

Gold-rich porphyry copper models - less developed potassic+magnetite alteration	
Buried	**Exposed**

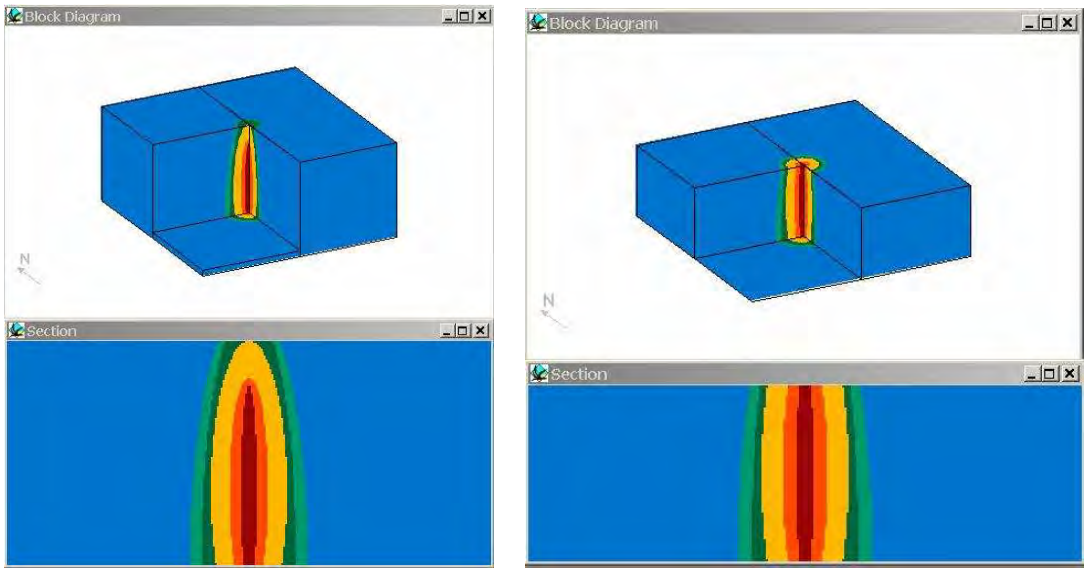

Inner and outer potassic zones are assigned susceptibilities of 0.18 and 0.08 respectively, corresponding to ~5 vol% (8.5 wt %) and 2.2 vol % (4 wt %) magnetite, which are typical values for the inner and outer potassic zones at Grasberg. Mafic-intermediate country rocks in outer zones have susceptibilities as given above. Felsic country rocks are assigned susceptibilities of 0.004 SI (unaltered), 0.003 (weak propylitic zone), 0.002 (strong propylitic zone) and 0.001 (phyllic zone).

A more realistic model of skarns developed within carbonates around a porphyry Cu-Au system consists of discrete magnetite-bearing skarn bodies, developed within favourable horizons and localised by overall zonation patterns and by structural controls. Models that incorporate discrete proximal and distal skarn bodies, in the inner garnet-rich zone and near the marble contact respectively, were developed. An example is shown below:

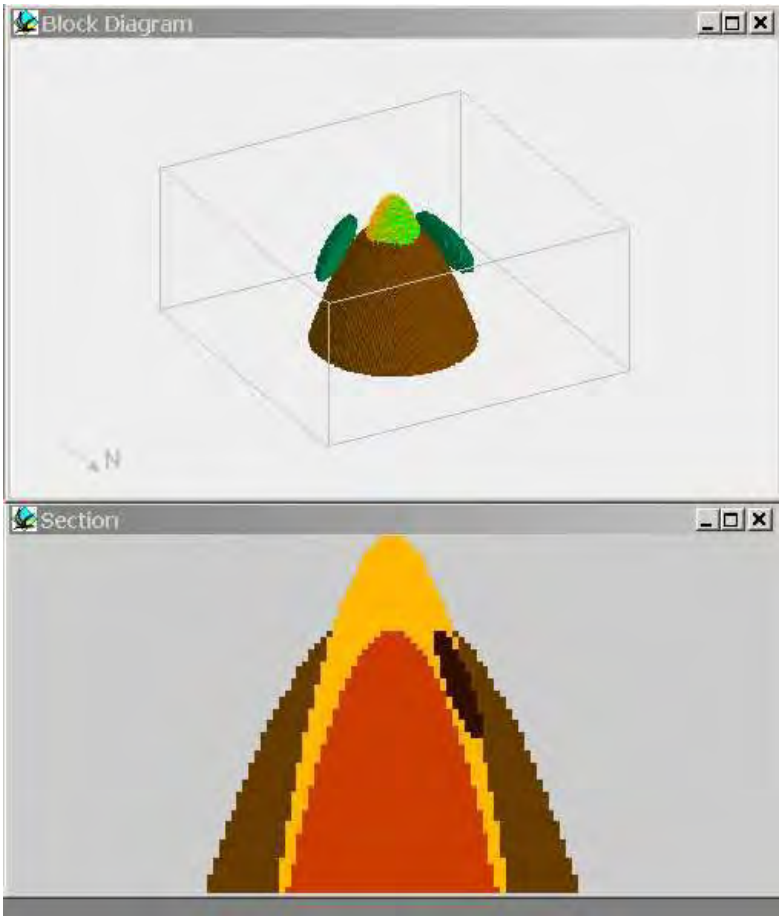

Porphyry Cu-Au model hosted by carbonate. Carbonate, main skarn zones and phyllically altered intrusion are non-magnetic. Potassically altered intrusion has k = 0.18. Distal Au-skarn has k = 0.3; proximal Cu-(Au) mt-skarn has k = 0.5.

12.2 Chilean (Atacama) Porphyry Copper Models

Giant porphyry copper deposits of the Chilean Andes are characterised by extensive magnetite-destructive alteration within their mineralised zones, which are surrounded by broad pyrite-rich propylitic halos. As a consequence of Late Tertiary-Recent physiography and climatic conditions of the Atacama desert they are generally overlain by thick supergene blankets that contribute much of their economic value. Supergene blankets are most developed over deposits that have abundant hypogene pyrite, which are also those that have the highest intensity and extent of magnetite-destructive alteration, such as phyllic, advanced argillic and sericite-chlorite alteration. Secondary magnetite is locally associated with early potassic alteration of relatively mafic rocks, but is much less developed than in gold-rich porphyry copper systems. The magnetic signatures are much weaker than those of gold-rich porphyry copper deposits and are distinctly different in character. The geometry of the basic Chilean porphyry copper model for an andesitic host is shown below. The Escondida deposit was used as a basis for this model (Padilla Garza et al. 2001).

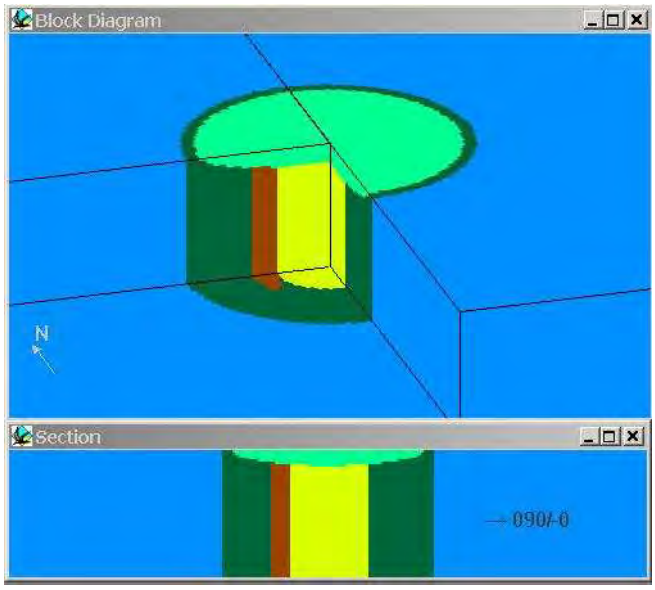

Chilean porphyry copper model (blue = andesite; olive = propylitic zone; brown = potassic; yellow = mt-destructive zone; pale green = supergene blanket)

The calc-alkaline andesitic rocks of this region generally have lower susceptibility than the high-K calc-alkaline to shoshonitic andesites of the Farallon Negro Volcanics that host the Alumbrera deposit, reducing the magnetisation contrast between the unaltered country rocks and the predominantly magnetite-destructive alteration within the deposit. The dimensions and susceptibilities of the zones are given below:

Zone	Diameter (m)	Width (m)	Depth extent (m)	Susceptibility (SI)
Mt-destructive Zone (phyllic, AA, ser-chl)	2600	2600	3500*	0.0001
Potassic		600×2000	3500*	0.018
Propylitic	6600	2000	4000	0.003
Supergene blanket	6000	6000	500*	0.0001
Andesite	Very large	Very large	4000	0.0055

* at thickest part of blanket

Alternative models include deposits hosted by different country rocks. The main categories considered in the Atlas are felsic igneous rocks, unreactive sedimentary rocks (e.g. quartzites), and carbonates. Felsic country rocks are assigned a susceptibility of 0.004 SI (unaltered), 0.002 (propylitic zone), 0.006 (potassic zone). Susceptibilities within the magnetite-destructive core and supergene blanket are as above (0.0001).

Carbonate host rocks and marble are assumed to have zero susceptibility. A 200 m wide skarn zone is assigned a susceptibility of 0.022. The 2600 m diameter magnetite-destructive zone has k = 0.0005. The supergene zone is more restricted in area, occurring only over mineralised igneous rocks rather than mineralised carbonates. Quartzite host rocks have zero susceptibility, including within the weakly developed propylitic zone. The local potassic zone is assigned a susceptibility of 0.001 and the magnetite-destructive core has k = 0.0005.

12.3 Quartz-monzonite Porphyry Copper Models

Quartz-monzonite type porphyry copper deposits that have substantial magnetite within their potassic zones are similar to the gold-rich porphyry copper models discussed above. These deposits tend to associated with intrusions that have lower sulphur contents than QM-type deposits that are characterised by extensive magnetite-destructive alteration. The Chilean-type porphyry copper models can be used to represent large, high sulphur QM-type deposits that have developed thick supergene blankets.

Areas that have thick continental crust that was underlain by a shallow subduction zone (e.g. the Laramide porphyry province of SW North America) tend to produce magmas with substantial crustal contamination, including high sulphur magmas. Such magmas often produce QM-type porphyry copper deposits with dominant magnetite-destructive alteration. Magnetite is relatively scarce in the potassic zones of such deposits, as it is mostly replaced by pyrite. For example, the Bingham Canyon porphyry Cu-Au-Mo deposit is notable among gold-rich porphyry coppers for having little magnetite within its potassic zone, which contains instead abundant pyrite.

For this type of deposit, the phyllic zones are well-developed in the intrusion and within suitable host rocks, and are surrounded by broad propylitic zones with extensive pyritisation of magnetite in country rocks. Thus the general signature of such deposits, if they are hosted by moderately or strongly magnetic rocks, is an alteration low. The situation is different if the intrusion is hosted by carbonate rocks. In this case extensive skarn formation occurs, often with associated zoned mineralisation. Some zones within the skarns tend to be strongly magnetic, producing a pronounced magnetisation contrast with both the weakly magnetic altered intrusion and unaltered sedimentary rocks.

The geometry of the high sulphur porphyry copper model hosted by andesitic rocks is shown below. In this case there has been insufficient erosion to expose the deposit. The top of the mineralisation lies 400m below the surface and the only sign of the mineralised system at the surface is a patch of propylitic alteration that could easily be overlooked or, if observed, assumed to be of little significance.

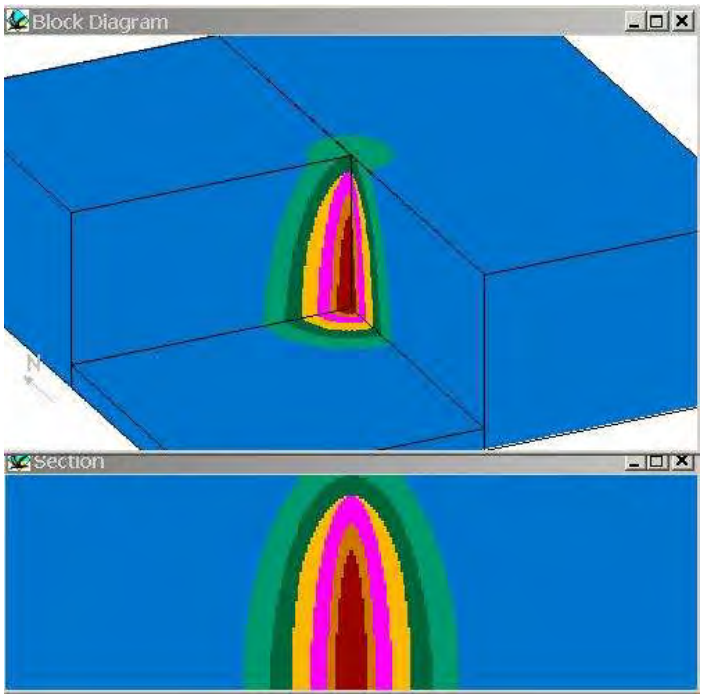

QM (high S) porphyry copper model, unexposed by erosion. Dark red is inner potassic zone, orange is outer potassic, pink is ore shell, yellow is phyllic (argillic), dark green is strong propylitic and light green is weak propylitic alteration. Host andesite is blue.

The dimensions and susceptibilities of the zones are given below:

Zone	Diameter* (m)	Width* (m)	Depth extent (m)	Susceptibility (SI)
Inner/deep potassic	600	600	2600	0.05
Outer/upper potassic	900	150	3100	0.0035
Ore shell	1500	300	3600	0.0025
Phyllic	2200	350	3600	0.003
Strong propylitic	3000	400	4000	0.003
Weak propylitic	4000	500	4000	0.015
Andesite	Very large	Very large	4000	0.03

* Diameters and widths of zones are maxima (at a depth 4000 m below the surface). The tops of the phyllic zone and ore shell are 400 m below the surface, the top of the outer/upper potassic zone is at 900m depth and the inner/deep potassic zone is buried 2400 m.

12.4 Alkalic Porphyry/Diorite Porphyry Models

Many alkalic porphyries and gold-rich porphyry copper systems in island arc and back-arc settings conform to the diorite model, i.e. the phyllic zone is suppressed and the potassic core passes outwards into propylitic alteration. Commonly, these deposits are hosted by mafic-intermediate rocks. In the Atlas, this type of deposit is represented by alkalic/diorite models of the type illustrated below. The mafic host rocks have a susceptibility of 0.05 SI. Weak propylitic, strong propylitic and potassic zones have susceptibilities of 0.04, 0.02 and 0.1 respectively. The potassic zone has a maximum diameter of 800m, at which depth the inner and outer propylitic zones are 200 m and 150 m wide respectively.

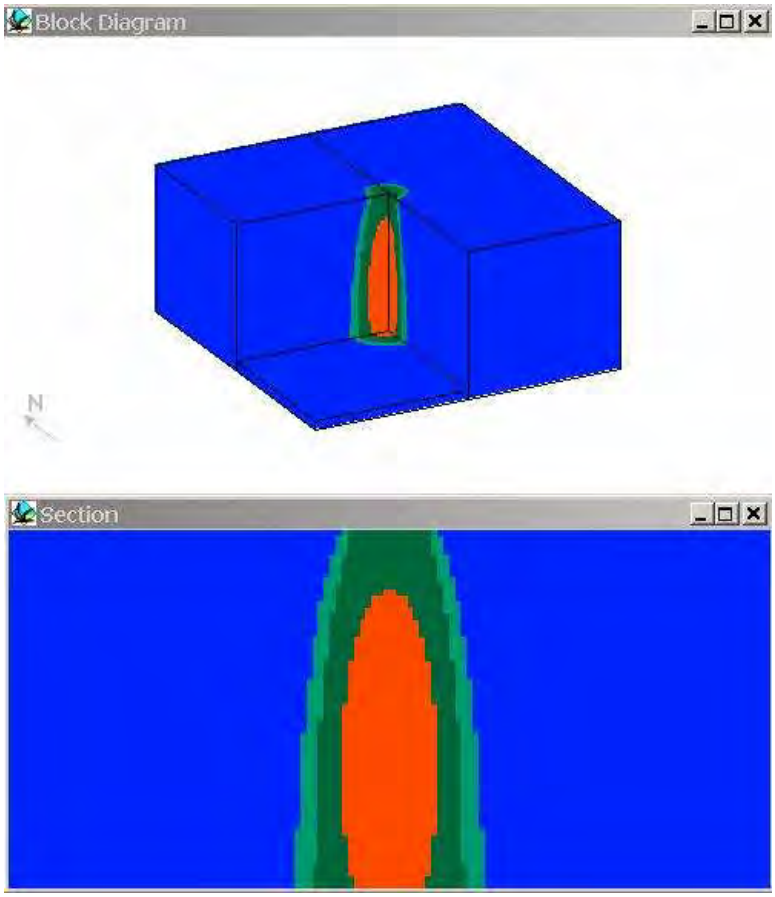

12.5 Inside-out Zoning Models

Porphyry systems formed at depth in batholithic settings tend to have zoning that is inside-out with respect to the classic Lowell-Guilbert pattern in their cores, i.e. the central zone is phyllically altered and is surrounded by potassic alteration, passing outwards into propylitic alteration. This type of zoning can result from emplacement along tectonically active structures, particularly intersecting structures, that remain active as the magmatic-hydrothermal system evolves. Phyllic alteration can then result either from evolved late-stage magmatic fluids injected into the deposit from below, or from meteoric fluids that descend along these structures during the waning phases of the hydrothermal system. The zones in this model are:

Zone	Diameter (m)	Width (m)	Depth extent (m)	Susceptibility (SI)
Inner QSP	200	400	2000	0
Chlorite zone	400	100	2000	0.007
Inner biotite	600	100	2000	0.047
Biotite-magnetite zone	3000	1200	2000	0.054
Quartz diorite	Very large	Very large	2000	0.047

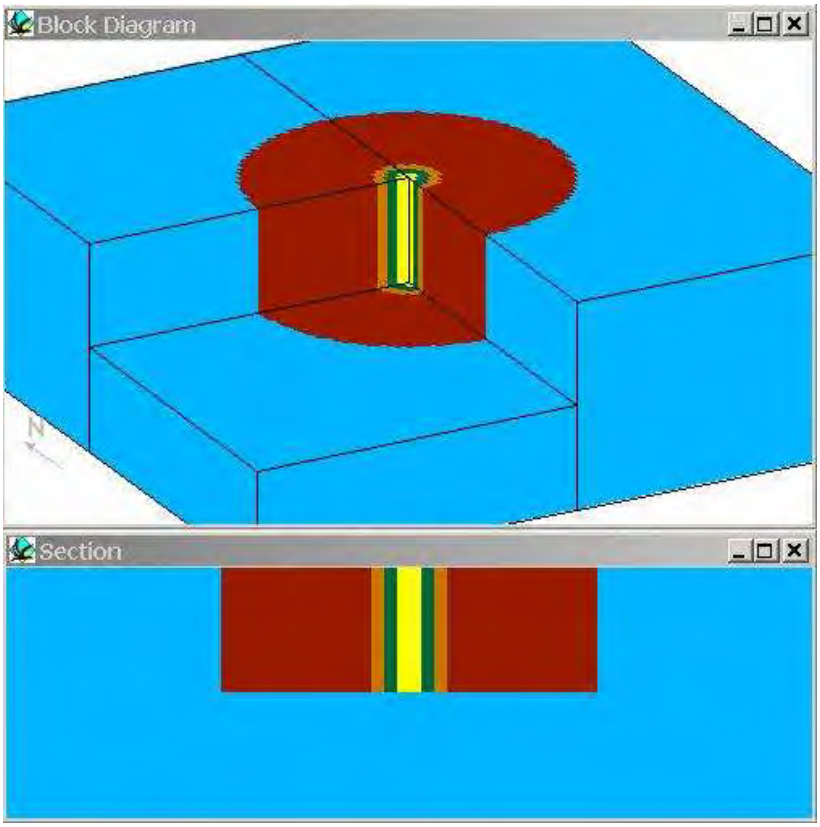

Batholithic porphyry deposit with inside-out zoning

Inside-out zoning also occurs with porphyry deposits of the volcanic morphological class. A classic example is afforded by the deposits of the Goonumbla Volcanic Complex. A simple model of this type of deposit is shown below.

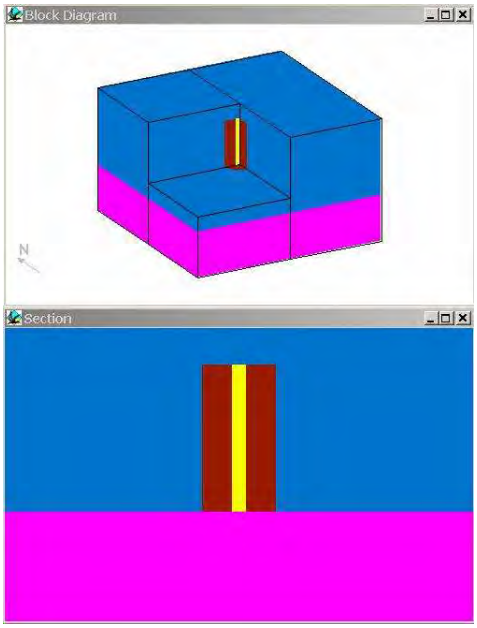

Volcanic model with inside-out zoning

The mafic-intermediate volcanic host rocks have susceptibility of 0.075 SI, the biotite zone (diameter 500 m) has k = 0.082 and the central phyllic zone (diameter 100 m has zero susceptibility). In this environment, the degree of development of the doughnout signature depends strongly on the width of the phyllic zone. In the GVC this is affected by the permeability of the host rocks, which is significantly greater for lavas than for volcaniclastic rocks. Profiles across a Goonumbla-type deposit with interlayed lava and volcaniclastic host rocks is shown below, with end members following.

RTP profile over a GVC-type deposit emplaced into interlayered lavas and volcaniclastics

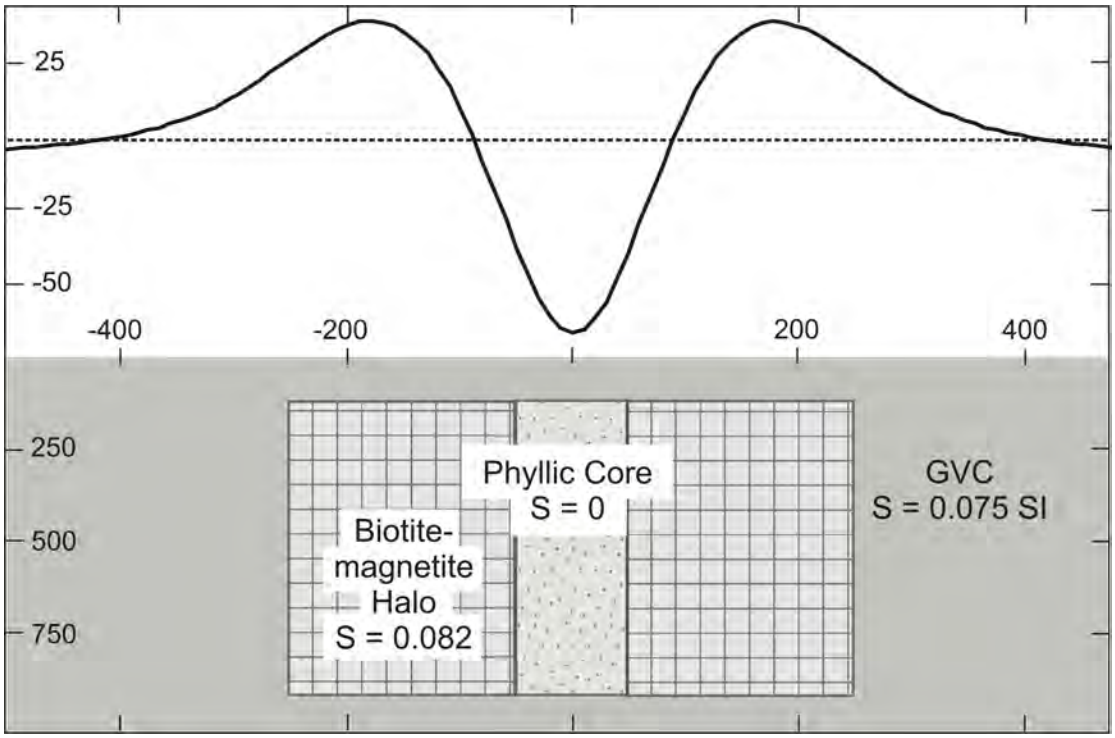

RTP profile over a GVC-type deposit emplaced into permeable, fractured lavas

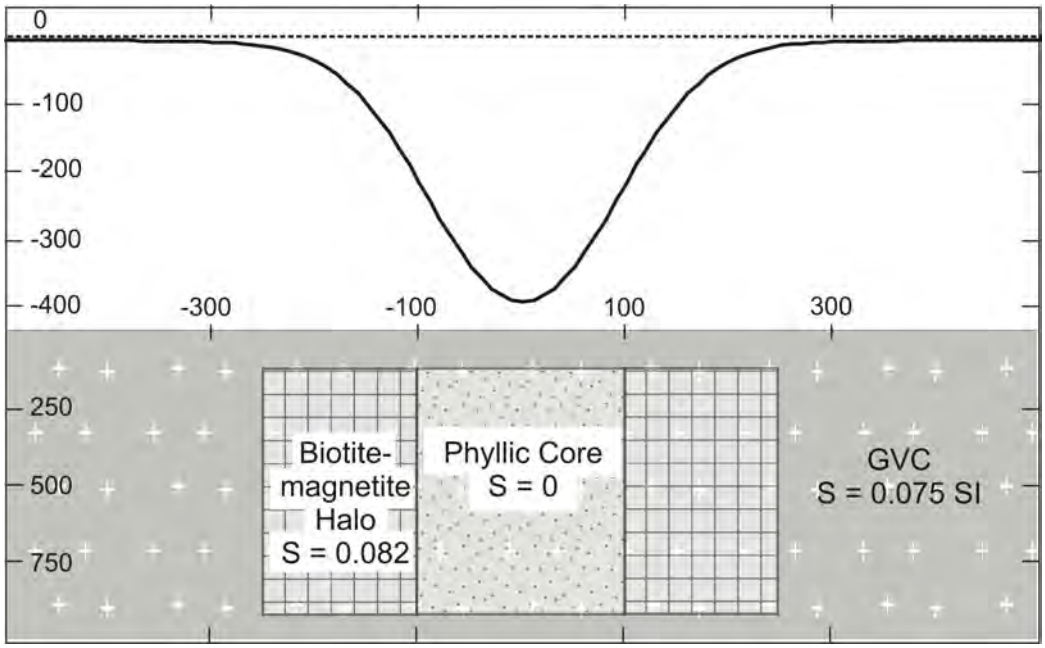

RTP profile over a GVC-type deposit emplaced into impermeable biotite-altered volcaniclastics

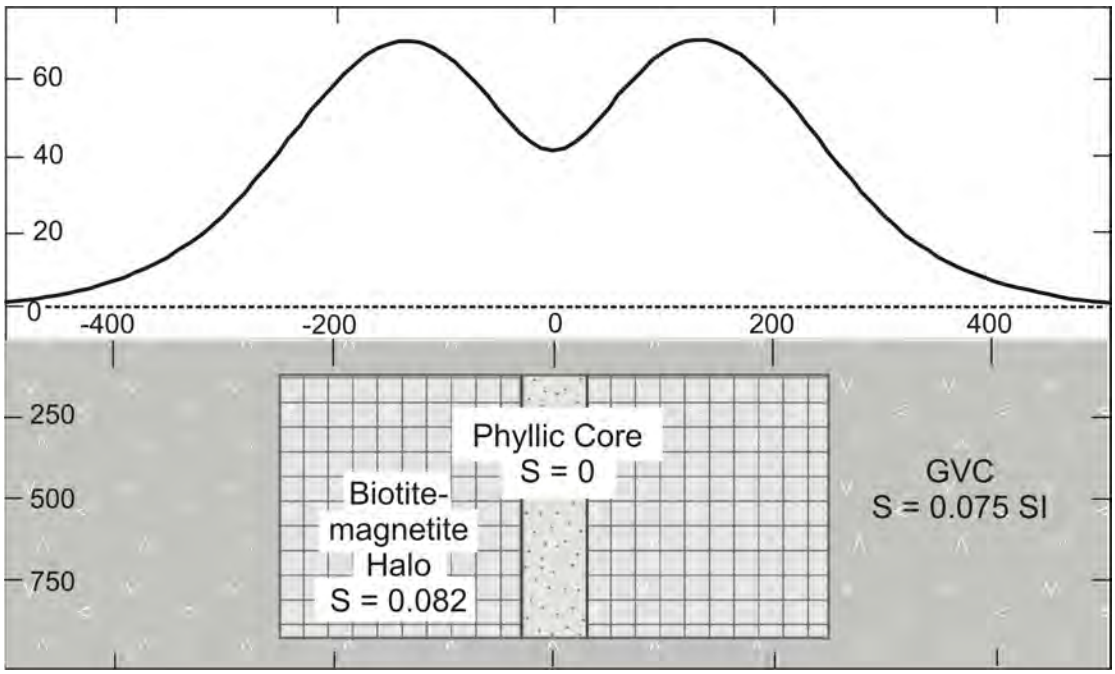

12.6 Reduced Porphyry Models

This model is based on deposits such as Copper Canyon, using magnetic property data on pyrrhotite-bearing rocks around the 17 Mile Hill deposit. It comprises a weakly magnetic (k = 0.001) reduced intrusion (pink) of maximum diameter 1000 m emplaced into weakly magnetic (k = 0.005) metasedimentary rocks (grey). A biotite hornfels (brown), 1100 m wide, of elevated susceptibility (k = 0.01) occurs around the intrusion. There is an enhanced pyrrhotite halo (yellow) of diameter 4000 m (i.e. 400 m wide) and susceptibility of 0.1, around the intrusion and hornfels. Distal massive pyrrhotite pods (orange), up to 400 m × 400 m× 200 m in size with effective k = 3.5 (including remanence), occur ~ 1 km from the margin of the intrusion.

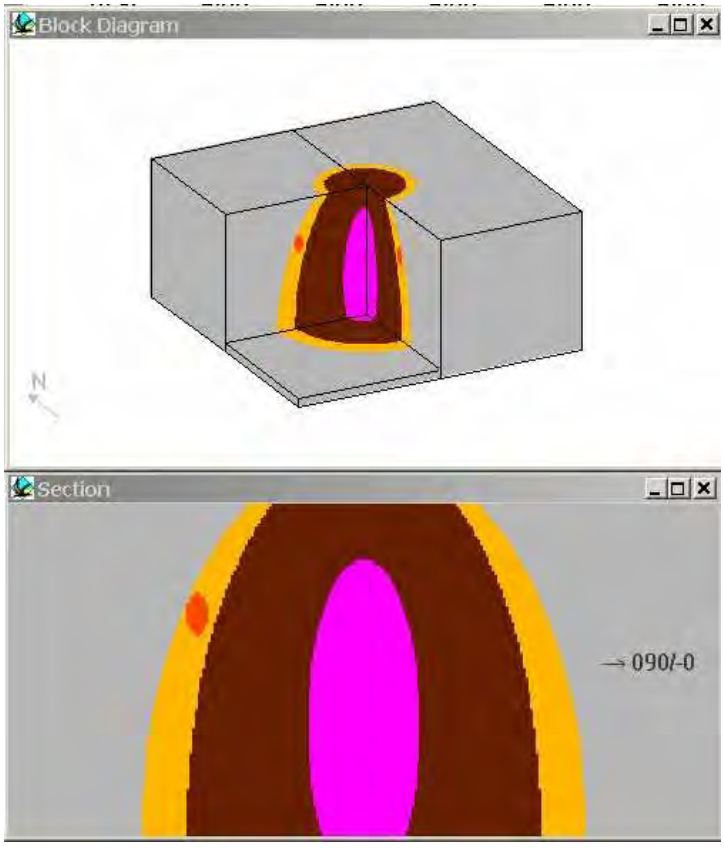

Reduced porphyry model with distal po-bearing mineralisation

12.7 Volcanic-hosted Epithermal Models

Epithermal models were based on information given by Bonham (1988) and Hedenquist et al. (1996). Both high-sulphidation and low-sulphidation epithermal systems are characterised by magnetite-destructive alteration in and around the mineralised zones, surrounded by propylitic alteration halos that are partially magnetite-destructive. Thus the magnetic signatures of the epithermal systems are generally smooth, flat magnetic lows within typically busy textured magnetic patterns of the host volcanics. The magnetisation contrast of the epithermal systems is therefore mainly dependent on the magnetisation of the unaltered host volcanics. Small epithermal systems, or those hosted by weakly magnetic volcanics, have indistinct magnetic signatures, whereas large systems within highly magnetic volcanics have easily detected signatures. Although the magnetic signature of the alteration system may be apparent, the location of the relatively small mineralised zones within the broader alteration envelope is usually difficult to pinpoint.

The geometry of the high-sulphidation epithermal model with a genetically linked deeper porphyry intrusion (possibly mineralised) is shown below, as a block model and long section. The model is analogous to the Lepanto-Far Southeast epithermal and porphyry deposits of the Phillipines, and other similar systems (Hedenquist et al., 1996).

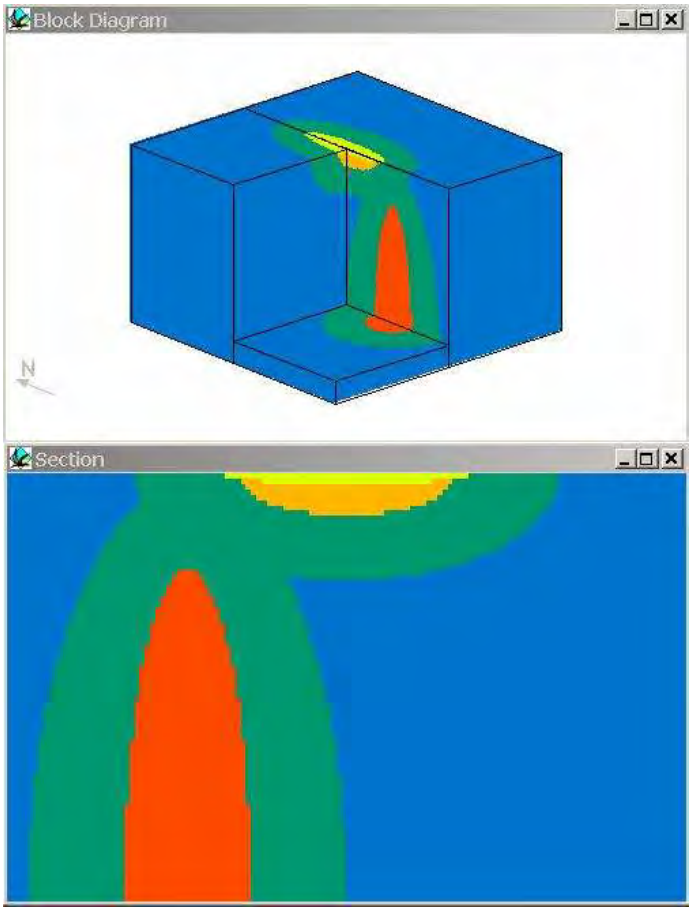

HS epithermal model (blue = andesitic host; green = propylitic alteration; red = porphyry intrusion with potassic alteration; dark yellow = mt-destructive alteration; pale yellow = acid-leached rock)

The dimensions and susceptibilities of the zones are given below:

Zone	Plan dimensions (m)	Width (m)	Depth extent (m)	Susceptibility (SI)
Acid-leached rock/silicification	2000 × 600	2000 × 600	100	0.0001
Mt-destructive zone (AA etc.)	1600 × 400	1600 × 400	300	0.0003
HS propylitic	4000 × 2000	800-1200	1000	0.021
Porphyry + Potassic	1200 × 1200	1200	3100	0.053
Porphyry-centred Propylitic	3000 × 3000	900	3900	0.021
Andesite Rhyolite	Very large	Very large	4000	0.047 0.003

Low-sulphidation epithermal systems are generally more distal to plutons that are the ultimate source of most of the metals, so in this case the model includes only the shallow epithermal alteration system, as shown below. Susceptibilities of corresponding zones are as given above. The block dimensions are also identical to the HS model. The adularia-sericite zone is 1600 m × 200 m in plan × 400 deep.

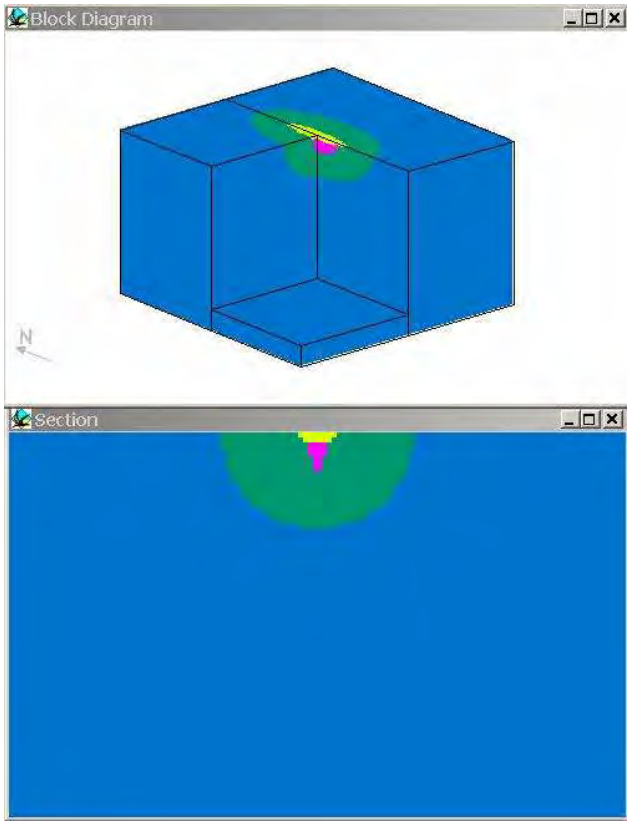

LS epithermal model (blue = andesitic host; green = propylitic zone; mauve = adularia-sericite alteration; yellow = acid-leached rock

12.8 Notes on Calculated Magnetic Signatures

Some signatures for specific models were calculated using ModelVision™ by ENCOM. The vast majority of models were calculated using the NODDY™ structural history-based modelling package. After checking of simple models against other packages and confirming the consistency of alternative calculation methods within NODDY for each basic model type, most models were calculated using the Fourier-based method, which was found to be quite accurate and much faster than the spatial convolution methods.

For each model the following signatures were calculated:

- Reduced-to-pole (RTP), which removes the effects of the geomagnetic inclination, provided remanence effects are negligible, and is the most useful presentation for high and moderate latitudes
- Reduced-to-equator (RTE), which produces more complex patterns, but provides a reasonable representation of predicted signatures in near equatorial regions, where RTP processing of observed data is impracticable
- Analytic signal (AS) of the RTP and RTE signatures, which emphasises areas with steep anomaly gradients, focusses on interfaces between regions of contrasting magnetisation and is relatively insensitive to remanence effects.

The calculated grids were exported in an ASCII format (Grid Exchange Format *. GXF). The analytic signal was calculated using a simple Fourier-based algorithm, without regularisation. Calculated AS images may therefore show some edge effects and in some cases are slightly noisy. Calculated signatures are presented as images (usually with linear stretches, unless specific features need to be emphasised with alternative stretches) and profiles, with some contour maps.

The analytic signal has the following features, some advantageous, others disadvantageous:

- AS has higher spatial resolution than RTP, emphasising shallow body boundaries and structural features,
- AS is much less sensitive to remanence effects than the RTP, so it can outline source geometry more reliably than RTP, if remanence is significant,
- On the other hand, dip information is degraded by the AS, whereas it is retained by RTP data, if the magnetisation direction is known, or correctly assumed,
- AS, like the TMI, is insensitive to N-S striking boundaries and structures in areas with shallow geomagnetic inclination. Thus radially symmetric sources, such as many of the porphyry models, produce asymmetric RTEAS signatures, whereas the same sources in high inclinations produce almost symmetric AS anomalies.
- Models with zoned or juxtaposed highs and lows are better resolved in the RTP images than the AS images. This is because the AS is indifferent to anomaly sign – RTP highs and lows both produce AS highs wherever the gradients are steep.

13. GEOPHYSICAL EXPLORATION CRITERIA FOR PORPHYRY, EPITHERMAL AND IRON OXIDE COPPER GOLD DEPOSITS

Indicators of tectonic setting

- In areas of extensive cover, regional potential field data sets, supplemented by seismic, magnetotelluric or other deep-penetrating methods, may be useful for delineating favourable geological environments for ore deposits of particular types.
- Subduction-related magmatic arcs are favourable settings for porphyry, epithermal and some, generally younger, ICOG deposits. These areas are characterised by linear parallel belts of gravity and magnetic highs and lows.
- Magnetic high zones correspond to belts of magnetite-series granitoids and are most favourable for porphyry Cu, Cu-Au, and Cu-Mo deposits, HS and LS epithermal deposits and ICOG deposits.
- Magnetic low belts may correspond to sedimentary basins (e.g. back arc basins), which can be recognised from their gravity lows, or to belts of reduced, ilmenite-series granitoids, which are prospective for Sn and also for intrusive-related Au and reduced porphyry Au-(Cu) deposits.
- Anorogenic settings, e.g. failed continental rifts and passive Atlantic-type continental margins, are favourable for ICOG deposits, particularly of Precambrian age. Buried terrains with this character may be recognisable from linear rift-parallel regional gravity and magnetic highs along the ancient continental margin, with a quiet magnetic zone outboard of the regional highs and relatively busy magnetic patterns inboard of the margin.
- Bimodal magmatism associated with anorogenic settings is characterised by contrasting highly magnetic and weakly magnetic intrusions, which are often evident in regional magnetic and gravity data.

Indicators of favourable structures

- at a regional scale major structures that control the emplacement of mineralising or heat-engine magmas, or channel flow of crustal fluids, are often evident in suitably processed gravity and magnetic data sets. These features may also be visible in satellite imagery. Intersections of lineaments appear to be particularly favourable for IOCG mineralisation.
- Structural controls at a range of scales, from province to prospect scale, may be evident in detailed magnetic data. Intersections of such lineaments appear to be favourable for porphyry and/or epithermal mineralisation.
- Identification of favourable orientations of structures may be possible if senses of movement, block rotations etc. are known. Anomaly offsets and abrupt changes of trend in magnetic images can help to define tectonic movements. Palaeomagnetic studies can also be useful for defining rotations and tilting within and around deposits.

Indicators of fractional crystallisation

- At a semi-regional scale, zoned plutons, with correspondingly zoned magnetic properties, densities and radioelement concentrations, are indicative of fractional crystallisation and suggest potential for development of magmatic-hydrothermal systems.
- Multiple/nested intrusions, with a substantial range of magnetic properties, densities and radioelement contents, particularly when there are geophysical indications of an underlying magma chamber , are also favourable indicators of fractional crystallisation.
- Well-developed contact aureoles are indicative of emplacement of high-temperature, melt-rich magma capable of undergoing substantial fractional crystallisation
- Strong contact aureole effects produce substantial mineralogical changes in the metamorphosed and metasomatised host rocks, often with pronounced changes in magnetic susceptibility (particularly increased susceptibility due to creation of secondary magnetite and/or pyrrhotite)
- strong remanent magnetisation of contact aureoles is diagnostic of high temperature emplacement or substantial metasomatism.

Understanding effects of primary composition and alteration on magnetic properties

- Understanding the effects of protolith composition and alteration type on magnetic properties is crucial for evaluating magnetic signatures of hydrothermal systems. Cu-Au is associated with more magnetic magmatic-hydrothermal systems than Cu-Mo; W-Mo-Bi and Au in tin provinces is much less magnetic. In oxidised Au-bearing systems, Au mineralisation is often associated with the felsic end of magmatic evolution and is then associated locally with a weaker magnetic character and higher radioelement contents.
- The P700 database is a tool for studying alteration effects on magnetic properties. Coupled with empirical observations and theoretical considerations, it has allowed generation of predictive models with plausible properties and geometries.
- Strong alteration zoning of magnetic character is favourable: early potassic alteration, particularly of mafic protoliths, is often magnetite-rich, contrasting strongly with phyllic overprinting, which is magnetite-destructive. Large zones of contrasting intense alteration suggest development and preservation of a mature hydrothermal system.

Superposed or Juxtaposed Gravity and Magnetic Anomalies

- Iron oxide copper-gold deposits occur within Fe-metasomatic systems that are typically zoned from magnetite-dominant to hematite-dominant.
- The primary zonation is usually from magnetite-dominant at depth to hematite-dominant at shallower levels, producing magnetic and gravity highs that are *superposed* not simply *coincident*, i.e. detailed analysis of the anomalies should reveal that the magnetic source is deeper than the gravity source.

- Tilting or faulting of an IOCG deposit may juxtapose the magnetite-dominant and hematite-dominant zones, producing *juxtaposed* gravity and magnetic anomalies
- Even without tilting or faulting, magnetite-enhanced alteration often occurs peripheral to hematite-dominant systems. This again will produce juxtaposed, rather than coincident, magnetic and gravity anomalies.
- Hematite-rich deposits that have undergone high-grade metamorphism to greater than ~650°C can be expected to carry intense remanence, with a strong magnetic anomaly. Either regional metamorphism to upper amphibolite-granulite grade or contact metamorphism due to a nearby intrusion could produce this effect. The form of the anomaly may be diagnostic of strong remanence, if the palaeofield recorded is oblique to the present field – which is very likely if the magnetisation is ancient.

Use of predictive models to prioritise targets

- The predictive models generated for the P700 Atlas are designed to assist recognition of deposit signatures that are appropriate for the local geological setting. Predicted signatures vary greatly depending on the deposit type, the host rocks, post-formation faulting or tilting and so on.
- The predictive models can also be used to assess the detectability of particular types of deposit in the local geological setting. For example, an intact gold-rich porphyry copper deposit buried beneath 100 m of magnetic volcanics should be detectable in most cases, whereas a typical giant porphyry copper of the Chilean Andes would be difficult to detect beneath such cover, although it should be visible beneath sedimentary overburden, provided it is emplaced into fairly magnetic rocks.
- The observed signatures depend not only on the local geological environment, but on local to semi-regional geomagnetic field gradients, which can distort the signatures substantially. The calculated grids generated for each model can be used to study the effects of geomagnetic field distortion and aid recognition of distorted signatures.

Other considerations

- Although magnetics can be a very useful tool for locating prospective hydrothermal systems, location of ore zones within the system often requires alternative methods. Electrical and, in some cases, electromagnetic methods, are generally more sensitive to sulphide-rich mineralisation.
- An empirical tendency for remanent magnetic signatures to be more common in mineralised intrusive systems than barren systems is suggested by case studies.
- Subtle alteration zoning of magnetic mineralogy may be detectable palaeomagnetically. For example the host rocks to the Mount Leyshon Au deposit carry syn-mineralisation overprints that are detectable well beyond the zone of visible alteration and are zoned from proximal magnetite to distal hematite.

14. ACKNOWLEDGMENTS

AMIRA International, in particular Mr Joe Cucuzza, are thanked for marketing of the P700 proposal and project management. Rio Tinto and BHP-Billiton supplied samples for inclusion in the database. Phelps Dodge, in particular Walter Martin and Candelaria mine staff are thanked for providing access to and data from the Candelaria deposit.

15. REFERENCES AND BIBLIOGRAPHY

Ade-Hall, J.M., Palmer, H.C. and Hubbard, T.P., 1971. The magnetic and opaque petrological response to regional hydrothermal alteration. Geophys. J. R. Astron. Soc., 24, 137-174.

Ague, J.J. and Brimhall, G.H., 1987. Granites of the batholiths of California: products of local assimilation and regional-scale crustal contamination. Geology, 15, 63-66.

Ague, J.J. and Brimhall, G.H., 1988a. Regional variations in bulk chemistry, mineralogy and the compositions of mafic and accesory minerals in the batholiths of California. Geol. Soc. Am. Bull., 100, 891-911.

Ague, J.J. and Brimhall, G.H., 1988b. Magmatic arc asymmetry and distribution of anomalous plutonic belts in the batholiths of California: effects of assimilation, crustal thickness, and depth of crystallization. Geol. Soc. Am. Bull., 100, 912-927.

Aguirre, L., 1974. Andean magmatism: its paleogeographic and structural setting in the central part (30°-35°S) of the Southern Andes. Pacific Geology, 8, 1-38.

Aguirre, L., 1983. Granitoids in Chile *in* J.A. Roddick (Ed.), Circum-Pacific Plutonic Terranes. Geol. Soc. Am. Memoir 159, 293-316 .

Albino, G.V., 1995. Porphyry copper deposits of the Great basin - Nevada, Utah, and adjacent California. *In*: F.W. Pierce and J.G. Bolm (Eds), Porphyry Copper Deposits of the American Cordillera. Arizona Geological Society Digest, 20, 267-296.

Allis, R.G., 1990. Geophysical anomalies over epithermal systems. J. Geochem. Explor., 36, 339-374.

Alva-Valdivia, L.M., Urrutia-Fucugauchi, J., Bo"hnel, H. and Morán-Zenteno, D.J., 1991. Aeromagnetic anomaliea and paleomagnetism in Jalisco and Michoachan, southern Mexico continental margin. Tectonophysics, 192, 169-190.

Anderson, R.G., 1985. An overview of some Mesozoic and Tertiary plutonic suites and their associated mineralization in the northern Canadian Cordillera *in* R.P. Taylor and D.F. Strong (eds), Granite-related Mineral Deposits, Geology, Petrogenesis and Tectonic Setting, CIM Geology Division.

Anderson, C.G. and Logan, K.J., 1992. The history and current status of geophysical exploration at the Osborne Cu & Au deposit, Mt. Isa. Explor. Geophys., 23, 1-8.

Andrew, A.S. and Baker, E.M., 1987. The nature of the ore-forming fluid in the Kidston gold deposit, north Queensland. Proceedings of the Pacific Rim 87 Congress, Gold Coast. Aus IMM, Melbourne, pp.13-16.

Arancibia, O.N. and Clark, A.H., 1995. Early magnetite-amphibole-plagioclase alteration-mineralization in the Island Copper porphyry copper-molybdenum-gold deposit, Vancouver Island, British Columbia. Econ. Geol., 91, 402-438.

Asami, N. and Britten, R.M., 1980. The porphyry copper deposits at the Frieda River prospect, Papua New Guinea. *In*: S. Ishihara and S. Takenouchi (Eds), Granitic Magmatism and Related Mineralization. Soc. Min. Geol. Japan, Special Issue 8, 117-140.

Atkinson, W.W. and Einaudi, M.T., 1978. Skarn formation and mineralization in the contact aureole at Carr Fork, Bingham, Utah. Econ. Geol., 1326-1365.

Babcock, R.C., Ballantyne, G.H. and Phillips, C.H., 1995. Summary of the geology of the Bingham district, Utah. *In*: F.W. Pierce and J.G. Bolm (Eds), Porphyry Copper Deposits of the American Cordillera. Arizona Geological Society Digest, 20, 316-335.

Bain, J.H.C., Oversby, B.S., MacKenzie, D.E., Moffat, P. and Withnall, I.W., 1985. Geology of the Georgetown region, Queensland. 1:250,000 Scale Map. BMR Australia.

Bajwah, Z.U., 1994. A contribution of geology, petrology and geochemistry to the Cullen Batholith and related hydrothermal activity responsible for mineralization, Pine Creek Geosyncline, Northern Territory. N.T. Geol. Surv, Report 8, 71p.

Bajwah, Z.U., 1994. Mineralogy and magnetic susceptibility of the Proterozoic granites, related to gold mineralisation, Pine Creek Geosyncline, Northern Territory, Australia. Proceedings of Aus. IMM Conference, Darwin, pp.57-67.

Baker, E.M. and Andrew, A.S., 1991. Geologic, fluid inclusion and stable isotope studies of the gold-bearing breccia hosted gold mineralization at Kidston, North Queensland, Australia. Econ. Geol., 86, 810-830.

Baker, E.M., 1987. Brecciation, mineralisation and alteration of the Kidston gold deposit. Proceedings of the Pacific Rim 87 Congress, Gold Coast. Aus IMM, Melbourne, pp.29-33.

Baker, E.M. and Andrew, A.S., 1988. Processes associated with the gold mineralisation within the Kidston Breccia Pipe, north Queensland. Proceedings of the Bicentennial Gold 88 Symposium, Melbourne, pp.102-109.

Baker, E.M. and Andrew, A.S., 1991. Geologic, fluid inclusion, and stable isotope studies of the gold-bearing breccia pipe at Kidston, Queensland, Australia. Econ. Geol., 86, 810-830.

Baker, E.M. and Tullemans, F.J., 1990. Kidston Gold Deposit. In: Geology of the Mineral Deposits of Australia and PNG (Ed F.E. Hughes), 1461-1465.

Ballantyne, G., Maughan, C.J. and Smith, T., 1995. The Bingham copper-gold-molybdenum deposit, Utah: why Bingham is a “super-giant”. *In*: A.H. Clark (Ed), Giant Ore Deposits - II, Controls on the Scale of Orogenic Magmatic-Hydrothermal Mineralization (Proceedings of the Second Giant Ore Deposits Workshop, Kingston, Ontario, Canada, April 25-27, 1995), pp. 334-349.

Balsey, J.R. and Buddington, A.F., 1958. Iron-titanium oxide minerals, rocks, and aeromagnetic anomalies of the Adirondack area, New York. Econ. Geol., 53, 777-805.

Banerjee, S.K., 1991. Magnetic properties of Fe-Ti oxides. In: Lindsley, D.H. (editor), Oxide minerals: petrologic and magnetic significance, Reviews in Mineralogy, 25, 489-509.

Barink, H.W., 1982. Decrease of cation-deficiency in rock-forming minerals as the cause of the retrogressive oxidation of accessory Fe-Ti oxides in deep-seated rocks; a new approach. N. Jb. Miner. Mh., H.1, 29-44.

Barker, F., 1981. Introduction to special issue on granites and rhyolites: a commentary for the nonspecialist. J. Geophys. Res., 86, 10,131-10,135.

Barton, P.B., 1984. Redox reactions in hydrothermal fluids. *In*: R.W. Henley, A.H. Truesdell and P.B. Barton, Fluid-mineral Equilibria in Hydrothermal Systems. Reviews in Economic Geology, v. 1, 99-113.

Barton, P.B. and Skinner, B.J., 1979. Sulifide mineral stabilities. *In*: Barnes, H.L. (Ed), Geochemistry of Hydrothermal Ore Deposits, Second Edition. Wiley-Interscience, New York, 278-403.

Bateman, P.C., 1983. A summary of critical relations in the Sierra Nevada batholith, California, U.S.A. *in* J.A. Roddick (Ed.), Circum-Pacific Plutonic Terranes. Geol. Soc. Am. Memoir 159, 241-254.

Bateman, P.C. and Chappell, B.W., 1979. Crystallization, fractionation, and solidification of the Tuolumne Intrusive Series, Yosemite National Park, California. Geol. Soc. Am. Bull., 90, 465-482.

Bateman, P.C. and Dodge, F.C.W., 1970. Variations of major chemical constituents across the central Sierra Nevada batholith. Geol. Soc. Am. Bull., 81, 409-420.

Bateman, P.C., Dodge, F.C.W. and Kistler, R.W., 1991. Magnetic susceptibility and relation to initial $^{87}Sr/^{86}Sr$ for granitoids of the central Sierra Nevada, California. J. Geophys. Res., 96, 19,555-19,568.

Battles, D.A., 1991. Hydrothermal alteration within the tilted Shamrock batholith, Yerington district, Nevada. *In*: Raines, G.L., Lisle, R.E., Schafer, R.W. and Willkinson, W.H., 1991 (Eds), Geology and Ore Deposits of the Great Basin (Symposium Proceedings, Reno, Nevada, April 1-5, 1990). Geol. Soc. Nevada, Reno, 351-353.

Beams, S.D., 1994. Geology and petrography of the Permian Tuckers Igneous Complex, Ravenswood Block, North Queensland. Report on field project for AMIRA P425.

Beane, R.E., 1994. A graphic view of hydrothermal mineral stability relations. *In*: D.R. Lentz (Editor), Alteration and Alteration Processes Associated with Ore-forming Systems. Geological Association of Canada Short Course Notes, v.11, 1-30.

Beane, R.E. and Titley, S.R., 1981. Porphyry copper deposits Part II. Hydrothermal alteration and mineralization. Econ. Geol., 75th Anniversary Volume, 235-269.

Behn, G., Camus, F., Carrasco, P. and Ware, H., 2001. Aeromagnetic signature of porphyry copper systems in northern Chile and its geologic implications. Econ. Geol., 96, 239-248.

Blakely, R.J. and Jachens, R.C., 1990. Concealed mineral deposits in Nevada - insights from three-dimensional analysis of gravity and magnetic anomalies. *In*: Raines, G.L., Lisle, R.E., Schafer, R.W. and Willkinson, W.H., 1991 (Eds), Geology and Ore Deposits of the Great Basin (Symposium Proceedings, Reno, Nevada, April 1-5, 1990). Geol. Soc. Nevada, Reno, 185-192.

Bleil, U. and Petersen, N., 1982. Magnetic properties of minerals *in* G. Angenheister (ed), Physical Properties of Rocks, Landolt-Bornstein Numerical Data and Functional Relationships in Science and Technology, Group V, Volume 1b. Springer-Verlag, Berlin.

Blevin, P.L., 1994a. Magnetic susceptibility of the Lachlan Fold Belt and New England Batholith granites. AMIRA Project P147B Final Report.

Blevin, P.L., 1994b. Identification of favourable exploration/resource areas in eastern Australia using magma compositions. New Developments in Geology and Metallogeny: Northern Tasman Orogenic Zone, Conference Proceedings, Townsville, 137-140.

Blevin, P.L., 1996. Using magnetic susceptibility meters to interpret the oxidation state of granitic rocks. 13th Australian Geological Convention, Geol. Soc. Aust., Abstracts, 41, 40.

Blevin, P.L., 1996. Chemical matching of intrusives related to gold mineralisation in North Queensland -final report. AMIRA P425 Report, May 1996.

Blevin, P.L. and Chappell, B.W., 1991. Relationships between granites and mineral deposits in the Lachlan Fold Belt.

Blevin, P.L. and Chappell, B.W., 1993. The influence of fractionation and magma redox on the distribution of mineralisation associated with the New England Batholith. *In*: Blevin, P.L. and Chappell, B.W., 1996. Controls on the distribution and character of the intrusive-metallogenic provinces of eastern Australia. 13th Australian Geological Convention, Geol. Soc. Aust., Abstracts, 41, 42.

Blevin, P.L. and Chappell, B.W., 1991. Some fundamental parameters in granitoid metallogeny: an eastern Australian perspective *in* Second Hutton Symposium on Granites and Related Rocks, BMR Record 1991/25, 10.

Blevin, P.L. and Chappell, B.W., 1992. The role of magma sources, oxidation states and fractionation in determining the granite metallogeny of eastern Australia: Trans. Roy. Soc. Edinburgh, Earth Sciences, 83, 305-316.

Blevin, P.L. and Chappell, B.W., 1995. Chemistry, origin and evolution of mineralized granites in the Lachlan Fold Belt, Australia; the metallogeny of I- and S-type granites: Econ. Geol., 90, 1604-1619.

Blevin, P.L., Chappell, B.W. and Allen, C.M., 1996. Intrusive metallogenic provinces in eastern Australia based on granite source and composition. Trans. Roy. Soc. Edinburgh, Earth Sciences, 87, 281-290.

Blevin, P.L., Candela, P.A. and Chappell, B.W., 1996. Magmatic controls on ore metal ratios across the Cu-Mo(Au) “porphyry” spectrum. 13th Australian Geological Convention, Geol. Soc. Aust., Abstracts, 41, 41.

Blevin, P.L., Morrison, G.W. and Chappell, B.W., 1997. Magmatic and Hydrothermal Evolution of Major Intrusive Related Gold Deposits: P425 Abstracts and Attachments for Final Meeting.

Bonham, H.F., 1988. Models for volcanic-hosted epithermal precious metal deposits. *In*: Schafer, R.W., Cooper, J.J. and Vikre, P.G. (Eds), Bulk Mineable Precious Metal Deposits of the Western United States. Geological Society of Nevada, Reno, 259-271.

Borisov, A.A. and Shapkin, A.I., 1990. A new empirical equation relating Fe^{3+}/Fe^{2+} in magmas to their composition, oxygen fugacity and temperature. Geochemistry International, 6, 111-116.

Bowden, P., Batchelor, R.A., Chappell, B.W., Didier, J. and Lameyre, J., 1984. Petrological, geochemical and source criteria for the classification of granitic rocks: a discussion: Phys. Earth. Planet. Inter., 35, 1-11.

Brant, A.A., 1966. Geophysics in the exploration for Arizona porphyry coppers. *In*: S.R. Titley and C.L. Hicks (Eds), Geology of the Porphyry Copper Deposits, Southwestern North America. University of Arizona Press, Tucson.

Brooks, J.W., Meinert, L.D., Kuyper, B.A. and Lane, M.L., 1991. Petrology and geochemistry of the McCoy gold skarn, Lander County, Nevada. *In*: Raines, G.L., Lisle, R.E., Schafer, R.W. and Willkinson, W.H., 1991 (Eds), Geology and Ore Deposits of the Great Basin (Symposium Proceedings, Reno, Nevada, April 1-5, 1990). Geol. Soc. Nevada, Reno, 419-442.

Brown, G.C., Thorpe, R.S. and Webb, P.C., 1984. The geochemical characteristics of granitoids in contrasting arcs and comments on magma sources. J. Geol. Soc. London, 141, 413-426.

Browne, P.R.L., 1978. Hydrothermal alteration in active geothermal fields. Ann. Rev. Earth Sci., 6, 229-250.

Buddington, A.F., 1951. Chemical petrology of some metamorphosed Adirondack gabbroic, syenitic and quartz syenitic rocks. Am J. Sci., Bowen Volume, 37-84.

Buddington, A.F. and Lindsley, D.H., 1964. Iron-titanium oxide minerals and synthetic equivalents. J. Petrology, 5, 310-357.

Burkhard, D.J.M., 1991. Temperature and redox path of biotite-bearing intrusives: a method of estimation applied to S- and I-type granites from Australia. Earth Planet. Sci. Lett., 104, 89-98.

Burnham, C.W., 1979. Magmas and hydrothermal fluids. *In*: Barnes, H.L. (Ed), Geochemistry of Hydrothermal Ore Deposits, Second Edition. Wiley-Interscience, New York, 71-136.

Burnham, C.W., 1997. Magmas and hydrothermal fluids. *In*: Barnes, H.L. (Ed), Geochemistry of Hydrothermal Ore Deposits, Third Edition. Wiley, New York, 63-123.

Burnham, C.W. and Ohmoto, H., 1980. Late stage processes of felsic magmatism. Mining Geology Special Issue, 8, 1-11.

Butler, R.F., 1992. Paleomagnetism: Magnetic Domains to Geologic Terranes. Blackwell, Boston, 319pp.

Cameron, E.M. and Carrigan, W.J., 1987. Oxygen of Archean felsic magmas: relationship to gold mineralization. Geol. Surv. Canada, Paper 87-1A, 281-298.

Cameron, E.M. and Hattori, K., 1987. Archean gold mineralization and oxidised hydrothermal fluids. Econ. Geol., 82, 1177-1191.

Cameron, G.H., Walshe, J.L., Heinrich, C.A. and Wall, V.J., 1996. Gold mineralization at the Porgera gold mine, Papua New Guinea, in response to adiabatic decompression and fluid mixing along the Roamane fault.

Candela, P.A., 1986. The evolution of aqueous vapour from igneous melts: effect on oxygen fugacity. Geochim. Cosmochim. Acta, 50, 1205-1211.

Candela, P.A., 198?. Felsic magmas, volatiles, and metallogenesis. *In*: Whitney, J.A. and Naldrett, A.J. (Eds), Ore Deposition Associated With Magmas. Rev. Econ. Geol., 4, 223-233.

Candela, P.W., 1991a. Controls on metal ratios in granite-related ore systems: an experimental and computational approach *in* Second Hutton Symposium on Granites and Related Rocks, BMR Record 1991/25, 10.

Candela, P.A., 1991b. Physics of aqueous phase evolution in plutonic environments. Am. Mineral., 76, 1081-1091.

Candela, P.A. and Blevin, P.L., 1995a. Physical and chemical controls on the size of magmatic-hydrothermal ore deposits. In: A.H. Clark (Ed), Giant Ore Deposits - II, Controls on the Scale of Orogenic Magmatic-Hydrothermal Mineralization (Proceedings of the Second Giant Ore Deposits Workshop, Kingston, Ontario, Canada, April 25-27, 1995), pp.2-42.

Candela, P.A. and Blevin, P.L., 1995b. Do some miarolitic granites preserve evidence of magmatic volatile phase permeability? Econ. Geol., 90, 2310-2316.

Cannon, R.L., Dave, J.V., Bezdek, J.C., and Trivedi, MM., 1986. Segmentation of a Thematic Mapper Image Using the Fuzzy C-Means Clustering Algorithm. IEEE Transactions on Geoscience and Remote Sensing, GE-24(3), 400-408.

Carlile, J.C. and Mitchell, A.H.G., 1994. Magmatic arcs and associated gold and copper mineralization in Indonesia. J. Geochem. Explor., 50, 91-142.

Carmichael, I.S.E., 1967. The iron-titanium oxides of salic volcanic rocks and their associated ferromagnesian silicates. Contrib. Mineral. Petrol., 14, 36-64.

Carmichael, I.S.E., 1972. The occurrence of magnesian pyroxene and magnetite in porphyritic acid glasses.

Carmichael, I.S.E., 1991. The redox states of basic and silicic magmas: a reflection of their source regions. Contrib. Mineral. Petrol., 106, 129-141.

Carroll, M.R. and Rutherford, M.J., 1985. Sufide and sulfate saturation in hydrous silicate melts. J. Geophys. Res., 90 (Supplement), C601-C612.

Carten, R.B., 1986. Sodium-calcium metasomatism: chemical, temporal and spatial relationships at the Yerington, Nevada, porphyry copper deposit. Econ. Geol., 81, 1495-1519.

Carten, R.B., White, W.H. and Stein, H.J., 1993. High-grade granite-related molybdenum systems: classification and origin. *In*: R.V. Kirkham, W.D. Sinclair, R.I. Thorpe and J.M. Duke (Eds), Mineral Deposit Modelling. Geological Association of Canada, Special Paper 40, 465-478.

Champion, D.C. and Heinemann, M.A., 1994. Igneous rocks of northern Queensland: 1:500 000 map and GIS explanatory notes. AGSO Record 1994/11.

Chappell, B.W., 1990. Granites and tectonics. Geol. Soc. Aust. Abstracts, 25, 260-261.

Chappell, B.W., 1991. Tectonic evolution of the Lachlan Fold Belt: petrological constraints.

Chappell, B.W. and Stephens, W.E., 1988. Origin of infracrustal (I-type) granite magmas. Trans. Roy. Soc. Edinburgh: Earth Sci., 79, 71-86.

Chappell, B.W. and White, A.J.R., 1974. Two contrasting granite types. Pac. Geol., 8, 173-174.

Chappell, B.W. and White, A.J.R., 1976. Plutonic rocks of the Lachlan Mobile Zone. 25th Int. Geol. Conf., Excursion Guide 13C, 40 pp.

Chappell, B.W., White, A.J.R. and Hine, R., 1988. Granite provinces and basement terranes in the Lachlan Fold Belt, southeastern Australia. Aust. J. earth Sci., 35, 505-521.

Chappell, B.W., White, A.J.R. and Williams, I.S., 1991. A transverse section through granites of the Lachlan Fold Belt. Second Hutton Symposium Excursion guide. BMR Record 1991/22.

Cheney, E.S. and Trammell, J.W., 1996. The “inside-out” Quartz Creek quartz dioritic, batholithic, copper deposit, central Cascade Range, Washington. *In*: A.R. Coyner and P.L. Fahey (Eds), Geology and Ore Deposits of the American Cordillera. Geol. Soc. Nevada Symposium Proceedings, p.1521-1532.

Chernyuk, M.V., 1971. Distribution of the magnetic susceptibility values of intrusive rocks. Izv. Phys. Solid Earth, 3, 225-229.

Chi, G.X., Guha, J. and Lu, H.Z., 1993. Separation mechanisms in the formation of proximal and distal tin polymetallic deposits, Xinlu ore field, southern China - evidence from fluid inclusion data. Econ. Geol., 88, 916-933.

Chinner, G.A., 1960. Pelitic gneisses with varying ferrous/ferric ratios from Glen Clova, Angus, Scotland. J. Petrology, 1, 178-217.

Chivas, A.R., 1981a. Geochemical evidence for magmatic fluids in porphyry copper mineralization. Part I. Mafic silicates from the Koloula Igneous Complex. Contrib. Mineral. Petrol., 78, 389-403.

Chivas, A.R., 1981b. Geochemical evidence for magmatic fluids in porphyry copper mineralization. Part II. Ion-probe analysis of Cu contents of mafic minerals, Koloula Igneous Complex. Contrib. Mineral. Petrol., 78, 389-403.

Clark, A.H., 1993. Are outsize porphyry copper deposits either anatomically or environmentally distinctive? *In*: Whiting, B.H., Mason, R. and Hodgson, C.J. (Eds), Giant Ore Deposits, Society of Economic Geologists, Special Publication 2, pp. 213-284.

Clark, A.H. and Arancibia, O.N., 1995. The occurrence, paragenesis and implications of magnetite-rich alteration-mineralization in calc-alkaline porphyry copper deposits. *In*: A.H. Clark (Ed), Giant Ore Deposits - II, Controls on the Scale of Orogenic Magmatic-Hydrothermal Mineralization (Proceedings of the Second Giant Ore Deposits Workshop, Kingston, Ontario, Canada, April 25-27, 1995), pp. 583-640.

Clark, D.A., 1983a. Comments on magnetic petrophysics. Bulletin of the Australian Society of Exploration Geophysicists, 14, 40-62.

Clark, D.A., 1983b. Magnetic Properties of Pyrrhotite - Applications to Geology and Geophysics. M.Sc. Thesis, University of Sydney, 256 pp.

Clark, D.A., 1984a. Hysteresis properties of sized dispersed monoclinic pyrrhotite grains. Geophys. Res. Lett., 11:173-176.

Clark, D.A., 1984b. Magnetic petrophysics of pyrrhotite-bearing rocks. CSIRO Division of Mineral Physics Restricted Investigation Report 1531R.

Clark, D.A., 1984c. Crystallography and mineralogy of the pyrrhotite group. CSIRO Division of Mineral Physics Restricted Investigation Report 1557R.

Clark, D.A., 1985. Intrinsic magnetic properties of pyrrhotite. CSIRO Division of Mineral Physics Restricted Investigation Report 1571R.

Clark, D.A., 1987. Theoretical rock magnetism of monoclinic pyrrhotite. CSIRO Division of Mineral Physics and Mineralogy Restricted Investigation Report 1693R.

Clark, D.A., 1988. Magnetic properties and magnetic signatures of the Trough Tank and Starra copper-gold deposits, Eastern Mt Isa Block. CSIRO Division of Mineral Physics and Mineralogy Restricted Investigation Report 1745R, 50p.

Clark. D.A., 1994. Magnetic properties and magnetite contents of ores from the Ernest Henry deposit, eastern Mount Isa Inlier. CSIRO Division of Exploration and Mining Report 23C, 79p.

Clark, D.A., 1996. Palaeomagnetism of the Mount Leyshon Intrusive Complex, the Tuckers Igneous Complex and the Ravenswood Batholith. CSIRO Exploration and Mining Report 318R, 141p.

Clark (1996). Palaeomagnetism of the Mount Leyshon Intrusive Complex, the Tuckers Igneous Complex and the Ravenswood Batholith. CSIRO Exploration and Mining Report 266R.

Clark, D.A., 1997. Magnetic petrophysics and magnetic petrology: Aids to geological interpretation of magnetic surveys: AGSO J. Aust. Geol. Geophys., 17, 83-103.

Clark, G.H., 1990. Panguna copper-gold deposit. *In*: F.E. Hughes (Ed.), Geology of the Mineral Deposits of Australia and Papua New Guinea, Aus. IMM, Melbourne, 1807-1816.

Clark, K.A., 1982. Mineral composition of rocks. In: R.S. Carmichael (Ed), CRC Handbook of Physical Properties of Rocks, Volume I, pp.1-215.

Clark, D.A. and Dickson, B.L.,1996. Magnetic and radiometric properties of the Mount Leyshon Intrusive Complex, the Tuckers Igneous Complex and the Ravenswood Batholith: implications for magnetic and radiometric interpretation. CSIRO Exploration and Mining Restricted Report 266R, 59p. + 2 floppy discs.

Clark, D.A. and Emerson, D.W., 1991. Notes on rock magnetization characteristics in applied geophysical studies: Explor. Geophys., 22, 547-555.

Clark, D.A. and Schmidt, P.W., 1993. Magnetic petrophysics, palaeomagnetism and tectonic rotations of the Porgera Intrusive Complex, Papua New Guinea. CSIRO Division of Exploration Geoscience Restricted Report 364R.

Clark, D.A. and Schmidt, P. W., 1994. Magnetic properties and magnetic signatures of BIFs of the Hamersley Basin and Yilgarn Block, Western Australia. *In*: Dentith, M.C., Frankombe, K.F., Ho, S.E., Shepherd, J.M., Groves, D.I. and Trench, A. (Eds), Geophysical Signatures of Western Australian Mineral Deposits. Geology and Geophysics Department (Key Centre) & UWA Extension, The University of Western Australia, Publication 26, and A.S.E.G. Special Publication 7, 343-354.

Clark, D.A. and Schmidt, P.W., 2001. Petrophysical properties of the Goonumbla Volcanic Complex, NSW: Implications for magnetic and gravity signatures of porphyry Cu-Au mineralisation. Explor. Geophys., 32, 171-175.

Clark, D.A. and Tonkin, C., 1987. Magnetic properties of ironstones and host rocks from the Tennant Creek area. CSIRO Division of Mineral Physics and Mineralogy Restricted Investigation Report 1691R, 124p.

Clark, D.A. and Tonkin, C., 1994. Magnetic anomalies due to pyrrhotite: examples from the Cobar area, N.S.W., Australia. Journal of Applied Geophysics, 32, 11-32.

Clark, D.A., French, D.H., Lackie, M.A. and Schmidt, P.W., 1992a. Rock Magnetism and Magnetic Petrology Applied to Geological Interpretation of Magnetic Surveys. CSIRO Division of Exploration Geoscience, Restricted Report 303R, 193p.

Clark, D.A., French, D.H., Lackie, M.A. & Schmidt, P.W., 1992b. Magnetic petrology: application of integrated rock magnetic and petrological techniques to geological interpretation of magnetic surveys: Explor. Geophys., 23, 65-68.

Clarke, D.E., 1971. Geology of the Ravenswood 1-mile Sheet area. Geological Survey of Queensland, Report 53.

Clarke, I., 1987. Early Palaeozoic shoshonitic volcanism associated with gold and copper mineralization in the Parkes area, New South Wales. Pacific Rim Congress 87, Brisbane, Proceedings, 697-700.

Collins, S., 1987. The geophysics of the Red Dome gold mine and surrounding areas: Explor. Geophys., 18, 19-20.

Collins, S., 1991. The role of geophysics in exploration at Junction Reefs and the Sheahan-Grants gold mine, central N.S.W. Explor. Geophys., 22, 65-70.

Collins, W.J., 1994. Upper- and middle-crustal response to delamination: an example from the Lachlan fold belt, eastern Australia. Geology, 22, 143,146.

Collins, W.J., Beams, S.D., White, A.J.R. and Chappell, B.W., 1982. Nature and origin of A-type granites with particular reference to southeastern Australia. Contrib. Mineral. Petrol., 80, 189-200.

Cook, N.J., Klemd, R. and Okrusch, 1994. Sulphide mineralogy, metamorphism and deformation in the Matchless massive sulphide deposit, Namibia. Mineral. Deposita, 29, 1-15.

Cox, D.P. and Singer, D.A. (Eds), 1992. Mineral Deposit Models. U.S. Geol. Surv. Bull. 1693.

Craig, J.R. and Vokes, F.M., 1992. Ore mineralogy of the Appalachian-Caledonian stratabound sulfide deposits. Ore Geology reviews, 7, 77-123.

Criss, R.E. and Champion, D.E., 1984. Magnetic properties of rocks from the southern half of the Idaho Batholith: influences of hydrothermal alteration and implications for aeromagnetic interpretation: J. Geophys. Res., 89, 7061-7076.

Criss, R.E., Champion, D.E. and McIntyre, D.H., 1985. Oxygen isotope, aeromagnetic, and gravity anomalies associated with hydrothermally altered zones in the Yankee Fork mining district, Custer County, Idaho. Econ. geol., 80, 1277-1296.

Cygan, G.L. and Candela, P.A., 1995. Preliminary study of gold partitioning among pyrrhotite, pyrite, magnetite, and chalcopyrite in gold-saturated chloride solutions at 600

to 700°C, 140 MPa (1400 bars). *In*: J.F.H. Thompson (Editor), Magmas, Fluids and Ore Deposits. Mineralogical Association of Canada, Short Course Series, v. 23, 101-137.

Czamanske, G.K. and Mihalik, P., 1972. Oxidation during magmatic differentiation, Finnamarka Complex, Oslo area, Norway: Part 1, the opaque oxides. J. Petrology, 13, 493-509.

Czamanske, G.K. and Wones,D.R., 1973. Oxidation during magmatic differentiation, Finnamarka Complex, Oslo area, Norway: Part 2, the mafic silicates. J. Petrology, 14, 349-380.

Czamanske, G.K., Ishihara, S. and Atkin, S.A., 1981. Chemistry of rock-forming minerals of the Cretaceous-Paleocene batholith in southwestern Japan and implications for magma genesis: J. Geophys. Res., 86, 10431-10469.

Day, R.W., Whitaker, W.G., Murray, C.G., Wilson, I.H. and Grimes, K.G., 1983. Queensland Geology. A companion volume to the 1:2500 000 scale geological map (1975). Geological Survey of Queensland Publication, 383.

Dekkers, M.J., 1988. Magnetic properties of natural pyrrhotite Part I: Behaviour of initial susceptibility and saturation-magnetization-related rock-magnetic parameters in a grain-size dependent framework. Physics of the Earth and Planetary Interiors, 52, 376-393.

Dekkers, M.J., 1989. Magnetic properties of natural pyrrhotite. II: High- and low-temperature behaviour of J_{rs} and TRM as a function of grain size. Physics of the Earth and Planetary Interiors, 57, 266-283.

Dentith, M.C., 2003. Geophysical Signatures of South Australian Mineral Deposits: Miscellaneous and minor deposits, *in* Dentith, M.C. (ed), Geophysical Signatures of South Australian Mineral Deposits. Centre for Global Metallogeny, University of Western Australia, Publication 31, pp.147-168.

Dickinson, W.R., Force, E.R. and Hagstrum, J.T., 1996. Tilting history of the San Manuel-Kalamazoo porphyry system, southeastern Arizona - a reply. Econ. Geol., 91, 2096-2098.

Dilles, J.H. and Einaudi, M.T., 1992. Wall rock alteration and hydrothermal flow paths about the Ann-Mason porphyry copper deposit, a 6 km vertical reconstruction. Econ. Geol., 87, 1963-2001.

Dilles, J.H. and Proffett, J.M., 1995. *In*: F.W. Pierce and J.G. Bolm (Eds), Porphyry Copper Deposits of the American Cordillera. Arizona Geological Society Digest, 20, 306-315.

Dilles, J.H., Farmer, G.L. and Field, C.W., 1995. Sodium-calcium alteration by non-magmatic saline fluids in porphyry copper deposits: results from Yerington, Nevada. *In*: J.F.H. Thompson (Editor), Magmas, Fluids and Ore Deposits. Mineralogical Association of Canada, Short Course Series, v. 23, 309-338.

Dodge, F.C.W., 1972. Variation of ferrous-ferric ratios in the central Sierra Nevada Batholith, U.S.A.: Proceedings of the 24th IGC, Section 10, 12-19.

Dodge, F.C.W., Smith, V.C. and Mays, R.E., 1969. Biotites from granitic rocks of the central Sierra Nevada batholith, California. J. Petrology, 10, 250-271.

Drummond, A.D. and Godwin, C.I., 1976. Hypogene mineralization - an epirical evaluation of alteration zoning. *In*: Sutherland Brown, A. (Ed), Porphyry Deposits of the Canadian Cordillera. Canadian Institute of Mining and Metallurgy, Special Volume 15, 52-63.

Drummond, S.E. and Ohmoto, H., 1985. Chemical evolution and mineral deposition in boiling hydrothermal systems. Econ. Geol., 80, 126-147.

Dunlop, D.J. and Özdemir, Ö., 1997. Rock Magnetism.

Einaudi, M.T., 1982a. Description of skarns associated with porphyry copper plutons: southwestern North America. *In*: S.R. Titley (Ed), Advances in Geology of the Porphyry Copper Deposits, Southwestern North America. University of Arizona Press, Tucson, 139-183.

Einaudi, M.T., 1982b. General features and origin of skarns associated with porphyry copper plutons: southwestern North America. *In*: S.R. Titley (Ed), Advances in Geology

of the Porphyry Copper Deposits, Southwestern North America. University of Arizona Press, Tucson, 185-209.

Einaudi, M.T., Meinert, L.D. and Newberry, R.J., 1981. Skarn deposits, Econ. Geol., 75th Anniversary Volume, 317-391.

Ellwood, B.B., 1981. Weathering effects on the magnetic properties of the Milledgeville granite, Georgia. Earth Planet. Sci. Lett., 55, 311-316.

Ellwood, B.B. and Wenner, D.B., 1981. Correlation of magnetic susceptibility with $^{18}O/^{16}O$ data in late orogenic granites of the southern Appalachian Piedmont. Earth Planet. Sci. Lett., 54, 200-202.

Elo,S. and Tuomi, A., 1989. Gravimetric, magnetic and seismic interpretations of rapakivi massifs in southeastern Finland *in* I. Haapala and Y. Kahkonen (eds). Symposium Precambrian Granitoids. Geol. Surv. Finland Spec. Paper 8, 45.

Elston, W.E., 1994. Siliceous volcanic centers as guides to mineral exploration: review and summary. Econ. Geol., 89, 1662-1686.

Emerson, D.W., 1986. Physical properties of skarns. Explor. Geophys., 17, 201-212.

Emerson, D.W., Embleton, B.J.J. and Clark, D.A., 1979. The Petrophysical and petrologic characteristics of the magnetic igneous intrusion at Mt Derriwong, N.S.W. Bull. Aust. Soc. Explor. Geophys., 10,67-78.

Eugster, H.P., 1959. Oxidation and reduction in metamorphism *in* P.H. Abelson (ed), Researches in Geochemistry, Wiey, New York, 397-426.

Eugster, H.P., 1972. Reduction and oxidation in metamorphism (II). 24th IGC, Abstracts with Programs, Section 10, 3-11.

Ewers, G.R. and Sun, S.S., 1988. Genesisi of the Red Dome deposit, northeast Queensland. Proceedings of Bicentennial Gold 88 Symposium, Melbourne, 110-115.

Ewers, G.R., Torrey, C.E. and Erceg, M.M., 1990. Red Dome gold deposit. *In*: F.E. Hughes (Ed.), Geology of the Mineral Deposits of Australia and Papua New Guinea, Aus. IMM, Melbourne, 1455-1460.

Fanning, C.M., 1996. SHRIMP U-Pb dating for AMIRA project P425. Report prepared for AMIRA P425, 11p.

Feebrey, C.A., Hishida, H., Yoshioka, K. and Nakayama, K., 1998. Geophysical expression of low sulphidation epithermal Au-Ag deposits and exploration implications - examples from the Hokusatsu Region of SW Kyushu, Japan. Resource Geology, 48, 75-86.

Ferenczi, P.A., 1994. Are Tennant Creek style ironstone-related gold-copper-bismuth deposits unique? A review of available data and a comparison with possible analogous deposits. Proceedings of Aus. IMM Conference, Darwin, pp.171-177.

Fershtater, G.B. and Chashchukhina, V.A., 1979. Granitoid mineral parageneses in various ferrofacies: Geochem. Int., 3, 48-61.

Fershtater, G.B., Borodina, N.S. and Chashchukhina, V.A., 1978. Granitoid ferrofacies: Geochem. Int., 2, 91-102.

Finn, C., 1990. geophysical constraints on Washington convergent margin structure. J. geophys. res., 95, 19,533 -19,546.

Finn, C., 1994. Aeromagnetic evidence for a buried Early Cretaceous magmatic arc, northeast Japan. J. Geophys. Res., 99, 22,165-22,185.

Fleet, M.E. and Pan, Y., 1995. Magmatism, metamorphism and deformation at Hemlo, Ontario, and the timing of Au-Mo mineralization in the Golden Giant mine - a discussion. Econ. Geol., 90, 1338-1341.

Flood, P.G. and Aitchison, J.C. (Eds), New England Orogen, Eastern Australia, University of New England, Armidale, 423-429.

Fleming, A.W., Handley, G.A., Williams, K.L., Hills, A.L. and Corbett, G.J., 1986. The Porgera gold deposit, Papua New Guinea. Econ. Geol., 81, 660-680.

Force, E.R., Dickinson, W.R., and Hagstrum, J.T., 1995. Tilting history of the San Manuel-Kalamazoo porphyry system, southeastern Arizona. Econ. Geol., 90, 67-80.

Froese, E. and Berman, R.G., 1994. Oxidation and sulphidation reactions. *In*: D.R. Lentz (Editor), Alteration and Alteration Processes Associated with Ore-forming Systems. Geological Association of Canada Short Course Notes, v. 11, 101-113.

Frost, B.R., 1988. A review of graphite-sulfide-oxide-silicate equilibria in metamorphic rocks. Rend. Soc. Ital. Mineral. Petrol., 43, 25-40.

Frost, B.R., 1991a. Magnetic petrology: factors that control the occurrence of magnetite in crustal rocks. In: Lindsley, D.H. (editor), Oxide minerals: petrologic and magnetic significance: Rev. Mineral., 25, 489-509.

Frost, B.R., 1991b. Introduction to oxidation fugacity and its petrologic importance. In: Lindsley, D.H. (editor), Oxide minerals: petrologic and magnetic significance: Rev. Mineral., 25, 489-509.

Frost, B.R., 1991c. Stability of oxide minerals in metamorphic rocks *in* D.H. Lindsley (ed), Oxide Minerals: petrologic and magnetic significance. Rev. Mineral., 25, 469-488.

Frost, B.R. and Lindsley, D.H., 1991. Occurrence of iron-titanium oxides in igneous rocks *in* D.H. Lindsley (ed), Oxide Minerals: petrologic and magnetic significance. Rev. Mineral., 25, 489-509.

Fudali, R.F., 1965. Oxygen fugacities of basaltic and andesitic magmas. Geochim. Cosmochi. Acta, 29, 1063-1075.

Garcia, J.S., 1991. Geology and mineralization characteristics of the Mankayan Mineral District, Benguet, Phillipines. Geol. Surv. Japan Rep., 277, 21-30.

Garrett, S.W., 1990. Interpretation of reconnaissance gravity and aeromagnetic surveys of the Antarctic Peninsula. J. Geophys. Res., 95, 6759-6777.

Gaucher, E.H.S., 1965. Quantitative interpretation of the "Montagne du Sorcier" magnetic anomaly, Chibougamau, Quebec. Geophysics, 30, 762-782.

Gay, S.P., 1972. Fundamental Characteristics of Aeromagnetic Lineaments, Their Geological Significance, and Their Significance to Geology. American Stereo Map Company, Salt Lake City, 94pp.

Gay, S.P. and Mardirosian, C.A., 1970. Aeromagnetics and Geology of 36 Copper and Molybdenum Porphyry Deposits in the Western United States and British Columbia. Privately Published, American Stereo Map Company, Salt Lake City, Utah.

Geissman, J.W., Van der Voo, R. and Howard, K.L., 1982. A paleomagnetic study of the structural deformation in the Yerington district, Nevada. Am. J. Sci., 282, 1042-1109.

Ghiorso, M.S. and Sack, R.O., 1991. Fe-Ti oxide geothermometry: thermodynamic formulation and the estimation of intensive variables in silicic magmas. Contrib. Mineral. Petrol., 108, 484-510.

Giggenbach, W.F., 1981. Geothermal mineral equilibria. Geochim. Cosmochim. Acta, 45, 393-410.

Giggenbach, W.F., 1991. Redox processes accompanying the deposition of minerals in volcanic-magmatic-hydrothermal systems. Geol. Surv. Japan Rep., 277, 91-96.

Giggenbach, W.F., 1992. Magma degassing and mineral deposition in hydrothermal systems along convergent plate boundaries. Econ. Geol., 87, 1927-1944.

Giggenbach, W.F., 1995. Magmatic components in hydrothermal fluids. *In*: J.F.H. Thompson (Editor), Magmas, Fluids and Ore Deposits. Mineralogical Association of Canada, Short Course Series, v. 23, 247-261.

Giggenbach, W.F., 1997. The origin and evolution of fluids in magmatic-hydrothermal systems. *In*: Barnes, H.L. (Ed), Geochemistry of Hydrothermal Ore Deposits, Wiley, New York, pp.737-796.

Gilligan, L.B., Lewis, P. and Suppel, D.W., 1990 (Eds). Gold Mines of Central Western New South Wales Excursion. NSW Department of Minerals and Energy.

Glen, R.A. and Watkins, J.J., 1994. The Orange 1:100 000 sheet: a preliminary account of stratigraphy, structure and tectonics, and implications for mineralisation. Geol. Surv. NSW,
Quarterly Notes, 95.

Goellnicht, N.M., Groves, D.I. and McNaughton, N.J., 1989. Granitoids as indicators of tectonic setting of the Telfer District, Paterson Province, Western Australia.

Goellnicht, N.M., Groves, D.I. and McNaughton, N.J., 1991. Late Proterozoic fractionated granitoids of the mineralized Telfer area, Paterson Province, Western Australia. Precam. Res., 51, 375-391.

Gondwana Consultants, 1995. Global Paleomagnetic Database, version 3.1. Gondwana Consultants, Hat Head, NSW, Australia.

Gordon, M.J., 1990. The geology of E.L. 2908, Molong; and mineralisation of the Endeavour 37 propspect, Goonumbla, N.S.W. B.Sc. (Hons) thesis, Australian National University.

Gow, P.A., Wall, V.J., Oliver, N.H.S. and Valenta, R.K., 1994. Proterozoic iron oxide (Cu-U-Au-REE) deposits: further evidence of hydrothermal origins. Geology, 22, 633-636.

Grant, F.S., 1985a. Aeromagnetics, geology and ore environments, I. Magnetite in igneous, sedimentary and metamorphic rocks: an overview. Geoexploration, 23, 303-333.

Grant, F.S., 1985b. Aeromagnetics, geology and ore environments, II. Magnetite and ore environments. Geoexploration, 23, 335-362.

Grasty, R.L. (1979). Gamma-ray spectrometric methods in uranium exploration - Theory and Operational procedures. In Geophysics and Geochemistry in the search for Metallic ores, (ed. P.J. Hood), pp. 147-59. Economic Geology Report 31, Geological Survey of Canada.

Grauch, V.J.S. and Bankey, V., 1991. Preliminary results of aeromagnetic studies of the Getchell disseminated gold deposit trend, Osgood mountains, north-central Nevada. *In*: Raines, G.L., Lisle, R.E., Schafer, R.W. and Willkinson, W.H., 1991 (Eds), Geology and Ore Deposits of the Great Basin (Symposium Proceedings, Reno, Nevada, April 1-5, 1990). Geol. Soc. Nevada, Reno, 781-791.

Gu, L.X. and Vokes, F.M., 1996. Intergrowths of hexagonal and monoclinic pyrrhotites in some sulphide ores from Norway. Mineralogical Magazine, 60, 303-316.

Guidotti, C.V. and Dyar, M.D., 1991. Ferric iron in metamorphic biotite and its petrologic and crystallochemical implications. Am. Mineral., 76, 161-175.

Guilbert, J.M., 1995. Geology, alteration, mineralization, and genesis of the Bajo de la Alumbrera porphyry copper-gold deposit, Catamarca Province, Argentina. *In*: F.W. Pierce and J.G. Bolm (Eds), Porphyry Copper Deposits of the American Cordillera. Arizona Geological Society Digest, 20, 646-656.

Guilbert, J.M. and Lowell, J.D., 1996. Tilting history of the San Manuel-Kalamazoo porphyry system, southeastern Arizona - a discussion. Econ. Geol., 91, 2094-2096.

Guilbert, J.M. and Park, C.F., 1986. The Geology of Ore Deposits. Freeman, New York,

Gustafson. L.B., 1995. Magmatism, metamorphism and deformation at Hemlo, Ontario, and the timing of Au-Mo mineralization in the Golden Giant mine - a discussion. Econ. Geol., 90, 1341-1342.

Gustafson, L.P. and Hunt, J.P., 1975. The porphyry copper deposit at El Salvador, Chile. Econ. Geol., 70, 857-912.

Gustafson, L.P. and Quiroga, G.J., 1995. Patterns of mineralization and alteration below the porphyry copper orebody at El Salvador, Chile. Econ. Geol., 90, 2-16.

Gwinn and Hess, 1989. Iron and titanium in peraluminous and peralkaline rhyolitic liquids. Contrib. Mineral. Petrol., 101, 326-338.

Haapala, I., 1974. Some petrological and geochemical characteristics of rapakivi granite varieties associated with greisen-type Sn, Be and W mineralization in the Eurajoki and

Kymi areas, southern Finland *in* Metallization Associated with Acid Magmatism, Geol. Surv. Czechoslovakia, Prague, pp. 159-169.

Haggerty, S.E., 1976a. Oxidation of opaque mineral oxides in basalts *in* D. Rumble (ed), Oxide Minerals. Mineral. Soc. Amer. Short Course Notes (Rev. Mineral.), 3, Hg-1 - Hg-100.

Haggerty, S.E., 1976b. Opaque mineral oxides in terrestrial igneous rocks *in* D. Rumble (ed), Oxide Minerals. Mineral. Soc. Amer. Short Course Notes (Rev. Mineral.), 3, Hg-101 - Hg-300.

Haggerty, S.E., 1979. The aeromagnetic mineralogy of igneous rocks. Can. J. Earth Sci., 16, 1281-1293.

Hall, R.J., Britten, R.M. and Henry, D.D., 1990. Frieda River copper-gold deposits. *In*: F.E. Hughes (Ed.), Geology of the Mineral Deposits of Australia and Papua New Guinea, Aus. IMM, Melbourne,
1709-1715.

Handley, G.A. and Henry, D.D., 1990. Porgera gold deposit. *In*: F.E. Hughes (Ed.), Geology of the Mineral Deposits of Australia and Papua New Guinea, Aus. IMM, Melbourne, 1717-1724.

Hanna, W.F., 1969. Negative aeromagnetic anomalies over mineralized areas of the Boulder Batholith, Montana. U.S. Geol. Surv. Prof. Paper 650-D, D159-D167.

Hannah, J.L. and Stein, H.J., 1990. Magmatic and hydrothermal processes in ore-bearing systems. Geol. Soc. Am., Special Paper 246, 1-9.

Harding, K.L., Morris, W.A., Balch, S.J., Lapointe, P. and A.G. Latham, 1988. A comparison of magnetic character and alteration in three granite drill cores from eastern Canada. Can. J. Earth Sci., 25, 1141-1150.

Harris, D.P. and Pan, G.C., 1991. Consistent geologic areas for epithermal gold-silver deposits in the Walker Lake quadrangle of Nevada and California: delineated by quantitative methods. Econ. Geol., 86, 142-165.

Harris, N.B.W., Pearce, J.A. and Tindle, A.G., 1986. Geochemical characteristics of collision zone magmatism *in* M.P.Coward and A.C. Ries (eds), Collision Tectonics, Geol. Soc. Spec. Pub., 19, 67-81.

Hattori, K., 1987. Magnetic felsic intrusions associated with Canadian Archean gold deposits. Geology, 15, 1107-1111.

Hattori, K., 1991. Archaean gold mineralization and granitoid intrusions in the Superior Province of Canada: a review *in* Second Hutton Symposium on Granites and Related Rocks, BMR Record 1991/25, 10.

Haywood, M.A., 1993. Analysis of magnetic susceptibility data for the Ravenswood Batholith. Queensland Geological Survey Record 1993/21.

Heald, P., Foley, N. and Hayba, D.O., 1987. Comparative anatomy of volcanic-hosted epithermal deposits: acid-sulfate and adularia-sericite types.

Hedenquist, J.W., 1995. The ascent of magmatic fluid: discharge versus mineralization. *In*: J.F.H. Thompson (Editor), Magmas, Fluids and Ore Deposits. Mineralogical Association of Canada, Short Course Series, v. 23, 263-289.

Hedenquist, J.W., Izawa, E., Arribas, A. and White, N.C., 1996. Epithermal gold deposits: Styles, characteristics, and exploration. Resource Geology Special Publication Number 1. Society of Resource Geology, Tokyo.

Hedenquist, J.W. and Lowenstern, J.B., 1994. The role of magmas in the formation of hydrothermal ore deposits. Nature, 370, 519-527.

Heitanen, A., 1986. Role of replacement in the genesis of anorthosite in Boehls Butte area, Idaho. Bull. Geol. Soc. Finland, 58, 71-79.

Heithersay, P.S. and Walshe, J.L., 1995. Endeavour 26N: a porphyry copper-gold deposit in the Late Ordovician, shoshonitic Goonumbla Volcanic Complex, NSW, Australia. Econ. Geol., 90, 1506-1532.

Heithersay, P.S., O'Neill, W.J., van der Helder, P., Moore, C.R. and Garbon, P.G., 1990. Goonumbla porphyry copper district - Endeavour 26 North, Endeavour 22 and

Endeavour 27 copper-gold deposits. *In*: F.E. Hughes (Ed), Geology of the Mineral Deposits of Australia and Papua New Guinea. Aus. I.M.M., Melbourne, pp.1385-1398.

Heithersay, P., Jones, G. and Love, M., 1996. The Goonumbla Lake Cowal porphyry copper belt. In: Porphyry Related Copper and Gold Deposits of the Asia Pacific Region, Conference Proceedings. Australian Mineral Foundation, Glenside, S.A., pp.15.1-15.10.

Hellinwerf, R.H. and Baker, J.H., 1985. Wall-rock alteration and tungsten and molybdenum mineralizations associated with older granites in western Bergslagen, Sweden. Econ. Geol., 80, 479-487.

Hemley, J.J., Cygan, G.L. and Fein, J.B., 1992a. Hydrothermal ore-forming processes in the light of studies in rock-buffered systems: I. Iron-copper-zinc-lead sulfide solubility relations. Econ. Geol., 87, 1-22.

Hemley, J.J., Cygan, G.L. and Fein, J.B., 1992b. Hydrothermal ore-forming processes in the light of studies in rock-buffered systems: II. Some general geologic applications. Econ. Geol., 87, 23-43.

Hendry, D.A.F., Chivas, A.R., Long, J.V.P. and Reed, S.J.B., 1985. Chemical differences between minerals from mineralizing and barren intrusions from some North American porphyry copper deposits. Contrib. Mineral. Petrol., 89, 317-329.

Henkel, H., 1991. Petrophysical properties (density and magnetization) of rocks from the northern part of the Baltic Shield. Tectonophysics, 192, 1-19.

Henkel, H., 1994. Standard diagrams of magnetic properties and density - a tool for understanding magnetic petrology. J. Appl. Geophys., 32, 43-53.

Henley, R.W., 1994. Epithermal deposition of gold during transition from propylitic to potassic alteration at Round Mountain, Nevada - a discussion. Econ. Geol., 86, 892-894.

Henley, R.W., 1996. Copper-gold: back to basics. *In*: Porphyry Related Copper and Gold deposits of the Asia Pacific Region (Conference Proceedings), Australian Mineral Foundation, 2.1-2.13.

Henry, D.D., 1988. Porgera - the first fifty years. Proceedings of Bicentennial Gold 88 Symposium, Melbourne, 144-149.

Hilyard, D., Drummond, M., Clare, A., Sanders, Y., Aung, Z., Glen, R., Ruszkowski, Fleming, G., Lewis, P. and Robson, D., 1996. Preliminary Palaeozoic bedrock interpretation of the Narromine and Nyngan 1:250 000 sheet areas. Geol. Surv. NSW, Quarterly Notes, 101, 1-16.

Hine, R., Williams, I.S. and Chappell, B.W., 1978. Contrasts between I- and S-type granitoids of the Kosciusko Batholith: J. Geol. Soc. Aust., 25, 219-234.

Hitzman, M.W., Oreskes, N. and Einaudi, M.T., 1992. Geological characteristics and tectonic setting of Proterozoic iron oxide (Cu-U-Au-REE) deposits. Precambrian Research, 58, 241-287.

Hollister, V.F., 1975. An appraisal of the nature and source of porphyry copper deposits. Min. Sci. Engng: 7, 225-233.

Hooper, B., Heithersay, P.S., Mills, M.B., Lindhorst, J.W. and Freyberg, J., 1996. Shoshonite-hosted Endeavour 48 porphyry copper-gold deposit, Northparkes, central New South Wales. Aust. J. Earth Sciences, 43, 279-288.

Hoover, D.B., Grauch, V.J.S., Pitkin, J.A., Krohn, D. and Pierce, H.A., 1991. Getchell trend airborne geophysics, an integrated geophysical study along the Getchell trend of gold deposits, north central Nevada. *In*: Raines, G.L., Lisle, R.E., Schafer, R.W. and Willkinson, W.H., 1991 (Eds), Geology and Ore Deposits of the Great Basin (Symposium Proceedings, Reno, Nevada, April 1-5, 1990). Geol. Soc. Nevada, Reno, 739-758.

Hughes, C.J., 1982. Igneous Petrology. Elsevier, Amsterdam.

Hunt, J.P., 1991. Porphyry copper deposits. *In*: Hutchinson, R.W. and Grauch, R.I. (Eds). Historical Perspectives of Genetic Concepts and Case Histories of Famous Discoveries. Economic Geology Monograph 8, 192-206.

Huston, D.L., Bolger, C. and Cozens, G., 1993. A comparison of mineral deposits at the Gecko and White Devil deposits: implications for ore genesis in the Tennant Creek district, Northern Territory, Australia. Econ. Geol., 88, 1198-1225.

Hutchison, C.S., 1982. The various granitoid series and their relationship to W and Sn mineralisation. Tungsten Geology Symposium, Jianxi. Geological Publishing House, Beijing.

Hutton, L.J., Rienks, I.P., Tenison Woods, K.L., Hartley, J.S. and Crouch, S.B.S., 1994. Geology of the Ravenswood Batholith, North Queensland. Queensland Geological Record 1994/4.

Hutton, L.J., Hartley, J.S. and Rienks, I.P., 1993. Geology of the Charters Towers region. Geol. Soc. Aust. Field Excursion Guidebook, Charters Towers, 12-14 June, 1993,

Hyndman, D.W., 1972. Petrology of Igneous and Metamorphic Rocks. McGraw Hill, New York.

Hyndman, D.W., 1981. Controls on source and depth of emplacement of granitic magma. Geology, 9, 244-249.

Idnurm, M. and Heinrich, C.A., 1993. A palaeomagnetic study of hydrothermal activity and uranium mineralization at Mt Painter, South Australia. Aust. J. Earth Sci., 40, 87-101.

Irvine, R.J. and Smith, M.J., 1990. Geophysical exploration for epithermal gold systems. J. Geochem. Explor., 36, 375-412.

Irvine, R.J. and Robertson, I., 1987. Interpretation of airborne geophysical data over the Ok Tedi porphyry copper-gold orebody using image processing techniques. Explor. geophys., 18, 103-107.

Ishihara, S., 1977. The magnetite-series and ilmenite-series granitic rocks. Min. Geol., 27, 293-305.

Ishihara, S., 1978. Metallogenesis in the Japanese island arc system. J. Geol. Soc. Lond., 135, 389-406.

Ishihara, S., 1979. Lateral variation of magnetic susceptibility of the Japanese granitoids. J. Geol. Soc. Japan, 85, 509-523.

Ishihara, S., 1981. The granitoid series and mineralization. Econ. Geol., 75th Anniversary Volume, 458-484.

Ishihara, S., 1982. Granitoid series and tungsten deposits in Japan. Tungsten Geology Symposium, Jianxi. Geological Publishing House, Beijing.

Ishihara, S., 1991. Opening remarks: necessity of ore deposit research for mineral exploration. Geol. Surv. Japan Rep., 277, 1-4.

Ishihara, S. and Sasaki, A., 1989. Sulfur isotpe ratios of the magnetite-series and ilmenite-series granitoids of the Sierra-Nevada batholith - a reconnaissance study. Geology, 17, 788-791.

Ishihara, S. and Terashima, S., 1989. Carbon contents of the magnetite-series and ilmenite-series granitoids of Japan. Geochim. J., 23, 25-36.

Ishihara, S., Sawata, H., Arpornsuwan, S., Busaracome, P. and Bungbrakearti, N., 1979. The magnetite-series and ilmenite-series granitoids and their bearing on tin mineralization, particularly of the Malay Peninsula region. Geol. Soc. Malaysia. Bull., 11, 103-110.

Ishihara, S., Sawata, H., Shibata, K., Terashima, S., Arrykul, S. and Sato, K., 1980. Granites and Sn-W deposits of peninsular Thailand. Min. Geol. Spec. Issue, 8, 223-241.

Ishihara, S., Terashima, S. and Tsukimura, K., 1987. Spatial distribution of magnetic susceptibility and ore elements, and cause of local reduction on magnetite-series granitoids and related ore deposits at Chichibu, central Japan. Min. Geol., 37, 15-28.

Jaeger, J.C., 1957. The temperature in the neighbourhood of a cooling intrusive sheet. Am. J. Sci., 255, 306-318.

Jaeger, J.C., 1959. Temperatures outside a cooling intrusive sheet. Am. J. Sci., 257, 44-54.

Jaeger, J.C., 1964. Thermal effects of intrusions. Rev. Geophys., 2, 443-466.

Jaireth, S., Heinrich, C.A. and Solomon, M., 1990. Chemical controls on hydrothermal tungsten transport in some magmatic systems and the precipitation of ferberite and scheelite. Geol. Soc. Aust. Abstracts, 25, 269-270.

James, A.H., 1971. Hypothetical diagrams of several porphyry copper deposits. Econ. Geol., 66, 43-47.

Jébrak, M., LeQuentrec, M.F., Mareschal, J-C and Blais, D., 1991. A gravity survey across the Bourlamaque massif, southeastern Abitibi greenstone belt, Québec, Canada: the relationship between the geometry of tonalite plutons and associated gold mineralization. Precambrian Research, 50, 261-268.

Jerome, S.E., 1966. Some features pertinent in exploration of porphyry copper deposits. *In*: S.R. Titley and C.L. Hicks (Eds), Geology of the Porphyry Copper Deposits, Southwestern North America. University of Arizona Press, Tucson.

John, E.C., 1978. Mineral zones in the Utah copper orebody. Econ. Geol., 73, 1250-1259.

John, D.A., 1989. Evolution of hydrothermal fluids in the Park Premier stock, central Wasatch mountains, Utah. Econ. Geol., 84, 879-902.

Johnson, A.C., 1996. Arc evolution: a magnetic perspective from the Antarctic peninsula. Geol. Mag., 133, 637-644.

Johnson, I.M. and Fujita, M., 1985. The Hishikari gold discovery: An airborne EM discovery. Can. Inst. Metall. Bull., 78, 61-66.

Johnson, J.P. and Cross, K.C., 1995. U-Pb geochronological constraints on the genesis of the Olympic Dam Cu-U-Au-Ag deposit, South Australia. Econ. Geol., 90, 1046-1063.

Johnson, P.R., Zietz, I. and Bond, K.R., 1990. U.S. west coast revisited: an aeromagnetic perspective. Geology, 18, 332-335.

Jones, G.J., 1985. The Goonumbla porphyry copper deposits, New South Wales. Econ. geol., 80, 591-613.

Jones, P. (Compiler), 1995. AGSO Phanerozoic timescale 1995: wallchart and explanatory notes. Oxford University Press, Melbourne, 32pp.

Jover, O., Rochette, P., Lorand, J.P., Maeder, M. and Bouchez, J.L., 1989. Magnetic mineralogy of some granites from the French Massif Central: origin of their low-field suceptibility. Phys. Earth Planet. Inter., 55, 79-92.

Kadushkin, A.P., 1988. Main findings on magnetism and other physical properties of rocks along southeast Asian tin belt *in* M.M. Purbo Hadiwidjoyo (ed) Application of Geophysics in the Tin Mining Industry, SE Asia Tin Research and Development Centre Technical Publication no. 7.

Kafafy, A.M., 1987. Preliminary results on the use of magnetic techniques on the study of the granite aureoles. J. Geomagn. Geoelectr., 39, 5443-550.

Kafay, A.M. and Tarling, D.H., 1985. Magnetic fabric in some granitic aureoles, Southern Uplands, Scotland. J. Geol. Soc. London, 142, 1007-1014.

Kanisawa, S., 1983. Chemical characteristics of biotites and hornblendes of Late Mesozoic to Early Tertiary granitic rocks in Japan *in* J.A. Roddick (Ed.), Circum-Pacific Plutonic Terranes. Geol. Soc. Am. Memoir 159, 129-134.

Kawakatsu, K. and Yamaguchi, Y., 1987. Succesive zoning of amphibole during progressive oxidation in the Daito-Yokota granitic complex, San-in belt, southwest Japan. Geochim. Cosmochim. Acta, 51, 535-540.

Kawasaki, T.W., Okada, K. and Kubota, R., 1986. Geophysical surveys in the Hishikari mine area. Mining Geology, 36, 131-147.

Keith, S.B. and Swan, M.M., 1995. Tectonic setting, petrology, and genesis of the Laramide porphyry copper cluster of Arizona, Sonora and New Mexico. *In*: F.W. Pierce and J.G. Bolm (Eds), Porphyry Copper Deposits of the American Cordillera. Arizona Geological Society Digest, 20, 339-347.

Keith, J.D., van Middelaar, W., Clark, A.H. and Hodgson, C.J., 1989. Granitoid textures, compositions, and volatile fugacities associated with the formation of tungsten-dominated skarn deposits. *In*: Whitney, J.A. and Naldrett, A.J. (Eds), Ore Deposition Associated With Magmas. Rev. Econ. Geol., 4, 235-250.

Kerrich, R., 1989. Archean gold: relation to granulite formation or felsic intrusions? Geology, 17, 1011-1015.

Khitrunov, A.T., 1985. Oxidation-reduction environment of formation of granitoid rocks with different ore concentrations. Doklady Earth Science Sections, 280, 201-204.

Kleinkopf, M.D., Peterson, D.L. and Gott, G., 1970. Geophysical studies of the Cripple Creek mining district, Colorado. Geophysics, 35, 490-500.

Klootwijk, C., Giddings, J. and Percival, P., 1993. Palaeomagnetic reconnaissance of Upper Palaeozoic volcanics, northeastern Queensland. AGSO Record 1993/36.

Klootwijk, C., Idnurm, M., Théveniaut, H. and Trench, A., 1993. Phanerozoic Magnetostratigraphy: a Contribution to the Timescales Project. AGSO Record 1994/45.

Knox-Robinson, C.M. and Wyborn, L.A.I., 1997. Towards a holistic exploration strategy: using Geographic Information Systems as a tool to enhance exploration. Aust. J. Earth Sci., 44, 453-463.

Kress, V.C. and Carmichael, I.S.E., 1988. Stoichiometry of the iron oxidation reaction in silicate melts. Am. Mineral., 73, 1267-1274.

Kress, V.C. and Carmichael, I.S., 1991. The compressibility of silicate liquids containing Fe_2O_3 and the effect of composition, temperature, oxygen fugacity and pressure on their redox states: Contrib. Mineral. Petrol., 108, 82-92.

Krutikhovskaya, Z.A., Silina, I.M., Bondareva, N.M. and Podolyanko, S.M., 1979. Relation of magnetic prperties of the rocks of the Ukrainian Shield to their composition and metamorphism. Can. J. earth Sci., 16, 984-991.

Kuhns, R.J., Sawkins, F.J. and Ito, E., 1994. Magmatism, metamorphism and deformation at Hemlo, Ontario, and the timing of Au-Mo mineralization in the Golden Giant mine. Econ. Geol., 89, 720-756.

Kuhns, R.J., Sawkins, F.J. and Ito, E., 1995. Magmatism, metamorphism and deformation at Hemlo, Ontario, and the timing of Au-Mo mineralization in the Golden Giant mine - a reply. Econ. Geol., 90, 1343-1344.

Kullerud, G., 1986. Monoclinic pyrrhotite. Bull. Geol. Soc. Finland, 58, 293-305.

Kuroda, Y., Yamada, T., Takano, O. and Matsuo, S., 1989. D/H study of the magnetite-series granitic plutons from the Kitakami district, northeast Japan. Chem. Geol., 73, 343-352.

Kwak, T.A.P., 1994. Hydrothermal alteration in carbonate-replacement deposits; oreskarns and distal equivalents. *In*: D.R. Lentz (Editor), Alteration and Alteration Processes Associated with Ore-forming Systems. Geological Association of Canada Short Course Notes, v.11, 69-99.

Kwak, T.A.P. and White, A.J.R., 1982. Contrasting W-Mo-Cu and W-Sn-F skarn types and related granitoids. Mining Geology, 32, 339-351.

Kwak, T.A.P., Taylor, R.G. and Plimer, I.R., 1982. Australian tungsten deposits. Tungsten Geology Symposium, Jiangxi, China, Geological Publishing House, Beijing, pp. 127-152.

Lackie, M.A., Clark, D.A. and French, D.H., 1991. Rock magnetism and palaeomagnetism of the Mount Leyshon gold mine in northeast Queensland. CSIRO Restricted Report 217R.

Lackie, M.A., Clark, D.A. and French, D.H., 1992a. A regional survey of the rock magnetic properties of the Ravenswood Igneous Complex, northeast Queensland. CSIRO Restricted Report 279R.

Lackie, M.A., French, D.H. and Clark, D.A., 1992b. Magnetic mineralogy of felsic volcanics of the Conway-Bimurra area, northeast Queensland: relationships to aeromagnetic anomalies and hydrothermal alteration. CSIRO Restricted Report 274R.

Laing, W.P., 1994. Palaeozoic structural framework and regional plumbing system of northeastern Queensland. *In*: New Developments in Geology and Metallogeny: Northern Tasman Orogenic Zone, Townsville, 21-22 July, 1994, pp.125-132.

Lalonde, A.E. and Bernard, P., 1993. Composition and color of biotite from granites: two useful properties in the characterization of plutonic suites from the Hepburn internal zone of Wopmay Orogen, Northwest Territories. Can. Mineral., 31, 203-217.

Lameyre, J. and Bowden, P., 1982. Plutonic rock series: discrimination of various granitoid series and related rocks. J. Volcan. Geotherm. Res., 14, 169-186.

Lang, J.R., Stanley, C.R., Thompson, J.F.H., 1992. Quartz-alkalic and nepheline-alkalic: two distinct types of porphyry deposits related to alkalic rocks. Geol. Soc. Am. Abstracts with Programs, 24, p.A143.

Lang, J.R., Stanley, C.R., Thompson, J.F.H. and Dunne, K.P.E., 1995a. Porphyry copper-gold deposits related to alkalic igneous rocks in the Triassic-Jurassic arc terranes of British Columbia. *In*: F.W. Pierce and J.G. Bolm (Eds), Porphyry Copper Deposits of the American Cordillera. Arizona Geological Society Digest, 20, 219-236.

Lang, J.R., Stanley, C.R., Thompson, J.F.H. and Dunne, K.P.E., 1995b. Na-K-Ca magmatic-hydrothermal alteration in alkalic porphyry Cu-Au deposits, British Columbia. *In*: J.F.H. Thompson (Editor), Magmas, Fluids and Ore Deposits. Mineralogical Association of Canada, Short Course Series, v. 23, 339-366.

Lanier, G.L., John, E.C., Swenson, A.J., Reid, J., Bard, C.E., Caddey, S.W. and Wilson, J.C., 1978a. General geology of the Bingham mine, Bingham Canyon, Utah. Econ. Geol., 73, 1228-1241.

Lanier, G., Raab, W.J., Folsom, R.B. and Cone, S., 1978b. Alteration of equigranular monzonite, Bingham mining district, Utah. Econ. Geol., 73, 1270-1286.

Latham, A.G., Harding, K.L., Lapointe, P., Morris, W.A. and Balch, S.J., 1989. On the lognormal distribution of oxides in igneous rocks, using magnetic susceptibility as a proxy for oxide mineral concentration. Geophys. J., 96, 179-184.

Lauer, H.V. and Morris, R.V., 1977. Redox equilibria of multivalent ions in silicate glasses. J. Amer. Ceram. Soc., 60, 443-451.

Lawrie, K.C. (Ed), 1997. Porphyry and epithermal deposits of the Lachlan Fold Belt - pre-conference field trip (27-29 January, 1997). Specialist Group in Economic Geology, Geological Society of Australia, 102 pp.

Leake, B.E., Brown, G.C. and Halliday, A.N., 1980. The origin of granite magmas: a discussion. J. Geol. Soc. London, 137, 93-97.

Le Bas, M.J. and Streckeisen, A.L., 1991. The IUGS systematics of igneous rocks. J. Geol. Soc. London, 148, 825-833.

Lentz, D.R., 1994. Exchange interactions in hydrothermally altered rocks: examples from biotite-bearing assemblages. *In*: D.R. Lentz (Editor), Alteration and Alteration Processes Associated with Ore-forming Systems. Geological Association of Canada Short Course Notes, v.11, 69-99.

Letros, S., Strangway, D.W., Tasillo-Hirt, A.M., Geissman, J.W. and Jensen, L.S., 1983. Aeromagnetic interpretation of the Kirkland Lake - Larder Lake portion of the Abitibi Greenstone Belt, Ontario. Can J. Earth Sci., 20, 548-560.

Lindsay, D.D., Zentilli, M. and Rojas de la Rivera, J., 1995. Evolution of an active ductile to brittle shear system controlling mineralization at the Chuquicamata porphyry copper deposit, northern Chile. Int. Geol. Rev., 37, 945-958.

Lindsley, D.H. (ed), 1991. Oxide Minerals: petrologic and magnetic significance. Rev. Mineral., 25, 509 pp.

Lishnevskiy, E.N., 1984. The magnetic field as an indicator of tin-ore and molybdenum provinces. Doklady Earth Sci. Sect., 266, 41-43.

Locke, C.A. and De Ronde, C.E.J., 1987. Delineation of gold-bearing hydrothermally altered rocks using gravity data - a New Zealand example. Geoexploration, 24, 471-481.

Logan, K., 1993. Porgera Detailed Magnetic Modelling, Processing and Interpretation: Implications for Exploration. Placer Exploration Ltd, Report 93/08.

Loutit, T.S., Wyborn, L.A., Hinman, M.C. and Idnurm, M., 1994. Palaeomagnetic, tectonic, magmatic and mineralisation events in the Proterozoic of northern Australia. Proceedings of Aus. IMM Conference, Darwin, pp.109-115.

Lowell, J.D. and Guilbert, J.M., 1970. Lateral and vertical alteration-mineralization zoning in porphyry copper deposits. Econ. Geol., 65, 373-408.

Lowenstern, J.B., Mahood, G.A., Rivers, M.L. and Sutton, S.R., 1991. Evidence for extreme partitioning of copper into a magmatic vapor phase. Science, 252, 1405-1409.

Lowrie, W., 1990. Identification of magnetic minerals in a rock by coercivity and unblocking temperature properties. Geophys. Res. Lett., 17, 159-162.

Lum, J.A., Clark, A.H. and Coleman, P.J., 1992. Gold potential of the Southwest Pacific. East-West Center, Honolulu.

Lynch, G. and Ortega, J. 1997. Hydrothermal alteration and tourmaline-albite equilibria at the Coxheath porphyry Cu-Mo-Au deposit, Nova Scotia. Can. Mineral., 35, 79-94.

Lynton, S.J., Candela, P.A. and Piccoli, P.M., 1993. An experimental study of the partitioning of copper between pyrrhotite and a high silica rhyolitic melt. Econ. Geol., 88, 901-915.

MacDonald, G.D. and Arnold, L.C., 1994. Geological and geochemical zoning of the Grasberg Igneous Complex, Irian Jaya, Indonesia. J. Geochem. Explor., 50, 179-202.

MacDonald, G.D. and Arnold, L.C., 1995. Factors responsible for extreme concentration of Cu and Au in the Grasberg deposit: a comparative look at the porphyry copper systems of the Ertsberg district, Indonesia. ??, 314-333.

MacDougall, R.E., 1965. The role of magnetics in a copper porphyry exploration program (abstract). Geophysics Yearbook, 1965, S.E.G., Tulsa, p.236.

Maniar, P.D. and Piccoli, P.M., 1989. Tectonic discrimination of granitoids. Geol.Soc. Am. Bull., 101, 635-643.

Marsh, J.S., 1975. Aenigmatite stability in silica-undersaturated rocks. Contrib. Mineral. Petrol., 50, 135-144.

Mason, D.R., 1978. Compositional variations in ferromagnesian minerals from porphyry copper-generating and barren intrusions of the Western Highlands, Papua New Guinea. Econ. geol., 73, 878-890.

Mason, D.R. and McDonald, J.A., 1978. Intrusive rocks and porphyry copper occurrences of the Papua New Guinea - Solomon Islands region: a reconnaissance study. Econ. Geol., 73, 857-877.

Mathez, E.A., 198?. Vapor associated with mafic magma and controls on its composition. *In*: Whitney, J.A. and Naldrett, A.J. (Eds), Ore Deposition Associated With Magmas. Rev. Econ. Geol., 4, 21-31.

Matthews, S.J., Jones, A.P. and Beard, A.D., 1994. Buffering of melt oxygen fugacity by sulphur redox reactions in calc-alkaline magmas. J. Geol. Soc. London, 151, 815-823.

McDowell, F.W., McMahon, T.P., Warren, P.Q. and Cloos, M., 1996. Pliocene Cu-Au-bearing igneous intrusions of the Gunung Bijih (Ertsberg) district, Irian Jaya, Indonesia: K-Ar geochronology. J. Geol., 104, 327-340.

McIntyre, J.I., 1980. Geological significance of magnetic patterns related to magnetite in sediments and metasediments - a review. Aust. Soc. Explor. Geophys. Bull., 11, 19-33.

McMahon, T.P., 1994. Pliocene intrusions in the Ertsberg (Gunung Bijih) mining district, Irian Jaya, Indonesia: petrography, geochemistry, and tectonic setting. Ph.D. dissertation, University of Texas at Austin, 299p.

McMillan,W.J. and Panteleyev, A.J., 1995. Porphyry copper deposits of the Canadian Cordillera. *In*: F.W. Pierce and J.G. Bolm (Eds), Porphyry Copper Deposits of the American Cordillera. Arizona Geological Society Digest, 20, 203-218.

McMillan,W.J., Thompson, J.F.H., Hart, C.J.R. and Johnston, S.T., 1995. Regional geological and tectonic setting of porphyry deposits in British Columbia and Yukon Territory. *In*: Schroeter, T.G. (Ed), Porphyry Deposits of the Northwestern Cordillera of North America. Can Inst. Min. Metall., Special Volume 46, 40-57.

Meinert, L.D., 1995. Compositional variation of igneous rocks asssociated with skarn deposits - chemical evidence for a genetic connection between petrogenesis and mineralization. *In*: J.F.H. Thompson (Editor), Magmas, Fluids and Ore Deposits. Mineralogical Association of Canada, Short Course Series, v. 23, 401-418.

Meinert, L.D., 1992. Skarns and skarn deposits. Geosci. Canada, 19, 145-162.

Meinert, L.D., 1993. Igneous petrogenesis and skarn deposits. *In*: R.V. Kirkham, W.D. Sinclair, R.I. Thorpe and J.M. Duke (Eds), Mineral Deposit Modeling. Geological Association of Canada, Special Paper 40, 403-417.

Meldrum, S.J., Aquino, R.S., Gonzales, R.I., Burke, R.J., Suyadi, A., Irianto, B., Clarke, D.S., 1994. The Batu Hijau porphyry copper-gold deposit, Sumbawa island, Indonesia. J. Geochem. Explor., 50, 203-220.

Menyeh, A. and O'Reilly, W., 1991. The magnetization process in monoclinic pyrrhotite (Fe_7S_8) particles containing few domains. Geophys. J. Int., 104, 387-399.

Merrill, R.T., 1975. Magnetic effects associated with chemical changes in igneous rocks. Geophys. Surv., 2, 277-311.

Mertig, H.J., Rubin, J.N. and Kyle, J.R., 1994. Skarn Cu-Au orebodies of the Gunung Bijih (Ertsberg) district, Irian Jaya, Indonesia. J. Geochem. Explor., 50, 179-202.

Meyer, C. and Hemley, J., 1967. Wall rock alteration. *In*: Barnes, H.L. (Ed), Geochemistry of Hydrothermal Ore Deposits, First Edition. Wiley-Interscience, New York, 166-235.

Miller, C.F., Watson, E.B. and Harrison, T,M., 1988. Perspectives on the source, segregation and transport of granitoid magmas. Trans. Roy. Soc. Edinburgh, Earth Sci., 79, 135-156.

Mohr, D.W. and Newton, R.C., 1983. Kyanite-staurolite metamorphism in sulfidic schists of the Anakeesta Formation, Great Smoky Mountains, North Carolina. Am. J. Sci., 283, 97-134.

Moore, W.J., 1978. Chemical characteristics of hydrothermal alteration at Bingham, Utah. Econ. Geol., 73, 1260-1269.

Morasse, S., Wasteneys, H.A., Cormier, M., Helmstaedt, H. and Mason. R., 1995. A pre-2686 Ma intrusion-related gold deposit at the Kiena mine, Val d'Or, Québec, southern Abitibi subprovince. Econ. Geol., 90, 1310-1321.

Morasse, S., Wasteneys, H.A., Cormier, M., Helmstaedt, H. and Mason. R., 1996a. A pre-2686 Ma intrusion-related gold deposit at the Kiena mine, Val d'Or, Québec, southern Abitibi subprovince - a reply. Econ. Geol., 91, 801-803.

Morasse, S., Wasteneys, H.A., Cormier, M., Helmstaedt, H. and Mason. R., 1996b. A pre-2686 Ma intrusion-related gold deposit at the Kiena mine, Val d'Or, Québec, southern Abitibi subprovince - a reply. Econ. Geol., 91, 807-811.

Morrison, G.W., 1980. Characteristics and tectonic setting of the shoshonite rock association. Lithos, 13, 97-108.

Morrison, G.W. and Blevin, P.L., 1995. Field trip guide: Magmatic and hydrothermal evolution of major intrusive related gold deposits - North Queensland. Report prepared for AMIRA P425, 102p.

Morrison, G.W. and Seed, M., 1993. Controls on the location of ore shoots in the Kidston breccia pipe - a model for exploration. Unpublished report to Kidston Gold Mines, 33p.

Morrison, G.W., Andrew, A.S. and Teale, G.S., 1988. Origin of gold mineralisation in the Mount Leyshon diatreme. Geol. Soc. Aust. Abstracts, 22, 116-120.

Morrison, G.W., Seed, M., Bobis, R. and Tullemans, F., 1996. The Kidston Gold Deposit, Queensland: a piston cylinder model for gold mineralisation in a porphyry Mo system. Geol. Soc. Aust. Abstr., v.41.

Mueller, R.F., 1971. Oxidative capacity of magmatic components. Am. J. Sci., 270, 236-243.

Müller, D. and Groves, D.I., 1995. Potassic igneous rocks and associated gold-copper mineralization. Springer-verlag, Berlin, 210 pp.

Müller, D., Heithersay, P.S. and Groves, D.I., 1994. The shoshonite porphyry Cu-Au association in the Goonumbla district, N.S.W., Australia. Mineral. Petrol., 51, 299-321.

Murata, M and Itaya, T., 1987. Sulfide and oxide minerals from S-type and I-type granitic rocks. Geochim. Cosmochim. Acta, 51, 497-507.

Mutschler, F.E. and Mooney, T.C., 1993. Precious-metal deposits related to alkalic igneous rocks: provisional classification, grade-tonnage data and exploration frontiers. *In*: R.V. Kirkham, W.D. Sinclair, R.I. Thorpe and J.M. Duke (Eds), Mineral Deposit Modeling. Geological Association of Canada, Special Paper 40, 465-478.

Mutschler, F.E., Mooney, T.C. and Johnson, D.C., 1991. Precious metal deposits related to alkaline igneous rocks - a space-time trip yhrough the Cordillera. Mng Eng., March 1991, 304-309.

Mutton, A.J. and Shaw, R.D., 1979. Physical property measurements as an aid to magnetic interpretation in basement terrains. Bull. Aust. Soc. Explor. Geophys., 10, 79-91.
Hollister, V.F., 1975. An appraisal of the nature and source of porphyry copper deposits. Minerals Sc. Engng, 7, 225-233.

Myers, G.L. and Meinert, L.D., 1991. Alteration, mineralization, and gold distribution in the Fortitude gold skarn. *In*: Raines, G.L., Lisle, R.E., Schafer, R.W. and Willkinson, W.H., 1991 (Eds), Geology and Ore Deposits of the Great Basin (Symposium Proceedings, Reno, Nevada, April 1-5, 1990). Geol. Soc. Nevada, Reno, 407-417.

Myers, G., Dennis, M.D., Wilkinson, W.H. and Wendt, C.J., 1991. Precious-metal distribution in the Mount Hamilton polymetallic skarn system, Nevada. *In*: Raines, G.L., Lisle, R.E., Schafer, R.W. and Willkinson, W.H., 1991 (Eds), Geology and Ore Deposits of the Great Basin (Symposium Proceedings, Reno, Nevada, April 1-5, 1990). Geol. Soc. Nevada, Reno, 393-403.

Nakamura, K., 1995. Case history of the discovery of the Hishikari gold deposit, Japan. Proceedings of the PACRIM '95 Conference, 429-434.

Nedachi, M., Enjoji, M., Urashima, Y. and Manser, W., 1984. Preliminary study on the rock magnetism of the intrusives from the Panguna ore deposit, Bouganville, Papua New Guinea. Kagoshima University Research Center for the South Pacific, Report 6, Subject I. Prompt Report of 3rd Scientific Survey of South Pacific.

Nedachi, M., Enjoji, M., Urashima, Y. and Manser, W., 1985. On the paleomagnetism of the intrusives from the Panguna porphyry copper deposit, Bouganville, Papua New Guinea. Kagoshima University Research Center for the South Pacific, Occasional Papers, 5, 13-26.

Neindorf, L., Dennis, R., Palmer, G. and Clark, A., 1993. Ravenswood gold mine, an experience of rapid exploration, development and production. Geol. Soc. Aust. Field Excursion Guidebook, Charters Towers, 12-14 June, 1993, 33-35.

Nesbitt, B.E., 1986a. Oxide-sulfide-silicate equilibria associated with metamorphosed ore deposits. Part I: theoretical considerations. Econ. Geol., 81, 831-840.

Nesbitt, B.E., 1986b. Oxide-sulfide-silicate equilibria associated with metamorphosed ore deposits. Part II: pelitic and felsic volcanic terrains. Econ. Geol., 81, 841-856.

Ney, C.S. and Hollister, V.F., 1976. Geologic setting of porphyry deposits of the Canadian Cordillera. *In*: Sutherland Brown, A. (Ed), Porphyry Deposits of the Canadian Cordillera. Canadian Institute of Mining and Metallurgy, Special Volume 15, 21-29.

Nielsen, R.L., 1968. Hypogene texture and mineral zoning in a copper-bearing granodiorite porphyry stock, Santa Rita, New Mexico. Econ. Geol., 63, 37-50.

Nilsson, K. and Peach, C.L., 1993. Sulfur speciation, oxidation state, and sulfur concentration in backarc magmas. Geochim. Cosmochim. Acta, 57, 3807-3813.

Okada, K., 1995. Geophysical exploration for epithermal gold deposits: case studies from the Hishikari gold mine, Kagoshima, Japan. Explor. Geophys., 26, 78-83.

Oldenburg, D.W., Li, Y. and Ellis, R.G., 1997. Inversion of geophysical data over a copper-gold porphyry deposit: a case history for Mt. Milligan. Geophysics, 62, 1419-1431.

Olesen, O., Henkel, H., Kaada, K. and Tveten, E., 1991. Petrophysical properties of a prograde amphibolite-granulite facies transition zone at Sigerfjord, Vesteralen, northern Norway. Tectonophysics, 192, 33-39.

Oliver, H.W., 1977. Gravity and magnetic investigations of the Sierra Nevada batholith, California. Geol. Soc. Am. Bull., 88, 445-461.

Opdyke, N.D., Clauoe-Long, J., Roberts, J. and Irving, E., 1996. Preliminary magnetostratigraphic results from the Carboniferous (Kiaman) of eastern Australia (abstract). Annales Geophysicae, 14, Suppl. 1, C142.

Oreskes, N. and Hitzman, M.W., 1993. A model for the origin of Olympic Dam-type deposits.
In: R.V. Kirkham, W.D. Sinclair, R.I. Thorpe and J.M. Duke (Eds), Mineral Deposit Modeling. Geological Association of Canada, Special Paper 40, 615-633.

Orr, T.H., 1994. The Mt Leyshon gold mine: geology and mineralisation. *In*: New Developments in Geology and Metallogeny: Northern Tasman Orogenic Zone, Townsville, 21-22 July, 1994, pp.29-35.

Orr, T.H., 1995. The Mt Leyshon gold mine: geology and mineralisation. *In*: Mineral Deposits of Northeast Queensland: Geology and Geochemistry. JCUNQ EGRU Contribution 52, pp.116-136.

Osborn, E.F., 1959. Role of oxygen pressure in the crystallization and differentiation of basaltic magma. Am. J. Sci., 257, 609-647.

Park, F.B., 1968. Remanent magnetism and the anomaly at Cottoner Mountain, Madison County, Missouri. Geophysics, 33, 613-620.

Pasteris, J.D., 1996. Mount Pinatubo volcano and “negative” porphyry copper deposits. Geology, 24, 1075-1078.

Paterson, N.R. and Hallof, P.G., 1993. Geophysical exploration for gold. *In*: R.P. Foster (Ed), Gold Metallogeny and Exploration, Chapman and Hall, London, pp. 361-398.

Patton, T.C., Grant, A.R. and Cheney, E.S., 1973. Hydrothermal alteration at the Middle Fork copper prospect, central Cascades, Washington. Econ. Geol., 68, 816-830.

Peccerillo, A. and Taylor, S.R., 1976. Geochemistry of Eocene calc-alkaline volcanic rocks from the Kastamonu area, northern Turkey. Contrib. Mineral. Petrol., 58, 63-81.

Pecherskiy, D.M., 1963. Statistical analysis of the reasons for the varying magnetization of the granitoids of the Verkhoyansk-Chutotka fold region and the Okhotsk-Chucotka belt. Inter. Geol. Rev., 7, 1963-1976.

Perelló, J.A., Fleming, J.A., O'Kane, K.P., Burt, P.D., Clarke, G.A., Himes, M.D. and Reeves, A.T., 1996. Porphyry copper-gold-molybdenum mineralization in the Island Copper cluster. *In*: Schroeter, T.G. (Ed), Porphyry Deposits of the Northwestern Cordillera of North America. Canadian Institute of Mining, Metallurgy and Petroleum, Special Volume 46, 214-238.

Perkins, C. and Wyborn, L., 1996. The age of Cu-Au mineralisation, Cloncurry district, Mount Isa Inlier, as determined by $^{40}A/^{39}A$ dating. AGSO Research Newsletter, 25, 8-9.

Perring, C.S., Groves, D.I. and Shellabear, J., 1989. The porphyry-gold association in the Yilgarn Block of Western Australia: spatial coincidence or genetic connection? *in* I. Haapala and Y. Kahkonen (eds). Symposium Precambrian Granitoids. Geol. Surv. Finland Spec. Paper 8, 100-101.

Peters, S.G., 1987. Geology and Lode Controls of the Charters Towers Goldfield, Northeastern Queensland. EGRU Contribution 19, James Cook University of North Queensland, Townsville.

Petersen, N. and Bleil, U., 1982. Magnetic properties of rocks *in* G. Angenheister (ed), Physical Properties of Rocks, Landolt-Bornstein Numerical Data and Functional Relationships in Science and Technology, Group V, Volume 1b. Springer-Verlag, Berlin.

Phillips, C.H., Gambell, N.A. and Fountain, D.S., 1974. Hydrothermal alteration, mineralization, and zoning in the Ray deposit. Econ. Geol., 69, 1237-1250.

Pilcher, S.H. and Mc Dougall, J.J., 1976. Characteristics of some Canadian Cordilleran porphyry prospects. *In*: Sutherland Brown, A. (Ed), Porphyry Deposits of the Canadian Cordillera. Canadian Institute of Mining and Metallurgy, Special Volume 15, 79-82.

Pitcher, W.S., 1979a. The nature, ascent and emplacement of granitic magmas. J. Geol. Soc. London, 136, 627-662.

Pitcher, W.S., 1979b. Comments on the geological environments of granites *in* Atherton, M.P. and Tarney, J., 1979 (eds). Origin of Granite Batholiths. Shiva Publishing, pp. 1-8.

Pitcher, W.S., 1983. Granite type and tectonic environment *in* K. Hsu (ed), Mountain Building Processes, Academic Press, London, pp. 19-40.

Plant, J.A., O'Brien, C., Tarney, J. and Hurdley, J., 1985. Geochemical criteria for the recognition of high heat production granites. *In*: High Heat Production (HHP) Granites, Hydrothermal Circulation and Ore Genesis. Inst. Min. Metall., London, pp.263-285.

Ponce, D.A., 1991. Gravity and magnetic anomalies in the Ely quadrangle, Nevada, and anomalies related to granitic plutons. *In*: Raines, G.L., Lisle, R.E., Schafer, R.W. and Willkinson, W.H., 1991 (Eds), Geology and Ore Deposits of the Great Basin (Symposium Proceedings, Reno, Nevada, April 1-5, 1990). Geol. Soc. Nevada, Reno, 103-106.

Popp, R.K., Gilbert, C.M. and Craig, J.R., 1977. Stability of Fe-Mg amphiboles with respect to oxygen fugacity. Am. Mineral., 62, 1-12.

Potter, D.R., 1996. What makes Grasberg anomalous, implications for future exploration. *In*: Porphyry Related Copper and Gold deposits of the Asia Pacific Region (Conference Proceedings), Australian Mineral Foundation, 10.1-10.13.

Power, L.F. and Fine, H.A., 1976. The iron-sulphur system. Part I. The structure and physical properties of the compounds of the low-temperature phase fields. Minerals Sci. Engng, 8:106-128.

Preece, R.K. and Beane, R.E., 1982. Contrasting evolutions of hydrothermal alteration in quartz monzonite and quartz diorite wall rocks at the Sierrita porphyry copper deposit, Arizona. Econ. Geol., 77, 1621-1641.

Princehouse, D.S. and Dilles, J.H., 1996. Mesozoic porphyry gold-copper mineralization at the Wheeler Mine, Pine Grove District, Nevada. *In*: A.R. Coyner and P.L. Fahey (Eds), Geology and Ore Deposits of the American Cordillera. Geol. Soc. Nevada Symposium Proceedings, p.1533-1556.

Pucher, R., 1994. Pyrrhotite-induced aeromagnetic anomalies in western Germany. J. Appl. Geophys., 32, 33-42.

Puffer, J.H., 1972. Iron-bearing minerals as indicators of intensive variables pertaining to granitic rocks from the Pegmatite Points area, Colorado. Am. J. Sci., 272, 273-289.

Puranen, R., 1989. Susceptibilities, iron and magnetite content of Precambrian rocks from Finland. Geol. Surv. Finland Rep. Inv. 90, 45 pp.

Putnis, A. and McConnell, J.D.C., 1980. Priniples of Mineral Behaviour. Blackwell, Oxford, 257pp.

Rajagopalan, S., Schmidt, P. and Clark, D., 1993. Rock magnetism and geophysical interpretation of the Black Hill Norite, South Australia. Explor. Geophys., 24, 209-212.

Rajagopalan, S., Clark, D. and Schmidt, P., 1995. Magnetic mineralogy of the Black Hill Norite and its aeromagnetic and palaeomagnetic implications. Explor. Geophys., 26, 215-220.

Reed, L.E., 1987. Geophysics in gold exploration - some examples. Exploration ‘87 Proceedings, 473-485.

Reed, M.H., 1997. Hydrothermal alteration and its relationship to ore fluid composition. *In*: Barnes, H.L. (Ed), Geochemistry of Hydrothermal Ore Deposits, Third Edition. Wiley, New York, 303-365.

Reyes, A.G., 1990. Petrology of Phillipne geothermal systems and the application of alteration mineralogy to their assessment. J. Volcan. Geotherm. Res., 43, 279-309.

Ribbe, P.H., 1974 (editor). Sulfide mineralogy. Mineralogical Society of America Short Course Notes, 1.

Richards, J.P., 1990. Petrology and geochemistry of alkalic intrusives at the Porgera gold deposit, Papua New Guinea. J. Geochem. Explor., 35, 141-190.

Richards, J.P., 1992. Magmatic-epithermal transitions in alkalic systems: Porgera gold deposit, Papua New Guinea. Geology, 20, 547-550.

Richards,J.P., 1995a. Controls on scale in Porgera-type porphyry/epithermal gold deposits associated with mafic alkalic magmatism. *In*: A.H. Clark (Ed), Giant Ore Deposits - II, Controls on the Scale of Orogenic Magmatic-Hydrothermal Mineralization (Proceedings of the Second Giant Ore Deposits Workshop, Kingston, Ontario, Canada, April 25-27, 1995), pp. 682-706.

Richards, J.P., 1995b. Alkalic-type epithermal gold deposits - a review. *In*: J.F.H. Thompson (Editor), Magmas, Fluids and Ore Deposits. Mineralogical Association of Canada, Short Course Series, v. 23, 367-400.

Richards, J.P. and Kerrich, R., 1993. The Porgera gold mine, Papua New Guinea: magmatic hydrothermal to epithermal evolution of an alkalic-type precious metal deposit. Econ. Geol., 88, 1017-1052.

Richards, J.P. and McDougall, I., 1990. Geochronology of the Porgera gold deposit, Papua New Guinea: resolving the effects of excess argon on K-Ar and $^{40}Ar/^{39}Ar$ age estimates for magmatism and mineralization. Geochim. Cosmochim. Acta, 54, 1397-1415.

Richards, J.P., Chappell, B.W. and McCulloch, M.T., 1990. Intraplate-type magmatism in a continent-island arc collision zone: Porgera intrusive complex, Papaua New Guinea. Geology, 18, 958-961.

Richards, J.P., McCulloch, M.T., Chappell, B.W. and Kerrich, R., 1991. Sources of metals in the Porgera gold deposit, Papua New Guinea: evidence from alteration, isotope, and noble metal geochemistry. Geochim. Cosmochim. Acta, 55, 565-580.

Rienks, I.P., Tenison Woods, K.L. and Wyborn, D., 1995. Geology of the southeast portion of the Ravenswood Batholith. Queensland Geological Record 1995/4.

Rimstidt, J.D., 1997. Gangue mineral transport and deposition. *In*: Barnes, H.L. (Ed), Geochemistry of Hydrothermal Ore Deposits, Third Edition. Wiley, New York, 487-515.

Robert, F., 1996. A pre-2686 Ma intrusion-related gold deposit at the Kiena mine, Val d'Or, Québec, southern Abitibi subprovince - a discussion. Econ. Geol., 91, 803-807.

Roberts, M.P. and Clemens, J.D., 1993. Origin of high-potassium, calc-alkaline, I-type granitoids. Geology, 21, 825-828.

Rollinson, H.R., 1980. Iron-titanium oxides as an indicator of the role of the fluid phase during the cooling of granites metamorphosed to granulite grade. Min. Mag., 43, 623-631.

Romberger, S.B., 1991. Transport and deposition of precious metals in epithermal deposits.
In: Raines, G.L., Lisle, R.E., Schafer, R.W. and Willkinson, W.H., 1991 (Eds), Geology and Ore Deposits of the Great Basin (Symposium Proceedings, Reno, Nevada, April 1-5, 1990). Geol. Soc. Nevada, Reno, 219-232.

Rona, P.A., 1978. Magnetic signatures of hydrothermal alteration and volcanogenic mineral deposits in oceanic crust. J. Volcan. Geotherm. Res., 3, 219-225.

Rose, A.W., 1970. Zonal relations of wallrock alteration and sulfide distribution at porphyry copper deposits. Econ. Geol., 65, 920-936.

Rose, A.W. and Baltosser, W.W., 1966. The porphyry copper deposit at Santa Rita, New Mexico.
In: S.R. Titley and C.L. Hicks (Eds), Geology of the Porphyry Copper Deposits, Southwestern North America. University of Arizona Press, Tucson, pp.205-220..

Rose, A.W. and Burt, D.M, 1979. Hydrothermal alteration. *In*: Barnes, H.L. (Ed), Geochemistry of Hydrothermal Ore Deposits, Second Edition. Wiley-Interscience, New York, 173-235.

Rotherham, J.F., 1997. A metasomatic origin for the iron-oxide Au-Cu Starra orebodies, Eastern Fold Belt, Mount Isa Inlier. Mineral. Deposita, 32, 205-218.

Rowins, S.M., Cameron, E.M., Lalonde, A.E. and Ernst, R.E., 1993. Petrogenesis of the Late Archean syenitic Murdock Creek pluton, Kirkland Lake, Ontario: evidence for a late extensional tectonic setting. Can. Mineral., 31, 219-244.

Rubin, J.N., 1996. Skarn formation and ore deposition at the Gunung Bijih Timur (Erstberg East) complex, Irian Jaya, Indonesia. Ph.D. dissertation, University of Texas at Austin, 311p.

Rush, P.M. and Seegers, H.J., 1990. Ok Tedi copper-gold deposits. *In*: F.E. Hughes (Ed.), Geology of the Mineral Deposits of Australia and Papua New Guinea, Aus. IMM, Melbourne, 1747-1754.

Rytuba, J.J., 1994. Evolution of volcanic and tectonic features in caldera settings and their importance in the localization of ore deposits. Econ. Geol., 89, 1687-1696.

Sander, M.V. and Einaudi, M.T., 1990. Epithermal deposition of gold during transition from propylitic to potassic alteration at Round Mountain, Nevada. Econ. Geol., 85, 285-311.

Sander, M.V. and Einaudi, M.T., 1991. Epithermal deposition of gold during transition from propylitic to potassic alteration at Round Mountain, Nevada - a reply. Econ. Geol., 86, 894-897.

Sanderson, D.D., 1974. Spatial distribution and origin of magnetite in an intrusive igneous mass. Geol. Soc. Am. Bull., 85, 1183-1188.

Sauck, W.A., 1972. Magnetic susceptibility and magnetite content. Econ. Geol., 67, 383-385.

Scheibner, E. and Basden, H., 1996. Geology of New South Wales - Synthesis. Volume 1, Structural Framework. Geol. Surv. NSW, Memoir Geology 13(1).

Schmidt, P.W., Clark, D.A. and Rajagopalan, S., 1993. An historical perspective of the Early Palaeozoic APWP of Gondwana: new results from the Early Ordovician Black Hill Norite, South Australia. Exploration Geophysics, 24, 257-262.

Schmidt, P.W., Clark, D.A. and Logan, K.J., 1997. Palaeomagnetism, magnetic petrophysics and magnetic signature of the Porgera Intrusive Complex, Papua New Guinea. Explor. Geophys., 28, 276-280.

Schroeter, T.G. (Ed), 1995. Porphyry Deposits of the Northwestern Cordillera of North America. Canadian Institute of Mining, Metallurgy and Petroleum, Special Volume 46.

Schwarz, E.J., 1991. Magnetic expressions of intrusions including magnetic aureoles. Tectonophysics, 192, 191-200.

Schwarz, E.J. and Broome, J., 1994. Magnetic anomalies due to pyrrhotite in Paleozoic metasediments in Nova Scotia, eastern Canada. J. Appl. Geophys., 32, 1-10.

Schwarz, E.J. and Buchan, K.L., 1989. Identifying types of remanent magnetization in igneous contact zones. Phys. Earth Planet. Inter., 158, 155-162.

Scott, K.M. and Dickson, B.L., 1991. Radioelements in rocks and soils in and about the Kidston gold deposit, N.E. Queensland. CSIRO Division of Exploration Geoscience Restricted Report 196R.

Seedorff, E., 1991a. Royston district, western Nevada - a Mesozoic porphyry copper system that was tilted and dismembered by Tertiary normal faults. *In*: Raines, G.L., Lisle, R.E., Schafer, R.W. and Willkinson, W.H., 1991 (Eds), Geology and Ore Deposits of the Great Basin (Symposium Proceedings, Reno, Nevada, April 1-5, 1990). Geol. Soc. Nevada, Reno, 359-391.

Seedorff, E., 1991b. Magmatism, extension, and ore deposits of Eocene to Holocene age in the Great Basin - mutual effects and preliminary proposed genetic relationships. *In*: Raines, G.L., Lisle, R.E., Schafer, R.W. and Willkinson, W.H., 1991 (Eds), Geology and Ore Deposits of the Great Basin (Symposium Proceedings, Reno, Nevada, April 1-5, 1990). Geol. Soc. Nevada, Reno, pp. 133-178.

Seraphim, R.H. and Hollister, V.F., 1976. Structural settings. *In*: Sutherland Brown, A. (Ed), Porphyry Deposits of the Canadian Cordillera. Canadian Institute of Mining and Metallurgy, Special Volume 15, 30-43.

Seward, T.M., 1993. The hydrothermal geochemistry of gold. *In*: R.P. Foster (Ed), Gold Metallogeny and Exploration, Chapman and Hall, London, pp.37-62.

Seward, T.M. and Barnes, H.L., 1997. Metal transport by hydrothermal fluids. *In*: Barnes, H.L. (Ed), Geochemistry of Hydrothermal Ore Deposits, Third Edition. Wiley, New York, 435-486.

Sexton, M.A., 1994. Geophysical characteristics of the Telfer gold deposits, Western Australia. *In*: Dentith, M.C., Frankombe, K.F., Ho, S.E., Shepherd, J.M., Groves, D.I. and Trench, A. (Eds), Geophysical Signatures of Western Australian Mineral Deposits. Geology and Geophysics Department (Key Centre) & UWA Extension, The University of Western Australia, Publication 26, and A.S.E.G. Special Publication 7, 199-212.

Sexton, M.A., Morrison, G.W., Orr, T.O.H., Foley, A.M. & Wormald, P.J., 1995. The Mt Leyshon magnetic anomaly. Explor. Geophys., 26, 84-91.

Shawe, D.R., 1991. Structurally controlled gold trends imply large gold resources in Nevada. *In*: Raines, G.L., Lisle, R.E., Schafer, R.W. and Willkinson, W.H., 1991 (Eds), Geology and Ore Deposits of the Great Basin (Symposium Proceedings, Reno, Nevada, April 1-5, 1990). Geol. Soc. Nevada, Reno, pp. 199-212.

Sheets, R.W., Nesbitt, B.E. and Muehlenbachs, K., 1996. Meteoric water component in magmatic fluids from porphyry copper mineralization, Babine Lake area, British Columbia. Geology, 24, 1091-1094.

Shinohara, H., Kazahaya, K. and Lowernstern, J.B., 1995. Volatile transport in a convecting magma column: implications for porphyry Mo mineralization. Geology, 23, 1091-1094.

Shive, P.N., 1989. Can remanent magnetization in the deep crust contribute to long wavelength magnetic anomalies? Geophys. Res. Lett., 16, 89-92.

Sillitoe, R.H., 1972. A plate tectonic model for the origin of porphyry copper deposits. Econ. Geol., 67, 184-197.

Sillitoe, R.H., 1973a. The tops and bottoms of porphyry copper deposits. Econ. Geol., 68, 799-815.

Sillitoe, R.H., 1973b. Geology of the Los Pelambres porphyry copper deposit, Chile. Econ. Geol., 68, 1-10.

Sillitoe, R.H., 1979. Some thoughts on gold-rich porphyry copper deposits: Mineral. Dep., 14, 161-1744.

Sillitoe, R.H., 1987. Copper, gold and subduction: a trans-Pacific perspective. Pacific Rim Congress 87 Proceedings, Gold Coast, 399-403.

Sillitoe, R.H., 1988a. Gold deposits in western Pacific island arcs: the magmatic connection.
In: Keays, R.R., et al., The Geology of Gold Deposits: the Perspective in 1988. Econ. Geol. Monograph 6, 274-291.

Sillitoe, R.H., 1988b. Gold and silver deposits in porphyry systems. *In*: Schafer, R.W., Cooper, J.J. and Vikre, P.G. (Eds), Bulk Mineable Precious Metal Deposits of the Western United States. Geological Society of Nevada, Reno, 233-257.

Sillitoe, R.H., 1990. Gold-rich porphyry copper deposits of the circum-Pacific region - an updated overview. Pacific Rim 90 Congress Proceedings, 119-126.

Sillitoe, R.H., 1993a. Giant and bonanza gold deposits in epithermal and subvolcanic settings. *In*: Whiting, B.H., Mason, R. and Hodgson, C.J.(Eds), Giant Ore Deposits, Society of Economic Geologists, Special Publication 2, pp. 232-236.

Sillitoe, R.H., 1993b. Epithermal models: genetic types, geometrical controls, and shallow features. *In*: Whiting, B.H., Mason, R. and Hodgson, C.J.(Eds), Giant Ore Deposits, Society of Economic Geologists, Special Publication 2, pp. 239-301.

Sillitoe, R.H., 1993c. Gold-rich porphyry copper deposits: geological model and exploration implications. *In*: Whiting, B.H., Mason, R. and Hodgson, C.J.(Eds), Giant Ore Deposits, Society of Economic Geologists, Special Publication 2, pp. 305-362.

Sillitoe, R.H., 1993d. Intrusion-related gold deposits. *In*: R.P. Foster (Ed), Gold Metallogeny and Exploration, Chapman and Hall, London, pp.165-209.

Sillitoe, R.H., 1993e. Epithermal models: genetic types, geometrical controls and shallow features. *In*: R.V. Kirkham, W.D. Sinclair, R.I. Thorpe and J.M. Duke (Eds), Mineral Deposit Modeling. Geological Association of Canada, Special Paper 40, 403-417.

Sillitoe, R.H., 1993f. Epithermal models: genetic types, geometrical controls and shallow features. *In*: R.V. Kirkham, W.D. Sinclair, R.I. Thorpe and J.M. Duke (Eds), Mineral Deposit Modeling. Geological Association of Canada, Special Paper 40, 465-478.

Sillitoe, R.H., 1994. Erosion and collapse of volcanoes: causes of telescoping in intrusion-centered ore deposits. Geology, 22, 945-948.

Sillitoe, R.H., 1995. The influence of magmatic-hydrothermal models on exploration strategies for volcano-plutonic arcs. *In*: J.F.H. Thompson (Editor), Magmas, Fluids and Ore Deposits. Mineralogical Association of Canada, Short Course Series, v. 23, 511-525.

Sillitoe, R.H., 1996. Characteristics and controls of the largest porphyry copper-gold and epithermal gold deposits in the circum-Pacific region. Aust J. Earth Sci., 44, 373-388.

Skewes, M.A. and Stern, C.R., 1995. Genesis of the giant Late Miocene to Pliocene copper deposits of central Chile in the context of Andean magmatic and tectonic evolution. Int. Geol. Rev., 37, 893-909.

Skilbrei, J.R., Skyseth, T. and Olesen, O., 1991. Petrophysical data and opaque mineralogy of high-grade and retrogressed lithologies: implications for the interpretation of aeromagnetic anomalies in northern Vestranden, central Norway. Tectonophysics, 192, 21-31.

Skinner, B.J., 1997. Hydrothermal mineral deposits: what we do and don’t know. *In*: Barnes, H.L. (Ed), Geochemistry of Hydrothermal Ore Deposits, Third Edition. Wiley, New York, 1-29.

Skirrow, R.G. and Walshe, J.L., 1994. Transport and deposition of gold, copper and bismuth in the Tennant Creek goldfield, N.T.: evidence for involvement of reducing and oxidising fluids. Geol. Soc. Aust. Abstracts, 37, 470.

Smith, R.J., 2002. Geophysics of iron oxide copper-gold deposits *in* Porter, T.M. (ed.) Hydrothermal Iron Oxide Copper-Gold & Related Deposits: A Global Perspective, Volume 2. PGC Publishing, Adelaide, 123-136.

Smithies, R.H. and Witt, W.K., 1997. Distinct basement terranes identified from granite geochemistry in late Archaean granite-greenstones, Yilgarn Craton, Western Australia. Precam. Res., 83, 185-201.

Solomon, M., 1990. Subduction, arc reversal, and the origin of porphyry copper-gold deposits in island arcs. Geology, 18, 630-633.

Speer, J.A., 1981. The nature and magnetic expression of isograds in the contact aureole of the Liberty Hill pluton, South Carolina: Geol. Soc. Am. Bull., Part I, 92, 603-609 and Part II, 92, 1262-1358.

Stewart, J.H., Moore, W.J. and Zietz, I., 1977. East-west patterns of Cenozoic igneous rocks, aeromagnetic anomalies, and mineral deposits, Nevada and Utah. Geol. Soc. Am. Bull., 88, 67-77.

Stolz, A.J. and Morrison, R.J., 1994. Proterozoic igneous activity in the Tennant Creek region, Northern Territory, Australia, and its relationship to Cu-Au-Bi mineralisation. Mineral. Deposita, 29, 261-274.

Studemeister, P.A., 1983. The redox state of iron: a powerful indicator of hydrothermal alteration: Geoscience Canada, 10, 189-194.

Stussi, J.-M., 1989. Granitoid chemistry and associated mineralization in the French Variscan. Econ. Geol., 84, 1363-1381.

Suppel, D.W., Warren, A.Y.E., Watkins, J.J., Chapman, J., Tenison Woods, K. and Barron, L., 1986. A reconnaisance study of the geology and gold deposits of the West Wyalong - Temora - Adelong district. N.S.W. Geol. Surv. Quart. Notes, 64, 1-23.

Susak, N.J., 1994. Alteration factors affecting ore deposition. *In*: D.R. Lentz (Editor), Alteration and Alteration Processes Associated with Ore-forming Systems. Geological Association of Canada Short Course Notes, v.11, 69-99.

Sutherland Brown, A., 1976. Morphology and classification. *In*: Sutherland Brown, A. (Ed), Porphyry Deposits of the Canadian Cordillera. Canadian Institute of Mining and Metallurgy, Special Volume 15, 44-51.

Takagi, T. and Nureki, T., 1994. Two T-f(O_2) paths in the Myoken-Zan magnetite-bearing granitic complex, San'yo Belt, southwestern Japan. Can Mineral., 32, 747-762.

Takagi, T. and Tsukimura, K., 1997. Genesis of oxidized- and reduced-type granites. Econ. Geol., 92, 81-86.

Takahashi, M., 1989. Neogene granitic magmatism in the South Fossa Magna collision zone, Central Japan. Modern Geology, 14, 127-143.

Takahashi, M., Aramaki, S. and Ishihara, S., 1980. Magnetite-series/ilmenite-series vs. I-type/S-type granitoids. Min. Geol. Spec. Issue, 8, 13-28.

Taner, M., 1996. A pre-2686 Ma intrusion-related gold deposit at the Kiena mine, Val d'Or, Québec, southern Abitibi subprovince - a discussion. Econ. Geol., 91, 799-801.

Tarling, D.H. & Hrouda, F., 1993. The magnetic anisotropy of rocks. Chapman and Hall, London.

Taylor, J.R. and Wall, V.J., 1990. The behaviour of tin in magmatic-hydrothermal systems. Geol. Soc. Aust. Abstracts, 25, 270-271.

Tenison Woods, K. and Rienks, I., 1992. New insights into the structure and subdivision of the Ravenswood Batholith - a geophysical perspective. Exploration Geophysics, 23, 353-359.

Tenison Woods, K. and Webster, S.S., 1985. Geophysical signature of gold and porphyry copper mineral deposits in the Lachlan Fold Belt, NSW. Explor. Geophys., 16, 279-283.

Thomson, G.F., Cornwell, J.D. & Collinson, D.W., 1991. Magnetic characteristics of some pyrrhotite-bearing rocks in the United Kingdom. Geoexploration, 28, 23-42.

Thompson, J.F.H., 1995. Exploration and research related to porphyry deposits. *In*: Schroeter, T.G. (Ed), Porphyry Deposits of the Northwestern Cordillera of North

America. Canadian Institute of Mining, Metallurgy and Petroleum, Special Volume 46, 857-870.

Thompson, J.F.H., Lang, J.R., Mortensen and Cassidy, K.F., 1995. Cu-Au metallogeny of Alkalic arc magmatism: examples from the Mesozoic arc terranes of the northern Canadian Cordillera and comparisons to the Tabar-Feni arc, PNG. *In*: A.H. Clark (Ed), Giant Ore Deposits - II, Controls on the Scale of Orogenic Magmatic-Hydrothermal Mineralization (Proceedings of the Second Giant Ore Deposits Workshop, Kingston, Ontario, Canada, April 25-27, 1995), pp. 725-731.

Titley, S.R., 1993a. Characteristics of porphyry copper occurrence in the American Southwest. *In*: R.V. Kirkham, W.D. Sinclair, R.I. Thorpe and J.M. Duke (Eds), Mineral Deposit Modeling. Geological Association of Canada, Special Paper 40, 433-464.

Titley, S.R., 1993b. Characteristics of high-temperature, carbonate-hosted massive sulphide ores in the United States, Mexico and Peru. *In*: R.V. Kirkham, W.D. Sinclair, R.I. Thorpe and J.M. Duke (Eds), Mineral Deposit Modeling. Geological Association of Canada, Special Paper 40, 585-614.

Titley, S.R., 1994. Evolutionary habits of hydrothermal and supergene alteration in intrusion-centred ore systems, southwestern North America. *In*: D.R. Lentz (Editor), Alteration and Alteration Processes Associated with Ore-forming Systems. Geological Association of Canada Short Course Notes, v.11, 69-99.

Titley, S.R., 1995. Geological summary and perspective of porphyry copper deposits in southwestern North America. *In*: F.W. Pierce and J.G. Bolm (Eds), Porphyry Copper Deposits of the American Cordillera. Arizona Geological Society Digest, 20, 6-20.

Titley, S.R., 1995?. Size aspects of porphyry copper systems southwestern North America. ?*In*: A.H. Clark (Ed), Giant Ore Deposits - II, Controls on the Scale of Orogenic Magmatic-Hydrothermal Mineralization (Proceedings of the Second Giant Ore Deposits Workshop, Kingston, Ontario, Canada, April 25-27, 1995), pp.374-401.

Titley, S.R. and Beane, R.E., 1981. Porphyry copper deposits Part I. Geologic settings, petrology and petrogenesis. Econ. Geol., 75th Anniversary Volume, 214-235.

Torrey, C.E., Karjalainen, H., Joyce, P.J., Erceg, M. and Stevens, M., 1986. Geology and mineralization of the Red Dome (Mungana) gold skarn deposit, North Queensland, Australia. Proceedings of Gold ‘86 Symposium, Toronto, 504-517.

Tracy, R.J. and Robinson, P., 1988. Silicate-sulfide-oxide-fluid reactions in granulite-grade pelitic rocks, central Massachusetts. Am. J. Sci., 288-A, 45-74.

Trench, A., Dentith, M.C. and Li, Z.X., 1992. palaeomagnetic dating of mineral deposits: a brief review and a Western Australian perspective. Explor. Geophys., 23, 373-380.

Trudu, A.G. and Bloom, M.S., 1988. A genetic model for the origin of hypogene gold in porphyry copper systems: the Tirad porphyry copper-gold deposit (Guinaoang, NW Luzon, Phillipines). Proceedings of Bicentennial Gold 88 Symposium, Melbourne, 211-216.

Urquhart, W.E.S., 1989. Field examples of controls on magnetite content. Explor. Geophys., 20, 93-97.

Urrutia-Fucugauchi, J. and Jurado-Chichay, Z., 1989. Palaeomagnetic correlation and dating of mineralization and intrusive events. Phys. Earth Planet. Inter., 55, 65-78.

Van Nort, S.D., Alwood, G.W., Collinson, T.B., Flint, D.C. and Potter, D.R., 1991. Geology and mineralization of the Grasberg porphyry copper-gold deposit, Irian Jaya, Indonesia. Mng Eng., March 1991, 300-303.

Vaughn, D.J. and Craig, J.R., 1997. Sulfide ore mineral stabilities, morphologies, and intergrowth textures. *In*: Barnes, H.L. (Ed), Geochemistry of Hydrothermal Ore Deposits, Third Edition. Wiley, New York, 1-29.

Vaughn, D.J. and Lennie, A.R., 1991. The iron sulphide minerals: their chemistry and role in nature. Sci. Progress Edinburgh, 75, 371-388.

Vernon, R.H., 1961. Magnetic susceptibility as a measure of total iron plus manganese in some ferromagnesian silicate minerals. Am. Mineral., 46, 1141-1153.

Vernon, R.H., Etheridge, M.A. and Wall, V.J., 1988. Shape and microstructure of micrgranitoid enclaves: indicators of magma mingling and flow. Lithos, 22, 1-11.

Wahl, W.G., 1960. An interpretative technique for delimiting mineral potential areas based on the magnetic susceptibility of source rocks. 21st International Geological Congress, Part 2, 200-215.

Wall, V.J. and Gow, P.A., 1995. Some copper-gold ore-forming systems: iron(ic) connections. *In*: A.H. Clark (Ed), Giant Ore Deposits - II, Controls on the Scale of Orogenic Magmatic-Hydrothermal Mineralization (Proceedings of the Second Giant Ore Deposits Workshop, Kingston, Ontario, Canada, April 25-27, 1995), pp.557-582.

Wall, V.J. and Taylor, 1990. Granite emplacement and temporally related gold mineralisation. Geol. Soc. Aust. Abstracts, 25, 264-265.

Wall, V.J. and Valenta, R.K., 1990. Ironstone-related gold-copper mineralisation: Tennant Creek and elsewhere. Pacific Rim 90 Congress Proceedings, Aus IMM, 855-863.

Wall, V.J., Clemens, J.D. and Clarke, D.B., 1987. Models for granitoid evolution and source compositions. J. Geology, 95, 731-749.

Wall, V.J., Munroe, S.M., Cameron, G.H., Heinrich, C.A., Cox, S.F. and Walshe, J.L., 1995. Porgera: plumbing and processes of gold mineralization. *In*: A.H. Clark (Ed), Giant Ore Deposits - II, Controls on the Scale of Orogenic Magmatic-Hydrothermal Mineralization (Proceedings of the Second Giant Ore Deposits Workshop, Kingston, Ontario, Canada, April 25-27, 1995), pp. 707-724.

Wallace, S.R., 1991. Model development: porphyry molybdenum deposits. *In*: Hutchinson, R.W. and Grauch, R.I. (Eds), Historical Perspectives of Genetic Concepts and Case Histories of Famous Discoveries. Econ. Geol. Monograph 8, 207-224.

Walshe, J.L., Heithersay, P.S. and Morrison, G.W., 1995. Toward an undestanding of the metallogeny of the Tasman fold belt system. Econ. Geol., 90, 1382-1401.

Wang, L.C., McNaughton, N.J. and Groves, D.I., 1991. Archaean granitoids in the Murchison Province, Western Australia: petrogenetic classification and relations to gold mineralisation *in* Second Hutton Symposium on Granites and Related Rocks, BMR Record 1991/25, 10.

Wang, L.C., McNaughton, N.J. and Groves, D.I., 1993. An overview of the relationship between granitoid intrusions and gold mineralisation in the Archaean granitoids in the Murchison Province, Western Australia. Mineral. deposita, 28, 482-494.

Ware, G.H., 1979. In-situ induced-polarization and magnetic susceptibility measurements - Yerington mine. Geophysics, 44, 1417-1428.

Washington, H.S. and Adams, L.H., 1951. The chemical and petrological composition of the Earth's crust. In: B. Gutenberg (Ed), Internal Constitution of the Earth, Dover, pp.81-106.

Webb, M. and Rowston, P., 1995. The geophysics of the Ernest Henry Cu-Au deposit (N.W.) Queensland. Explor. Geophys., 26, 51-59.

Webster, J.D., 1997. Exsolution of magmatic volatile phases fron Cl-enriched mineralizing granitic magmas and implications for ore transport. Geochim. Cosmochim. Acta, 61, 1017-1029.

Webster, S.S., 1984. A magnetic signature for tin deposits in south-east Australia: Explor. Geophys., 15, 15-31.

Webster, S., 2003. A geophysical signature for tin deposits in south-eastern Australia - revisited. ASEG 16th Geophysical Conference, Adelaide, Extended Abstracts.

Webster, S.S. and E. Scheibner, 1984. Introduction to the magnetic properties of New England granitoids. Explor. Geophys., 15, 67-73.

Wellman, P., 1988. Development of the Australian Proterozoic crust as inferred from gravity and magnetic anomalies. Precambrian Research, 40/41, 89-100.

Wellman, P., 1992. A geological interpretation of the regional gravity and magnetic features of north Queensland. Explor. Geophys., 23, 423-428.

Wellman, P., 1994. Mapping large-scale hydrothermal systems using coincident magnetic and gamma-ray spectrometric anomalies. AGSO Research Newsletter, 20, 16-17.

Wellman, P., 1995. Tasman Orogenic System: a model for its subdivision and growth history based on gravity and magnetic anomalies. Econ. Geol., 90, 1430-1442.

Whalen, J.B. and Chappell, B.W., 1988. Opaque mineralogy and mafic mineral chemistry of I- and S-type granites of the Lachlan Fold Belt, southeast Australia. Am. Mineral., 73, 281-296.

Whalen, J.B., Currie, K.L. and Chappell, B.W., 1987. A-type granites: geochemical characteristics, discrimination and petrogenesis: Contrib. Mineral. Petrol., 95, 407-419.

White, A.J.R., Wyborn, D. and Chappell, B.W., 1991. A granite classification for the economic geologist.

White, W.H., Bookstrom, A.A., Kamilli, R.J., Ganster, M.W., Smith, R.P., Ranta, D.E. and Steininger, R.C., 1981. Character and origin of Climax-type molybdenum deposits. Econ. Geol., 75th Anniversary Volume, 270-316.

Whiting, T.H., 1986. Aeromagnetics as an aid to geological mapping - a case history from the Arunta Inlier, Northern Territory. Austr J. Earth Sci., 33, 271-286.

Whiting, T.H., 1988. Magnetic mineral petrogenesis, rock magnetism and aeromagnetic response in the eastern Arunta Inlier, Northern Territory. Explor. Geophys., 19, 377-383.

Whitney, J.A., 1984. Fugacities of sulfurous gases in pyrrhotite-bearing silicic magmas. Am. Mineral., 69, 69-78.

Whitney, J.A., 1988. Composition and activity of sulfurous species in quenched magmatic gases associated with pyrrhotite-bearing silicic systems. Econ. Geol., 83, 86-92.

Whitney, J.A., 198?. Origin and evolution of silicic magmas. *In*: Whitney, J.A. and Naldrett, A.J. (Eds), Ore Deposition Associated With Magmas. Rev. Econ. Geol., 4, 183-201.

Whitney, J.A. and Stormer, J.C., 1976. Geothermometry and geobarometry in epizonal granitic intrusions: a comparison of iron-titanium oxides and coexisting feldspars. Am. Mineral., 61, 751-761.

Whitney, J.A., Hemley, J.A. and Simon, F.O., 1985. The concentration of iron in chloride solutions equilibrated with synthetic granitic compositions: the sulfur-free system. Econ. Geol., 80, 444-460.

Wilkins, J. and Heidrick, T.L., 1995. Post Laramide extension and rotation of porphyry copper deposits, southwestern United States. *In*: F.W. Pierce and J.G. Bolm (Eds), Porphyry Copper Deposits of the American Cordillera. Arizona Geological Society Digest, 20, 109-127.

Williams, P.J., 1994a. Iron mobility during synmetamorphic alteration in the Selwyn Range area, NW Queensland: implications for origin of ironstone-hosted Au-Cu deposits. Mineral. Deposita, 29, 250-260.

Williams, P.J., 1994b. Diverse nature of hematization (‘Red Rock Alteration’) in the Cloncurry district, northwest Queensland. Aust. J. Earth Sci., 41, 381-382.

Williams, D.L. and Finn, C., 1987. Evidence for a shallow pluton beneath the Goat Rocks wilderness, Washington, from gravity and magnetic data. J. Geophys. Res., 92, 4867-4880.

Wilt, J.C., 1995. Correspondence of alkalinity and ferric/ferrous ratios of igneous rocks associated with various types of porphyry copper deposits. *In*: F.W. Pierce and J.G. Bolm (Eds), Porphyry Copper Deposits of the American Cordillera. Arizona Geological Society Digest, 20, 180-201.

Wones, D.R., 1980. Contributions of crystallography, mineralogy and petrology to the geology of the Lucerne pluton, Hancock County, Maine. Am. Mineral., 65, 411-437.

Wones, D.R., 1989. Significance of the assemblage titanite + magnetite + quartz in granitic rocks. Am. Mineral., 74, 744-749.

Wones, D.R. and Gilbert, M.C., 1982. Amphiboles in the igneous environment *in* D.R. Veblen and P.H. Hill (Eds), Amphiboles: petrology and experimental phase relations. Reviews of Mineralogy, 355 -390.

Woodward, D.J. and Caldwell, T.G., 1992. Apparent magnetisation from aeromagnetic data. Explor. Geophys., 23, 447-452.

Woodward, D.J. and Mumme, T.C., 1993. Variation of magnetisation on White Island, New Zealand.
N.Z. J. Geol. Geophys., 36, 447-451.

Worm, H.U., 1989. Comment on "Can remanent magnetization in the deep crust contribute to long wavelength magnetic anomalies?" by Peter N. Shive. Geophys. Res. Lett., 16, 595-597.

Worm, H.-U., 1991. Multidomain susceptibility and anomalously strong low field dependence of induced magnetization in pyrrhotite. Physics of the Earth and Planetary Interiors, 69, 112-118.

Worm, H.-U., Clark, D. & Dekkers, M.J., 1993. Magnetic susceptibility of pyrrhotite: grain size, field and frequency dependence. Geophysical Journal International, 114, 127-137.

Wormald, P.J., 1993. Geology of the Mount Leyshon Gold Deposit, Australia: a study of breccia pipe formation, facies and brecciation mechanisms. Ph.D. thesis, James Cook University.

Wormald, R.J. and Price, R.C., 1990. The gabbro-quartz monzodiorite-alkali granite association in southern NSW: implications for intrusive related gold mineralisation. Geol. Soc. Aust. Abstracts, 25, 265-266.

Wormald, P.J., Orr, T.O.H. and Hodkinson, I.P., 1991. The Mount Leyshon gold mine (NE Queensland), an intrusive breccia and igneous complex. Proceedings of the World Gold ‘91 Symposium, Cairns, April 21-25.

Wyatt, D.H., Paine, A.G.L., Clarke, D.E., Gregory, C.M. and Harding, R.R., 1971. Geology of the Charters Towers 1:250,000 Sheet area, Queensland. Bureau of Mineral Resources, Australia, Report 137.

Wyborn, D., 1983. A comparison of restite control and fractional crystallisation in granites. Sixth Australian Geological Convention, Canberra, Geol. Soc. Aust. Abstracts, 9, 183-184.

Wyborn, D., 1992a. The tectonic significance of Ordovician magmatism in the eastern Lachlan Fold Belt. Tectonophysics, 214, 177-192.

Wyborn, D., 1992b. Stratigraphy and geochemistry of Ordovician volcanics from the Lachlan Fold Belt in central New South Wales. In: B.D. Webby and J.R. Laurie (Eds), Global Perspectives on Ordovician Geology. Balkema, Rotterdam, pp.495-497.

Wyborn, L.A.I., 1988. Petrology, geochemistry and origin of a major Australian 1880-1840 Ma felsic volcano-plutonic suite: a model for intracratonic felsic magma generation. Precam. Res., 40/41, 37-60.

Wyborn, L., 1992c. The Williams and Naraku Batholiths, Mt Isa Inlier: an analogue of the Olympic Dam Granites? BMR Research Newsletter, 16, 13-16.

Wyborn, L., 1992d. New results from the BMR Yilgarn granite database: implications for metallogeny, tectonics and lower crustal structure. BMR Research Newsletter, 16, 5-6.

Wyborn, L.A.I., 1993. Potential applications of palaeomagnetism in mineral exploration in northern Australia. Explor. Geophys., 124, 219-222.

Wyborn, L.A.I., 1994. Exploration criteria to determine which Australian Proterozoic granites may be associated with gold ± base metal mineralisation. Geol. Soc. Aust. Abstracts, 37, 12th Australian Geological Convention, Perth, 471.

Wyborn, L., 1996. An overview of temporal geochemical changes in Australian igneous rocks: implications for crustal evolution and metallogeny. Geol. Soc. Aust. Abstracts, 41, 482.

Wyborn, L.A. and Drummond, B.J., 1991. Australian Proterozoic granites: important indicators of crustal evolution *in* Second Hutton Symposium on Granites and Related Rocks, BMR Record 1991/25, 10.

Wyborn, L.A. and Heinrich, C., 1993a. The relationship between late-tectonic felsic intrusives and Cu-Au mineralisation in the Eastern Fold Belt, Mount Isa Inlier: In: Symposium on Recent Advances in the Mount Isa Block, Aust. Inst. Geosci. Bulletin, 13, 27-30.

Wyborn, L.A. and Heinrich, C., 1993b. Empirical observations on granite-associated gold ± base-metal mineral deposits in the Proterozoic of Australia. AGSO Research Newsletter, 19, 3-4.

Wyborn, L. and Stuart-Smith, P., 1993. The relationship between granite composition, host rock types, and Au ± base-metal mineralisation in the Cullen Mineral Field, Pine Creek Inlier. AGSO Research Newsletter, 19, 5-8.

Wyborn, D. and Sun, S-S., 1993. Nd-isotopic 'fingerprinting' of Cu/Au mineralisation in the Lachlan Fold Belt. AGSO Research Newsletter, 19, 13-14.

Wyborn, D. and Sun, S-S., 1994. Sulphur-undersaturated magmatism - a key factor for generating magma-related copper-gold deposits. AGSO Research Newsletter, 21, 7-8.

Wyborn, D., Chappell, B.W. and Johnston, R.M., 1981. Three S-type volcanic suites from the Lachlan Fold Belt, southeast Australia. J. Geophys. Res., 86, 10,355-10,348.

Wyborn, D., Turner, B.S. and Chappell, B.W., 1987. The Boggy Plain Supersuite: a distinctive belt of I-type igneous rocks of potential economic significance in the Lachlan Fold Belt. Aust. J. Earth Sci., 34, 21-43.

Wyborn, L., Idnurm, M. and Giddings, J., 1993. Potential applications of palaeomagnetism to mineral exploration in the Proterozoic of northern Australia. AGSO Research Newsletter, 19, 1-2.

Wyborn, L.A., Heinrich, C. and Jaques, A.L., 1994. Australian Proterozoic mappable systems: essential ingredients and mappable criteria. Proceedings of Aus. IMM Conference, Darwin, pp.109-115.

Wyllie, P.W., 1984. Sources of granitoid magmas at convergent plate boundaries. Phys. Earth Planet. Inter., 35, 12-18.

Wyllie, P.J., Huang, W.L., Stern, C.R. and Maalo/e S., 1976. Granitic magmas: possible and impossible sources, water contents, and crystallization sequences. Can. J. Earth Sci., 13, 1007-1019.

Yang, K. and Bodnar, R.J., 1994. Magmatic-hydrothermal evolution in the “bottoms” of porphyry copper systems: evidence from silicate melt and aqueous fluid inclusions in granitoid intrusions in the Gyeongsang Basin, South Korea. Int. Geol. Rev., 36, 608-628.

Yeates, A.N., Wyatt, B.W. and Tucker, D.H., 1982. Application of gamma ray spectrometry to prospecting for tin and tungsten granites, particularly within the Lachlan Fold Belt, New South Wales. Econ. Geol., 77, 1725-1738.

Yudin, B.A. and Katseblin, P.I., 1978. Petrophysical characteristics of gabbro-labradorite complexes, Kola Peninsula. Int. Geol. Rev., 23, 517-523.

Yudintsev, S.V., 1992. The valency of uranium in a granitic magma. Geochem. Int., 29(11), 130-133.

Zaluski, G., Nesbitt, B. and Muehlenbachs, K.,1994. Hydrothermal alteration and stable isotope systematics of the Babine porphyry Cu deposits, British Columbia: implications for fluid evolution of porphyry systems. Econ. Geol., 89, 1518-1541.

Zen, E-an, 1988. Phase relations of peraluminous granitic rocks and their petrogenetic implications. Ann. Rev. Earth Planet. Sci., 16, 21-51.

Zorpi, M.J., Coulon, C., Orsini, J.B. and Cocirta, C., 1989. Magma mingling, zoning and emplacement in calc-alkaline granitoid plutons. Tectonophysics, 157, 315-329.

APPENDIX A - PRODUCTS DISTRIBUTED TO SPONSORS

1. P700 relational database of geological, geophysical and petrophysical characteristics of deposits (Access)
2. P700 Atlas of geophysical signatures (empirical and predictive)
3. P700 Short Course Manual (this document)
4. Miscellaneous items on CD: Visual Basic program (Palaeo) to calculate remanence directions from palaeopoles and other geomagnetic and tectonic calculations; Global Palaeomagnetic Database; Susceptibility ready reckoner (Excel spreadsheet to calculate susceptibility from magnetite or monoclinic pyrrhotite content).